Applications of Group Theory

to the Physics of Solids

M. S. Dresselhaus

8.510J

6.734J

SPRING 2002

ii

Contents

Chapter 1

Basic Mathematical Background – Introduction

In this chapter we consider mainly mathematical definitions and concepts that are basic to group theory and the classification of symmetry properties.

1.1   Definition of a Group

A collection of elements $A, B, C, \ldots$ form a group when the following four conditions are satisfied:

1. The product of any two elements of the group is itself an element of the group. For example, relations of the type $AB = C$ are valid for all members of the group.

2. The associative law is valid – i.e., $(AB)C = A(BC)$.

3. There exists a unit element E (also called the identity element) such that the product of E with any group element leaves that element unchanged $AE = EA = A$.

4. For every element there exists an inverse, $A^{-1}A = AA^{-1} = E$.

It is not necessary that elements of the group commute. In general, the elements will not commute $AB \neq BA$. But if all elements of a group commute, the group is then called an **Abelian** group.

1
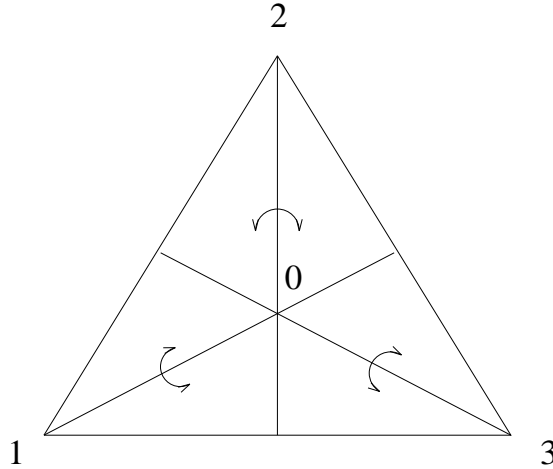
Figure 1.1: The symmetry operations on an equilateral triangle, are the rotations by $\pm 2\pi/3$ about the origin 0 and the rotations by π about the axes 01, 02, and 03.

1.2   Simple Example of a Group

As a simple example of a group, consider the permutation group for three elements, $P(3)$. Below are listed the 3!=6 possible permutations that can be carried out; the top row denotes the initial arrangement of the three numbers and the bottom row denotes the final arrangement.

$$E = \begin{pmatrix} 1 & 2 & 3 \\ 1 & 2 & 3 \end{pmatrix} \quad A = \begin{pmatrix} 1 & 2 & 3 \\ 2 & 1 & 3 \end{pmatrix} \quad B = \begin{pmatrix} 1 & 2 & 3 \\ 1 & 3 & 2 \end{pmatrix}$$

$$C = \begin{pmatrix} 1 & 2 & 3 \\ 3 & 2 & 1 \end{pmatrix} \quad D = \begin{pmatrix} 1 & 2 & 3 \\ 3 & 1 & 2 \end{pmatrix} \quad F = \begin{pmatrix} 1 & 2 & 3 \\ 2 & 3 & 1 \end{pmatrix} \tag{1.1}$$

This group is identical with the symmetry operations on a equilateral triangle shown in Fig. 1.1. What then are the symmetry operations of an equilateral triangle?

We can also think of the elements in Eq. 1.1 in terms of the 3 points of the triangle in the initial state and the bottom line as the effect of the six distinct symmetry operations that can be performed on these three points. We can call each symmetry operation an **element** of the group.

Table 1.1: Multiplication† table for permutation group of 3 elements; $P(3)$

	E	A	B	C	D	F
E	E	A	B	C	D	F
A	A	E	D	F	B	C
B	B	F	E	D	C	A
C	C	D	F	E	A	B
D	D	C	A	B	F	E
F	F	B	C	A	E	D

† $AD = B$ defines use of multiplication table.

It is convenient to classify the products of group elements. We write these products using a **multiplication table**. In Table 1.1 a multiplication table is written out for the symmetry operations on an equilateral triangle or equivalently for the permutation group of 3 elements. It can easily be shown that the symmetry operations given in Eq. 1.1 satisfy the four conditions in §1.1 and therefore form a group. Each symmetry element of the permutation group $P(3)$ has a one-to-one correspondence to the symmetry operations of an equilateral triangle and we therefore say that these two groups are **isomorphic** to each other. We furthermore can use identical group theoretical procedures in dealing with physical problems associated with either of these groups, even though the two groups arise from totally different physical situations. It is this generality that makes group theory so useful as a general way to classify symmetry operations arising in physical problems.

We illustrate the use of the notation in Table 1.1 by verifying the **associative law** $(AB)C = A(BC)$ for a few elements:

$$
\begin{aligned}
(AB)C &= DC = B \\
A(BC) &= AD = B
\end{aligned}
\tag{1.2}
$$

Often, when we deal with symmetry operations in a crystal, the geometrical visualization of repeated operations becomes difficult. Group theory is designed to help with this problem. Suppose that the symmetry operations in practical problems are elements of a group; this is

generally the case. Then if we can associate each element with a matrix that obeys the same multiplication table as the elements themselves, that is, if the elements obey $AB = D$, then the matrices representing the elements must obey

$$M(A)\, M(B) = M(D). \tag{1.3}$$

If this relation is satisfied, then we can carry out all geometrical operations analytically in terms of arithmetic operations on matrices, which are usually easier to perform. The one-to-one identification of a generalized symmetry operation with a matrix is the basic idea of a **representation** and why group theory plays such an important role in the solution of practical problems.

A set of matrices that satisfy the multiplication table (Table 1.1) for the group $P(3)$ are:

$$E = \begin{pmatrix} 1 & 0 \\ 0 & 1 \end{pmatrix} \qquad A = \begin{pmatrix} 1 & 0 \\ 0 & -1 \end{pmatrix} \qquad B = \begin{pmatrix} -\frac{1}{2} & \frac{\sqrt{3}}{2} \\ \frac{\sqrt{3}}{2} & \frac{1}{2} \end{pmatrix}$$

$$C = \begin{pmatrix} -\frac{1}{2} & -\frac{\sqrt{3}}{2} \\ -\frac{\sqrt{3}}{2} & \frac{1}{2} \end{pmatrix} \quad D = \begin{pmatrix} -\frac{1}{2} & \frac{\sqrt{3}}{2} \\ -\frac{\sqrt{3}}{2} & -\frac{1}{2} \end{pmatrix} \quad F = \begin{pmatrix} -\frac{1}{2} & -\frac{\sqrt{3}}{2} \\ \frac{\sqrt{3}}{2} & -\frac{1}{2} \end{pmatrix} \tag{1.4}$$

We note that the matrix corresponding to the identity operation is always a unit matrix. The matrices in Eq. 1.4 constitute a matrix representation of the group that is isomorphic to $P(3)$ and to the symmetry operations on an equilateral triangle.

1.3   Basic Definitions

Definition: The **order of a group** $\equiv$ the number of elements in the group. We will be mainly concerned with finite groups. As an example, $P(3)$ is of order 6.

Definition: A **subgroup** $\equiv$ a collection of elements within a group that by themselves form a group.

Examples of subgroups in $P(3)$:

$$
\begin{array}{lll}
E & (E, A) & (E, D, F) \\
& (E, B) & \\
& (E, C) &
\end{array}
$$

Theorem: If in a finite group, an element X is multiplied by itself enough times (n), the identity $X^n = E$ is eventually recovered.

Proof: If the group is finite, and any arbitrary element is multiplied by itself repeatedly, the product will eventually give rise to a repetition. For example, for $P(3)$ which has six elements, seven multiplications must give a repetition. Let Y represent such a repetition:

$$Y = X^p = X^q \qquad \text{where } p > q. \tag{1.5}$$

Then let $p = q + n$ so that

$$X^p = X^n X^q = X^q = E X^q \tag{1.6}$$

from which it follows that

$$X^n = E. \tag{1.7}$$

Definition: The **order of an element** $\equiv$ the smallest value of n in the relation $X^n = E$.

We illustrate the order of an element using $P(3)$ where:

- E is of order 1

- A, B, C are of order 2

- D, F are of order 3

Definition: The **period of an element** $X \equiv$ collection of elements $E,\ X,\ X^2,\ \ldots, X^{n-1}$ where n is the order of the element. The period forms an **Abelian subgroup**.

Some examples of periods based on the group $P(3)$ are:

$$
\begin{array}{l}
E, A \\
E, B \\
E, C \\
E, D, F = E, D, D^2
\end{array}
\tag{1.8}
$$

1.4   Rearrangement Theorem

The rearrangement theorem is fundamental and basic to many theorems to be proven subsequently.

Rearrangement Theorem: If $E, A_1, A_2, \ldots, A_h$ are the elements of a group, and if A_k is an arbitrary group element, then the assembly of elements

$$A_k E, A_k A_1, \ldots, A_k A_h \qquad (1.9)$$

contains each element of the group once and only once.

Proof: 1. We show first that every element is contained.

Let X be an arbitrary element. If the elements form a group there will be an element $A_r = A_k^{-1} X$. Then $A_k A_r = A_k A_k^{-1} X = X$. Thus we can always find X after multiplication of the appropriate group elements.

2. We now show that X occurs only once. Suppose that X appears twice in the assembly $A_k E, A_k A_1, \ldots, A_k A_h$, say $X = A_k A_r = A_k A_s$. Then by multiplying on the left by A_k^{-1} we get $A_r = A_s$ which implies that two elements in the original group are identical, contrary to the original listing of the group elements.

Because of the rearrangement theorem, every row and column of a multiplication table contains each element once and only once.

1.5   Cosets

Definition: If $\mathcal{B}$ is a subgroup of the group G, and X is an element of G, then the assembly $EX, B_1 X, B_2 X, \ldots, B_g X$ is the **right coset of $\mathcal{B}$**, where $\mathcal{B}$ consists of $E, B_1, B_2, \ldots, B_g$.

A coset need not be a subgroup. A coset will be a subgroup if X is an element of $\mathcal{B}$.

Theorem: Two right cosets of given subgroup either contain exactly the same elements, or else have no elements in common.

Proof: Clearly two right cosets either contain no elements in common
or at least one element in common. We show that if there is one
element in common, all elements are in common.

Let $\mathcal{B}X$ and $\mathcal{B}Y$ be two right cosets. If $B_k X = B_\ell Y =$ one
element that the two cosets have in common, then

$$B_\ell^{-1} B_k = Y X^{-1} \qquad (1.10)$$

and YX^{-1} is in $\mathcal{B}$, since the product on the right hand side of
Eq. 1.10 is in $\mathcal{B}$. And also contained in $\mathcal{B}$ is EYX^{-1}, $B_1 Y X^{-1}$,
$B_2 Y X^{-1}$,..., $B_g Y X^{-1}$. Furthermore, according to the rearrange-
ment theorem, these elements are, in fact, identical with $\mathcal{B}$ except
for possible order of appearance. Therefore the elements of $\mathcal{B}Y$
are identical to the elements of $\mathcal{B}Y X^{-1} X$ which are also identical
to the elements of $\mathcal{B}X$ so that all elements are in common.

We now give some examples of cosets using the group $P(3)$.
Let $\mathcal{B} = E, A$ be a subgroup. Then the right cosets of $\mathcal{B}$ are

$$\begin{array}{ll}
(E,A)E \rightarrow E,A & (E,A)C \rightarrow C,F \\
(E,A)A \rightarrow A,E & (E,A)D \rightarrow D,B \\
(E,A)B \rightarrow B,D & (E,A)F \rightarrow F,C
\end{array} \qquad (1.11)$$

so that there are three distinct right cosets of (E,A), namely

$$\begin{array}{ll}
(E,A) & \text{which is a subgroup} \\
(B,D) & \text{which is not a subgroup} \\
(C,F) & \text{which is not a subgroup.}
\end{array}$$

Similarly there are three left cosets of (E,A):

$$\begin{array}{l}
(E,A) \\
(C,D) \\
(B,F)
\end{array} \qquad (1.12)$$

To multiply two cosets, we multiply constituent elements of each coset
in proper order. Such multiplication either yields a coset or joins two
cosets.

Theorem: The order of a subgroup is a divisor of the order of the group.

Proof: If an assembly of all the distinct cosets of a subgroup is formed (n of them), then n multiplied by the number of elements in a coset, $\mathcal{C}$, is exactly the number of elements in the group. Each element must be included since cosets have no elements in common.

For example, for the group $P(3)$, the subgroup (E, A) is of order 2, the subgroup (E, D, F) is of order 3 and both 2 and 3 are divisors of 6, which is the order of $P(3)$.

1.6 Conjugation and Class

Definition: An element B **conjugate** to A is by definition $B \equiv XAX^{-1}$, where X is an arbitrary element of the group.
For example,

$$A = X^{-1}BX = YBY^{-1} \quad \text{where} \quad BX = XA \quad \text{and} \quad AY = YB.$$

The elements of an **Abelian** group are all **self-conjugate**.

Theorem: If B is conjugate to A and C is conjugate to B, then C is conjugate to A.

Proof: By definition of conjugation, we can write

$$B = XAX^{-1}$$
$$C = YBY^{-1}.$$

Thus, upon substitution we obtain

$$C = YXAX^{-1}Y^{-1} = YXA(YX)^{-1}.$$

Definition: A **class** is the totality of elements which can be obtained from a given group element by conjugation.

For example in $P(3)$, there are three classes:
(i) E;   (ii) A, B, C;   (iii) D, F.
Consistent with this class designation is

$$ABA^{-1} \ = AF \ = C \qquad\qquad (1.13)$$
$$DBD^{-1} \ = DA \ = C \qquad\qquad (1.14)$$

Note that each class corresponds to a physically distinct kind of symmetry operation such as rotation of π about equivalent two-fold axes, or rotation of $2\pi/3$ about equivalent three-fold axes. The identity symmetry element is always in a class by itself. An **Abelian** group has as many classes as elements. The identity element is the only class forming a group, since none of the other classes contain the identity.

Theorem: All elements of the same class have the same order.

Proof: The order of an element n is defined by $A^n = E$. An arbitrary conjugate of A is $B = XAX^{-1}$. Then $B^n = (XAX^{-1})(XAX^{-1})\ldots$ n times gives $XA^nX^{-1} = XEX^{-1} = E$.

1.6.1   Self-Conjugate Subgroups

Definition: A subgroup $\mathcal{B}$ is **self-conjugate** if $X\mathcal{B}X^{-1}$ is identical with $\mathcal{B}$ for all possible choices of X in the **group**.

For example (E, D, F) forms a self-conjugate subgroup of $P(3)$, but (E, A) does not. The subgroups of an Abelian group are self-conjugate subgroups. We will denote self-conjugate subgroups by $\mathcal{N}$. To form a self-conjugate subgroup, it is necessary to include entire classes in this subgroup.

Definition: A group with no self-conjugate subgroups $\equiv$ a **simple** group.

Theorem: The right and left cosets of a self-conjugate subgroup $\mathcal{N}$ are the same.

Proof: If N_k is an arbitrary element of the group, then the left coset is found by elements $XN_k = XN_kX^{-1}X = N_jX$, where the right coset is formed by the elements N_jX where $N_j = XN_kX^{-1}$.

For example in the group $P(3)$, one of the right cosets is $(E, D, F)A = (A, C, B)$ and one of the left cosets is $A(E, D, F) = (A, B, C)$ and both cosets are identical except for the listing of the elements.

Theorem: The multiplication of the elements of two right cosets of a self-conjugate subgroup gives another right coset.

Proof: Let $\mathcal{N}X$ and $\mathcal{N}Y$ be two right cosets. Then multiplication of two right cosets gives

$$
\begin{aligned}
(\mathcal{N}X)(\mathcal{N}Y) \Rightarrow N_kXN_\ell Y &= N_k(XN_\ell)Y \\
= N_k(N_mX)Y = (N_kN_m)(XY) &\Rightarrow \mathcal{N}(XY)
\end{aligned}
\tag{1.15}
$$

and $\mathcal{N}(XY)$ denotes a right coset.

The elements in one right coset of $P(3)$ are $(E, D, F)A = (A, C, B)$ while $(E, D, F)D = (D, F, E)$ is another right coset. The product $(A, C, B)(D, F, E)$ is (A, B, C) which is a right coset. Also the product of the two right cosets $(A, B, C)(A, B, C)$ is (D, F, E) which is a right coset.

1.7   Factor Groups

Definition: The **factor group** of a self-conjugate subgroup is the collection of cosets of the self-conjugate subgroup, each coset being considered an element of the factor group. The factor group satisfies the four rules of §1.1 and is therefore a group.

1. multiplication – $(\mathcal{N}X)(\mathcal{N}Y) = \mathcal{N}XY$

2. associative law – holds because it holds for the elements.

3. identity – $E\mathcal{N}$ where E is the coset that contains the identity element

4. inverse – $(X\mathcal{N})(X^{-1}\mathcal{N}) = (\mathcal{N}X)(X^{-1}\mathcal{N}) = \mathcal{N}^2 = E\mathcal{N}$

Definition: The **index** of a subgroup $\equiv$ total number of cosets $=$ (order of group)/(order of subgroup).

The order of the factor group is the index of the self-conjugate subgroup.

In §1.6 we saw that (E, D, F) forms a self-conjugate subgroup, $\mathcal{N}$. The only other coset of this subgroup $\mathcal{N}$ is (A, B, C), so that the order of this factor group $= 2$. Let $(A, B, C) = \mathcal{A}$ and $(E, D, F) = \mathcal{E}$ be the two elements of the factor group. Then the multiplication table for this factor group is

	$\mathcal{E}$	$\mathcal{A}$
$\mathcal{E}$	$\mathcal{E}$	$\mathcal{A}$
$\mathcal{A}$	$\mathcal{A}$	$\mathcal{E}$

which is also the multiplication table for the group for the permutation of 2 objects $P(2)$. $\mathcal{E}$ is the identity element of this factor group. $\mathcal{E}$ and $\mathcal{A}$ are their own inverses. From this illustration you can see how the four group properties (see §1.1) apply to the factor group. The multiplication table is easily found by taking an element in each coset, carrying out the multiplication of the elements and finding the coset of the resulting element.

1.8 Selected Problems

1. (a) Show that the trace of an arbitrary square matrix X is invariant under a similarity transformation UXU^{-1}.

   (b) Given a set of matrices that represent the group G, denoted by $D(R)$ (for all R in G), show that the matrices obtainable by a similarity transformation $UD(R)U^{-1}$ also are a representation of G.

2. (a) Show that the operations of $P(3)$ in Eq. 1.1 of the class notes form a group, referring to the rules in §1.1.

   (b) Multiply the two left cosets of subgroup (E, A): (B, F) and (C, D), referring to §1.5 of the class notes. Is the result another coset?

(c) Prove that in order to form a normal subgroup it is necessary to include entire classes in this subgroup.

(d) Demonstrate that the normal subgroup of $P(3)$ includes entire classes.

3. (a) What are the symmetry operations for the molecule AB_4, where the B atoms lie at the corners of a square and the A atom is at the center and is not coplanar with the B atoms.

   (b) Find the multiplication table.

   (c) List the subgroups. Which subgroups are self-conjugate?

   (d) List the classes.

   (e) Find the multiplication table for the factor group for the self-conjugate subgroup(s) of (c).

4. The group defined by the permutations of 4 objects, $P(4)$, is isomorphic with the group of symmetry operations of a regular tetrahedron (T_d). The symmetry operations of this group are sufficiently complex so that the power of group theoretical methods can be appreciated. For notational convenience, the elements of this group are listed below.

$$
\begin{array}{llll}
e = (1234) & g = (3124) & m = (1423) & s = (4213) \\
a = (1243) & h = (3142) & n = (1432) & t = (4231) \\
b = (2134) & i = (2314) & o = (4123) & u = (3412) \\
c = (2143) & j = (2341) & p = (4132) & v = (3421) \\
d = (1324) & k = (3214) & q = (2413) & w = (4312) \\
f = (1342) & l = (3241) & r = (2431) & y = (4321)
\end{array}
$$

Here we have used a shorthand notation to denote the elements: for example $j = (2341)$ denotes

$$
\begin{pmatrix}
1 & 2 & 3 & 4 \\
2 & 3 & 4 & 1
\end{pmatrix}
$$

that is, the permutation which takes objects in the order 1234 and leaves them in the order 2341.

(a) What is the product vw? wv?

(b) List the subgroups of this group which correspond to the symmetry operations on an equilateral triangle.

(c) List the right and left cosets of the subgroup (e, a, k, l, s, t).

(d) List all the symmetry classes for $P(4)$, and relate them to symmetry operations on a regular tetrahedron.

(e) Find the factor group and multiplication table formed from the self-conjugate sub-group (e, c, u, y). Is this factor group isomorphic to $P(3)$?

Chapter 2

Representation Theory and Basic Theorems

In this chapter we introduce the concept of a representation of an abstract group and prove a number of important theorems relating to irreducible representations, including the "Wonderful Orthogonality Theorem".

2.1 Important Definitions

Definition: Two groups are **isomorphic** or **homomorphic** if there exists a correspondence between their elements such that

$$A \to \hat{A}$$
$$B \to \hat{B}$$
$$AB \to \hat{A}\hat{B}$$

where the plain letters denote elements in one group and the letters with carets denote elements in the other group. If the two groups have the same order (same number of elements), then they are **isomorphic**.

For example, the permutation group of three numbers $P(3)$ is **isomorphic** to the symmetry group of the equilateral triangle and **homomorphic** to its factor group, as shown in Table 2.1. Thus, the

Table 2.1: Table of homomorphic mapping.

Permutation group element		Factor group
E, D, F	$\rightarrow$	$\mathcal{E}$
A, B, C	$\rightarrow$	$\mathcal{A}$

homomorphic representations in Table 2.1 are **unfaithful**. Isomorphic representations are **faithful**, because they maintain the one-to-one correspondence.

Definition: A **representation** of an abstract group is a substitution group (matrix group with square matrices) such that the substitution group is homomorphic (or isomorphic) to the abstract group. We assign a matrix $D(A)$ to each element A of the abstract group such that $D(AB) = D(A)D(B)$.

The matrices of Eq. 1.4 are an isomorphic representation of the permutation group $P(3)$. In considering the representation

$$\left. \begin{array}{c} E \\ D \\ F \end{array} \right\} \rightarrow \quad (1) \qquad \qquad \left. \begin{array}{c} A \\ B \\ C \end{array} \right\} \rightarrow \quad (-1)$$

the one-dimensional matrices (1) and (–1) are a homomorphic representation of $P(3)$ and an isomorphic representation of the factor group $\mathcal{E}, \mathcal{A}$ (see §1.7). The homomorphic one-dimensional representation (1) is a representation for any group, though an unfaithful one.

In quantum mechanics, the matrix representation of a group is important for several reasons. First of all, we will find that the eigenfunctions for a quantum mechanical problem will transform under a symmetry operation according to some matrix representation of a group. Secondly, quantum mechanical operators are usually written in terms of a matrix representation, and thus it is convenient to write symmetry operations using the same kind of matrix representation. Finally, matrix algebra is often easier to manipulate than geometrical symmetry operations.

2.2 Matrices

Definitions: Hermitian matrices are defined by: $\tilde{A} = A^*$, $\tilde{A}^* = A$,
or $A^\dagger = A$ (where the symbol $*$ denotes complex conjugation, $\sim$
denotes transposition, and $\dagger$ denotes taking the adjoint)

$$A = \begin{pmatrix} a_{11} & a_{12} & \cdots \\ a_{21} & a_{22} & \cdots \\ \vdots & \vdots & \end{pmatrix} \tag{2.1}$$

$$\tilde{A} = \begin{pmatrix} a_{11} & a_{21} & \cdots \\ a_{12} & a_{22} & \cdots \\ \vdots & \vdots & \end{pmatrix} \tag{2.2}$$

Unitary matrices are defined by: $\tilde{A}^* = A^\dagger = A^{-1}$
Orthonormal matrices are defined by: $\tilde{A} = A^{-1}$

Definition: The dimensionality of a representation is equal to the di-
mensionality of each of its matricies, which is in turn equal to the
number of rows or columns of the matrix.

These representations are **not unique**. For example, by performing
a similarity (or equivalence, or canonical) transformation $UD(A)U^{-1}$
we generate a new set of matrices which provides an equally good rep-
resentation. We can also generate another representation by taking one
or more representations and combining them according to

$$\begin{pmatrix} D(A) & \mathcal{O} \\ \mathcal{O} & D'(A) \end{pmatrix} \tag{2.3}$$

where $\mathcal{O} = (m \times n)$ matrix of zeros, not necessarily a square zero matrix.
The matrices $D(A)$ and $D'(A)$ can be either two distinct representations
or they can be identical representations.

To overcome the difficulty of non-uniqueness of a representation
with regard to a similarity transformation, we often just deal with the
traces of the matrices which are invariant under similarity transfor-
mations. The **trace** of a matrix is defined as the sum of the diagonal
matrix elements.

2.3   Irreducible Representations

To overcome the difficulty of the ambiguity of representations in general, we introduce the concept of **irreducible** representations. Consider the representation made up of two distinct or identical representations for every element in the group

$$\left(\begin{array}{cc} D(A) & \mathcal{O} \\ \mathcal{O} & D'(A) \end{array} \right).$$

This is a reducible representation because the matrix corresponding to each and every element of the group is in the same block form. We could now carry out a similarity transformation which would mix up all the elements so that the matrices are no longer in block form. But still the representation is reducible. Hence the definition:

Definition: If by one and the same equivalence transformation, all the matrices in the representation of a group can be made to acquire the same block form, then the representation is said to be **reducible**; otherwise it is **irreducible**. Thus, an irreducible representation cannot be expressed in terms of representations of lower dimensionality.

We will now consider three irreducible representations for the permutation group $P(3)$:

$$
\begin{array}{cccc}
 & E & A & B \\
\Gamma_1 : & (1) & (1) & (1) \\
\Gamma_{1'} : & (1) & (-1) & (-1) \\
\Gamma_2 : & \left(\begin{array}{cc} 1 & 0 \\ 0 & 1 \end{array} \right) & \left(\begin{array}{cc} 1 & 0 \\ 0 & -1 \end{array} \right) & \left(\begin{array}{cc} -\frac{1}{2} & \frac{\sqrt{3}}{2} \\ \frac{\sqrt{3}}{2} & \frac{1}{2} \end{array} \right) \\
 & C & D & F \\
\Gamma_1 : & (1) & (1) & (1) \\
\Gamma_{1'} : & (-1) & (1) & (1) \\
\Gamma_2 : & \left(\begin{array}{cc} -\frac{1}{2} & -\frac{\sqrt{3}}{2} \\ -\frac{\sqrt{3}}{2} & \frac{1}{2} \end{array} \right) & \left(\begin{array}{cc} -\frac{1}{2} & \frac{\sqrt{3}}{2} \\ -\frac{\sqrt{3}}{2} & -\frac{1}{2} \end{array} \right) & \left(\begin{array}{cc} -\frac{1}{2} & -\frac{\sqrt{3}}{2} \\ \frac{\sqrt{3}}{2} & -\frac{1}{2} \end{array} \right)
\end{array}
\tag{2.4}
$$

A reducible representation containing these three irreducible representations is:

$$
\Gamma_R : \quad
\overset{E}{
\begin{pmatrix}
1 & 0 & 0 & 0 \\
0 & 1 & 0 & 0 \\
0 & 0 & 1 & 0 \\
0 & 0 & 0 & 1
\end{pmatrix}
}
\quad
\overset{A}{
\begin{pmatrix}
1 & 0 & 0 & 0 \\
0 & -1 & 0 & 0 \\
0 & 0 & 1 & 0 \\
0 & 0 & 0 & -1
\end{pmatrix}
}
\quad
\overset{B}{
\begin{pmatrix}
1 & 0 & 0 & 0 \\
0 & -1 & 0 & 0 \\
0 & 0 & -\frac{1}{2} & \frac{\sqrt{3}}{2} \\
0 & 0 & \frac{\sqrt{3}}{2} & \frac{1}{2}
\end{pmatrix}
}
\quad etc.
$$

$$(2.5)$$

where Γ_R is of the form

$$
\left(
\begin{array}{c|c|c}
\Gamma_1 & 0 & \mathcal{O} \\
\hline
0 & \Gamma_{1'} & \mathcal{O} \\
\hline
\mathcal{O} & \mathcal{O} & \Gamma_2
\end{array}
\right). \tag{2.6}
$$

It is customary to list the irreducible representations contained in a reducible representation Γ_R as

$$
\Gamma_R = \Gamma_1 + \Gamma_{1'} + \Gamma_2. \tag{2.7}
$$

In working out problems of physical interest, each irreducible representation describes the transformation properties of a set of eigenfunctions and corresponds to a distinct energy eigenvalue. Assume Γ_R is a reducible representation for some group G but an irreducible representation for some other group G'. If Γ_R contains the irreducible representations $\Gamma_1 + \Gamma_{1'} + \Gamma_2$ as illustrated above for the group $P(3)$, this indicates that some interaction is breaking up a four-fold degenerate level in group G' into three energy levels in group G: two nondegenerate ones and a doubly degenerate one. Group theory doesn't tell us what these energies are, nor their ordering. Group theory only specifies the symmetries and degeneracies of the energy levels. In general, the higher the symmetry, the higher the degeneracy. Thus when a perturbation is applied to lower the symmetry, the degeneracy of the energy levels tends to be reduced. Group theory provides a systematic method for determining how the degeneracy is lowered.

Representation theory is useful for the treatment of physical problems because of certain orthogonality theorems which we will now discuss. To prove the orthogonality theorems we need first to prove some other theorems (including the unitarity of representations in §2.4 and the two Schur lemmas in §2.5 and §2.6.)

2.4   The Unitarity of Representations

This theorem which shows that in most physical cases, the elements of a group can be represented by unitary matrices. This theorem is then used to prove lemmas leading to the proof of the "Wonderful Orthogonality Theorem".

Theorem: Every representation with matrices having non-vanishing determinants can be brought into unitary form by an equivalence transformation.

Proof: By unitary form we mean that the matrix elements obey the relation $(A^{-1})_{ij} = A^{\dagger}_{ij} = A^{*}_{ji}$ where A is an arbitrary matrix of the representation. The proof is carried out be finding the corresponding unitary matrices if the A_{ij} matrices are not already unitary matrices.

Let $A_1, A_2, \cdots, A_h$ denote matrices of the representation. We start by forming the matrix sum

$$H = \sum_{x=1}^{h} A_x A_x^{\dagger} \tag{2.8}$$

where the sum is over all the elements in the group and where the adjoint of a matrix is the transposed complex conjugate matrix $(A_x^{\dagger})_{ij} = (A_x)_{ji}^{*}$. The matrix H is Hermitian because

$$H^{\dagger} = \sum_{x}(A_x A_x^{\dagger})^{\dagger} = \sum_{x} A_x A_x^{\dagger}. \tag{2.9}$$

Any Hermitian matrix can be diagonalized by a suitable unitary transformation. Let U be a unitary matrix made up of the orthonormal eigenvectors which diagonalize H to give the diagonal matrix d:

$$d = U^{-1}HU = \sum_{x} U^{-1} A_x A_x^{\dagger} U = \sum_{x} U^{-1} A_x U U^{-1} A_x^{\dagger} U = \sum_{x} \hat{A}_x \hat{A}_x^{\dagger} \tag{2.10}$$

where we define $\hat{A}_x = U^{-1} A_x U$ for all x. The diagonal matrix d is a **special** kind of matrix and contains only real, positive diagonal

elements since

$$
\begin{aligned}
d_{kk} &= \sum_x \sum_j (\hat{A}_x)_{kj} (\hat{A}_x^\dagger)_{jk} \\
&= \sum_x \sum_j (\hat{A}_x)_{kj} (\hat{A}_x)_{kj}^* \\
&= \sum_x \sum_j |(\hat{A}_x)_{kj}|^2.
\end{aligned}
\tag{2.11}
$$

One can form out of the diagonal matrix d two matrices ($d^{1/2}$ and $d^{-1/2}$) such that

$$
d^{1/2} \equiv
\begin{pmatrix}
\sqrt{d_{11}} & & \mathcal{O} \\
& \sqrt{d_{22}} & \\
\mathcal{O} & & \ddots
\end{pmatrix}
\tag{2.12}
$$

and

$$
d^{-1/2} \equiv
\begin{pmatrix}
\frac{1}{\sqrt{d_{11}}} & & \mathcal{O} \\
& \frac{1}{\sqrt{d_{22}}} & \\
\mathcal{O} & & \ddots
\end{pmatrix}
\tag{2.13}
$$

where $d^{1/2}$ and $d^{-1/2}$ are real, diagonal matrices. We note that the generation of $d^{-1/2}$ from $d^{1/2}$ requires that none of the d_{kk} vanish. These matrices clearly obey the relations

$$
(d^{1/2})^\dagger = d^{1/2} \tag{2.14}
$$

$$
(d^{-1/2})^\dagger = d^{-1/2} \tag{2.15}
$$

$$
(d^{1/2})(d^{1/2}) = d \tag{2.16}
$$

so that

$$
d^{1/2}d^{-1/2} = d^{-1/2}d^{1/2} = 1 = \text{unit matrix.} \tag{2.17}
$$

We can also from Eq. 2.10 write

$$
d = d^{1/2}d^{1/2} = \sum_x \hat{A}_x \hat{A}_x^\dagger. \tag{2.18}
$$

We now define a new set of matrices

$$
\hat{\hat{A}}_x \equiv d^{-1/2} \hat{A}_x d^{1/2} \tag{2.19}
$$

and

$$
\hat{A}_x^\dagger = (U^{-1} A_x U)^\dagger = U^{-1} A_x^\dagger U \tag{2.20}
$$

$$\hat{\hat{A}}_x^\dagger = (d^{-1/2}\hat{A}_x d^{1/2})^\dagger = d^{1/2}\hat{A}_x^\dagger d^{-1/2}. \qquad (2.21)$$

We now show that the matrices $\hat{\hat{A}}_x$ are unitary:

$$
\begin{aligned}
\hat{\hat{A}}_x \hat{\hat{A}}_x^\dagger &= (d^{-1/2}\hat{A}_x d^{1/2})(d^{1/2}\hat{A}_x^\dagger d^{-1/2}) \\
&= d^{-1/2}\hat{A}_x d\hat{A}_x^\dagger d^{-1/2} \\
&= d^{-1/2}\sum_y \hat{A}_x \hat{A}_y \hat{A}_y^\dagger \hat{A}_x^\dagger d^{-1/2} \\
&= d^{-1/2}\sum_y (\hat{A}_x \hat{A}_y)(\hat{A}_x \hat{A}_y)^\dagger d^{-1/2} \\
&= d^{-1/2}\sum_z \hat{A}_z \hat{A}_z^\dagger\, d^{-1/2} \qquad (2.22)
\end{aligned}
$$

by the rearrangement theorem. But from the relation

$$d = \sum_z \hat{A}_z \hat{A}_z^\dagger \qquad (2.23)$$

it follows that $\hat{\hat{A}}_x \hat{\hat{A}}_x^\dagger = 1$ so that $\hat{\hat{A}}_x$ is unitary.

Therefore we have demonstrated how we can always construct a unitary representation by the transformation:

$$\hat{\hat{A}}_x = d^{-1/2}U^{-1}A_x U d^{1/2} \qquad (2.24)$$

where

$$H = \sum_{x=1}^h A_x A_x^\dagger \qquad (2.25)$$

$$d = \sum_{x=1}^h \hat{A}_x \hat{A}_x^\dagger \qquad (2.26)$$

U is the unitary matrix that diagonalizes the Hermitian matrix H and $\hat{A}_x = U^{-1}A_x U$.

Note: On the other hand, not all symmetry operations can be represented by a unitary matrix; an example of an operation which cannot be represented by a unitary matrix is the time inversion operator. Time inversion symmetry is represented by an anti-unitary matrix rather than an unitary matrix. It is thus not possible to represent all symmetry operations by a unitary matrix. Time inversion symmetry is discussed later in the book.

2.5   Schur's Lemma (Part I)

Schur's lemmas on irreducible representations are proved in order to prove the "Wonderful Orthogonality Theorem" in §2.7.

Lemma: A matrix which commutes with all matrices of an irreducible representation is a constant matrix, i.e., a constant times the unit matrix. Therefore, if a non-constant commuting matrix exists, the representation is reducible; if none exists, the representation is irreducible.

Proof: Let M be a matrix which commutes with all the matrices of the representation $A_1, A_2, \ldots, A_h$

$$MA_x = A_x M. \tag{2.27}$$

Take the adjoint of both sides of Eq. 2.27 to obtain

$$A_x^\dagger M^\dagger = M^\dagger A_x^\dagger. \tag{2.28}$$

Since A_x can in all generality be taken to be unitary (see §2.4), multiply on the right and left of Eqs. 2.28 by A_x to yield

$$M^\dagger A_x = A_x M^\dagger \tag{2.29}$$

so that if M commutes with A_x so does $M^\dagger$, and so do the Hermitian matrices H_1 and H_2 defined by

$$H_1 = M + M^\dagger$$
$$\tag{2.30}$$
$$H_2 = i(M - M^\dagger),$$

$$H_j A_x = A_x H_j \quad \text{where} \quad j = 1, 2. \tag{2.31}$$

We will now show that a commuting Hermitian matrix is a constant matrix from which it follows that $M = H_1 - iH_2$ is also a constant matrix.

Since H_j $(j = 1, 2)$ is a Hermitian matrix, it can be diagonalized. Let U be the matrix that diagonalizes H_j (for example H_1) to give the diagonal matrix d

$$d = U^{-1} H_j U. \tag{2.32}$$

We now perform the unitary transformation on the matrices A_x of the representation $\hat{A}_x = U^{-1}A_xU$. From the commutation relations Eqs. 2.27, 2.28 and 2.31, a unitary transformation on all matrices $H_iA_x = A_xH_i$ yields

$$\underbrace{(U^{-1}H_jU)}_{d}\underbrace{(U^{-1}A_xU)}_{\hat{A}_x} = \underbrace{(U^{-1}A_xU)}_{\hat{A}_x}\underbrace{(U^{-1}H_jU)}_{d}. \qquad (2.33)$$

So now we have a diagonal matrix d which commutes with all the matrices of the representation. We now show that this diagonal matrix d is a constant matrix, if the $\hat{A}_x$ matrices (and thus also the A_x matrices) form an irreducible representation. Thus, starting with Eq. 2.33

$$d\hat{A}_x = \hat{A}_xd \qquad (2.34)$$

we take the ij element of both sides of Eq. 2.34

$$d_{ii}(\hat{A}_x)_{ij} = (\hat{A}_x)_{ij}d_{jj} \qquad (2.35)$$

so that

$$(\hat{A}_x)_{ij}(d_{ii} - d_{jj}) = 0 \qquad (2.36)$$

for all the matrices A_x.

If $d_{ii} \neq d_{jj}$, so that the matrix d is not a constant diagonal matrix, then $(\hat{A}_x)_{ij}$ must be 0 for all the $\hat{A}_x$. This means that the similarity transformation $U^{-1}A_xU$ has brought all the matrices of the representation into the same block form, showing that the representation A_x is reducible. But we have assumed the A_x to be irreducible – therefore $d_{ii} = d_{jj}$ and Schur's lemma **part 1** is proved.

2.6   Schur's Lemma (Part 2)

Lemma: If the matrix representations $D^{(1)}(A_1), D^{(1)}(A_2), \ldots, D^{(1)}(A_h)$ and $D^{(2)}(A_1), D^{(2)}(A_2), \ldots, D^{(2)}(A_h)$ are two irreducible representations of a given group of dimensionality ℓ_1 and ℓ_2, respectively, then, if there is a matrix of ℓ_1 columns and ℓ_2 rows M such that

$$MD^{(1)}(A_x) = D^{(2)}(A_x)M \qquad (2.37)$$

for all A_x, then M must be the null matrix ($M = \mathcal{O}$) if $\ell_1 \neq \ell_2$. If $\ell_1 = \ell_2$, then either $M = \mathcal{O}$ or the representations $D^{(1)}(A_x)$ and $D^{(2)}(A_x)$ differ from each other by an equivalence or similarity transformation.

Proof: Since the matrices which form the representation can always be transformed into unitary form, we can in all generality assume that the matrices of both representations $D^{(1)}(A_x)$ and $D^{(2)}(A_x)$ have already been brought into unitary form.

Assume $\ell_1 \leq \ell_2$, and take the adjoint of Eq. 2.37

$$[D^{(1)}(A_x)]^\dagger M^\dagger = M^\dagger [D^{(2)}(A_x)]^\dagger. \tag{2.38}$$

The unitary property of the representation implies $[D(A_x)]^\dagger = [D(A_x)]^{-1} = D(A_x^{-1})$, since the matrices form a substitution group for the elements A_x of the group. Therefore we can write Eq. 2.38 as

$$D^{(1)}(A_x^{-1})M^\dagger = M^\dagger D^{(2)}(A_x^{-1}). \tag{2.39}$$

Then multiplying Eq. 2.39 on the left by M yields:

$$MD^{(1)}(A_x^{-1})M^\dagger = MM^\dagger D^{(2)}(A_x^{-1}) = D^{(2)}(A_x^{-1})MM^\dagger \tag{2.40}$$

which follows from applying Eq. 2.37 to the element A_x^{-1} which is also an element of the group:

$$MD^{(1)}(A_x^{-1}) = D^{(2)}(A_x^{-1})M. \tag{2.41}$$

We have now shown that if $MD^{(1)}(A_x) = D^{(2)}(A_x)M$ then $MM^\dagger$ commutes with all the matrices of representation (2) and $M^\dagger M$ commutes with all matrices of representation (1). But if $MM^\dagger$ commutes with all matrices of a representation, then by Schur's lemma (part 1), $MM^\dagger$ is a constant matrix of dimensionality ($\ell_2 \times \ell_2$):

$$MM^\dagger = c\,\hat{1}, \tag{2.42}$$

where $\hat{1}$ is the unit matrix.

First we consider the case $\ell_1 = \ell_2$. Then M is a square matrix, with an inverse:

$$M^{-1} = \frac{M^\dagger}{c}, \quad c \neq 0. \tag{2.43}$$

Then if $M^{-1} \neq \mathcal{O}$, multiplying Eq. 2.37 by M^{-1} on the left yields:

$$D^{(1)}(A_x) = M^{-1}D^{(2)}(A_x)M \tag{2.44}$$

and the two representations differ by an equivalence transformation.

However, if $c = 0$ then we cannot write Eq. 2.43, but instead we have to consider $MM^\dagger = 0$:

$$\sum_k M_{ik}M_{kj}^\dagger = 0 = \sum_k M_{ik}M_{jk}^* \tag{2.45}$$

for all ij elements. In particular, for $i = j$ we can write

$$\sum_k M_{ik}M_{ik}^* = \sum_k |M_{ik}|^2 = 0 \tag{2.46}$$

Therefore each element $M_{ik} = 0$ and M is a null matrix. This completes proof of the case $\ell_1 = \ell_2$ and $M = \mathcal{O}$.

Finally we prove that for $\ell_1 \neq \ell_2$, then $M = \mathcal{O}$. Suppose that $\ell_1 \neq \ell_2$, then we can arbitrarily take $\ell_1 < \ell_2$. Then M has ℓ_1 columns and ℓ_2 rows. We can make a square $(\ell_2 \times \ell_2)$ matrix out of M by adding $(\ell_2 - \ell_1)$ columns of zeros

$$\ell_2 \text{ rows} \begin{pmatrix} & & \overbrace{}^{\ell_1 \text{ columns}} & & \\ & & 0 & 0 & 0 \\ & & 0 & 0 & 0 \\ M & & 0 & 0 & 0 \\ & & \vdots & \vdots & \vdots \\ & & 0 & 0 & 0 \end{pmatrix} = N = \text{square } (\ell_2 \times \ell_2) \text{ matrix.} \tag{2.47}$$

The adjoint of Eq. 2.47 is then written as

$$\begin{pmatrix} & & M^\dagger & & \\ 0 & 0 & 0 & \cdots & 0 \\ 0 & 0 & 0 & \cdots & 0 \\ \vdots & \vdots & \vdots & & \vdots \\ 0 & 0 & 0 & \cdots & 0 \end{pmatrix} = N^\dagger \tag{2.48}$$

so that
$$NN^\dagger = MM^\dagger = c\,\hat{1} \qquad \textbf{dimension } (\ell_2 \times \ell_2). \qquad (2.49)$$

$$\sum_k N_{ik}N_{ki}^\dagger = \sum_k N_{ik}N_{ik}^* = c$$

$$\sum_{ik} N_{ik}N_{ik}^* = c\ell_2.$$

But if we sum over i we see by direct computation $\sum_{k,i} N_{ik}N_{ik}^* = 0$, so that $c = 0$. But this implies that every element $N_{ik} = 0$ and therefore also $M_{ik} = 0$, so that M is a null matrix, completing the proof of Schur's lemma (part 2).

2.7 Wonderful Orthogonality Theorem

The orthogonality theorem which we now prove is so central to the application of group theory to quantum mechanical problems that it was named the "Wonderful Orthogonality Theorem" by Van Vleck, and is widely known by this name.

Theorem: The orthonormality relation

$$\sum_R D_{\mu\nu}^{(\ell_2)}(R)D_{\nu'\mu'}^{(\ell_1)}(R^{-1}) = \frac{h}{\ell_1}\delta_{\Gamma_1,\Gamma_2}\delta_{\mu,\mu'}\delta_{\nu,\nu'} \qquad (2.50)$$

is obeyed for all the inequivalent, irreducible representations of a group, where the summation is over all h group elements $A_1, A_2, \ldots, A_h$ and ℓ_i $(i = 1, 2)$ is the dimensionality of representation Γ_i. If the representations are unitary, the orthonormality relation becomes

$$\sum_R D_{\mu\nu}^{(\ell_2)}(R)\left[D_{\mu'\nu'}^{(\ell_1)}(R)\right]^* = \frac{h}{\ell_1}\delta_{\Gamma_1,\Gamma_2}\delta_{\mu,\mu'}\delta_{\nu,\nu'}. \qquad (2.51)$$

Proof: Consider the $\ell_2 \times \ell_1$ matrix

$$M = \sum_R D^{(\ell_2)}(R)XD^{(\ell_1)}(R^{-1}) \qquad (2.52)$$

where X is an arbitrary matrix with ℓ_2 rows and ℓ_1 columns so that M is a rectangular matrix of dimensionality $(\ell_2 \times \ell_1)$.

Multiply M by $D^{(\ell_2)}(S)$ for some element S in the group:

$$\underbrace{D^{(\ell_2)}(S)M}_{\ell_2 \times \ell_1} = \sum_R D^{(\ell_2)}(S)D^{(\ell_2)}(R) \; X \; D^{(\ell_1)}(R^{-1}) \qquad (2.53)$$

Then carrying out the multiplication of two elements in a group

$$\underbrace{D^{(\ell_2)}(S)M}_{\ell_2 \times \ell_1} = \sum_R D^{(\ell_2)}(SR) \; X \; D^{(\ell_1)}(R^{-1}S^{-1})D^{(\ell_1)}(S) \quad (2.54)$$

where we have used the group properties of the representations Γ_1 and Γ_2. By the rearrangement theorem, the above equation can be rewritten

$$D^{(\ell_2)}(S)M = \underbrace{\sum_R D^{(\ell_2)}(R) \; X \; D^{(\ell_1)}(R^{-1})}_{M} \, D^{(\ell_1)}(S) = M \, D^{(\ell_1)}(S).$$

$$(2.55)$$

Now apply Schur's lemma part 2 for the various cases.

Case 1 $\ell_1 \neq \ell_2$ or if $\ell_1 = \ell_2$, and the representations are not equivalent.

Since $D^{(\ell_2)}(S)M = MD^{(\ell_1)}(S)$, then by Schur's lemma part 2, M must be a null matrix. From the definition of M we have

$$0 = M_{\mu\mu'} = \sum_R \sum_{\gamma,\lambda} D^{(\ell_2)}_{\mu\gamma}(R)X_{\gamma\lambda}D^{(\ell_1)}_{\lambda\mu'}(R^{-1}). \qquad (2.56)$$

But X is an arbitrary matrix. By choosing X to have an entry 1 in the $\nu\nu'$ position and 0 everywhere else, we write:

$$X = \begin{pmatrix} 0 & 0 & 0 & 0 & 0 & 0 & \cdots \\ 0 & 0 & 0 & 1 & 0 & 0 & \cdots \\ 0 & 0 & 0 & 0 & 0 & 0 & \cdots \\ 0 & 0 & 0 & 0 & 0 & 0 & \cdots \\ \vdots & \vdots & \vdots & \vdots & \vdots & \vdots & \end{pmatrix}. \qquad X_{\gamma\lambda} = \delta_{\gamma\nu}\delta_{\lambda\nu'} \qquad (2.57)$$

It then follows by substituting Eq. 2.57 into Eq. 2.56 that

$$0 = \sum_R D^{(\ell_2)}_{\mu\nu}(R)D^{(\ell_1)}_{\nu'\mu'}(R^{-1}). \qquad (2.58)$$

Case 2 $\ell_1 = \ell_2$ **and the representations** Γ_1 **and** Γ_2 **are equivalent**

If the representations Γ_1 and Γ_2 are equivalent, then $\ell_1 = \ell_2$ and Schur's lemma part 1 tells us that $M = c\hat{1}$. The definition for M in Eq. 2.52 gives

$$M_{\mu\nu'} = c\delta_{\mu\mu'} = \sum_R \sum_{\gamma,\lambda} D^{(\ell_2)}_{\mu\gamma}(R) X_{\gamma\lambda} D^{(\ell_2)}_{\lambda\mu'}(R^{-1}). \tag{2.59}$$

Choose X in Eq. 2.57 as above to have a non-zero entry at $\nu\nu'$ and 0 everywhere else. Then $X_{\gamma\lambda} = c'_{\nu\nu'}\delta_{\gamma\nu}\delta_{\lambda\nu'}$ so that

$$c''_{\nu\nu'}\delta_{\mu\mu'} = \sum_R D^{(\ell_2)}_{\mu\nu}(R)\ D^{(\ell_2)}_{\nu'\mu'}(R^{-1}) \tag{2.60}$$

where $c''_{\nu\nu'} = c/c'_{\nu\nu'}$. To evaluate $c''_{\nu\nu'}$ choose $\mu = \mu'$ in Eq. 2.60 and sum on μ:

$$c''_{\nu\nu'}\underbrace{\sum_\mu \delta_{\mu\mu}}_{\ell_2} = \sum_R \sum_\mu D^{(\ell_2)}_{\mu\nu}(R)\ D^{(\ell_2)}_{\nu'\mu}(R^{-1}) = \sum_R D^{(\ell_2)}_{\nu'\nu}(R^{-1}R)$$

$$\tag{2.61}$$

since $D^{(\ell_2)}(R)$ is a representation of the group and follows the multiplication table for the group. Therefore we can write

$$c''_{\nu\nu'}\ell_2 = \sum_R D^{(\ell_2)}_{\nu'\nu}(R^{-1}R) = \sum_R D^{(\ell_2)}_{\nu'\nu}(E) = D^{(\ell_2)}_{\nu'\nu}(E)\sum_R 1. \tag{2.62}$$

But $D^{(\ell_2)}_{\nu'\nu}(E)$ is a unit $(\ell_2 \times \ell_2)$ matrix and the $\nu'\nu$ matrix element is $\delta_{\nu'\nu}$. The sum of unity over all the group elements is h. Therefore we obtain

$$c''_{\nu\nu'} = \frac{h}{\ell_2}\delta_{\nu\nu'}. \tag{2.63}$$

Substituting Eq. 2.63 into Eq. 2.60 gives:

$$\frac{h}{\ell_2}\delta_{\mu\mu'}\delta_{\nu\nu'} = \sum_R D^{(\ell_2)}_{\mu\nu}(R)\ D^{(\ell_2)}_{\nu'\mu'}(R^{-1}). \tag{2.64}$$

We can write the results of case 1 and case 2 in compact form

$$\sum_R D^{(\ell_j)}_{\mu\nu}(R)\ D^{(\ell_{j'})}_{\nu'\mu'}(R^{-1}) = \frac{h}{\ell_j}\delta_{\Gamma_j,\Gamma_{j'}}\delta_{\mu\mu'}\delta_{\nu\nu'}. \tag{2.65}$$

For a unitary representation Eq. 2.65 can also be written as:

$$\sum_R D_{\mu\nu}^{(\ell_j)}(R) \, D_{\mu'\nu'}^{(\ell_{j'})*}(R) = \frac{h}{\ell_j}\delta_{\Gamma_j,\Gamma_{j'}}\delta_{\mu\mu'}\delta_{\nu\nu'}. \qquad (2.66)$$

This completes the proof of the wonderful orthogonality theorem.

2.8   Representations and Vector Spaces

Let us spend a moment and consider what the representations in Eq. 2.66 mean as an orthonormality relation in a vector space of dimensionality h. Here h is the order of the group which equals the number of group elements. In this space, the representations $D_{\mu\nu}^{(\ell_j)}(R)$ can be considered as elements in this h-dimensional space:

$$V_{\mu,\nu}^{(\ell_j)} = \left[D_{\mu\nu}^{(\ell_j)}(A_1), D_{\mu\nu}^{(\ell_j)}(A_2), \ldots, D_{\mu\nu}^{(\ell_j)}(A_h) \right]. \qquad (2.67)$$

The three indices $\Gamma_{\ell_j}, \mu, \nu$ label a particular vector. All distinct vectors in this space are orthogonal. Thus two representations are orthogonal if any one of their three indices is different. But in an h-dimensional vector space, the maximum number of orthogonal vectors is h. We now ask how many vectors $V_{\mu,\nu}^{(\ell_j)}$ can we make? For each representation, we have ℓ_j choices for μ and ν so that the total number of vectors we can have is $\sum_j \ell_j^2$ where we are now summing over representations. This argument yields the important result

$$\sum_j \ell_j^2 \leq h. \qquad (2.68)$$

We will see later that it is the **equality** that holds in Eq. 2.68.

The result in Eq. 2.68 is extremely helpful in finding the totality of irreducible (non-equivalent) representations. In our example of $P(3)$ we have $h = 6$. Therefore $\sum_j \ell_j^2 = 6$. The representations we found in §2.3 were two one-dimensional and one two-dimensional representation. Therefore $\sum_j \ell_j^2 = 1^2 + 1^2 + 2^2 = 1 + 1 + 4 = 6$. This tells us that no matter how hard we try, we will not find any more irreducible representations for $P(3)$ – we have them all.

2.9 Suggested Problems

1. Show that every symmetry operator for every group can be represented by the (1×1) unit matrix. Is it also true that every symmetry operator for every group can be represented by the (2×2) unit matrix? If so, does such a representation satisfy the Wonderful Orthogonality Theorem? Why?

Chapter 3

Character of a Representation

We have already discussed the arbitrariness of a representation with regard to similarity or equivalence transformations. Namely, if $D^{(\ell_j)}(R)$ is a representation of a group, so is $U^{-1}D^{(\ell_j)}(R)U$. To get around this arbitrariness we introduce the use of the trace (or character) of a matrix representation which remains invariant under a similarity transformation. In this chapter we define the character of a representation, derive the most important theorems for the character, summarize the conventional notations used to denote symmetry operations and groups and list some of the most important character tables for the point groups.

3.1 Definition of Character

Definition: The **character** of the matrix representation $\chi^{\ell_j}(R)$ for a symmetry operation R in a representation $D(R)$ is the **trace** (or the sum over diagonal matrix elements) of the matrix of the representation:

$$\chi^{(\ell_j)}(R) = \text{trace } D^{(\ell_j)}(R) = \sum_{\mu=1}^{\ell_j} D^{(\ell_j)}(R)_{\mu\mu} \qquad (3.1)$$

where ℓ_j is the dimensionality of the representation Γ_j and j is a representation index. From the definition, it follows that repre-

sentation Γ_j will have h characters, one for each element in the group. Since the trace of a matrix is invariant under a similarity transformation, the character is invariant under such a transformation.

3.2   Characters and Class

We relate concepts of class (see §1.6) and character by the following theorem.

Theorem: The character for each element in a class is the same.

Proof: Let A and B be elements in the same class. By the definition of class this means that A and B are related by conjugation (see §1.6)

$$A = Y^{-1}BY \tag{3.2}$$

where Y is an element of the group. Each element can always be represented by a unitary matrix D (see §2.4), so that

$$D(A) = D(Y^{-1})\, D(B)\, D(Y) = D^{-1}(Y)\, D(B)\, D(Y). \tag{3.3}$$

And since a similarity transformation leaves the trace invariant, we have the desired result for characters in the same class: $\chi(A) = \chi(B)$, which completes the proof.

The property that all elements in a class have the same character is responsible for what Van Vleck called "**the great beauty of character**". If two elements of a group are in the same class, this means that they correspond to similar symmetry operations – e.g., the class of two-fold axes of rotation of the equilateral triangle, or the class of three-fold rotations for the equilateral triangle.

Sometimes a given group will have more than one kind of two-fold symmetry axis. To test whether these two kinds of axes are indeed symmetrically inequivalent, we check whether or not not they have the same characters.

We summarize the information on the characters of the representations of a group in the celebrated **character table**. In a character

Table 3.1: Character table for the permutation group $P(3)$: Group "D_3".

Class $\rightarrow$		$\mathcal{C}_1$	$3\mathcal{C}_2$	$2\mathcal{C}_3$
irreducible		$\chi(E)$	$\chi(A,B,C)$	$\chi(D,F)$
representation	Γ_1	1	1	1
$\downarrow$	$\Gamma_{1'}$	1	-1	1
	Γ_2	2	0	-1

Table 3.2: Classes for the permutation group $P(3)$: Group "D_3".

	D_3		$P(3)$
Class 1 E (identity)	$1\mathcal{C}_1$	(identity class)	$(1)(2)(3)$
Class 2 A, B, C (3 elements)	$3\mathcal{C}_2$	(rotation of π about 2-fold axis)	$(1)(23)$
Class 3 D, F (2 elements)	$2\mathcal{C}_3$	(rotation of 120° about 3-fold axis)	(123)

table we list the representations in column form (for example, the left hand column of the character table) and the class as rows (top row labels the class). For example, the character table for the permutation group $P(3)$ (see §1.2) is shown in Table 3.1. (Sometimes you will see character tables with the columns and rows interchanged relative to this display.) We will later see that the name for this point group is D_3 (Schoenflies notation). In Table 3.1 the notation $N_k\mathcal{C}_k$ is used in the character table to label each class $\mathcal{C}_k$, and N_k is the number of elements in $\mathcal{C}_k$. If a representation is irreducible, then we say that its character is **primitive**. In a character table we limit ourselves to the primitive characters. The classes for group D_3 and $P(3)$ are listed in Table 3.2.

Now that we have introduced character and character tables, let us see how to use the character tables. To appreciate the power of the character tables we present a few fundamental theorems for character.

3.3   Wonderful Orthogonality Theorem for Character

The "Wonderful Orthogonality Theorem" for character follows directly from the wonderful orthogonality theorem (see §2.7). There is also a second orthogonality theorem for character which is discussed below (see §3.6).

Theorem: The **primitive** characters of an irreducible representation obey the orthogonality relation

$$\sum_R \chi^{(\Gamma_1)}(R^{-1})\,\chi^{(\Gamma_2)}(R) = h\delta_{\Gamma_1,\Gamma_2} \tag{3.4}$$

or

$$\sum_R \chi^{(\ell_j)}(R)^*\,\chi^{(\ell_{j'})}(R) = h\delta_{\Gamma_j,\Gamma_{j'}} \tag{3.5}$$

where Γ_j denotes irreducible representation j with dimensionality ℓ_j. This theorem says that unless the representations are identical or equivalent, the characters are orthogonal in h-dimensional space, where h is the order of the group.

Proof: The proof of the wonderful orthogonality theorem for character follows from the Wonderful Orthogonality Theorem (see §2.7) itself. Consider the wonderful orthogonality theorem (Eq. 2.51)

$$\sum_R D_{\mu\nu}^{(\ell_j)}(R)D_{\nu'\mu'}^{(\ell_{j'})}(R^{-1}) = \frac{h}{\ell_j}\delta_{\Gamma_j,\Gamma_{j'}}\delta_{\mu,\mu'}\delta_{\nu,\nu'}. \tag{3.6}$$

Take the diagonal elements of Eq. 3.6:

$$\sum_R D_{\mu\mu}^{(\ell_j)}(R)D_{\mu'\mu'}^{(\ell_{j'})}(R^{-1}) = \frac{h}{\ell_j}\delta_{\Gamma_j,\Gamma_{j'}}\delta_{\mu\mu'}\delta_{\mu'\mu}. \tag{3.7}$$

Now sum Eq. 3.7 over μ and μ' to calculate the traces or characters

$$\sum_R \sum_\mu D_{\mu\mu}^{(\ell_j)}(R)\sum_{\mu'} D_{\mu'\mu'}^{(\ell_{j'})}(R^{-1}) = \frac{h}{\ell_j}\delta_{\Gamma_j,\Gamma_{j'}}\sum_{\mu\mu'}\delta_{\mu\mu'}\delta_{\mu'\mu} \tag{3.8}$$

where we note that

$$\sum_{\mu\mu'} \delta_{\mu\mu'}\delta_{\mu'\mu} = \sum_{\mu} \delta_{\mu\mu} = \ell_j \qquad (3.9)$$

so that

$$\sum_R \chi^{(\ell_j)}(R)\chi^{(\ell_{j'})}(R^{-1}) = h\delta_{\Gamma_j,\Gamma_{j'}}, \qquad (3.10)$$

completing the proof. Equation 3.10 implies that the primitive characters of an irreducible representation form a set of **orthogonal** vectors in **group-element** space. Since any arbitrary representation is equivalent to some unitary representation (and the character is preserved under a unitary transformation), Eq. 3.10 can also be written as

$$\sum_R \chi^{(\ell_j)}(R)\left[\chi^{(\ell_{j'})}(R)\right]^* = h\delta_{\Gamma_j,\Gamma_{j'}}. \qquad (3.11)$$

Since the character is the same for each element in the class, the summation in Eq. 3.11 can be written over classes k to obtain

$$\sum_k N_k \chi^{(\ell_j)}(\mathcal{C}_k)\left[\chi^{(\ell_{j'})}(\mathcal{C}_k)\right]^* = h\delta_{\Gamma_j,\Gamma_{j'}} \qquad (3.12)$$

where N_k denotes the number of elements in class k.

The importance of the results in Eqs. 3.10, 3.11, and 3.12 cannot be over-emphasized:

1. Character tells us if a representation is irreducible or not. If a representation is reducible then the characters are not primitive and will generally not obey this orthogonality relation (and other orthogonality relations that we will soon discuss).

2. Character tells us whether or not we have found all the irreducible representations. For example, the permutation group $P(3)$ could not contain a three-dimensional irreducible representation, since by Eq. 2.68

$$\sum_j \ell_j^2 \le h, \qquad (3.13)$$

and if $P(3)$ contained one 3D irreducible representation then:

$$1^2 + 3^2 > 6 \tag{3.14}$$

contrary to Eq. 3.13.

We will now demonstrate the use of the Wonderful Orthogonality Theorem for Character for the permutation group $P(3)$. Let $\Gamma_{\ell_j} = \Gamma_1$ and $\Gamma_{\ell'_j} = \Gamma_{1'}$. Then use of Eq. 3.12 yields

$$\sum_k N_k \chi^{(\ell_j)}(\mathcal{C}_k)\left[\chi^{(\ell_{j'})}(\mathcal{C}_k)\right]^* = \underbrace{(1)(1)(1)}_{\text{class of }E} + \underbrace{(3)(1)(-1)}_{\text{class of }A,B,C} + \underbrace{(2)(1)(1)}_{\text{class of }D,F}$$

$$= 1 - 3 + 2 = 0. \tag{3.15}$$

It can likewise be verified that the Wonderful Orthogonality Theorem works for all possible combinations of Γ_{ℓ_j} and $\Gamma_{\ell'_j}$ in the group $P(3)$. Character allows us to check the uniqueness of an irreducible representation, using the following theorem.

Theorem: A necessary and sufficient condition that two irreducible representations be equivalent is that the characters be the same.

Proof: Necessary condition: If they are equivalent, then the characters are the same – we have demonstrated this already since the trace of a matrix is invariant under an equivalence transformation.
Sufficient condition: If the characters are the same, the vectors for each of the irreducible representations in h-dimensional space can't be orthogonal, so the representations must be equivalent.

3.4   Reducible Representations

We now prove a theorem that forms the basis for setting up the characters of a **reducible** representation in terms of the primitive characters for the irreducible representations. This theoretical background will also be used in constructing irreducible representations and character tables, and is essential to most of the practical applications of group theory to solid state physics.

Theorem: The reduction of any reducible representation into its irreducible constituents is **unique**.

Thus, if $\chi(\mathcal{C}_k)$ is the character for some class in a reducible representation, then this theorem claims that we can write the character for the reducible representation $\chi(\mathcal{C}_k)$ as a linear combination of characters for the **irreducible** representations of the group $\chi^{(\Gamma_i)}(\mathcal{C}_k)$

$$\chi(\mathcal{C}_k) = \sum_{\Gamma_i} a_i \chi^{(\Gamma_i)}(\mathcal{C}_k) \tag{3.16}$$

where the a_i coefficients are non-negative integers which denote the number of times the irreducible representation Γ_i is contained in the reducible representation. Furthermore we show here that the a_i coefficients are unique.

Proof: In proving that the a_i coefficients are unique, we explicitly determine the a_i's which constitute the characters for a reducible representation.

Consider the sum over classes k:

$$\sum_k N_k \left[\chi^{(\Gamma_j)}(\mathcal{C}_k)\right]^* \chi(\mathcal{C}_k) = S_j. \tag{3.17}$$

Since $\chi(\mathcal{C}_k)$ is reducible, we write the linear combination for $\chi(\mathcal{C}_k)$ in Eq. 3.17 using Eq. 3.16:

$$S_j = \sum_k N_k \left[\chi^{(\Gamma_j)}(\mathcal{C}_k)\right]^* \sum_{\Gamma_i} a_i \chi^{(\Gamma_i)}(\mathcal{C}_k)$$
$$= \sum_{\Gamma_i} a_i \left\{ \sum_k N_k \left[\chi^{(\Gamma_j)}(\mathcal{C}_k)\right]^* \chi^{(\Gamma_i)}(\mathcal{C}_k) \right\}. \tag{3.18}$$

We now apply the Wonderful Orthogonality Theorem for Characters Eq. 3.12 to get

$$\sum_{\Gamma_i} a_i h \delta_{\Gamma_i, \Gamma_j} = a_j h = \sum_k N_k \left[\chi^{(\Gamma_j)}(\mathcal{C}_k)\right]^* \chi(\mathcal{C}_k) = S_j \tag{3.19}$$

yielding the decomposition relation

$$a_j = \frac{1}{h} \sum_k N_k \left[\chi^{(\Gamma_j)}(\mathcal{C}_k)\right]^* \chi(\mathcal{C}_k) = \frac{S_j}{h} \tag{3.20}$$

and completing the proof of the theorem. Thus the coefficients a_i in Eq. 3.16 are uniquely determined. In other words, the number of times the various irreducible representations are contained in a given reducible representation can be obtained directly from the character table for the group.

This sort of decomposition of the character for a reducible representation is important for the following type of physical problem. Consider a **cubic crystal**. A cubic crystal has many symmetry operations and therefore many classes and many irreducible representations. Now suppose that we squeeze this crystal and lower its symmetry. Let us further suppose that the energy levels for the cubic crystal are degenerate for certain points in the Brillouin zone. This squeezing would most likely lift some of the level degeneracies. To find out how the degeneracy is lifted, we take the representation for the cubic group that corresponds to the unperturbed energy and treat this representation as a reducible representation in the group of lower symmetry. Then the decomposition formulae (Eqs. 3.16 and 3.20) tell us immediately the degeneracy and symmetry types of the split levels in the perturbed or stressed crystal.

3.5   The Number of Irreducible Representations

We now come to another extremely useful theorem.

Theorem: The number of irreducible representations is equal to the number of classes.

Proof: The Wonderful Orthogonality Theorem for character is

$$\sum_{k'=1}^{k} N_{k'} \left[\chi^{(\Gamma_i)}(\mathcal{C}_{k'}) \right]^* \chi^{(\Gamma_j)}(\mathcal{C}_{k'}) = h\, \delta_{\Gamma_i, \Gamma_j} \qquad (3.21)$$

or

$$\sum_{k'=1}^{k} \left[\sqrt{\frac{N_{k'}}{h}}\, \chi^{(\Gamma_i)}(\mathcal{C}_{k'}) \right]^* \left[\sqrt{\frac{N_k}{h}}\, \chi^{(\Gamma_j)}(\mathcal{C}_{k'}) \right] = \delta_{\Gamma_i, \Gamma_j}. \qquad (3.22)$$

Each term $\sqrt{\frac{N_{k'}}{h}}\,\chi^{(\Gamma_i)}(\mathcal{C}_{k'})$ in Eq. 3.22 gives the k'th component of a k-dimensional vector. There can be only k such vectors in a k-dimensional space, since the $(k+1)$st vector would be linearly dependent on the other k vectors. If there were less than k such vectors, then the number of independent vectors would not be large enough to span the k-dimensional space. To express a reducible representation in terms of its irreducible components requires that the vector space be spanned by irreducible representations. Therefore the number of irreducible representations must be k, the number of classes.

For our example of the permutation group of three objects, we have three classes and therefore only three irreducible representations. We have already found these irreducible representations and we now know that any additional representations that we might find are either **equivalent** to these representations or they are **reducible**. Knowing the number of distinct irreducible representations is very important in setting up character tables.

3.6 Second Orthogonality Relation for Characters

We now prove a second orthogonality theorem for characters which sums over the irreducible representations and is extremely valuable for constructing character tables.

Theorem: The summation over all irreducible representations

$$\sum_{\Gamma_j} \chi^{(\ell_j)}(\mathcal{C}_k)\left[\chi^{(\ell_j)}(\mathcal{C}_{k'})\right]^* N_k = h\delta_{k,k'} \qquad (3.23)$$

yields a second orthogonality relation for the characters. Thus, the Wonderful Orthogonality Theorem for Character yields an orthogonality relation between **rows** in the character table while the second orthogonality theorem gives a similar relation between the **columns** of the character table.

Proof: Construct the matrix

$$Q = \begin{pmatrix} \chi^{(1)}(\mathcal{C}_1) & \chi^{(1)}(\mathcal{C}_2) & \cdots \\ \chi^{(2)}(\mathcal{C}_1) & \chi^{(2)}(\mathcal{C}_2) & \cdots \\ \chi^{(3)}(\mathcal{C}_1) & \chi^{(3)}(\mathcal{C}_2) & \\ & \vdots & \vdots \end{pmatrix} \qquad (3.24)$$

where the irreducible representations label the rows and the classes label the columns. Q is a square matrix since by Eq. 3.22 the number of classes (designating the column index) is equal to the number of irreducible representations (designating the row index). We now also construct the square matrix

$$Q' = \frac{1}{h} \begin{pmatrix} N_1 \chi^{(1)}(\mathcal{C}_1)^* & N_1 \chi^{(2)}(\mathcal{C}_1)^* & \cdots \\ N_2 \chi^{(1)}(\mathcal{C}_2)^* & N_2 \chi^{(2)}(\mathcal{C}_2)^* & \cdots \\ N_3 \chi^{(1)}(\mathcal{C}_3)^* & N_3 \chi^{(2)}(\mathcal{C}_3)^* & \cdots \\ & \vdots & \vdots \end{pmatrix} \qquad (3.25)$$

where the classes label the rows, and the irreducible representations label the columns. The ij matrix element of the product QQ' summing over classes is then

$$(QQ')_{ij} = \sum_k \frac{N_k}{h} \chi^{(\Gamma_i)}(\mathcal{C}_k) \left[\chi^{(\Gamma_j)}(\mathcal{C}_k) \right]^* = \delta_{\Gamma_i, \Gamma_j} \qquad (3.26)$$

using the Wonderful Orthogonality Theorem for Character (Eq. 3.12). Therefore $QQ' = \hat{1}$ or $Q' = Q^{-1}$ and $Q'Q = \hat{1}$ since $QQ^{-1} = Q^{-1}Q = \hat{1}$ where $\hat{1}$ is the unit matrix. Now we will write $Q'Q$ in terms of components, but now summing over the irreducible representations

$$(Q'Q)_{kk'} = \delta_{kk'} = \sum_{\Gamma_i} \frac{N_k}{h} \chi^{(\Gamma_i)}(\mathcal{C}_k) \left[\chi^{(\Gamma_i)}(\mathcal{C}_{k'}) \right]^* \qquad (3.27)$$

so that

$$\sum_{\Gamma_i} \chi^{(\Gamma_i)}(\mathcal{C}_k) \left[\chi^{(\Gamma_i)}(\mathcal{C}_{k'}) \right]^* = \frac{h}{N_k} \delta_{k,k'} \qquad (3.28)$$

which completes the proof of the second orthogonality theorem.

Table 3.3: Multiplication table for the group $P(3)$ used to generate the regular representation.

	E	A	B	C	D	F
$E = E^{-1}$	E	A	B	C	D	F
$A = A^{-1}$	A	E	D	F	B	C
$B = B^{-1}$	B	F	E	D	C	A
$C = C^{-1}$	C	D	F	E	A	B
$F = D^{-1}$	F	B	C	A	E	D
$D = F^{-1}$	D	C	A	B	F	E

3.7   Regular Representation

The regular representation provides a recipe for finding all the irreducible representations of a group. It is not always the fastest method for finding the irreducible representations, but it will always work.

The **regular representation** is found directly from the multiplication table by rearranging the rows and columns so that the identity element is always along the main diagonal. When this is done, the group elements label the columns and their inverses label the rows. We will illustrate this with the permutation group of three objects $P(3)$ for which the multiplication table is given in Table 1.1. Application of the rearrangement theorem to give the identity element along the main diagonal gives Table 3.3. Then the matrix representation for an element X in the regular representation is obtained by putting 1 wherever X appears in the multiplication Table 3.3 and 0 everywhere else. Thus we obtain

$$D^{\text{reg}}(E) = \begin{pmatrix} 1 & 0 & 0 & 0 & 0 & 0 \\ 0 & 1 & 0 & 0 & 0 & 0 \\ 0 & 0 & 1 & 0 & 0 & 0 \\ 0 & 0 & 0 & 1 & 0 & 0 \\ 0 & 0 & 0 & 0 & 1 & 0 \\ 0 & 0 & 0 & 0 & 0 & 1 \end{pmatrix} \tag{3.29}$$

which is always the unit matrix of dimension $(h \times h)$. For one of

the other elements in the regular representation we obtain

$$D^{\text{reg}}(A) = \begin{pmatrix} 0 & 1 & 0 & 0 & 0 & 0 \\ 1 & 0 & 0 & 0 & 0 & 0 \\ 0 & 0 & 0 & 0 & 0 & 1 \\ 0 & 0 & 0 & 0 & 1 & 0 \\ 0 & 0 & 0 & 1 & 0 & 0 \\ 0 & 0 & 1 & 0 & 0 & 0 \end{pmatrix} \tag{3.30}$$

and so on. By construction, only $D^{\text{reg}}(E)$ has a non-zero trace!

We now show that the regular representation is indeed a representation. This means that the regular representation obeys the multiplication table (either Table 1.1 or 3.3). Let us for example show

$$D^{\text{reg}}(BC) = D^{\text{reg}}(B)D^{\text{reg}}(C). \tag{3.31}$$

It is customary to denote the matrix elements of the regular representation directly from the definition $D^{\text{reg}}(X)_{A_k^{-1},A_i}$ where A_k^{-1} labels the rows and A_i labels the columns using the notation

$$D^{\text{reg}}(X)_{A_k^{-1},A_i} = \begin{cases} 1 & \text{if} \quad A_k^{-1}A_i = X \\ \\ 0 & \text{otherwise.} \end{cases} \tag{3.32}$$

Using this notation, we have to show that:

$$D^{\text{reg}}(BC)_{A_k^{-1},A_i} = \sum_{A_j} D^{\text{reg}}(B)_{A_k^{-1},A_j} D^{\text{reg}}(C)_{A_j^{-1},A_i}. \tag{3.33}$$

Now look at the rearranged multiplication table given in Table 3.3. By construction, we have for each of the matrices:

$$D^{\text{reg}}(B)_{A_k^{-1},A_j} = \begin{cases} 1 & \text{if} \quad A_k^{-1}A_j = B \\ \\ 0 & \text{otherwise} \end{cases} \tag{3.34}$$

$$D^{\text{reg}}(C)_{A_j^{-1},A_i} = \begin{cases} 1 & \text{if} \quad A_j^{-1}A_i = C \\ \\ 0 & \text{otherwise} \end{cases} \tag{3.35}$$

Therefore in the sum of Eq. 3.33 over A_j, namely $\sum_{A_j} D^{\text{reg}}(B)_{A_k^{-1},A_j} D^{\text{reg}}(C)_{A_j^{-1},A_i}$, we have only non-zero entries when

$$BC = (A_k^{-1} \underbrace{A_j)(A_j^{-1}}_{1} A_i) = A_k^{-1} A_i. \tag{3.36}$$

But this coincides with the definition of $D^{\text{reg}}(BC)$:

$$D^{\text{reg}}(BC)_{A_k^{-1},A_i} = \begin{cases} 1 & \text{if} \quad A_k^{-1} A_i = BC \\ \\ 0 & \text{otherwise} \end{cases} \tag{3.37}$$

Therefore D^{reg} is, in fact, a representation of the group $A_1, \ldots A_h$, completing the proof.

The following theorem allows us to find all the irreducible representations from the regular representation.

Theorem: The regular representation contains each irreducible representation a number of times equal to the dimensionality of the representation. (For the group $P(3)$, this theorem says that D^{reg} contains $D^{(\Gamma_1)}$ once, $D^{(\Gamma_{1'})}$ once and $D^{(\Gamma_2)}$ twice so that the regular representation of $P(3)$ would be of dimensionality 6.)

Proof: Since D^{reg} is a reducible representation, we can write for the characters (see Eq. 3.16)

$$\chi^{\text{reg}}(\mathcal{C}_k) = \sum_{\Gamma_i} a_i \chi^{(\Gamma_i)}(\mathcal{C}_k) \tag{3.38}$$

where $\sum_{\Gamma_i}$ is the sum over the irreducible representations and the a_i coefficients have been shown to be unique (Eq. 3.20) and given by

$$a_i = \frac{1}{h} \sum_k N_k \left[\chi^{(\Gamma_i)}(\mathcal{C}_k) \right]^* \chi^{\text{reg}}(\mathcal{C}_k). \tag{3.39}$$

We note that $N_E = 1$ for the identity element, which is in a class by itself. But by construction $\chi^{\text{reg}}(\mathcal{C}_k) = 0$ unless $\mathcal{C}_k = E$ in which case $\chi^{\text{reg}}(E) = h$. Therefore $a_i = \chi^{\Gamma_i}(E) = \ell_i$, where χ^{Γ_i} is the trace of an ℓ_i dimensional unit matrix, thereby completing the proof.

The theorem (Eq. 3.38) that we have just proven tells us that the regular representation contains each irreducible representation of the group at least once. To obtain these irreducible representations explicitly, we have to carry out a similarity transformation which brings the matrices of the regular representation into block diagonal form. It turns out to be very messy to extract the matrices of the regular representation – in fact, it is so tedious to do this operation that it doesn't even make an instructive homework problem. It is much easier to write down the matrices which generate the symmetry operations of the group directly.

Consider for example the permutation group of three objects $P(3)$ which is isomorphic to the symmetry operations of a regular triangle. The matrices for D and F generate rotations by $\pm 2\pi/3$ about the z axis, which is $\perp$ to the plane of the triangle. The A matrix represents a rotation by $\pm\pi$ about the x axis while the B and C matrices represent rotations by $\pm\pi$ about axes in the $x - y$ plane which are $\pm 120°$ away from the x axis. In setting up a representation, it is advantageous to write down those matrices which can be easily written down – such as E, A, D, F. The remaining matrices such as B and C can then be found through the multiplication table.

We will now make use of the regular representation to prove a useful theorem for setting up character tables. This is the most useful application of the regular representation for our purposes.

Theorem: The order of a group h and the dimensionality ℓ_j of its irreducible representations Γ_j are related by

$$\sum_j \ell_j^2 = h. \tag{3.40}$$

We had previously found (Eq. 2.68) that $\sum_j \ell_j^2 \leq h$. The regular representation allows us to prove that it is the equality that applies.

Proof: By construction, the regular representation is of dimensionality h which is the number of elements in the group and in the multiplication table. But each irreducible representation of the group

is contained ℓ_j times in the regular representation (see Eq. 3.38) so that

$$\chi^{\text{reg}}(E) = h = \sum_{\Gamma_j} \underbrace{a_j}_{\ell_j} \underbrace{\chi^{\Gamma_j}(E)}_{\ell_j} = \sum_{\Gamma_j} \ell_j^{\,2} \qquad (3.41)$$

where the first ℓ_j is the number of times each irreducible representation is contained in the regular representation and the second ℓ_j is the dimension of the irreducible representation Γ_j.

We thus obtain the result:

$$\sum_j \ell_j^2 = h. \qquad (3.42)$$

where $\sum_j$ is the sum over irreducible representations. For example for $P(3)$, we have $\ell_1 = 1$, $\ell_{1'} = 1$, $\ell_2 = 2$ so that $\sum \ell_j^2 = 6 = h$.

3.8 Setting up Character Tables

For many applications it is sufficient to know just the character table without the actual matrix representations for a particular group. So far, we have only set up the character table by taking traces of the irreducible representations – i.e., from the definition of χ. For the most simple cases, the character table can be constructed using the results of the theorems we have just proved – without knowing the representations themselves. In practice, the character tables that are needed to solve a given problem are found either in books or in journal articles. The examples in this section are thus designed to show the reader how character tables are constructed, should this be necessary. Our goal is further to give some practice in using the theorems proven in Chapter 3.

A summary of useful rules for the construction of character tables is given below.

1. The number of irreducible representations is equal to the number of classes. (§3.5) The number of classes is found most conveniently from the classification of the symmetry operations of the group. Another way to find the classes is to compute all possible

conjugates for all group elements using the group multiplication table.

2. The dimensionalities of the irreducible representations are found from $\sum_i \ell_i^2 = h$ (see Eq. 3.42). For most cases, this relation uniquely determines the dimensionalities of the irreducible representations. For example, the permutation group of three objects $P(3)$ has three classes and therefore three irreducible representations. One of these must be 1-dimensional (i.e., the matrix for each element of the group is unity). So this gives $1^2 + ?^2 + ?^2 = 6$. This equation only has one solution, namely $1^2 + 1^2 + 2^2 = 6$. No other solution works!

3. There is always a whole row of 1's in the character table for the identity representation.

4. The first column of the character table is always the trace for the unit matrix representing the identity element or class. This character is always ℓ_1, the dimensional of the $(\ell_i \times \ell_i)$ unit matrix. Therefore, the first column of the character table is also filled in.

5. For all representations other than the identity representation Γ_1, the following relation is satisfied:

$$\sum_k N_k \chi^{(\Gamma_i)}(\mathcal{C}_k) = 0. \tag{3.43}$$

where $\sum_k$ denotes the sum on classes. Equation 3.43 follows from the wonderful orthogonality theorem for character and taking the identity representation Γ_1 as one of the irreducible representations.

If there are only a few classes in the group, Eq. 3.43 often uniquely determines the characters for several of the irreducible representations; particularly for the 1-dimensional representations.

6. The Wonderful Orthogonality Theorem for Character works on rows of the character table:

$$\sum_k \left[\chi^{(\Gamma_i)}(\mathcal{C}_k) \right]^* \chi^{(\Gamma_j)}(\mathcal{C}_k) N_k = h \delta_{\Gamma_i, \Gamma_j} \tag{3.44}$$

This theorem can be used both for orthogonality (different rows) or for normalization (same rows) of the characters in an irreducible representation.

7. The second orthogonality theorem works for columns of the character table:

$$\sum_{\Gamma_i} \left[\chi^{(\Gamma_i)}(\mathcal{C}_k) \right]^* \chi^{(\Gamma_i)}(\mathcal{C}_{k'}) = \frac{h}{N_k} \delta_{k,k'}. \tag{3.45}$$

This relation can be used both for orthogonality (different columns) or normalization (same columns), as the wonderful orthogonality theorem for character.

8. From the second orthogonality theorem for character, and from the character for the identity class

$$\chi^{(\Gamma_i)}(E) = \ell_i \tag{3.46}$$

we see that the characters for all the other classes obey the relation

$$\sum_{\Gamma_i} \chi^{(\Gamma_i)}(\mathcal{C}_k)\ell_i = 0 \tag{3.47}$$

where $\sum_{\Gamma_i}$ denotes the sum on irreducible representations and ℓ_i is the dimensionality of representation Γ_i. Equation 3.47 follows from the wonderful orthogonality theorem for character, and it uses as one of the irreducible representations, any but the identity representation ($\Gamma_i \neq \Gamma_1$).

With all this machinery it is often possible to complete the character tables for simple groups without an explicit determination of the matrices for a representation.

Let us illustrate the use of the rules for setting up character tables with the permutation group of three objects, $P(3)$.

We fill in the first row and first column of the character table immediately from rules #3 and #4 in the above list.

	$\mathcal{C}_1$	$3\mathcal{C}_2$	$2\mathcal{C}_3$
Γ_1	1	1	1
$\Gamma_{1'}$	1		
Γ_2	2		

	$\mathcal{C}_1$	$3\mathcal{C}_2$	$2\mathcal{C}_3$
Γ_1	1	1	1
$\Gamma_{1'}$	1	−1	1
Γ_2	2		

In order to satisfy #5, we know that $\chi^{(\Gamma_{1'})}(\mathcal{C}_2) = -1$ and $\chi^{(\Gamma_{1'})}(\mathcal{C}_3) = 1$, which we add to the character table.

Now apply the second orthogonality theorem using columns 1 and 2 and then again with columns 1 and 3, and this completes the character table, thereby obtaining:

	$\mathcal{C}_1$	$3\mathcal{C}_2$	$2\mathcal{C}_3$
Γ_1	1	1	1
$\Gamma_{1'}$	1	−1	1
Γ_2	2	0	−1

Let us give another example of a character table which illustrates another principle – not all entries in a character table need to be real. Such a situation can occur in the case of cyclic groups. Consider a group with three symmetry operations:

- E – identity

- C_3 – rotation by $\frac{2\pi}{3}$

- C_3^2 – rotation by $\frac{4\pi}{3}$

See Table 3.4 for the multiplication Table for this group. All three operations in this cyclic group are in separate classes as can be easily seen by conjugation of the elements. Hence there are three classes and three irreducible representations to write down. The character table we start with is obtained by following Rules #3 and #4.

	E	C_3	C_3^2
Γ_1	1	1	1
Γ_2	1	a	b
Γ_3	1	c	d

Orthogonality of Γ_2 to Γ_1 yields the algebraic relation: $1 + a + b = 0$.

Since $C_3^2 = C_3$ and $C_3^2 C_3 = E$, it follows that $b = a^2$ and $ab = a^3 = 1$, so that $a = e^{\frac{2\pi i}{3}}$. From this information we can readily complete the character table

Table 3.4: Multiplication table for the cyclic group of 3 rotations by $2\pi/3$ about a common axis.

	E	C_3	C_3^2
E	E	C_3	C_3^2
C_3	C_3	C_3^2	E
C_3^2	C_3^2	E	C_3^2

	E	C_3	C_3^2
Γ_1	1	1	1
Γ_2	1	ω	ω^2
Γ_3	1	ω^2	ω

where $\omega = \exp[\frac{2\pi i}{3}]$. In a physical problem with time inversion, the energy levels corresponding to Γ_2 and Γ_3 are degenerate.

This idea of the cyclic group can be applied to a 4-element group: E, C_2, C_4, C_4^3 – to a 5-element group: E, C_5, C_5^2, C_5^3, C_5^4 – and to a 6-element group: E, C_6, C_3, C_2, C_3^2, C_6^5, etc. For the case of Bloch's theorem we have an N-element group with characters that comprise the Nth roots of unity $\omega = \exp[\frac{2\pi i}{N}]$.

All these cyclic groups are Abelian so that each element is in a class by itself. The representations for these groups correspond to the multiplication tables, which therefore contain the appropriate collections of roots of unity.

3.9 Symmetry Notation

We make use of the following point group notation for the symmetry operations in the character tables printed in books and journals:

- $E =$ Identity

- $C_n =$ rotation through $2\pi/n$. For example C_2 is a rotation of $180°$. Likewise C_3 is a rotation of $120°$, while C_6^2 represents a rotation of $60°$ followed by another rotation of $60°$ about the
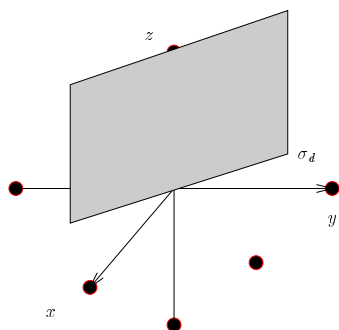
Figure 3.1: Schematic illustration of a dihedral symmetry axis. The reflection plane containing the diagonal of the square and the four-fold axes is called a dihedral plane. For this geometry $\sigma_d(x, y, z) = (-y, -x, z)$.

same axis so that $C_6^2 = C_3$. In a Bravais lattice it can be shown that n in C_n can only assume values of n=1, 2, 3, 4, and 6. The observation of a diffraction pattern with five-fold symmetry in 1984 was therefore completely unexpected, and launched the field of quasicrystals.

- $\sigma =$ reflection in a plane.

- $\sigma_h =$ reflection in a "horizontal" plane. The reflection plane here is perpendicular to the axis of highest rotational symmetry.

- $\sigma_v =$ reflection in a "vertical" plane. The reflection plane here contains the axis of highest symmetry.

- $\sigma_d =$ reflection in a diagonal plane. The reflection plane here is a vertical plane which bisects the angle between the two fold axes $\perp$ to the principal symmetry axis. An example of a diagonal plane is shown in Fig. 3.1. σ_d is also called a dihedral plane.

- $i =$ inversion which takes

$$\begin{cases} x \rightarrow -x \\ y \rightarrow -y \\ z \rightarrow -z \end{cases}$$

- $S_n =$ improper rotation through $2\pi/n$, which consists of a rotation by $2\pi/n$ followed by a reflection in a horizontal plane.

- iC_n = compound rotation-inversion, which consists of a rotation followed by an inversion.

In addition to these point group symmetry operations, there are several space group symmetry operations, such as translations, glide planes, screw axes, etc., which are discussed in Chapter 12. The notation used in the list above for the symmetry operations is called the **Schoenflies** notation. Based on this symmetry notation is a point group notation. There are **32 common point groups** and the character tables for these 32 point groups are given in any standard group theory text. For convenience we also list the character tables for the 32 point groups in the notes at the end of Chapter 3 (see Tables 3.8 – 3.34 on pp. 63-70). For example, groups $C_1, C_2, \ldots, C_6$ only have n-fold rotations about a simple symmetry axis C_n (see Tables 3.8 – 3.13 on pp. 63-64). Groups C_{nv} have, in addition to the n-fold axes, vertical reflection planes σ_v (see Tables 3.14 – 3.18 on pp. 64-66). Groups C_{nh} have, in addition to the n-fold axes (see Tables 3.19 and 3.21 pp. 66-67), horizontal reflection planes σ_h and include each operation C_n together with the compound operations C_n followed by σ_h. The groups S_2, S_4 and S_6 have mostly (see Tables 3.22 – 3.23) compound operations. The groups denoted by D_n are dihedral groups and have (see Tables 3.24 – 3.28 pp. 68-69) non-equivalent symmetry axes in perpendicular planes. The group of the operations of a square is D_4 and has in addition to the principal four-fold axes, two sets of non-equivalent two-fold axes. When non-equivalent axes are combined (see Tables 3.29 – 3.31 on p. 69) with mirror planes we get groups like D_{2h}, D_{3h}, etc. There are 5 cubic groups T, O, T_d, T_h and O_h. These groups have no principal axis but instead have four three-fold axes (see Tables 3.32 – 3.34).

There is also a second notation for symmetry operations and groups – namely the **Hermann–Mauguin** or **international notation**, referring to the International Tables for X-Ray Crystallography, a standard structural and symmetry reference book. The international notation is what is usually found in crystallography textbooks and various materials science journals, and for that reason it is also necessary to become familiar with this notation. The general correspondence between the two notations is shown in Table 3.5 for rotations and mirror planes. The Hermann–Mauguin notation $\bar{n}$ means iC_n which is equivalent to a

Table 3.5: Comparison between Schoenflies and Hermann-Mauguin notation.

	Schoenflies	**Hermann-Mauguin**
rotation	C_n	n
rotation-inversion	iC_n	$\bar{n}$
mirror plane	σ	m
horizontal reflection plane $\perp$ to $n-$fold axes	σ_h	n/m
$n-$fold axes in vertical reflection plane	σ_v	nm
two non $-$ equivalent vertical reflection planes	$\sigma_{v'}$	nmm

rotation followed by or preceded by an inversion. A string of numbers like 422 (see Table 3.26 on p. 68) means that there is a four-fold major symmetry axis (C_4 axis), and perpendicular to this axis are 2 inequivalent two-fold axes $C_{2'}$ and $C_{2''}$, such as occur in the group of the square (D_4). If there are several inequivalent horizontal mirror planes like

$$\frac{2}{m}, \frac{2}{m}, \frac{2}{m},$$

an abbreviated notation mmm is sometimes used [see notation for the group D_{2h} below (Table 3.29 on p. 69)]. The notation $4mm$ (see Table 3.16 on p. 65) denotes a four-fold axis and two sets of vertical mirror planes, one set through the axes C_4 and denoted by $2\sigma_v$ and the other set through the bisectors of the $2\sigma_v$ planes and denoted by the dihedral vertical mirror planes $2\sigma_d$.

Table 3.6 is useful in relating the two kinds of notations for rotations and improper rotations.

Some useful relations on the commutativity of symmetry operations are:

1. Inversion commutes with all point symmetry operations.

2. All rotations about the same axis commute.

3. All rotations about an arbitrary rotation axis commute with reflections across a plane perpendicular to this rotation axis.

Table 3.6: Comparison of notation for proper and improper rotations in the Schoenflies and International systems.

Proper Rotations		Improper Rotations	
International	**Schoenflies**	**International**	**Schoenflies**
1	C_1	$\bar{1}$	S_2
2	C_2	$\bar{2} \equiv m$	σ
3	C_3	$\bar{3}$	S_6^{-1}
3_2	C_3^{-1}	$\bar{3}_2$	S_6
4	C_4	$\bar{4}$	S_4^{-1}
4_3	C_4^{-1}	$\bar{4}_3$	S_4
6	C_6	$\bar{6}$	S_3^{-1}
6_5	C_6^{-1}	$\bar{6}_5$	S_3

4. Two two-fold rotations about perpendicular axes commute.

5. Two reflections in perpendicular planes will commute.

6. Any two of the symmetry elements σ_h, S_2, C_n ($n = $ even) implies the third.

If we have a major symmetry axis $C_n(n \geq 2)$ and there are either two-fold axes C_2 or vertical mirror planes σ_v, then there will generally be more than one C_2 or σ_v.

The classification of the 32 point symmetry groups shown in Table 3.7 is often useful in making practical applications of character tables in textbooks and journal articles to specific materials. In Table 3.7 the first symbol in the Hermann-Mauguin notation denotes the principal axis or plane. The second symbol denotes an axis (or plane) perpendicular to this axis, except for the cubic groups where the second symbol refers to a $\langle 111 \rangle$ axis. The third symbol denotes an axis or plane that is $\perp$ to the first axis and at an angle of π/n with respect to the second axis.

It is also convenient to picture group symmetries with stereograms (e.g., Tinkham p.55), which are here reproduced in Fig. 3.2. The stereogram is a mapping of a general point on a sphere onto a plane going through the center of the sphere. If the point on the sphere is above

Table 3.7: The 32 point groups and their symbols. In the Hermann–Mauguin notation, the symmetry axes parallel to and the symmetry planes perpendicular to each of the "principal" directions in the crystal are named in order. When there is both an axis parallel to and a plane normal to a given direction, these are indicated as a fraction; thus $6/m$ means a six-fold rotation axis standing perpendicular to a plane of symmetry, while $\bar{4}$ denotes a four-fold rotary inversion axis. In some classifications, the rhombohedral (trigonal) groups are listed with the hexagonal groups.

The 32 Point Groups and Their Symbols			
System	Schoenflies symbol	Hermann-Mauguin symbol		Examples
		Full	Abbreviated	
Triclinic	C_1	1	1	
	$C_i, (S_2)$	$\bar{1}$	$\bar{1}$	Al_2SiO_5
Monoclinic	$C_{2v}, (C_{1h}), (S_1)$	m	m	KNO_2
	C_2	2	2	
	C_{2h}	$2/m$	$2/m$	
Orthorhombic	C_{2v}	$2mm$	mm	
	$D_2, (V)$	222	222	
	$D_{2h}, (V_h)$	$2/m\,2/m\,2/m$	mmm	I, Ga
Tetragonal	S_4	4	4	
	C_4	4	4	
	C_{4h}	$4/m$	$4/m$	$CaWO_4$
	$D_{2d}, (V_d)$	$\bar{4}2m$	$\bar{4}2m$	
	C_{4v}	$4mm$	$4mm$	
	D_4	422	42	
	D_{4h}	$4/m\,2/m\,2/m$	$4/mmm$	$TiO_2, In, \beta-Sn$
Rhombohedral	C_3	3	3	AsI_3
	$C_{3i}, (S_6)$	$\bar{3}$	$\bar{3}$	$FeTiO_3$
	C_{3v}	$3m$	$3m$	
	D_3	32	32	Se
	D_{3d}	$\bar{3}2/m$	$\bar{3}m$	Bi, As, Sb, Al_2O_3
Hexagonal	$C_{3h}, (S_3)$	$\bar{6}$	$\bar{6}$	
	C_6	6	6	
	C_{6h}	$6/m$	$6/m$	
	D_{3h}	$\bar{6}2m$	$\bar{6}2m$	
	C_{6v}	$6mm$	$6mm$	ZnO, NiAs
	D_6	622	62	CeF_3
	D_{6h}	$6/m\,2/m\,2/m$	$6/mmm$	Mg, Zn, graphite
Cubic	T	23	23	$NaClO_3$
	T_h	$2/m\bar{3}$	$m3$	FeS_2
	T_d	$\bar{4}3m$	$\bar{4}3m$	ZnS
	O	432	43	β-Mn
	O_h	$4/m\,\bar{3}\,2/m$	$m3m$	NaCl, diamond, Cu
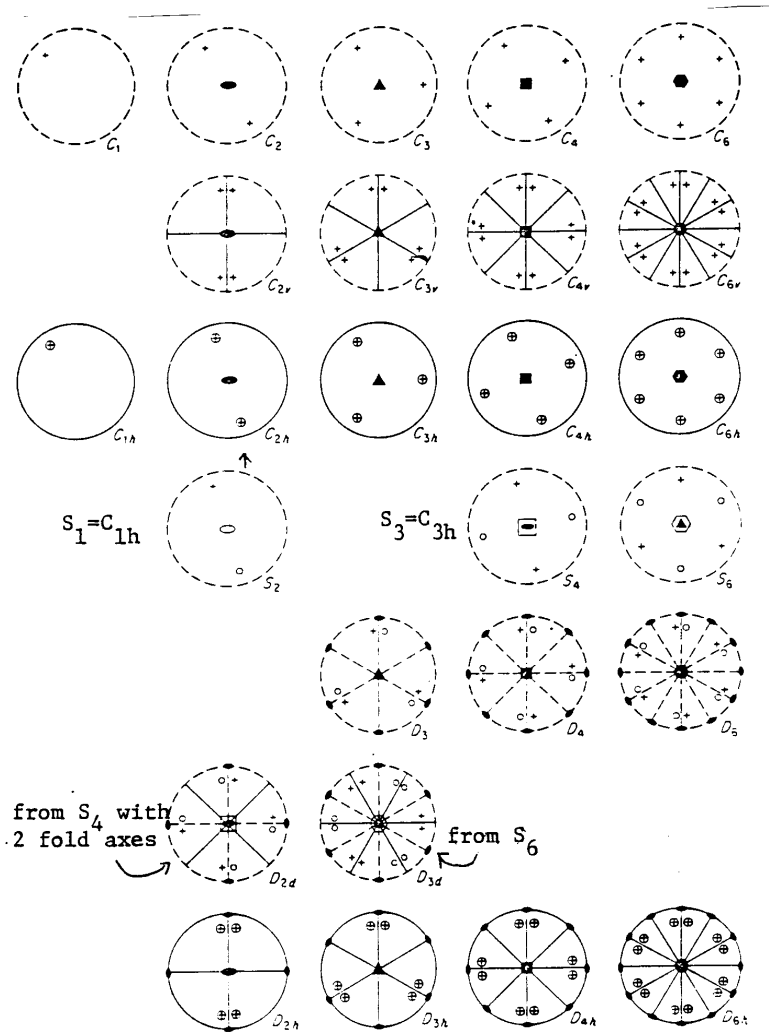
Figure 3.2: Stereographic projections of simple point groups. For the case of icosahedral symmetry projections for C_5, C_{5v}, D_{5h}, and D_{5d} are useful.

the plane it is indicated as a +, if below as a ∘. In general, the polar axis of the stereogram coincides with the principal axis of symmetry.

The 5 stereograms on the first row pertaining to groups with a single axis of rotation show the effect of 2-, 3-, 4-, and 6-fold rotation axes on a point +. These groups are cyclic groups with only n-fold axes. Note the symmetry of the central point for each group. On the second row we have added vertical mirror planes which are indicated by the solid lines. Since the "vertical" and "horizontal" planes are not distinguishable for C_1, the addition of a mirror plane to C_1 is given in the third row, showing the groups which result from the first row upon addition of horizontal planes. The symbols ⊕ indicate the coincidence of the projection of points above and below the plane, characteristic of horizontal mirror planes.

If instead of proper rotations as in the first row, we have improper rotations, then the groups on row 4 are generated. Since S_1 is identical with C_{1h}, it is not shown separately; this also applies to $S_3 \Rightarrow C_{3h}$. It is of interest to note that S_2 and S_6 have inversion symmetry but S_4 does not.

The addition of two-fold axes ⊥ to the principal symmetry axis for the groups in the first row yields the stereograms of the fifth row where the two-fold axes appear as dashed lines. Here we see that the higher the symmetry of the principal symmetry axis, the greater the number of two-fold axes.

The addition of two-fold axes to the groups on the 4th row yields the stereograms of the 6th row, where D_{2d} comes from S_4, and D_{3d} from S_6. The addition of two-fold axes to S_2 results in C_{2h}. The stereograms on the last row are obtained by adding two-fold axes ⊥ to C_n to the stereograms on the 3rd row. The effect of adding a two-fold axis to C_{1h} is to produce C_{2v}.

The remaining 5 point symmetry groups not shown in Fig. 3.2 have higher symmetry and have no single principal axis. The resulting stereograms are very complicated and for this reason are not given in Fig. 3.2. We give some of the symmetry elements for these groups below.

The group T (or 23 using the International notation) has 12 symmetry elements which include:
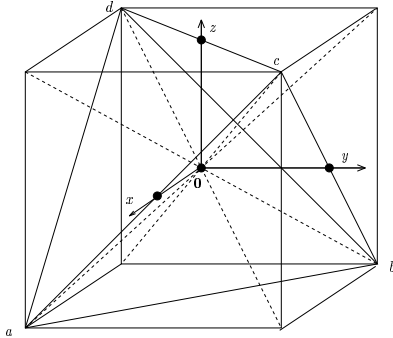
Figure 3.3: Schematic diagram for the symmetry operations of the group T_d.

1	identity	
3	two-fold axes	(x, y, z)
4	three-fold axes	(body diagonals–positive rotation)
4	three-fold axes	(body diagonals–negative rotations)
12	symmetry elements	

The point group T_h (denoted by $m3$ in the abbreviated International notation or by $2/m3$ in the full International notation) contains all the symmetry operations of T and inversion as well, and is written as $T_h \equiv T \otimes i$, indicating the direct product of the group T and the group C_i having 2 symmetry elements E, i. This is equivalent to adding a horizontal plane of symmetry, hence the notation $2/m$; the symbol 3 means a three-fold axis (see Table 3.6). Thus T_h has 24 symmetry elements.

The point group T_d ($\bar{4}3m$) contains the symmetry operations of the regular tetrahedron (see Fig. 3.3), which correspond to the point symmetry for diamond and the zincblende (III–V and II–VI) structures. We list below the 24 symmetry operations of T_d.

Symmetry Operations of T_d

- Identity

- 8 C_3 about body diagonals corresponding to rotations of $\pm\frac{2\pi}{3}$

- 3 C_2 about x, y, z directions
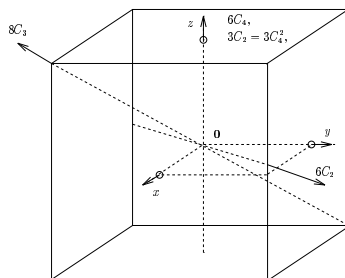
Figure 3.4: Schematic for the symmetry operations of the group O.

- 6 S_4 about x, y, z corresponding to rotations of $\pm \frac{\pi}{2}$

- 6 σ_d planes that are diagonal reflection planes

The cubic groups are O (432) and O_h ($m3m$) and are shown schematically in Fig. 3.4. The operations for group O are shown in Fig. 3.4 and are $E, 8C_3, 3C_2 = 3C_4^2, 6C_2$ and $6C_4$. To get O_h we combine these 24 operations with inversion to give 48 operations in all. We note that the second symbol in the Hermann-Mauguin (International) notation for all 5 cubic groups is for the $\langle 111 \rangle$ axes rather than for an axis $\perp$ to the principal symmetry axis.

At this point we are ready to understand the notation used in the character tables of the texts (e.g., Tinkham) and journal articles. As we examine the character tables we observe that not all the entries are real. However, in the 11 point groups where there are representations with complex characters, there is always another representation that is the complex conjugate of the first.

In addition to the 32 point groups, the character tables contain listings for $C_{\infty v}$ and $D_{\infty h}$ which have full rotational symmetry around a single axis, and therefore have an ∞ number of symmetry operations and classes. These two groups are sometimes called the semi-infinite groups because they have an infinite number of operations about the major symmetry axis. An example of the $C_{\infty v}$ group is the CO molecule shown in Fig. 3.5. Here the symmetry operations are $E, 2C_\phi$ and σ_v. The notation C_ϕ denotes an axis of full rotational symmetry and σ_v denotes the corresponding infinite array of vertical planes. The group $D_{\infty h}$ has in addition the inversion operation which is compounded with each of the operations in $C_{\infty v}$, and this is written as $D_{\infty h} = C_{\infty v} \otimes i$.
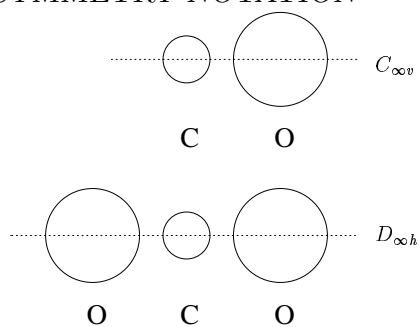
Figure 3.5: Schematic diagram of the CO molecule with symmetry $C_{\infty v}$ and symmetry operations $E, 2C_\phi, \sigma_v$, and the linear CO_2 molecule in which the inversion operation is also present to give the group $D_{\infty h}$.
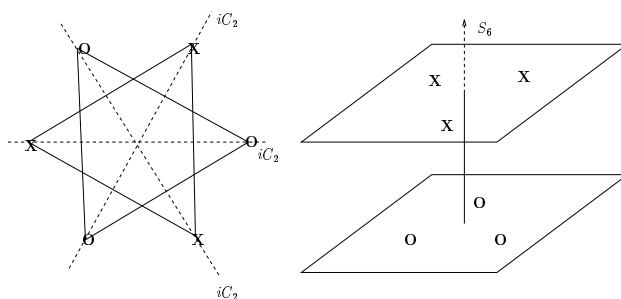
Figure 3.6: Schematic diagram of an X_3O_3 molecule.

An example of a molecule with $D_{\infty h}$ symmetry in the CO_2 molecule (see Fig. 3.5).

To make use of group theory for describing physical properties of molecules, we classify the symmetry operations of a molecule in terms of a point group. We illustrate this problem by considering a molecule X_3O_3 shown in the schematic diagram of Fig. 3.6.

The symmetry operations for the molecule in Fig. 3.6 are:

E

C_3

σ_h (only for planar molecule)

σ_v

σ_d (only for planar molecule)

i (X goes into O)

S_6 (X goes into O)

iC_3 (X goes into O)

Thus, if the X and O atoms are distinct, the appropriate group is C_{3v}. If X and O are the same, the group is D_{3d}. If the A_3B_3 molecule is planar but X and O are distinct the appropriate group is D_{3h} and if X and O are the same the group is D_{6h}.

In Tables 3.8 – 3.34, we give the character tables for the 32 point groups, following Tinkham's tables. These are followed by Tables 3.35 and 3.36 for the semi-infinite groups $C_{\infty v}$ and $D_{\infty h}$. Tables 3.37–3.40 are for groups with five-fold symmetry axes not readily found in group theory books, but have recently become important because of the discovery of quasi-crystals and C_{60} and related molecules. Note that the tables for five-fold symmetry are: C_5 (Table 3.12); C_{5v} (Table 3.17); $C_{5h} \equiv C_5 \otimes \sigma_h$; D_5 (Table 3.27); D_{5d} (Table 3.37); D_{5h} (Table 3.38); I (Table 3.39); and I_h (Table 3.40). Recurrent in these tables is the "golden mean", $\tau = (1 + \sqrt{5})/2$ where $\tau - 1 = 2\cos(2\pi/5) = 2\cos 72°$.

At this point there are many features of the character tables which have not yet been explained in the book. Future chapters that will address these features are on the topics of basis functions (Chapter 4), direct products (Chapter 4), linear molecules (Chapter 4) and icosahedral symmetry (Chapter 4). Furthermore, as we use the various character tables in physical applications, the notation will become more clear and more familiar to the reader.

Table 3.8: Character Table for Group C_1

C_1 (1)	E
A	1

Table 3.9: Character Table for Group C_2

C_2 (2)			E	C_2
x^2, y^2, z^2, xy	R_z, z	A	1	1
xz, yz	$\begin{matrix}(x,y)\\(R_x, R_y)\end{matrix}\Big\}$	B	1	-1

Table 3.10: Character Table for Group C_3

$C_3(3)$			E	C_3	C_3^2
$x^2 + y^2, z^2$	R_z, z	A	1	1	1
$\left.\begin{matrix}(xz, yz)\\(x^2 - y^2, xy)\end{matrix}\right\}$	$\left.\begin{matrix}(x,y)\\(R_x, R_y)\end{matrix}\right\}$	E	$\left\{\begin{matrix}1\\1\end{matrix}\right.$	$\begin{matrix}\omega\\\omega^2\end{matrix}$	$\begin{matrix}\omega^2\\\omega\end{matrix}$

where $\omega = e^{2\pi i/3}$

Table 3.11: Character Table for Group C_4

C_4 (4)			E	C_2	C_4	C_4^3
$x^2 + y^2, z^2$	R_z, z	A	1	1	1	1
$x^2 - y^2, xy$		B	1	1	-1	-1
(xz, yz)	$\left.\begin{matrix}(x,y)\\(R_x, R_y)\end{matrix}\right\}$	E	$\left\{\begin{matrix}1\\1\end{matrix}\right.$	$\begin{matrix}-1\\-1\end{matrix}$	$\begin{matrix}i\\-i\end{matrix}$	$\begin{matrix}-i\\i\end{matrix}$

Table 3.12: Character Table for Group C_5

C_5 (5)			E	C_5	C_5^2	C_5^3	C_5^4
$x^2 + y^2, z^2$	R_z, z	A	1	1	1	1	1
(xz, yz)	(x, y) (R_x, R_y)	E'	1	ω	ω^2	ω^3	ω^4
			1	ω^4	ω^3	ω^2	ω
$(x^2 - y^2, xy)$		E''	1	ω^2	ω^4	ω	ω^3
			1	ω^3	ω	ω^4	ω^2

where $\omega = e^{2\pi i/5}$

Table 3.13: Character Table for Group C_6

C_6 (6)			E	C_6	C_3	C_2	C_3^2	C_6^5
$x^2 + y^2, z^2$	R_z, z	A	1	1	1	1	1	1
		B	1	-1	1	-1	1	-1
(xz, yz)	(x, y) (R_x, R_y)	E'	1	ω	ω^2	ω^3	ω^4	ω^5
			1	ω^5	ω^4	ω^3	ω^2	ω
$(x^2 - y^2, xy)$		E''	1	ω^2	ω^4	1	ω^2	ω^4
			1	ω^4	ω^2	1	ω^4	ω^2

where $\omega = e^{2\pi i/6}$

Table 3.14: Character Table for Group C_{2v}

C_{2v} (2mm)			E	C_2	σ_v	σ_v'
x^2, y^2, z^2	z	A_1	1	1	1	1
xy	R_z	A_2	1	1	-1	-1
xz	R_y, x	B_1	1	-1	1	-1
yz	R_x, y	B_2	1	-1	-1	1

Table 3.15: Character Table for Group C_{3v}

C_{3v} (3m)			E	$2C_3$	$3\sigma_v$
x^2+y^2, z^2	z	A_1	1	1	1
	R_z	A_2	1	1	-1
$\left.\begin{array}{l}(x^2-y^2, xy)\\(xz, yz)\end{array}\right\}$	$\left.\begin{array}{l}(x, y)\\(R_x, R_y)\end{array}\right\}$	E	2	-1	0

Table 3.16: Character Table for Group C_{4v}

C_{4v} (4mm)			E	C_2	$2C_4$	$2\sigma_v$	$2\sigma_d$
x^2+y^2, z^2	z	A_1	1	1	1	1	1
	R_z	A_2	1	1	1	-1	-1
x^2-y^2		B_1	1	1	-1	1	-1
xy		B_2	1	1	-1	-1	1
$\left.\begin{array}{l}(x^2-y^2, xy)\\(xz, yz)\end{array}\right\}$	$\left.\begin{array}{l}(x, y)\\(R_x, R_y)\end{array}\right\}$	E	2	-2	0	0	0

Table 3.17: Character Table for Group C_{5v}

C_{5v} (5m)			E	$2C_5$	$2C_5^2$	$5\sigma_v$
$x^2+y^2, z^2, z^3, z(x^2+y^2)$	z	A_1	1	1	1	1
	R_z	A_2	1	1	1	-1
$z(x, y), z^2(x, y), (x^2+y^2)(x, y)$	$\left.\begin{array}{l}(x, y)\\(R_x, R_y)\end{array}\right\}$	E_1	2	$2\cos\alpha$	$2\cos 2\alpha$	0
$(x^2-y^2, xy), z(x^2-y^2, xy), [x(x^2-3y^2), y(3x^2-y^2)]$		E_2	2	$2\cos 2\alpha$	$2\cos 4\alpha$	0

where $\alpha = \frac{2\pi}{5} = 72°$.
Note that $\tau = (1+\sqrt{5})/2$ so that $\tau = -2\cos 2\alpha = -2\cos 4\pi/5$ and
$\tau - 1 = 2\cos\alpha = 2\cos 2\pi/5$.

Table 3.18: Character Table for Group C_{6v}

C_{6v} (6mm)			E	C_2	$2C_3$	$2C_6$	$3\sigma_d$	$3\sigma_v$
$x^2 + y^2, z^2$	z	A_1	1	1	1	1	1	1
	R_z	A_2	1	1	1	1	-1	-1
		B_1	1	-1	1	-1	-1	1
		B_2	1	-1	1	-1	1	-1
(xz, yz)	(x, y) (R_x, R_y) $\big\}$	E_1	2	-2	-1	1	0	0
$(x^2 - y^2, xy)$		E_2	2	2	-1	-1	0	0

Table 3.19: Character Table for Group C_{1h}

$C_{1h}(m)$			E	σ_h
x^2, y^2, z^2, xy	R_z, x, y	A'	1	1
xz, yz	R_x, R_y, z	A''	1	-1

Table 3.20: Character Table for Group C_{2h}

C_{2h} (2/m)			E	C_2	σ_h	i
x^2, y^2, z^2, xy	R_z	A_g	1	1	1	1
	z	A_u	1	1	-1	-1
xz, yz	R_x, R_y	B_g	1	-1	-1	1
	x, y	B_u	1	-1	1	-1

Table 3.21: Character Table for Group C_{3h}

$C_{3h} = C_3 \otimes \sigma_h$ ($\bar{6}$)			E	C_3	C_3^2	σ_h	S_3	($\sigma_h C_3^2$)
$x^2 + y^2, z^2$	R_z	A'	1	1	1	1	1	1
	z	A''	1	1	1	-1	-1	-1
$(x^2 - y^2, xy)$	(x, y)	E'	1	ω	ω^2	1	ω	ω^2
			1	ω^2	ω	1	ω^2	ω
(xz, yz)	(R_x, R_y)	E''	1	ω	ω^2	-1	$-\omega$	$-\omega^2$
			1	ω^2	ω	-1	$-\omega^2$	$-\omega$

where $\omega = e^2\pi i/3$

$$
\begin{aligned}
C_{4h} &= C_4 \otimes i & (4/m) \\
C_{5h} &= C_5 \otimes \sigma_h & (\bar{10}) \\
C_{6h} &= C_6 \otimes i & (6/m)
\end{aligned}
$$

Table 3.22: Character Table for Group S_2

S_2 ($\bar{1}$)			E	i
$x^2, y^2, z^2, xy, xz, yz$	R_x, R_y, R_z	A_g	1	1
	x, y, z	A_u	1	-1

Table 3.23: Character table for Group S_4

S_4 ($\bar{4}$)			E	C_2	S_4	S_4^3
$x^2 + y^2, z^2$	R_z	A	1	1	1	1
	z	B	1	1	-1	-1
(xz, yz) $\}$ $(x^2 - y^2, xy)$	(x, y) $\}$ (R_x, R_y)	E	1	-1	i	$-i$
			1	-1	$-i$	i

$$
S_6 = C_3 \otimes i \quad (\bar{3})
$$

Table 3.24: Character Table for Group D_2

D_2 (222)			E	C_2^z	C_2^y	C_2^x
x^2, y^2, z^2		A_1	1	1	1	1
xy	R_z, z	B_1	1	1	-1	-1
xz	R_y, y	B_2	1	-1	1	-1
yz	R_x, x	B_3	1	-1	-1	1

Table 3.25: Character Table for Group D_3

D_3 (32)			E	$2C_3$	$3C_2'$
$x^2 + y^2, z^2$		A_1	1	1	1
	R_z, z	A_2	1	1	-1
$\left.\begin{array}{l}(xz, yz)\\(x^2 - y^2, xy)\end{array}\right\}$	$\left.\begin{array}{l}(x, y)\\(R_x, R_y)\end{array}\right\}$	E	2	-1	0

Table 3.26: Character Table for Group D_4

D_4 (422)			E	$C_2 = C_4^2$	$2C_4$	$2C_2'$	$2C_2''$
$x^2 + y^2, z^2$		A_1	1	1	1	1	1
	R_z, z	A_2	1	1	1	-1	-1
$x^2 - y^2$		B_1	1	1	-1	1	-1
xy		B_2	1	1	-1	-1	1
(xz, yz)	$\left.\begin{array}{l}(x, y)\\(R_x, R_y)\end{array}\right\}$	E	2	-2	0	0	0

Table 3.27: Character Table for Group D_5

D_5 (52)			E	$2C_5$	$2C_5^2$	$5C_2'$
$x^2 + y^2, z^2$		A_1	1	1	1	1
	R_z, z	A_2	1	1	1	-1
(xz, yz)	$\left.\begin{array}{l}(x, y)\\(R_x, R_y)\end{array}\right\}$	E_1	2	$2\cos\alpha$	$2\cos 2\alpha$	0
$(x^2 - y^2, xy)$		E_2	2	$2\cos 2\alpha$	$2\cos 4\alpha$	0

where $\alpha = 2\pi/5 = 72°$.
Note that $\tau = (1 + \sqrt{5})/2$ so that $\tau = -2\cos 2\alpha = -2\cos 4\pi/5$ and $\tau - 1 = 2\cos\alpha = 2\cos 2\pi/5$.

Table 3.28: Character Table for Group D_6

D_6 (622)			E	C_2	$2C_3$	$2C_6$	$3C_2'$	$3C_2''$
$x^2 + y^2, z^2$		A_1	1	1	1	1	1	1
	R_z, z	A_2	1	1	1	1	-1	-1
		B_1	1	-1	1	-1	1	-1
		B_2	1	-1	1	-1	-1	1
(xz, yz)	(x,y) (R_x, R_y) $\Big\}$	E_1	2	-2	-1	1	0	0
$(x^2 - y^2, xy)$		E_2	2	2	-1	-1	0	0

Table 3.29: Character Table for Group D_{2d}

D_{2d} ($\bar{4}2m$)			E	C_2	$2S_4$	$2C_2'$	$2\sigma_d$
$x^2 + y^2, z^2$		A_1	1	1	1	1	1
	R_z	A_2	1	1	1	-1	-1
$x^2 - y^2$		B_1	1	1	-1	1	-1
xy	z	B_2	1	1	-1	-1	1
(xz, yz)	(x,y) (R_x, R_y) $\Big\}$	E	2	-2	0	0	0

$$D_{2h} = D_2 \otimes i \quad (mmm)$$
$$D_{5d} = D_5 \otimes i \quad (\bar{5}m) \text{ see Table 3.37}$$

Table 3.30: Character Table for Group D_{3d}

$D_{3d} = D_3 \otimes i$ ($\bar{3}m$)			E	$2C_3$	$3C_2'$	i	$2iC_3$	$3iC_2'$
$x^2 + y^2, z^2$		A_{1g}	1	1	1	1	1	1
	R_z	A_{2g}	1	1	-1	1	1	-1
$(xz, yz), (x^2 - y^2, xy)$	(R_x, R_y)	E_g	2	-1	0	2	-1	0
		A_{1u}	1	1	1	-1	-1	-1
	z	A_{2u}	1	1	-1	-1	-1	1
	(x,y)	E_u	2	-1	0	-2	1	0

Table 3.31: Character Table for Group D_{3h}

$D_{3h} = D_3 \otimes \sigma_h$ ($\bar{6}m2$)			E	σ_h	$2C_3$	$2S_3$	$3C_2'$	$3\sigma_v$
$x^2 + y^2, z^2$		A_1'	1	1	1	1	1	1
	R_z	A_2'	1	1	1	1	-1	-1
		A_1''	1	-1	1	-1	1	-1
	z	A_2''	1	-1	1	-1	-1	1
$(x^2 - y^2, xy)$	(x,y)	E'	2	2	-1	-1	0	0
(xz, yz)	(R_x, R_y)	E''	2	-2	-1	1	0	0

$$
\begin{aligned}
D_{4h} &= D_4 \otimes i \quad (4/mmm) \\
D_{5h} &= D_5 \otimes \sigma_h \quad (\overline{10}m2) \quad \text{see Table 3.38} \\
D_{6h} &= D_6 \otimes i \quad (6/mmm)
\end{aligned}
$$

Table 3.32: Character Table for Group T

T (23)		E	$3C_2$	$4C_3$	$4C_3'$
	A	1	1	1	1
	E $\begin{cases} \\ \\ \end{cases}$	$\begin{matrix} 1 \\ 1 \end{matrix}$	$\begin{matrix} 1 \\ 1 \end{matrix}$	$\begin{matrix} \omega \\ \omega^2 \end{matrix}$	$\begin{matrix} \omega^2 \\ \omega \end{matrix}$
$\left. \begin{matrix} (R_x, R_y, R_z) \\ (x, y, z) \end{matrix} \right\}$	T	3	-1	0	0

where $\omega = \exp(2\pi i/3)$

$$T_h = T \otimes i \quad (m3)$$

Table 3.33: Character Table for Group O

O (432)		E	$8C_3$	$3C_2 = 3C_4^2$	$6C_2'$	$6C_4$
$(x^2 + y^2 + z^2)$	A_1	1	1	1	1	1
	A_2	1	1	1	-1	-1
$(x^2 - y^2, 3z^2 - r^2)$	E	2	-1	2	0	0
$\left. \begin{matrix} (R_x, R_y, R_z) \\ (x, y, z) \end{matrix} \right\}$	T_1	3	0	-1	-1	1
(xy, yz, zx)	T_2	3	0	-1	1	-1

$$O_h = O \otimes i \quad (m3m)$$

Table 3.34: Character Table for Group T_d

T_d ($\overline{4}3m$)		E	$8C_3$	$3C_2$	$6\sigma_d$	$6S_4$
	A_1	1	1	1	1	1
	A_2	1	1	1	-1	-1
	E	2	-1	2	0	0
(R_x, R_y, R_z)	T_1	3	0	-1	-1	1
(x, y, z)	T_2	3	0	-1	1	-1

Table 3.35: Character Table for Group $C_{\infty v}$

$C_{\infty v}$ (∞m)			E	$2C_\phi$	σ_v
$(x^2 + y^2, z^2)$	z	$A_1(\Sigma^+)$	1	1	1
	R_z	$A_2(\Sigma^-)$	1	1	-1
(xz, yz)	$\begin{matrix}(x,y)\\(R_x, R_y)\end{matrix}$	$E_1(\Pi)$	2	$2\cos\phi$	0
$(x^2 - y^2, xy)$		$E_2(\Delta)$	2	$2\cos 2\phi$	0
			$\vdots$	$\vdots$ $\vdots$	$\vdots$

Table 3.36: Character Table for Group $D_{\infty h}$

$D_{\infty h}$ (∞/mm)			E	$2C_\phi$	C_2'	i	$2iC_\phi$	iC_2'
$x^2 + y^2, z^2$		$A_{1g}(\Sigma_g^+)$	1	1	1	1	1	1
		$A_{1u}(\Sigma_u^-)$	1	1	1	-1	-1	-1
	R_z	$A_{2g}(\Sigma_g^-)$	1	1	-1	1	1	-1
	z	$A_{2u}(\Sigma_u^+)$	1	1	-1	-1	-1	1
(xz, yz)	(R_x, R_y)	$E_{1g}(\Pi_g)$	2	$2\cos\phi$	0	2	$2\cos\phi$	0
	(x, y)	$E_{1u}(\Pi_u)$	2	$2\cos\phi$	0	-2	$-2\cos\phi$	0
$(x^2 - y^2, xy)$		$E_{2g}(\Delta_g)$	2	$2\cos 2\phi$	0	2	$2\cos 2\phi$	0
		$E_{2u}(\Delta_u)$	2	$2\cos 2\phi$	0	-2	$-2\cos 2\phi$	0
			$\vdots$	$\vdots$	$\vdots$	$\vdots$	$\vdots$	$\vdots$

Table 3.37: Character table for D_{5d}.

D_{5d}	E	$2C_5$	$2C_5^2$	$5C_2'$	i	$2S_{10}^{-1}$	$2S_{10}$	$5\sigma_d$	$(h = 20)$
A_{1g}	$+1$	$+1$	$+1$	$+1$	$+1$	$+1$	$+1$	$+1$	$(x^2 + y^2), z^2$
A_{2g}	$+1$	$+1$	$+1$	-1	$+1$	$+1$	$+1$	-1	R_z
E_{1g}	$+2$	$\tau - 1$	$-\tau$	0	$+2$	$\tau - 1$	$-\tau$	0	$z(x + iy, x - iy)$
E_{2g}	$+2$	$-\tau$	$\tau - 1$	0	$+2$	$-\tau$	$\tau - 1$	0	$[(x + iy)^2, (x - iy)^2]$
A_{1u}	$+1$	$+1$	$+1$	$+1$	-1	-1	-1	-1	
A_{2u}	$+1$	$+1$	$+1$	-1	-1	-1	-1	$+1$	z
E_{1u}	$+2$	$\tau - 1$	$-\tau$	0	-2	$1 - \tau$	$+\tau$	0	$(x + iy, x - iy)$
E_{2u}	$+2$	$-\tau$	$\tau - 1$	0	-2	$+\tau$	$1 - \tau$	0	

Note: $D_{5d} = D_5 \otimes i$, $iC_5 = S_{10}^{-1}$ and $iC_5^2 = S_{10}$. Also $iC_2' = \sigma_d$.
where $\alpha = 2\pi/5 = 72°$.
Note also that $\tau = (1 + \sqrt{5})/2$ so that $\tau = -2\cos 2\alpha = -2\cos 4\pi/5$
and $\tau - 1 = 2\cos\alpha = 2\cos 2\pi/5$.

Table 3.38: Character table for D_{5h}.

D_{5h} $(\overline{10}m2)$	E	$2C_5$	$2C_5^2$	$5C_2'$	σ_h	$2S_5$	$2S_5^3$	$5\sigma_v$	$(h=20)$
A_1'	$+1$	$+1$	$+1$	$+1$	$+1$	$+1$	$+1$	$+1$	x^2+y^2, z^2
A_2'	$+1$	$+1$	$+1$	-1	$+1$	$+1$	$+1$	-1	R_z
E_1'	$+2$	$\tau-1$	$-\tau$	0	$+2$	$\tau-1$	$-\tau$	0	$(x,y), (xz^2,yz^2), [x(x^2+y^2),y(x^2+y^2)]$
E_2'	$+2$	$-\tau$	$\tau-1$	0	$+2$	$-\tau$	$\tau-1$	0	$(x^2-y^2,xy), [y(3x^2-y^2),x(x^2-3y^2)]$
A_1''	$+1$	$+1$	$+1$	$+1$	-1	-1	-1	-1	
A_2''	$+1$	$+1$	$+1$	-1	-1	-1	-1	$+1$	$z, z^3, z(x^2+y^2)$
E_1''	$+2$	$\tau-1$	$-\tau$	0	-2	$1-\tau$	$+\tau$	0	$(R_x,R_y), (xz,yz)$
E_2''	$+2$	$-\tau$	$\tau-1$	0	-2	$+\tau$	$1-\tau$	0	$[xyz, z(x^2-y^2)]$

Note that $\tau = (1+\sqrt{5})/2$ so that $\tau = -2\cos 2\alpha = -2\cos 4\pi/5$ and $\tau - 1 = 2\cos\alpha = 2\cos 2\pi/5$.

Table 3.39: Character table for I.

I (532)	E	$12C_5$	$12C_5^2$	$20C_3$	$15C_2$	$(h=60)$
A	$+1$	$+1$	$+1$	$+1$	$+1$	$x^2+y^2+z^2$
F_1	$+3$	$+\tau$	$1-\tau$	0	-1	$(x,y,z); (R_x,R_y,R_z)$
F_2	$+3$	$1-\tau$	$+\tau$	0	-1	
G	$+4$	-1	-1	$+1$	0	
H	$+5$	0	0	-1	$+1$	$\begin{cases} 2z^2-x^2-y^2 \\ x^2-y^2 \\ xy \\ xz \\ yz \end{cases}$

Note that $\tau = (1+\sqrt{5})/2$ so that $\tau = -2\cos 2\alpha = -2\cos 4\pi/5$ and $\tau - 1 = 2\cos\alpha = 2\cos 2\pi/5$.

Table 3.40: Character table for I_h.

I_h	E	$12C_5$	$12C_5^2$	$20C_3$	$15C_2$	i	$12S_{10}^3$	$12S_{10}$	$20S_6$	15σ	$(h = 120)$
A_g	$+1$	$+1$	$+1$	$+1$	$+1$	$+1$	$+1$	$+1$	$+1$	$+1$	$x^2 + y^2 + z^2$
F_{1g}	$+3$	$+\tau$	$1-\tau$	0	-1	$+3$	τ	$1-\tau$	0	-1	R_x, R_y, R_z
F_{2g}	$+3$	$1-\tau$	$+\tau$	0	-1	$+3$	$1-\tau$	τ	0	-1	
G_g	$+4$	-1	-1	$+1$	0	$+4$	-1	-1	$+1$	0	
H_g	$+5$	0	0	-1	$+1$	$+5$	0	0	-1	$+1$	$\begin{cases} 2z^2 - x^2 - y^2 \\ x^2 - y^2 \\ xy \\ xz \\ yz \end{cases}$
A_u	$+1$	$+1$	$+1$	$+1$	$+1$	-1	-1	-1	-1	-1	
F_{1u}	$+3$	$+\tau$	$1-\tau$	0	-1	-3	$-\tau$	$\tau-1$	0	$+1$	(x, y, z)
F_{2u}	$+3$	$1-\tau$	$+\tau$	0	-1	-3	$\tau-1$	$-\tau$	0	$+1$	
G_u	$+4$	-1	-1	$+1$	0	-4	$+1$	$+1$	-1	0	
H_u	$+5$	0	0	-1	$+1$	-5	0	0	$+1$	-1	

where $\tau = (1 + \sqrt{5})/2$.

Note: C_5 and C_5^{-1} are in different classes, labeled $12C_5$ and $12C_5^2$ in the character table. Then $iC_5 = S_{10}^{-1}$ and $iC_5^{-1} = S_{10}$ are in the classes labeled $12S_{10}^3$ and $12S_{10}$, respectively. Also $iC_2 = \sigma_v$.

3.10   Selected Problems

1. (a) Explain the symmetry operations pertaining to each class of the point group D_{3h}. You may find the stereograms on useful.

   (b) Prove that the following irreducible representations are orthonormal:
   - E_1 and E_2 in the group D_5 (see Table 3.27).
   - F_{2g} and G_u in the group I_h (see Table 3.39).

   (c) Given the group T (see Table 3.31), verify that the equality

   $$\sum_j \ell_j^2 = h$$

   is satisfied. What is the meaning of the two sets of characters given for the two-dimensional irreducible representation E? Are they orthogonal to each other or are they part of the same irreducible representation?

(d) Which symmetry operation results from multiplying the operations σ_v and σ_d in group C_{4v}? Can you obtain this information from the character table? If so, how?

2. Make stereographic sketches for groups C_5, C_{5v}, D_{5h}, and D_{5d}, such as are given in Fig. 3.2.

3. Consider the point group D_6

   (a) Construct the character table for $D_{6h} = D_6 \otimes i$ (see Table 3.28).

   (b) How many two-dimensional irreducible representations are there in D_6? and in D_{6h}?

   (c) Consider the groups D_{3h}, C_3, and C_{3v} as subgroups of D_{6h}: for which group (or groups) are the two two-dimensional representations of D_6 no longer irreducible? If the representations are reducible, into which irreducible representations of the lower symmetry group do they reduce?

4. (a) What are the symmetry operations of a regular hexagon?

   (b) Find the classes. Why are not all the 2-fold axes in the same class?

   (c) Find the self-conjugate subgroups, if any.

   (d) Identify the appropriate character table.

   (e) For some representative cases (two cases are sufficient), check the validity of the "Wonderful Orthogonality and Second Orthogonality Theorems" on character, using the character table in (d).

5. Suppose that you have the following set of characters: $\chi(E) = 4$, $\chi(\sigma_h) = 2$, $\chi(C_3) = 1$, $\chi(S_3) = -1$, $\chi(C_2') = 0$, $\chi(\sigma_v) = 0$.

   (a) Do these characters correspond to a representation of the point group D_{3h}? Is it irreducible?

   (b) If the representation is reducible, find the irreducible representations contained therein.

   (c) Give an example of a molecule with D_{3h} symmetry.

Chapter 4

Basis Functions

In the previous Chapters we have discussed symmetry elements, their matrix representations and the properties of the characters of these representations. In this discussion we saw that the matrix representations are not unique though their characters are unique. Because of the uniqueness of the characters of each irreducible representation, the characters for each group are tabulated in character tables. Also associated with each irreducible representation are "basis functions" which can be used to generate the matrices that represent the symmetry elements of a particular irreducible representation. Because of the importance of basis functions, it is customary to list the most important basis functions in the character tables.

4.1 Symmetry Operations and Basis Functions

Suppose that we have a group G with symmetry elements R and symmetry operators $\hat{P}_R$. We denote the representations by $\Gamma_n j$ where n (or Γ_n) labels the representation and j labels the component or partner of the representation — e.g., if we have a two-dimensional representation then $j = 1, 2$. We can then define a set of basis vectors denoted by $|\Gamma_n j\rangle$. These basis vectors relate the symmetry operator $\hat{P}_R$ with its

matrix representation denoted by $D^{\Gamma_n}(R)$ through the relation

$$\hat{P}_R|\Gamma_n\alpha\rangle = \sum_j D^{\Gamma_n}(R)_{j\alpha}|\Gamma_n j\rangle. \tag{4.1}$$

Each vector $|\Gamma_n j\rangle$ of an irreducible representation Γ_n is called a partner and all partners collectively generate the matrix representation $D^{\Gamma_n}(R)$. The basis vectors can be abstract vectors; a very important type of basis vector is a **basis function** which we define here as a basis vector expressed explicitly in coordinate space. **Wavefunctions** in quantum mechanics which are basis functions for symmetry operators are a special but important example of such basis functions.

In quantum mechanics, each energy eigenvalue of Schrödinger's equation is labeled according to its symmetry classification, which is specified according to an irreducible representation of a symmetry group. If the dimensionality of the representation is $j > 1$, the energy eigenvalue will correspond to a j-fold degenerate state, with j linearly independent wave-functions. The effect of the symmetry operator $\hat{P}_R$ on one of these wavefunctions (e.g., the αth wavefunction) will generally be the formation of a linear combination of the j wavefunctions, as is seen in Eq. 4.1.

Like the matrix representations and the characters, the basis vectors also satisfy orthogonality relations

$$\langle \Gamma_n j | \Gamma_{n'} j' \rangle = \delta_{n,n'} \delta_{j,j'}, \tag{4.2}$$

as is shown in Tinkham p. 41-2 and will be proved in §7.1 in connection with selection rules. In quantum (wave) mechanics, this orthogonality relation would be written in terms of the orthogonality for the wavefunctions

$$\int \psi_{n,j}^*(\vec{r})\psi_{n',j'}(\vec{r})d^3r = \delta_{n,n'}\delta_{j,j'} \tag{4.3}$$

where the wave functions $\psi_{n,j}$ and $\psi_{n',j'}$ correspond to different energy eigenvalues (n, n') and to different components (j, j') of a particular degenerate state, and the integration is performed in 3D space. The orthogonality relation (Eq. 4.3) allows us to generate matrices for an irreducible representation from a complete set of basis vectors, as is demonstrated in §4.2.

4.2 Use of Basis Functions to Generate Irreducible Representations

In this section we demonstrate how basis functions can be used to generate the matrices for an irreducible representation.

Multiplying Eq. 4.1 on the left by the basis vector $\langle \Gamma_{n'} j' |$ (corresponding in wave mechanics to $\psi_{n',j'}^*(\vec{r})$), we obtain using the orthogonality relation for basis functions (Eq. 4.2):

$$\langle \Gamma_{n'} j' | \hat{P}_R | \Gamma_n \alpha \rangle = \sum_j D^{(\Gamma_n)}(R)_{j\alpha} \langle \Gamma_{n'} j' | \Gamma_n j \rangle = D^{(\Gamma_{n'})}(R)_{j'\alpha} \delta_{nn'} \quad (4.4)$$

from which we see that the matrix elements of a symmetry operator are diagonal in each irreducible representation, which correspond to symmetry quantum numbers. From Eq. 4.4 we obtain a relation between each matrix element of $D^{(\Gamma_n)}(R)_{j\alpha}$ and the effect of the symmetry operation on the basis functions:

$$D^{(\Gamma_n)}(R)_{j\alpha} = \langle \Gamma_n j | \hat{P}_R | \Gamma_n \alpha \rangle. \quad (4.5)$$

Thus by taking matrix elements of a symmetry operator $\hat{P}_R$ between all possible partners of an irreducible representation as shown by Eq. 4.5 the matrix representation $D^{\Gamma_n}(R)_{j\alpha}$ can be generated. In practice, this turns out to be the easiest way to obtain these matrix representations for the symmetry elements.

As an example of how basis vectors or basis functions can generate the matrices for an irreducible representation, consider a planar molecule with three-fold symmetry such that the symmetry operations are isomorphic to those of an equilateral triangle and also isomorphic to $P(3)$. Thus there are 6 symmetry operations and 6 operators $\hat{P}_R$. (See §3.2. The proper point group to describe the symmetry operations of a regular planar triangle is D_{3h}.) Group theory tells us that the energy levels can never be more than two-fold degenerate. Thus no three-fold or six-fold levels can occur because the largest dimensionality of an irreducible representation of $P(3)$ is 2. For the 1-dimensional representation Γ_1, the operator $\hat{P}_R$ leaves every basis vector invariant. Thus any constant such as 1 forms a suitable basis function. For many practical problems we like to express our basis functions in terms of functions
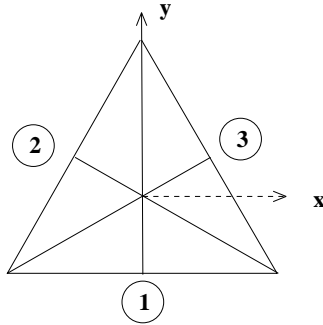
Figure 4.1: Symmetry operations of an equilateral triangle. The notation of this diagram defines the symmetry operations in Table 4.1.

Table 4.1: Symmetry operations of the group of the equilateral triangle on basis functions.

$\hat{P}_R/f(x,y,z)$	x	y	z	x^2	y^2	z^2
$E = E$	x	y	z	x^2	y^2	z^2
$C_3 = F$	$\frac{1}{2}(-x+\sqrt{3}y)$	$\frac{1}{2}(-y-\sqrt{3}x)$	z	$\frac{1}{4}(x^2+3y^2-2\sqrt{3}xy)$	$\frac{1}{4}(y^2+3x^2+2\sqrt{3}xy)$	z^2
$C_3^{-1} = D$	$\frac{1}{2}(-x-\sqrt{3}y)$	$\frac{1}{2}(-y+\sqrt{3}x)$	z	$\frac{1}{4}(x^2+3y^2+2\sqrt{3}xy)$	$\frac{1}{4}(y^2+3x^2-2\sqrt{3}xy)$	z^2
$C_{2(1)} = A$	$-x$	y	$-z$	x^2	y^2	z^2
$C_{2(2)} = B$	$\frac{1}{2}(x-\sqrt{3}y)$	$\frac{1}{2}(-y-\sqrt{3}x)$	$-z$	$\frac{1}{4}(x^2+3y^2-2\sqrt{3}xy)$	$\frac{1}{4}(y^2+3x^2+2\sqrt{3}xy)$	z^2
$C_{2(3)} = C$	$\frac{1}{2}(x+\sqrt{3}y)$	$\frac{1}{2}(-y+\sqrt{3}x)$	$-z$	$\frac{1}{4}(x^2+3y^2+2\sqrt{3}xy)$	$\frac{1}{4}(y^2+3x^2-2\sqrt{3}xy)$	z^2

of the coordinates (x, y, z). Some explanation is needed here about the meaning of (x, y, z) as a basis function. To satisfy the orthogonality requirement, the basis functions are vectors with unit length and the matrices which represent the symmetry operations are unitary matrices. Thus (x, y, z) would generally correspond to the x, y, and z components of a vector of unit length. The transformation properties of the x, y, and z components of an arbitrary vector under the symmetry operations of the group are the same as those for the unit vectors x, y, and z.

In this connection it is convenient to write out a basis function table such as Table 4.1. On the top row we list the functions to be investigated; in the first column we list all the symmetry operations of the group (see Fig. 4.1 for notation). If we denote the entries in the table by $f'(x, y, z)$, then Table 4.1 can be summarized as:

$$\hat{P}_R f(x, y, z) = f'(x, y, z) \tag{4.6}$$

where the symmetry operations $\hat{P}_R$ label the rows. From Table 4.1 we can then write down the matrix representations for each irreducible representation. In the trivial case of the identity representation, the (1×1) matrix 1 satisfies $\hat{P}_R 1 = 1$ for all $\hat{P}_R$ so that this homomorphic representation always applies, i.e., $|\Gamma_1\rangle = 1$.

To find the basis functions for the $\Gamma_{1'}$ representation (i.e., the representation of the factor group for $P(3)$), we note that (E, D, F) leaves z invariant while (A, B, C) takes z into $-z$, so that z forms a suitable basis function for $\Gamma_{1'}$, which we write as $|\Gamma_{1'}\rangle = z$. Then application of Eq. 4.5 yields the matrices for the irreducible representation $\Gamma_{1'}$

$$\langle z|(E, D, F)|z\rangle = 1 \qquad\qquad \langle z|(A, B, C)|z\rangle = -1. \qquad (4.7)$$

Thus the characters (1) and (-1) for the (1×1) irreducible representations are obtained for $\Gamma_{1'}$. We note that **in the case of (1×1) representations, the characters and the representations are identical.**

To find the 2-dimensional representation Γ_2 we note that all the group operations take (x, y) into (x', y'). Table 4.1 can be used to find the matrix representation for Γ_2 by taking as basis functions $|\Gamma_2, 1\rangle = |x\rangle$ and $|\Gamma_2, 2\rangle = |y\rangle$. We now illustrate the use of Table 4.1 to generate the matrix $D^{(\Gamma_2)}(C_3 = F)$ where F is a counter clockwise rotation of $2\pi/3$ about the z axis:

$F|x\rangle = \frac{1}{2}(-x + \sqrt{3}y)$ yields first column of matrix representation
$F|y\rangle = -\frac{1}{2}(y + \sqrt{3}x)$ yields second column of matrix representation
so that

$$F\begin{pmatrix} x \\ y \end{pmatrix} = (x \ \ y)D^{\Gamma_2}(F) \quad \text{gives the matrix } D^{(\Gamma_2)}(F) \text{ using Eq. 4.1:}$$

$$D^{(\Gamma_2)}(C_3 = F) = \begin{pmatrix} -\frac{1}{2} & -\frac{\sqrt{3}}{2} \\ \frac{\sqrt{3}}{2} & -\frac{1}{2} \end{pmatrix} \qquad (4.8)$$

To clarify how we obtain all the matrices for the irreducible representations with Γ_2 symmetry, we repeat the operations leading to Eq. 4.8 for each of the symmetry operations $\hat{P}_R$. We thus obtain for the other 5 symmetry operations of the group $\hat{P}_R$ using the same basis functions

(x, y) and the notation of Fig. 4.1:

$$D^{(\Gamma_2)}(E) = \begin{pmatrix} 1 & 0 \\ 0 & 1 \end{pmatrix} \tag{4.9}$$

$$D^{(\Gamma_2)}(C_2(2) = B) = \begin{pmatrix} \frac{1}{2} & -\frac{\sqrt{3}}{2} \\ -\frac{\sqrt{3}}{2} & -\frac{1}{2} \end{pmatrix} \tag{4.10}$$

$$D^{(\Gamma_2)}(C_3^{-1} = D) = \begin{pmatrix} -\frac{1}{2} & \frac{\sqrt{3}}{2} \\ -\frac{\sqrt{3}}{2} & -\frac{1}{2} \end{pmatrix} \tag{4.11}$$

$$D^{(\Gamma_2)}(C_2(1) = A) = \begin{pmatrix} -1 & 0 \\ 0 & 1 \end{pmatrix} \tag{4.12}$$

$$D^{(\Gamma_2)}(C_2(3) = C) = \begin{pmatrix} \frac{1}{2} & \frac{\sqrt{3}}{2} \\ \frac{\sqrt{3}}{2} & -\frac{1}{2} \end{pmatrix} \tag{4.13}$$

As mentioned before, x and y are both basis functions for representation Γ_2 and are called the **partners** of this irreducible representation. The number of partners is equal to the dimensionality of the representation.

In Table 4.1 we have included entries for $\hat{P}_R x^2$, $\hat{P}_R y^2$, $\hat{P}_R z^2$ and these entries are obtained as illustrated below by the operation $F = C_3$:

$$Fx^2 = (-\frac{x}{2} + \frac{\sqrt{3}}{2}y)^2 = (\frac{x^2}{4} - \frac{\sqrt{3}}{2}xy + \frac{3}{4}y^2) \tag{4.14}$$

$$Fy^2 = (-\frac{y}{2} - \frac{\sqrt{3}}{2}x)^2 = (\frac{y^2}{4} + \frac{\sqrt{3}}{2}xy + \frac{3}{4}x^2) \tag{4.15}$$

$$F(x^2 + y^2) = x^2 + y^2 \tag{4.16}$$

$$F(xy) = (-\frac{x}{2} + \frac{\sqrt{3}}{2}y)(-\frac{y}{2} - \frac{\sqrt{3}}{2}x)$$

$$= \frac{1}{4}(-2xy + \sqrt{3}[x^2 - y^2]) \tag{4.17}$$

$$F(x^2 - y^2) = -\frac{1}{4}(2[x^2 - y^2] + 4\sqrt{3}xy) \tag{4.18}$$

$$F(xz) = (-\frac{x}{2} + \frac{\sqrt{3}}{2}y)z \tag{4.19}$$

$$F(yz) = (-\frac{y}{2} - \frac{\sqrt{3}}{2}x)z \tag{4.20}$$

Using Eq. 4.1 we see that $\hat{P}_R(x^2 + y^2) = (x^2 + y^2)$ for all $\hat{P}_R$ so that $(x^2 + y^2)$ is a basis function for Γ_1 or as we often say transforms according to the irreducible representation Γ_1. Correspondingly $z(x^2 + y^2)$ transforms as $\Gamma_{1'}$ and z^2 transforms as Γ_1. These transformation properties will be used extensively for many applications of group theory. It is found that many important basis functions are given directly in the published character tables. Like the matrix representations, the basis functions are not unique. However corresponding to a given set of basis functions, the matrix representation which is generated by these basis functions will be unique.

As before, the characters for a given representation are found by taking the sum of the diagonal elements of each matrix in a given representation:

$$\chi^{(\Gamma_n)}(R) \equiv tr\ D^{(\Gamma_n)}(R) = \sum_j D^{(\Gamma_n)}(R)_{jj} = \sum_j \langle \Gamma_n j | \hat{P}_R | \Gamma_n j \rangle. \quad (4.21)$$

Since the trace is invariant under a similarity transformation, the character is independent of the particular choice of basis functions or matrix representations.

If instead of a basis function (which generates irreducible representations) we use an arbitrary function f, then a reducible representation will result, in general. We can express an arbitrary function as a linear combination of the basis functions. For example, any linear function of x, y, z such as $f(x, y, z)$ can be expressed in terms of linear combinations of basis vectors x, y, z and likewise any quadratic function is expressed in terms of basis functions which transform as irreducible representations of the group. For example for the group $P(3)$ (see Table 4.1), quadratic forms which serve as basis functions are $(x^2 + y^2)$ and z^2 which both transform as Γ_1; z transforms as $\Gamma_{1'}$; (xz, yz) and $(xy, x^2 - y^2)$ both transform as Γ_2.

If we now inspect the character table $D_3(32)$ found in Table 3.25 we find that these basis functions are listed. The basis functions labeled R_α represent the angular momentum component around axis α. For the two dimensional irreducible representations both partners of the basis functions are listed, for example (xz, xy) and $(x^2 - y^2, xy)$, etc. The reason why (x, y, z) and (R_x, R_y, R_z) often transform as different irreducible representations (not the case for the group $D_3(32)$) is that

x, y, z transforms as a radial vector (such as coordinate, momentum) while R_x, R_y, R_z transforms as an axial vector (such as angular momentum $\vec{r} \times \vec{p}$).

$D_3(32)$			E	$2C_3$	$3C_2'$
$x^2 + y^2, z^2$		A_1	1	1	1
	R_z, z	A_2	1	1	-1
$\left.\begin{array}{l}(xz, yz)\\(x^2 - y^2, xy)\end{array}\right\}$	$\left.\begin{array}{l}(x, y)\\(R_x, R_y)\end{array}\right\}$	E	2	-1	0

(The full symmetry of an equilateral triangle is $D_{3h} = D_3 \otimes \sigma_h$. Since the triangle is a 2D object, the horizontal mirror plane is not an important symmetry operation and we can simplify the algebra by using the group D_3.)

4.3 Projection Operators $\hat{P}_{kl}^{(\Gamma_n)}$

The previous discussion of basis vectors assumed that we already knew how to write down the basis vectors. In many cases, representative basis functions are tabulated in the character tables. However, suppose that we have to find basis functions for the following cases:

1. an irreducible representation for which no basis functions are listed in the character table; or

2. an arbitrary function.

In such cases the basis functions can often be found using **projection operators** $\hat{P}_{k\ell}$, not to be confused with the symmetry operators $\hat{P}_R$. We define the projection operator $\hat{P}_{k\ell}^{(\Gamma_n)}$ as transforming one basis vector $|\Gamma_n\ell\rangle$ into another basis vector $|\Gamma_n k\rangle$ of the same irreducible representation Γ_n:

$$\hat{P}_{k\ell}^{(\Gamma_n)}|\Gamma_n\ell\rangle \equiv |\Gamma_n k\rangle. \tag{4.22}$$

The utility of projection operators is mainly to project out basis functions for a given partner of a given irreducible representation from an arbitrary function.

The discussion of this topic focuses on the following issues:

1. The relation of the projection operator to symmetry operators of the group and to the matrix representation of these symmetry operators for an irreducible representation.

2. The effect of projection operators on an arbitrary function.

As an example, we illustrate in §4.6 how to find basis functions from an arbitrary function for the case of the group of the equilateral triangle (see §4.2).

4.4   Derivation of an Explicit Expression for $\hat{P}_{k\ell}^{(\Gamma_n)}$

In this section we find an explicit expression for the projection operators $\hat{P}_{kl}^{(\Gamma_n)}$ by considering the relation of the projection operator to symmetry operators of the group. We will find that the coefficients of this expression give the matrix representations of each of the symmetry elements.

Let the projection operator $\hat{P}_{k\ell}^{(\Gamma_n)}$ be written as a linear combination of the symmetry operators $\hat{P}_R$:

$$\hat{P}_{k\ell}^{(\Gamma_n)} = \sum_R A_{k\ell}(R)\hat{P}_R \tag{4.23}$$

where the $A_{k\ell}(R)$ are arbitrary expansion coefficients to be determined. Substitution of Eq. 4.23 into Eq. 4.22 yields

$$\hat{P}_{k\ell}^{(\Gamma_n)}|\Gamma_n\ell\rangle \equiv |\Gamma_n k\rangle = \sum_R A_{k\ell}(R)\hat{P}_R|\Gamma_n\ell\rangle. \tag{4.24}$$

Multiply Eq. 4.24 on the left by $\langle\Gamma_n k|$ to yield

$$\langle\Gamma_n k|\Gamma_n k\rangle = 1 = \sum_R A_{k\ell}(R)\underbrace{\langle\Gamma_n k|\hat{P}_R|\Gamma_n\ell\rangle}_{D^{(\Gamma_n)}(R)_{k\ell}}. \tag{4.25}$$

But the Wonderful Orthogonality Theorem (Eq. 2.50) specifies that

$$\sum_R D^{(\Gamma_n)}(R)_{k\ell}^* D^{(\Gamma_n)}(R)_{k\ell} = \frac{h}{\ell_n} \tag{4.26}$$

where h is the number of symmetry operators in the group and ℓ_n is the dimensionality of the irreducible representation Γ_n, so that we can identify $A_{k\ell}(R)$ with the matrix element of the representation for the symmetry element R:

$$A_{k\ell}(R) = \frac{\ell_n}{h} D^{(\Gamma_n)}(R)_{k\ell}^*. \tag{4.27}$$

Thus the projection operator is explicitly given in terms of the symmetry operators of the group by the relation:

$$\hat{P}_{k\ell}^{(\Gamma_n)} = \frac{\ell_n}{h} \sum_R D^{(\Gamma_n)}(R)_{k\ell}^* \hat{P}_R. \tag{4.28}$$

From the explicit form for $\hat{P}_{k\ell}^{(\Gamma_n)}$ in Eq. 4.28 and from Eq. 4.22 we see how to find the partners of an irreducible representation Γ_n from any single known basis vector, provided that the matrix representation for all the symmetry operators $D^{(\Gamma_n)}(R)$ is known.

As a special case, the projection operator $\hat{P}_{kk}^{(\Gamma_n)}$ transforms $|\Gamma_n k\rangle$ into itself and can be used to check that $|\Gamma_n k\rangle$ is indeed a basis function. We note that the relation of $\hat{P}_{kk}^{(\Gamma_n)}$ to the symmetry operators $\hat{P}_R$ involves only the **diagonal elements of the matrix representations** (though not the trace):

$$\hat{P}_{kk}^{(\Gamma_n)} = \frac{\ell_n}{h} \sum_R D^{(\Gamma_n)}(R)_{kk}^* \hat{P}_R \tag{4.29}$$

where

$$\hat{P}_{kk}^{(\Gamma_n)} |\Gamma_n k\rangle \equiv |\Gamma_n k\rangle. \tag{4.30}$$

4.5 The Effect of Projection Operations on an Arbitrary Function

The projection operators $\hat{P}_{kk}^{(\Gamma_n)}$ defined in Eq. 4.30 are of special importance because they can project the kth partner of irreducible representation Γ_n from an arbitrary function. Any arbitrary function F can

be written as a linear combination of a complete set of basis functions $f_{j'}^{(\Gamma_{n'})}$:

$$F = \sum_{\Gamma_{n'}} \sum_{j'} f_{j'}^{(\Gamma_{n'})} |\Gamma_{n'} j'\rangle. \tag{4.31}$$

We can then write from Eq. 4.29:

$$\hat{P}_{kk}^{(\Gamma_n)} F = \frac{\ell_n}{h} \sum_R D^{(\Gamma_n)}(R)_{kk}^* \hat{P}_R F \tag{4.32}$$

and substitution of Eq. 4.31 into 4.32 then yields

$$\hat{P}_{kk}^{(\Gamma_n)} F \;=\; \frac{\ell_n}{h} \sum_R \sum_{\Gamma_{n'}} \sum_{j'} f_{j'}^{(\Gamma_{n'})} D^{(\Gamma_n)}(R)_{kk}^* \; \hat{P}_R |\Gamma_{n'} j'\rangle \tag{4.33}$$

But substitution of Eq. 4.1 into 4.33 and use of the Wonderful Orthogonality Theorem (Eq. 2.50):

$$\sum_R D^{(\Gamma_{n'})}(R)_{jj'} D^{(\Gamma_n)}(R)_{kk}^* = \frac{h}{\ell_n} \delta_{\Gamma_n \Gamma_{n'}} \delta_{jk} \delta_{j'k} \tag{4.34}$$

yields

$$\hat{P}_{kk}^{(\Gamma_n)} F = f_k^{(\Gamma_n)} |\Gamma_n k\rangle \tag{4.35}$$

where

$$\hat{P}_{kk}^{(\Gamma_n)} = \frac{\ell_n}{h} \sum_R D^{(\Gamma_n)}(R)_{kk}^* \hat{P}_R. \tag{4.36}$$

We note that the projection operator does not yield normalized basis functions. One strategy to find basis functions is to start with an arbitrary function F.

1. We then use $\hat{P}_{kk}^{(\Gamma_n)}$ to project out one basis function $|\Gamma_n k\rangle$.

2. We can then use the projection operator $\hat{P}_{k\ell}^{(\Gamma_n)}$ to project out all other partners $|\Gamma_n \ell\rangle$ orthogonal to $|\Gamma_n k\rangle$ in irreducible representation Γ_n. Or alternatively we can use $\hat{P}_{\ell\ell}^{(\Gamma_n)}$ to project out each of the partners ℓ of the representation, whichever method works most easily in a given case.

If we do not know the explicit representations $D_{k\ell}^{(\Gamma_n)}(R)^*$, but only know the characters, then we can still project out basis functions which transform according to the irreducible representations (using the argument given below in §4.5), though we cannot in this case project out specific partners but only linear combinations of the partners of these irreducible representations.

If we only know the characters of an irreducible representation Γ_n, we define the projection operator for this irreducible representation as $\hat{P}^{(\Gamma_n)}$:

$$\hat{P}^{(\Gamma_n)} \equiv \sum_k \hat{P}_{kk}^{(\Gamma_n)} = \frac{\ell_n}{h} \sum_R \sum_k D^{(\Gamma_n)}(R)_{kk}^* \hat{P}_R \qquad (4.37)$$

so that

$$\hat{P}^{(\Gamma_n)} = \frac{\ell_n}{h} \sum_R \chi^{(\Gamma_n)}(R)^* \hat{P}_R \qquad (4.38)$$

and using Eq. 4.35 we then obtain

$$\hat{P}^{(\Gamma_n)} F = \sum_k \hat{P}_{kk}^{(\Gamma_n)} F = \sum_k f_k^{(\Gamma_n)} |\Gamma_n k\rangle \qquad (4.39)$$

which projects out a function transforming as Γ_n but not a specific partner of Γ_n.

In dealing with physical problems it is useful to use physical insight in guessing at an appropriate "arbitrary function" to initiate this process for finding the basis functions and matrix representations for specific problems.

4.6   Linear Combinations of Atomic Orbitals for 3 Equivalent Atoms at the Corners of an Equilateral Triangle

As an example of finding basis functions for an arbitrary function, we will consider forming linear combinations of atomic orbitals which transform as irreducible representations of the symmetry group.

In many of the applications that we will be making of group theory to solid state physics, we will have equivalent atoms at different sites. We use the symmetry operations of the group to show which irreducible
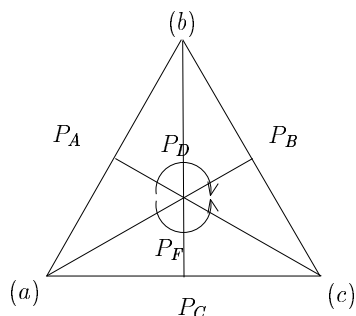
Figure 4.2: Equilateral triangle and arbitrary functions defining the notation used in §4.6.

representations result when the equivalent atoms transform into each other under the symmetry operations of the group. The discussion of projection operators of an arbitrary function applies to this very important case.

As an example of this application, suppose that we have 3 equivalent atoms at the 3 corners of an equilateral triangle (see Figure 4.2) and that each atom is in the same spherically symmetric ground state described by a wave function $\psi_0(\vec{r}_i)$, where the subscript i is a site index which can apply to any of the 3 sites. As a short-hand notation for $\psi_0(\vec{r}_a), \psi_0(\vec{r}_b), \psi_0(\vec{r}_c)$ we will here use a, b, c so that the arbitrary function is written as

$$F = \begin{pmatrix} a \\ b \\ c \end{pmatrix}. \tag{4.40}$$

We now want to combine these atomic orbitals to make a molecular orbital that transforms according to the irreducible representations of the group. To do this we use the results on the projection operator to find out which irreducible representations are contained in the function F. According to the above discussion, we can project out a basis function for representation Γ_n by considering the action of $\hat{P}_{kk}^{(\Gamma_n)}$ on one of the atomic orbitals, as for example orbital a:

$$\hat{P}_{kk}^{(\Gamma_n)} a = \frac{\ell_n}{h} \sum_R D^{(\Gamma_n)}(R)_{kk}^* \, \hat{P}_R a = f_k^{(\Gamma_n)} |\Gamma_n k\rangle \tag{4.41}$$

in which we have used the definition for $\hat{P}_{kk}^{(\Gamma_n)}$ given by Eq. 4.35 and the expression for $\hat{P}_{kk}^{(\Gamma_n)}$ given by Eq. 4.36. If the representation Γ_n is one-dimensional, then we can obtain $D^{(\Gamma_n)}(R)$ directly from the character table, and Eq. 4.41 then becomes

$$\hat{P}^{(\Gamma_n)}a = \frac{\ell_n}{h} \sum_R \chi^{(\Gamma_n)}(R)^* \hat{P}_R a = f^{(\Gamma_n)}|\Gamma_n\rangle \qquad (4.42)$$

For the appropriate symmetry operators for this problem we refer to §1.2 where we have defined: $E \equiv$ identity; $(A, B, C) \equiv \pi$ rotations about two-fold axes in the plane of triangle; $(D, F) \equiv 2\pi/3$ rotations about the three-fold axis $\perp$ to the plane of the triangle. These symmetry operations are also indicated in Fig. 4.2.

For the identity representation Γ_1 the characters and matrix representations are all unity so that

$$\begin{aligned} \hat{P}^{(\Gamma_1)}a &= \frac{1}{6}(\hat{P}_E a + \hat{P}_A a + \hat{P}_B a + \hat{P}_C a + \hat{P}_D a + \hat{P}_F a) \\ &= \frac{1}{6}(a + b + a + c + b + c) \\ &= \frac{1}{3}(a + b + c), \end{aligned} \qquad (4.43)$$

a result which is intuitively obvious. Each atom site must contribute equally to the perfectly symmetrical molecular representation Γ_1. This example illustrates how starting with an arbitrary function a (or $\psi(\vec{r}_a)$) we have found a linear combination that transforms as Γ_1. Likewise, we obtain the same result by selecting b or c as the arbitrary function

$$\hat{P}^{(\Gamma_1)}b = \hat{P}^{(\Gamma_1)}c = \frac{1}{3}(a + b + c). \qquad (4.44)$$

We now apply a similar analysis for representation $\Gamma_{1'}$ to illustrate another important point. In this case the matrix representations and characters are $+1$ for (E, D, F), and -1 for (A, B, C). Thus

$$\begin{aligned} \hat{P}^{(\Gamma_{1'})}a &= \frac{1}{6}(\hat{P}_E a - \hat{P}_A a - \hat{P}_B a - \hat{P}_C a + \hat{P}_D a + \hat{P}_F a) \\ &= \frac{1}{6}(a - b - a - c + c + b) = 0 \end{aligned} \qquad (4.45)$$

which states that no molecular orbital with $\Gamma_{1'}$ symmetry can be made by taking a linear combination of the a, b, c orbitals. This is verified by considering

$$\hat{P}^{(\Gamma_{1'})}b = \hat{P}^{(\Gamma_{1'})}c = 0. \tag{4.46}$$

The same approach also yields the 2-dimensional irreducible representations. To carry out the evaluations, we use the (11) and (22) elements of the matrix representation given by Eq. 1.4 in §1.2 for Γ_2 and the symmetry operations. We will see below that only the irreducible representations of $\Gamma_1 + \Gamma_2$ are contained in the linear combination of atomic orbitals for a, b, c. This makes sense since we have 3 atomic orbitals which split into a non-degenerate and a 2-dimensional representation in trigonal symmetry through the symmetry operations $\hat{P}_R$ on the equivalent site functions $a, \ b, \ c$:

$$\hat{P}_R \begin{pmatrix} a \\ b \\ c \end{pmatrix}. \tag{4.47}$$

Equations 4.36 and 4.39 then yield:

$$
\begin{aligned}
\hat{P}_{11}^{(\Gamma_2)}a &= \frac{2}{6}\left[1\hat{P}_E a + 1\hat{P}_A a - \frac{1}{2}\hat{P}_B a - \frac{1}{2}\hat{P}_C a - \frac{1}{2}\hat{P}_D a - \frac{1}{2}\hat{P}_F a\right] \\
&= \frac{1}{3}\left[a + b - \frac{1}{2}a - \frac{1}{2}c - \frac{1}{2}b - \frac{1}{2}c\right] \\
&= \frac{1}{3}\left[\frac{1}{2}a + \frac{1}{2}b - c\right] = |\Gamma_2 1\rangle
\end{aligned} \tag{4.48}
$$

and

$$
\begin{aligned}
\hat{P}_{22}^{(\Gamma_2)}a &= \frac{2}{6}\left[1\hat{P}_E a - 1\hat{P}_A a + \frac{1}{2}\hat{P}_B a + \frac{1}{2}\hat{P}_C a - \frac{1}{2}\hat{P}_D a - \frac{1}{2}\hat{P}_F a\right] \\
&= \frac{1}{3}\left[a - b + \frac{1}{2}a + \frac{1}{2}c - \frac{1}{2}b - \frac{1}{2}c\right] \\
&= \frac{1}{3}\left[\frac{3}{2}a - \frac{3}{2}b\right] = \frac{1}{2}[a - b] = |\Gamma_2 2\rangle.
\end{aligned} \tag{4.49}
$$

The orthogonality of the basis functions $|\Gamma_2 1\rangle$ and $|\Gamma_2 2\rangle$ can be checked by inspection. The representations corresponding to these basis functions are found from the main definition (Eq. 4.1). For example, the

operation of $\hat{P}_B$ on the basis functions found in Eqs. 4.48 and 4.49 also provide basis functions for $\hat{P}_B$ as shown explicitly in Eqs. 4.50 and 4.51

$$\hat{P}_B(\psi_1 \quad \psi_2) = (\psi_1 \quad \psi_2) \begin{pmatrix} -\frac{1}{2} & \frac{3}{2} \\ \frac{1}{2} & \frac{1}{2} \end{pmatrix} \tag{4.50}$$

$$\hat{P}_B \left[\frac{1}{6}a + \frac{1}{6}b - \frac{1}{3}c \right] = \left[\frac{1}{6}a + \frac{1}{6}c - \frac{1}{3}b \right] = -\frac{1}{2}\left[\frac{1}{6}a + \frac{1}{6}b - \frac{1}{3}c \right] + \frac{1}{2}\left[\frac{1}{2}a - \frac{1}{2}b \right]$$

$$\hat{P}_B \left[\frac{1}{2}a - \frac{1}{2}b \right] = \left[\frac{1}{2}a - \frac{1}{2}c \right] = \frac{3}{2}\left[\frac{1}{6}a + \frac{1}{6}b - \frac{1}{3}c \right] + \frac{1}{2}\left[\frac{1}{2}a - \frac{1}{2}b \right] \tag{4.51}$$

These basis functions are applied equally well to all the other group elements: C, D, F, E. In terms of the basis functions $|\Gamma_2 1\rangle$ and $|\Gamma_2 2\rangle$ given in Eqs. 4.48 and 4.49 we obtain by a similar procedure, as was used to obtain Eq. 4.51, the following matrix representation:

$$D^{(\Gamma_2)}(E) = \begin{pmatrix} 1 & 0 \\ 0 & 1 \end{pmatrix} \tag{4.52}$$

$$D^{(\Gamma_2)}(A) = \begin{pmatrix} 1 & 0 \\ 0 & -1 \end{pmatrix} \tag{4.53}$$

$$D^{(\Gamma_2)}(B) = \begin{pmatrix} -\frac{1}{2} & \frac{3}{2} \\ \frac{1}{2} & \frac{1}{2} \end{pmatrix} \tag{4.54}$$

$$D^{(\Gamma_2)}(C) = \begin{pmatrix} -\frac{1}{2} & -\frac{3}{2} \\ -\frac{1}{2} & \frac{1}{2} \end{pmatrix} \tag{4.55}$$

$$D^{(\Gamma_2)}(D) = \begin{pmatrix} -\frac{1}{2} & -\frac{3}{2} \\ \frac{1}{2} & -\frac{1}{2} \end{pmatrix} \tag{4.56}$$

$$D^{(\Gamma_2)}(F) = \begin{pmatrix} -\frac{1}{2} & \frac{3}{2} \\ -\frac{1}{2} & -\frac{1}{2} \end{pmatrix}. \tag{4.57}$$

It is readily checked that these matrices obey the multiplication table given in Table 1.1 on p. 3.

The basis functions given by Eqs. 4.48 and 4.49 and the corresponding representation given by Eqs. 4.50 and 4.52–4.57 are not unique. Two sets of equally good basis functions are:

$$\left[\frac{1}{6}b + \frac{1}{6}c - \frac{1}{3}a \right] \quad \text{and} \quad \frac{1}{2}[b - c] \tag{4.58}$$

or

$$\left[\frac{1}{6}c + \frac{1}{6}a - \frac{1}{3}b\right] \quad \text{and} \quad \frac{1}{2}\left[c - a\right]. \tag{4.59}$$

All of these basis functions lack aesthetic symmetry and do not give rise to unitary matrix representations.

To obtain a more symmetrical set of basis functions for this problem, we start with an arbitrary function that is like one of the symmetry operations of the group (e.g., a three-fold rotation $\hat{P}_D$)

$$|\Gamma_2\alpha\rangle = a + \omega b + \omega^2 c \tag{4.60}$$

where $\omega = e^{2\pi i/3}$ and we note that $\hat{P}_D|\Gamma_2\alpha\rangle = \omega^2|\Gamma_2\alpha\rangle$

Thus $|\Gamma_2\alpha\rangle$ is already a basis function. Clearly the partner of $|\Gamma_2\alpha\rangle$ is $|\Gamma_2\alpha\rangle^*$ since $\hat{P}_D|\Gamma_2\alpha\rangle^* = \hat{P}_D(a+\omega^2 b+\omega c) = \omega(a+\omega^2 b+\omega c) = \omega|\Gamma_2\beta\rangle$ where we have used the notation (α, β) to denote another set of partners of the Γ_2 representation:

$$|\Gamma_2\alpha\rangle = a + \omega b + \omega^2 c \qquad\qquad |\Gamma_2\beta\rangle = a + \omega^2 b + \omega c. \tag{4.61}$$

The two partners in Eq. 4.61 are complex conjugates of each other. Corresponding to these basis functions, the matrix representation for each of the group elements is simple and symmetrical

$$E = \begin{pmatrix} 1 & 0 \\ 0 & 1 \end{pmatrix} \quad A = \begin{pmatrix} 0 & \omega^2 \\ \omega & 0 \end{pmatrix} \quad B = \begin{pmatrix} 0 & 1 \\ 1 & 0 \end{pmatrix} \tag{4.62}$$

$$C = \begin{pmatrix} 0 & \omega \\ \omega^2 & 0 \end{pmatrix} \quad D = \begin{pmatrix} \omega^2 & 0 \\ 0 & \omega \end{pmatrix} \quad F = \begin{pmatrix} \omega & 0 \\ 0 & \omega^2 \end{pmatrix}. \tag{4.63}$$

By inspection the representation given by Eq. 4.61 is **unitary** while that corresponding to the basis functions $|\Gamma_2 1\rangle$ and $|\Gamma_2 2\rangle$ is not. By inspection we further see that the basis functions $|\Gamma_2 1\rangle$ and $|\Gamma_2 2\rangle$ are linear combinations of the basis functions $|\Gamma_2\alpha\rangle$ and $|\Gamma_2\beta\rangle$:

$$\begin{aligned}
|\Gamma_2 1\rangle &= \frac{1}{6}(a + b - 2c) = -\frac{1}{6}[\omega(a + \omega b + \omega^2 c) + \omega^2(a + \omega^2 b + \omega c)] \\
&= -\frac{1}{6}\left[\omega|\Gamma_2\alpha\rangle + \omega^2|\Gamma_2\beta\rangle\right], \tag{4.64} \\
|\Gamma_2 2\rangle &= \frac{1}{2}(a - b) = -\frac{i}{2\sqrt{3}}[\omega(a + \omega b + \omega^2 c) - \omega^2(a + \omega^2 b + \omega c)] \\
&= -\frac{i}{2\sqrt{3}}\left[\omega|\Gamma_2\alpha\rangle - \omega^2|\Gamma_2\beta\rangle\right] \tag{4.65}
\end{aligned}$$

or

$$|\Gamma_2\alpha\rangle = -3\omega^2|\Gamma_21\rangle + i\sqrt{3}\omega^2|\Gamma_22\rangle \qquad (4.66)$$

$$|\Gamma_2\beta\rangle = -3\omega|\Gamma_21\rangle - i\sqrt{3}\omega|\Gamma_22\rangle = |\Gamma_2\alpha\rangle^* \qquad (4.67)$$

In general, the more symmetric the choice of basis functions, the easier the use of the representation.

Icosahedral symmetry will be covered in Chapter 23.

4.7 Selected Problems

1. (a) What are the matrix representations for $(xy, x^2 - y^2)$ and (R_x, R_y) in the point group D_3?

   (b) Using the results in (a), find the unitary transformation which transforms the matrices for the representation corresponding to the basis functions $(xy, x^2 - y^2)$ into the representation corresponding to the basis functions (x, y).

   (c) Using projection operators, check that xy forms a proper basis function of the two-dimensional irreducible representation Γ_2 in point group D_3. Using the matrix representation found in (a) and projection operators, find the partner of xy.

   (d) Using the basis functions in the character table for D_{3h}, write a set of (2×2) matrices for the two 2-dimensional representations E' and E''.

2. (a) Explain the Hermann–Manguin notation $T_d(\bar{4}3m)$.

   (b) What are the irreducible representations and partners of the following basis functions in T_d symmetry? (i) $\omega x^2 + \omega^2 y^2 + z^2$, where $\omega = \exp(2\pi i/3)$; (ii) xyz; and (iii) $x^2 yz$.

   (c) Using the results of (b) and the basis functions in the character table for the point group T_d, give one set of basis functions for each irreducible representation of T_d.

   (d) Using the basis function $\omega x^2 + \omega^2 y^2 + z^2$ and its partner (or partners), find the matrix for an S_4 rotation about the x axis in this irreducible representation.

3. Consider the cubic group O_h. Find the basis functions for all the irreducible representations of the point group O_h.

4. Consider the hypothetical molecule CH_4 where the four H atoms are at the corners of a square $(\pm a, 0, 0)$ and $(0, \pm a, 0)$ while the C atom is at $(0, 0, z)$, where $z \ll a$. What are the symmetry ele-

ments?
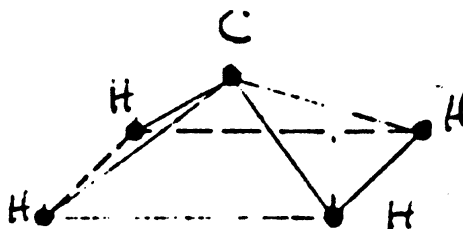
(a) Identify the appropriate character table.

(b) Using the basis functions in the character table, write down a set of (2×2) matrices which provide a representation for the two-dimensional irreducible representation of this group.

(c) Find the 4 linear combinations of the four H orbitals (assume identical s-functions at each H site) that transform as the irreducible representations of the group. What are their symmetry types?

(d) What are the basis functions that generate the irreducible representations.

(e) Check that xz forms a proper basis function for the two dimensional representation of this point group and find its partner.

(f) What are the irreducible representations and partners of the following basis functions in the point group (the hydrogens lie in the xy plane): (i) xyz, (ii) $x^2 y$, (iii) $x^2 z$, (iv) $x + iy$.

(g) What additional symmetry operations result in the limit that all H atoms are coplanar with atom C? What is now the appropriate group and character table? (The stereograms in Table 3.2 of the class notes may be useful.)

5. Consider a molecule AB_6 where the A atom lies in the central plane and three B atoms indicated by "o" lie in a plane at a

distance c above the central plane and the B atoms indicated by "×" lie in a plane below the central plane at a distance $-c$. When projected onto the central plane, all B atoms occupy the corners of a hexagon.
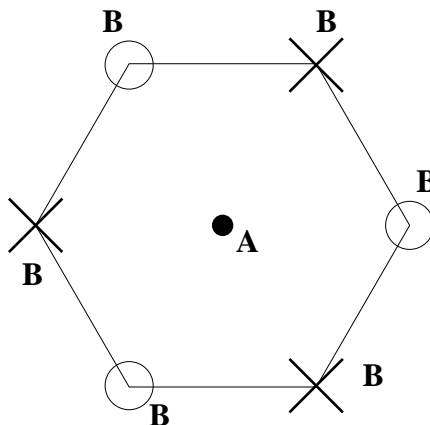
(a) Find the symmetry elements and classes.

(b) Construct the character table. To which point group (Chapter 3 does this molecule correspond? How many irreducible representations are there? How many are one-dimensional and how many are of higher dimensionality?

(c) Using the basis functions in the character table for this point group, find a set of matrices for each irreducible representation of the group.

(d) Find the linear combinations of the six s-orbitals of the B atoms that transform as the irreducible representations of the group.

(e) What additional symmetry operations result in the limit that all B atoms are coplanar with A? What is now the appropriate group and character table for this more symmetric molecule?

(f) Indicate which stereogram in Fig. 3.2 is appropriate for the case where the B atoms are not coplanar with A, and the case where they are coplanar.

Chapter 5

Group Theory and Quantum Mechanics

In this brief chapter we consider the connection between group theory and quantum mechanics. For many practical problems we calculate the solution of Schrödinger's equation for a Hamiltonian displaying various symmetries, which implies that the system is invariant under the action of both the Hamiltonian $\mathcal{H}$ and the symmetry operation $\hat{P}_R$.

5.1 Overview

We define the "Group of Schrödinger's Equation" as the group of all $\hat{P}_R$ such that

$$\left[\mathcal{H}, \hat{P}_R\right] = 0. \tag{5.1}$$

If $\mathcal{H}$ and $\hat{P}_R$ commute, and if $\hat{P}_R$ is a Hermitian operator, then $\mathcal{H}$ and $\hat{P}_R$ can be simultaneously diagonalized. In this Chapter we show that:

1. The elements $\hat{P}_R$ satisfy the group property.

2. If ψ_n is an eigenfunction corresponding to the energy eigenvalue E_n then $\hat{P}_R\psi_n$ and $\hat{P}_R\hat{P}_S\psi_n$, etc. are also eigenfunctions corresponding to the same eigenvalue.

3. If E_n is a k-fold degenerate level, then the matrix representation (irreducible) of $\hat{P}_R$ is given by

$$\hat{P}_R \psi_{n\alpha} = \sum_{j=1}^{k} \psi_{nj} \, D^{(n)}(R)_{j\alpha}. \tag{5.2}$$

4. The operation of $\hat{P}_R$ on a general vector consisting of a complete set of eigenfunctions yields a matrix representation of R in block diagonal form.

5.2   The Group of Schrödinger's Equation

We have now learned enough to start making applications of group theory to physical problems. In such problems we typically have a system described by a Hamiltonian which may be very complicated. Symmetry often allows us to make certain simplifications, without knowing the detailed Hamiltonian. To make a connection between group theory and quantum mechanics, we consider the group of symmetry operators $\hat{P}_R$ which leave the Hamiltonian invariant. These operators $\hat{P}_R$ are symmetry operations of the system and the $\hat{P}_R$ commute with the Hamiltonian (see Eq. 5.1). The operators $\hat{P}_R$ are said to form **the group of Schrödinger's equation**.

We now show that these operators form a group. The identity element clearly exists (leaving the system unchanged). Each symmetry operator $\hat{P}_R$ has an inverse $\hat{P}_R^{-1}$ to undo the operation $\hat{P}_R$ and from physical considerations the element $\hat{P}_R^{-1}$ is also in the group. The product of 2 operators of the group is still an operator of the group, since we can consider these separately as acting on the Hamiltonian. The associative law clearly holds. Thus the requirements for forming a group are satisfied.

Whether the operators $\hat{P}_R$ be rotations, reflections, translations or permutations, these symmetry operations do not alter the Hamiltonian or its eigenvalues. If $\mathcal{H}\psi_n = E_n\psi_n$ is a solution to Schrödinger's equation and $\mathcal{H}$ and $\hat{P}_R$ commute, then

$$\hat{P}_R \mathcal{H} \psi_n = \hat{P}_R E_n \psi_n = \mathcal{H}(\hat{P}_R \psi_n) = E_n(\hat{P}_R \psi_n) \tag{5.3}$$

Thus $\hat{P}_R \psi_n$ is as good an eigenfunction of $\mathcal{H}$ as ψ_n itself. Furthermore, both ψ_n and $\hat{P}_R \psi_n$ correspond to the **same** eigenvalue E_n. Thus,

starting with a particular eigenfunction, we can generate all other eigenfunctions of the same degenerate set (same energy) by applying all the symmetry operations that commute with the Hamiltonian (or leave it invariant). Similarly, if we consider the product of two symmetry operators we again generate an eigenfunction of the Hamiltonian $\mathcal{H}$

$$\hat{P}_R\hat{P}_S\mathcal{H}=\mathcal{H}\hat{P}_R\hat{P}_S$$
$$\hat{P}_R\hat{P}_S\mathcal{H}\psi_n=\hat{P}_R\hat{P}_S E_n\psi_n = E_n(\hat{P}_R\hat{P}_S\psi_n) = \mathcal{H}(\hat{P}_R\hat{P}_S\psi_n) \tag{5.4}$$

in which $\hat{P}_R\hat{P}_S\psi_n$ is an eigenfunction of $\mathcal{H}$. We also note that the action of $\hat{P}_R$ on an arbitrary vector consisting of ℓ eigenfunctions, yields a $\ell \times \ell$ matrix representation of $\hat{P}_R$ that is in block diagonal form, with each block having the dimensions of the corresponding irreducible representation.

Suppose E_n is a k-fold degenerate level of the group of Schrödinger's equation. Then any linear combination of the eigenfunctions $\psi_{n1}, \psi_{n2}, \ldots, \psi_{nk}$ is also a solution of Schrödinger's equation. We can write the operation $\hat{P}_R\psi_{n\alpha}$ on one of these eigenfunctions as

$$\hat{P}_R\psi_{n\alpha} = \sum_j \psi_{nj} D^{(n)}(R)_{j\alpha} \tag{5.5}$$

where $D^{(n)}(R)_{j\alpha}$ is an irreducible matrix which defines the linear combination, n labels the energy index, α labels the degeneracy index.

Equation 5.5 is identical with the more general equation for a basis function (Eq. 4.1) where the states $|\Gamma_n\alpha\rangle$ and $|\Gamma_n j\rangle$ are written symbolically rather than explicitly as they are in Eq. 5.5.

We show here that the matrices $D^{(n)}(R)$ form an ℓ_n dimensional irreducible representation of the group of Schrödinger's equation where ℓ_n denotes the degeneracy of the energy eigenvalue E_n. Let R and S be two symmetry operations which commute with the Hamiltonian and let RS be their product. Then from Eq. 5.5 we can write

$$\hat{P}_{RS}\psi_{n\alpha}=\hat{P}_R\hat{P}_S\psi_{n\alpha} = \hat{P}_R \sum_j \psi_{nj}D^{(n)}(S)_{j\alpha}$$

$$=\sum_{jk} \psi_{nk}D^{(n)}(R)_{kj}D^{(n)}(S)_{j\alpha} = \sum_k \psi_{nk} \left[D^{(n)}(R)D^{(n)}(S)\right]_{k\alpha} \tag{5.6}$$

after carrying out the indicated matrix multiplication. But by definition, the product operator RS can be written as:

$$\hat{P}_{RS}\psi_{n\alpha} = \sum_k \psi_{nk}D^{(n)}(RS)_{k\alpha} \qquad (5.7)$$

so that

$$D^{(n)}(RS) = D^{(n)}(R)D^{(n)}(S) \qquad (5.8)$$

and the matrices $D^{(n)}(R)$ form a representation for the group. We label quantum mechanical states typically by a state vector (basis vector) $|\alpha, \Gamma_n, j\rangle$ where Γ_n labels the irreducible representation, j the component or partner of the irreducible representation, and α labels the other quantum numbers that do not involve the symmetry of the $\hat{P}_R$ operators.

The dimension of the irreducible representation is equal to the degeneracy of the eigenvalue E_n. The representation $D^{(n)}(R)$ generated by $\hat{P}_R\psi_{n\alpha}$ is an irreducible representation if all the ψ_{nk} correspond to a single eigenvalue E_n. For otherwise it would be possible to form linear combinations of the type

$$\underbrace{\psi'_{n1}, \psi'_{n2}, \ldots, \psi'_{ns}}_{\text{subset 1}} \underbrace{\psi'_{n,s+1}, \ldots, \psi'_{nk}}_{\text{subset 2}} \qquad (5.9)$$

whereby the linear combinations within the subsets would transform amongst themselves. But if this happened, then the eigenvalues for the 2 subsets would be different, except for the rare case of accidental degeneracy. Thus, the transformation matrices for the symmetry operations form an **irreducible** representation for the group of Schrödinger's equation.

5.3 The Application of Group Theory

It is convenient at this point to classify the ways that group theory is used to solve quantum mechanical problems. Group theory is used both to obtain exact results and in applications of perturbation theory. In the category of exact results, we have as examples:
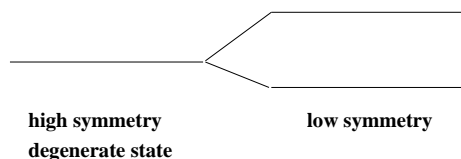
Figure 5.1: The effect of lowering the symmetry often results in a lowering of the degeneracy of degenerate energy states.

high symmetry degenerate state   **low symmetry**

1. The irreducible representations of the symmetry group of Schrödinger's equation **label the states and specify their degeneracies** (e.g., an atom in a crystal field).

2. Group theory is useful in following the changes in the degeneracies of the energy levels as the **symmetry** is lowered. This case can be thought of in terms of a Hamiltonian

$$\mathcal{H} = \mathcal{H}_0 + \mathcal{H}' \tag{5.10}$$

where $\mathcal{H}_0$ has high symmetry corresponding to the group G, and $\mathcal{H}'$ is a perturbation having lower symmetry and corresponding to a group G' of lower order (fewer symmetry elements). Normally group G' is a subgroup of Group G. Here we find first which symmetry operations of G are contained in G'; the irreducible representations of G' label the states of the lower symmetry situation exactly. In going to lower symmetry we want to know what happens to the degeneracy of the various states in the initial higher symmetry situation (see Fig. 5.1). We say that in general the irreducible representation of the **higher symmetry group forms reducible representations for the lower symmetry group**.

The degeneracy of states may either be lowered as the symmetry is lowered or the degeneracy may be unchanged. Group theory tells us exactly what happens to these degeneracies. We are also interested in finding the basis functions for the lower symmetry group G'. For those states where the degeneracy is unchanged, the basis functions are generally unchanged. When the degeneracy is reduced, then by proper choice of the form of the partners, the basis functions for the degenerate state will also be basis functions

for the states in the lower symmetry situation; e.g., if (x, y, z) are basis functions for a 3-dimensional representation in the cubic group, then lowering the symmetry to tetragonal with z as the main symmetry direction will give a 2-dimensional representation with basis functions (x, y) and a one-dimensional representation with basis function z. However, if the symmetry is lowered to tetragonal along a z' direction (different from z), then linear combinations of (x, y, z) must be taken to obtain a vector along z' and two others that are mutually orthogonal. The lowering of degeneracy is a very general topic and will enter the discussion of many applications of group theory.

3. Group theory is helpful in finding the correct **linear combination of wavefunctions** that is needed to diagonalize the Hamiltonian. This procedure involves the concept of equivalence which applies to situations where equivalent atoms sit at symmetrically equivalent sites.

We elaborate on these concepts in the following chapters.

5.4 Selected Problems

1. Consider the hypothetical XH_{12} molecule which has I_h icosahedral symmetry, and the X atom is at the center. The lines connecting the X and H atoms are 5-fold axes.
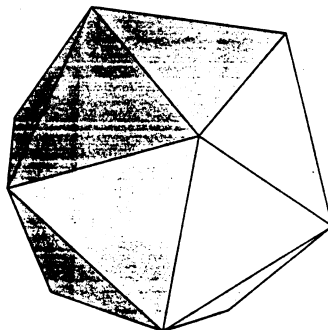
   (a) Suppose that we stretch the XH_{12} molecule along one of the 5-fold axes. What are the resulting symmetry elements of the stretched molecule?

(b) What is the appropriate point group?

(c) Consider the G_u and H_g irreducible representations of group I_h as a reducible representation of the lower symmetry group. Find the symmetries of the lower symmetry group that were contained in a 4-fold energy level that transforms as G_u and in a 5-fold level that transforms as H_g in the I_h group. Assuming the basis functions given in the character table for the I_h point group, give the corresponding basis functions for each of the levels in the multiplets for the stretched molecule.

(d) Suppose that the symmetry of the XH_{12} molecule is described in terms of hydrogen atoms placed at the center of each pentagon of a regular dodecahedron. A regular dodecahedron has 12 regular pentagonal faces, 20 vertices and 30 edges. What are the symmetry classes for the regular dodecahedron. Suppose that the XH_{12} molecule is stretched along one of its 5-fold axes as in (a). What are the symmetry elements of the stretched XH_{12} molecule when viewed from the point of view of a distortion from dodecahedral symmetry?
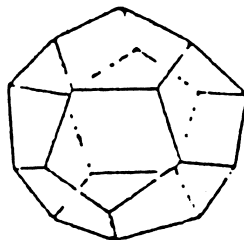
Chapter 6

Application of Group Theory to Crystal Field Splitting

This is the first of several chapters aimed at presenting some **general applications** of group theory while further developing theoretical concepts and amplifying on those given in the first 5 chapters. The first application of group theory is made to crystal field splittings because of the relative simplicity of this application and because it provides a good example of going from higher to lower symmetry, a procedure used very frequently in applications of group theory to solid state physics. In this chapter we also consider irreducible representations of the full rotation group.

6.1   Introduction

The study of crystal field theory is relevant for physics and engineering applications in situations where it is desirable to exploit the sharp, discrete energy levels that are characteristic of atomic systems together with the larger atomic densities that are typical of solids. As an example, consider the variety of powerful lasers whose operation is based on the population inversion of impurity levels of rare earth ions in a transparent host crystal. The energy levels of an electron moving in the field of an ion embedded in such a solid are approximately the same as for an electron moving in the field of a free ion. The interaction of the

impurity ion with the host crystal is small enough so that the electrons can be localized and identified in a tight binding sense with an impurity ion. Thus the interaction between the ion and the host crystal can be treated in perturbation theory. Group theory plays a major role in finding the degeneracy and the symmetry types of the electronic levels in the crystalline field.

Recently the topic of crystal field splittings has attracted considerable attention with the very important technical breakthrough of erbium-doped silica-based optical glass fiber amplifiers for use in optical communications systems. With the arrival of a wave packet of photons having a frequency within the linewidth of an optical transition, optical amplification occurs when there are more ions in the upper state than in the lower state. The ground state of Er^{3+} is a $^4I_{15/2}$ level ($s = 3/2$, $l = 6$, $j = 15/2$) and in the silica host the only radiative transition is the $^4I_{13/2} \rightarrow^4 I_{15/2}$ transition. In the actual optical fibers, this transition is a broad line centered at $1.55 \, \mu$m, and is homogeneously broadened. The optical amplifier can be pumped by InGaAs or InGaAsP laser diodes to create the population inversion. Some characteristics of the erbium-doped fiber amplifier include: low insertion loss (< 0.5 dB), high gain (30–45 dB) with no polarization sensitivity, high saturation power outputs (> 10 dBm), slow gain dynamics (100 μs – 1 ms) giving negligible cross talk at frequencies greater than 100 kHz, and quantum-limited noise figures. This technological breakthrough provides added motivation for understanding the splitting of the energy levels of an impurity ion in a crystal field.

In this chapter the point group symmetry of an impurity ion in a crystal is presented. The crystal potential V_{xtal} determines the point group symmetry. Following the discussion on the form of the crystal potential, some properties of the full rotation group are given, most importantly the characters $\chi^{(\ell)}(\alpha)$ for rotations through an angle α and $\chi^{(\ell)}(i)$ for inversions. The expression for $\chi^{(\ell)}(\alpha)$ is given by

$$\chi^{(\ell)}(\alpha) = \frac{\sin(\ell + 1/2)\alpha}{\sin(\alpha/2)} \qquad \text{for rotations.} \tag{6.1}$$

In general, inversion is not equivalent to a C_2 operation. For the inversion operation i, we have

$$iY_{\ell m}(\theta, \phi) = Y_{\ell m}(\pi - \theta, \pi + \phi) = (-1)^\ell Y_{\ell m}(\theta, \phi) \tag{6.2}$$

and therefore

$$\chi^{(\ell)}(i) = \sum_{m=-\ell}^{m=\ell} (-1)^\ell = (-1)^\ell (2\ell + 1), \qquad (6.3)$$

where ℓ denotes the angular momentum quantum number.

Irreducible representations of the full rotation group are generally found to be reducible representations of a point group of lower symmetry which is a subgroup of the higher symmetry group. If the representation is reducible, then crystal field splittings of the energy levels occur. If, however, the representation is irreducible, then no crystal field splittings occur. Examples of each type of representation are presented.

We focus explicitly on giving examples of going from higher to lower symmetry. In so doing, we consider the:

1. Splitting of the energy levels.

2. Symmetry types of the split levels.

3. Choice of basis functions to bring the Hamiltonian $\mathcal{H}$ into block diagonal form. Spherical symmetry results in spherical harmonics $Y_{\ell m}(\theta, \phi)$ for basis functions. Proper linear combinations of the spherical harmonics $Y_{\ell m}(\theta, \phi)$ are taken to make appropriate basis functions for the point group of lower symmetry.

In crystal field theory we write down the Hamiltonian for the impurity ion in a crystalline solid as

$$\mathcal{H} = \sum_i \left\{ \frac{p_i^2}{2m} - \frac{Ze^2}{r_{i\mu}} + \sum_j{}' \frac{e^2}{r_{ij}} + \sum_j \xi_{ij} \vec{\ell}_i \cdot \vec{s}_j + \gamma_{i\mu} \vec{j}_i \cdot \vec{I}_\mu \right\} + V_{\text{xtal}} \quad (6.4)$$

where the first term is the kinetic energy of the electrons associated with the ion and the second term represents the Coulomb attraction of the electrons of the ion to their nucleus and the third term represents the mutual Coulomb repulsion of the electrons associated with the impurity ion, and the sum on j denotes a sum on pairs of electrons. These three quantities are denoted by $\mathcal{H}_0$ the electronic Hamiltonian of the free atom without spin-orbit interaction. $\mathcal{H}_0$ is the dominant term in the

total Hamiltonian $\mathcal{H}$. The remaining terms are treated in perturbation theory in some order. Here $\xi_{ij}\vec{\ell_i} \cdot \vec{s_j}$ is the spin-orbit interaction of electrons on the impurity ion and $\gamma_{i\mu}\vec{j_i} \cdot \vec{I_\mu}$ is the hyperfine interaction of electrons on the ion. The perturbing crystal potential V_{xtal} of the host ions acts on the impurity ion and lowers its spherical symmetry.

Because of the various perturbation terms appearing in Eq. 6.4, it is important to distinguish the two limiting cases of weak and strong crystal fields.

1. Weak field case – In this case, the perturbing crystal field V_{xtal} is considered to be small compared with the spin-orbit interaction. In this limit, we find the energy levels of the free impurity ion with spin-orbit interaction and at this point we consider the crystal field as an additional perturbation. These approximations are appropriate to rare earth ions in ionic host crystals. We will deal with the group theoretical aspects of this case in §19.4, after we have learned how to deal with the spin on the electron in the context of group theory.

2. Strong field case – In this case, the perturbing crystal field V_{xtal} is strong compared with the spin-orbit interaction. We now consider V_{xtal} as the major perturbation on the energy levels of $\mathcal{H}_0$. Examples of the strong field case are transition metal ions (Fe, Ni, Co, Cr, etc.) in a host crystal. It is this limit that we will consider first, and is the focus of this Chapter.

6.2   Comments on the Form of Crystal Fields

To construct the crystal field, we consider the electrostatic interaction of the neighboring host ions at the impurity site. To illustrate how this is done, consider the highly symmetric case of an impurity ion in a cubic environment provided by ions at $x = \pm a$, $y = \pm a$, $z = \pm a$. The contribution from an ion at $x = -a$ at the field point (x, y, z) is (see Fig. 6.1):

$$V_{x=-a} = \frac{e}{a\sqrt{(1 + x/a)^2 + (y/a)^2 + (z/a)^2}} = \frac{e}{a\sqrt{1 + \varepsilon}} \qquad (6.5)$$
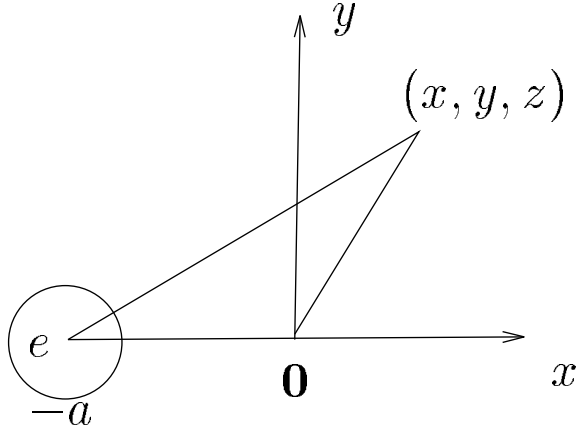
Figure 6.1: Coordinate system used for expansion of the impurity ion potential.

where e is the charge on the electron and ε is a small dimensionless quantity. Then using the binomial expansion:

$$(1+\varepsilon)^{-\frac{1}{2}} = 1 - \frac{1}{2}\varepsilon + \frac{3}{8}\varepsilon^2 - \frac{5}{16}\varepsilon^3 + \frac{35}{128}\varepsilon^4 + ... \qquad (6.6)$$

we obtain the contribution to the potential for charges e at $x = a$ and $x = -a$:

$$\begin{aligned}
V_{x=-a} + V_{x=a} = {} & \frac{2e}{a}[1 - \frac{1}{2}(r^2/a^2) + \frac{3}{2}(x^2/a^2) + \frac{3}{8}(r^4/a^4) \\
& - \frac{15}{4}(x^2/a^2)(r^2/a^2) + \frac{35}{8}(x^4/a^4) + ...].
\end{aligned} \qquad (6.7)$$

For a cubic field with charges e at $x = \pm a$, $y = \pm a$, $z = \pm a$ we get for $V_{\text{total}} = V_{\text{xtal}}$:

$$V_{\text{total}} = \frac{2e}{a}[3 + \frac{35}{8a^4}(x^4 + y^4 + z^4) - \frac{21}{8}(r^4/a^4) + ...] \qquad (6.8)$$

so that the perturbation that will lift the degeneracy of the free atom is of the form

$$V_{\text{cubic}} = \frac{35e}{4a^5}\left[(x^4 + y^4 + z^4) - \frac{3}{5}r^4\right]. \tag{6.9}$$

From these expressions it also follows that for a rhombic field where the charges are at $x = \pm a, y = \pm b, z = \pm c$ (where $a \neq b \neq c$)

$$V_{\text{total}} = \frac{2e}{a} + \frac{2e}{b} + \frac{2e}{c} + ex^2\left[\frac{2}{a^3} - \frac{1}{b^3} - \frac{1}{c^3}\right] + ey^2\left[\frac{2}{b^3} - \frac{1}{a^3} - \frac{1}{c^3}\right] + ez^2\left[\frac{2}{c^3} - \frac{1}{a^3} - \frac{1}{b^3}\right] \tag{6.10}$$

so that the perturbation that will lift the degeneracy of the free atom is of the form

$$V_{\text{rhombic}} = Ax^2 + By^2 - (A + B)z^2. \tag{6.11}$$

We note that V_{cubic} contains no terms of order x^2 whereas V_{rhombic} does.

It is sometimes useful to express the crystal field potential in terms of spherical harmonics since the unperturbed states for the free impurity ion are expressed in that way. Here we make use of the fact that the crystal field potential is generated by a collection of point sources and in the intervening space we are "outside" the field sources so that the potential must satisfy the Laplace equation $\nabla^2 V = 0$. Solutions to Laplace's equation are of the form $r^\ell Y_{\ell m}(\theta, \phi)$. Let us then recall the form of the spherical harmonics $Y_{\ell m}(\theta, \phi)$ which are the basis functions for the full rotation group:

$$Y_{\ell m}(\theta, \phi) = \left[\frac{2\ell + 1}{4\pi}\frac{(\ell - |m|)!}{(\ell + |m|)!}\right]^{\frac{1}{2}} P_\ell^m(\cos\theta)e^{im\phi} \tag{6.12}$$

where the associated Legendre polynomial is written as

$$P_\ell^m(x) = (1 - x^2)^{\frac{1}{2}|m|}\frac{d^{|m|}}{dx^{|m|}}P_\ell(x) \tag{6.13}$$

and the Legendre polynomial $P_\ell(x)$ is generated by

$$1/\sqrt{1 - 2sx + s^2} = \sum_{\ell=0}^{\infty} P_\ell(x)s^\ell. \tag{6.14}$$

From these definitions it is clear that for a cubic field, the only spherical harmonics that will enter V_{cubic} are $Y_{4,0}, Y_{4,4}$ and $Y_{4,-4}$ since $(z/4)^4$ involves only $Y_{4,0}$ while

$$[(x/4)^4 + (y/4)^4]$$

involves only $Y_{4,4}$ and $Y_{4,-4}$. Following this example, we conclude that the crystal field potential V_{xtal} can be written in terms of spherical harmonics, the basis functions normally used to describe the potential of the free ion which has full spherical symmetry.

More generally, we can write any function (e.g., any arbitrary V_{xtal}) in terms of a complete set of basis functions, such as the spherical harmonics. One important role of group theory in the solution of quantum mechanical problems is to determine the degeneracy of the eigenvalues and which choice of basis functions yields the eigenvalues most directly. This information is available without the explicit diagonalization of the Hamiltonian. In the case of the crystal field problem, we determine V_{xtal} for a specific crystal symmetry using the appropriate basis functions for the relevant point group.

We note that the crystal potential V_{xtal} lowers the full rotational symmetry of the free atom to cause level splittings relative to those of the free atom. We show here how group theory tells us the degeneracy of the resulting levels and the appropriate basis functions to use in diagonalizing the crystal field Hamiltonian. The first step in this process is to consider the irreducible representation of the higher symmetry group (the full rotation group) as a reducible representation of the lower symmetry group (the crystal field group). We now consider in §6.3 some of the fundamental properties of the full rotation group. These results are liberally used in later Chapters.

6.3   Characters for the Full Rotation Group

The free atom has full rotational symmetry and the number of symmetry operations which commute with the Hamiltonian is infinite. That is, all C_ϕ rotations about any axis are symmetry operations of the full rotation group. We are not going to discuss infinite or continuous groups in any detail, but we will adopt results that we have used in quantum
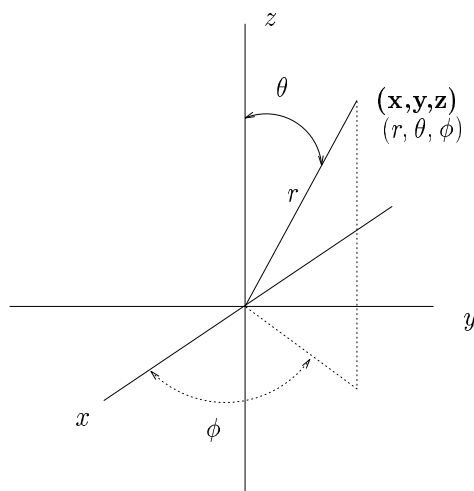
Figure 6.2: Polar coordinate system defining the angles θ and ϕ.

mechanics without rigorous proofs. It can be shown that the spherical harmonics (angular momentum eigenfunctions) can be written in the form:

$$Y_{\ell,m}(\theta,\phi) = CP_\ell^m(\theta)\, e^{im\phi} \tag{6.15}$$

where C is a normalization constant and $P_\ell^m(\theta)$ is an associated Legendre polynomial given explicitly in Eq. 6.12. The coordinate system used to define the polar and azimuthal angles is shown in Fig. 6.2. The $Y_{\ell,m}(\theta,\phi)$ spherical harmonics generate odd-dimensional representations of the rotation group and these representations are irreducible representations. For $\ell = 0$, we have a 1-dimensional representation; $\ell = 1(m = 1, 0, -1)$ gives a 3-dimensional irreducible representation; $\ell = 2(m = 2, 1, 0, 1, -2)$ gives a 5-dimensional representation, etc. So for each value of the angular momentum, the spherical harmonics provide us with a representation of the proper $2\ell + 1$ dimensionality.

These irreducible representations are found from the so-called **addition theorem for spherical harmonics** which tells us that if we change the polar axis (i.e., the axis of quantization), then the "old" spherical harmonics $Y_{\ell,m}(\theta,\phi)$ and the "new" $Y_{\ell',m'}(\theta',\phi')$ are related by a <u>linear transformation</u> of basis functions when <u>$\ell' = \ell$</u>:

$$\hat{P}_R Y_{\ell,m}(\theta',\phi') = \sum_{m'} Y_{\ell,m'}(\theta,\phi) D^{(\ell)}(R)_{m'm} \tag{6.16}$$

where $\hat{P}_R$ denotes a rotation operator that changes the polar axis, and the matrix $D^{(\ell)}(R)_{m'm}$ provides an ℓ-dimensional matrix representation of element R in the full rotation group. Let us assume that the reader has previously seen this expansion for spherical harmonics which is a major point in the development of the irreducible representations of the rotation group.

In any system with full rotational symmetry, the choice of the z axis is arbitrary. We thus choose the z axis as the axis about which the operator $\hat{P}_\alpha$ makes the rotation α. Because of the form of the spherical harmonics $Y_{\ell,m}(\theta, \phi)$ (see Eq. 6.15) and the choice of the z axis, the action of $\hat{P}_\alpha$ on the $Y_{\ell m}(\theta, \phi)$ basis functions only affects the ϕ dependence of the spherical harmonic (not the θ dependence). The effect of this rotation on the function $Y_{\ell,m}(\theta, \phi)$ is equivalent to a rotation of the axes in the opposite sense by the angle $-\alpha$

$$\hat{P}_\alpha Y_{\ell,m}(\theta, \phi) = Y_{\ell,m}(\theta, \phi - \alpha) = e^{-im\alpha} Y_{\ell,m}(\theta, \phi) \tag{6.17}$$

in which the second equality results from the explicit form of $Y_{\ell,m}(\theta, \phi)$. But Eq. 6.17 gives the linear transformation of $Y_{\ell,m}(\theta, \phi)$ resulting from the action by the operator $\hat{P}_\alpha$. Thus by comparing Eqs. 6.16 and 6.17, we see that the matrix $D^{(\ell)}(\alpha)_{m'm}$ is diagonal in m so that we can write $D^{(\ell)}(\alpha)_{m'm} = e^{-im\alpha} \delta_{m'm}$ where $-\ell \le m \le \ell$, yielding

$$D^{(\ell)}(\alpha) = \begin{pmatrix} e^{-i\ell\alpha} & & & \mathcal{O} \\ & e^{-i(\ell-1)\alpha} & & \\ & & \ddots & \\ \mathcal{O} & & & e^{i\ell\alpha} \end{pmatrix} \tag{6.18}$$

where $\mathcal{O}$ represents all the zero entries in the off-diagonal positions. The character of the rotations C_α is given by the geometric series

$$
\begin{aligned}
\chi^{(\ell)}(\alpha) &= \text{trace } D^{(\ell)}(\alpha) = e^{-i\ell\alpha} + ... + e^{i\ell\alpha} \\
&= e^{-i\ell\alpha}\left[1 + e^{i\alpha} + ... + e^{2i\ell\alpha}\right] \\
&= e^{-i\ell\alpha} \sum_{k=0}^{2\ell} (e^{ik\alpha}) \\
&= e^{-i\ell\alpha}\left[\frac{e^{i(2\ell+1)\alpha} - 1}{e^{i\alpha} - 1}\right]
\end{aligned}
$$

$$= \frac{e^{i(\ell+\frac{1}{2})\alpha} - e^{-i(\ell+\frac{1}{2})\alpha}}{e^{i\alpha/2} - e^{-i\alpha/2}} = \frac{\sin(\ell+\frac{1}{2})\alpha}{\sin(\frac{1}{2})\alpha}. \tag{6.19}$$

Thus we show that the character for rotations α about the z axis is

$$\chi^{(\ell)}(\alpha) = \frac{\sin(\ell+\frac{1}{2})\alpha}{\sin\alpha/2} \tag{6.20}$$

which is identical with Eq. 6.1. To obtain the character $\chi^{(\ell)}(i)$ for the inversion operator, we use the result $(-1)^\ell(2\ell+1)$ given in Eq. 6.3.

We now give a general result for an improper rotation defined by

$$S_n = C_n \otimes \sigma_h \tag{6.21}$$

S_n can be a product of $C(\alpha) \otimes i$, as for example, $S_6 = C_3 \otimes i$, or $S_3 = C_6 \otimes i$, ... etc. where $\otimes$ denotes the direct product of the two symmetry operations appearing at the left and right of the symbol $\otimes$. If we now apply Eqs. 6.1 and 6.2, we obtain

$$\chi^{(\ell)}(S_n) = \chi^{(\ell)}(C(\alpha) \otimes i) = (-1)^\ell \frac{\sin(\ell+\frac{1}{2})\alpha}{\sin\alpha/2}. \tag{6.22}$$

In the case of mirror planes, such as σ_h, σ_d, or σ_v we can make use of relations such as

$$\sigma_h = C_2 \otimes i \tag{6.23}$$

to obtain the character for mirror planes in the full rotation group.

But we are free to choose the z axis in any arbitrary way in the full rotation group. Therefore, the formula for the character given by Eq. 6.20 is applicable to any arbitrary rotation of α about any axis whatsoever. Furthermore, it can be shown that there are no equivalent irreducible representations of odd order for the full rotation group and thus the character given by Eq. 6.20 is unique.

Now we are going to place our free ion into a crystal field which does not have full rotational symmetry operations, but rather has the symmetry operations of a crystal which include rotations about finite angles, inversions and a finite number of reflections. The **full rotation group contains all these symmetry operations**. Therefore, the representation $D^{(\ell)}(\alpha)$ given above is a representation of the crystal

point group if α is a symmetry operation in that point group. But $D^{(\ell)}(\alpha)$ is, in general, a <u>reducible</u> representation of the lower symmetry group. Therefore the $(2\ell + 1)$ fold degeneracy of each level will in general be partially lifted. We can find out how the degeneracy of each level is lifted by asking what are the irreducible representations contained in $D^{(\ell)}(\alpha)$ in terms of the group of lower symmetry for the crystal. The actual calculation of the crystal field splittings depends on setting up a suitable Hamiltonian and solving it, usually in some approximation scheme. But the energy level **degeneracy** does not depend on the detailed Hamiltonian, but only on its symmetry. Thus, the decomposition of the level degeneracies in a crystal field is exact and is a consequence of the symmetry of the crystal field.

6.4 Example of a Cubic Crystal Field Environment for a Paramagnetic Transition Metal Ion

Imagine that we place our paramagnetic ion (e.g., an iron impurity) in a cubic host crystal. Assume further that this impurity goes into a substitutional lattice site, and is surrounded by a regular octahedron of negative ions - symmetry type O (see Fig. 6.3). The character table for O is shown in Table 6.1 (see also Table 3.33). From all possible rotations on a sphere only 24 symmetry operations remain in the group O.

Reviewing the **notation** in Table 6.1, the Γ notations for the irreducible representations are the usual ones used in solid state physics and are due to Bouckaert, Smoluchowski and Wigner, Phys. Rev. <u>50</u>, 58 (1936). The second column in Table 6.1 follows the notation usually found in molecular physics and chemistry applications, which also make lots of use of symmetry and group theory. The key to the notation is that A denotes 1 dimensional representations, E denotes 2 dimensional representations, and T denotes 3 dimensional representations. Papers on lattice dynamics of solids often use the A, E, T symmetry notation to make contact with the molecular analog. The subscripts in Table 6.1 refer to the conventional indexing of the representations. The pertinent

Table 6.1: Character table for O

O		E	$8C_3$	$3C_2 = 3C_4^2$	$6C_2$	$6C_4$
Γ_1	A_1	1	1	1	1	1
Γ_2	A_2	1	1	1	-1	-1
Γ_{12}	E	2	-1	2	0	0
$\Gamma_{15'}$	T_1	3	0	-1	-1	1
$\Gamma_{25'}$	T_2	3	0	-1	1	-1
$\Gamma_{\ell=0}$	A_1	1	1	1	1	1
$\Gamma_{\ell=1}$	T_1	3	0	-1	1	-1
$\Gamma_{\ell=2}$	$E + T_2$	5	-1	1	1	-1
$\Gamma_{\ell=3}$	$A_1 + T_1 + T_2$	7	-1	-1	1	1
$\Gamma_{\ell=4}$	$A_1 + E + T_1 + T_2$	9	0	1	1	1
$\Gamma_{\ell=5}$	$E + 2T_1 + T_2$	11	-1	-1	-1	1

symmetry operations can be found from Fig. 6.3, and the classes associated with these symmetry operations label the various columns where the characters in Table 6.1 appear. The various types of rotational symmetry operations are listed as:

- The $8C_3$ rotations are about the axes through face centroids of the octahedron.

- The $6C_4$ rotations are about the corners of the octahedron.

- The $3C_2$ rotations are also about the corners of the octahedron, with $C_2 = C_4^2$.

- The $6C_2$ rotations are two-fold rotations about a (110) axis passing through the midpoint of the edges (along the 110 directions of the cube).

To be specific, suppose that we have a magnetic impurity atom with angular momentum $\ell = 2$. We first find the characters for all the symmetry operations which occur in the O group for an irreducible representation of the full rotation group. The representation of the full
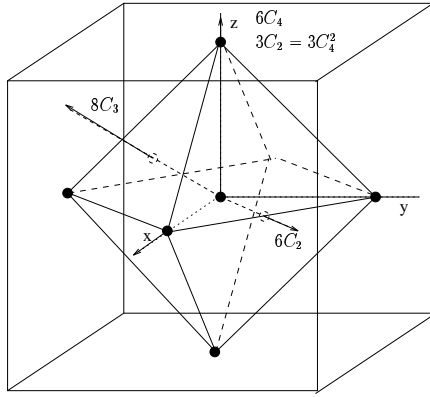
Figure 6.3: A regular octahedron inscribed in a cube, illustrating the symmetry operations of group O.

Table 6.2: Classes and characters for the group O.

Class	α	$\chi^{(2)}(\alpha)$
$8C_3$	$2\pi/3$	$\frac{\sin(5/2)\cdot(2\pi/3)}{\sin((2\pi)/(2\cdot3))} = (-\sqrt{3}/2)/(\sqrt{3}/2) = -1$
$6C_4$	$2\pi/4$	$\frac{\sin(5/2)\cdot(\pi/2)}{\sin(\pi/4)} = (-1/\sqrt{2})/(1/\sqrt{2}) = -1$
$3C_2$ and $6C_2$	$2\pi/2$	$\frac{\sin(5/2)\pi}{\sin(\pi/2)} = 1$

rotation group will be a representation of group O, but in general this representation will be <u>reducible</u>.

Since the character for a general rotation α in the full rotation group is found using Eq. (6.20), the identity class (or $\alpha = 0$) yields get the characters

$$\chi^{(\ell)}(0) = \frac{\ell + \frac{1}{2}}{1/2} = 2\ell + 1. \tag{6.24}$$

For our case $l = 2$, and by applying Eq. 6.24 to the symmetry operations in each class we obtain the results summarized in Table 6.2. To compare with the character table for group O (Table 6.1), we list the characters found in Table 6.2 for the $\Gamma_{\text{rot}}^{(2)}$ of the full rotation group

$(l = 2)$ according to the classes listed in the character table for group O (see Tables 6.1 and 3.33):

	E	$8C_3$	$3C_2$	$6C_2'$	$6C_4$
$\Gamma_{\text{rot}}^{(2)}$	5	-1	1	1	-1

We note that $\Gamma_{\text{rot}}^{(2)}$ is a reducible representation of group O because group O has no irreducible representations with dimensions $\ell_n > 3$. To find the irreducible representations contained in $\Gamma_{\text{rot}}^{(2)}$ we use the decomposition formula for reducible representations Eq. 3.20:

$$a_j = \frac{1}{h} \sum_k N_k \chi^{(\Gamma_j)}(\mathcal{C}_k)^* \chi^{\text{reducible}}(\mathcal{C}_k) \tag{6.25}$$

where we have used the expression

$$\chi^{\text{reducible}}(\mathcal{C}_k) = \sum_j a_j \chi^{(\Gamma_j)}(\mathcal{C}_k) \tag{6.26}$$

in which $\chi^{(\Gamma_j)}$ is an irreducible representation and the characters for the reducible representation $\Gamma_{\text{rot}}^{(2)}$ are written as $\chi^{\text{reducible}}(\mathcal{C}_k) \equiv \chi^{\Gamma_{\text{rot}}^{(2)}}(\mathcal{C}_k)$. We now ask how many times is A_1 contained in $\Gamma_{\text{rot}}^{(2)}$? Using Eq. 6.25 we obtain:

$$a_{A_1} = \frac{1}{24}[5 - 8 + 3 + 6 - 6] = 0 \tag{6.27}$$

which shows that the irreducible representation A_1 is not contained in $\Gamma_{\text{rot}}^{(2)}$. We then apply Eq. 6.25 to the other irreducible representations of group O:

$$
\begin{array}{lllll}
A_2: & a_{A_2} & = & \frac{1}{24}[5 - 8 + 3 - 6 + 6] & = & 0 \\
E: & a_E & = & \frac{1}{24}[10 + 8 + 6 + 0 - 0] & = & 1 \\
T_1: & a_{T_1} & = & \frac{1}{24}[15 + 0 - 3 - 6 - 6] & = & 0 \\
T_2: & a_{T_2} & = & \frac{1}{24}[15 + 0 - 3 + 6 + 6] & = & 1 \\
\end{array}
$$

so that finally we write

$$\Gamma_{\text{rot}}^{(2)} = E + T_2$$

which means that the reducible representation $\Gamma_{\text{rot}}^{(2)}$ breaks into the irreducible representations E and T_2 in cubic symmetry. In other words,
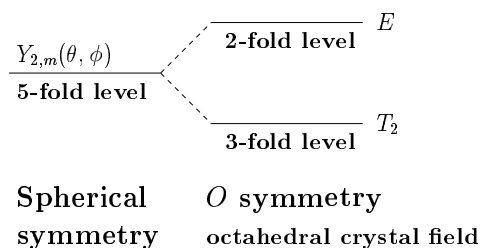
Figure 6.4: The splitting of the d–levels (five-fold) in an octahedral crystal field.

an atomic d–level in a cubic O_h crystal field splits into an E_g and a T_{2g} level, where the g denotes evenness under inversion. Group theory doesn't provide any information about the ordering of the levels (see Fig. 6.4). For general utility, we have included in Table 6.1 the characters for the angular momentum states $\ell = 0, 1, 2, 3, 4, 5$ for the full rotation group expressed as reducible representations of the group O. The splittings of these angular momentum states in cubic group O symmetry are also included in Table 6.1.

We can now carry the passage from higher to lower symmetry by going one step further. Suppose that the presence of the impurity strains the crystal. Let us further imagine (for the sake of argument) that the new local symmetry of the impurity site is D_4 (see Table 3.26), which is a proper subgroup of the full rotation group. Then the levels E and T_2 given above may be split further in D_4 (tetragonal) symmetry (for example by stretching the molecule along the 4-fold axis). We now apply the same technique to investigate this tetragonal field splitting. We start again by writing the character table for the group D_4 which is of order 8. We then consider the representations E and T_2 of the group O as reducible representations of group D_4 and write down the characters for the E, C_4, C_4^2, C_2' and C_2'' operations from the character table for O given above, noting that the C_2'' in the group D_4 refers to three of the (110) axes $6C_2'$ of the cubic group O:
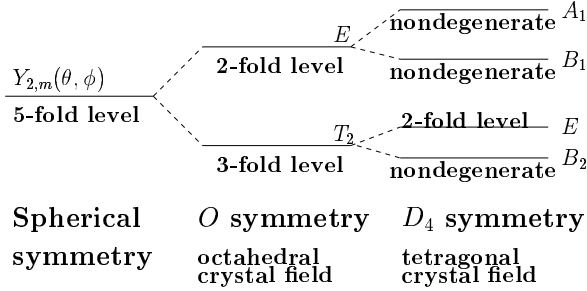
Figure 6.5: d-level splitting in octahedral and D_4 crystal fields

Character Table for D_4	E	$C_2 = C_4^2$	$2C_4$	$2C_2'$	$2C_2''$	
$\Gamma_1 \quad A_1$	1	1	1	1	1	
$\Gamma_{1'} \quad A_2$	1	1	1	-1	-1	
$\Gamma_2 \quad B_1$	1	1	-1	1	-1	
$\Gamma_{2'} \quad B_2$	1	1	-1	-1	1	
$\Gamma_3 \quad E$	2	-2	0	0	0	
reducible representations from O group						
E	2	2	0	2	0	$\equiv A_1 + B_1$
T_2	3	-1	-1	-1	1	$\equiv E + B_2$

Using the decomposition theorem, Eq. 3.20, we find that E splits into the irreducible representations $A_1 + B_1$ in the group D_4 while T_2 splits into the irreducible representations $E + B_2$ in the group D_4, as summarized in Fig. 6.5.

We note that the C_2 operations in D_4 is a π rotation about the z axis and the $2C_2'$ are π rotations about the x and y axes. The $2C_2''$ are π rotations about (110) axes. To check the decomposition of the $\ell = 2$ level in D_4 symmetry, we add up the characters for $A_1 + B_1 + B_2 + E$ for group D_4 and we get

	E	C_2	$2C_4$	$2C_2'$	$2C_2''$	
$\Gamma_{\text{rot}}^{(2)}$	5	1	-1	1	1	$A_1 + B_1 + B_2 + E$

which are the characters for the spherical harmonics considered as a reducible representation of group D_4, so that this result checks.
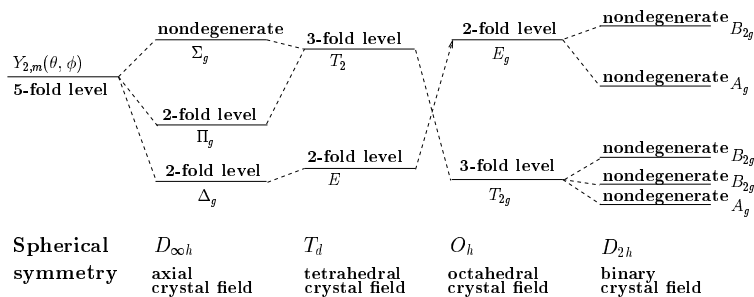
Figure 6.6: *d*-level splitting in various crystal fields

Suppose now that instead of applying a strain along a (001) direction, we apply a strain along a (110) direction. This will give a two-fold axis along a (110) direction and another two-fold axis at right angles in the ($\bar{1}$10) direction. The other right angle direction (001) now also becomes a two-fold axis to give the group D_2 (see Table 6.3 and Fig. 6.7) which has only 1-dimensional representations. Therefore, application of a stress along a (110) direction will lift all the degeneracies of the levels in the octahedral field, while the tetragonal distortion will not. Figure 6.6 shows the splitting of the $\ell = 2$ level in going from full rotational symmetry to various lower symmetries, including $D_{\infty h}$, T_d, O_h, and D_{2h}, showing in agreement with the above discussion, the lifting of all the degeneracy of the $\ell = 2$ level in D_{2h} symmetry. The symmetry axis and stereographic projections for the group D_2 (222) are shown in Fig. 6.7.

6.5   Comments on Basis Functions

Although group theory tells us how the impurity ion energy levels are split by the crystal field, it doesn't tell us the ordering of these levels. Often a simple physical argument can be given to decide which levels ought to lie lower. Consider the case of a *d*–electron in a cubic field, where the host ions are at $x = \pm a$, $y = \pm a$, $z = \pm a$. Assume that the impurity ion enters the lattice substitutionally, so that it is replacing one of the cations. Then the nearest neighbor host ions are all anions. The charge distributions for the *d*–states are shown in Fig. 6.8. Re-

Table 6.3: Character table for the group D_2 (222).

$D_2(222)$			E	$C_2^{z(a)}$	$C_2^{y(b)}$	$C_2^{x(c)}$	
x^2, y^2, z^2		A_1	1	1	1	1	
xy	R_z, z	B_1	1	1	-1	-1	
xz	R_y, y	B_2	1	-1	1	-1	
yz	R_z, x	B_3	1	-1	-1	1	
		$\chi_E^{O_h}$	2	2	0	0	$\rightarrow A_1 + B_1$
		$\chi_{T_2}^{O_h}$	3	-1	1	1	$\rightarrow A_1 + B_2 + B_3$
		$\Gamma_{\text{rot}}^{(2)}$	5	1	1	1	$\rightarrow 2A_1 + B_1 + B_2 + B_3$

[a] $C_2(001)$ corresponds to C_2^z
[b] $C_2(110)$ corresponds to C_2^y
[c] $C_2(\bar{1}10)$ corresponds to C_2^x

D_2
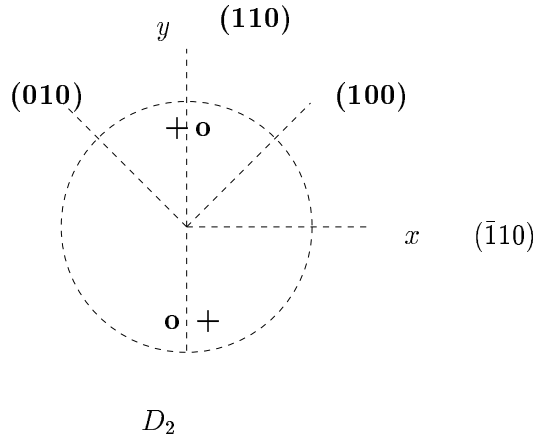
Figure 6.7: Symmetry axes and stereograph for D_2 symmetry.
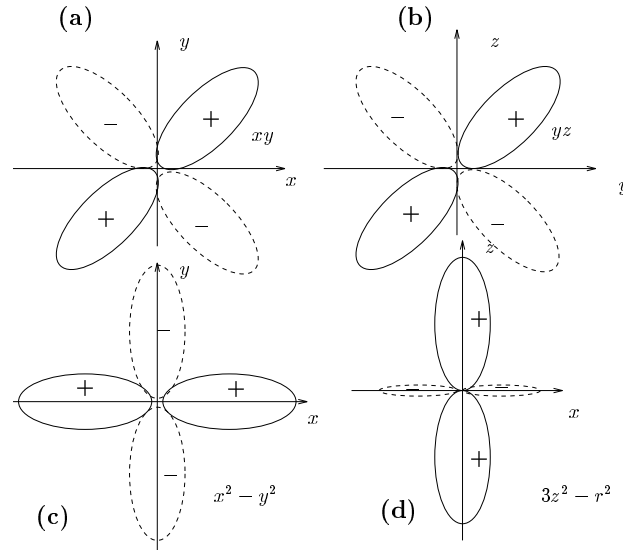
Figure 6.8: The angular parts of d–wave functions in cubic crystals are shown as labeled by the basis functions for the partners of the irreducible representations.
(a) $xy/r^2 \Rightarrow \quad (\Gamma_{25}^+, \quad T_{2g})$
(b) $yz/r^2 \Rightarrow \quad (\Gamma_{25}^+, \quad T_{2g})$
(c) $(x^2 - y^2)/r^2 \Rightarrow \quad (\Gamma_{12}^+, \quad E_g)$
(d) $(3z^2 - r^2)/r^2 \Rightarrow \quad (\Gamma_{12}^+, \quad E_g)$.

ferring to the basis functions for O which are listed in Table 3.33, we see that for the irreducible representation Γ_{12}^+ we have basis functions $(x^2 - y^2, \ 3z^2 - r^2)$ and for Γ_{25}^+ we have basis functions (xy, yz, zx). For the basis functions which transform as the Γ_{25}^+ representation, the charge distributions do not point to the host ions and hence the crystal field interaction is relatively weak. For the d–functions which transform as Γ_{12}^+, the interaction will be stronger since the charge distributions now <u>do</u> point to the host ion sites. If, however, the interaction is repulsive, then the E level will lie higher than the T_2 level. A more quantitative way to determine the ordering of the levels is to solve the eigenvalue problem explicitly. In carrying out this solution it is convenient to use basis functions that transform as the irreducible representations of the crystal field group.

$$\underset{\textbf{5-fold level}}{\underline{Y_{2,m}(\theta,\phi)}} \diagup \underset{\textbf{2-fold level}}{\overline{}} \begin{cases} x^2 - y^2 \\ 3z^2 - r^2 \end{cases}$$

$$\underset{\textbf{3-fold level}}{\overline{}} \begin{cases} xy \\ yz \\ zx \end{cases}$$
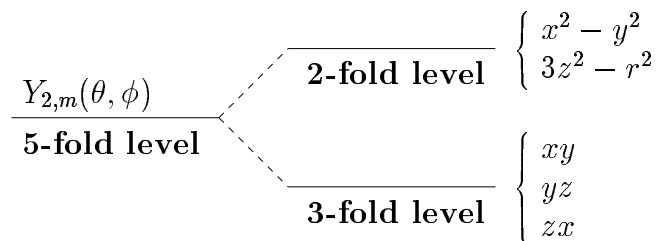
Figure 6.9: Schematic energy level splitting for the five-fold $\ell = 2$ level into two-fold and three-fold levels in an environment where bonding is along the {110} directions. The E_g and T_{2g} levels are labeled by the basis functions (partners) for each if the irreducible representations of O_h.

We now look at the basis functions which provide irreducible representations for these cases of lower symmetry. In going from the full rotation group to the cubic group O_h, we obtain the irreducible representations E_g and T_{2g} shown in Fig. 6.9 in terms of the basis functions for these irreducible representations. We note that these basis functions bring the crystal field potential into block form, but need not completely diagonalize the Hamiltonian. There are various forms of the crystal field potential that have O_h symmetry (e.g., octahedral sites, cubic sites, etc.), and in each case the appropriate set of basis functions that transform as irreducible representations of the group will bring the secular equation into block form.

Upon lowering the symmetry further to D_4 symmetry, the T_{2g} and E_g levels split further according to $T_{2g} \rightarrow E + B_2$ and $E_g \rightarrow A_1 + B_1$ (see Fig. 6.5). The appropriate basis functions for these levels can be identified with the help of the character table for group D_4 in Table 3.26:

$$E \begin{cases} yz \\ zx \end{cases}, \qquad B_2 \{ xy \quad, \qquad B_1 \{ x^2 - y^2 \quad, \qquad A_1 \{ z^2. \qquad (6.28)$$

As a further example we can consider the case of going from cubic O_h symmetry to D_2 symmetry by applying a stress along the $(1\ 1\ 0)$ direction. Here the appropriate coordinate system is chosen with the z–axis taken along the $(0\ 0\ 1)$ direction, and the (y, x)-axes taken along the $(1\ 1\ 0)$ and $(\bar{1}\ 1\ 0)$ directions, respectively, as shown in Fig. 6.7.
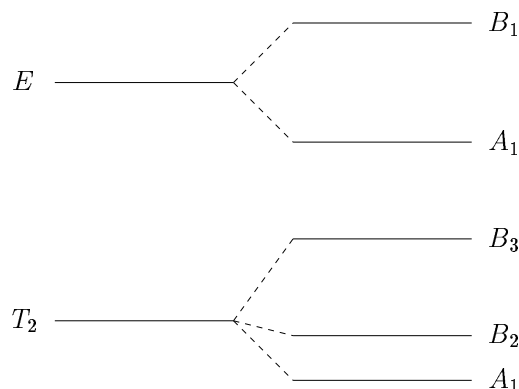
Figure 6.10: Schematic diagram of level splitting of the d-levels in going from cubic O_h symmetry to D_2 symmetry.

The character table for the group D_2 is given in Table 3.24 and in Table 6.3. To help with the assignment of the two-fold axes, we use the stereogram for D_2 from Fig. 3.2, which is shown in more detail in Fig. 6.7.

We can see immediately from Fig. 6.10 how the irreducible representations E_g and T_{2g} of the cubic group O_h become reducible representations for the group D_2 with the following basis functions referred to the axes shown in Fig. 6.7:

$$
\begin{array}{cc}
A_1 & x^2 - y^2 \\
A_1 & 3z^2 - r^2 \\
B_1 & xy \\
B_2 & xz \\
B_3 & yz
\end{array}
$$

Because all these basis functions ultimately relate to the $\ell = 2$ level $Y_{2,m}(\theta, \phi)$ with full rotational symmetry, we have the opportunity to choose the coordinate system for D_2 group symmetry in any way that is convenient.

In §6.4 and §6.5 we consider the spherical harmonics for $\ell = 2$ as reducible representations of the point groups O_h, O, D_4, and D_2. In this connection, Table 6.4 gives the decomposition of the various spherical harmonics for angular momentum $\ell \leq 15$ into irreducible

representations of the cubic group O_h. We note that the lowest angular momentum state to contain the A_{1g} irreducible representation of O_h is $\ell = 4$, consistent with Eq. (6.9). The corresponding table for icosahedral symmetry is Table 6.5, where it is seen that the angular momentum state for $\ell = 6$ is the lowest ℓ value to contain the A_{1g} irreducible representation of the I_h group.

6.6 Characters for Other Symmetry Operators in the Rotation Group

In dealing with the symmetry operations of the full rotation group, the inversion operation frequently occurs. This operation also occurs in the lower symmetry point groups either as a separate operation i or in conjunction with other compound operations (e.g., $S_6 = i \otimes C_3^{-1}$). A compound operation (like an improper rotation or a mirror plane) can be represented as a product of a proper rotation followed by inversion. The character for the inversion operation is $+1$ for <u>even</u> angular momentum states ($\ell =$ even in $Y_{\ell,m}(\theta, \phi)$) and -1 for <u>odd</u> angular momentum states (see Eq. 6.3). This idea of compound operations will become clearer after we have discussed in Chapter 7 the direct product groups and direct product representations. A listing of the decompositions of the spherical harmonics for various ℓ values into irreducible representations of the icosahedral is given below (for $\ell \leq 6$) and in Table 6.5 for higher values of $\ell \leq 10$.

$$
\begin{aligned}
\Gamma_{\ell=0} &\longrightarrow (A_g)_{I_h} \\
\Gamma_{\ell=1} &\longrightarrow (F_{1u})_{I_h} \\
\Gamma_{\ell=2} &\longrightarrow (H_g)_{I_h} \\
\Gamma_{\ell=3} &\longrightarrow (F_{2u})_{I_h} + (G_u)_{I_h} \\
\Gamma_{\ell=4} &\longrightarrow (G_g)_{I_h} + (H_g)_{I_h} \\
\Gamma_{\ell=5} &\longrightarrow (F_{1u})_{I_h} + (G_u)_{I_h} \\
\Gamma_{\ell=6} &\longrightarrow (A_{1g})_{I_h} + (G_g)_{I_h}
\end{aligned}
\tag{6.29}
$$

Table 6.4: Splitting of angular momentum in cubic symmetry O_h.

ℓ	A_{1g}	A_{2g}	E_g	T_{1g}	T_{2g}	A_{1u}	A_{2u}	E_u	T_{1u}	T_{2u}
0	1									
1									1	
2			1		1					
3							1		1	1
4	1		1	1	1					
5								1	2	1
6	1	1	1	1	2					
7							1	1	2	2
8	1		2	2	2					
9						1	1	1	3	2
10	1	1	2	2	3					
11							1	2	3	3
12	2	1	2	3	3					
13						1	1	2	4	3
14	1	1	3	3	4					
15						1	2	2	4	4

Table 6.5: Splitting of angular momentum in icosahedral symmetry I_h.

ℓ	A_g	T_{1g}	T_{2g}	G_g	H_g	A_u	T_{1u}	T_{2u}	G_u	H_u
0	1									
1							1			
2					1					
3								1	1	
4				1	1					
5							1	1		1
6	1	1		1	1					
7							1	1	1	1
8			1	1	2					
9							1	1	2	1
10	1	1	1	1	2					

6.7   Selected Problems

1. Consider the hydrogen atom, described by the Schrödinger equation

$$\mathcal{H}\Psi_{n\ell m} = \left\{ -\frac{\hbar^2}{2m}\nabla_r^2 - \frac{L^2}{r^2} + V(r) \right\}\Psi_{n\ell m} = E_{n\ell}\Psi_{n\ell m}$$

   (a) Does $\mathcal{H}$ commute with any arbitrary rotation about the origin? Explain your answer.

   (b) If the electron is in a d-orbital ($\ell = 2$) described by the eigenfunction

$$\Psi_{n2m}(r, \theta, \phi) = R_n(r)Y_{2,m}(\theta, \phi)$$

   where $Y_{2,m}(\theta, \phi)$ is a spherical harmonic for $\ell = 2$. What is the effect on $\Psi_{n2m}(r, \theta, \phi)$ of rotating the system by θ around the origin? Is the new wave function still an eigenfunction of the Hamiltonian with the same eigenvalue? Explain.

2. Suppose that an iron (Fe) impurity is introduced into a two-dimensional honeycomb lattice of an insulating host material. A honeycomb lattice is a hexagonal lattice with atoms at the hexagon corners but not at the center. Suppose that the Fe impurity is placed first in a substitutional location and second in an interstitial location at the center of the hexagon.
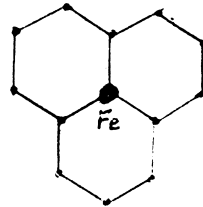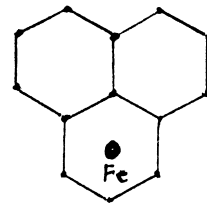
substitutional   interstitial

   (a) What is the difference in crystal potential (include only nearest neighbors) between the substitutional and interstitial locations?

(b) For the interstitial case, express your result in part (a) in terms of spherical harmonics for the lowest order terms with angular dependencies.

(c) What is the proper point group symmetry and character table in each case?

(d) Give the crystal field splitting of the 5-fold d-levels of the Fe impurity in the crystal fields in part (a).

(e) Identify the basis functions associated with each of the levels in part (d).

(f) Since the bonding orbitals lie lower in energy than the antibonding orbitals, indicate how the ordering of the levels might indicate whether the Fe impurity is located substitutionally or interstitially in the honeycomb lattice.

3. Suppose that an iron (Fe) impurity is introduced into a substitutional site in the high T_c superconductor $YCu_2Ba_3O_7$. Assume that the material is in the tetragonal phase ($a = b \neq c$).

(a) What is the difference in crystal potential (include only nearest neighbors) between substitutional and interstitial sites?

(b) What is the proper point group symmetry and character table for a single molecule of $YCu_2Ba_3O_7$?

(c) Give the crystal field splitting of the 5-fold d-levels of the Fe impurity in the crystal field in (a). Consider all three cases regarding the relative size of the crystal field and the spin-orbit interaction.

(d) Identify the basis functions associated with each of the levels of the Fe impurity in (a).

(e) Suppose that you measure the reflectivity of this material with polarized light and determine the energy levels. How could you distinguish if the Fe impurity is in a Cu(1) site, a Cu(2) site or an Y site, making use of the crystal symmetry?

4. Show (by finding the characters of the rotation group) that the d-level for a transition metal impurity in a metal cluster with I_h point symmetry is not split by the icosahedral crystal field.

Chapter 7

Application of Group Theory to Selection Rules and Direct Products

Our second general application of group theory to physical problems will be to selection rules. In considering selection rules we always involve some interaction $\mathcal{H}'$ matrix that couples two states ψ_α and ψ_β. Group theory is often invoked to decide whether or not these states are indeed coupled and this is done by testing whether or not the matrix element $(\psi_\alpha, \mathcal{H}'\psi_\beta)$ vanishes by symmetry. The simplest case to consider is the one where the perturbation $\mathcal{H}'$ does not destroy the symmetry operations of the group of the Schrödinger equation. Since these matrix elements transform as scalars (numbers), $(\psi_\alpha, \mathcal{H}'\psi_\beta)$ must exhibit the full group symmetry, and must transform as the fully symmetric representation Γ_1. These matrix elements of the interaction Hamiltonian must be invariant under all the symmetry operations of the group of Schrödinger's equation. Thus, if $(\psi_\alpha, \mathcal{H}'\psi_\beta)$ does not transform as a number, it vanishes. To exploit these symmetry properties, we thus choose ψ_α^* and ψ_β to be symmetry eigenfunctions for the unperturbed Hamiltonian - i.e., basis functions for irreducible representations of the group of Schrödinger's equation. We then determine how $\mathcal{H}'\psi_\beta$ transforms - i.e., according to which irreducible representations of the group. (This involves the direct product of two representations and the theory behind the direct product of two repre-

sentations will be given in this chapter.) If $\mathcal{H}'\psi_\beta$ is orthogonal to ψ_α, then the matrix element vanishes by symmetry; otherwise the matrix element need not vanish, and the transition may occur.

In considering various selection rules that arise in physical problems, we often have to consider matrix elements of a perturbation Hamiltonian which lowers the symmetry of the unperturbed problem, as for example $\mathcal{H}'_{\text{em}}$ describing the electromagnetic field

$$\mathcal{H}'_{\text{em}} = \left(-\frac{e}{mc} \right) \vec{p} \cdot \vec{A}. \tag{7.1}$$

Such a perturbation Hamiltonian is generally <u>not</u> invariant under the symmetry operations of the group of Schrödinger's equation which is determined by the unperturbed Hamiltonian $\mathcal{H}_0$. Therefore we must consider the transformation properties of $\mathcal{H}'\psi_\beta$ where ψ_β is an eigenfunction that is chosen to transform as one partner $\psi_j^{(\Gamma_i)}$ of an irreducible representation Γ_i of the unperturbed Hamiltonian $\mathcal{H}_0$. In general, the action of $\mathcal{H}'$ on $\psi_j^{(\Gamma_i)}$ will mix in all other partners of the representation Γ_i since any arbitrary function can be expanded in terms of a complete set of functions such as the $\psi_j^{(\Gamma_i)}$. In group theory, the transformation properties of $\mathcal{H}'\psi_j^{(\Gamma_i)}$ are handled through what is called the direct product. Even though $\mathcal{H}'$ need not transform as the totally symmetric representation (e.g., $\mathcal{H}'_{\text{em}}$ transforms as a vector x, y, z), the matrix element $(\psi_i(\Gamma_i), \mathcal{H}'\psi_j(\Gamma_i))$ may not vanish, since it may contain a term that transforms as a scalar (number).

The discussion of the selection rules in this chapter is organized around the following topics:

1. Summary of the important symmetry rules for basis functions

2. Theory of the Direct Product of Groups and Representations

3. The Selection Rule concept in Group Theoretical Terms

4. Example of Selection Rules for electric dipole transitions in a system with O_h symmetry.

7.1 Summary of Important Results for Basis Functions

The basis functions $\psi_\alpha^{(i)}$ for a given irreducible representation i are defined by (see Eq. 4.1 of notes):

$$\hat{P}_R \psi_\alpha^{(i)} = \sum_{j=1}^{\ell_i} \psi_j^{(i)} D^{(i)}(R)_{j\alpha} \tag{7.2}$$

where $\hat{P}_R$ is the symmetry operator, $\psi_\alpha^{(i)}$ denotes the basis functions for an l_i-dimensional irreducible representation (i) and $D^{(i)}(R)_{j\alpha}$ is the matrix representation for symmetry element R in irreducible representation (i).

To exploit the symmetry properties of a given problem, we want to find eigenfunctions which form basis functions for the irreducible representations of the group of Schrödinger's equation. We can find such eigenfunctions using the symmetry operator and projection operator techniques discussed in §4.1 and §4.3. In this chapter, we will then assume that the eigenfunctions have been chosen to transform as irreducible representations of the group of Schrödinger's equation for $\mathcal{H}_0$. The application of group theory to selection rules then depends on the following orthogonality theorem. This orthogonality theorem can be considered as the selection rule for the identity operator.

Theorem: Two basis functions which belong either to different irreducible representations or to different columns (rows) of the same representation are orthogonal.

Proof: Let $\phi_\alpha^{(i)}$ and $\psi_{\alpha'}^{(i')}$ be two basis functions belonging respectively to irreducible representations (i) and (i') and corresponding to columns α and α' of their respective representations. By definition:

$$\begin{aligned}
\hat{P}_R \phi_\alpha^{(i)} &= \sum_{j=1}^{\ell_i} \phi_j^{(i)} D^{(i)}(R)_{j\alpha} \\
\hat{P}_R \psi_{\alpha'}^{(i')} &= \sum_{j'=1}^{\ell_{i'}} \psi_{j'}^{(i')} D^{(i')}(R)_{j'\alpha'}.
\end{aligned} \tag{7.3}$$

Because the scalar product (or the matrix element of unity taken between the two states) is independent of coordinate system, we can write the scalar product:

$$
\begin{aligned}
(\phi_\alpha^{(i)}, \psi_{\alpha'}^{(i')}) &= (\hat{P}_R)\phi_\alpha^{(i)}, \hat{P}_R\psi_{\alpha'}^{(i')}) \\
&= \sum_{j,j'} D^{(i)}(R)_{j\alpha}^* D^{(i')}(R)_{j'\alpha'}(\phi_j^{(i)}, \psi_{j'}^{(i')}) \\
&= \frac{1}{h}\sum_{j,j'}\sum_{R} D^{(i)}(R)_{j\alpha}^* D^{(i')}(R)_{j'\alpha'}(\phi_j^{(i)}, \psi_{j'}^{(i')}) \quad (7.4)
\end{aligned}
$$

since the left hand side of Eq. 7.4 is independent of R, and h is the order of the group. Now apply the Wonderful Orthogonality Theorem

$$
\frac{1}{h}\sum_{R} D^{(i)}(R)_{j\alpha}^* D^{(i')}(R)_{j'\alpha'} = \frac{1}{\ell_i}\delta_{ii'}\delta_{jj'}\delta_{\alpha\alpha'} \qquad (7.5)
$$

to Eq. 7.4, which yields:

$$
(\phi_\alpha^{(i)}, \psi_{\alpha'}^{(i')}) = \frac{1}{\ell_i}\delta_{i,i'}\delta_{\alpha,\alpha'}\sum_{j=1}^{\ell_i}(\phi_j^{(i)}, \psi_j^{(i)}). \qquad (7.6)
$$

Thus according to Eq. 7.6, if the basis functions $\phi_\alpha^{(i)}$ and $\psi_{\alpha'}^{(i')}$ correspond to two different irreducible representations $i \neq i'$ they are orthogonal. If they correspond to the same representation $(i = i')$, they are still orthogonal <u>if</u> they correspond to different columns (or rows) – i.e., if they correspond to different partners. We further note that the right hand side of Eq. 7.6 is independent of α so that the **scalar product is the same for all components** α, thereby completing the proof.

In general, selection rules deal with the matrix elements of an operator different from the identity operator. Clearly if the operator is invariant under all of the symmetry operations of the group of Schrödinger's equation then it transforms like the identity operator. For example, if

$$
\mathcal{H}_0\psi_{\alpha'}^{(i')} = E_{\alpha'}^{(i')}\psi_{\alpha'}^{(i')} \qquad (7.7)
$$

then $E_{\alpha'}^{(i')}$ is a number which is independent of any coordinate system. If $\psi_{\alpha'}^{(i')}$ and $\phi_{\alpha}^{(i)}$ are both eigenfunctions of the Hamiltonian $\mathcal{H}_0$ and are also basis functions for irreducible representations (i') and (i), then the **matrix element** $(\phi_{\alpha}^{(i)}, \mathcal{H}_0 \psi_{\alpha'}^{(i')})$ vanishes unless $i = i'$ and $\alpha = \alpha'$, which is a result familiar to us from quantum mechanics. In the more general case when we have a perturbation $\mathcal{H}'$, the perturbation need not have the full symmetry of $\mathcal{H}_0$. In general $\mathcal{H}'\psi$ **transforms differently from** ψ.

7.2 Direct Product of Two Groups

We now define the **direct product of two groups.** Let $G_A = E, A_2, \ldots, A_{h_a}$ and $G_B = E, B_2, \ldots, B_{h_b}$ be two groups such that all operators A_R commute with all operators B_S. Then the direct product group is

$$G_A \otimes G_B = E, A_2, \ldots, A_{h_a}, B_2, A_2 B_2, \ldots, A_{h_a} B_2, \ldots, A_{h_a} B_{h_b} \quad (7.8)$$

and has $(h_a \times h_b)$ elements. It is easily shown that if G_A and G_B are groups, then the direct product group $G_A \otimes G_B$ is a group. Examples of direct product groups that are frequently encountered involve products of groups with the group of inversions (group C_i with two elements E, i) and reflections (group C_σ with two elements E, σ). For example, we can make a direct product group D_{3d} from the group D_3 by compounding all the operations of D_3 with (E, i) where i is the inversion operation (see Table 3.30). An example of the group D_{3d} is a triangle with finite thickness. We write the direct product group when compounding the initial group with the inversion operation

$$D_{3d} = D_3 \otimes i \quad (7.9)$$

or with the mirror reflection in a horizontal plane (see Table 3.31):

$$D_{3h} = D_3 \otimes \sigma. \quad (7.10)$$

The full cubic group O_h is a direct product group of $O \otimes i$.

7.3   Direct Product of Two Irreducible Representations

In addition to **direct product groups** we have the **direct product of two representations** which is defined in terms of the direct product of two matrices. From algebra, we have the definition of the direct product of two matrices $A \otimes B = C$, whereby every element of A is multiplied by every element of B. Thus, the direct product matrix C has a double set of indices

$$A_{ij}B_{k\ell} = C_{ik,j\ell} \tag{7.11}$$

Thus, if A is a (2×2) matrix and B is a (3×3) matrix, then C is a (6×6) matrix.

Theorem: The direct product of the representations of the groups A and B forms a representation of the direct product group.

Proof: To prove this theorem we need to show that

$$D^{a\otimes b}(A_k B_\ell) \, D^{a\otimes b}(A_{k'} B_{\ell'}) = D^{a\otimes b}(A_i B_j) \tag{7.12}$$

where

$$A_i = A_k A_{k'} \qquad B_j = B_\ell B_{\ell'}. \tag{7.13}$$

Since the elements of group A commute with those of group B by the definition of the direct product group, the multiplication property of elements in the direct product group is

$$A_k B_\ell \, A_{k'} B_{\ell'} = A_k A_{k'} \, B_\ell B_{\ell'} = A_i B_j \tag{7.14}$$

where $A_k B_\ell$ is a typical element of the direct product group. We must now show that the representations reproduce this multiplication property. By definition:

$$D^{a\otimes b}(A_k B_\ell) \, D^{a\otimes b}(A_{k'} B_{\ell'}) = \Big[D^{(a)}(A_k) \otimes D^{(b)}(B_\ell) \Big] \Big[D^{(a)}(A_{k'}) \otimes D^{(b)}(B_{\ell'}) \Big].$$
$$\tag{7.15}$$

To proceed with the proof, we write Eq. (7.15) in terms of components:

$$
\begin{aligned}
&\left[D^{a\otimes b}(A_k B_\ell) D^{a\otimes b}(A_{k'} B_{\ell'}) \right]_{ip,jq} \\
&= \sum_{sr} \left(D^{(a)}(A_k) \otimes D^{(b)}(B_\ell) \right)_{ip,sr} \quad \times \left(D^{(a)}(A_{k'}) \otimes D^{(b)}(B_{\ell'}) \right)_{sr,jq} \\
&\qquad = \sum_s D^{(a)}_{is}(A_k) D^{(a)}_{sj}(A_{k'}) \quad \times \sum_r D^{(b)}_{pr}(B_\ell) D^{(b)}_{rq}(B_{\ell'}) \\
&\qquad\qquad = D^{(a)}_{ij}(A_i) D^{(b)}_{pq}(B_j) \quad = \left(D^{(a\otimes b)}(A_i B_j) \right)_{ip,jq}
\end{aligned}
$$
$$(7.16)$$

This completes the proof.

It can be further shown that the direct product of two <u>irreducible</u> representations of groups G_A and G_B yields an <u>irreducible</u> representation of the direct product group so that all irreducible representations of the direct product group can be generated from the irreducible representations of the original groups before they are joined. We can also take direct products between 2 representations of the same group. Essentially the same proof as given in this section shows that the direct product of two representations of the same group is also a representation of that group, though in general, it is a reducible representation. The proof proceeds by showing

$$
[D^{(\ell_1 \otimes \ell_2)}(A) D^{(\ell_1 \otimes \ell_2)}(B)]_{ip,jq} = D^{(\ell_1 \otimes \ell_2)}(AB)_{ip,jq} \qquad (7.17)
$$

where ℓ_1 and ℓ_2 denote irreducible representations with the corresponding dimensionalities. The direct product representation $D^{(\ell_1 \otimes \ell_2)}(R)$ will in general be reducible even though ℓ_1 and ℓ_2 are irreducible.

7.4 Characters for the Direct Product of Groups and Representations

In this section we find the characters for direct product groups and representations.

Theorem: The simplest imaginable formulae are assumed by the characters in direct product groups or in taking the direct product of two representations.

1. If the direct product occurs between two groups, then the characters for the irreducible representations in the direct product group are obtained by multiplication of the characters of the irreducible representations of the original groups according to:

$$\chi^{(a\otimes b)}(A_k B_\ell) = \chi^{(a)}(A_k)\, \chi^{(b)}(B_\ell) \qquad (7.18)$$

2. If the direct product is taken between two representations of the same group, then the character for the direct product representation is written as

$$\chi^{(\ell_1\otimes\ell_2)}(R) = \chi^{(\ell_1)}(R)\, \chi^{(\ell_2)}(R). \qquad (7.19)$$

Proof: Consider the diagonal matrix element of an element in the direct product group. From the definition of the direct product of two groups, we write

$$D^{(a\otimes b)}(A_k B_\ell)_{ip,jq} = D_{ij}^{(a)}(A_k)D_{pq}^{(b)}(B_\ell). \qquad (7.20)$$

Taking the diagonal matrix elements of Eq. 7.20 and summing over these matrix elements, we obtain

$$\sum_{ip} D^{(a\otimes b)}(A_k B_\ell)_{ip,ip} = \sum_{i} D_{ii}^{(a)}(A_k) \sum_{p} D_{pp}^{(b)}(B_\ell) \qquad (7.21)$$

which can be written in terms of the traces:

$$\chi^{(a\otimes b)}(A_k B_\ell) = \chi^{(a)}(A_k)\chi^{(b)}(B_\ell). \qquad (7.22)$$

This completes the proof of the theorem for the direct product of two groups.

The result of Eq. 7.22 holds equally well for classes (i.e., $R \to \mathcal{C}$), and thus can be used to find the character tables for direct product groups as is explained below.

Exactly the same proof as given above can be applied to find for the direct product of two representations of the same group

$$\chi^{(\ell_1 \otimes \ell_2)}(R) = \chi^{(\ell_1)}(R)\chi^{(\ell_2)}(R). \qquad (7.23)$$

The direct product representation is irreducible only if $\chi^{(\ell_1 \otimes \ell_2)}$ is identical to one of the irreducible representations of the group $\ell_1 \otimes \ell_2$. In general, if we take the direct product between 2 irreducible representations of a group, then the resulting direct product representation will be reducible. If it is reducible, the direct product can then be written as a linear combination of the irreducible representations of the group:

$$\chi^{(\lambda)}(R)\chi^{(\mu)}(R) = \sum_{\nu} a_{\lambda\mu\nu}\chi^{(\nu)}(R) \qquad (7.24)$$

where from Eq. 3.20 we can write the coefficients $a_{\lambda\mu\nu}$ as:

$$a_{\lambda\mu\nu} = \frac{1}{h}\sum_{\mathcal{C}_\alpha} N_{\mathcal{C}_\alpha}\left[\chi^{(\lambda)}(\mathcal{C}_\alpha)\chi^{(\mu)}(\mathcal{C}_\alpha)\right]\chi^{(\nu)}(\mathcal{C}_\alpha)^* \qquad (7.25)$$

where $\mathcal{C}_\alpha$ denotes classes and $N_{\mathcal{C}_\alpha}$ denotes the number of elements in class $\mathcal{C}_\alpha$. In applications of group theory to selection rules, constant use is made of Eqs. 7.24 and 7.25.

Finally we use the result of Eq. 7.22 to show how the character tables for the original groups G_A and G_B are used to form the character table for the direct product group. First we form the elements and classes of the direct product group and then we use the character tables of G_A and G_B to form the character table for $G_A \otimes G_B$. In many important cases one of the groups (e.g., G_B) has only two elements (such as the group C_i with elements E, i) and two irreducible representations Γ_1 with characters $(1,1)$ and $\Gamma_{1'}$ with characters $(1,-1)$. We illustrate such a case below for the direct product group $C_{4h} = C_4 \otimes i$. In the character table for group C_{4h} shown below we use the notation g to denote representations that are even (German, gerade) under inversion, and u to denote representations that are odd (German, ungerade) under inversion.

$$C_{4h} \equiv C_4 \otimes i \quad (4/m)$$

	E	C_2	C_4	C_4^3	i	iC_2	iC_4	iC_4^3	
A_g	1	1	1	1	1	1	1	1	
B_g	1	1	-1	-1	1	1	-1	-1	even under
E_g	1	-1	i	$-i$	1	-1	i	$-i$	inversion (g)
	1	-1	$-i$	i	1	-1	$-i$	i	
A_u	1	1	1	1	-1	-1	-1	-1	
B_u	1	1	-1	-1	-1	-1	1	1	odd under
E_u	1	-1	i	$-i$	-1	1	$-i$	i	inversion (u)
	1	-1	$-i$	i	-1	1	i	$-i$	

We note that the upper left hand quadrant contains the character table for the group C_4. The 4 classes obtained by multiplication of the classes of C_4 by i are listed on top of the upper right columns. The characters in the upper right hand and lower left hand quadrants are the same as in the upper left hand quadrant, while the characters in the lower right hand quadrant are all multiplied by (-1) to produce the odd (ungerade) irreducible representations.

7.5   The Selection Rule Concept in Group Theoretical Terms

Having considered the background for taking direct products, we are now ready to consider the selection rules for the matrix element

$$(\psi_{\alpha'}^{(i')}, \mathcal{H}' \phi_\alpha^{(i)}). \tag{7.26}$$

This matrix element can be computed by integrating the indicated scalar product over all space. Group theory then tells us that when any or all the symmetry operations of the group are applied, this **matrix element must transform as a constant**. Conversely, if the matrix element is not invariant under the symmetry operations which form the group of Schrödinger's equation, then the matrix element must vanish. We will now express the same physical concepts in terms of the direct product formalism.

Let the wave functions $\phi_\alpha^{(i)}$ and $\psi_{\alpha'}^{(i')}$ transform, respectively, as partners α and α' of irreducible representations Γ_i and $\Gamma_{i'}$, and let $\mathcal{H}'$ transform as representation Γ_j. Then if the direct product $\Gamma_j \otimes \Gamma_i$ is orthogonal to $\Gamma_{i'}$ the matrix element vanishes, or equivalently if $\Gamma_{i'} \otimes \Gamma_j \otimes \Gamma_i$ does not contain the fully symmetrical representation Γ_1, the matrix element vanishes. In particular, if $\mathcal{H}'$ transforms as Γ_1 (i.e., the perturbation does not lower the symmetry of the system), then $\phi_\alpha^{(i)}$ and $\psi_{\alpha'}^{(i')}$ must correspond to the same irreducible representation and the same partners of that representation because of the orthogonality theorem for basis functions.

To illustrate the meaning of these statements for a more general case, we will apply these selection rule concepts to the case of electric dipole transitions in §7.6 below. First we express the perturbation $\mathcal{H}'$ (in this case due to the electromagnetic field) in terms of the irreducible representations that $\mathcal{H}'$ contains in the group of Schrödinger's equation:

$$\mathcal{H}' = \sum_{j,\beta} f_\beta^{(j)} \mathcal{H}_\beta'^{(j)} \tag{7.27}$$

where j denotes the irreducible representations Γ_j of the Hamiltonian $\mathcal{H}'$ and β denotes the partners of Γ_j. Then $\mathcal{H}'\phi_\alpha^{(i)}$ transforms as the direct product representation formed by taking direct products $\mathcal{H}_\beta'^{(j)} \otimes \phi_\alpha^{(i)}$ in accordance with Eq. 7.27. The matrix element $(\psi_{\alpha'}^{(i')}, \mathcal{H}'\phi_\alpha^{(i)})$ vanishes if and only if $\psi_{\alpha'}^{(i')}$ is orthogonal to all the basis functions that occur in the decomposition of $\mathcal{H}'\phi_\alpha^{(i)}$ into irreducible representations. An equivalent expression of the same concept is obtained by considering the triple direct product $\psi_{\alpha'}^{(i')} \otimes \mathcal{H}_\beta'^{(j)} \otimes \phi_\alpha^{(i)}$. In order for the matrix element in Eq. 7.26 to be non-zero, this triple direct product must contain a term that transforms as a scalar or a constant number – i.e., according to the irreducible representation Γ_1.

7.6 Example of Selection Rules for Electric Dipole Transitions in a System with O_h Symmetry

The electromagnetic interaction giving rise to electric dipole transitions is

$$\mathcal{H}'_{\text{em}} = -\frac{e}{2mc}\vec{p}\cdot\vec{A} \qquad (7.28)$$

in which $\vec{p}$ is the momentum of the electron and $\vec{A}$ is the vector potential of an external electromagnetic field. The momentum operator is part of the physical "system" under consideration while the vector $\vec{A}$ acts like the "bath" or "reservoir" in a thermodynamic sense. Thus $\vec{p}$ acts like an operator with respect to Schrödinger's equation but $\vec{A}$ does not. Therefore, in terms of group theory, $\mathcal{H}'_{\text{em}}$ for the electromagnetic interaction transforms like a vector in the context of the group of Schrödinger's equation for the unperturbed system $\mathcal{H}_0\psi = E\psi$. If we have unpolarized radiation, we must then consider all three components of the vector $\vec{p}$ (i.e., p_x, p_y, p_z). In cubic symmetry, all 3 components of the vector transform as the same irreducible representation. If instead we had a system which exhibits tetragonal symmetry, then p_x and p_y would transform as one of the two-dimensional irreducible representations and p_z would transform as one of the one-dimensional irreducible representations.

To find the particular irreducible representations that are involved in cubic symmetry we consult the character table for $O_h = O \otimes i$. In the cubic group O_h the vector (x, y, z) transforms according to the irreducible representation T_{1u} and so does (p_x, p_y, p_z), because both are radial vectors and both are odd under inversion. We note that the character table for O_h (Table 3.33) gives the irreducible representation for vectors, and the same is true for most of the other character tables in Chapter 3. To obtain the character table for the direct product group $O_h = O \otimes i$ we note that each symmetry operation in O is also compounded with E and i to yield 48 symmetry operations and 10 classes.

For the O_h group there will then be 10 irreducible representations, 5 of which are even and 5 are odd. For the even irreducible represen-

Table 7.1: Character Table for O (432)

$O(432)$		E	$8C_3$	$3C_2 = 3C_4^2$	$6C_2$	$6C_4$
	A_1	1	1	1	1	1
	A_2	1	1	1	−1	−1
$(x^2 - y^2, 3z^2 - r^2)$	E	2	−1	2	0	0
$\left.\begin{array}{l}(R_x, R_y, R_z) \\ (x, y, z)\end{array}\right\}$	T_1	3	0	−1	−1	1
(xy, yz, zx)	T_2	3	0	−1	1	−1

$$O_h = O \otimes i$$

tations, the same characters are obtained for class $\mathcal{C}$ and class $i\mathcal{C}$. For the odd representations the characters for $\mathcal{C}$ and $i\mathcal{C}$ have opposite signs. Even representations are denoted by the subscript g and odd representations by the subscript u. The radial vector $\mathbf{p}$ transforms as an odd irreducible representation since $\mathbf{p} \to -\mathbf{p}$ under inversion.

To find selection rules we must also specify the initial and final states. For example, if the system is initially in a state with symmetry T_{2g} then the direct product $\mathcal{H}'_{\text{em}} \otimes \psi_{T_{2g}}$ contains the irreducible representations found by taking the direct product $\chi_{T_{1u}} \otimes \chi_{T_{2g}}$. The characters for $\chi_{T_{1u}} \otimes \chi_{T_{2g}}$ are given below:

E	$8C_3$	$3C_2$	$6C_2$	$6C_4$	i	$8iC_3$	$3iC_2$	$6iC_2$	$6iC_4$
9	0	1	−1	−1	−9	0	−1	1	1

We consider $\chi_{T_{1u}} \otimes \chi_{T_{2g}}$ as a reducible representation of the group O_h. Then using the decomposition formula Eq. 7.25 yields:

$$T_{1u} \otimes T_{2g} = A_{2u} + E_u + T_{1u} + T_{2u}. \tag{7.29}$$

Thus we obtain the selection rules that electric dipole transitions to a state T_{2g} can only be made from states with A_{2u}, E_u, T_{1u}, and T_{2u} symmetry. Furthermore, since $\mathcal{H}'_{\text{em}}$ is an odd function, electric dipole transitions will couple only states with opposite parity. The same arguments as given above can be used to find selection rules between any

initial and final states for the case of cubic symmetry. For example, from Table 7.1, we can write the following direct products as:

$$\left.\begin{array}{l} E_g \otimes T_{1u} = T_{1u} + T_{2u} \\ T_{1u} \otimes T_{1u} = A_{1g} + E_g + T_{1g} + T_{2g} \end{array}\right\}.$$

Suppose that we now consider the situation where we lower the symmetry from O_h to D_{4h}. Referring to the character table for D_4 in Table 3.26 and below, we can form the direct product group D_{4h} by taking the direct product $D_{4h} = D_4 \otimes i$.

D_4 (422)			E	$C_2 = C_4^2$	$2C_4$	$2C_2'$	$2C_2''$
$x^2 + y^2, z^2$		A_1	1	1	1	1	1
	R_z, z	A_2	1	1	1	−1	−1
$x^2 - y^2$		B_1	1	1	−1	1	−1
xy		B_2	1	1	−1	−1	1
(xz, yz)	$\left.\begin{array}{l}(x, y) \\ (R_x, R_y)\end{array}\right\}$	E	2	−2	0	0	0

We note here the important result that the vector in $D_{4h} = D_4 \otimes i$ symmetry does not transform as a single irreducible representation but rather as the irreducible representations:

$$\left.\begin{array}{l} z \rightarrow A_{2u} \\ (x, y) \rightarrow E_u \end{array}\right\}$$

so that T_{1u} in O_h symmetry goes into: $A_{2u} + E_u$ in D_{4h} symmetry.

Furthermore a state with symmetry T_{2g} in the O_h group goes into states with $E_g + B_{2g}$ symmetries in D_{4h} (see discussion in §6.4). Thus for the case of the D_{4h} group, electric dipole transitions will only couple an A_{1g} state to states with E_u and A_{2u} symmetries. For a state with E_g symmetry according to group D_{4h} the direct product with the vector yields

$$E_g \otimes (A_{2u} + E_u) = E_u + (A_{1u} + A_{2u} + B_{1u} + B_{2u}), \qquad (7.30)$$

so that for the D_{4h} group, electric dipole transitions from an E_g state can be made to any odd parity state. This analysis points out that as

we reduce the amount of symmetry, there are fewer selection rules and more transitions become allowed.

Polarization effects also are significant when considering selection rules. For example, if the electromagnetic radiation is polarized along the z direction in the case of the D_{4h} group, then the electromagnetic interaction involves only p_z which transforms according to A_{2u}. With the p_z polarization, the following states are coupled by electric dipole radiation (i.e., by matrix elements of p_z):

initial state	final state
A_{1g}	A_{2u}
A_{2g}	A_{1u}
B_{1g}	B_{2u}
B_{2g}	B_{1u}
E_g	E_u
A_{1u}	A_{2g}
A_{2u}	A_{1g}
B_{1u}	B_{2g}
B_{2u}	B_{1g}
E_u	E_g

If, on the other hand, the radiation is polarized in the x direction, then the basis function is a single partner x of the E_u representation. Then if the initial state has A_{1g} symmetry, the electric dipole transition will be to a state which transforms as the x partner of the E_u representation. If the initial state has A_{2u} symmetry (transforms as z), then the general selection rule gives $A_{2u} \otimes E_u = E_g$ while polarization considerations indicate that the transition couples the A_{2u} level with the xz partner of the E_g representation. If the initial state has E_u symmetry, the general selection rule gives

$$(E_u \otimes E_u) = A_{1g} + A_{2g} + B_{1g} + B_{2g}. \tag{7.31}$$

The polarization x couples the partner E_u^x to $A_{1g}^{x^2+y^2}$ and $B_{1g}^{x^2-y^2}$ while the partner E_u^y couples to A_{2g}^{xy-yx} and B_{2g}^{xy}. Thus polarization effects further restrict the states that are coupled in electric dipole transitions. If the polarization direction is not along one of the (x, y, z) directions,

$\mathcal{H}'_{\text{em}}$ will transform as a linear combination of the irreducible representations $A_{2u} + E_u$ even though the incident radiation is polarized.

Selection rules can be applied to a variety of perturbations $\mathcal{H}'$ other than the electric dipole interactions, such as uniaxial stress, hydrostatic pressure and the magnetic dipole interaction. In these cases, the special symmetry of $\mathcal{H}'$ in the group of Schrödinger's equation must be considered.

7.7   Selected Problems

1. (a) The (2×2) matrices B and C form the direct product $A = B \otimes C$, where

$$B = \begin{pmatrix} b_{11} & b_{12} \\ b_{21} & b_{22} \end{pmatrix} \qquad \text{and} \qquad C = \begin{pmatrix} c_{11} & c_{12} \\ c_{21} & c_{22} \end{pmatrix}$$

to give a 4×4 matrix labeled A.

   (b) Show that if G_A with elements $E, A_2, \ldots, A_{h_a}$ and G_B with elements $E, B_2, \ldots, B_{h_b}$ are groups, then the direct product group $G_A \otimes G_B$ is also a group. Use the notation $B_{ij}C_{kl} = (B \otimes C)_{ik,jl}$ to label the rows and columns of the direct product matrix.

   (c) In going from higher to lower symmetry, if the inversion operation is preserved, show that even representations remain even and the odd representations remain odd.

2. (a) Consider electric dipole transitions in full cubic O_h symmetry for transitions between an initial state with A_{1g} symmetry (s-state) and a final state with T_{1u} symmetry (p-state). [Note that one of these electric dipole matrix elements is proportional to a term $(1|p_x|x)$, where $|1)$ denotes the s-state and $|x)$ denotes the x partner of the p-state.] Of the 9 possible matrix elements that can be formed, how many are non-vanishing? Of those that are non-vanishing, how many are equivalent?

(b) If the initial state has E_g symmetry (rather than A_{1g} symmetry), repeat part (a). You will find it convenient to use as basis functions for the E_g level the two partners $x^2 + \omega y^2 + \omega^2 z^2$ and $x^2 + \omega^2 y^2 + \omega z^2$ where $\omega = \exp(2\pi i/3)$.

(c) Repeat part (a) for the case of electric dipole transitions from an s-state to a p-state in tetragonal D_{4h} symmetry. Consider the light polarized first along the z direction and then in the $x - y$ plane. Note that as the symmetry is lowered, the selection rules become less stringent.

Chapter 8

Electronic States of Molecules and Directed Valence

In this chapter we consider the electronic states of molecules, the formation of molecular bonds and the simplifications that are introduced through the use of group theory. We organize our discussion in this chapter in terms of a general discussion of molecular energy levels; the general concept of equivalence; the concept of directed valence bonding; the application of the directed valence bond concept to various molecules, including H_2, CO, NH_3, CH_4, "SH_6", SF_6, and $B_{12}H_{12}$; bond strengths in directed valence bonds; and finally σ and π bonding.

8.1 Introduction

The energy levels of molecules are basically more complicated than those for atoms because:

1. there are several centers of positive charge which serve to attract a given electron,

2. these center are themselves in relative motion.

Since the nuclei are very massive relative to the electrons, we can utilize the Born-Oppenheimer approximation which separates out the

electronic motion from the nuclear or ionic motion. In this approximation, the electrons move in a potential generated by the equilibrium positions of the nuclei. As for the nuclei, they can be involved in some form of relative motion, giving rise to molecular vibrations in the isolated molecules or to lattice modes in the solid. Also possible in the case of isolated molecules are molecular rotations or translations. Since the translational motion corresponds to plane wave solutions and the eigenvalues form a continuous spectrum, these solutions do not give rise to molecular spectra and need not be considered further. We are thus left with 3 kinds of molecular motion:

1. electronic-most energetic

2. vibrational-less energetic

3. rotational-least energetic

If these motions are in fact independent and can be decoupled (this is not always the case), then we can write for the wave functions and the energies as:

$$\psi_{\text{total}} \;\; = \;\; \psi_{\text{electronic}} \times \psi_{\text{vibrational}} \times \psi_{\text{rotational}} \tag{8.1}$$

and

$$E_{\text{total}} \;\; = \;\; E_{\text{electronic}} + E_{\text{vibrational}} + E_{\text{rotational}}. \tag{8.2}$$

In this chapter we consider the electronic energy levels of some typical molecules, and in Chapter 9 we consider the vibrational and rotational levels of molecules

The effective one-electron potential $V(\vec{r})$ for an electron in a molecule must be invariant under all symmetry operations which leave the molecule invariant. If we did not exploit the symmetry explicitly through group theory, we would then solve the Schrödinger equation to find the energy eigenvalues and the corresponding eigenfunctions of the molecule taking into account all the valence electrons for all the atoms in the molecule. This would require solution of a large secular equation of the form:

$$|\langle \psi_i | \mathcal{H} | \psi_j \rangle - E\delta_{ij}| = 0. \tag{8.3}$$

The utilization of symmetry (as for example using group theoretical methods) allows us to choose our basis functions wisely, so that many of the matrix elements in the secular equation vanish through symmetry arguments and the secular equation breaks up into block diagonal form. Thus by using symmetry, we have to solve much smaller secular equations for only those states which transform according to the same irreducible representations, because it is only those states of like symmetry that are coupled in the secular equation.

Group theory is used in yet another way for solving the electronic problem. Many molecules contain more than one equivalent atom. Symmetry is used to simplify the secular equation by forming linear combinations of atomic orbitals that transform according to the irreducible representations of the group of Schrödinger's equation. Using such linear combinations of atomic orbitals, the secular equation can more readily be brought into block diagonal form. In this chapter we show how to form linear combinations of atomic orbitals that transform as irreducible representations of the appropriate symmetry group, and we will show how the equivalence concept is used in forming these linear combinations.

In the free atom, the electronic orbitals display the symmetry of a $(1/r)$ potential, and therefore the free-atom orbitals are eigenfunctions which transform according to irreducible representations of the **full rotation group**. In a molecule or in a solid, the electrons tend to spend more time between the ion cores in the bonding state and the increased probability of finding the electron between two nuclei (see Fig. 8.1) is called a chemical bond. These bonds display the known symmetry of the molecule (or the solid). For this reason, the wavefunctions for the electrons in the molecule (or the solid) transform as irreducible representations of the appropriate symmetry group, which in general will be of lower symmetry than the full rotation group. From elementary considerations, we know that molecular bonds arise from the **exchange interaction** whose magnitude depends on the extent of the overlap of the charge clouds between neighboring atoms. Because these orbitals concentrate the charge along preferred directions, the bonding is called **directed valence bonding**, and exhibits the symmetry of the molecule or of the solid. We use the directed valence bonding concepts to identify the kind of symmetries needed to make the desired orbitals.
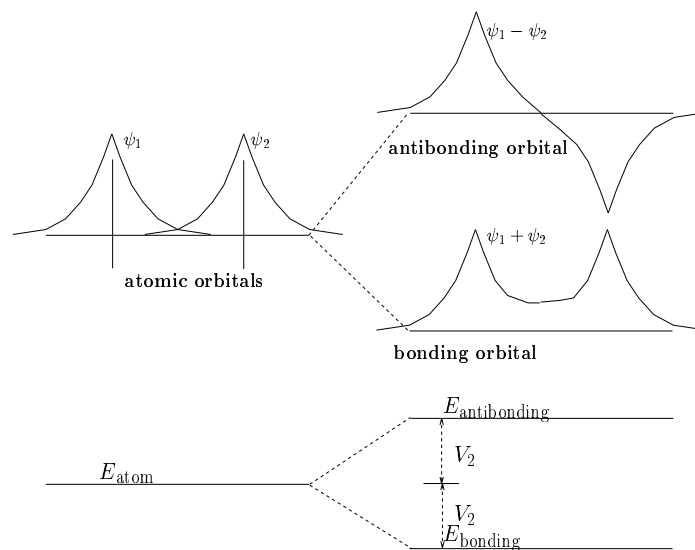
Figure 8.1: Electronic wave functions for a diatomic molecule. The formation of bonding and antibonding states is indicated. To find the energy splitting between the bonding and antibonding states (indicated schematically), the solution of Schrödinger's equation is necessary.

Symmetry enters the electronic problem of molecules in yet another way, namely through the Pauli principle and the effect of permutation of the electrons on the electron wavefunctions. This topic is discussed in Chapter 10 for many-electron states.

8.2 General Concept of Equivalence

Equivalent bonding orbitals are required to transform into one another under all the symmetry operations of the point group with no more change than a possible change of phase. The transformation which takes one **equivalent function** into another generates a representation for the point group called the equivalence transformation. The equivalence representation will in general be reducible. We denote the representation that generates the transformation between equivalent atom sites by $\Gamma^{\text{atom sites}}$ and its characters by $\chi^{\text{atom sites}}$. (To save space, we sometimes use the abbreviation $a.s. \equiv$ atomic sites.) In this section we present the equivalence concept, show how to find the irreducible representations contained in the equivalence representation (i.e., $\chi^{\text{atom sites}}$) and then give a few examples.

The matrices $D^{(\text{atom sites})}(R)_{ji}$ for the equivalence representation $\Gamma^{\text{atom sites}}$ are found from the general definition

$$\hat{P}_R \psi_i = \sum_j \psi_j D^{(\text{atom sites})}(R)_{ji} \qquad (8.4)$$

or written in matrix form

$$\hat{P}_R(\psi_1, \psi_2, \dots \psi_n) = (\psi_1, \psi_2, \dots \psi_n)(D^{(\text{atom sites})}(R)). \qquad (8.5)$$

Explicitly, the $D^{(\text{atom sites})}(R)_{ij}$ matrices are found by entering unity into the i, j position in the matrix if $\hat{P}(R)$ takes site i into an equivalent site j and zero otherwise. From this argument we readily see that the characters for the equivalence representation can be found by counting the number of points which are left unaffected by the symmetry operation, because it is only those points that will give a contribution to the matrix on diagonal positions and contribute to the character for that representation. To obtain the characters for $\chi^{\text{atom sites}}$ we take a

representative member of each class and consider the number of points that are left unchanged under action of the representative symmetry operator.

The representation $\Gamma^{\text{atom sites}}$ is in general reducible. The pertinent symmetry types for the problem are then found by decomposing $\Gamma^{\text{atom sites}}$ into its irreducible representations. To illustrate this concept, consider the example of 3 identical atoms at the corners of an equilateral triangle as for example the 3 hydrogen atoms in the NH_3 molecule. The symmetry group is C_{3v}, and the character table is given in Table 8.2. Referring to Fig. 4.2, where the 3 equivalent sites are labeled by (a, b, c) we obtain $D^{(\text{atom sites})}(R)$ for some typical symmetry operators:

$$D^{(a.s.)}(E) = \begin{pmatrix} 1 & 0 & 0 \\ 0 & 1 & 0 \\ 0 & 0 & 1 \end{pmatrix} \tag{8.6}$$

$$D^{(a.s.)}(C_3) = \begin{pmatrix} 0 & 1 & 0 \\ 0 & 0 & 1 \\ 1 & 0 & 0 \end{pmatrix} \tag{8.7}$$

$$D^{(a.s.)}(\sigma_v) = \begin{pmatrix} 1 & 0 & 0 \\ 0 & 0 & 1 \\ 0 & 1 & 0 \end{pmatrix} \tag{8.8}$$

in which the rows and columns correspond to the sequence of atoms (a, b, c). From these matrices we can compute the characters for each of the classes for the $\Gamma^{\text{atom sites}}$ representation in group $C_{3v}(3m)$. The character $\chi^{\text{atom sites}}(R)$ is always the number of sites that are left unchanged by the operation $\hat{P}_R$ so that $\chi^{\text{atom sites}}(E) = 3$, $\chi^{\text{atom sites}}(C_3) = 0$ and $\chi^{\text{atom sites}}(\sigma_v) = 1$. These results are summarized below and

	E	$2C_3$	$3\sigma_v$	
$\Gamma^{\text{atom sites}}$	3	0	1	$\Rightarrow \Gamma_1 + \Gamma_2 = A_1 + E$

from Table 8.2 we see immediately that $\Gamma^{\text{atom sites}} = \Gamma_1 + \Gamma_2$, in agreement with the explicit orbitals found in §4.6. The orbitals on the nitrogen atom are then chosen to bond to the atomic orbitals of the 3 hydrogen atoms as discussed in §8.5.1.

Table 8.1: Character Table for the Group C_{1h}

$C_{1h}(m)$			E	σ_h
x^2, y^2, z^2, xy	R_z, x, y	A' (Γ_1)	1	1
xz, yz	R_x, R_y, z	A'' (Γ_1')	1	-1
		$\chi^{\text{atom sites}}$	2	$0 \Rightarrow \Gamma_1 + \Gamma_1' \equiv A' + A''$

8.3 Directed Valence Bonding

For diatomic molecules we know immediately, without recourse to group theory, how to make a bond out of the atomic orbitals. We need simply to take the symmetrical combination $(\psi_a + \psi_b)$ to pile up charge in the directed valence bond (see Fig. 8.1).

For the case of the homopolar diatomic molecule, we thus form a bonding state $(\psi_a + \psi_b)$ and an antibonding state of higher energy $(\psi_a - \psi_b)$ which is generally unoccupied. Suppose that this diatomic molecule only has 2 symmetry operations, the identity E and the mirror plane reflections m. These are the 2 symmetry elements of the group C_{1h}. (In §8.4 we will consider the semi-infinite groups $D_{\infty h}$ and $C_{\infty v}$ which give the full symmetry of typical homogeneous and heterogeneous diatomic molecules.) Taking ψ_a as an arbitrary function, and noting that $\hat{P}_m \psi_a = \psi_b$, the projection operator for 1-dimensional irreducible representations (see Eq. 4.38) can be written as:

$$\hat{P}^{(\Gamma_n)} = \frac{l_n}{h} \sum_R \chi^{(\Gamma_n)}(R)^* \hat{P}_R. \tag{8.9}$$

The basic formula (Eq. 8.9) for finding linear combinations of atomic orbitals when acting on the wave function ψ_a yields:

$$\hat{P}^{(\Gamma_1)}\psi_a = \tfrac{1}{2}[(1)\hat{P}_E\psi_a + (1)\hat{P}_m\psi_a] = \tfrac{1}{2}[\psi_a + \psi_b] \qquad \text{bonding}$$

$$\hat{P}^{(\Gamma_1')}\psi_a = \tfrac{1}{2}[(1)\hat{P}_E\psi_a + (-1)\hat{P}_m\psi_a] = \tfrac{1}{2}[\psi_a - \psi_b] \qquad \text{antibonding} \tag{8.10}$$

for the bonding and anti-bonding states, so that the bonding orbitals will have Γ_1 symmetry and the antibonding orbitals Γ_1' symmetry. Since

there are only two initial wave functions ψ_a and ψ_b, the combinations in Eq. 8.10 are all the independent linear combinations that can be formed.

Our discussion of the use of projection operators (see §4.5 and §4.6) illustrated how linear combinations of atomic orbitals could be found such that the resulting orbitals transform according to irreducible representations of the point group. This process is simplified by using the **directed valence representation** $\Gamma_{D.V.}$ which introduces two kinds of simplifications:

1. $\Gamma_{D.V.}$ gives all the irreducible representations for the molecular orbitals before the molecular orbitals are found explicitly. This saves time because the projection operator $\hat{P}^{(\Gamma_n)}$ need not then be applied to irrelevant representations, but only to those irreducible representations contained in $\Gamma_{D.V.}$.

2. If we are only interested in finding the number of distinct eigenvalues and their degeneracies, this follows directly from the characters $\chi_{D.V.}$ of the representation $\Gamma_{D.V.}$. To obtain this kind of information it is not necessary to solve Schrödinger's equation or even to find the linear combination of molecular orbitals as in §4.3.

8.4   Diatomic Molecules

8.4.1   Homonuclear Diatomic Molecules in General

The simplest molecules are the homonuclear diatomic molecules. For homonuclear molecules (such as H_2) the appropriate symmetry group is $D_{\infty h}$ and the character table for $D_{\infty h}$ is shown below. We now summarize the main points about this character table.

$D_{\infty h}$ (∞/mm)			E	$2C_\phi$	C_2'	i	$2iC_\phi$	iC_2'
$x^2 + y^2, z^2$		$A_{1g}(\Sigma_g^+)$	1	1	1	1	1	1
		$A_{1u}(\Sigma_u^-)$	1	1	1	-1	-1	-1
	R_z	$A_{2g}(\Sigma_g^-)$	1	1	-1	1	1	-1
	z	$A_{2u}(\Sigma_u^+)$	1	1	-1	-1	-1	1
(xz, yz)	(R_x, R_y)	$E_{1g}(\Pi_g)$	2	$2\cos\phi$	0	2	$2\cos\phi$	0
	(x, y)	$E_{1u}(\Pi_u)$	2	$2\cos\phi$	0	-2	$-2\cos\phi$	0
$(x^2 - y^2, xy)$		$E_{2g}(\Delta_g)$	2	$2\cos 2\phi$	0	2	$2\cos 2\phi$	0
		$E_{2u}(\Delta_u)$	2	$2\cos 2\phi$	0	-2	$-2\cos 2\phi$	0
		$\vdots$	$\vdots$	$\vdots$	$\vdots$	$\vdots$	$\vdots$	$\vdots$

C_ϕ denotes an arbitrary rotation about the linear molecular axis (z-axis) and C_2' is a two-fold axis $\perp$ to C_ϕ. In the group $D_{\infty h}$, each of the operations E, C_ϕ and C_2' is also combined with inversion. We further note that σ_v is a plane through the molecular axis, so that $\sigma_v = iC_{2'}$. The subscripts g and u refer to the evenness and oddness of functions under the inversion operation while the superscripts $+$ and $-$ refer to the evenness and oddness of functions under reflection in a mirror plane. The characters for σ_v in the $D_{\infty h}$ group are found most conveniently by considering the effect of the operation σ_v on the basis functions which correspond to a given irreducible representation —e.g., σ_v changes (x, y) into $(-x, y)$ yielding a transformation matrix

$$D(\sigma_v) = \begin{pmatrix} -1 & 0 \\ 0 & 1 \end{pmatrix} \tag{8.11}$$

and the corresponding character for σ_v is $\chi(\sigma_v) = 0$ for the E_{1u} irreducible representation.

For a homogeneous diatomic molecule (such as H_2) we have the following characters for the equivalence transformation:

	E	$2C_\phi$	$C_{2'} = i\sigma_v$	i	$2iC_\phi$	$iC_{2'} = \sigma_v$	
$\chi^{\text{atom sites}}$	2	2	0	0	0	2	$\Rightarrow A_{1g} + A_{2u}$ $\Rightarrow \Sigma_g^+ + \Sigma_u^+$

When forming LCAO from s functions on the two equivalent atomic

sites (see §8.3), the normalized bonding orbital $\psi_S = (\psi_a + \psi_b)/\sqrt{2}$ has Σ_g^+ or A_{1g} symmetry and the normalized antibonding orbital $\psi_A = (\psi_a - \psi_b)/\sqrt{2}$ has Σ_u^+ or A_{2u} symmetry. Using the equivalence concept in §8.3, we can construct a linear combination of atomic orbitals which transform as irreducible representations of the group of Schrödinger's equation. Thus ψ_S and ψ_A form such basis functions and the Hamiltonian for the homogeneous diatomic molecule will not couple states ψ_S and ψ_A to each other. This follows from the argument that the product $(\mathcal{H}\psi_S)$ transforms as A_{1g} since $\mathcal{H}$ transforms as A_{1g} and so does ψ_S; also ψ_A transforms as A_{2u}. The selection rules thus tell us that the matrix element $(\psi_A|\mathcal{H}|\psi_S)$ must vanish. Thus to bring the secular equation into block diagonal form, we have to make a unitary transformation on the atomic basis functions (ψ_a, ψ_b) to bring them into the form (ψ_S, ψ_A):

$$\left(\begin{array}{c} \psi_S \\ \psi_A \end{array} \right) = \underbrace{U}_{\text{unitary matrix}} \left(\begin{array}{c} \psi_a \\ \psi_b \end{array} \right) = \left(\begin{array}{cc} \frac{1}{\sqrt{2}} & \frac{1}{\sqrt{2}} \\ \frac{1}{\sqrt{2}} & -\frac{1}{\sqrt{2}} \end{array} \right) \left(\begin{array}{c} \psi_a \\ \psi_b \end{array} \right). \qquad (8.12)$$

Applying the unitary transformation $U\mathcal{H}U^\dagger$ to the original matrix (written in terms of the original ψ_a and ψ_b) will bring the secular matrix into block diagonal form. Bringing the secular equation into block diagonal form greatly simplifies the solution of the secular equation – in this simple case from a coupled (2×2) secular equation to two decoupled (1×1) secular equations.

8.4.2   The Hydrogen Molecule H_2

In this case we can put each electron in a $(\sigma_g 1s)$ orbital and construct bonding and antibonding orbitals. For H_2, the bonding orbital σ_g is occupied with electrons having opposite spin states and the antibonding σ_u orbital is unoccupied. The $(\sigma_g 1s)$ state is symmetric under both inversion i and reflection σ_v. Hence the symmetry for each of the separated atoms is Σ_g^+ so that the symmetry for the molecule is $\Sigma_g^+ \otimes \Sigma_g^+ = \Sigma_g^+$. We write this state as $^1\Sigma_g^+$ where the superscript 1 denotes a singlet $(s = 0)$ with a total spin degeneracy of $(2s + 1) = 1$. By making spatial bonding orbitals that are symmetric under exchange

of the electrons, the spin state must be antisymmetric:

$$\frac{1}{\sqrt{2}} \left[\alpha(1)\beta(2) - \alpha(2)\beta(1) \right]. \tag{8.13}$$

8.4.3 The Helium Molecule He$_2$

Suppose we could make a bound diatomic molecule out of 2 helium atoms and containing 4 electrons. This molecule would have, on the separated atom model, a configuration $(\sigma_g 1s)^2 (\sigma_u 1s)^2$ and would be in a $^1\Sigma_g^+$ state, all spins being antiparallel in pairs. Here σ_u denotes the antibonding orbital for the $1s$ states. In this case, both the bonding and antibonding states need to be occupied to make a He$_2$ molecule and the resulting symmetry is $\Sigma_g^+ \otimes \Sigma_g^+ \otimes \Sigma_u^+ \otimes \Sigma_u^+ = \Sigma_g^+$. Since the He$_2$ molecule is not formed under ordinary circumstances we know that the antibonding state lies sufficiently high in energy so that it is not energetically favorable to form the He$_2$ molecule. On the other hand, H$_2^-$ involves occupation of an antibonding state and does indeed form a bound state. Group Theory gives us the symmetry designation for each molecule, but does not give definitive information as to whether or not a bound state is formed.

8.4.4 Heterogeneous Diatomic Molecules

We illustrate the case of a linear heterogeneous diatomic molecule with CO. Since the electronic wave functions on each site are not equivalent (see Fig. 8.2), there is no inversion symmetry. The appropriate symmetry group for CO is $C_{\infty v}$ which has the following character table:

$C_{\infty v}$ (∞m)			E	$2C_\phi$	σ_v
$(x^2 + y^2, z^2)$	z	$A_1(\Sigma^+)$	1	1	1
	R_z	$A_2(\Sigma^-)$	1	1	-1
(xz, yz)	$\begin{array}{c}(x, y) \\ (R_x, R_y)\end{array} \Big\}$	$E_1(\Pi)$	2	$2\cos\phi$	0
$(x^2 - y^2, xy)$		$E_2(\Delta)$	2	$2\cos 2\phi$	0
		$\vdots$	$\vdots$	$\vdots$	$\vdots$

Figure 8.2: The wave functions for a heteropolar diatomic molecule and their formation of bonding and antibonding states. If $2V_3$ is the energy separation between the anion and cation for large interatomic distance, the splitting resulting from an interaction energy $2V_2$ is shown.

The symmetry operations of $C_{\infty v}$ have already been covered when discussing the symmetry operations of $D_{\infty h}$ (see §8.4.1). Using the equivalence operation on the carbon and oxygen atoms in CO, we have the result $\chi^{\text{atom sites}} = 2A_1$ (see also $\chi^{\text{atom sites}}$ for H_2 with $D_{\infty h}$ symmetry in §8.4.2). Now the C atom has the electronic configuration $2s^2 2p^2$ while O has the configuration $2s^2 2p^4$. We will then make bonding and antibonding molecular orbitals from $2s, 2p_z$ and $2p_{x,y}$ atomic orbitals. From the basis functions given in the character table for $C_{\infty v}$ we see that the irreducible representations for these atomic orbitals (for group $C_{\infty v}$) are:

$$
\begin{aligned}
2s &\rightarrow A_1 \\
2p_z &\rightarrow A_1 \\
2p_{x,y} &\rightarrow E_1
\end{aligned}
$$

To find the direct products using the character table for $C_{\infty v}$ we note that

$$\cos^2 \phi = \left(\frac{1}{2}\right)(1 + \cos 2\phi)$$

which allows us to evaluate the direct product $\pi \otimes \pi$ or $E_1 \otimes E_1$ to obtain

$$\pi \otimes \pi = {}^1\Sigma^+ + {}^3\Sigma^- + {}^1\Delta^+$$

or

$$E_1 \otimes E_1 = A_1 + A_2 + E_2.$$

The secular equation implied by the interactions in Fig. 8.2 is

$$
\begin{vmatrix}
V_3 - E & V_2 \\
V_2 & -V_3 - E
\end{vmatrix} = 0 \tag{8.14}
$$

which gives $-(V_3^2 - E^2) - V_2^2 = 0$ or $E^2 = V_2^2 + V_3^2$ so that

$$E = \pm\sqrt{V_2^2 + V_3^2} \tag{8.15}$$

as shown in Fig. 8.2.

Referring to Fig. 8.3 the number of electrons which form bonds in CO are 4+6=10. We note from Fig. 8.3 that the occupied levels
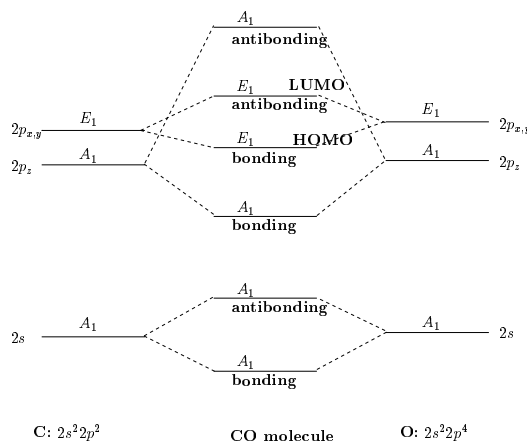
Figure 8.3: Bonding and antibonding molecular levels for the CO molecule.

include the $2s$ A_1 bonding and antibonding orbitals and the $2p$ A_1 and E_1 bonding orbitals. The $2p$ A_1 and E_1 antibonding orbitals will remain unoccupied. Since the p_z orbitals are directed along the molecular axis, the bonding-antibonding interaction (and level splitting) will be largest for the p_z orbitals, as shown in Fig. 8.3.

The symmetry of the s-function orbitals for a diatomic molecule are found directly from the transformation properties of $\chi^{\text{atom sites}}$. However, for p-function orbitals we must take the direct product of $\chi^{\text{atom sites}} \otimes \chi^{\text{vector}}$ since the p-functions transform as vectors. For the case of the heterogeneous CO molecule with $C_{\infty v}$ symmetry $\chi^{\text{atom sites}} = 2A_1 = 2\Sigma^+$ and $\chi^{\text{vector}} = A_1 + E_1 = \Sigma^+ + \Pi$. With regard to the p_z orbital, both the bonding and antibonding orbitals (see Fig. 8.3) have A_1 or Σ^+ symmetry. For the bonding p_z orbital, there is a maximum of the charge accumulation between the C and O atoms as shown in Fig. 8.3. For the (p_x, p_y) orbitals, the bonding and antibonding levels both have E_1 or Π symmetry (see Character Table 3.35 for notation).

The symmetry types of each of the molecular orbitals determines the form of the secular equation. The block structure of the secular equation then assumes the form shown in Fig. 8.4, in which the coupling terms appear in the blocks indicated.

$$
\begin{array}{|ccc|ccc|}
\hline
\mathcal{H}^{\text{C,C}}_{A_1,A_1}(ss) & \mathcal{H}^{\text{C,C}}_{A_1,A_1}(sz) & \mathcal{O} & \mathcal{H}^{\text{C,O}}_{A_1,A_1}(ss) & \mathcal{H}^{\text{C,O}}_{A_1,A_1}(sz) & \mathcal{O} \\
\mathcal{H}^{\text{C,C}}_{A_1,A_1}{}^{\dagger}(zs) & \mathcal{H}^{\text{C,C}}_{A_1,A_1}(zz) & \mathcal{O} & \mathcal{H}^{\text{C,O}}_{A_1,A_1}{}^{\dagger}(zs) & \mathcal{H}^{\text{C,O}}_{A_1,A_1}(zz) & \mathcal{O} \\
\mathcal{O} & \mathcal{O} & \mathcal{H}^{\text{C,C}}_{E_1,E_1}(xy,xy) & \mathcal{O} & \mathcal{O} & \mathcal{H}^{\text{C,O}}_{E_1,E_1}(xy,xy) \\
\hline
\mathcal{H}^{\text{C,O}}_{A_1,A_1}{}^{\dagger}(ss) & \mathcal{H}^{\text{C,O}}_{A_1,A_1}{}^{\dagger}(sz) & \mathcal{O} & \mathcal{H}^{\text{O,O}}_{A_1,A_1}(ss) & \mathcal{H}^{\text{O,O}}_{A_1,A_1}(sz) & \mathcal{O} \\
\mathcal{H}^{\text{C,O}}_{A_1,A_1}(zs) & \mathcal{H}^{\text{C,O}}_{A_1,A_1}{}^{\dagger}(zz) & \mathcal{O} & \mathcal{H}^{\text{O,O}}_{A_1,A_1}{}^{\dagger}(zs) & \mathcal{H}^{\text{O,O}}_{A_1,A_1}(zz) & \mathcal{O} \\
\mathcal{O} & \mathcal{O} & \mathcal{H}^{\text{C,O}}_{E_1,E_1}{}^{\dagger}(xy,xy) & \mathcal{O} & \mathcal{O} & \mathcal{H}^{\text{O,O}}_{E_1,E_1}(xy,xy) \\
\hline
\end{array}
$$

Figure 8.4: Schematic diagram of the matrix Hamiltonian for molecular orbitals for the CO molecule.

Table 8.2: Character Table for Group C_{3v} $(3m)$

$C_{3v}(3m)$			E	$2C_3$	$3\sigma_v$
$x^2 + y^2, z^2$	z	A_1 (Γ_1)	1	1	1
	R_z	A_2 (Γ_1')	1	1	−1
$(x^2 - y^2, xy)$ $\Big\}$ (xz, yz)	(x, y) $\Big\}$ (R_x, R_y)	E (Γ_2)	2	−1	0

8.5   Electronic Orbitals for Multi-atomic Molecules

In this section we consider the electronic levels for various multi-atomic molecules, each selected for particular pedagogic purposes.

8.5.1   The NH_3 Molecule

We have already seen in §4.6 how to construct LCAO's for the three equivalent atoms at the corners of an equilateral triangle (e.g., the hydrogen atoms in NH_3). In this case we use group C_{3v} (see Fig. 8.5) and obtain the irreducible representations $A_1 + E$ for the directed valence representation.

To bond to the H atoms, the N atom must make orbitals directed to the 3 hydrogens. We refer to this as the directed valence bonds of the nitrogen atoms. The directed valence bonds $\Gamma_{D.V.}$ for the nitrogen must therefore exhibit the symmetry of $\Gamma^{\text{atom sites}}$ for the hydrogens. Thus $\Gamma_{D.V.}$ for the nitrogen atom is written as $\Gamma_{D.V.} = \Gamma_1 + \Gamma_2$ or $A_1 + E$.

We now explore the orbitals that can be made at the nitrogen site. Nitrogen has the electronic configuration $1s^2 2s^2 2p^3$. The $1s$ and $2s$ electrons will lie low in energy, and bonding orbitals to the hydrogens will be made with the three p electrons. Since p electrons have angular momentum $l = 1$, they transform like the vector (x, y, z) and the character table for C_{3v} shows that the p_x and p_y functions will transform as $E(\Gamma_2)$ and the p_z as $A_1(\Gamma_1)$ (see Fig. 8.5). The states with like symmetries will interact to form bonding and antibonding orbitals, as shown
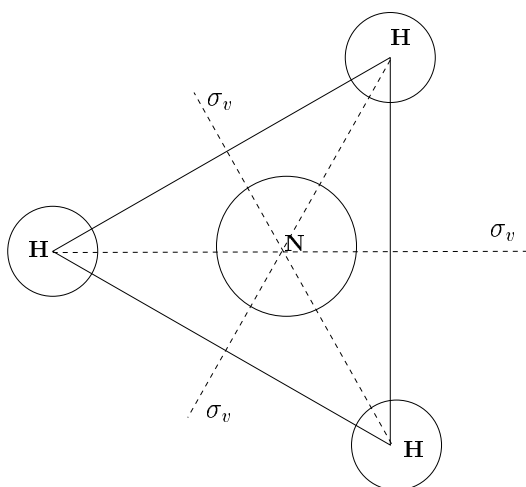
Figure 8.5: Schematic diagram of the symmetry operations for an NH_3 molecule (group C_{3v}) where the three hydrogen atoms are at the corners of an equilateral triangle and the N atom is along the normal through the midpoint of this triangle but not coplanar with the hydrogens.

schematically in Fig. 8.6. **States with unlike symmetries do not interact**. Thus the Nitrogen has three p electrons for bonding and the H_3 likewise has 3 electrons for bonding. The A_1 bonding states will hold 2 electrons and the E bonding state will hold 4 electrons. These bonds then can accommodate all 6 electrons. All the antibonding states will be unoccupied.

8.5.2 The CH_4 Molecule

In this example we consider generally how carbon atoms will form tetrahedral bonds. One example of such tetrahedral bonds for carbon is in the diamond structure. This problem is identical to the formation of tetrahedral valence bonds in the CH_4 molecule. The methane molecule forms a regular tetrahedron (see Fig. 3.3), where the carbon atom is at the center of the tetrahedron, and the four H atoms are at the tetrahedral vertices; this structure has T_d point symmetry (see Table 3.34).

What are the features of the electronic configuration that will produce this bond geometry? The ground state of the carbon atom is $1s^2 2s^2 2p^2$. Can tetrahedral bonds be formed in this ground state, or does the C atom have to go into an excited state?

We can see by inspection that a bond can be formed by superim-

(a)
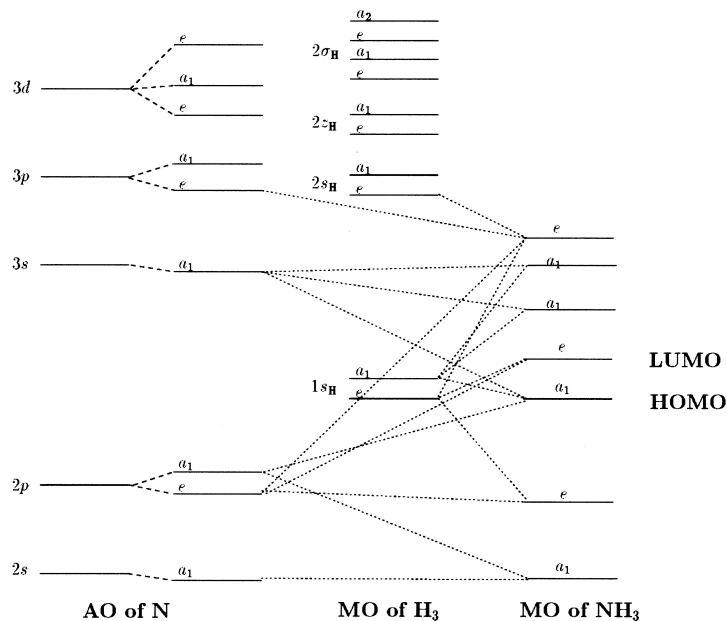
(b)
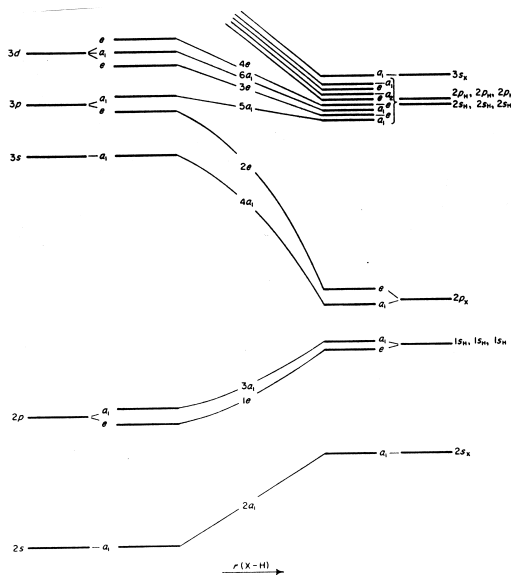
Figure 8.6: (a)Schematic energy level diagram for the XH_3 molecule (N=X for the ammonia molecule). Energy states are shown for the atomic orbitals (AO) of nitrogen and the molecular orbitals (MO) for the cluster of three hydrogen atoms. Finally on the right are shown the molecular orbitals for the NH_3 molecule. The spin $\uparrow$ and spin $\downarrow$ electrons in the nitrogen $2s$ state are paired. The three electrons in the p state form bonds to the three hydrogen atoms. The higher levels are all antibonding states. HOMO denotes the "highest occupied molecular orbital" and LUMO denotes the "lowest unoccupied molecular orbital". (b) Same plot from Herzberg's book.

posing (or making a linear combination of) an s and a p wave function shown schematically in Fig. 8.7. In superimposing s and p functions we can make linear combinations of s, p_x, p_y and p_z functions so that the bonds will lie along each of the (111) directions. The matrices, which transform the directed valence orbitals ψ_i ($i = 1, \ldots 4$) associated with the carbon atom into one another, form a 4-dimensional directed valence representation of group T_d. The matrices for the directed valence representation from the 4 hydrogen atoms to the central carbon atom are found by considering the permutations of points a, b, c, d in Fig. 3.3.

The 24 symmetry operations of T_d are described in §3.9 and in Fig. 3.3. If we now consider each of the symmetry operations the group T_d acting on the points a, b, c, d (see Fig. 3.3) we obtain the equivalence representation for the hydrogen orbital $\Gamma^{\text{atom sites}}$ or equivalently the directed valence representation from the hydrogens to the carbon atom at the center of the tetrahedron. Some typical matrices for the symmetry operations of T_d in the equivalence representation $\Gamma^{\text{atom sites}}$ are:

$$D^{a.s.}(E) = \begin{pmatrix} 1 & 0 & 0 & 0 \\ 0 & 1 & 0 & 0 \\ 0 & 0 & 1 & 0 \\ 0 & 0 & 0 & 1 \end{pmatrix} \tag{8.16}$$

$$D^{a.s.}(C_3) = \begin{pmatrix} 1 & 0 & 0 & 0 \\ 0 & 0 & 1 & 0 \\ 0 & 0 & 0 & 1 \\ 0 & 1 & 0 & 0 \end{pmatrix} \tag{8.17}$$

where the rows and columns relate to the array (a b c d) of Fig. 3.3. The results for the characters of the equivalence representation formed from transforming the atom sites $\chi^{a.s.}$ are summarized below just under the character table for T_d and are related to irreducible representations of T_d:
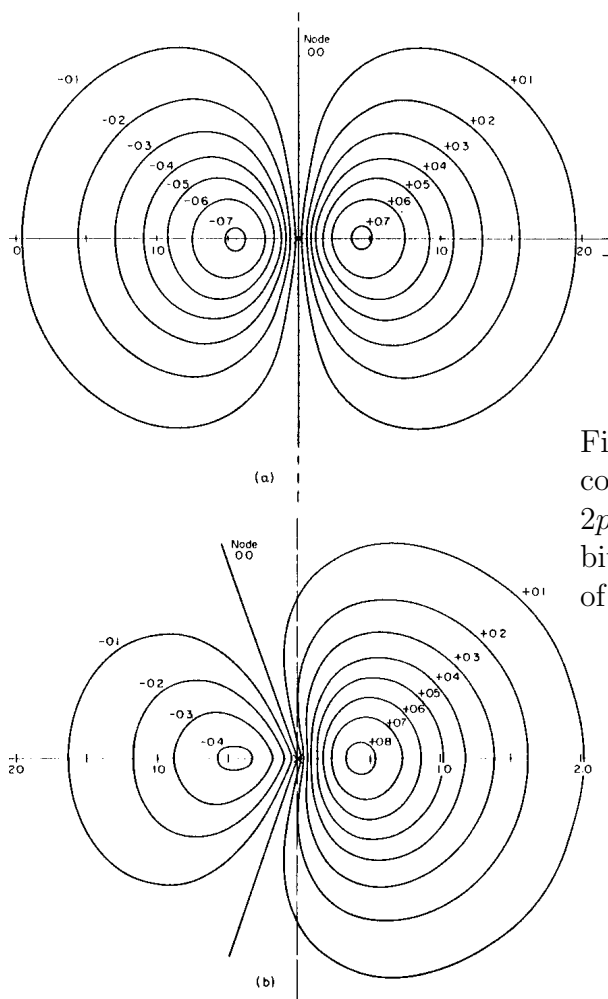
Figure 8.7: Schematic picture of the constant charge contours of (a) a $2p_x$ orbital and (b) a directed orbital arising from the superposition of $[(1/2)\psi_s + (\sqrt{3}/2)\psi_{p_x}]$.

$T_d(43m)$		E	$8C_3$	$3C_2$	$6\sigma_d$	$6S_4$	
	A_1	1	1	1	1	1	
	A_2	1	1	1	-1	-1	
	E	2	-1	2	0	0	
(R_x, R_y, R_z)	T_1	3	0	-1	-1	1	
(x, y, z)	T_2	3	0	-1	1	-1	
	$\chi^{a.s.}$	4	1	0	2	0	$\Rightarrow A_1 + T_2$

The characters $\chi^{a.s.}$ are for the atom sites for the 4 hydrogen atoms H_4 and $\chi_{D.V.} = \chi^{a.s.}$ gives the characters for the directed valence representation for C at the center of the regular tetrahedron.

From the point of view of the 4 hydrogens, $\chi^{a.s.}$ gives the symmetries for the linear combination of atomic orbitals (LCAO). The appropriate LCAO's in normalized form are found using the procedure given in §4.6 yielding for the A_1 representation:

$$\psi(A_1) = \frac{1}{2}(\psi_a + \psi_b + \psi_c + \psi_d) \qquad (8.18)$$

and for the three degenerate partners of the T_2 representation:

$$\begin{aligned}
\psi_1(T_2) &= \tfrac{1}{2}(\psi_a + \psi_b - \psi_c - \psi_d) \\
\psi_2(T_2) &= \tfrac{1}{2}(-\psi_a + \psi_b + \psi_c - \psi_d) \\
\psi_3(T_2) &= \tfrac{1}{2}(\psi_a - \psi_b + \psi_c - \psi_d).
\end{aligned} \qquad (8.19)$$

How did we get this result?

The linear combination that transforms as A_1 is clearly the sum of the atomic orbitals. The T_2 orbitals must be orthogonal and are obtained from Eq. 8.9 using the characters for the T_2 irreducible representation:

$$\begin{aligned}
\hat{P}^{(\Gamma_n)}a &= \frac{3}{24}\Big[3a - (b + c + d) + (a + c + a + d + a + b) \\
&\quad - (d + b + b + c + d + c)\Big] \\
&= \frac{3}{24}\Big[6a - 2b - 2c - 2d\Big]. \qquad (8.20)
\end{aligned}$$

In reduced form Eq. 8.20 is written as

$$\hat{P}^{(\Gamma_n)}a = \frac{1}{4}[3a - b - c - d] \qquad (8.21)$$

Taking cyclic permutations, we write:

$$\hat{P}^{(\Gamma_n)}b = \frac{1}{4}[3b - c - d - a] \tag{8.22}$$

$$\hat{P}^{(\Gamma_n)}c = \frac{1}{4}[3c - d - a - b] \tag{8.23}$$

$$\hat{P}^{(\Gamma_n)}d = \frac{1}{4}[3d - a - b - c]. \tag{8.24}$$

To obtain LCAO's that are more symmetric and orthogonal, consider:

$$\hat{P}^{(\Gamma_n)}a + \hat{P}^{(\Gamma_n)}c = \tfrac{1}{2}[a - b + c - d]$$

$$\hat{P}^{(\Gamma_n)}a + \hat{P}^{(\Gamma_n)}b = \tfrac{1}{2}[a + b - c - d] \tag{8.25}$$

$$-\hat{P}^{(\Gamma_n)}a - \hat{P}^{(\Gamma_n)}d = \tfrac{1}{2}[-a + b + c - d]$$

which are (except for a normalization factor) the results given in Eq. 8.19.

Since the symmetries for the directed valence orbitals from the central carbon atom are the same as those from the four hydrogen orbitals, interactions between orbitals with like symmetry will occur so that bonding and antibonding orbitals will be produced. These symmetries in the directed valence orbitals can be related conveniently to angular momentum states for carbon. This is done for the general case by considering the characters for rotations and inversions (see Eqs. 6.1 and 6.3):

$$\chi(\alpha) = \frac{\sin(\ell + \frac{1}{2})}{\sin(\alpha/2)} \qquad \text{for pure rotations}$$

$$\chi(i\alpha) = (-1)^\ell \frac{\sin(\ell + \frac{1}{2})\alpha}{\sin(\alpha/2)} \qquad \text{for improper rotations.}$$

We thus obtain the characters for the angular momentum states in the T_d group and list them in Table 8.3, where we have made use of the fact that

$$\begin{cases} \sigma_d = iC_2 \\ S_4 = iC_4. \end{cases}$$

The results in Table 8.3 could equally well have been obtained by looking at the character table for group T_d (see Table 3.34) and making the following identifications:

Table 8.3: Characters and symmetries for the angular momentum states in T_d symmetry.

	E	$8C_3$	$3C_2$	$6\sigma_d$	$6S_4$		
$\chi_\ell = 0$	1	1	1	1	1	A_1	$A_1 \to s$ state
$\chi_\ell = 1$	3	0	-1	1	-1	T_2	$T_2 \to p$ state
$\chi_\ell = 2$	5	-1	1	1	-1	$E + T_2$	

		basis functions
$\ell = 0$	s-state	1
$\ell = 1$	p-state	(x, y, z)
$\ell = 2$	d-state	$\underbrace{(xy, yz, zx}_{T_2}, \underbrace{x^2 - y^2, 3z^2 - r^2)}_{E}$

and associating the various basis functions of the angular momentum states with the appropriate irreducible representations for the T_d group.

If we now apply this discussion to the CH_4 molecule we see that the directed valence orbitals for the carbon are made from one $2s$ (A_1) state and three $2p$ (T_2) states (see Fig. 8.8) and involve 8 valence electrons for the molecule. A set of 4 mutually orthogonal functions for the linear combination of hydrogen orbitals is given in Eq. 8.19. Using the same form as these orbitals, we obtain the corresponding directed valence orbitals emanating from the carbon atom:

$$\Psi(1, 1, 1) = \tfrac{1}{2}(\psi_s + \psi_{p_x} + \psi_{p_y} + \psi_{p_z})$$

$$\Psi(1, -1, -1) = \tfrac{1}{2}(\psi_s + \psi_{p_x} - \psi_{p_y} - \psi_{p_z})$$

$$\Psi(-1, 1, -1) = \tfrac{1}{2}(\psi_s - \psi_{p_x} + \psi_{p_y} - \psi_{p_z})$$

$$\Psi(-1, -1, 1) = \tfrac{1}{2}(\psi_s - \psi_{p_x} - \psi_{p_y} + \psi_{p_z}) \tag{8.26}$$

Equations 8.26 also represent normalized functions for tetrahedral bonding orbitals in common semiconductors. Bonding states are made between the A_1 carbon orbital and the A_1 orbital of the four hydrogens

(a)
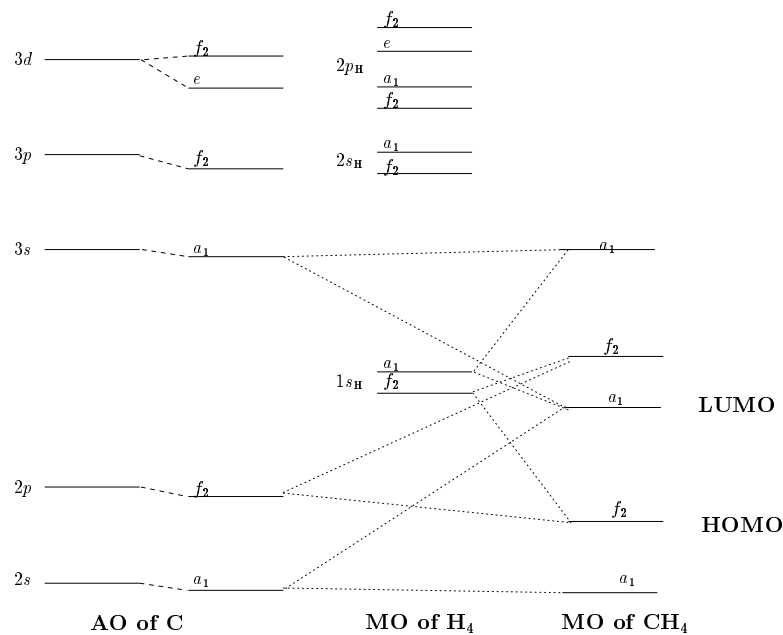
(b)
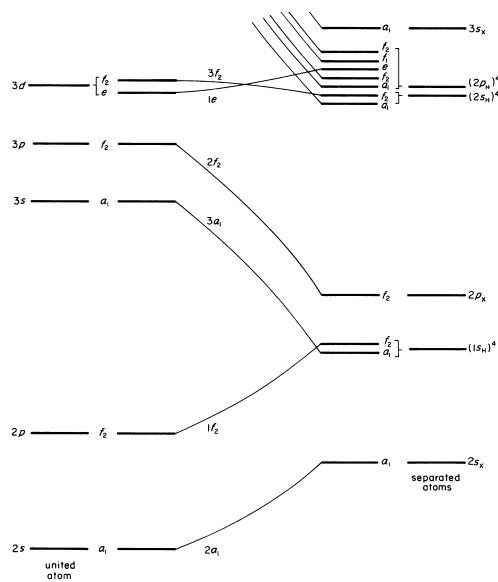
Figure 8.8: (a)Schematic diagram for the energy levels in the XH_4 molecule (C=X) as they are formed from C and H_4 orbitals. In this diagram the A_1 state is labeled a_1 and the T_2 state in labeled f_2 to follow the Herzberg notation, and both bonding and antibonding states are shown. The molecular orbitals labeled a_1 and f_2 can accommodate the 8 valence electrons of CH_4. (b) Same plot from Herzberg's book.

and between the corresponding T_2 carbon and hydrogen orbitals (see Fig. 8.8). Although the carbon electrons must be promoted to the excited sp^3 configuration to satisfy the bonding orbitals in the molecule, the bonding energy due to the CH_4 bonds more than compensates for the electronic excitation. The directed valence can only be considered as approximate since the electronic orbitals in the molecular states are strongly hybridized, rather than being atomic-like, as is assumed in forming LCAO's.

8.5.3   The Hypothetical SH_6 Molecule

Consider a hypothetical molecule SH_6 where the six identical H atoms are arranged on a regular hexagon (e.g., the benzene ring has this basic symmetry) and the sulfur is at the center. For the hydrogens, we have 6 distinct atomic orbitals. To simplify the secular equation we use group theory to make appropriate linear combinations of atomic orbitals:

$$\begin{pmatrix} \psi_a \\ \psi_b \\ \psi_c \\ \psi_d \\ \psi_e \\ \psi_f \end{pmatrix} \tag{8.27}$$

so that the transformed linear combinations are proper basis functions for irreducible representations of the point symmetry group D_{6h} which applies to this problem. We see that the largest dimension for an irreducible representation in D_{6h} is $n = 2$. We show below that the use of symmetry will result in a secular equation with block diagonal form, having blocks with dimensions no greater than (2×2).

The characters for $\chi^{\text{atom sites}}(R)$ for the six H orbitals in D_{6h} symmetry are found by considering how many atom sites go into each other under the various symmetry operations of the group. The results are given at the bottom of the character table below for D_6 where $D_{6h} = D_6 \otimes i$.
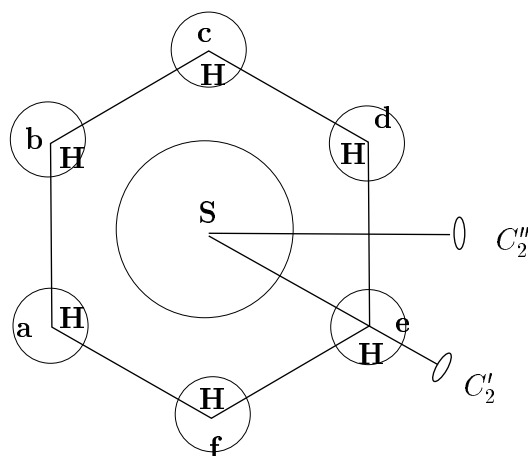
Figure 8.9: Geometry of the hypo-
thetical SH_6 molecule with 6 hydro-
gens at the corners of a hexagon and
the sulfur atom at the center (D_{6h}
symmetry).

D_6		E	C_2	$2C_3$	$2C_6$	$3C_2'$	$3C_2''$	
$x^2 + y^2, z^2$	$\Gamma_1(A_1)$	1	1	1	1	1	1	
z	$\Gamma_2(A_2)$	1	1	1	1	-1	-1	
	$\Gamma_3(B_1)$	1	-1	1	-1	1	-1	
	$\Gamma_4(B_2)$	1	-1	1	-1	-1	1	
$(x^2 - y^2, xy)$	$\Gamma_5(E_2)$	2	2	-1	-1	0	0	
$(xz, yz), (x, y)$	$\Gamma_6(E_1)$	2	-2	-1	1	0	0	
$\chi^{\text{atom sites}}$		6	0	0	0	2	0	$\Rightarrow \Gamma_1 + \Gamma_3 + \Gamma_5 + \Gamma_6$

We now set up the appropriate linear combinations. This can be
done by projection operators or by inspection (see §4.3), utilizing the
correspondence of this problem with the nth roots of unity, in this
case, the 6th roots of unity. We will denote the 6th roots of unity
by $1, \Omega, \omega, -1, \omega^2, \Omega^5$ where $\omega = e^{2\pi i/3}$ and $\Omega = e^{2\pi i/6}$. For simplicity
we will denote the atomic orbitals at a site α by ψ_α and use the abbre-
viated notation α. In terms of the site notation (a, b, c, d, e, f), the 6
orthogonal linear combinations formed by taking the 6th roots of unity
are:

$$\psi_1 \qquad a + b + c + d + e + f \quad \text{transforms as } \Gamma_1$$
$$\psi_2 \qquad a + \Omega b + \omega c - d + \omega^2 e + \Omega^5 f$$
$$\psi_3 \qquad a + \omega b + \omega^2 c + d + \omega e + \omega^2 f$$

$$\psi_4 \qquad a - b + c - d + e - f \qquad \text{transforms as } \Gamma_3$$
$$\psi_5 \qquad a + \omega^2 b + \omega c + d + \omega^2 e + \omega f$$
$$\psi_6 \qquad a + \Omega^5 b + \omega^2 c - d + \omega e + \Omega f$$

where $\Omega = e^{2\pi i/6}$ and $\omega = e^{2\pi i/3}$.

To obtain the symmetries of the functions $\psi_1, \ldots, \psi_6$ we examine $R\psi_i$ where R is a symmetry operation in group D_6. Clearly ψ_2 and ψ_6 are partners since $\psi_2^* = \psi_6$, and similarly ψ_3 and ψ_5 are partners since $\psi_3^* = \psi_5$, so these provide good candidates for representing the Γ_5 and Γ_6 irreducible representations. By inspection ψ_1 is invariant under all the symmetry operations of the group and thus ψ_1 transforms as Γ_1. As for ψ_4, application of $C_6(\psi_4) = -\psi_4$, and $C_3\psi_4 = \psi_4$ etc., verifies that ψ_4 transforms as Γ_3. Inspection of the character table shows differences between Γ_5 and Γ_6 under the operations in classes C_2 and $2C_6$. It is clear that the basis formed by ψ_2 and ψ_6 transforms under C_6 as:

$$C_6(\psi_2, \psi_6) = (\psi_2, \psi_6) \begin{pmatrix} \Omega^5 & 0 \\ 0 & \Omega \end{pmatrix} \qquad (8.28)$$

since $a \to b, b \to c, c \to d$ etc. Thus the trace of the matrix is

$$\Omega + \Omega^5 = e^{2\pi i/6} + e^{-2\pi i/6} = 2\cos\frac{2\pi}{6} = 1 \qquad (8.29)$$

which is the proper character for Γ_6. As a check, we see that $C_2(\psi_2, \psi_6)$ results in a trace $= \Omega^3 + \Omega^{15} = \Omega^3 + \Omega^3 = 2\cos\pi = -2$, and this also checks.

Similarly we see that the transformation matrix for

$$C_6(\psi_3, \psi_5) = (\psi_3, \psi_5)D^{\Gamma_5}(C_6)$$

again sends $a \to b, b \to c, c \to d$ etc. and yields a trace of $\omega + \omega^2 = -1$ while $C_2(\psi_3, \psi_5)$ yields a trace of $\omega^3 + \omega^6 = 2$. The unitary transformation U which takes the original basis a, b, c, d, e, f, g into a basis that exhibits D_6 symmetry

$$U \begin{pmatrix} a \\ b \\ c \\ d \\ e \\ f \end{pmatrix} = \begin{pmatrix} \psi_1 \\ \psi_4 \\ \psi_2 \\ \psi_6 \\ \psi_3 \\ \psi_5 \end{pmatrix} \qquad (8.30)$$

$$
\begin{array}{c|c|c|c}
\mathcal{H}_{\Gamma_1,\Gamma_1} & \mathcal{O} & \mathcal{O} & \mathcal{O} \\
\hline
\mathcal{O} & \mathcal{H}_{\Gamma_3,\Gamma_3} & \mathcal{O} & \mathcal{O} \\
\hline
\mathcal{O} & \mathcal{O} & \mathcal{H}_{\Gamma_5,\Gamma_5} & \mathcal{O} \\
\hline
\mathcal{O} & \mathcal{O} & \mathcal{O} & \mathcal{H}_{\Gamma_6,\Gamma_6}
\end{array}
$$

Figure 8.10: Schematic of the secular equation for 6 hydrogen orbitals at the corners of a regular hexagon. Outside of the block structure, all entries are zeros. The Γ_1 and Γ_3 are 1-dimensional representations and the Γ_5 and Γ_6 are 2-dimensional representations.

brings the one-electron molecular secular matrix into the block diagonal form shown in Fig. 8.10, and zeros in all the off-diagonal positions coupling these blocks.

Just as we used some intuition to write down the appropriate basis functions, we can use physical arguments to guess at the ordering of the energy levels. The fully symmetric state yields a maximum charge density **between** the atom sites and therefore results in maximum bonding. On the other hand, the totally antisymmetric state yields a minimum bonding and therefore should be the highest energy state. The doubly degenerate levels have an intermediate amount of wave function overlap.

Since the total energy of the states in the 6-atom system is conserved, the center of gravity of the energy of the LCAO's is at the center of the atomic orbitals (see Fig. 8.11). The 6 symmetric orbitals that we make can be populated by 12 electrons. But we only have 6 electrons at our disposal and these go into the lowest energy states. For this reason, the molecule produces a lower energy state than the free atoms. One can then make directed valence orbitals from the S at the
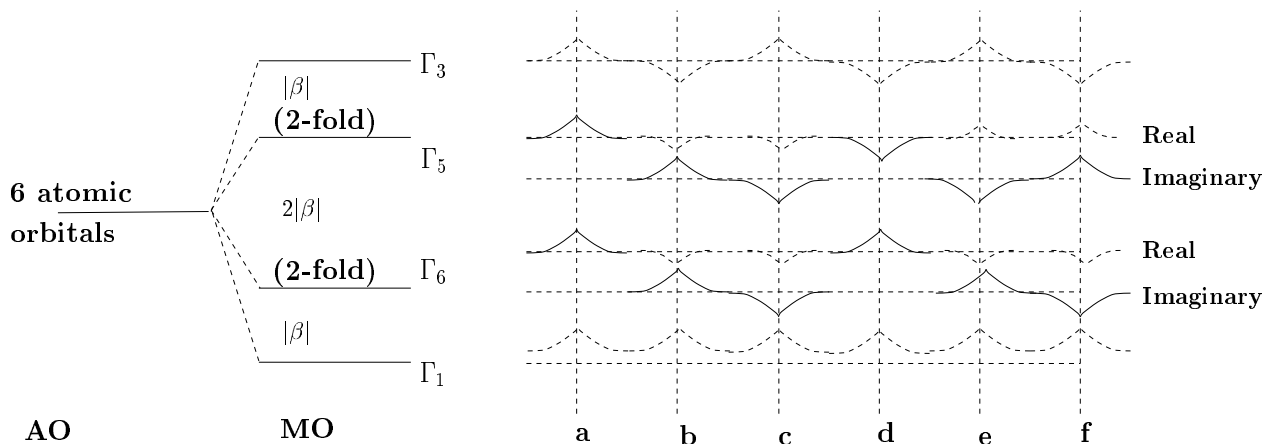
Figure 8.11: Energies of the LCAO's formed by six hydrogen atoms at the corners of a hexagon. Also shown is a schematic summary of the wave functions for the various orbitals.

center of the hexagon to the 6 hydrogens.

An isolated S atom is in a $1s^2 2s^2 2p^6 3s^2 3p^4$ configuration which is compatible with the $\Gamma_1 + \Gamma_2 + \Gamma_6$ irreducible representations of group D_6. For the directed valence orbitals from the sulfur atom to the 6 hydrogen atoms in a plane, higher angular momentum states are needed to obtain orbitals with Γ_3 and Γ_5 symmetry. To obtain Γ_5 symmetry a d function ($\ell = 2$) is needed while Γ_3 symmetry requires an f function ($\ell = 3$) which first occurs in a $4f$ state, since the $\ell = 2$ angular momentum state in full rotational symmetry reduces to the $\Gamma_1 + \Gamma_5 + \Gamma_6$ irreducible representations in D_6 symmetry, and $\ell = 3$ reduces to $\Gamma_2 + \Gamma_3 + \Gamma_4 + \Gamma_5 + \Gamma_6$ in D_6 symmetry. Therefore the planar geometry is not favorable for forming the SH_6 molecule on the basis of directed valence bonding arguments.

8.5.4 The SF_6 Molecule

We next give an example of SF_6 with a molecular configuration that involves octahedral bonding (see Fig. 8.12). The octahedral configuration is very common in solid state physics.

If we now use the symmetry operations of O_h we get the characters for the equivalence representation $\chi^{\text{atom sites}}$ for the six atoms which sit
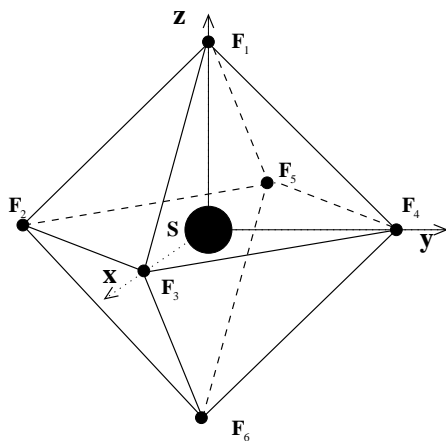
Figure 8.12: Schematic diagram of the SF_6 molecule which exhibits octahedral bonding.

at the corners of the octahedron (see Fig. 8.12):

	E	$8C_3$	$3C_2$	$6C_2'$	$6C_4$	i	$8iC_3$	$3iC_2$	$6iC_2'$	$6iC_4$	
$\chi^{a.s.}$	6	0	2	0	2	0	0	4	2	0	$\Rightarrow A_{1g} + E_g + T_{1u}$

The decomposition of the reducible representation $\chi^{\text{atom sites}}$ for the six equivalent fluorine atoms gives

$$\chi^{a.s.} = A_{1g} + E_g + T_{1u} \tag{8.31}$$

If we (hypothetically) put s-functions on each of the six fluorine sites, then we can write $\chi_s(F_6) = \chi^{a.s.}$. However, if we put p-functions on each fluorine site then $\chi_p(F_6) = \chi^{a.s.} \otimes \chi_{T_{1u}}$. This general concept of taking the direct product of the transformation of the sites with the symmetry of the orbital on each site is frequently used in applications of the equivalence principle.

Table 8.4: Characters for angular momentum states and their irreducible representations in O_h symmetry.

	E	$8C_3$	$3C_2$	$6C_2'$	$6C_4$	i	$8iC_3$	$3iC_2$	$6iC_2'$	$6iC_4$	
$\ell = 0$	1	1	1	1	1	1	1	1	1	1	$\Rightarrow A_{1g}$
$\ell = 1$	3	0	-1	-1	1	-3	0	1	1	-1	$\Rightarrow T_{1u}$
$\ell = 2$	5	-1	1	1	-1	5	-1	1	1	-1	$\Rightarrow E_g + T_{2g}$
$\ell = 3$	7	1	-1	-1	-1	-7	-1	1	1	1	$\Rightarrow A_{2u} + T_{1u} + T_{2u}$
$\ell = 4$	9	0	1	1	1	-9	0	-1	-1	-1	$\Rightarrow A_{1g} + E_g + T_{1g} + T_{2g}$

$O(432)$		E	$8C_3$	$3C_2 = 3C_4^2$	$6C_2'$	$6C_4$
	A_1	1	1	1	1	1
	A_2	1	1	1	-1	-1
$(x^2 - y^2, 3z^2 - r^2)$	E	2	-1	2	0	0
$\left. \begin{array}{c} (R_x, R_y, R_z) \\ (x, y, z) \end{array} \right\}$	T_1	3	0	-1	-1	1
(xy, yz, zx)	T_2	3	0	-1	1	-1

$$O_h \equiv O(m3m) \otimes i$$

We will now look at the orbitals for electrons on the sulfur site. Bonding orbitals are found by setting the directed valence representation equal to the symmetries found from the equivalence transformation. For simplicity let us assume that $\chi_s(F_6) = \chi^{a.s.} = \chi_{D.V.}$. We then need to identify the irreducible representations contained in $\chi_{D.V.}$ with angular momentum states. The characters for the angular momentum states in O_h symmetry are then found from:

$$\chi(\alpha) = \frac{\sin(\ell + \frac{1}{2})\alpha}{\sin(\alpha/2)} \tag{8.32}$$

and using the character table for O_h. The results are tabulated in Table 8.4. To produce $\chi_{D.V.} = A_{1g} + E_g + T_{1u}$ as in Eq. 8.31 we can use an s state $\ell = 0$ for the A_{1g} symmetry, a p state ($\ell = 1$) for the T_{1u} symmetry, and a d state ($\ell = 2$) for the E_g symmetry in Eq. 8.31. Thus sp^3d^2 orbitals are required for the directed valence of the sulfur ion, which ordinarily has an atomic ground state configuration $3s^23p^4$.

Thus to make the necessary bonding, we must promote the S atom to an excited state, namely to a $3d$ state. This type of excitation is called *configuration mixing*. Still this configuration is more stable than that for a planar SH_6 molecule.

8.5.5   The $B_{12}H_{12}$ Molecule

Since the point groups for icosahedral symmetry have become of interest recently, and these groups are not discussed in many of the standard group theory text books, we give an example here of this symmetry group for pedagogic reasons.

Five-fold rotation axes are known to occur in molecules (e.g., IF_7 with symmetry D_{5h}; $Fe(C_2H_5)_2$ with symmetry D_{5d}; and $(B_{12}H_{12})$ with icosahedral symmetry I_h). In 1985 interest in the icosahedral group was kindled by the observation in a new type of matter called quasi-crystals which require two sets of basis vectors rather than the single set that is used to describe crystals following one of the 230 possible space groups. The discovery of how to prepare gram quantities of C_{60} (in 1990), an insulating form of carbon with icosahedral symmetry, has made five-fold symmetry an important current topic in condensed matter physics and materials science. These C_{60} species are found to be very stable in the gas phase and form a "soccerball" structure (see Fig. 8.13) with a diameter of ~ 7 Å. This arrangement of the carbon atoms at the 60 corners of a truncated icosahedron leaves no dangling bonds. In some cases the "soccerball" is filled with a single transition metal or rare earth metal atom; such carbon cages for metal atoms have now been reported for $C_{60}La$, but are also found for other metal atoms (Ca, Ba, and Sr).

Five-fold symmetry also occurs in clusters and in liquids. For example, DNA is known to exhibit five-fold coordination. However, it was commonly believed that there would be no five-fold axes in condensed matter physics because it is not possible to fill a Bravais lattice with structures based on five-fold point-group symmetry. (We will prove this theorem in a later chapter, when we discuss space groups for periodic lattices.)

The molecule $B_{12}H_{12}$ is a relatively simple molecule with icosahedral symmetry. The molecule is shown schematically in Fig. 8.14 in terms of

Figure 8.13: Truncated icosahedron showing pentagonal and hexagonal faces (the "soccerball"). This is the proposed structure for C_{60}, a sixty atom stable carbon molecule. A carbon atom is located at each vertex, which occurs at the intersection of one pentagonal face with two hexagonal faces.
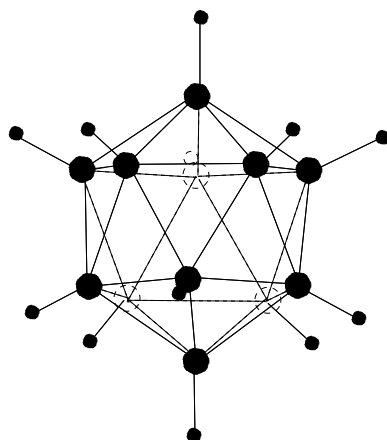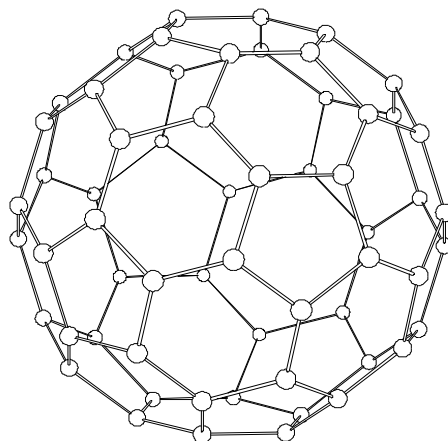
Figure 8.14: The $B_{12}H_{12}$ molecule has I_h icosahedral symmetry (see text). Shown in the figure is a regular icosahedron before the truncation that forms the figure in Fig. 8.13. The big bullets denote the 12 boron atoms and the small bullets denote the 12 hydrogens.

the regular icosahedron, where each B atom is at one of the 12 corners of the icosahedron. The $B_{12}H_{12}$ molecule could also be described in terms of the regular dodecahedron where each B atom (or H atom) sits over the center of a pentagonal face. The hydrogens are all sticking out from the borons on either side of each of the six C_5 axes (see Fig. 8.14). The symmetry operations of the group I_h include: six C_5 axes, ten C_3 axes, fifteen C_2 axes, inversion, six S_{10} axes (coincident with the C_5 axes) and ten S_6 axes (coincident with the C_3 axes) and fifteen mirror planes. The symmetry operations are summarized in the character table for I_h shown in Table 3.40. The symmetry operations of the regular dodecahedron and the regular icosahedron are the same, and each of these figures is said to be the dual of the other. The golden mean $\tau = (1 + \sqrt{5})/2 = 1.618$ appears in the characters for the 3–dimensional representations of group I_h and arises from the five-fold rotations which involve the angle of $2\pi/5 = 72°$. We note here that $\tau - 1 = 2\cos(2\pi/5)$. The number of symmetry elements in the group I_h is 120. We note that the icosahedral group contains some representations of dimensionality 4 and 5. The number of elements of the icosahedral group I is 60 which is equal to the sum of the squares of the dimensionality of the representations $h = \sum_i n_i^2 = 1^2 + 3^2 + 3^2 + 4^2 + 5^2 = 60$.

From Fig. 8.14, we can compute the characters $\Gamma^{\text{atom sites}}$ for the 12 hydrogens (or the 12 borons) corresponding to each of the classes for this reducible representation in group I_h, and the results are given in Table 8.5. From the characters in Table 8.5 and the character table for I_h (Table 3.40), we use Eq. 3.20 to obtain the irreducible representation for $\chi^{a.s.}$ for the 12 hydrogen orbitals in the $B_{12}H_{12}$ molecule:

$$\Gamma^{\text{atom sites}} = A_g + H_g + F_{1u} + F_{2u}.$$

In the $B_{12}H_{12}$ molecule the local symmetry at the B site is C_{5v}.

Also included in Table 8.5 are $\chi^{a.s.}$ for 20 and 30 atoms, respectively, at the 20 vertices and the centers of the 30 edges of the dodecahedron. With regard to the regular icosahedron, C_{20} and C_{30} would respectively have atoms at the centers of each of the 20 triangular faces or at the centers of the 30 edges (see Fig. 8.14). Also $\chi^{a.s.}$ is given in Table 8.5 for 60 atoms at the 60 vertices of the regular truncated icosahedron to form the C_{60} molecule.

Table 8.5: Characters for the equivalence transformation $\Gamma^{\text{atom sites}}$ of various LCAO's in icosahedral symmetry.

I_h	E	$12C_5$	$12C_5^2$	$20C_3$	$15C_2$	i	$12S_{10}$	$12S_{10}^3$	$20S_6$	15σ	
H_{12}	12	2	2	0	0	0	0	0	0	4	$\Rightarrow$ $A_g + H_g$ $+F_{1u} + F_{2u}$
C_{20}	20	0	0	2	0	0	0	0	0	4	$\Rightarrow$ $A_g + G_g + H_g$ $+F_{1u} + F_{2u} + G_u$
C_{30}	30	0	0	0	2	0	0	0	0	4	$\Rightarrow$ $A_g + G_g + 2H_g$ $+F_{1u} + F_{2u} + G_u + H_u$
C_{60}	60	0	0	0	0	0	0	0	0	4	$\Rightarrow$ $A_g + F_{1g} + F_{2g} + 2G_g + 3H_g$ $+2F_{1u} + 2F_{2u} + 2G_u + 2H_u$

In the C_{20} molecule the local symmetry at the C site in C_{3v}. The directed valence representation for this symmetry has $\chi_{\text{d.v.}} = A + E$ which suggests that the sp^2 atomic configuration would give the necessary directed orbitals. The irreducible representations contained in $\Gamma^{\text{atom sites}}$ for the C_{20} molecule are tabulated in Table 8.5.

8.6 Bond Strengths

In this section we show that the amplitudes of the wave functions are in fact maxima along the bond directions, consistent with the concept of a directed valence bond. Let us then consider the angular parts of the wave functions and demonstrate that the directed valence bond is a maximum in the bond direction. The $(1, 1, 1)$ directed valence bond for CH_4 is written as the first equation in Eq. 8.26. We express each of the terms of this equation in terms of spherical harmonics, using the coordinate system of Fig. 8.15. For angular momentum $l = 0$ and $l = 1$ the spherical harmonics yield

$$\psi_s = 1 \qquad\qquad \psi_{p_y} = \sqrt{3} \sin\theta \sin\phi$$

$$\text{(8.33)}$$

$$\psi_{p_x} = \sqrt{3} \sin\theta \cos\phi \qquad \psi_{p_z} = \sqrt{3} \cos\theta.$$

We can thus write the angular dependence of the directed valence bond
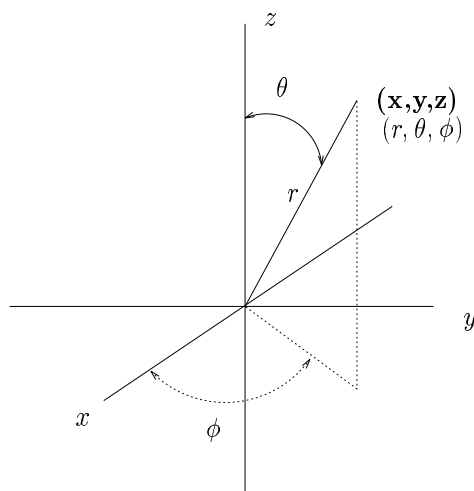
Figure 8.15: Polar coordinate system defining the angles θ and ϕ.

along (111) as:

$$\Psi(1,1,1)|_{(\theta,\phi)} = \frac{f(r)}{2}\left[1 + \sqrt{3}\sin\theta(\cos\phi + \sin\phi) + \sqrt{3}\cos\theta\right]. \quad (8.34)$$

By differentiation with respect to ϕ, we can find the maximum:

$$\frac{\partial\Psi(1,1,1)}{\partial\phi} = 0 = \left[-\sin\phi + \cos\phi\right]f(r)\sqrt{3}\sin\theta, \quad (8.35)$$

so that at the maximum:

$$\tan\phi = 1 \quad \text{or} \quad \phi = \frac{\pi}{4} \quad (8.36)$$

from which it follows that

$$\sin\phi = \cos\phi = \frac{1}{\sqrt{2}}. \quad (8.37)$$

Then differentiating $\Psi(1,1,1)$ with respect to θ to get the maximum with respect to θ gives

$$\frac{\partial\Psi(1,1,1)}{\partial\theta} = 0 = f(r)\sqrt{3}\left[\cos\theta(\cos\phi + \sin\phi) - \sin\theta\right] \quad (8.38)$$

which when evaluated at $\phi = \frac{\pi}{4}$ yields

$$\tan\theta = \frac{2}{\sqrt{2}} = \sqrt{2} \quad \text{and} \quad \theta = \tan^{-1}\sqrt{2}. \tag{8.39}$$

But these are the values of (θ, ϕ) which denote the $(1, 1, 1)$ direction, along which

$$\psi_{p_x} = \sqrt{3}\sin\theta\cos\phi = \sqrt{3}(\sqrt{\frac{2}{3}})(\frac{1}{\sqrt{2}}) = 1 = \psi_{p_y} \tag{8.40}$$

$$\psi_{p_z} = \sqrt{3}\cos\theta = \sqrt{3}(\frac{1}{\sqrt{3}}) = 1. \tag{8.41}$$

Thus the maximum value for $\Psi(1, 1, 1)$ is along a $(1,1,1)$ direction:

$$\Psi(1, 1, 1)|_{(1,1,1)} = \frac{f(r)}{2}(1 + 1 + 1 + 1) = 2f(r) \tag{8.42}$$

and $2f(r)$ is the maximum value that $\Psi(1, 1, 1)$ can have.

If we consider the value of $\Psi(1, 1, 1)$ along a different $\{1,1,1\}$ direction, we will get a smaller amplitude. For example, along a $(\bar{1}, \bar{1}, \bar{1})$ direction:

$$\Psi(1, 1, 1)|_{(\bar{1},\bar{1},\bar{1})} = \frac{f(r)}{2}[1 + \sqrt{3}(\sqrt{\frac{2}{3}})(-\frac{1}{\sqrt{2}} - \frac{1}{\sqrt{2}}) + \sqrt{3}(\frac{-1}{\sqrt{3}})] = -f(r) \tag{8.43}$$

and along a $(\bar{1}, \bar{1}, 1)$ direction:

$$\Psi(1, 1, 1)|_{(\bar{1},\bar{1},1)} = \frac{f(r)}{2}[1 + \sqrt{3}(\sqrt{\frac{2}{3}})(-\frac{1}{\sqrt{2}} - \frac{1}{\sqrt{2}}) + \sqrt{3}(\frac{1}{\sqrt{3}})] = 0 \tag{8.44}$$

and along a $(\bar{1}, 1, 1)$ direction:

$$\Psi(\bar{1}, 1, 1)|_{(\bar{1},1,1)} = \frac{f(r)}{2}[1 + \sqrt{3}(\sqrt{\frac{2}{3}})(-\frac{1}{\sqrt{2}} + \frac{1}{\sqrt{2}}) + \sqrt{3}(\frac{1}{\sqrt{3}})] = f(r). \tag{8.45}$$

This analysis shows that $\Psi(1, 1, 1)$ has a large lobe along $(1,1,1)$. Since the derivatives of $\Psi(1, 1, 1)$ along the $(\bar{1}, \bar{1}, \bar{1})$, $(\bar{1}, \bar{1}, 1)$ and $(\bar{1}, 1, 1)$ all vanish, $\Psi(1, 1, 1)$ has 3 smaller lobes, making tetrahedral angles with

one another along $(\bar{1},\bar{1},\bar{1})$, $(\bar{1},1,1),(1,\bar{1},1)$ and $(1,1,\bar{1})$. In the directions where the other three functions of Eq. 8.30 have their largest lobes, $\Psi(1,1,1)$ has a node (i.e., vanishes)– namely along $(\bar{1},\bar{1},1)$, $(\bar{1},1,\bar{1})$ and $(1,\bar{1},\bar{1})$. Furthermore, the wave function for this tetrahedrally directed valence bond is larger than for other types of bonding schemes for CH_4. For example, we will soon investigate the trigonal bonding of carbon. In this connection we will see that tetrahedral bonding is stronger than trigonal bonding. Also we will see that for trigonal bonding, the planar (p_x, p_y) bonding is stronger than the p_z bonding. Hence, **diamond (tetrahedral bonds) has strong binding in 3 dimensions, while graphite (trigonal bonds) only has strong binding in the layer planes**.

8.7 σ- and π-bonds

We now discuss the difference between σ- and π-bonds which are defined in the diagram in Fig. 8.16. The situation which we have considered until now is bonding by s-functions or by p-functions in the direction of the bond and this is denoted by σ-bonding, as shown in Fig. 8.16. We can also obtain some degree of bonding by directing our p-functions $\perp$ to the bond direction, as also shown in Fig. 8.16, and this is called π-bonding. We note that there are two equivalent mutually perpendicular directions that are involved in π-bonding. From considerations of overlapping wavefunctions, we would expect π-bonding to be much weaker than σ-bonding.

Just as group theory tells us which linear combinations of atomic orbitals (LCAO) are needed to form σ-bonds, group theory also provides corresponding information about the linear combination of atomic orbitals that form π-bonds. We will describe the procedure for finding both σ-bonds and π-bonds in this section.

Let us first review the situation for the σ-bonds. To find a σ-bond, we consider the atomic wave function at each equivalent site to be degenerate with the corresponding wave functions on the other sites and we find the transformation matrices that transform equivalent sites into one another according to the symmetry operations of the group. To find out if an entry in this matrix is 1 or 0 we ask the question whether or not
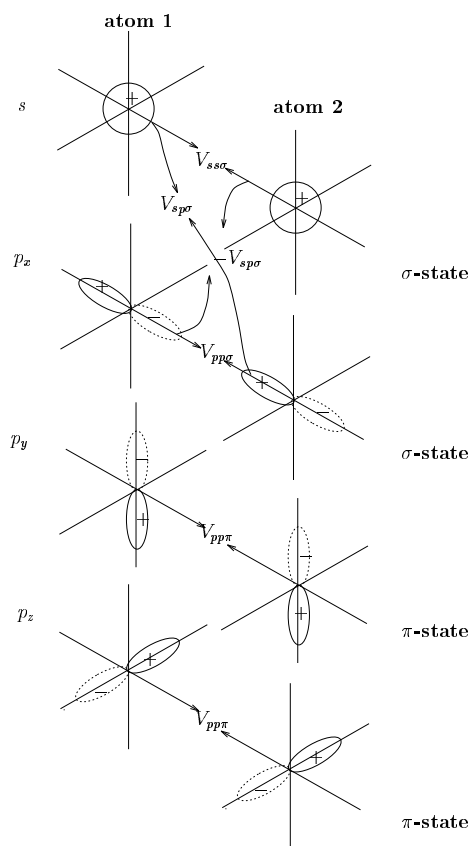
Figure 8.16: Schematic diagram of σ-bonding by s-functions and by longitudinally oriented p-functions. π-bonding with transverse p-functions is also shown.

a site goes into itself under a particular symmetry operation. If it goes into itself we produce a 1 on the diagonal, otherwise a 0. Therefore by asking how many sites go into themselves, we obtain the character for each symmetry operation. This is the procedure we have used throughout the chapter to find $\chi^{\text{atom sites}}$ which denotes the equivalence transformation.

To find the characters for a π-bond, we have to consider how many vectors normal to the bond direction remain invariant under the symmetry operations of the group. The simplest way to obtain the characters for the σ-bonds and π-bonds is to consider the transformation as the product of 2 operations: the transformation of one equivalent site into another, followed by the transformation of the vector on a site. The character for such a transformation is most easily found from the theory of the direct product of two representations:

$$\chi(R)^{\text{atom sites}} \otimes \chi(R)_{\text{general vector}} = \chi(R)^{\text{atom sites}} \otimes \chi(R)_{\text{vector}\perp \text{ to }\sigma-\text{bonds}}$$

$$+ \chi(R)^{\text{atom sites}} \otimes \chi(R)_{\text{vector }\parallel\text{ to }\sigma-\text{bonds}}$$
$$(8.46)$$

But

$$\chi(R)_{D.V.\ \sigma-\text{bonds}} \equiv \chi(R)^{\text{atom sites}} \otimes \chi(R)_{(\text{vector }\parallel\text{ to }\sigma-\text{bonds})}.$$

Thus:

$$\chi(R)_{D.V.\ \pi-\text{bonds}} = \chi(R)^{\text{atom sites}} \otimes \chi(R)_{\text{general vector}} - \chi(R)_{D.V.\ \sigma-\text{bonds}}$$
$$(8.47)$$

and we thus obtain the desired result:

$$\chi(R)_{D.V.\pi-\text{bonds}} = \chi(R)^{\text{atom sites}} \otimes \chi(R)_{\text{vector }\perp\text{ to }\sigma-\text{bonds}}. \qquad (8.48)$$

As an example of σ-bonds and π-bonds let us consider the problem of **trigonal bonding** of a hypothetical C_4 cluster where one carbon atom is at the center of an equilateral triangle and the other 3 carbon atoms are at the corners of the triangle, as shown in Fig. 8.17. The pertinent character table is D_{3h} which is given below. For this group σ_h denotes an x-y reflection plane and σ_v denotes a reflection plane containing the three-fold axis and one of the two-fold axes.
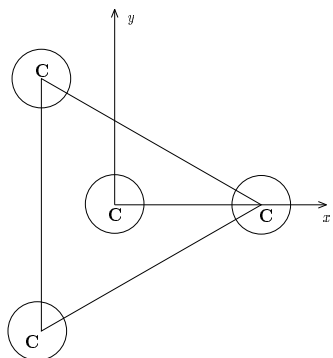
Figure 8.17: Schematic diagram of a carbon atom forming bonds to 3 other carbon atoms at the corners of an equilateral triangle.

$D_{3h}(6m2) \equiv D_3 \otimes \sigma_h$			E	σ_h	$2C_3$	$2S_3$	$3C_2'$	$3\sigma_v$
$x^2 + y^2, z^2$		A_1'	1	1	1	1	1	1
	R_z	A_2'	1	1	1	1	−1	−1
		A_1''	1	−1	1	−1	1	−1
	z	A_2''	1	−1	1	−1	−1	1
$(x^2 - y^2, xy)$	(x, y)	E'	2	2	−1	−1	0	0
(xz, yz)	(R_x, R_y)	E''	2	−2	−1	1	0	0

Consider the linear combination of atomic orbitals made out of the 3 carbon atoms at the corners of the equilateral triangle. From the equivalence transformation for these 3 carbons, we obtain $\chi^{\text{atom sites}}$:

	E	σ_h	$2C_3$	$2S_3$	$3C_2'$	$3\sigma_v$	
$\chi^{\text{atom sites}}$	3	3	0	0	1	1	$\Rightarrow A_1' + E'$

Clearly if each of the orbitals at the corners of the equilateral triangle were s-functions, then the appropriate linear combination of atomic orbitals would transform as $A_1' + E'$

$$A_1' \quad : \quad \psi_1 + \psi_2 + \psi_3 \tag{8.49}$$

$$E' \quad : \quad \begin{cases} \psi_1 + \omega\psi_2 + \omega^2\psi_3 \\ \psi_1 + \omega^2\psi_2 + \omega\psi_3 \end{cases} \tag{8.50}$$

where

$$\omega = \exp(\frac{2\pi i}{3}). \tag{8.51}$$

In transforming wavefunctions corresponding to higher angular momentum states, we must include the transformation of a tensor (vector) on each of the equivalent sites. This is done formally by considering the direct product of $\chi^{\text{atom sites}}$ with χ_{tensor}, where χ_{tensor} gives the transformation properties of the orbital: a scalar for s-functions, a vector for p-functions, a tensor for d-functions, etc.

We now illustrate the construction of LCAO's from s and p-functions, noting that from the character table for the group D_{3h}, s-functions transform as A_1', p_z functions as A_2'' and (p_x, p_y) functions as E'. We thus obtain for the transformation properties of the three s-functions at the corners of an equilateral triangle:

$$\chi^{\text{atom sites}} \otimes \chi_s = (A_1' + E') \otimes A_1' = A_1' + E' \tag{8.52}$$

for the p_z functions which transform as A_2'' we have for the direct product:

$$\chi^{\text{atom sites}} \otimes \chi_{p_z} = (A_1' + E') \otimes A_2'' = A_2'' + E''. \tag{8.53}$$

Finally for the $p_{x,y}$ functions which transform as E' we obtain

$$\chi^{\text{atom sites}} \otimes \chi_{p_x,p_y} = (A_1' + E') \otimes E' = A_1' + A_2' + 2E'. \tag{8.54}$$

We will see below that the $A_1' + E'$ symmetries correspond to σ-bonds and the remaining $(A_2' + E') + (A_2'' + E'')$ correspond to π-bonds, as shown in Fig. 8.18.

For the carbon atom at the center of the equilateral triangle (see Fig. 8.17) we make directed valence orbitals to the carbon atoms at sites (1), (2), and (3) from states with A_1' and E' symmetry, which in accordance with the character table for D_{3h}, transform as the ψ_s and ψ_{p_x}, ψ_{p_y} wave functions. The directed orbitals from the central carbon atom are thus:

$$
\begin{aligned}
\psi_1 &= \alpha\psi_s + \beta\psi_{p_x} \\
\psi_2 &= \alpha\psi_s + \beta\left[-\frac{1}{2}\psi_{p_x} + \frac{\sqrt{3}}{2}\psi_{p_y} \right] \\
\psi_3 &= \alpha\psi_s + \beta\left[-\frac{1}{2}\psi_{p_x} - \frac{\sqrt{3}}{2}\psi_{p_y} \right].
\end{aligned}
\tag{8.55}
$$
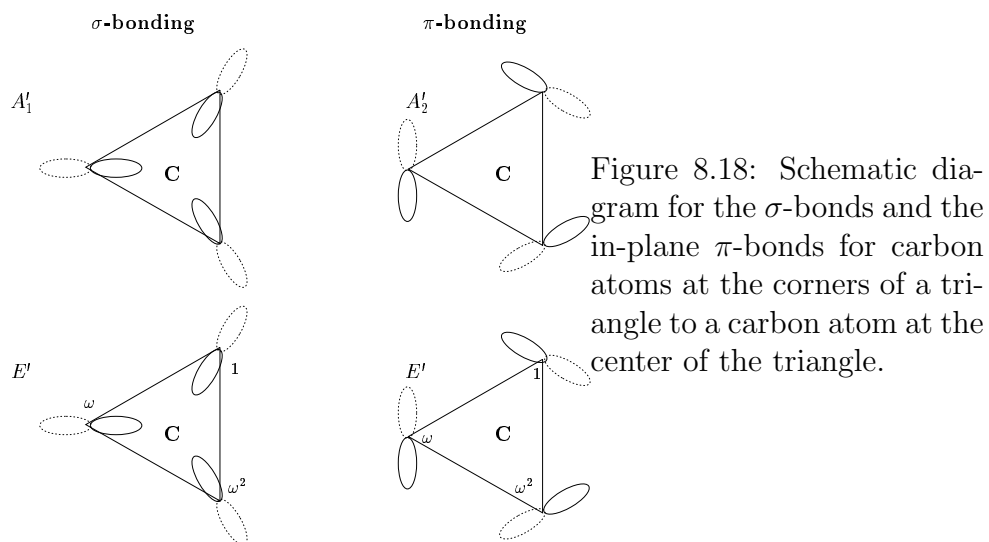
Figure 8.18: Schematic diagram for the σ-bonds and the in-plane π-bonds for carbon atoms at the corners of a triangle to a carbon atom at the center of the triangle.

The orthonormality condition on the three waves functions in Eqs. 8.55, gives

$$\alpha^2 + \beta^2 = 1 \qquad \beta^2 = 2\alpha^2 \tag{8.56}$$

or

$$\alpha = \frac{1}{\sqrt{3}} \qquad \beta = \sqrt{\frac{2}{3}} \tag{8.57}$$

so that

$$
\begin{aligned}
\psi_1 &= \sqrt{\frac{1}{3}}\psi_s + \sqrt{\frac{2}{3}}\psi_{p_x} \\
\psi_2 &= \sqrt{\frac{1}{3}}\psi_s - \sqrt{\frac{1}{6}}\psi_{p_x} + \sqrt{\frac{1}{2}}\psi_{p_y} \\
\psi_3 &= \sqrt{\frac{1}{3}}\psi_s - \sqrt{\frac{1}{6}}\psi_{p_x} - \sqrt{\frac{1}{2}}\psi_{p_y}.
\end{aligned}
\tag{8.58}
$$

Using the basis functions in the character table for D_{3h} and the classification of angular momentum states in Table 8.6, we can make σ-bonding orbitals with the following orbitals for the central carbon atom, neglecting for the moment the energetic constraints on the problem:

Table 8.6: Characters for the angular momentum states and their irreducible representations for the group D_{3h}.

	E	$\sigma_h = iC_2$	$2C_3$	$2S_3 = 2iC_6$	$3C_2'$	$3\sigma_v = iC_2$	
$\ell = 0$	1	1	1	1	1	1	A_1'
$\ell = 1$	3	1	0	-2	-1	1	$A_2'' + E'$
$\ell = 2$	5	1	-1	1	1	1	$A_1' + E' + E''$
$\ell = 3$	7	1	1	1	-1	1	$A_1' + A_2' + A_2'' + E' + E''$

$$
\begin{array}{ll}
2s2p^2 & s + (p_x, p_y) \\
2s3d^2 & s + (d_{xy}, d_{x^2-y^2}) \\
3d2p^2 & d_{3z^2-r^2} + (p_x, p_y) \\
3d^3 & d_{3z^2-r^2} + (d_{xy}, d_{x^2-y^2}) \ .
\end{array}
$$

It is clear from the list in Table 8.6 that the lowest energy σ-bond is made with the $2s2p^2$ configuration. The carbon atom has 4 valence electrons, 3 of which make the in-plane trigonal σ-bonds. The 4th electron is free to bond in the z direction. This bonding involves π-bonds.

To obtain π-bonds from the central carbon atom to the atoms at the corners of the triangle, we look at the character table to see how the vector (x, y, z) transforms. From the character table, we have the result

$$\chi_{\text{vector}} = E' + A_2''. \tag{8.59}$$

We then take the direct product:

$$
\begin{aligned}
\chi^{\text{a.s.}} \otimes \chi_{\text{vector}} \ &= \ \overbrace{(A_1' + E')}^{\chi^{\text{atom sites}}} \otimes \underbrace{(E' + A_2'')}_{\chi_{\text{vector}}} \\
&= \ (A_1' \otimes E') + (A_1' \otimes A_2'') + (E' \otimes E') + (E' \otimes A_2'') \\
&= \ (E') + (A_2'') + (E' + A_1' + A_2') + (E'') \\
&= \ (A_1' + E') + (E' + A_2'' + A_2' + E''). \tag{8.60}
\end{aligned}
$$

Since the irreducible representations for the σ-bonds are A_1' and E', we have the desired result that the irreducible representations for the

π-bonds are:

$$E' + A_2'' + A_2' + E''.$$

We can now go one step further by considering the polarization of the π-bonds by considering the irreducible representations that are even and odd under the horizontal mirror plane σ_h:

$$\chi_{D.V.\ \pi-bonds} = \overbrace{A_2' + E'}^{\text{even under } \sigma_h} + \underbrace{A_2'' + E''}_{\text{odd under } \sigma_h}. \tag{8.61}$$

The above polarization analysis identifies the bonds given in Eqs. 8.52–8.54.
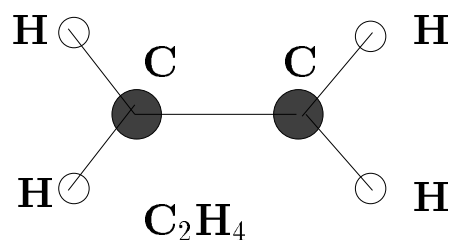
To find the representations contained in the directed valence for the π-bonds we have to go to rather high angular momentum states: $\ell = 2$ for an E'' state and $\ell = 3$ for an A_2' state. Such high angular momentum states correspond to much higher energy. Therefore π-bonding will be much weaker than σ-bonding. The irreducible representations $A_2'' + E''$ correspond to π-bonding in the z direction while the $A_2' + E'$ representations correspond to π-bonding in the plane of the triangle, but $\perp$ to the σ-bonding directions. We further note that the symmetries $A_2'' + E''$ correspond to p_z and d_{xz}, d_{yz} orbitals for angular momentum 1 and 2, respectively. On the other hand, the symmetries $A_2' + E'$ require $\ell = 3$ states, and therefore correspond to higher energies than the $A_2'' + E''$ orbitals. A diagram showing the orbitals for the σ-bonds and π-bonds for the various carbon atoms is given in Fig. 8.18.

8.8   Selected Problems

1. Consider a hypothetical SF_6 molecule with octahedral symmetry (p. 171 of class notes).
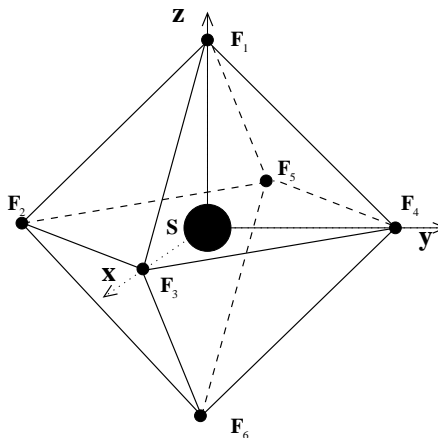
   (a) Using $\chi^{\text{atom sites}}$, construct the linear combination of atomic orbitals for the six fluorine atoms which transform according to the 3 irreducible representations contained in $\chi^{\text{atom sites}}$, assuming for the moment s functions on the six fluorine sites.

   (b) What are the symmetries for the six LCAO's in (a) if we assume that we have p-functions on each of the fluorine sites?

   (c) What are the irreducible representations corresponding to σ-bonds and π-bonds for the central sulfur atom to the 6 fluorine atoms? Sketch the orientation of these bonding orbitals.

   (d) What are the angular momentum states required to bond the sulfur to the fluorine.

2. C_2H_4 (ethylene) is a planar molecule which has the configuration shown on the diagram below:

C_2H_4

(a) Identify the appropriate point group for C_2H_4.

(b) Find $\chi^{\text{atom sites}}$ for the 2 carbon atoms and for the 4 hydrogen atoms.

(c) Give the block diagonal structure for the secular equation for the electronic energy levels of ethylene.

(d) How do the carbon atoms satisfy their bonding requirements? Which angular momentum states are needed to form bonding orbitals from each carbon atom?

3. Suppose that we have a hypothetical CdH_{12} molecule where the Cd $(4s^2 4p^6 4d^{10} 5s^2)$ is located at the center of a regular truncated icosahedron and 12 hydrogens are at the centers of the pentagonal faces.

   (a) Find a linear combination of atomic orbitals for the 12 hydrogen atoms that transform as irreducible representations of group I_h.

   (b) To make chemical bonds to the hydrogen atoms, what are the symmetries and angular momentum states that are needed to form the directed valence orbitals from the Cd atom to the 12 hydrogen atoms? Would you expect the hypothetical CdH_{12} molecule to be stable and why?

4. (a) Consider the hypothetical molecule XH_{12} where the 12 hydrogen atoms are at the vertices of a regular icosahedron and the atom X is at the center of the icosahedron. What are the symmetries and degeneracies of the 12 linear combinations of atomic orbitals (LCAO's) associated with the 12 equivalent hydrogen atoms?

(b) Give the linear combination of atomic orbitals (LCAO's) for the hydrogen atoms.

(c) What are the angular momentum states involved with each of the directed valence orbitals from the central atom X?

Chapter 9

Molecular Vibrations, Infrared, and Raman Activity

In this chapter we review molecular vibrations and present the use of group theory to identify the symmetry and degeneracy of the normal modes. Selection rules for infrared and Raman activity are also discussed and are illustrated for a variety of molecules selected for pedagogic purposes.

9.1 Molecular Vibrations – Background

A molecule having its ions at their equilibrium sites is in an energy minimum. If the ions are displaced from their equilibrium positions, a restoring force will be exerted which will tend to bring the ions back to equilibrium. If the displacement is small, the restoring forces will be harmonic. The vibrational motion of the molecule will thus be harmonic in the limit of small displacements.

Suppose that a molecule contains N ions and suppose further that the potential function is known from solution of the electronic problem (see Chapter 8). The potential function for the electronic problem is expressed in terms of the $3N$ coordinates for the N ions, $V(\vec{R}_1, \ldots, \vec{R}_N)$. We are particularly interested in $V(\vec{R}_1, \ldots, \vec{R}_N)$ about its equilibrium

value at $\vec{R}_1^\circ, \ldots, \vec{R}_N^\circ$. In solving the molecular vibration problem, we expand V about its equilibrium value, utilizing the fact that a minimum in energy implies the vanishing of the first derivative of the potential. We can conveniently take our zero of energy at the potential minimum and obtain a Hamiltonian for molecular vibrations in terms of displacements from equilibrium:

$$\mathcal{H} = \underbrace{\sum_k \frac{1}{2} m_k \dot{\xi}_k^2}_{\text{kinetic energy}} + \underbrace{\sum_{k,\ell} \frac{1}{2} \frac{\partial^2 V}{\partial \xi_k \partial \xi_\ell} \xi_k \xi_\ell}_{\text{potential energy}} \tag{9.1}$$

where m_k denotes the mass of the kth ion, ξ_k denotes its displacement coordinate, and the potential energy depends of the second derivative of $V(\vec{R}_1, \ldots, \vec{R}_N)$. The Hamiltonian in Eq. 9.1 gives rise to a $(3N \times 3N)$ secular equation. The roots of this secular equation are the eigenfrequencies ω_k^2 and the eigenvector is the normal mode linear combination of the displacements.

The usual procedure for finding the normal modes involves one transformation:

$$q_k = \sqrt{m_k} \, \xi_k \tag{9.2}$$

to eliminate the mass term in the kinetic energy, and a second transformation to express q_k in terms of the normal mode coordinates Q_K:

$$q_k = \sum_K a_{kK} Q_K \tag{9.3}$$

where a_{kK} denotes the amplitude of each normal mode Q_K that is contained in q_k.

Thus, by proper choice of the a_{kK} amplitudes we can use Eqs. 9.2 and 9.3 to reduce the potential energy to a sum of squares of the form $\omega_K^2 Q_K^2 / 2$. These transformations yield for the potential function in Eq. 9.1:

$$V = \frac{1}{2} \sum_{\substack{k,\,\ell \\ K,\,L}} \left(\frac{\partial^2 V}{\partial q_k \partial q_\ell} \right) a_{kK} a_{\ell L} Q_K Q_L = \frac{1}{2} \sum_K \omega_K^2 Q_K^2 \tag{9.4}$$

Table 9.1: Correspondence between the electronic problem and the molecular vibration problem.

Quantity	Electronic	Molecular Vibration
Matrix element	$H_{k\ell}$	$\frac{\partial^2 V}{\partial q_k \partial q_\ell}$
Eigenvalue	E_n	ω_K^2
Eigenfunction†	$\psi_n(r)$	a_{kK}

† For the molecular vibration problem, the eigenfunction is the normal mode amplitude while for the electronic problem it is the wavefunction.

———-

where the coefficients a_{kK} are chosen to form a unitary matrix satisfying Eq. 9.4. Thus we obtain the relations $a_{Kk}^\dagger = a_{Kk}^{-1} = a_{kK}$ if the matrix elements of a_{kK} are real. The a_{kK} coefficients are thus chosen to solve the eigenvalue problem defined in Eq. 9.4. To achieve the diagonalization implied by Eq. 9.4 we must solve the secular equation

$$\sum_{k,\ell} a_{Kk}^{-1} \left(\frac{\partial^2 V}{\partial q_k \partial q_\ell} \right) a_{\ell L} = \omega_K^2 \delta_{KL}. \tag{9.5}$$

Solution of the secular equation (Eq. 9.5) yields the eigenvalues or normal mode frequencies ω_K^2 and the eigenfunctions or normal mode amplitudes a_{kK} for $K = 1, \ldots, 3N$. From the form of the secular equation we can immediately see the correspondence between the electronic problem and the molecular vibration problem shown in Table 9.1.

9.2 Application of Group Theory to Molecular Vibrations

In an actual solution to a molecular vibration problem, group theory helps us to classify the normal modes and to find out which modes are coupled when electromagnetic radiation is incident on the molecule, either through electric dipole transitions (infrared activity) or in light scattering (Raman effect). We discuss all of these issues in this chapter.

We make use of the symmetry of the molecule by noting that the molecule remains invariant under a symmetry operation of the group of Schrödinger's equation. Therefore application of a symmetry operation $\hat{P}_R$ to an eigenfunction of a normal mode f_q just produces a linear combination of other normal modes of the same frequency ω_q. That is, f_q forms a basis for a representation for the symmetry operators $\hat{P}_R$

$$\hat{P}_R f_q^{(i)} = \sum_{q'} f_{q'}^{(i)} D^{(i)}(R)_{q'q} \tag{9.6}$$

where $D^{(i)}(R)_{q'q}$ is the matrix representation for symmetry operator R and i is the label for the irreducible representation which labels both the matrix and the basis function (normal mode coordinate in this case). Since different irreducible representations do not couple to each other, group theory helps to bring the normal mode matrix into block diagonal form, with each eigenvalue and its corresponding normal mode labeled by its appropriate irreducible representation. This is in concept similar to the solution of the electronic eigenvalue problem discussed in Chapter 8, except that every atom (or ion) in the molecule has 3 degrees of freedom, so that the vibration itself must transform as a vector. Thus the molecular vibration problem is analogous to the electronic problem for p-functions, since the p-functions also transform as a vector.

Therefore to find the normal modes for the vibration problem, we carry out the following steps:

1. Identify the symmetry operations and appropriate symmetry group G to describe the molecule in its equilibrium position.

2. Find $\chi_{\text{equivalence}} = \chi^{\text{atom sites}}$, the characters for the equivalence transformation, which represents the number of atoms that are invariant under the symmetry operations of the group. But since $\chi^{\text{atom sites}}$ is in general a reducible representation in group G, we must decompose $\chi^{\text{atom sites}}$ into its irreducible representations.

3. We now use the concept that a molecular vibration involves the transformation properties of a vector. In group theoretical terms, this means that the molecular vibrations are found by taking the direct product of $\chi^{\text{atom sites}}$ with the irreducible representations

for a polar vector. The characters for the molecular vibrations are thus found according to the relation

$$\chi_{\text{molecular vibrations}} = \left(\chi^{\text{atom sites}} \otimes \chi_{\text{vector}}\right) - \chi_{\text{translations}} - \chi_{\text{rotations}}$$
(9.7)

where the simple translations of the center of mass or rotations of the molecule about the center of mass do not contribute to the degrees of freedom for the molecular vibrations themselves. The characters found from Eq. 9.7 in general correspond to a reducible representation of Group G. We therefore express $\chi_{\text{molecular vibrations}}$ in terms of the **irreducible** representations of group G to obtain the normal modes. Each eigenmode is labeled by one of these irreducible representations, and the degeneracy of each eigenfrequency is the dimensionality of the corresponding irreducible representation. The characters for $\chi_{\text{translation}}$ are found by identifying the irreducible representations of the group G corresponding to the basis functions (x, y, z) for the radial vector. The characters for χ_{rotation} are found by identifying the irreducible representations corresponding to the basis functions (R_x, R_y, R_z) for the axial vector (e.g., angular momentum). Every standard character table normally lists the irreducible representations for the 6 basis functions for (x, y, z) and (R_x, R_y, R_z).

4. From the characters for the irreducible representations for the molecular vibrations, we find the normal modes. The normal modes for a molecule are constrained to contain **no translations or rotations** and to be orthogonal to each other.

5. We use the techniques for selection rules (see Chapter 7) to find out whether or not each of the vibrational modes is infrared active (can be excited by electromagnetic radiation, see §9.5) or Raman-active (see §9.8).

To illustrate the procedure for finding molecular vibrations, we will consider the molecular vibrations of an isolated H_2O water molecule.

(a)

A_1 **mode of** H_2O

(b)

A_1 **mode of** H_2O

(c)
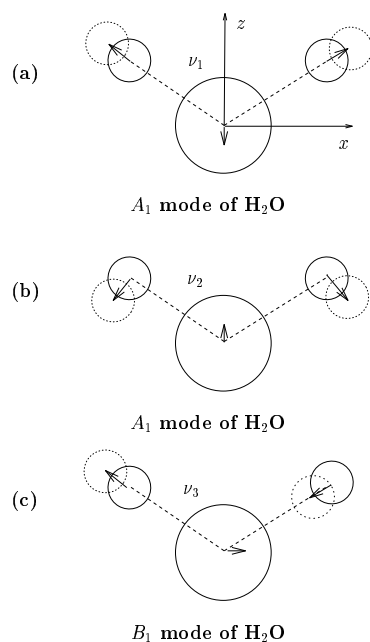
B_1 **mode of** H_2O

Figure 9.1: Normal modes for the H_2O molecule with 3 vibrational degrees of freedom. (a) The breathing mode with symmetry A_1, which changes only bond lengths. (b) The symmetric stretch mode of H_2O with A_1 symmetry, which changes bond angles. (c) The anti-symmetric stretch mode with B_1 symmetry.

9.3   Molecular Vibrations in H_2O

The four symmetry operations for the H_2O molecule (see Fig. 9.1) include E the identity operation, a $180°$ rotation C_2 around the z-axis, a reflection plane σ_v in the plane of molecule and a σ'_v reflection perpendicular to the plane of the molecule. The σ_v plane is a vertical reflection plane rather than a σ_h plane since the xz plane contains the highest symmetry axis C_2 rather than being $\perp$ to the highest symmetry axis and similarly for the σ'_v plane. The reflection plane $\sigma_{v'}$ which goes through C_2 is $\perp$ to the plane of the molecule. In labelling the axes, the plane of the H_2O molecule is denoted by xz, with the x axis parallel to a line going through the two hydrogens, and the perpendicular y axis goes through the oxygen atom. The appropriate point group for the H_2O molecule is the group C_{2v} and the character table is given below.

C_{2v} (2mm)			E	C_2	σ_v	σ_v'
x^2, y^2, z^2	z	A_1	1	1	1	1
xy	R_z	A_2	1	1	-1	-1
xz	R_y, x	B_1	1	-1	1	-1
yz	R_x, y	B_2	1	-1	-1	1

Next we find $\chi^{\text{atom sites}}$. For H_2O we have to consider the transformation of three atoms under the symmetry operations of the group. In writing down $\chi^{\text{atom sites}}$ we recall that for each site that is invariant under a symmetry operation, a contribution of $+1$ is made to the character of that operation; otherwise the contribution is zero. Thus, we obtain $\chi^{\text{atom sites}}(H_2O)$ for all 3 atoms in the H_2O molecule as given below:

	E	C_2	σ_v	$\sigma_{v'}$	
$\chi^{\text{atom sites}}(H_2O)$	3	1	3	1	$\Rightarrow 2A_1 + B_1$
$\chi^{\text{atom sites}}(2H)$	2	0	2	0	$\Rightarrow A_1 + B_1$

Also given in the above listing is $\chi^{\text{atom sites}}(2H)$ for the two hydrogens only. In both cases, the irreducible representations of group C_{2v} contained in $\chi^{\text{atom sites}}$ are listed. We note that for the 2 hydrogens considered by themselves, $\chi^{\text{atom sites}}(2H) = A_1 + B_1$, so that for the electronic problem, the appropriate LCAOs for the two hydrogen atoms are the bonding orbital $(\psi_{H_1} + \psi_{H_2})$ which transforms as A_1 and the antibonding orbital $(\psi_{H_1} - \psi_{H_2})$ which transforms as B_1.

From the character table we see that the vector transforms as

$$\chi_{\text{vector}} = A_1 + B_1 + B_2$$

where z, x, y, respectively, transform as A_1, B_1 and B_2. Likewise the irreducible representations for the rotations are $A_2 + B_1 + B_2$ corresponding to R_z, R_y, and R_x, respectively. We then calculate the irreducible representations contained in the molecular vibrations:

$$
\begin{aligned}
\chi_{\text{molecular vibrations}} &= \chi^{\text{atom sites}} \otimes \chi_{\text{vector}} - \chi_{\text{translations}} - \chi_{\text{rotations}} \\
&= (2A_1 + B_1) \otimes (A_1 + B_1 + B_2) - (A_1 + B_1 + B_2)
\end{aligned}
$$

$$-(A_2 + B_1 + B_2)$$
$$= \quad [3A_1 + 3B_1 + 2B_2 + A_2] - (A_1 + B_1 + B_2)$$
$$-(A_2 + B_1 + B_2)$$

$$\chi_{\text{molecular vibrations}} \quad = \quad 2A_1 + B_1$$

The 3 modes in $\chi_{\text{molecular vibrations}}$ are all 1-dimensional irreducible representations and therefore have non-degenerate or distinct vibrational frequencies. The 2 normal modes with A_1 symmetry must leave the symmetry undisturbed and this can be accomplished by the stretching of bonds and bond angles. These modes are the breathing and symmetric stretch modes (see Fig. 9.1).

We must now find the normal modes corresponding to each eigenfrequency. All molecules have a "breathing" mode which leaves the symmetry unchanged. To get the eigenvectors for the breathing mode of the H_2O molecule, assume that one of the hydrogen atoms is displaced in some way (as shown below). With A_1 symmetry this implies (under operation C_2) that the other H atom must be correspondingly displaced (see Fig. 9.1a). To prevent translations and rotations of the molecule, O must be displaced as shown. (The actual vibration amplitude for each atom is constrained to avoid translation and rotation of the molecule).

The same arguments can be applied to obtain the A_1 symmetric stretch mode shown in Fig. 9.1b. The H atom motion is taken so that the two A_1 modes are orthogonal. Since the breathing mode and symmetric stretch mode have the same symmetry they can mix (or couple to each other) and for this reason the directions of the H atom motion for each of the modes in Fig. 9.1a and Fig. 9.1b are not uniquely specified.

To obtain the normal mode for B_1 symmetry, we observe that the character for the C_2 operation is -1, so that the two hydrogen atoms must move in opposite directions relative to the OH bond. Likewise, the motion of the O atom must be odd under C_2. These arguments determine the normal B_1 mode shown in Fig. 9.1c.

As mentioned above, all molecules have a breathing mode which transforms as A_1 and preserves the molecular symmetry. As a practical matter in checking whether or not the calculated normal modes are proper normal modes, it is useful to verify that the normal mode motion

preserves the center of mass (conservation of linear momentum), that no torques are applied (angular momentum must be conserved), and that all normal modes are orthogonal to each other.

To identify which normal modes are infrared-active, we must consider the selection rules for the electromagnetic interaction. This is described in §9.5 in general terms, and is then illustrated for several types of molecules for illustrative purposes. In §9.8 the Raman selection rules are discussed and several illustrations are given.

9.4 Overtones and Combination Modes

The non-linear elastic constants in the equations of motion for the molecular vibrations give rise to overtones and combination modes which can be observed by either infrared or Raman spectroscopy.

The mode frequencies for the overtone modes (or harmonics) are at $\sim 2\omega_{\Gamma_i}$ and the symmetries are given by the direct product $\Gamma_i \otimes \Gamma_i$ where Γ_i corresponds to the symmetry of the fundamental mode at frequency ω_{Γ_i}. The combination modes are at frequencies $\sim (\omega_{\Gamma_i} + \omega_{\Gamma_j})$ and have symmetries given by $\Gamma_i \otimes \Gamma_j$. Some of these modes for the methane molecule CH_4 are given in Table 9.2 (see §9.8.4).

9.5 Infrared Activity

If electromagnetic radiation is incident on a molecule in its ground state, then the radiation will excite those vibrational modes which give rise to a dipole moment. In the ground state, the molecule has A_1 symmetry in accordance with the invariance of the Hamiltonian for the electronic ground state under the symmetry operations of the group of Schrödinger's equation. We can use group theory to decide whether or not an electromagnetic transition will occur. The perturbation Hamiltonian for the interaction of the molecule with the electromagnetic (infrared) interaction is

$$\mathcal{H}'_{\text{infrared}} = -\vec{E} \cdot \vec{u} = -\frac{e}{mc}\, \vec{p} \cdot \vec{A} \tag{9.8}$$

Table 9.2: Observed vibrational frequencies for the methane molecule.

Assignment	Symmetry	mode	Frequency (cm^{-1})
$\nu_1(A_1)$	A_1	fundamental	2914.2
$\nu_2(E)$	E	fundamental	1526
$\nu_3(T_2)$	T_2	fundamental	3020.3
$\nu_4(T_2)$	T_2	fundamental	1306.2
$2\nu_2$	$A_1 + E$	overtone[†]	3067.0
$2\nu_3$	$(A_1 + E) + T_2$	overtone[†]	6006
$3\nu_3$	$(A_1 + T_1) + 2T_2$	overtone[‡]	9047
$2\nu_4$	$(A_1 + E) + T_2$	overtone[†]	2600
$\nu_4 - \nu_3$	T_2	combination	1720
$\nu_2 + \nu_4$	$(T_1) + T_2$	combination	2823

[†] For overtones, only the symmetric combinations are Raman allowed.
[‡] For $3\nu_3$ the symmetric combinations correspond to the angular momentum states $L = 1$ which transforms as T_2 and $L = 3$ which transforms as $A_1 + T_1 + T_2$.

—

where $\vec{E}$ is the incident oscillating electric field, $\vec{u}$ is the induced dipole moment arising from atomic displacements, and $\vec{p}$ is the electronic momentum of the molecule. In this interaction, $\vec{u}$ and $\vec{p}$ transform like vectors. To find out whether incident electromagnetic radiation will excite a particular vibrational mode, we must examine the selection rule for the process. This means that we must see whether or not the matrix element for the excitation $(\psi_f|\vec{u}|\psi_i)$ vanishes, where ψ_f denotes the normal mode which we are trying to excite, $\vec{u}$ is the vector giving the transformation properties of $\mathcal{H}'_{\text{infrared}}$, and ψ_i denotes the initial state of the molecule, which for most cases is the ground state. The ground state has no vibrations and is represented by the totally symmetric state A_1.

We use the usual methods for finding out whether or not a matrix element vanishes. That is, we ask whether the direct product $\Gamma_{\text{vector}} \otimes \Gamma_i$ contains the representation Γ_f; if $(\Gamma_{\text{vector}} \otimes \Gamma_i)$ does not contain Γ_f, then the matrix element $\equiv 0$. Since molecular vibrations are typically excited at infrared frequencies we say that a molecule is **infrared active** if any molecular vibrations can be excited by the absorption of electromagnetic radiation. The particular modes that are excited are called **infrared-active modes**. Correspondingly, the modes that cannot be optically excited are called **infrared inactive**.

As applied to the H_2O molecule (see §9.3) we have the following identification of terms in the electromagnetic matrix element: ψ_1 has A_1 symmetry for the unexcited molecule, the vector $\vec{u}$ transforms as

$$\vec{u} \rightarrow A_1 + B_1 + B_2$$

corresponding to the transformation properties of z, x, y, respectively. Thus, we obtain

$$\chi_{\mathcal{H}'_{\text{infrared}}} \otimes \chi_{\psi_i} = (A_1 + B_1 + B_2) \otimes (A_1) = A_1 + B_1 + B_2 \qquad (9.9)$$

Therefore the two A_1 modes and the B_1 mode of water are all infrared-active. Each of the three vibrations corresponds to an oscillating dipole moment. As far as polarization selection rules are concerned, we can excite either of the two A_1 modes with an optical electric field in the z direction, the two-fold axis of the molecule. To excite the B_1

mode, the optical electric field must be along the x direction, the direction of a line connecting the two hydrogen atoms. An electric field in the y direction (perpendicular to the plane of the molecule) does not excite any vibrational modes. Since all vibrational modes of the water molecule can be excited by an arbitrarily directed $\vec{E}$ field, all the vibrational modes of the water molecule are infrared-active. It is not always the case that **all** vibrational modes of a molecule are infrared-active. It can also happen that for some molecules only a few of the modes are infrared-active. This situation occurs in molecules having a great deal of symmetry.

To observe infrared activity in the second-order infrared spectra, we require that the combination of two vibrational modes be infrared-active. From a group theoretical standpoint, the symmetry of the combination mode arising from constituent modes of symmetries Γ_i and Γ_j is given by the direct product $\Gamma_i \otimes \Gamma_j$. Since groups containing inversion symmetry have only odd parity infrared-active modes, such symmetry groups have no overtones in the second-order infrared spectrum.

9.6   Vibrations for Linear Molecules

The procedure for dealing with the molecular vibrations of linear molecules such as CO (Fig. 9.2) is slightly different from what has been described above. We now present a method for handling the linear molecules and give some examples.

For a linear molecule, the irreducible representations for the rotations just involves the rotations R_x and R_y, assuming the molecular axis to be along $\hat{z}$. Thus for the linear molecule, only two degrees of freedom are removed by $\chi_{\text{rotations}}$. We now illustrate this point with the CO molecule, followed by other linear molecules, each selected to demonstrate additional issues.

9.6.1   The CO Molecule

The appropriate symmetry group for CO is $C_{\infty v}$ (see §8.4.4). The symmetry operations $2C_\phi$ denote rotations about the $\hat{z}$ axis in clockwise and counter-clockwise senses by an arbitrary angle ϕ. Thus C_ϕ is a class

ν_1

A_1 mode of CO
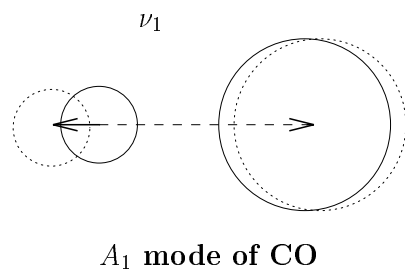
Figure 9.2: CO molecule having only an A_1 breathing mode.

with an ∞ number of members. The symmetry plane σ_v is a vertical plane through the molecular axis at an angle ϕ with respect to an arbitrary direction denoted by $\phi = 0$. Since the $2C_\phi$ and σ_v classes are of infinite order, the number of irreducible representations is also infinite.

The first step in finding $\chi_{\text{molecular vibrations}}$ for a linear molecule is to compute $\chi^{\text{atom sites}}$. For the CO molecule $\chi^{\text{atom sites}}$ becomes:

	E	$2C_\phi$	σ_v	
$\chi^{\text{atom sites}}$	2	2	2	$\Rightarrow 2A_1$

from which we find the irreducible representations for the molecular vibrations of CO remembering that $\chi_{\text{rotations}}$ only contains rotations in the xy plane:

$$
\begin{aligned}
\chi_{\text{molecular vibrations}} &= \chi^{\text{atom sites}} \otimes \chi_{\text{vector}} - \chi_{\text{translations}} - \chi_{\text{rotations}} \\
&= (2A_1) \otimes (A_1 + E_1) - (A_1 + E_1) - E_1 = A_1.
\end{aligned}
$$

The A_1 mode is the breathing mode for the CO molecule (see Fig. 9.2).
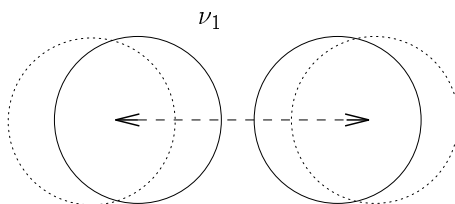
A_{1g} **mode of O$_2$**

Figure 9.3: The O$_2$ molecule having only an A_{1g} breathing mode.

9.6.2   The O$_2$ Molecule

If we now consider the O$_2$ molecule (see Fig. 9.3), we have a homonuclear molecule following the symmetry group $D_{\infty h}$ (see character Table 3.36). In this case

	E	$2C_\phi$	$2C_2'$	i	$2iC_\phi$	iC_2'	
$\chi^{\text{atom sites}}$	2	2	0	0	0	2	$\Rightarrow A_{1g} + A_{2u}$

Thus the irreducible representations for the molecular vibrations of O$_2$ become:

$$\chi_{\text{molecular vibrations}} = \chi^{\text{atom sites}} \otimes \chi_{\text{vector}} - \chi_{\text{translations}} - \chi_{\text{rotations}}$$

$$\chi_{\text{molecular vibrations}} = (A_{1g} + A_{2u}) \otimes (A_{2u} + E_{1u}) - (A_{2u} + E_{1u}) - E_{1g} = A_{1g}$$

Because of the inversion symmetry of the O$_2$ molecule, all the normal modes have either even (gerade) or odd (ungerade) symmetries.

Thus, for O$_2$ the breathing mode (see Fig. 9.3) has A_{1g} symmetry and is infrared-inactive. From simple physical considerations the breathing mode for O$_2$ has no oscillating dipole moment and hence should not couple to an electromagnetic field through an electric dipole

(a)

ν_1 **breathing**

A_{1g} **mode of CO$_2$**

(b)

ν_2 **stretch**

A_{2u} **mode of CO$_2$**

(c)

ν_3 **bending**
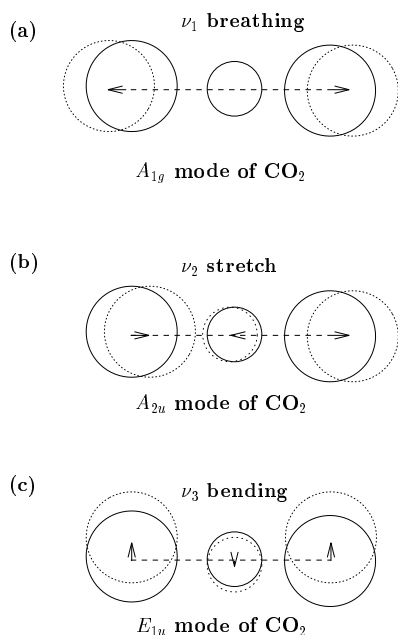
E_{1u} **mode of CO$_2$**

Figure 9.4: The CO$_2$ molecule having 3 vibrational normal modes: (a) the breathing mode of A_{1g} symmetry, (b) the antisymmetric stretch mode of A_{2u} symmetry, and (c) the doubly degenerate E_{1u} mode where the mode displacements for the two partners are orthogonal.

interaction, in agreement with our group theoretical result. In contrast, for the case of the CO molecule, there is an oscillating dipole moment and thus the CO molecule would be expected to be infrared-active, also in agreement with the group theoretical result.

9.6.3 The CO$_2$ Molecule

The CO$_2$ molecule is chosen for discussion to show the various types of modes that can be expected for linear molecules involving 3 or more atoms. In §9.6.4 we consider another molecule (C$_2$H$_2$) described by the same symmetry group $D_{\infty h}$ but having slightly more complexity.

For the case of CO$_2$ (see Fig. 9.4), we again have a linear molecule with $D_{\infty h}$ symmetry and now $\chi^{\text{atom sites}}$ corresponds to a three-dimensional representation:

	E	$2C_\phi$	C_2'	i	$2iC_\phi$	iC_2'	
$\chi^{\text{atom sites}}$	3	3	1	1	1	3	$\Rightarrow 2A_{1g} + A_{2u}$

so that

$$
\begin{aligned}
\chi_{\text{molecular vibrations}} \;=\;& \chi^{\text{atom sites}} \otimes \chi_{\text{vector}} - \chi_{\text{translations}} - \chi_{\text{rotations}} \\
=\;& (2A_{1g} + A_{2u}) \otimes (A_{2u} + E_{1u}) - (A_{2u} + E_{1u}) - E_{1g} \\
=\;& A_{1g} + A_{2u} + E_{1u}
\end{aligned}
$$

In this case the A_{2u} and E_{1u} modes are infrared-active while the symmetric A_{1g} mode is infrared-inactive. The normal modes for CO_2 are easily found with the help of the character table, and are shown in Fig. 9.4. The A_{1g} mode is the breathing mode, the A_{2u} mode is the antisymmetric stretch mode and the E_{1u} mode is a doubly degenerate bending mode where the displacements of the carbon and the two oxygens are normal to the molecular axis for each partner of the E_{1u} bending mode.

9.6.4   The C_2H_2 Molecule

For the case of the linear C_2H_2 molecule also following group $D_{\infty h}$ symmetry, we obtain:

$$
\chi^{\text{atom sites}} = 2A_{1g} + 2A_{2u} \tag{9.10}
$$

using the result for O_2 obtained in §9.6.2. Thus $\chi_{\text{molecular vibrations}}$ $(\chi_{m.v.})$ for the C_2H_2 molecule becomes:

$$
\begin{aligned}
\chi_{m.v.} \;=\;& (2A_{1g} + 2A_{2u}) \otimes (A_{2u} + E_{1u}) - (A_{2u} + E_{1u}) - E_{1g} \\
=\;& 2A_{1g} + A_{2u} + E_{1u} + E_{1g}
\end{aligned}
$$

The five normal modes for the molecular vibrations of C_2H_2 are shown in Fig. 9.5, again illustrating the breathing, antisymmetric stretch and bending modes corresponding to 5 different vibrational frequencies. These concepts can of course be generalized to give normal modes for more complex linear molecules.

(a)

ν_1 **breathing** ν_2 **breathing**

A_{1g} **modes of C$_2$H$_2$**

(b) ν_3 **stretch**

A_{2u} **mode of C$_2$H$_2$**

(c)

ν_4 **bending** ν_5 **bending**

E_{1g} **mode of C$_2$H$_2$** E_{1u} **mode of C$_2$H$_2$**
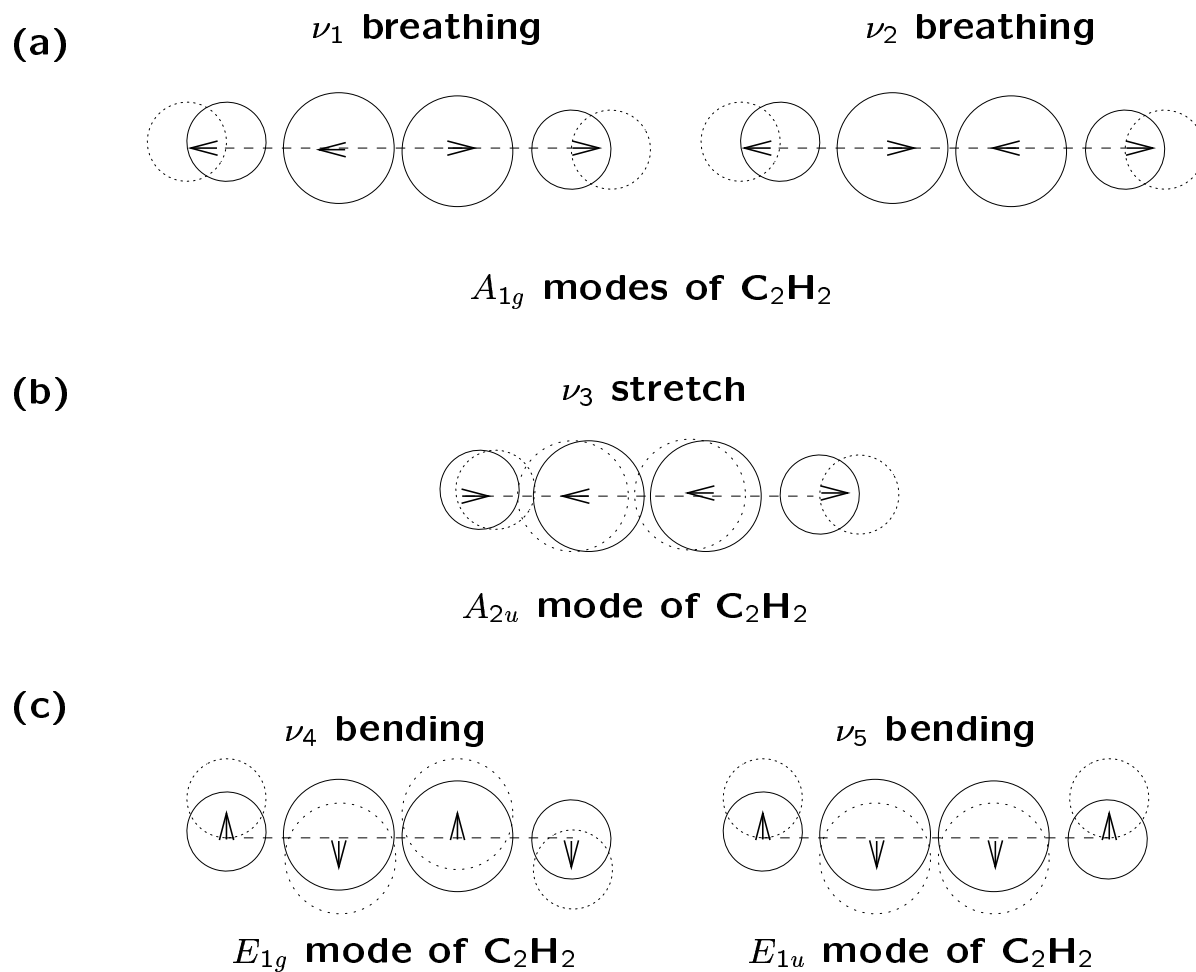
Figure 9.5: Schematic diagram of the normal modes of the linear C$_2$H$_2$ molecule: (a) two breathing modes of A_{1g} symmetry, (b) an antisymmetric stretch mode of A_{2u} symmetry, and (c) and (d) two doubly-degenerate bending modes of E_{1g} and E_{1u} symmetries.

9.7 Molecular Vibrations in Other Molecules

In this section we illustrate how symmetry is used in molecular vibration problems for several cases of pedagogic interest.

9.7.1 Vibrations of the NH_3 Molecule

To illustrate some features of degenerate normal modes, let us consider the NH_3 molecule (see Fig. 9.6). The hydrogen atoms in NH_3 are at the corners of an equilateral triangle and the nitrogen atom is either above or below the center of the triangle. If the molecule were planar it would have D_{3h} symmetry, but because the N atom is not coplanar with the hydrogens, the appropriate symmetry group is C_{3v} (see Table 3.15). To obtain the molecular vibrations we find $\chi^{\text{atom sites}} = \chi_{\text{a.s.}}$ first for all four atoms and then for the three hydrogen atoms separately:

	E	$2C_3$	$3\sigma_v$	
$\chi_{\text{a.s.}}^{\text{total}}$	4	1	2	$\Rightarrow 2A_1 + E$
$\chi_{\text{a.s.}}^{\text{H}}$	3	0	1	$\Rightarrow A_1 + E$

$$
\begin{aligned}
\chi_{\text{molecular vibrations}} &= \chi^{\text{atom sites}} \otimes \chi_{\text{vector}} - \chi_{\text{translations}} - \chi_{\text{rotations}} \\
&= (2A_1 + E) \otimes (A_1 + E) - (A_1 + E) - (A_2 + E) \\
&= 2A_1 + 2E
\end{aligned}
$$

The two modes of NH_3 with A_1 symmetry are breathing modes both in-plane and in the z-direction as shown in Fig. 9.6.

- One mode of the NH_3 molecule with A_1 symmetry is the breathing mode where the nitrogen atom is at rest and the equilateral triangle expands and contracts.

- For the A_1 out-of-plane breathing mode, the H atoms move in the $+z$ direction while the N atom moves in the $-z$ direction such that no translation results.
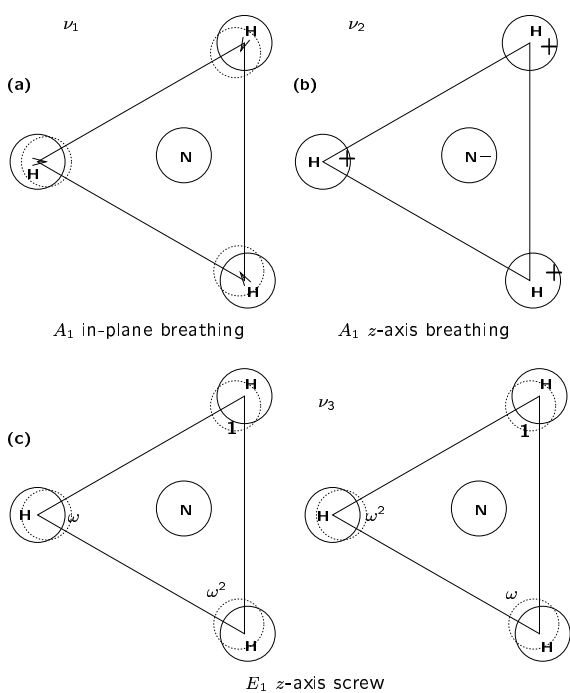
Figure 9.6: Normal modes for the NH_3 molecule: (a) the in-plane breathing mode, (b) the z-axis breathing mode, and (c) one partner of the in-plane mode of E symmetry; the second partner (complex conjugate of the first) is not shown. Also the other doubly-degenerate E mode for z-axis motion is not shown.

- One of the E modes is a doubly-degenerate in-plane mode. One eigenvector is made from the linear combination of hydrogen atom motions, $H_a + \omega H_b + \omega^2 H_c$ where the motion of each H atom bears a phase relation of $\omega = e^{2\pi i/3}$ relative to the next H atom. The second eigenvector is $H_a + \omega^2 H_b + \omega H_c$ which is orthogonal to the first. The nitrogen atom moves in the xy plane in such a way as to prevent translation of the center of mass and rotation of the molecule.

- For the second doubly degenerate E mode, the hydrogen atoms move along the z-direction with a phase difference between adjacent hydrogen atoms of $\omega = e^{2\pi i/3}$ for one partner and $\omega^2 = e^{4\pi i/3}$ for the other partner. The nitrogen atom again moves in the $x-y$ plane to prevent translations or rotations of the molecule.

The molecular vibrations for the NH_3 molecule illustrate the concept of phase relations between the motions of various atoms in executing a normal mode. Though it should be emphasized that in the case of degenerate modes, the normal mode (basis function) picture is not unique, and linear combinations of modes of the same symmetry are possible.

Since the normal modes for the NH_3 molecules have A_1 and E symmetries and since $\chi_{\text{vector}} = A_1 + E$, all the vibrational modes for NH_3 are infrared-active with one of the two A_1 modes excited by polarization $\vec{E} \parallel \hat{z}$, the other being excited by polarization $\vec{E} \perp \hat{z}$ and likewise for the two E modes.

9.7.2   Vibrations of the CH_4 Molecule

The CH_4 molecule is chosen for discussion to show that not all modes are infrared-active and to give more practice with T_d symmetry because of the importance of this symmetry to semiconductor physics.

In the case of the CH_4 molecule $\chi^{\text{atom sites}}$ for all the hydrogens and the carbon atom (see Fig. 9.7) contains the irreducible representations of the point group T_d: $(2A_1 + T_2)$ (see §8.2). In T_d symmetry, the vector transforms as T_2 while the angular momentum transforms as T_1. We thus get for the symmetry types in the molecular vibrations

$\chi_{\text{molecular vibrations}} = \chi_{\text{m.v.}}$ (see Fig. 9.7):

$$\chi_{\text{m.v.}} = [(2A_1 + T_2) \otimes (T_2)] - \underbrace{T_2}_{\text{translations}} - \overbrace{T_1}^{\text{rotations}}$$
$$= 2T_2 + (T_1 + T_2 + E + A_1) - T_2 - T_1$$
$$= A_1 + E + 2T_2$$

For many molecules of interest, the normal modes are given in Herzberg's book on IR and Raman Spectra, though you may find the diagrams difficult to understand. We give in Fig. 9.7 the normal modes found in Herzberg, as well as our own version.

9.7.3   Vibrations of the $B_{12}H_{12}$ Molecule

In this subsection we consider the molecular vibrations for a molecule with many atoms and this example also provides more practice with the use of the icosahedral group I_h.

Referring to Table 3.40 and §8.5.5, where the symmetry of the electronic states of the $B_{12}H_{12}$ molecule is discussed, we find that the equivalence transformation for the twelve B atoms or the 12 H atoms is the same and each gives:

$$\chi^{\text{atom sites}} = A_g + H_g + F_{1u} + F_{2u} \tag{9.11}$$

so that together the $B_{12}H_{12}$ molecule gives $2(A_g + H_g + F_{1u} + F_{2u})$ for $\chi^{\text{atom sites}}$. From the character table for icosahedral symmetry (Table 3.40), we see that the vector in I_h symmetry transforms as F_{1u}. We can now find the vibrational modes for $B_{12}H_{12}$ for $\chi_{\text{molecular vibrations}} = \chi_{\text{m.v.}}$ as

$$\chi_{\text{m.v.}}(B_{12}H_{12}) = \chi^{\text{atom sites}} \otimes \chi_{\text{vector}} - \chi_{\text{translations}} - \chi_{\text{rotations}}$$
$$= \left[2(A_g + H_g + F_{1u} + F_{2u}) \otimes F_{1u}\right] - F_{1u} - F_{1g}$$

Taking the indicated direct products we obtain

$$\chi_{\text{m.v.}}(B_{12}H_{12}) = 2(A_g \otimes F_{1u}) + 2(H_g \otimes F_{1u}) + 2(F_{2u} \otimes F_{1u})$$
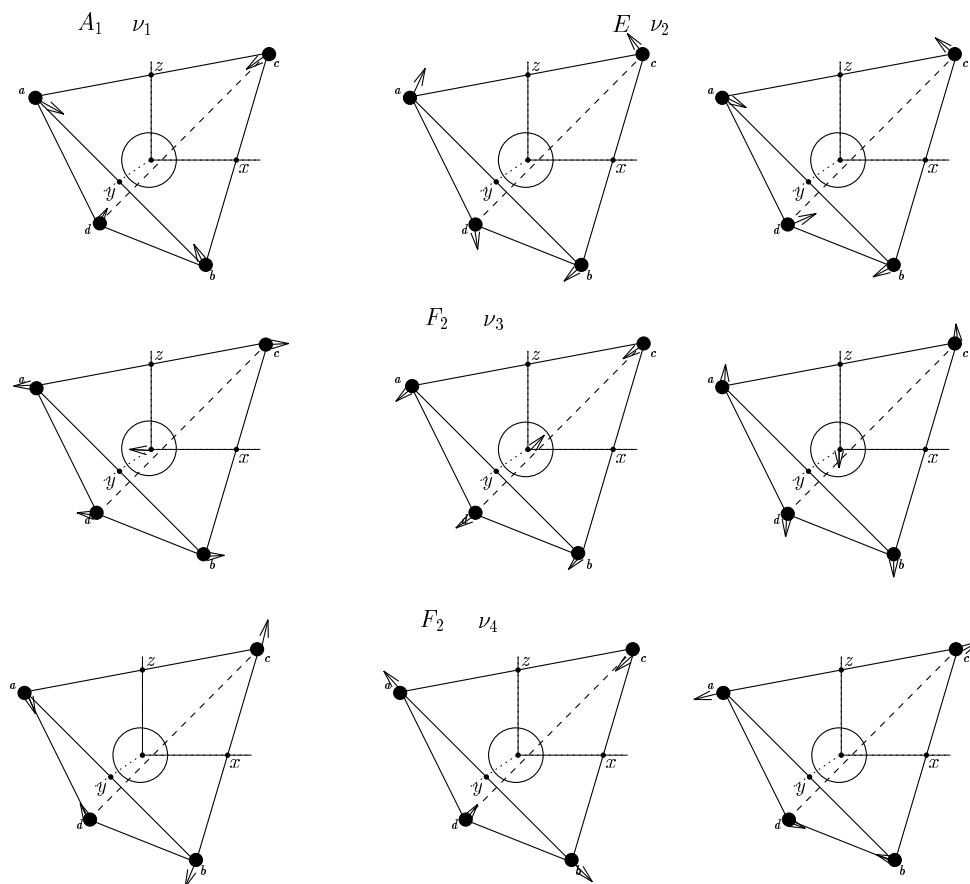
Figure 9.7: Normal vibrations of a tetrahedral XY_4 molecule such as methane taken from Herzberg's book. The three two-fold axes (dot-dash lines) are chosen as the x, y, and z axes.
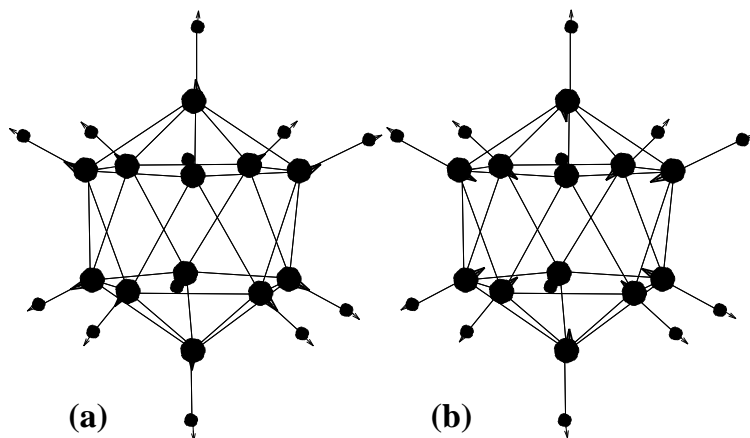
Figure 9.8: Displacement for the (a) A_g (B and H vibrating in phase) and (b) A_g (B and H vibrating out of phase) normal modes for the $B_{12}H_{12}$ molecule.

$$
\begin{aligned}
&+2(F_{1u} \otimes F_{1u}) - F_{1u} - F_{1g} \\
=\ & 2F_{1u} + 2(F_{1u} + F_{2u} + G_u + H_u) + 2(A_g + H_g + F_{1g}) \\
&+2(G_g + H_g) - F_{1u} - F_{1g} \\
=\ & 2A_g + F_{1g} + 2G_g + 4H_g \\
&+3F_{1u} + 2F_{2u} + 2G_u + 2H_u \qquad\qquad (9.12)
\end{aligned}
$$

representing 66 degrees of freedom. The symmetries of these 66 modes are tabulated in Table 9.3 where we also have listed the symmetries of the normal modes for the vibrations of C_{20}, C_{30}, and C_{60} clusters. The symmetries in $\chi^{\text{atom sites}}$ for these clusters are tabulated in Table 8.5. For the $B_{12}H_{12}$ molecule, we have 3 infrared-active F_{1u} modes (also called T_{1u} in some references), each of which is three-fold degenerate. Therefore polarization selection rules will be important for the IR spectra of $B_{12}H_{12}$. The A_g normal mode (see Fig. 9.8) is a breathing mode where all atoms are moving in phase and this mode is not infrared active.

Equation 9.12 shows that for the 66 modes, we have 18 distinct frequencies, only three of which will be seen on the infrared spectra. In §9.8 we discuss the symmetries of the Raman-active modes.

Table 9.3: Vibrational modes for clusters in I_h symmetry

Molecule	A_g	F_{1g}	F_{2g}	G_g	H_g	A_u	F_{1u}	F_{2u}	G_u	H_u
B_{12}	1			1	2		1	1	1	1
$B_{12}H_{12}$	2	1		2	4		3	2	2	2
C_{20}	1		1	2	3		1	2	2	2
C_{30}	1	1	2	3	4		2	3	3	3
C_{60}	2	3	4	6	8	1	4	5	6	7

9.8   Raman Effect

In the Raman effect we look at the light scattered from a system placed in an electromagnetic field. The **induced** dipole moment is

$$\vec{u} = \overset{\leftrightarrow}{\alpha} \cdot \vec{E}_0 \cos \omega t \tag{9.13}$$

where $\overset{\leftrightarrow}{\alpha}$ is the polarizability tensor, a second rank symmetric tensor. Because the incident light can excite molecular vibrations, the polarization tensor will have frequency dependent contributions at the molecular vibration frequencies ω_v

$$\overset{\leftrightarrow}{\alpha} = \overset{\leftrightarrow}{\alpha}_0 + \overset{\leftrightarrow}{\Delta\alpha} \cos \omega_v t \tag{9.14}$$

so that

$$
\begin{aligned}
\vec{u} &= \left(\overset{\leftrightarrow}{\alpha}_0 + \overset{\leftrightarrow}{\Delta\alpha} \cos \omega_v t \right) \cdot \vec{E}_0 \cos \omega t \\
&= \overset{\leftrightarrow}{\alpha}_0 \cdot \vec{E}_0 \cos \omega t + \frac{\overset{\leftrightarrow}{\Delta\alpha}}{2} \left[\cos(\omega - \omega_v)t + \cos(\omega + \omega_v)t \right] \cdot \vec{E}_0
\end{aligned}
$$

where the first term is the Rayleigh component at incident frequency ω, the second term is the Stokes component at frequency $(\omega - \omega_v)$, and the third term is the anti-Stokes component at frequency $(\omega + \omega_v)$. In observing the first-order Raman effect, the scattered light is examined for the presence of Stokes components at frequencies $(\omega - \omega_v)$ and of

anti-Stokes components at frequencies $(\omega+\omega_v)$. Not all normal modes of the molecule will yield scattered light at $(\omega\pm\omega_v)$, although if the Stokes component is excited, symmetry requires the anti-Stokes component to be present also.

To find the selection rules for the Raman effect we observe that the polarizability $\overleftrightarrow{\alpha}$ in Eq. 9.13 is a **second rank symmetric tensor** and has the same transformation properties as a general quadratic form— e.g., $x^2, y^2, z^2, xy, yz, zx$. We note here that the symmetric off-diagonal components correspond to combinations $(xy + yx)/2$ and the corresponding terms for yz and zx. The antisymmetric terms correspond to $(xy - yx)/2$ and its partners, which transform as the angular momentum. The basis functions for the angular momentum are given in the character table by R_x, R_y, and R_z.

In this section we will find the Raman activity for the molecules considered previously in this chapter. To find whether or not a vibrational mode is Raman active, we ask whether or not the matrix element for the Raman perturbation Hamiltonian vanishes. The Raman perturbation Hamiltonian is of the $-\vec{u}\cdot\vec{E}$ form and using Eq. 9.13, $\mathcal{H}'_{\text{Raman}}$ is written as:

$$\mathcal{H}'_{\text{Raman}} = -\frac{\overleftrightarrow{\Delta\alpha}}{2}\ \vec{E}\vec{E}\cos(\omega\pm\omega_v)t \qquad (9.15)$$

where the transformation properties of $\mathcal{H}'_{\text{Raman}}$ are those of a second rank symmetric tensor, since the tensor $(\vec{E}\vec{E})$ is external to the molecular system and it is only the polarizability tensor that pertains to the molecule. To find out whether a given normal mode is Raman active we consider the matrix element:

$$(\psi_f|\mathcal{H}'_{\text{Raman}}|\psi_i) \qquad (9.16)$$

where ψ_f is the final state corresponding to a normal mode we are trying to excite, $\mathcal{H}'_{\text{Raman}}$ is the Raman perturbation Hamiltonian which has the transformation properties of a symmetric 2nd rank tensor, and ψ_i is the initial state generally taken as the ground state which has the full symmetry of the group of Schrödinger's equation. A vibrational mode is Raman active if the direct product $(\Gamma_i\otimes\Gamma_{\text{2nd rank symmetric tensor}})$ contains the irreducible representation for the final state Γ_f. This is the basic selection rule for Raman activity.

In quantum mechanics, the Raman process is a second order process involving an intermediate state. This means that the Raman process involves the coupling by a vector interaction $\vec{V}$ of an initial state i to an intermediate state m and then from this intermediate state m to a final state f : $(i|\vec{V}|m)(m|\vec{V}|f)$. In terms of the spectroscopy of molecular systems with inversion symmetry, the Raman effect is especially important because it is a **complementary technique to infrared spectroscopy**. Since the infrared excitation is a first-order process and the dipole operator in $\mathcal{H}'_{\text{Raman}}$ transforms as a vector, selection rules for a vector interaction couple states with opposite parity. On the other hand, the Raman process being a second-order process is characterized by an interaction Hamiltonian $\mathcal{H}'_{\text{Raman}}$ which is even under inversion and therefore couples an initial and final state of similar parity. Thus infrared spectroscopy probes molecular vibrations with odd parity, while Raman spectroscopy probes modes with even parity.

The use of **polarized light** plays a major role in the assignment of experimentally observed Raman lines to specific Raman-active modes. In Raman experiments with polarized light, it is customary to use the notation: $\vec{k}_i(\vec{E}_i\ \vec{E}_s)\vec{k}_s$ to denote the incident propagation direction $\vec{k}_i$, the incident and scattered polarization directions $(\vec{E}_i\vec{E}_s)$ and the scattered propagation direction $\vec{k}_s$. From Eq. 9.15 we see that the Raman interaction Hamiltonian $\mathcal{H}'_{\text{Raman}}$ depends on both $\vec{E}_i$ and $\vec{E}_s$ and on the change in the polarizability tensor $\overleftrightarrow{\Delta\alpha}$, where $\vec{E}_i$ and $\vec{E}_s$ are, respectively, the incident and the scattered electric fields. It is customary to designate the scattered light as having **diagonal** Raman components $(\vec{E}_i \parallel \vec{E}_s)$, or **off-diagonal** Raman components $(\vec{E}_i \perp \vec{E}_s)$.

In the second-order Raman spectra, a combination mode or overtone will be observable if $\Gamma_i \otimes \Gamma_j$ for modes i and j contains irreducible representations that are themselves Raman-active. Some silent modes that cannot be found in the first-order spectrum can thus be observed in the second-order spectrum.

In the following subsections we discuss the Raman effect for the specific molecules previously discussed in this chapter, and in so doing, we will also include comments on the polarization selection rules.

9.8.1 The Raman Effect for H_2

The Raman effect is simplest for the homo-polar diatomic molecule H_2. The symmetry group in this case is $D_{\infty h}$. The only vibrational mode in this case has A_{1g} symmetry. Since $x^2 + y^2$ and z^2 all transform as A_{1g}, this mode will be Raman-active and the Raman tensor will have only diagonal components ($\vec{E}_i \parallel \vec{E}_s$), thereby giving the polarization selection rules.

9.8.2 The Raman Effect for H_2O

This molecule has C_{2v} point group symmetry. We take the initial state Γ_i to be the unexcited state which has A_1 symmetry, since the unexcited state always has the full symmetry of the molecule, which in the case of H_2O is the group C_{2v} (see §9.3). From the character table for C_{2v} in §9.3, we can write down the irreducible representations contained in the 2nd rank symmetric tensor (denoted here by Γ_{Raman}):

$$\Gamma_{\text{Raman}} = (3A_1 + A_2 + B_1 + B_2) \tag{9.17}$$

where $3A_1$ arises from the x^2, y^2, z^2 components, A_2 from the xy component, B_1 from the xz component, and B_2 from the yz component. Since $(\Gamma_i \otimes \Gamma_{\text{Raman}})$ contains all the symmetry types of group C_{2v}, all the normal modes for the H_2O molecule are Raman-active. Specifically the symmetries of the molecular vibrations for H_2O are $2A_1 + B_1$ and from Eq. 9.17 all of these modes are Raman-active.

The A_1 modes are observed when the incident (i) and scattered (s) light have polarization directions ($\vec{E}_i \parallel \vec{E}_s$), while the B_1 mode is observed for $\vec{E}_i \parallel \hat{x}$ and $\vec{E}_s \parallel \hat{z}$ or for $\vec{E}_i \parallel \hat{z}$ and $\vec{E}_s \parallel \hat{x}$. We thus say that the Raman tensor for the A_1 modes is diagonal, while for the B_1 mode it is off-diagonal.

9.8.3 The Raman Effect for NH_3

For the case of the NH_3 molecule which has C_{3v} symmetry (see §9.7.1), the Raman-active modes have the symmetries A_1 for $x^2 + y^2, z^2$ and E for $(x^2 - y^2, xy)$ and (xz, yz) so that all the normal modes for the NH_3 molecule ($2A_1 + 2E$) are Raman-active. Polarization selection rules

imply that the A_1 modes are diagonal (i.e., scattering occurs when $\vec{E}_i \parallel \vec{E}_s$) while the E modes are off-diagonal (i.e., scattering occurs when $\vec{E}_i \perp \vec{E}_s$).

9.8.4   The Raman Effect for CH$_4$

The appropriate symmetry group in this case is T_d (see §8.5.2 for the character table and notation). From §9.7.2, the molecular vibrations have $A_1 + E + 2T_2$ symmetries. Here again the unexcited state Γ_i has A_1 symmetry and the irreducible representations contained within the Raman second rank symmetric tensor include:

$$\Gamma_{\text{Raman}} = T_2 + E + A_1 \tag{9.18}$$

where (xy, yz, zx) transforms as T_2 and the basis functions $x^2 - y^2$, and $3z^2 - r^2$ transform as E while r^2 transforms as A_1. Thus we obtain

$$\Gamma_i \otimes \Gamma_{\text{Raman}} = A_1 + E + T_2 \tag{9.19}$$

which contains all the symmetries of the molecular vibrations. Thus all the normal modes are Raman-active for CH$_4$. The modes A_1 and E have diagonal Raman tensor components while the T_2 modes are fully off-diagonal. It is not always the case that all the normal modes are Raman-active. We illustrate this below. Examples of harmonics and combination modes that can be observed in the second-order Raman and infrared spectra are given in Table 9.2. In this table the frequencies of the four lines in the Raman spectra are given. We note that the T_2 modes are observed in the first-order infrared spectrum for CH$_4$. Some of the direct products of importance in interpreting the second-order spectra are

$$E \otimes E = A_1 + A_2 + E$$

and

$$T_2 \otimes T_2 = A_1 + E + T_1 + T_2.$$

9.8.5   The Raman Effect for CO$_2$ and C$_2$H$_2$

From §9.6.3 and §9.6.4 we see that $\chi_{\text{molecular vibrations}}$ for the two linear molecules CO$_2$ and C$_2$H$_2$ contains the irreducible representations for

the group $D_{\infty h}$:

$$\begin{aligned}
\mathrm{CO_2} &: \quad A_{1g} + A_{2u} + E_{1u} \\
\mathrm{C_2H_2} &: \quad 2A_{1g} + A_{2u} + E_{1u} + E_{1g}
\end{aligned}$$

$$(9.20)$$

From the character table for $D_{\infty h}$, the Raman tensor transforms as

$$A_{1g}(x^2 + y^2, z^2) + E_{1g}(xz, yz) + E_{2g}(x^2 - y^2, xy) \qquad (9.21)$$

where the subscripts on the coefficients give the pertinent symmetry types associated with the indicated basis functions. Thus for $\mathrm{CO_2}$ the only Raman-active mode is A_{1g}, while for $\mathrm{C_2H_2}$, the two A_{1g} modes and the E_{1g} mode are all Raman-active. Both of these molecules have inversion symmetry and therefore the modes $A_{2u} + E_{1u}$ are odd and are not Raman-active. These modes however are infrared-active. All Raman-active modes have even parity for systems with inversion symmetry.

9.8.6 The Raman Effect for Planar $\mathrm{XH_3}$

Consider a planar version of the ammonia molecule $\mathrm{NH_3}$, which we denote for illustrative purposes by $\mathrm{XH_3}$. The symmetry group in this case is D_{3h}. From §9.8.3, the irreducible representations contained in $\chi^{\mathrm{a.s.}}$ are: $A_1' + E'$ and those in χ_{vector} are $A_2'' + E'$. Then we can write for the irreducible representations for the normal modes:

$$\begin{aligned}
\chi_{\text{molecular vibrations}} &= \chi^{\mathrm{a.s.}} \otimes \chi_{\mathrm{vector}} - \chi_{\mathrm{trans}} - \chi_{\mathrm{rot}} \\
&= (A_1' + E') \otimes (A_2'' + E') - (A_2'' + E') - (A_1' + E'') \\
&= A_1' + A_2' + 2E'.
\end{aligned}$$

Of these modes, the E' mode is IR-active and the A_1' and E' modes are Raman-active. The A_2' mode is neither IR nor Raman-active, and is called a **silent** mode.

9.8.7 The Raman Effect for $\mathrm{B_{12}H_{12}}$

The vibrational levels were discussed in §9.7.3. The normal modes for the 66 degrees of freedom were found to be

$$2A_g + F_{1g} + 2G_g + 4H_g + 3F_{1u} + 2F_{2u} + 2G_u + 2H_u.$$

From the character table for group I_h we see that Γ_{Raman} contains the irreducible representations $A_g + H_g$ so that only six of the 18 eigen-frequencies of $B_{12}H_{12}$ are Raman active. The A_g mode is seen in the polarization $\vec{E}_i \parallel \vec{E}_s$, whereas the H_g mode is seen for all polarizations. Since the three F_{1u} mode frequencies correspond to infrared active vibrations, nine of the vibrational frequencies for $B_{12}H_{12}$ are silent in the first-order Raman and infrared spectra.

9.9   Rotational Energy Levels

In practice all molecules have rotational levels (labeled by quantum number J) very close in energy to the vibrational states. Since it is the total symmetry of the rotational-vibrational state that enters the selection rule, one expects to observe many Raman lines associated with each molecular vibration. We discuss the rotational energy levels in this section and the coupling between the rotational and vibrational levels in §9.10.

In the approximation that we can discuss the rotational motion as distinct from the translational motion, we consider the rotational motion of molecules to be much slower than the vibrational motion, and of course **very** much slower than the electronic motion. Typical rotational energies are of the order of ~ 1 meV and occur at far-infrared frequencies.

For some problems, it is adequate to consider the molecule as a rigid rotator, neglecting the effect of the molecular vibrations. The Hamiltonian is then written as:

$$\mathcal{H} = \frac{J_x^2}{2I_x} + \frac{J_y^2}{2I_y} + \frac{J_z^2}{2I_z} \qquad (9.22)$$

where I_x, I_y, I_z are the principal moments of inertia and J_x, J_y, J_z are the angular momentum components. The coordinates x, y, z are chosen so that the z axis is along the **figure** axis or the main symmetry axis of rotation of the molecule. If we have a diatomic molecule, one principal moment of inertia vanishes while the other two become equal. In this

case the Hamiltonian is simply

$$\mathcal{H}' = \frac{J^2}{2I} \tag{9.23}$$

and has eigenvalues

$$E_j = \hbar^2 j(j+1)/2I.$$

Unlike the vibrational energy levels which are all equally spaced with a level separation $\hbar\omega_v$, the rotational energy levels are unequally spaced:

$$E_{j+1} - E_j = \mathcal{C}[(j+1)(j+2) - j(j+1)] = 2\mathcal{C}(j+1). \tag{9.24}$$

and the level spacing depends on the quantum number j (see Fig. 9.9). If the molecule contains a permanent electric dipole moment, then it is possible to excite the molecule into higher rotational energy states by electric dipole transitions. For light polarized along the principal axis of rotation, the selection rule for electric dipole transitions is $\Delta j = 0$ while for light polarized in the plane $\perp$ to this axis, the selection rule is $\Delta j = \pm 1$ (Wigner–Eckart theorem, which is discussed in §9.11).

Thus, the first rotational transition will have energy $2\mathcal{C}$, the second $4\mathcal{C}$, the third $6\mathcal{C}$, etc. This pattern is indicated in Fig. 9.9, and is in contrast with the vibrational levels which have a constant separation energy of $\hbar\omega_v$. It is clear that diatomic molecules like H_2 have a **center of inversion** and hence **no permanent dipole moment**. Thus, molecules of this type do not exhibit any rotational infrared spectra. On the other hand, molecules like CO can exhibit rotational infrared spectra.

Also of interest are molecules which are more complex than the linear molecules. One class of molecules that are of interest and have sufficient symmetry to make the use of group theory helpful is the **symmetric top molecule**. Here we have 2 principal moments of inertia that are equal, $I_y = I_x$, and a third non-vanishing moment of inertia I_z that is unequal to the others. When we now quantize the angular momentum, we must not only quantize the total angular momentum J^2, but we must also quantize the component of angular momentum about the figure axis J_z. The quantum numbers that are used are K for J_z along the figure axis

$$(jK|J_z|jK) = \hbar K \tag{9.25}$$
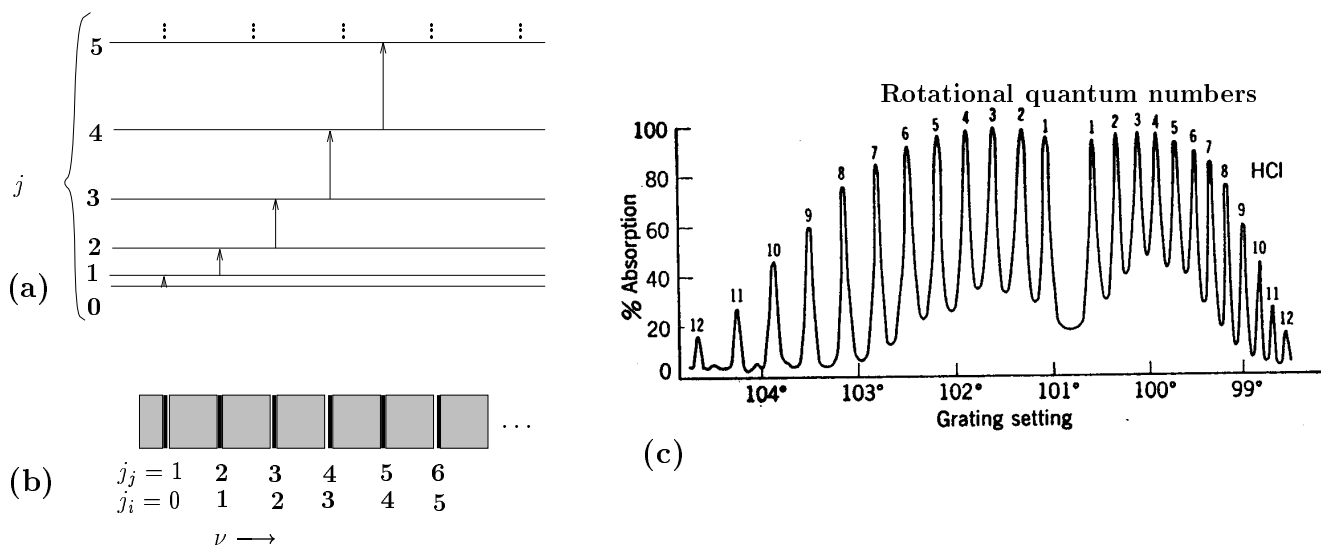
Figure 9.9: (a) Rotational levels of a diatomic molecule. (b) Energy separation between sequential rotational levels. (c) The rotational absorption spectrum for gaseous HCl.

where the integer K can assume values from $-j$ up to j. The total angular momentum obeys the relation

$$\left(jK|J^2|jK\right) = \hbar^2 j(j+1) \tag{9.26}$$

so that by writing the Hamiltonian for the symmetric top molecules as

$$\mathcal{H} = \frac{J_x^2 + J_y^2}{2I_x} + \frac{J_z^2}{2I_z} = \frac{J^2 - J_z^2}{2I_x} + \frac{J_z^2}{2I_z} \tag{9.27}$$

we obtain the energy eigenvalues

$$E(j, K) = \frac{\hbar^2 j(j+1)}{2I_x} + \frac{\hbar^2 K^2}{2}\left(\frac{1}{I_z} - \frac{1}{I_x}\right). \tag{9.28}$$

The selection rules for electric dipole transitions in symmetric top molecules occurring between purely rotational states are $\Delta K = 0$, along with $\Delta j = 0, \pm 1$, as for the case of diatomic molecules.

From a group theoretical standpoint the various angular momentum states will correspond to different irreducible representations and

the selection rules follow from determination of the vanishing or non-vanishing of the matrix element coupling the initial state (no rotation, $J = 0$) to the final rotational state.

9.10 Vibrational-Rotational Interaction

Since the nuclei of a molecule are actually in vibrational motion, there is consequently an interaction between the vibrational and rotational motions. Let us illustrate this coupling in terms of the diatomic molecule, where we write for the Hamiltonian

$$\mathcal{H} = \frac{p^2}{2\mu} + \frac{J^2}{2\mu R^2} + a_2 \xi^2 + a_3 \xi^3 \tag{9.29}$$

in which the first term is the kinetic energy (and μ is the reduced mass of the molecule). The second term denotes the rotational energy of the molecule, while $a_2 \xi^2$ is the harmonic restoring force for the vibrational energy, and $a_3 \xi^3$ is an anharmonic restoring term arising in the vibrational problem. The distance between the nuclei is now modified by the vibrational displacements from equilibrium

$$\frac{R - R_{\text{eq}}}{R_{eq}} = \xi \qquad \text{where} \qquad R = R_{\text{eq}}(1 + \xi). \tag{9.30}$$

We therefore write

$$\frac{1}{R^2} = \frac{1}{R_{\text{eq}}^2 (1 + \xi)^2} = \frac{1}{R_{\text{eq}}^2} \left[1 - 2\xi + 3\xi^2 + \ldots\right] \tag{9.31}$$

so that we can express the Hamiltonian in terms of an unperturbed term $\mathcal{H}_0$ and a perturbation term $\mathcal{H}'$:

$$\mathcal{H} = \mathcal{H}_0 + \mathcal{H}' \tag{9.32}$$

where

$$\mathcal{H}_0 = \frac{p^2}{2\mu} + B_{\text{eq}} J^2 + a_2 \xi^2 \tag{9.33}$$

and

$$B_{\text{eq}} = \frac{1}{2\mu R_{\text{eq}}^2}. \tag{9.34}$$

The first term in Eq. 9.33 denotes the kinetic energy and the second term defines the rotational energy when the molecule is in its equilibrium configuration, while the third term denotes the vibrational potential energy for the harmonic restoring forces. Thus $\mathcal{H}_0$ gives the energies for the vibrational and rotational motion in the limit where the vibrational and rotational motions are decoupled. For the $\mathcal{H}_0$ limit the selection rules are the same as if the vibrations and rotations occurred independently. The perturbation Hamiltonian then becomes

$$\mathcal{H}' = a_3\xi^3 - 2B_{\text{eq}}\xi J^2 + 3B_{\text{eq}}\xi^2 J^2 \tag{9.35}$$

where the first term is an anharmonic term that gives rise to overtones and combination modes in the vibrational spectrum. The second and third terms in Eq. 9.35 are associated with coupling between rotational and vibrational levels and give corrections to the rotational levels. The term in ξJ^2 makes a contribution in 2nd-order perturbation theory, while the term in $\xi^2 J^2$ makes a contribution in 1st-order perturbation theory which is proportional to

$$\left(n + \frac{1}{2}\right)\hbar\omega_v j(j+1).$$

Thus, the application of perturbation theory results in energy levels for the vibrational-rotational problem:

$$E_{n,j} = \underbrace{\hbar\omega_v\left(n + \frac{1}{2}\right)}_{\text{pure vibrational}} + \underbrace{\mathcal{A}_1 j(j+1)}_{\text{pure rotational}} + \underbrace{\mathcal{A}_2\,\hbar\omega_v\left(n + \frac{1}{2}\right)j(j+1) + \dots}_{\text{interaction terms}} \tag{9.36}$$

in which $\mathcal{A}_1$ and $\mathcal{A}_2$ are constants. For the diatomic molecule $\mathcal{A}_1 = (\hbar/2I)$ in accordance with Eq. 9.23. From a group theoretical point of view, the interaction terms modify the selection rules and new features in the IR and Raman specta can be seen. In general the symmetry of an interacting vibrational and rotational level is given by the direct product $\Gamma_{\text{vib}} \otimes \Gamma_{\text{rot}}$.

In making rotational transitions on absorption between different vibrational levels, we not only can have $\Delta j = 1$ **(the R branch)** but we also can have $\Delta j = -1$ **(the P branch)**. This is illustrated in the vibrational-rotational spectrum shown in Figure 9.10 for the HCl

Figure 9.10: P and R branches of the rotational structure of the HCl vibrational-rotational band near 2885 cm^{-1}.

molecule. We note here that the spectral lines in the R branch (up-shifted in frequency) are not symmetrically spaced with respect to the down-shifted P branch. The **Q branch** ($\Delta j = 0$) occurs very close to the central frequency ν_0, and would in fact be coincident with ν_0 if the moment of inertia would be independent of the vibrational state. Study of the Q branch requires high resolution laser spectroscopy.

If there were no vibrational-rotational interaction, the spacing of all spectral lines (shown in the top portion of Figure 9.10) would be the same for all vibrational levels n. For the case of diatomic molecules and for the polarization where $\vec{E}$ is along the molecular axis, then the selection rules $\Delta n = +1$ and $\Delta j = 0$ determine the vibrational-rotational spectrum, while for $\vec{E} \perp$ to the main symmetry axis of the molecule, the selection rules are $\Delta n = 0$ and $\Delta j = +1$.

Rotational Raman Spectra are also observed. Here the transitions with $\Delta j = 2$ are excited for the pure rotational transitions, $\Delta n = 0$ (see Figs. 9.9 and 9.10). This series is called the **S branch**.

When vibrational-rotational Raman spectra are excited, transitions with $\Delta j = 0$ and $\Delta j = -2$ are also possible and these are called the O **branches**. Because of the anharmonic terms in the Hamiltonian, there are vibrational-rotational spectra which occur between vibrational states separated by $\Delta n = 2, 3, \ldots$, etc. These anharmonic transitions would be expected to have lower intensity.

The above discussion focused on the vibrational degrees of freedom. There are in addition the electronic levels which generally are separated by much greater energies than are the vibrational and rotational levels. There is however some interaction also between the vibrational and rotational states and the electronic levels. **Interactions between the electronic and rotational levels** give rise to "Λ-doubling" of the rotational levels, and **coupling between the electronic and vibrational levels** gives rise to **vibronic levels**.

9.11   Wigner–Eckart Theorem and Selection Rules

For proof of the Wigner–Eckart theorem see Tinkham p. 131-2. This theorem deals with the matrix elements of a tensor T_μ^ω where ω is the rank of the tensor and μ is a component index, to be discussed further below. The theorem is discussed for angular momentum states which correspond (through the group of Schrödinger's equation) to the full rotation group.

The full rotation group has only odd–dimensional representations:

1-dimensional	$\ell = 0$	s-states
3-dimensional	$\ell = 1$	p-states
5-dimensional	$\ell = 2$	d-states

Thus, a scalar ($\ell = 0$) corresponds to a tensor with $\omega = 0$ and $\mu = 0$. A vector corresponds to a tensor with $\omega = 1$, $\ell = 1$ and $\mu = \pm 1, 0$, the three m_ℓ values for $\ell = 1$. A second rank tensor can be considered as the direct product

$$\Gamma^{\ell=1} \otimes \Gamma^{\ell=1} = \Gamma^{\ell=0} + \Gamma^{\ell=1} + \Gamma^{\ell=2} \tag{9.37}$$

having dimensions $3 \times 3 = 1 + 3 + 5 = 9$. Thus the second rank tensor will have a part which transforms as $\omega = 0$ and $\mu = 0$, another part which transforms as $\omega = 1$, $\mu = \pm 1, 0$ and a third part which transforms as $\omega = 2$, $\mu = \pm 2, 1, 0$. The part that transforms as $\omega = 0$ and $\omega = 2$ constitute the symmetric components and the parts that transforms as $\omega = 1$ corresponds to the anti-symmetric components of a second rank tensor.

The Wigner–Eckart Theorem gives the selection rules for a tensor operator T_μ^ω between states having full rotational symmetry

$$\left(N'j'm' \left| T_\mu^\omega \right| Njm \right) = A_{m\mu}^{j\omega j'} \delta_{m',m+\mu} \left(N'j' ||T^\omega|| Nj \right) \tag{9.38}$$

where j' lies in the range

$$|j - \omega| \leq j' \leq (j + \omega). \tag{9.39}$$

In Eq. 9.38, N and N' are principal quantum numbers, j and j' are quantum numbers for the total angular momentum, while m and m' are quantum numbers for the z component of the angular momentum. The coefficients $A_{m\mu}^{j\omega j'}$ are called Wigner coefficients and are tabulated in group theory texts. The reduced matrix element $(N'j'||T^\omega||Nj)$ in Eq. 9.38 is independent of μ, m and m' and can therefore be found for the simplest case $\mu = m' = m = 0$.

Thus the Wigner–Eckart Theorem gives selection rules on both j and m. Rewriting the restrictions implied by Eqs. 9.38 and 9.39 yields the selection rules

$$
\begin{aligned}
|\Delta j| &= |j - j'| \leq \omega \\
|\Delta m| &= |m' - m| = \mu \leq \omega.
\end{aligned}
\tag{9.40}
$$

We now write down special cases of Eq. 9.40. For electric dipole transitions ($\omega = 1$) for which the dipole is induced, we have the selection rules:

$$
\begin{aligned}
\Delta j &= 0, \pm 1 \\
\Delta m &= 0 \text{ for } \vec{E} \parallel \hat{z} \\
\Delta m &= \pm 1 \text{ for } \vec{E} \perp \hat{z}
\end{aligned}
\tag{9.41}
$$

where $\vec{E} \parallel \hat{z}$ refers to linear polarization along the quantization axis and $\vec{E} \perp \hat{z}$ refers to circular polarization about the quantization axis. For Raman transitions (where $\mathcal{H}'_{\text{Raman}}$ transforms as a second rank symmetric tensor) we have either $\omega = 0$ or $\omega = 2$ and the corresponding selection rules:

$$\begin{aligned} \omega = 0 : \qquad &\Delta j = 0 \qquad \Delta m = 0 \\ \omega = 2 : \qquad &\Delta j = 0, \pm 1, \pm 2 \quad \Delta m = 0, \pm 1, \pm 2 \end{aligned} \qquad (9.42)$$

In specific geometries, not all of these transitions are possible.

In applying the Wigner–Eckart theorem to the **rotational selection rules** for a **linear diatomic molecule**, we know that the dipole moment must be along the molecular z axis, so that only $\mu = 0$ applies. In this case the **Wigner–Eckart Theorem** gives the selection rules

$$\begin{aligned} \Delta j = 0, \pm 1; \quad &\Delta m = 0 \quad \text{for I.R. activity} \\ \Delta j = 0, \pm 2; \quad &\Delta m = 0 \quad \text{for Raman activity} \end{aligned} \qquad (9.43)$$

Since $\mu = 0$ is the only applicable component for the symmetric top molecule, the same selection rules (Eq. 9.43) as given for the linear diatomic molecule also apply to the symmetric top molecule. The case $\Delta j = \pm 1$ does not occur for Raman scattering because the Raman tensor only contains the symmetric components of the second rank tensor, whereas $\Delta j = \pm 1$ corresponds to the antisymmetric components of the second rank tensor.

9.12   Selected Problems

1. C_2H_4 (ethylene) is a planar molecule which has the configuration shown on the diagram below:

C_2H_4

(a) Using the point group and $\chi^{\text{atom sites}}$ found in Problem 2 of §8.8, find the symmetries of the allowed molecular vibrations.

(b) Sketch the normal mode displacements for each of the allowed molecular vibrations in (a).

(c) Which modes are infrared-active? Which are Raman-active? What are the polarization selection rules?

2. Both CO_2 and N_2O are linear molecules, but have different equilibrium arrangements:

CO_2

N_2O
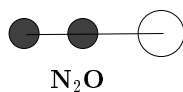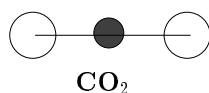
(a) What are the appropriate point groups for CO_2 and N_2O?

(b) What symmetries are involved for the bonding and antibonding states for these molecules?

(c) What are the differences in the symmetries of the normal modes for these two molecules?

(d) Show schematically the atomic displacements for the normal modes of each molecule.

(e) What are the expected differences in their IR spectra? Raman spectra?

3. Study the proof of the Wigner-Eckart theorem (e.g., Tinkham, p. 131-2).

4. (a) We will now find the molecular vibrations for the hypothetical molecule XH_{12} (see Problem 4 of §8.8) where the 12 hydrogen atoms are at the vertices of a regular icosahedron and the atom X is at the center of the icosahedron. Find $\chi^{\text{atom sites}}$ for XH_{12} for the icosahedral group I_h.

    (b) What are the symmetries for the normal modes? Which are infrared-active? Raman active?

    (c) What are the polarization selection rules for infrared? for Raman?

Chapter 10

Permutation Groups and Many-Electron States

In this chapter we discuss the properties of permutation groups, which are known as the "Symmetric Group" in the mathematics literature. Although permutation groups are quite generally applicable to many-body systems, they are used in this chapter to classify the symmetry in many-electron states. This discussion applies to the symmetries of both the spin and orbital states. In Chapter 11 we apply the results of Chapter 10 for the permutation groups to help classify the symmetry properties for tensors.

The main application of the permutation group in this chapter is to isolated atoms with full rotational symmetry. We give explicit results for two, three, four and five electron systems. Whereas two electron systems can be handled without group theory, the power of group theory is evident for three, four, five, and even larger electron systems. With a 5-electron system, we can treat all multi-electron states arising from s, p, and d electrons, since 5 electrons fill half of a d level, and a more than half-filled level is equivalent to the presence of hole states. To deal with all multi-electron states that could be made with f electrons we would need to also consider the permutation groups for 6 and 7 objects. In the solid state, multi-electron states occur predominantly in the context of crystal fields, as for example the substitution of a transition metal ion (having d electrons) on a crystal site with cubic symmetry. The crystal field lowers the full rotational symmetry of the free ion giving rise to

crystal field splittings. In this case the effect of the crystal field must be considered once the symmetry of the electronic configuration of the free ion has been determined using the permutation groups discussed in this chapter.

10.1   Introduction

In the physics of a many-electron atom or molecule we are interested in solutions to a Hamiltonian of the form

$$\mathcal{H}(\vec{r}_1, ..., \vec{r}_n) = \sum_{i=1}^{n} \left(\frac{p_i^2}{2m} + V(\vec{r}_i) \right) + \frac{1}{2} \sum_{i \neq j} \frac{e^2}{r_{ij}} \qquad (10.1)$$

where $V(\vec{r}_i)$ is a one-electron potential and the Coulomb electron-electron interaction term is explicitly included. The one-electron potential determines the rotational and translational symmetry of the Hamiltonian.

In addition to symmetry operations in space, the Hamiltonian in Eq. 10.1 is invariant under interchanges of electrons, i.e., permutation operations P of the type

$$P = \left(\begin{array}{cccc} 1 & 2 & \dots & n \\ a_1 & a_2 & \dots & a_n \end{array} \right), \qquad (10.2)$$

where the operation P replaces 1 by a_1, 2 by a_2, etc. We have already seen that these permutation operations form a group, i.e., there exists the inverse operation

$$P^{-1} = \left(\begin{array}{cccc} a_1 & a_2 & ... & a_n \\ 1 & 2 & ... & n \end{array} \right), \qquad (10.3)$$

and the identity element is given by

$$E = \left(\begin{array}{cccc} 1 & 2 & ... & n \\ 1 & 2 & ... & n \end{array} \right) \qquad (10.4)$$

which leaves the n electrons unchanged. Multiplication involves sequential permutation operations of the type given by Eq. 10.2. The

number of symmetry operations in a permutation group of n objects is $n!$ which gives the order of the permutation group to be $n!$.

The solutions of the many-electron Hamiltonian (Eq. 10.1) are denoted by $\Psi_{\Gamma_i}(\vec{r}_1, ..., \vec{r}_n)$. Since all electrons are indistinguishable, the permutation P commutes with the Hamiltonian, and we therefore can classify the wave functions of the group of the Schrödinger equation according to an irreducible representation Γ_i of the permutation or the symmetric group. Some permutations give rise to symmetric states, others to antisymmetric states, and the remainder are neither. In some cases, all possible states are either symmetric or antisymmetric, and there are no states that are neither fully symmetric nor fully antisymmetric.

For the permutation group of n objects amongst the various possible irreducible representations there are two special 1-dimensional irreducible representations: one that is symmetric and one that is antisymmetric under the interchange of two particles. The basis function for the symmetric representation Γ_1^s of an orbital state is just the product wave function

$$\Psi_{\Gamma_1^s}(\vec{r}_1, \vec{r}_2, \ldots, \vec{r}_n) = \frac{1}{\sqrt{n!}} \sum_{\text{permutations}} \psi_1(\vec{r}_1)\psi_2(\vec{r}_2)\ldots\psi_n(\vec{r}_n). \quad (10.5)$$

The total wave function for a many-electron system is the product of the orbital and spin wave functions. The basis function for the antisymmetric representation Γ_1^a is conveniently written in terms of the Slater determinant:

$$\Psi_{\Gamma_1^a}(\vec{x}_1, \vec{x}_2 \ldots, \vec{x}_n) = \frac{1}{\sqrt{n!}} \begin{vmatrix} \psi_1(\vec{r}_1, \sigma_1) & \psi_1(\vec{r}_2, \sigma_2) & \ldots & \psi_1(\vec{r}_n, \sigma_n) \\ \psi_2(\vec{r}_1, \sigma_1) & \psi_2(\vec{r}_2, \sigma_2) & \ldots & \psi_2(\vec{r}_n, \sigma_n) \\ \vdots & \vdots & \ddots & \vdots \\ \psi_n(\vec{r}_1, \sigma_1) & \psi_n(\vec{r}_2, \sigma_2) & \ldots & \psi_n(\vec{r}_n, \sigma_n) \end{vmatrix}$$

$$(10.6)$$

where $\vec{x}_i$ denotes a generalized coordinate, consisting of $\vec{r}_i$, the spatial coordinate and σ_i, the spin coordinate. When written in this form, the many-body wave function automatically satisfies the Pauli Principle since the repetition of either a row or a column results in a zero determinant thereby guaranteeing that every electron is in a different state.

The higher dimensional irreducible representations of the permutation group are also important in determining many-electron states which satisfy the Pauli principle. For example, in the $\vec{L} \cdot \vec{S}$ coupling scheme, one must take combinations of n spins to get a total S. These must be combined with the orbital angular momentum combinations to get a total L. Both the spin states and the orbital states will transform as some irreducible representation of the permutation group. When combined to make a total J, only those combinations with transform as the antisymmetric representation Γ_1^a are allowed by the Pauli principle. We will illustrate these concepts with several examples in this chapter including the 3-electron p^3 state and the 4-electron p^4 state.

In this chapter we will use the permutation groups to yield information about the symmetry and the degeneracy of the states for a many-electron system. We emphasize that in contrast to the case of rotational invariance, the ground state of Eq. 10.1 does not transform as the totally symmetric representation of the permutation group Γ_1^s. But rather for electrons (or half integral spin (Fermions) particles), the ground state and all allowed excited states transform as the antisymmetric one-dimensional irreducible representation Γ_1^a since any physical permutation $\mathcal{H}'$ will not distinguish between like particles. The perturbation itself transforms as the totally symmetric irreducible representation of the permutation group. Only integral spin particles (Bosons) have ground states that transform as the totally symmetric irreducible representation Γ_1^s.

Mathematicians are presently studying a new aspect of permutations called braids. A schematic picture for braids is shown in Fig. 10.1 where both the permutation and the ordered sequence of the permutation is part of the definition of the group element. At present, the mathematicians cannot express the irreducible representations for braids and the physics implications of braids are also unexplored at this time.

In this chapter we first discuss the classes of the permutation groups (§10.2), their irreducible representations (§10.3), and their basis functions (§10.4). Applications of the permutation groups are then made (§10.5) to classify 2-electron, 3-electron, 4-electron and 5-electron states.
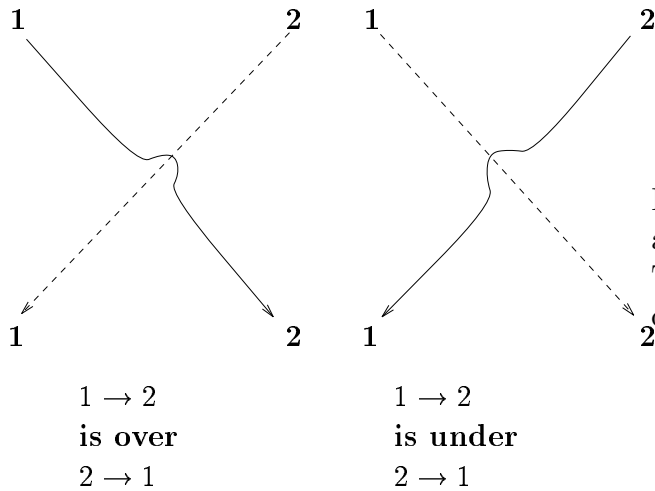
Figure 10.1: The symmetry operations on a braid of two strands. The solid curve (line) is over the dotted line (curve).

$1 \to 2$
is over
$2 \to 1$

$1 \to 2$
is under
$2 \to 1$

10.2 Classes of Permutation Groups

Of particular interest to the symmetry properties of permutation groups are cyclic permutations. If we have q objects, an example of a cyclic permutation of q objects is:

$$\begin{pmatrix} 1 & 2 & 3 & \ldots & (q-1) & q \\ 2 & 3 & 4 & \ldots & q & 1 \end{pmatrix} \equiv (23\ldots q1),$$

where $(123\ldots q)$ denotes the identity element. It is clear that the cyclic permutations of q identical objects are all related to one another by an equivalence transformation

$$(123...q) \;=\; (234...q1) \;=\; (34...q12) \;=\; \text{etc.} \qquad (10.7)$$

since all of these group elements imply that $1 \to 2$, $2 \to 3$, $3 \to 4$, etc., and therefore represent the same physics.

Any permutation can be decomposed into cycles. For example the permutation

$$P_i = \begin{pmatrix} 1 & 2 & 3 & 4 & 5 & 6 & 7 \\ 4 & 3 & 2 & 5 & 7 & 6 & 1 \end{pmatrix} \equiv (1457)(23)(6) \qquad (10.8)$$

can be decomposed into 3 cycles as indicated in Eq. 10.8. The decomposition of a permutation into cycles is unique, since different arrangements of cycles correspond to different permutations.

Let us assume that a permutation of q objects is decomposed into cycles as follows: there are λ_1 cycles of length 1, λ_2 cycles of length 2, ..., λ_n cycles of length n:

$$q = \lambda_1 + 2\lambda_2 + ... + n\lambda_n. \tag{10.9}$$

It is easily seen that there are

$$\frac{q!}{1^{\lambda_1}\lambda_1!\,2^{\lambda_2}\lambda_2!...n^{\lambda_n}\lambda_n!} \tag{10.10}$$

permutations that have the same cycle structure.

As an example consider the cycle $(abc)(d)$ of the permutation group $P(4)$. The class $(abc)(d)$ which in the isomorphic point group T_d for the symmetry operations of a regular tetrahedron, corresponds to the rotation about a 3-fold axis. The number of symmetry operations in this class according to Eq. 10.10 is

$$\frac{4!}{(1^1)(1!)(3^1)(1!)} = 8.$$

Another example is finding the number of symmetry operations in the class $(ab)(cd)$ of the point group $P(4)$, corresponding to the two-fold axes aroung x, y, z. From Eq. 10.10 the number of elements in this class is

$$\frac{4!}{(2^2)(2!)} = 3.$$

Theorem: Permutations with the same cycle structure belong to the same class.

Proof: Consider two permutations P and P' with the same cycle structure given by

$$\begin{aligned} P &= (a_1a_2\ldots a_{\lambda_1})(b_1b_2\ldots b_{\lambda_2})\ldots(d_1d_2\ldots d_{\lambda_r}) \\ P' &= (a'_1a'_2\ldots a'_{\lambda_1})(b'_1b'_2\ldots b'_{\lambda_2})\ldots(d'_1d'_2\ldots d'_{\lambda_r}). \end{aligned} \tag{10.11}$$

Here P takes $a_1 \to a_2$, etc., $b_1 \to b_2$, etc., $d_1 \to d_2$, etc. while P' does the corresponding permutation for the primed quantities. Now we introduce the permutation operation T which takes the primed quantities into the unprimed quantities (e.g., $a'_i \to a_i$)

$$T = \begin{pmatrix} a'_1 & \cdots & a'_{\lambda_1} & b'_1 & \cdots & b'_{\lambda_2} & \cdots & d'_1 & \cdots & d'_{\lambda_r} \\ a_1 & \cdots & a_{\lambda_1} & b_1 & \cdots & b_{\lambda_2} & \cdots & d_1 & \cdots & d_{\lambda_r} \end{pmatrix} \quad (10.12)$$

and T^{-1} takes $a_i \to a'_i$. Thus $T^{-1}PT$ does the following sequence: $a'_i \to a_i$, $a_i \to a_{i+1}$ and finally $a_{i+1} \to a'_{i+1}$. But this is equivalent to $a'_i \to a'_{i+1}$ which is precisely the permutation P'. Therefore

$$T^{-1}PT = P'$$

and P' is related to P by conjugation, thus completing the proof of the theorem. The number of elements in each class is found from Eq. 10.10.

From the above theorem it follows that the number of different classes (and hence the number of irreducible representations) of the permutation group of q objects is the number of different cycle structures that can be formed. Thus, the number of classes is just the number of ways in which the number q can be written as the sum of positive integers. For example, $q = 4$ objects can be constituted into 5 different cycle structures as enumerated below:

$$
\begin{array}{lll}
q = 4 & 4 = 4 & (1,2,3,4) \\
& 4 = 3 + 1 & (1,2,3)(4) \\
& 4 = 2 + 1 + 1 & (1,2)(3)(4) \qquad (10.13) \\
& 4 = 2 + 2 & (1,2)(3,4) \\
& 4 = 1 + 1 + 1 + 1 & (1)(2)(3)(4)
\end{array}
$$

giving rise to 5 classes. As an example of the notation, $4 = 3 + 1$ denotes a cycle structure $(123)(4)$. In the same way, $q = 5$ objects can

be constituted in 7 different cycle structures giving rise to 7 classes:

$$q = 5 \quad
\begin{array}{lll}
5 = 5 & & (1,2,3,4,5) \\
5 = 4 + 1 & & (1,2,3,4)(5) \\
5 = 3 + 2 & & (1,2,3)(4,5) \\
5 = 3 + 1 + 1 & & (1,2,3)(4)(5) \\
5 = 2 + 1 + 1 + 1 & & (1,2)(3)(4)(5) \\
5 = 2 + 2 + 1 & & (1,2)(3,4)(5) \\
5 = 1 + 1 + 1 + 1 + 1 & & (1)(2)(3)(4)(5)
\end{array}
\tag{10.14}$$

Correspondingly $q = 6$ gives rise to 11 classes, $q = 7$ gives rise to 15 classes, $q = 8$ gives rise to 22 classes, etc.

10.3   The Number of Irreducible Representations of Permutation Groups

Since permutation groups are finite groups, we can appeal to our experience regarding finite groups and use the theorem (Eq. 3.40)

$$h = \sum_i \ell_i^2 \tag{10.15}$$

where ℓ_i is the dimensionality of the representation i, and h is the order of the group. For a permutation group of q objects, the order of the group is $h = q!$. Since the number of classes is equal to the number of irreducible representations, we can construct Table 10.1 where $P(q)$ labels the permutation group of q objects. From Table 10.1 we note that $P(3)$ is isomorphic with group C_{3v} or alternatively group D_3. Similarly $P(4)$ is isomorphic with the tetrahedral group T_d. Although the groups $P(5)$ and I_h both have 120 symmetry operations, $P(5)$ is not isomorphic to the icosahedral group I_h since the two groups have different numbers of classes. The number of classes of $P(5)$ is 7 while the number of classes of I_h is 10. The dimensions ℓ_i of the 7 classes in the group $P(5)$ are listed in Table 10.1, and include two irreducible representations with $\ell_i = 1$, two with $\ell_i = 4$, two with $\ell_i = 5$, and one with $\ell_i = 6$. The 10 irreducible representations of I_h have the following dimensionalities: $2[1 + 3 + 3 + 4 + 5]$. Making use of the isomorphism of $P(3)$ and $P(4)$ mentioned above, matrix representations for the symmetry operations of these groups are easily written down.

Table 10.1: The number of classes and a listing of the dimensionalities of the irreducible representations.

Group	Classes	Number of group elements $\sum_i \ell_i^2$
$P(1)$	1	$1! = 1^2 = 1$
$P(2)$	2	$2! = 1^2 + 1^2 = 2$
$P(3)$	3	$3! = 1^2 + 1^2 + 2^2 = 6$
$P(4)$	5	$4! = 1^2 + 1^2 + 2^2 + 3^2 + 3^2 = 24$
$P(5)$	7	$5! = 1^2 + 1^2 + 4^2 + 4^2 + 5^2 + 5^2 + 6^2 = 120$
$P(6)$	11	$6! = 1^2 + 1^2 + 5^2 + 5^2 + 5^2 + 5^2 + 9^2 + 9^2 + 10^2 + 10^2 + 16^2 = 720$
$P(7)$	15	$7! = 1^2 + 1^2 + 6^2 + 6^2 + 14^2 + 14^2 + 14^2 + 14^2 + 15^2 + 15^2 + 21^2 + 21^2 +$
		$+35^2 + 35^2 + 20^2 = 5040$
$P(8)$	22	$8! = 1^2 + 1^2 + 7^2 + 7^2 + 14^2 + 14^2 + 20^2 + 20^2 + 21^2 + 21^2 + 28^2 + 28^2 +$
		$+35^2 + 35^2 + 56^2 + 56^2 + 64^2 + 64^2 + 70^2 + 70^2 + 42^2 + 90^2 = 40320$

$\vdots$

10.4 Basis Functions of Permutation Groups

The one-electron Hamiltonian

$$\mathcal{H}_0(\vec{r}_1) = \frac{p_1^2}{2m} + V(\vec{r}_1) \tag{10.16}$$

has one-electron solutions $\psi_0(\vec{r}_1)$, $\psi_1(\vec{r}_1)$, etc. Thus the solutions of the many-electron problem can be expanded in terms of products of the one-electron wave functions for the Hamiltonian in Eq. 10.16. Below, we write down the ground state many-electron wave function formed by putting all electrons in the ground state, and the lowest excited states formed by putting 1 electron in an excited state.

Ground State: (Boson gas)

The many-particle ground state wave function Ψ_0 is found by putting all the particles into the one-particle ground state:

$$\Psi_0 = \psi_0(\vec{r}_1)\psi_0(\vec{r}_2)\ldots\psi_0(\vec{r}_n) \rightarrow \Gamma_1^s \tag{10.17}$$

and from a group theoretical point of view this orbital state transforms at the totally symmetric representation Γ_1^s.

Single Excitation: (e.g., "phonons" or "magnons")

To form the first excited state, consider the functions g_i found by

placing the ith particle in the first excited state $\psi_1(\vec{r}_i)$:

$$
\begin{aligned}
\psi_1(\vec{r}_1)\psi_0(\vec{r}_2)\ldots\psi_0(\vec{r}_n) &= g_1 \\
\psi_0(\vec{r}_1)\psi_1(\vec{r}_2)\ldots\psi_0(\vec{r}_n) &= g_2 \\
&\vdots \\
\psi_0(\vec{r}_1)\psi_0(\vec{r}_2)\ldots\psi_1(\vec{r}_n) &= g_n
\end{aligned}
\tag{10.18}
$$

The basis functions given by Eqs. 10.18 transform as an n-dimensional reducible representation. Decomposition of this reducible representation yields:

$$
\Gamma_n(\text{reducible}) = \Gamma_1^s + \Gamma_{n-1},
$$

where Γ_1^s refers to the totally symmetric representation. Denoting the many-body wave function for the excited state by Ψ' to distinguish it from the ground state function in Eq. 10.17, the basis functions for the totally symmetric combination with Γ_1^s symmetry is:

$$
\Psi'_{\Gamma_1^s} = \frac{1}{\sqrt{n}} \sum_{i=1}^{n} g_i \to \Gamma_1^s
\tag{10.19}
$$

and the other representation depends on the ensemble of phase factors forming all possible n^{th} roots of unity:

$$
\Psi'_{\Gamma_{n-1}} = \left\{
\begin{array}{c}
\frac{1}{\sqrt{n}} \sum_{i=1}^{n} \omega^{(i-1)} g_i \\
\frac{1}{\sqrt{n}} \sum_{i=1}^{n} \omega^{2(i-1)} g_i \\
\vdots \\
\frac{1}{\sqrt{n}} \sum_{i=1}^{n} \omega^{n(i-1)} g_i
\end{array}
\right\} \to \Gamma_{n-1}
\tag{10.20}
$$

where ω are phase factors given by $\omega = e^{\frac{2\pi i}{n}}$.

For the special case $n = 2$, where $\omega = -1$, we obtain

$$
\Psi'_{\Gamma_1} = \frac{1}{\sqrt{2}} [\psi_1(r_1)\psi_0(r_2) - \psi_0(r_1)\psi_1(r_2)].
$$

For the case $n = 3$, where $\omega = e^{2\pi i/3}$, we obtain

$$
\Psi'_{\Gamma_2} = \frac{1}{\sqrt{3}} (\psi_1(r_1)\psi_0(r_2)\psi_0(r_3) + \omega\psi_0(r_1)\psi_1(r_2)\psi_0(r_3) + \omega^2\psi_0(r_1)\psi_0(r_2)\psi_1(r_3))
$$

and its partner

$$\Psi''_{\Gamma_2} = \frac{1}{\sqrt{3}}(\psi_1(r_1)\psi_0(r_2)\psi_0(r_3)+\omega^2\psi_0(r_1)\psi_1(r_2)\psi_0(r_3)+\omega\psi_0(r_1)\psi_0(r_2)\psi_1(r_3))$$

for the two dimensional irreducible representation. The $(n-1)$ cyclic permutations $(1)(2\ 3\ldots n)$, $(1)(n23\ldots(n-1))$, ... all commute with each other. Hence the eigenfunctions can be chosen so that these matrices are diagonal - the $(n-1)$ eigenvalues being

$$e^{\frac{2\pi i}{n}(\frac{n-2}{2})},\ldots,e^{\frac{-2\pi i}{n}(\frac{n-2}{2})}$$

Regular Representation:
    If all n functions in a Slater determinant are distinct, then the Slater determinant does not vanish. The Slater determinant is the unique basis function for the antisymmetric representation Γ_1^a. For the case where all n functions are distinct, the $n!$ functions form a regular representation of the permutation group and the character for the identity element for the regular representation is the order of the group and according to Eq. 3.42 we have

$$\chi^{\text{regular}} = \sum_j^q \ell_j \, \chi^{\Gamma_j} = h = n! \tag{10.21}$$

where ℓ_j is the dimension of the irreducible representation Γ_j and each representation occurs a number of times which is equal to the dimension of the representation, and h is the order of the group $= n!$. If two of the n functions are identical then the irreducible representation that is odd under the exchange of the two identical particles (namely Γ_1^a) does not occur.

10.5   Pauli Principle in Atomic Spectra

We will in the following subsections of §10.5 apply the results in §10.4 to specify the symmetry of many-body wavefunctions formed by two electrons, three electrons, etc.

10.5.1 Two-Electron States

For the case of two electrons, the use of group theory is not especially needed for selecting the proper linear combinations of wave functions and the same results can be found just from consideration of even and odd states, since there are only two classes and two irreducible representations for $P(2)$. We discuss this case here largely for review and pedagogic reasons.

The Slater determinant for the two-electron problem can be written as:

$$\Psi(\vec{x}_1, \vec{x}_2) = \frac{1}{\sqrt{2}} \begin{vmatrix} \psi_1(\vec{r}_1, \sigma_1) & \psi_1(\vec{r}_2, \sigma_2) \\ \psi_2(\vec{r}_1, \sigma_1) & \psi_2(\vec{r}_2, \sigma_2) \end{vmatrix} \qquad (10.22)$$

where $\Psi(\vec{x}_1, \vec{x}_2)$ denotes the many-electron wave function for the many-electron problem and $\psi_2(\vec{r}_1, \sigma_1)$ denotes a one-electron wave function that has an orbital part and a spin part. We use the vector $\vec{x}_i$ to denote both the orbital and spin variables $(\vec{r}_i, \sigma_i)$.

The lowest energy state for the two-electron problem is achieved by putting both electrons in $1s$ states, taking the **symmetric (s)** linear combination of spatial orbitals and taking the spins antiparallel. Multiplying out the Slater determinant in this case yields:

$$\Psi(1, 2) = \frac{1}{\sqrt{2}} \psi_s^{1s}(1) \psi_s^{1s}(2) [\alpha(1)\beta(2) - \alpha(2)\beta(1)] \qquad (10.23)$$

where the spin up state is denoted by α and the spin down state by β, and $\Psi(1, 2)$ denotes the two-electron ground state. The function $[\alpha(1)\beta(2) - \alpha(2)\beta(1)]$ denotes the antisymmetric spin function for the two electrons.

Let us now consider the transformation properties of these two electrons more generally, including their excited states. The possible spin states for two electrons are $S = 0, 1$. The phase factor for the two-electron problem is $\omega = e^{2\pi i/2} = -1$ so that the linear combinations simply involve ± 1. For the two-electron problem we can form a symmetric and an antisymmetric combination of α and β as given in Table 10.2. For the antisymmetric combination ($S = 0$) as in Eq. 10.23, we can have only $M_S = 0$ and the corresponding linear combination of spin states is given in Table 10.2. For the symmetric combination ($S = 1$), we can have 3 linear combinations. Only the $M_S = 1$

Table 10.2: Transformation properties of two-electron states under permutations. The symmetries of the irreducible representations of the permutation group $P(2)$ label the various spin and orbital angular momentum states. To obtain the states allowed by the Pauli Principle the direct product of the symmetries between the orbital and spin states must contain Γ_1^a.

Configuration	State	Irreducible Representations	Allowed States
$(\alpha_1\beta_2 - \beta_1\alpha_2)/\sqrt{2}$	$S = 0$	Γ_1^a	
$(\alpha_1\alpha_2 + \alpha_2\alpha_1)/\sqrt{2}, \ldots$	$S = 1$	Γ_1^s	
s^2	$L = 0$	Γ_1^s	^1S
$1s2s$	$L = 0$	$\Gamma_1^s + \Gamma_1^a$	$^1S, {}^3S$
sp	$L = 1$	$\Gamma_1^s + \Gamma_1^a$	$^1P, {}^3P$
p^2	$L = 0$	Γ_1^s	^1S
p^2	$L = 1$	Γ_1^a	^3P
p^2	$L = 2$	Γ_1^s	^1D
d^2	$L = 0$	Γ_1^s	^1S
d^2	$L = 1$	Γ_1^a	^3P
d^2	$L = 2$	Γ_1^s	^1D
d^2	$L = 3$	Γ_1^a	^3F
d^2	$L = 4$	Γ_1^s	^1G
f^2	$L = 0$	Γ_1^s	^1S
f^2	$L = 1$	Γ_1^a	^3P
f^2	$L = 2$	Γ_1^s	^1D
f^2	$L = 3$	Γ_1^a	^3F
f^2	$L = 4$	Γ_1^s	^1G
f^2	$L = 5$	Γ_1^a	^3H
f^2	$L = 6$	Γ_1^s	^1I

combination $(\alpha_1\alpha_2 + \alpha_2\alpha_1)/\sqrt{2}$ is listed explicitly in Table 10.2. The $M_S = 0$ combination $(\alpha_1\beta_2 + \beta_1\alpha_2)/\sqrt{2}$ and the $M_S = -1$ combination $(\beta_1\beta_2 + \beta_2\beta_1)/\sqrt{2}$ do not appear in the table.

We also make entries in Table 10.2 for the symmetries of the orbital angular momentum states. If the two electrons are in the same symmetric orbital s state ($L = 0$), then the spin functions must transform as an antisymmetric linear combination Γ_1^a in Table 10.2 and corresponding to the spectroscopic notation ^1S as in Eq. 10.23. However, if the two s electrons have different principal quantum numbers, then we can make both a symmetric and an antisymmetric combination of orbital states, as is illustrated here for the two electrons occupying $1s$ and $2s$ states, where the symmetric and antisymmetric combinations are

$$(\psi_{1s}(\vec{r}_1)\psi_{2s}(\vec{r}_2) + \psi_{1s}(\vec{r}_2)\psi_{2s}(\vec{r}_1))/\sqrt{2}$$

which transforms at Γ_1^s and

$$(\psi_{1s}(\vec{r}_1)\psi_{2s}(\vec{r}_2) - \psi_{1s}(\vec{r}_2)\psi_{2s}(\vec{r}_1))/\sqrt{2}$$

which transforms at Γ_1^a. Because of the Pauli principle, the orbital Γ_1^s combination goes with the Γ_1^a spin state leading to an ^1S level, while the Γ_1^a orbital state goes with the Γ_1^s spin state leading to an ^3S level (see Table 10.2).

We now consider the next category of entries in Table 10.2. If one electron is in an s state and the second is in a p state (configuration labeled sp), the total L value must be $L = 1$. We however have two choices for the orbital states: a symmetric Γ_1^s state or an antisymmetric Γ_1^a state. The symmetric combination of orbital wave functions (Γ_1^s) must then correspond to the $S = 0$ antisymmetric spin state (Γ_1^a), resulting in the ^1P level, whereas the antisymmetric orbital combination (transforming as Γ_1^a) goes with the symmetric triplet Γ_1^s spin state and yields the ^3P level (see Table 10.2).

Placing two electrons in p states with the same principal quantum number (configuration p^2 in Table 10.2) allows for a total angular momentum of $L = 0$ (which must have Γ_1^s symmetry), of $L = 1$ (with Γ_1^a symmetry) and of $L = 2$ (again with Γ_1^s symmetry). Each electron can be in one of the 3 states (p^+, p^0, p^-), corresponding to $m_l = 1, 0, -1$,

respectively for each one-electron state. Combining the p^+p^+ product yields an $M_L = 2$ state which belongs exclusively to the $L = 2$ multiplet, whereas combining the p^+p^0 states symmetrically yields the $M_L = 1$ state of the $L = 2$ multiplet. (We use the notation p^+p^0 to denote $\psi_{p^+}(\vec{r}_1)\psi_{p^0}(\vec{r}_2)$.) However combining p^+p^0 antisymmetrically yields the $M_L = 1$ state of the $L = 1$ multiplet. The formation of the two-electron states for the various L and M_L values occurring for the p^2 configuration is given below. Since the orbital functions for the $L = 1$ state transform as Γ_1^a the spin functions transform as Γ_1^s and the $L = 1$ multiplet is a triplet spin state ^3P. The $L = 0$ and $L = 2$ states both transform as Γ_1^s and thus the allowed spin states must be the singlet spin state $S = 0$ (see Table 10.2).

The wave functions for the p^2 configuration sketched above can be found in many standard Quantum mechanics text books and are:

$L = 2$ symmetry (Γ_1^s) going with Γ_1^a for the spins to yield a ^1D state

$$\begin{aligned}
\Psi(L = 2, M_L = 2) &= (p^+p^+) \\
\Psi(L = 2, M_L = 1) &= (p^0p^+ + p^+p^0)/\sqrt{2} \\
\Psi(L = 2, M_L = 0) &= [(p^0p^0) + (p^+p^- + p^-p^+)/\sqrt{2}]/\sqrt{2} \\
\Psi(L = 2, M_L = -1) &= (p^0p^- + p^-p^0)/\sqrt{2} \\
\Psi(L = 2, M_L = -2) &= (p^-p^-)
\end{aligned}$$

$$(10.24)$$

$L = 1$ symmetry (Γ_1^a) going with a symmetric spin state (Γ_1^s) to yield a ^3P state.

$$\begin{aligned}
\Psi(L = 1, M_L = 1) &= (p^0p^+ - p^+p^0)/\sqrt{2} \\
\Psi(L = 1, M_L = 0) &= (p^+p^- - p^-p^+)/\sqrt{2} \\
\Psi(L = 1, M_L = -1) &= (p^0p^- - p^-p^0)/\sqrt{2}
\end{aligned}$$

$$(10.25)$$

$L = 0$ symmetry (Γ_1^s) going with an antisymmetric spin state (Γ_1^a) to yield a ^1S state.

$$\Psi(L = 0, M_L = 0) = [(p^0p^0) - (p^+p^- + p^-p^+)/\sqrt{2}]/\sqrt{2} \quad (10.26)$$

Following this explanation for the p^2 configuration, the reader can now fill in the corresponding explanations for the states formed from two-electron states derived from the pd, d^2 or f^2 configurations listed in Table 10.2.

Table 10.3: Extended character table for permutation group $P(3)$.

	$\chi(E)$	$\chi(A,B,C)$	$\chi(D,F)$	
$P(3)$	(1^3)	$3(2,1)$	$2(3)$	
Γ_1^s	1	1	1	
Γ_1^a	1	-1	1	
Γ_2	2	0	-1	
$\chi_{\text{perm.}}(\psi_1\psi_1\psi_1)$	1	1	1	$\Rightarrow \Gamma_1^s$
$\chi_{\text{perm.}}(\psi_1\psi_1\psi_2)$	3	1	0	$\Rightarrow \Gamma_1^s + \Gamma_2$
$\chi_{\text{perm.}}(\psi_1\psi_2\psi_3)$	6	0	0	$\Rightarrow \Gamma_1^s + \Gamma_1^a + 2\Gamma_2$

10.5.2 Three-Electron States

For the case of three electrons, the use of group theory becomes more important. In this case we have the permutation group of three objects $P(3)$ which has 6 elements, 3 classes and 3 irreducible representations (see Table 10.3). In the extended character table above, we label the class (1^3) to denote the cyclic structure $(1)(2)(3)$ and class $(2,1)$ to denote the cyclic structure $(12)(3)$ and class (3) to denote the cyclic structure (123). The correspondence between the elements E, A, B, C, D, F and these three classes is immediate and is given in the table explicitly. Also given below the character table proper are all the possible symmetries of the permutations for three-electron wave functions. Because of these additional listings, we call this an extended character table. The first possibility for the 3-electron state is that all the one-electron states are the same $(\psi_1\psi_1\psi_1)$. This function is invariant under any of the 6 permutations of the group, so that all characters are 1 and the function $(\psi_1\psi_1\psi_1)$ transforms as Γ_1^s. In the second possible case, one of the electrons is in a different state $(\psi_1\psi_1\psi_2)$, and since there are 3 possible combinations that can be formed with the ψ_2 one-electron wave function, we have three distinct functions that can be obtained from permutation of the electrons. Hence $(\psi_1\psi_1\psi_2)$ transforms as a three-dimensional reducible representation of the permutation group $P(3)$ with 3 partners for this state. The identity leaves the three partners invariant so we get a character 3. Each of the permutation operations

$[3(2, 1)]$ leaves one of the partners invariant, so we get a character of 1, while the cyclic permutations change all partners yielding a character of 0. The reduction of this reducible representation to its irreducible components yields $\Gamma_1^s + \Gamma_2$ as indicated on the table. Finally, we consider the case when all 3 electrons are in different states $(\psi_1 \psi_2 \psi_3)$. This gives rise to 6 partners, and it is only the identity operation which leaves the partners $(\psi_1 \psi_2 \psi_3)$ invariant. This reducible representation (like the regular representation can be expressed in terms of its irreducible constituents using the relation $h = \sum_i \ell_i^2$) contains $\Gamma_1^s + \Gamma_1^a + 2\Gamma_2$, which can be directly verified by adding the characters. In the following chapter, there will be a great deal more discussion of the equivalence principle that is used here to form the reducible representations given in Table 10.3 which is the extended character table for $P(3)$.

Let us now look at the spin states that can be made from 3 electrons. Referring to §10.4 we can make a symmetric state

$$(\alpha_1 \alpha_2 \alpha_3)$$

with symmetry Γ_1^s that corresponds to the $S = 3/2$ and $M_S = 3/2$ spin state. To obtain the linear combination of spin states for the three other M_S values ($M_S = 1/2, -1/2, -3/2$), we must apply lowering operators to the $M_S = 3/2$ state $(\alpha_1 \alpha_2 \alpha_3)$. With regard to the $S = 1/2$ state, Eq. 10.18 tells us that this state is a 2-dimensional representation with partners:

$$\Psi'_{\Gamma_2} = \begin{cases} (g_1 + \omega g_2 + \omega^2 g_3) \\ \\ (g_1 + \omega^2 g_2 + \omega g_3) \end{cases} \tag{10.27}$$

where $\omega = \exp(2\pi i/3)$ and where the functions g_i are assembled by sequentially selecting the spin down state β at each of the sites 1, 2 or 3. This explains the first two entries in Table 10.4.

Now let us examine the spatial states. Putting all three electrons in the same s state would yield a state with $L = 0$, $M_L = 0$ and having Γ_1^s symmetry. Taking the direct product between Γ_1^s for the orbital $L = 0$ state and either of the spin states $\Gamma_1^s \otimes (\Gamma_1^s + \Gamma_2)$ does not yield a state with Γ_1^a symmetry, and therefore the s^3 configuration is not allowed because of the Pauli principle. This is a group theoretical statement of the fact that a particular s level can only accommodate one spin up

Table 10.4: Transformation properties of three-electron states under permutations. The symmetries of the irreducible representations of the permutation group $P(3)$ label the various spin and orbital angular momentum states. To obtain the states allowed by the Pauli Principle the direct product of the symmetries between the orbital and spin states must contain Γ_1^a.

Configuration	State	Irreducible Representation	Allowed State
$(\uparrow\uparrow\downarrow)$	$S = 1/2$	Γ_2	
$(\uparrow\uparrow\uparrow)$	$S = 3/2$	Γ_1^s	
s^3	$L = 0$	Γ_1^s	$-$
$1s^2 2s$	$L = 0$	$\Gamma_1^s + \Gamma_2$	^2S
$s^2 p$	$L = 1$	$\Gamma_1^s + \Gamma_2$	^2P
sp^2	$L = 0$	$\Gamma_1^s + \Gamma_2$	^2S
sp^2	$L = 1$	$\Gamma_1^a + \Gamma_2$	$^2P, \, ^4P$
sp^2	$L = 2$	$\Gamma_1^s + \Gamma_2$	^2D
$(2p)^2(3p)$	$L = 0$	$\Gamma_1^a + \Gamma_2$	$^2S, \, ^4S$
$(2p)^2(3p)$	$L = 1$	$2\Gamma_1^s + \Gamma_1^a + 3\Gamma_2$	$^2P, \, ^2P, \, ^2P, \, ^4P$
$(2p)^2(3p)$	$L = 2$	$\Gamma_1^s + \Gamma_1^a + 2\Gamma_2$	$^2D, \, ^2D, \, ^4D$
$(2p)^2(3p)$	$L = 3$	$\Gamma_1^s + \Gamma_2$	^2F
p^3	$L = 0$	Γ_1^a	^4S
p^3	$L = 1$	$\Gamma_1^s + \Gamma_2$	^2P
p^3	$L = 2$	Γ_2	^2D
p^3	$L = 3$	Γ_1^s	$-$
d^3	$L = 0$	Γ_1^s	$-$
d^3	$L = 1$	$\Gamma_1^a + \Gamma_2$	$^2P, \, ^4P$
d^3	$L = 2$	$\Gamma_1^s + 2\Gamma_2$	$^2D, \, ^2D$
d^3	$L = 3$	$\Gamma_1^s + \Gamma_1^a + \Gamma_2$	$^2F, \, ^4F$
d^3	$L = 4$	$\Gamma_1^s + \Gamma_2$	^2G
d^3	$L = 5$	Γ_2	^2H
d^3	$L = 6$	Γ_1^s	$-$
f^3	$L = 0$	Γ_1^a	^4S
f^3	$L = 1$	$\Gamma_1^s + \Gamma_2$	^2P
f^3	$L = 2$	$\Gamma_1^a + 2\Gamma_2$	$^2D, \, ^2D, \, ^4D$
f^3	$L = 3$	$2\Gamma_1^s + \Gamma_1^a + 2\Gamma_2$	$^2F, \, ^2F, \, ^4F$
f^3	$L = 4$	$\Gamma_1^s + \Gamma_1^a + 2\Gamma_2$	$^2G, \, ^2G, \, ^4G$
f^3	$L = 5$	$\Gamma_1^s + 2\Gamma_2$	$^2H, \, ^2H$
f^3	$L = 6$	$\Gamma_1^s + \Gamma_1^a + \Gamma_2$	$^2I, \, ^4I$
f^3	$L = 7$	$\Gamma_1^s + \Gamma_2$	^2J
f^3	$L = 8$	Γ_2	^2K
f^3	$L = 9$	Γ_1^s	$-$

and one spin down electron. If now one of the electrons is promoted to a $2s$ state, then we can make an Γ_1^s state and a Γ_2 state in accordance with §10.4 and with the character table for $P(3)$ in Table 10.3, taking $g_1 = \psi_{2s}(\vec{r}_1)\psi_{1s}(\vec{r}_2)\psi_{1s}(\vec{r}_3)$, etc. and forming states such as given in Eqs. 10.19 and 10.20. The direct product

$$\Gamma_2 \otimes \Gamma_2 = \Gamma_1^s + \Gamma_1^a + \Gamma_2$$

then ensures that a state with Γ_1^a symmetry can be assembled to satisfy the Pauli principle. Since the spin state with Γ_2 symmetry corresponds to a Pauli-allowed component $S = 1/2$, the allowed $1s^2 2s$ state will be a doublet ^2S state as shown in Table 10.4. Similar arguments apply to the formation of $s^2 p$ states with $L = 1$.

For the sp^2 configuration the orbital angular momentum can be $L = 0$, $L = 1$ and $L = 2$. This corresponds to $(2 \times 6 \times 6 = 72)$ possible states in the multiplet. We show below using the Pauli principle and group theory arguments that the number of allowed states is 30. The spatial states for the sp^2 configuration with $L = 2$ are formed from products of the type sp^+p^+ for the $M_L = 2$ state (see Eqs. 10.24–10.26). Once again from the character table (Table 10.3) for $P(3)$, the symmetries which are contained in the three-electron wave function sp^+p^+ (denoting $\psi_s(\vec{r}_1)\psi_{p^+}(\vec{r}_2)\psi_{p^+}(\vec{r}_3)$) are Γ_1^s and Γ_2 just as was obtained for the $1s^2 2s$ configuration. The only possible allowed state for $L = 2$ has $S = 1/2$ which results in the ^2D state listed in the table. The $M_L = 1$ states are linear combinations of the sp^+p^0 functions which have the symmetries $\Gamma_1^s + \Gamma_1^a + 2\Gamma_2$, since this case corresponds to $(\psi_1\psi_2\psi_3)$ in the character table. Of these symmetry types the $\Gamma_1^s + \Gamma_2$ states are associated with the $M_L = 1$ state of the $L = 2$ multiplet, since the irreducible representation is specified by the quantum number L and the M_L only specify the partners of that irreducible representation. After this subtraction has been performed the symmetry types $\Gamma_1^a + \Gamma_2$ for the $L = 1$, $M_L = 1$ level are obtained.

Referring to Table 10.4, the symmetry for the $L = 0$ state of the sp^2 configuration could arise from a sp^0p^0 state which is of the $(\psi_1\psi_1\psi_2)$ form and therefore transforms according to $\Gamma_1^s + \Gamma_2$ symmetry [see the character table (Table 10.3) for $P(3)$]. These orbital states go with the spin states Γ_1^a.

For the $L = 1$ state, the orbital Γ_1^a irreducible representation goes with the Γ_1^s spin 3/2 state to give rise to a quartet ^4P state while the Γ_2 orbital state can only go with the Γ_2 spin state to give a Γ_1^a state when taking the direct product of the symmetries of the orbital and spin states $(\Gamma_2 \otimes \Gamma_2)$.

The case of the p^3 configuration is an instructive example where we can see how group theory can be used to simplify the analysis of the symmetries of multi-electron states. As the number of electrons increases, the use of group theory becomes essential to keep track of the symmetries that are possible by the addition of angular momentum and the symmetries that are allowed by the Pauli principle. For the p^3 configuration, we can have a total of $6 \times 6 \times 6 = 216$ states. We will show below that if all electrons have the same principal quantum number only 20 of these states are allowed by the Pauli principle and we will here classify their symmetry types.

For the p^3 configuration we can have $L = 3$, 2, 1 and 0 total orbital angular momentum states. In the discussion that follows we will assume that all electrons have the same principal quantum number (e.g., $2p^3$). For the $L = 3$ state to be allowed, we must be able to put all 3 electrons into a $(p^+p^+p^+)$ state to make the $M_L = 3$ state. From the extended character table (Table 10.3) for $P(3)$, we see that $L = 3$ must transform as Γ_1^s. Since the direct product of the orbital and spin states $\Gamma_1^s \otimes (\Gamma_1^s + \Gamma_2)$ does not contain Γ_1^a this state is not allowed. The $L = 2$ multiplet is constructed from an $M_L = 2$ state having $p^+p^+p^0$ combinations which [from the character table (Table 10.3) for $P(3)$ on p. 250] transform as $\Gamma_1^s + \Gamma_2$. Since $M_L = 2$ also contributes to the $L = 3$ state with symmetry Γ_1^s, we must subtract Γ_1^s from $\Gamma_1^s + \Gamma_2$ to get the symmetry Γ_2 for the $L = 2$ state. If we take a direct product of the orbital and spin states for this case, we obtain

$$\Gamma_2 \otimes (\Gamma_1^s + \Gamma_2) = \Gamma_1^s + \Gamma_1^a + 2\Gamma_2,$$

but it is only the direct product $\Gamma_2 \otimes \Gamma_2$ which contributes a state with Γ_1^a symmetry that is allowed by the Pauli principle. Thus only the ^2D state is symmetry-allowed as indicated in Table 10.4. To get the symmetry of the $L = 1$ state, consider the combinations $p^+p^0p^0$ and $p^+p^+p^-$ which contribute to the $M_L = 1$ state. In this case the $M_L = 1$

Table 10.5: Character Table for Group $P(4)$

$P(4)$	(1^4)	$8(3,1)$	$3(2^2)$	$6(2,1^2)$	$6(4)$	
Γ_1^s	1	1	1	1	1	
Γ_1^a	1	1	1	−1	−1	
Γ_2	2	−1	2	0	0	
Γ_3	3	0	−1	1	−1	
$\Gamma_{3'}$	3	0	−1	−1	1	
$\chi_{\text{perm.}}(\psi_1\psi_1\psi_1\psi_1)$	1	1	1	1	1	$\Rightarrow \Gamma_1^s$
$\chi_{\text{perm.}}(\psi_1\psi_1\psi_1\psi_2)$	4	1	0	2	0	$\Rightarrow \Gamma_1^s + \Gamma_3$
$\chi_{\text{perm.}}(\psi_1\psi_1\psi_2\psi_2)$	6	0	2	2	0	$\Rightarrow \Gamma_1^s + \Gamma_2 + \Gamma_3$
$\chi_{\text{perm.}}(\psi_1\psi_1\psi_2\psi_3)$	12	0	0	2	0	$\Rightarrow \Gamma_1^s + \Gamma_2 + 2\Gamma_3 + \Gamma_{3'}$
$\chi_{\text{perm.}}(\psi_1\psi_2\psi_3\psi_4)$	24	0	0	0	0	$\Rightarrow \Gamma_1^s + \Gamma_1^a + 2\Gamma_2 + 3\Gamma_3 + 3\Gamma_{3'}$

state contains irreducible representations $2(\Gamma_1^s+\Gamma_2)$. Since $M_L = 1$ also appears for $L = 2$ and $L = 3$, we need to subtract $(\Gamma_1^s + \Gamma_2)$ to obtain $(\Gamma_1^s+\Gamma_2)$ for the symmetries of the orbital $L = 1$ state (see Table 10.4). For the $M_L = 0$ levels we have the combinations $p^0p^0p^0$ and $p^+p^-p^0$, the first transforming as Γ_1^s and the second as $\Gamma_1^s + \Gamma_1^a + 2\Gamma_2$ to give a total of $2\Gamma_1^s+\Gamma_1^a+2\Gamma_2$. However $M_L = 0$ is also present in the $L = 3$, 2 and 1 multiplets, so we must subtract the irreducible representations $(\Gamma_1^s) + (\Gamma_2) + (\Gamma_1^s+\Gamma_2)$ to obtain Γ_1^a for the $L = 0$ state. For an orbital angular momentum with symmetry Γ_1^a, it is only the $S = 3/2$ Γ_1^s spin state that is allowed by the Pauli principle (see Table 10.4).

The same procedure can be used to obtain all the other entries in Table 10.4, as well as the many 3-electron states not listed. As the angular momentum increases (e.g., for the case of d^3 or f^3 configurations), group theoretical concepts become increasingly important.

10.5.3 Four-Electron States

In consideration of the 4-electron problem we must consider the permutation group $P(4)$. The character table for the group $P(4)$ is given in Table 10.5. Also shown in Table 10.5 are the transformation properties for the various products of functions. These transformation properties

are obtained in the same way as for the case of the group $P(3)$ discussed in §10.5.2. The various 4-electron states of a free ion or atom that are consistent with the Pauli principle are formed with the help of these tables.

We first consider the possible spin states for the 4-electron configuration. The transformation of the spin states under the operations of the permutation group are shown in Table 10.6. The 4 spins can be arranged to give a total spin of $S = 2$, $S = 1$ and $S = 0$. The fully symmetric ($\alpha_1\alpha_2\alpha_3\alpha_4$) state, which appears in Table 10.5 as $\chi_{\mathrm{perm.}}(\psi_1\psi_1\psi_1\psi_1)$, has $S = 2$ and clearly transforms as Γ_1^s. The $S = 1$ state is formed from a combination ($\alpha_1\alpha_2\alpha_3\beta_4$) with $M_S = 1$ and is of the form $\chi_{\mathrm{perm.}}(\psi_1\psi_1\psi_1\psi_2)$, which from the extended character table in Table 10.5 transforms as $\Gamma_1^s + \Gamma_3$. But $M_S = 1$ also contributes to the $S = 2$ state which transforms as Γ_1^s. Thus by subtraction, $S = 1$ transforms as Γ_3. Likewise, the $S = 0$ state is formed from a configuration ($\alpha_1\alpha_2\beta_3\beta_4$) with $M_S = 0$ which from the extended character Table 10.5 is of the form $\chi_{\mathrm{perm.}}(\psi_1\psi_1\psi_2\psi_2)$ and transforms as $\Gamma_1^s + \Gamma_2 + \Gamma_3$. Upon subtraction of the symmetry types for the $S = 1$ and $S = 2$ states ($\Gamma_3 + \Gamma_1^s$), we obtain the symmetry Γ_2 for the $S = 0$ state, as shown in Table 10.6. This completes the discussion for the spin entries to Table 10.5.

With regard to the symmetries of the s^4, $1s^3 2s$ and $1s^2 2s^2$ orbital states, these follow from the discussion in §10.5.2. Some similarity is also found for the sp^3 states in Table 10.6.

We illustrate the 4-electron problem with the p^4 electron configuration, assuming the same principal quantum number for all 4 electrons as for example in a $(2p^4)$ state. Here we can have $L = 4$, 3, 2, 1 and 0 (see Table 10.6). Starting with the $L = 4$ multiplet, the $M_L = 4$ state $p^+p^+p^+p^+$ would have Γ_1^s symmetry. This state is forbidden by the Pauli principle since the direct product of the orbital and spin states $\Gamma_1^s \otimes (\Gamma_1^s + \Gamma_2 + \Gamma_3)$ does not contain Γ_1^a symmetry. To find the symmetry for the $L = 3$ multiplet, we consider the $M_L = 3$ states which arise from a $p^+p^+p^+p^0$ configuration and from Table 10.5 [giving the character table for $P(4)$], we see that ($\psi_1\psi_1\psi_1\psi_2$) contains the irreducible representations $\Gamma_1^s + \Gamma_3$. Thus subtracting Γ_1^s for the $L = 4$ state gives the symmetry Γ_3 for the $L = 3$ multiplet. The direct product of the

Table 10.6: Transformation properties of four-electron states under permutations. The symmetries of the irreducible representations of the permutation group $P(4)$ label the various spin and orbital angular momentum states. To obtain the states allowed by the Pauli Principle the direct product of the symmetries between the orbital and spin states must contain Γ_1^a.

Configuration	State	Irreducible Representation	Allowed State
$(\uparrow\uparrow\downarrow\downarrow)$	$S = 0$	Γ_2	
$(\uparrow\uparrow\uparrow\downarrow)$	$S = 1$	Γ_3	
$(\uparrow\uparrow\uparrow\uparrow)$	$S = 2$	Γ_1^s	
s^4	$L = 0$	Γ_1^s	$-$
$1s^3 2s$	$L = 0$	$\Gamma_1^s + \Gamma_3$	$-$
$1s^2 2s^2$	$L = 0$	$\Gamma_1^s + \Gamma_2 + \Gamma_3$	^1S
sp^3	$L = 0$	$\Gamma_1^a + \Gamma_{3'}$	$^3S, \, ^5S$
sp^3	$L = 1$	$\Gamma_1^s + \Gamma_2 + 2\Gamma_3 + \Gamma_{3'}$	$^1P, \, ^3P$
sp^3	$L = 2$	$\Gamma_2 + \Gamma_3 + \Gamma_{3'}$	$^1D, \, ^3D$
sp^3	$L = 3$	$\Gamma_1^s + \Gamma_3$	$-$
$(2p)^3(3p)$	$L = 0$	$\Gamma_1^s + \Gamma_2 + 2\Gamma_3 + \Gamma_{3'}$	$^1S, \, ^3S$
$(2p)^3(3p)$	$L = 1$	$\Gamma_1^s + \Gamma_1^a + 2\Gamma_2 + 3\Gamma_3 + 3\Gamma_{3'}$	$^1P, \, ^1P, \, ^3P, \, ^3P, \, ^3P, \, ^5P$
$(2p)^3(3p)$	$L = 2$	$2\Gamma_1^s + 2\Gamma_2 + 4\Gamma_3 + 2\Gamma_{3'}$	$^1D, \, ^1D, \, ^3D, \, ^3D$
$(2p)^3(3p)$	$L = 3$	$\Gamma_1^s + \Gamma_2 + 2\Gamma_3 + \Gamma_{3'}$	$^1F, \, ^3F$
$(2p)^3(3p)$	$L = 4$	$\Gamma_1^s + \Gamma_3$	$-$
p^4	$L = 0$	$\Gamma_1^s + \Gamma_2$	^1S
p^4	$L = 1$	$\Gamma_3 + \Gamma_{3'}$	^3P
p^4	$L = 2$	$\Gamma_1^s + \Gamma_2 + \Gamma_3$	^1D
p^4	$L = 3$	Γ_3	$-$
p^4	$L = 4$	Γ_1^s	$-$
d^4	$L = 0$	$\Gamma_1^s + 2\Gamma_2$	$^1S, \, ^1S$
d^4	$L = 1$	$2\Gamma_3 + 2\Gamma_{3'}$	$^3P, \, ^3P$
d^4	$L = 2$	$2\Gamma_1^s + \Gamma_1^a + 2\Gamma_2 + 2\Gamma_3 + \Gamma_{3'}$	$^1D, \, ^1D, \, ^3D, \, ^5D$
d^4	$L = 3$	$\Gamma_2 + 3\Gamma_3 + 2\Gamma_{3'}$	$^1F, \, ^3F, \, ^3F$
d^4	$L = 4$	$2\Gamma_1^s + 2\Gamma_2 + 2\Gamma_3 + \Gamma_{3'}$	$^1G, \, ^1G, \, ^3G$
d^4	$L = 5$	$\Gamma_1^s + 2\Gamma_3 + \Gamma_{3'}$	^3H
d^4	$L = 6$	$\Gamma_1^s + \Gamma_2 + \Gamma_3$	^1I
d^4	$L = 7$	Γ_3	$-$
d^4	$L = 8$	Γ_1^s	$-$
f^4	$L = 0$	$2\Gamma_1^s + \Gamma_1^a + 3\Gamma_3$	^5S
f^4	$L = 1$	$2\Gamma_2 + 3\Gamma_3 + 3\Gamma_{3'}$	$^1P, \, ^1P, \, ^3P, \, ^3P, \, ^3P$
f^4	$L = 2$	$2\Gamma_1^s + \Gamma_1^a + 4\Gamma_2 + 3\Gamma_3 + 2\Gamma_{3'}$	$^1D, \, ^1D, \, ^1D, \, ^1D, \, ^3D, \, ^3D, \, ^5D$
f^4	$L = 3$	$\Gamma_1^s + \Gamma_1^a + \Gamma_2 + 5\Gamma_3 + 4\Gamma_{3'}$	$^1F, \, ^3F, \, ^3F, \, ^3F, \, ^3F, \, ^5F$
f^4	$L = 4$	$3\Gamma_1^s + \Gamma_1^a + 4\Gamma_2 + 4\Gamma_3 + 3\Gamma_{3'}$	$^1G, \, ^1G, \, ^1G, \, ^1G, \, ^3G, \, ^3G, \, ^3G, \, ^5G$
f^4	$L = 5$	$\Gamma_1^s + 2\Gamma_2 + 5\Gamma_3 + 4\Gamma_{3'}$	$^1H, \, ^1H, \, ^3H, \, ^3H, \, ^3H$
f^4	$L = 6$	$3\Gamma_1^s + \Gamma_1^a + 3\Gamma_2 + 4\Gamma_3 + 2\Gamma_{3'}$	$^1I, \, ^1I, \, ^1I, \, ^3I, \, ^3I, \, ^5I$
f^4	$L = 7$	$\Gamma_1^s + \Gamma_2 + 4\Gamma_3 + 2\Gamma_{3'}$	$^1J, \, ^3J, \, ^3J$
f^4	$L = 8$	$2\Gamma_1^s + 2\Gamma_2 + 2\Gamma_3 + \Gamma_{3'}$	$^1K, \, ^1K, \, ^3K$
f^4	$L = 9$	$\Gamma_1^s + 2\Gamma_3 + \Gamma_{3'}$	^3L
f^4	$L = 10$	$\Gamma_1^s + \Gamma_2 + \Gamma_3$	^1M
f^4	$L = 11$	Γ_3	$-$
$\vdots$	$\vdots$	$\vdots$	
f^4	$L = 12$	Γ_1^s	$-$

orbital and spin states

$$\Gamma_3 \otimes (\Gamma_1^s + \Gamma_2 + \Gamma_3) = \Gamma_1^s + \Gamma_2 + 3\Gamma_3 + 2\Gamma_{3'}$$

again does not contain Γ_1^a and therefore is not allowed by the Pauli principle. However the $L = 2$ state is allowed and gives rise to a ^1D level since $M_L = 2$ arises from $p^+p^+p^0p^0$ or $p^+p^+p^+p^-$ which respectively correspond to the symmetries

$$(\Gamma_1^s + \Gamma_2 + \Gamma_3) + (\Gamma_1^s + \Gamma_3).$$

Thus subtracting the contributions of $M_L = 2$ to the $L = 3$ and $L = 4$ states gives $(\Gamma_1^a + \Gamma_2 + \Gamma_3)$. Now taking the direct product between the orbital and spin states

$$(\Gamma_1^s + \Gamma_2 + \Gamma_3) \otimes (\Gamma_1^s + \Gamma_2 + \Gamma_3) = 3\Gamma_1^s + \Gamma_1^a + 4\Gamma_2 + 5\Gamma_3 + 3\Gamma_{3'}$$

does contain the Γ_1^a symmetry arising from the direct product of $\Gamma_2 \otimes \Gamma_2$ and corresponding to the $S = 0$ spin state which is a singlet state. Likewise the symmetries of the ^3P and ^1S states for $L = 1$ and $L = 0$, respectively, can be found, and the results are given in Table 10.6. Since a p^4 electron configuration is equivalent to a p^2 hole configuration the allowed states for p^4 should be the same as for p^2. This can be verified by comparing p^2 in Table 10.2 with p^4 in Table 10.6.

It is left to the reader to verify the other entries in Table 10.6 and to explore the symmetries of other 4-electron combinations not listed. In finding these entries it should be noted that

$$\Gamma_2 \otimes \Gamma_2 = \Gamma_1^s + \Gamma_1^a + \Gamma_2$$

and

$$\Gamma_3 \otimes \Gamma_{3'} = \Gamma_1^a + \Gamma_2 + \Gamma_3 + \Gamma_{3'}$$

so that the spatial functions with Γ_1^a, Γ_2 and $\Gamma_{3'}$ all can give rise to states allowed by the Pauli principle.

10.5.4   Five-Electron States

The character table for the permutation group of 5 particles is shown in Table 10.7. Also listed in Table 10.7 are the characters for all possible

Table 10.7: Character table for the permutation group of five particles $P(5)$ (the symmetric group of order 5)

$P(5)$ or S_5	(1^5)	$10(2,1^3)$	$15(2^2,1)$	$20(3,1^2)$	$20(3,2)$	$30(4,1)$	$24(5)$
Γ_1^s	1	1	1	1	1	1	1
Γ_1^a	1	−1	1	1	−1	−1	1
Γ_4	4	2	0	1	−1	0	−1
$\Gamma_{4'}$	4	−2	0	1	1	0	−1
Γ_5	5	1	1	−1	1	−1	0
$\Gamma_{5'}$	5	−1	1	−1	−1	1	0
Γ_6	6	0	−2	0	0	0	1
$\chi_{\text{perm.}}(\psi_1\psi_1\psi_1\psi_1\psi_1)$	1	1	1	1	1	1	1
$\chi_{\text{perm.}}(\psi_1\psi_1\psi_1\psi_1\psi_2)$	5	3	1	2	0	1	0
$\chi_{\text{perm.}}(\psi_1\psi_1\psi_1\psi_2\psi_2)$	10	4	2	1	1	0	0
$\chi_{\text{perm.}}(\psi_1\psi_1\psi_1\psi_2\psi_3)$	20	6	0	2	0	0	0
$\chi_{\text{perm.}}(\psi_1\psi_1\psi_2\psi_2\psi_3)$	30	6	2	0	0	0	0
$\chi_{\text{perm.}}(\psi_1\psi_1\psi_2\psi_3\psi_4)$	60	6	0	0	0	0	0
$\chi_{\text{perm.}}(\psi_1\psi_2\psi_3\psi_4\psi_5)$	120	0	0	0	0	0	0

distinct products of 5 functions considered within the equivalence representation. The irreducible representations of $P(5)$ contained in the decomposition of the reducible equivalence representation are listed below:

S_5	Irreducible representations
$\chi_{\text{perm.}}(\psi_1\psi_1\psi_1\psi_1\psi_1)$	$\Rightarrow \Gamma_1^s$
$\chi_{\text{perm.}}(\psi_1\psi_1\psi_1\psi_1\psi_2)$	$\Rightarrow \Gamma_1^s + \Gamma_4$
$\chi_{\text{perm.}}(\psi_1\psi_1\psi_1\psi_2\psi_2)$	$\Rightarrow \Gamma_1^s + \Gamma_4 + \Gamma_5$
$\chi_{\text{perm.}}(\psi_1\psi_1\psi_1\psi_2\psi_3)$	$\Rightarrow \Gamma_1^s + 2\Gamma_4 + \Gamma_5 + \Gamma_6$
$\chi_{\text{perm.}}(\psi_1\psi_1\psi_2\psi_2\psi_3)$	$\Rightarrow \Gamma_1^s + 2\Gamma_4 + 2\Gamma_5 + \Gamma_{5'} + \Gamma_6$
$\chi_{\text{perm.}}(\psi_1\psi_1\psi_2\psi_3\psi_4)$	$\Rightarrow \Gamma_1^s + 3\Gamma_4 + \Gamma_{4'} + 3\Gamma_5 + 2\Gamma_{5'} + 3\Gamma_6$
$\chi_{\text{perm.}}(\psi_1\psi_2\psi_3\psi_4\psi_5)$	$\Rightarrow \Gamma_1^s + \Gamma_1^a + 4\Gamma_4 + 4\Gamma_{4'} + 5\Gamma_5 + 5\Gamma_{5'} + 6\Gamma_6$

With the help of these tables, the entries in Table 10.8 can be obtained for the spin and orbital symmetries of a number of 5-electron states that are listed in this table. The possible spin states are $S = 1/2$ which occurs 5 times, the $S = 3/2$ which occurs 4 times and the $S = 5/2$ which occurs once. In making the antisymmetric combinations it should be noted that

$$\Gamma_4 \otimes \Gamma_{4'} = \Gamma_1^a + \Gamma_{4'} + \Gamma_{5'} + \Gamma_6$$

and

$$\Gamma_5 \otimes \Gamma_{5'} = \Gamma_1^a + \Gamma_4 + \Gamma_{4'} + \Gamma_5 + \Gamma_{5'} + \Gamma_6$$

so that the spatial functions with Γ_1^a, $\Gamma_{4'}$ and $\Gamma_{5'}$ all give rise to states that are allowed by the Pauli Principle. Five-electron states occur in a half-filled d level. Such half-filled d levels are important in describing the magnetic ions in magnetic semiconductors formed by the substitution of Mn^{2+} for Cd in CdTe or CdSe.

10.6   Discussion

The Pauli-allowed states for n electrons in a more than half filled p shell and for $6 - n$ holes are the same. For example, referring to Table 10.8, the only Pauli-allowed state for p^5 is an $L = 1$, ^2P state. But this corresponds to a single hole in a p-shell, which has the same allowed angular momentum states as a single p electron ($S = 1/2$) in a p-shell.

Table 10.8: Transformation properties of five-electron states under permutations. The symmetries of the irreducible representations of the permutation group $P(5)$ label the various spin and orbital angular momentum states. To obtain the states allowed by the Pauli Principle the direct product of the symmetries between the orbital and spin states must contain Γ_1^a.

Configuration	State	Irreducible Representation	Allowed State
$(\uparrow\uparrow\uparrow\downarrow\downarrow)$	$S = 1/2$	Γ_5	
$(\uparrow\uparrow\uparrow\uparrow\downarrow)$	$S = 3/2$	Γ_4	
$(\uparrow\uparrow\uparrow\uparrow\uparrow)$	$S = 5/2$	Γ_1^s	
s^5	$L = 0$	Γ_1^s	$-$
$1s^4 2s$	$L = 0$	$\Gamma_1^s + \Gamma_4$	$-$
$1s^2 2s^2 3s$	$L = 0$	$\Gamma_1^s + 2\Gamma_4 + 2\Gamma_5 + \Gamma_{5'} + \Gamma_6$	^2S
p^5	$L = 0$	Γ_6	$-$
p^5	$L = 1$	$\Gamma_1^s + \Gamma_4 + \Gamma_5 + \Gamma_{5'}$	^2P
p^5	$L = 2$	$\Gamma_4 + \Gamma_5 + \Gamma_6$	$-$
p^5	$L = 3$	$\Gamma_1^s + \Gamma_4 + \Gamma_5$	$-$
p^5	$L = 4$	Γ_4	$-$
p^5	$L = 5$	Γ_1^s	$-$
d^5	$L = 0$	$\Gamma_1^a + \Gamma_4 + \Gamma_{5'} + \Gamma_6$	$^2S, \, ^6S$
d^5	$L = 1$	$\Gamma_1^s + 2\Gamma_4 + \Gamma_{4'} + 3\Gamma_5 + \Gamma_{5'} + 2\Gamma_6$	$^2P, \, ^4P$
d^5	$L = 2$	$2\Gamma_1^s + 3\Gamma_4 + \Gamma_{4'} + 4\Gamma_5 + 3\Gamma_{5'} + 2\Gamma_6$	$^2D, \, ^2D, \, ^2D, \, ^4D$
d^5	$L = 3$	$\Gamma_1^s + 4\Gamma_4 + \Gamma_{4'} + 3\Gamma_5 + 2\Gamma_{5'} + 4\Gamma_6$	$^2F, \, ^2F, \, ^4F$
d^5	$L = 4$	$2\Gamma_1^s + 4\Gamma_4 + \Gamma_{4'} + 4\Gamma_5 + 2\Gamma_{5'} + 2\Gamma_6$	$^2G, \, ^2G, \, ^4G$
d^5	$L = 5$	$\Gamma_1^s + 3\Gamma_4 + 3\Gamma_5 + \Gamma_{5'} + 3\Gamma_6$	^2H
d^5	$L = 6$	$2\Gamma_1^s + 3\Gamma_4 + 2\Gamma_5 + \Gamma_{5'} + \Gamma_6$	^2I
d^5	$L = 7$	$\Gamma_1^s + 2\Gamma_4 + \Gamma_5 + \Gamma_6$	$-$
d^5	$L = 8$	$\Gamma_1^s + \Gamma_4 + \Gamma_5$	$-$
d^5	$L = 9$	Γ_4	$-$
d^5	$L = 10$	Γ_1^s	$-$

We can denote both of these states by p^1 corresponding to the level designation ^2P. Using the same arguments p^2 and p^4 have the same allowed states. Similarly, the states for the d^6 electron configuration are identical to those for the d^4 hole configuration which are worked out in the Table 10.6, etc. In this sense, the tables that are provided in this chapter are sufficient to handle all atomic s, p and d levels. To treat the f levels completely we would need to construct tables for the permutation groups $P(6)$ and $P(7)$.

In solids and molecules where point group symmetry rather than full rotational symmetry applies, the application of permutation groups to the many-electron states is identical. Thus the $3d$ levels of a transition metal ion in a crystal field of cubic symmetry are split into a E_g and a T_{2g} level and the allowed d^2 levels would be either a ^1E_g or a $^1T_{2g}$, $^3T_{2g}$ level. In general, crystal field splittings are applied to the many-electron states whose symmetries are given in Tables 10.2, 10.4, 10.6 and 10.8. The d states in icosahedral symmetry do not experience any crystal field splitting and all the arguments of this chapter apply directly.

10.7 Selected Problems

1. Use the following character table for the permutation group $P(5)$.

$P(5)$ or S_5	(1^5)	$10(2, 1^3)$	$15(2^2, 1)$	$20(3, 1^2)$	$20(3, 2)$	$30(4, 1)$	$24(5)$
Γ_1^s	1	1	1	1	1	1	1
Γ_1^a	1	-1	1	1	-1	-1	1
Γ_4	4	2	0	1	-1	0	-1
$\Gamma_{4'}$	4	-2	0	1	1	0	-1
Γ_5	5	1	1	-1	1	-1	0
$\Gamma_{5'}$	5	-1	1	-1	-1	1	0
Γ_6	6	0	-2	0	0	0	1
$\chi_{\mathrm{perm.}}(\psi_1\psi_1\psi_1\psi_1\psi_1)$	1	1	1	1	1	1	1
$\chi_{\mathrm{perm.}}(\psi_1\psi_1\psi_1\psi_1\psi_2)$	5	3	1	2	0	1	0
$\chi_{\mathrm{perm.}}(\psi_1\psi_1\psi_1\psi_2\psi_2)$	10	4	2	1	1	0	0
$\chi_{\mathrm{perm.}}(\psi_1\psi_1\psi_1\psi_2\psi_3)$	20	6	0	2	0	0	0
$\chi_{\mathrm{perm.}}(\psi_1\psi_1\psi_2\psi_2\psi_3)$	30	6	2	0	0	0	0
$\chi_{\mathrm{perm.}}(\psi_1\psi_1\psi_2\psi_3\psi_4)$	60	6	0	0	0	0	0
$\chi_{\mathrm{perm.}}(\psi_1\psi_2\psi_3\psi_4\psi_5)$	120	0	0	0	0	0	0

(a) Show that there are 10 symmetry elements in the class $(2, 1^3)$ and 20 symmetry elements in class $(3, 2)$ for this permutation group.

(b) What are the characters for the equivalence transformation for a state where 3 of the 5 electrons are in one state (e.g.,

a d-state) and 2 electrons are in another state (e.g., a p-state)? Explain how you obtained your result. What irreducible representations are contained in this equivalence transformation?

2. (a) Consider the addition of Mn^{2+} as a substitutional magnetic impurity for CdTe. Since Mn^{2+} has five $3d$ electrons, use the permutation group $P(5)$ to find the Pauli-allowed states for the Mn^{2+} ion in CdTe. Of these Pauli-allowed d^5 states, which is the ground state based on Hund's rule?

   (b) Using the electric dipole selection rule for optical transitions, find the allowed transitions from the ground state in (a) to Pauli-allowed states in the $3d^4 4p$ configuration.

3. Use the following character table for the permutation group $P(6)$.

$P(6)$	1 (1^6)	15 $(2,1^4)$	45 $(2^2,1^2)$	15 (2^3)	40 $(3,1^3)$	120 $(3,2,1)$	40 (3^2)	90 $(4,1^2)$	90 $(4,2)$	144 $(5,1)$	120 (6)
Γ_1^s	1	1	1	1	1	1	1	1	1	1	1
Γ_1^a	1	-1	1	-1	1	-1	1	-1	1	1	-1
Γ_5	5	3	1	-1	2	0	-1	1	-1	0	-1
$\Gamma_{5'}$	5	-3	1	1	2	0	-1	-1	-1	0	1
$\Gamma_{5''}$	5	1	1	-3	-1	1	2	-1	-1	0	0
$\Gamma_{5'''}$	5	-1	1	3	-1	-1	2	1	-1	0	0
Γ_9	9	3	1	3	0	0	0	-1	1	-1	0
$\Gamma_{9'}$	9	-3	1	-3	0	0	0	1	1	-1	0
Γ_{10}	10	2	-2	-2	1	-1	1	0	0	0	1
$\Gamma_{10'}$	10	-2	-2	2	1	1	1	0	0	0	-1
Γ_{16}	16	0	0	0	-2	0	-2	0	0	1	0

(a) Show that there are 45 symmetry elements in the class $(2^2, 1^2)$ and 40 symmetry elements in class $(3, 1^3)$.

(b) Show that the irreducible representations Γ_5''' and Γ_9 as given in the character table are orthogonal. (This is a check that the character table is correct.) Which of the four 5-dimensional irreducible representations correspond to the basis functions $\Psi_{\Gamma_{n-1}}'$ in Eq. 10.19?

(c) What are the symmetries for the spin angular momentum states $S = 3, 2, 1, 0$? To solve this problem, you will have to find the equivalence transformations corresponding to selected permutations of spin configurations that are needed to construct the various spin angular momentum states. (See

Tables 10.5 and 10.6 for the permutation group $P(5)$ to provide guidance for solving this problem for $P(6)$.)

(d) According to Hund's rule, what are the S, L and J values for placing 6 electrons in a d^6 electronic configuration. To which irreducible representations of $P(6)$ do the spin and spatial parts of this Hund's rule ground state correspond?

4. Review the proof of the Wigner-Eckart theorem (e.g., Tinkham, p. 131-2). No written work is expected.

5. Both CO_2 and N_2O are linear molecules, but have different equilibrium arrangements:

CO_2

N_2O
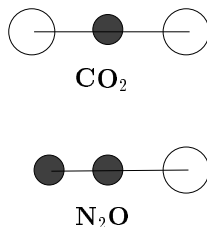
(a) What are the appropriate point groups for CO_2 and N_2O?

(b) What are the differences in the symmetries of the normal mode vibrations for these two molecules?

(c) Show schematically the atomic displacements for the normal mode vibrations of each molecule.

(d) What are the expected differences in their IR vibrational spectra? Raman vibrational spectra?

(e) What are the expected differences in the rotational spectra of these two molecules?

(f) Which of these rotational modes can be excited by infrared or Raman spectroscopy?

6. (a) We will now find the molecular vibrations for the hypothetical molecule XH_{12} (see Problem 4 of §3) where the 12 hydrogen atoms are at the vertices of a regular icosahedron

and the atom X is at the center of the icosahedron. Find $\chi^{\text{atom sites}}$ for XH_{12} for the icosahedral group I_h.

(b) What are the symmetries for the normal modes? Which are infrared-active? Raman active?

(c) What are the polarization selection rules for the infrared-active modes? for the Raman-active modes?

7. Use the following character table for the permutation group $P(5)$.

$P(5)$ or S_5	(1^5)	$10(2,1^3)$	$15(2^2,1)$	$20(3,1^2)$	$20(3,2)$	$30(4,1)$	$24(5)$
Γ_1^s	1	1	1	1	1	1	1
Γ_1^a	1	-1	1	1	-1	-1	1
Γ_4	4	2	0	1	-1	0	-1
$\Gamma_{4'}$	4	-2	0	1	1	0	-1
Γ_5	5	1	1	-1	1	-1	0
$\Gamma_{5'}$	5	-1	1	-1	-1	1	0
Γ_6	6	0	-2	0	0	0	1
$\chi_{\text{perm.}}(\psi_1\psi_1\psi_1\psi_1\psi_1)$	1	1	1	1	1	1	1
$\chi_{\text{perm.}}(\psi_1\psi_1\psi_1\psi_1\psi_2)$	5	3	1	2	0	1	0
$\chi_{\text{perm.}}(\psi_1\psi_1\psi_1\psi_2\psi_2)$	10	4	2	1	1	0	0
$\chi_{\text{perm.}}(\psi_1\psi_1\psi_1\psi_2\psi_3)$	20	6	0	2	0	0	0
$\chi_{\text{perm.}}(\psi_1\psi_1\psi_2\psi_2\psi_3)$	30	6	2	0	0	0	0
$\chi_{\text{perm.}}(\psi_1\psi_1\psi_2\psi_3\psi_4)$	60	6	0	0	0	0	0
$\chi_{\text{perm.}}(\psi_1\psi_2\psi_3\psi_4\psi_5)$	120	0	0	0	0	0	0

(a) Multiply element

$$P_i = \begin{pmatrix} 1 & 2 & 3 & 4 & 5 \\ 3 & 2 & 1 & 4 & 5 \end{pmatrix}$$

by element

$$P_j = \begin{pmatrix} 1 & 2 & 3 & 4 & 5 \\ 4 & 2 & 5 & 1 & 3 \end{pmatrix}$$

to form P_iP_j and P_jP_i. Are your results consistent with the character table?

(b) Show that there are 10 symmetry elements in the class $(2,1^3)$ and 20 symmetry elements in class $(3,2)$ for this permutation group. Give an example of a symmetry element in each class.

(c) Verify the results given in Table 10.6 for the Pauli-allowed states for p^5 by considering unfilled states (holes) in the p-shell.

(d) Referring to Table 10.6, what are the irreducible representations for the spin configuration $(\uparrow\uparrow\downarrow\downarrow)$?

(e) Using Hund's rule, what are the total spin and orbital angular momenta values for the d^5 configuration? Explain how to find the irreducible representations for this configuration from Table 10.6. You will make use of some of the results in (e) when you work parts (h) and (i).

(f) What are the characters for the equivalence transformation for a state where 3 of the 5 electrons are in a p-state and 2 electrons are in a d-state? Explain how you obtained your result. What irreducible representations are contained in this equivalence transformation?

(g) What are the Pauli allowed states (as would be given in Table 10.6) with the largest L value for the $p^3 d^2$ configuration?

(h) Consider the addition of Mn^{2+} as a substitutional magnetic impurity for CdTe. Since Mn^{2+} has five $3d$ electrons, use the permutation group $P(5)$ to find the Pauli-allowed states for the Mn^{2+} ion in CdTe. Of these Pauli-allowed d^5 states, which is the ground state based on Hund's rule (see part e)?

(i) Using the electric dipole selection rule for optical transitions, find the allowed transitions from the ground state for Mn^{2+} in CdTe in (a) to Pauli-allowed states in the $3d^4 4p$ configuration.

Chapter 11

Transformation of Tensors

In theories and experiments involving physical systems with high symmetry, one frequently encounters the question of how many independent terms are required by symmetry to specify a tensor of given rank for each symmetry group. These questions have simple group theoretical answers. This chapter deals with the transformation properties of tensors, with particular attention given to those tensors of rank 2 and higher that arise in non-linear optics and in elasticity theory. In this analysis we consider the symmetry implied by the permutation group which gives the number of independent components in the case of no point group symmetry. We then consider the additional symmetry that is introduced by the presence of symmetry elements such as rotations, reflections and inversions. We explicitly discuss full rotational symmetry and several point group symmetries.

Reference:
"Tensors and group theory for physical properties of crystals", W.A. Wooster, Clarendon Press, Oxford.

11.1   Introduction

We start by listing a few commonly occurring examples of tensors of rank 2, 3, and 4 that occur in solid state physics. Second rank symmetric tensors occur in the constitutive equations of Electromagnetic Theory, as for example in the linear equations relating the current den-

267

sity to the electric field intensity

$$\vec{J}^{(1)} = \overset{\leftrightarrow}{\sigma}^{(1)} \cdot \vec{E} \tag{11.1}$$

where the conductivity $\overset{\leftrightarrow}{\sigma}^{(1)}$ is a symmetric second rank tensor. A similar situation holds for the relation between the polarization and the electric field

$$\vec{P}^{(1)} = \overset{\leftrightarrow}{\alpha}^{(1)} \cdot \vec{E} \tag{11.2}$$

where the polarizability $\overset{\leftrightarrow}{\alpha}^{(1)}$ is a symmetric second rank tensor, and where $\overset{\leftrightarrow}{\alpha}^{(1)} \equiv \overset{\leftrightarrow}{\chi}_E^{(1)}$ is often called the electrical susceptibility. A similar situation also holds for the relation between the magnetization and the magnetic field

$$\vec{M}^{(1)} = \overset{\leftrightarrow}{\chi}_H^{(1)} \cdot \vec{H} \tag{11.3}$$

where the magnetic susceptibility $\overset{\leftrightarrow}{\chi}_H^{(1)}$ is a symmetric second rank tensor. These relations all involve second rank tensors: $\overset{\leftrightarrow}{\sigma}^{(1)}$, $\overset{\leftrightarrow}{\alpha}^{(1)}$ and $\overset{\leftrightarrow}{\chi}_H^{(1)}$. Each second rank tensor T_{ij} has 9 components (6 symmetric and 3 antisymmetric combinations under the interchange of the indices i and j). Thus, a symmetric second rank tensor, such as the polarizability tensor or the Raman tensor, has only 6 independent components. In this chapter we are concerned with the symmetry properties of these tensors under permutations and point group symmetry operations.

As an example of higher rank tensors, consider non-linear optical phenomena, where the polarization in Eq. 11.2 is further expanded to higher order terms in $\vec{E}$ as

$$\vec{P} = \vec{P}^{(1)} + \overset{\leftrightarrow}{\alpha}^{(2)} \cdot \vec{E}\vec{E} + \overset{\leftrightarrow}{\alpha}^{(3)} \cdot \vec{E}\vec{E}\vec{E} + \dots \tag{11.4}$$

where we can consider the polarizability tensor to be field dependent

$$\overset{\leftrightarrow}{\alpha} = \overset{\leftrightarrow}{\alpha}^{(1)} + \overset{\leftrightarrow}{\alpha}^{(2)} \cdot \vec{E} + \overset{\leftrightarrow}{\alpha}^{(3)} \cdot \vec{E}\vec{E} + \dots \tag{11.5}$$

More will be said about the symmetry of the various $\overset{\leftrightarrow}{\alpha}^{(i)}$ tensors under permutations and point group operations in §11.2. Similar expansions can be made for Eqs. 11.1 and 11.3.

Let us now consider the number of tensor components. As stated above $\overset{\leftrightarrow(1)}{\alpha}$ has $3^2 = 9$ coefficients (6 for the symmetric components, $\alpha_{ij} = \alpha_{ji}$). There are $3^3 = 27$ coefficients (10 symmetric) in $\overset{\leftrightarrow(2)}{\alpha}$, $3^4 = 81$ coefficients (only 15 symmetric) in $\overset{\leftrightarrow(3)}{\alpha}$, and $3^5 = 243$ coefficients (21 symmetric) in $\overset{\leftrightarrow(4)}{\alpha}$, etc. How many tensor components are independent? Which components are related to one another? How many independent experiments must be carried out to completely characterize these tensors? These are important questions that occur in many fields of physics and materials science. We address these questions in this chapter.

As another example, consider the **piezoelectric** tensor which is a 3rd rank tensor relating polarization per unit volume $\vec{P}$ to the strain tensor, $\overset{\leftrightarrow}{e}$, where $\vec{P}$ is given by

$$\vec{P} = \overset{\leftrightarrow(2)}{d} \cdot \overset{\leftrightarrow}{e}, \tag{11.6}$$

which can be rewritten to show the rank of each tensor explicitly

$$P_k = \sum_{i,j} d_{kij} \frac{\vec{u}_i}{\vec{x}_j} \tag{11.7}$$

in which $\vec{u}$ is the change in the length of $\vec{x}_i$. We note that there are 27 components in the tensor $\overset{\leftrightarrow(2)}{d}$ without taking into account symmetry under permutation operations. A frequently used 4th rank tensor is the elastic constant tensor $\overset{\leftrightarrow(3)}{C}$ defined by

$$\overset{\leftrightarrow}{T} = \overset{\leftrightarrow(3)}{C} \cdot \overset{\leftrightarrow}{e} \tag{11.8}$$

where the stress tensor $\overset{\leftrightarrow}{T}$ and strain tensor $\overset{\leftrightarrow}{e}$ (i.e., the gradient of the displacement) are related through the fourth rank elastic constant tensor $\overset{\leftrightarrow(3)}{C}$ (or C_{ijkl}) which neglecting permutation symmetry would have 81 components. More will be said about the elastic constant tensor below (see §11.6).

These tensors and many more are discussed in "Physical Properties of Crystals" by J.F. Nye. The discussion of tensors which we give

here is group theoretical, whereas Nye's book gives tables of the tensors which summarize many of the results which we can deduce from our group theoretical analysis. In §11.2, we discuss the reduction in the number of independent components of tensors obtained from point group symmetry (rotations, reflections and inversion) while in §11.3 we discuss the corresponding reduction arising from symmetries associated with the permutation of tensor indices. The number of independent coefficients for the case of complete isotropy (full rotational symmetry) is considered in §11.4, while lower point group symmetries are treated in §11.5. The independent coefficients of the elastic modulus tensor $\mathcal{C}_{ijkl}$ are discussed in §11.6.

11.2　Independent Components of Tensors – Point Symmetry Groups

In this section we discuss a very general group theoretical result for tensor components arising from point group symmetry operations such as rotations, reflections and inversions. These symmetry operations greatly reduce the number of independent coefficients that need to be introduced for the various tensors in crystals having various point group symmetry. In §11.3 we consider the reduction in the number of independent coefficients through symmetry under permutation group operations.

Let us consider a relation between a tensor of arbitrary rank $J_{ij\ldots}$ and another tensor $F_{i'}F_{j'}\ldots$ also of arbitrary rank and arbitrary form

$$J_{ij\ldots} = \sum_{i'j'\ldots} \{t_{ij\ldots,i'j'\ldots}\}F_{i'}F_{j'}\ldots \tag{11.9}$$

The number of independent non-zero tensor components $t_{ij\ldots,i'j'\ldots}$ allowed by point group symmetry in Eq. 11.9 is determined by finding the irreducible representations contained in both $\{\Gamma_{J_{ij\ldots}}\} = \sum \alpha_i \Gamma_i$ and $\{\Gamma_{F_{i'}F_{j'}\ldots}\} = \sum \beta_j \Gamma_j$. The only non-vanishing couplings between $\vec{J}_{\Gamma_i}$ and $\{\vec{F}, \vec{F}\ldots\}_{\Gamma_j}$ are between partners transforming according to the same irreducible representation because only these lead to matrix elements that are invariant under the symmetry operations of the group.

We therefore transform Eq. 11.9 to make use of the symmetrized form

$$\{\vec{J}\}_{\Gamma_i} = t_{\Gamma_1^+} \, \{\vec{F}, \vec{F}\dots\}_{\Gamma_i} \tag{11.10}$$

where the $\vec{J}_{\Gamma_i}$ and $\{\vec{F}, \vec{F}\dots\}_{\Gamma_i}$ correspond to the same partners of the same irreducible representation and $t_{\Gamma_1^+}$ transforms as a scalar which has Γ_1^+ symmetry. Thus the number of independent matrix elements in the tensor $t_{ij\dots i'j'\dots}$ is the number of times the scalar representation Γ_1^+ occurs in the decomposition of

$$\{\Gamma_{\vec{J}}\} \otimes \{\Gamma_{\vec{F},\vec{F}\dots}\} = \sum_i \alpha_i \Gamma_i \otimes \sum_j \beta_j \Gamma_j = \sum_k \gamma_k \Gamma_k. \tag{11.11}$$

In most cases of interest, permutational symmetry requirements on the products $\{\vec{F}, \vec{F}, \dots\}$ further limit the number of independent matrix elements of a tensor matrix, as discussed below (§11.3).

11.3 Independent Components of Tensors under Permutation Group Symmetry

In this section we consider the effect of permutation symmetry on reducing the number of independent components of tensors. For example, second-rank symmetric tensors occur frequently in solid state physics. In this case, the permutation symmetry $\alpha_{ij} = \alpha_{ji}$ restricts the off-diagonal matrix elements to follow this additional relation, thereby reducing the number of allowed off-diagonal elements from 6 to 3 since the symmetric combinations $(\alpha_{ij} + \alpha_{ji})/2$ are allowed and the $(\alpha_{ij} - \alpha_{ji})/2$ vanish by symmetry. Furthermore, the three elements $(\alpha_{ij} - \alpha_{ji})/2$ constitute the 3 components of an antisymmetric 2nd rank tensor, also called an axial vector; the angular momentum (listed in character tables as R_i) is an example of an antisymmetric second-rank tensor. To deal with the symmetry of a second-rank tensor under permutation operations, group theory is not needed. However, as the rank of the tensor increases, group theory becomes increasingly helpful in this symmetry classification.

Table 11.1: Transformation properties of various tensors under permutations. The irreducible representations associated with the designated permutation group, configuration and state are listed.

Tensor	Configuration	State	Irreducible Representation	Group
$C_{(ij)(kl)}$	SS	$L=0$	Γ_1^s	$P(2)$
	SD	$L=2$	$\Gamma_1^s + \Gamma_1^a$	$P(2)$
	DD	$L=0$	Γ_1^s	$P(2)$
	DD	$L=1$	Γ_1^a	$P(2)$
	DD	$L=2$	Γ_1^s	$P(2)$
	DD	$L=3$	Γ_1^a	$P(2)$
	DD	$L=4$	Γ_1^s	$P(2)$
$d_{i(jk)}$	pS	$L=1$	$\Gamma_1^s + \Gamma_1^a$	$P(2)$
	pD	$L=1$	$\Gamma_1^s + \Gamma_1^a$	$P(2)$
	pD	$L=2$	$\Gamma_1^s + \Gamma_1^a$	$P(2)$
	pD	$L=3$	$\Gamma_1^s + \Gamma_1^a$	$P(2)$
$\alpha^{(1)}$	p^2	$L=0$	Γ_1^s	$P(2)$
	p^2	$L=1$	Γ_1^a	$P(2)$
	p^2	$L=2$	Γ_1^s	$P(2)$
$\alpha^{(2)}$	p^3	$L=0$	Γ_1^a	$P(3)$
	p^3	$L=1$	$\Gamma_1^s + \Gamma_2$	$P(3)$
	p^3	$L=2$	Γ_2	$P(3)$
	p^3	$L=3$	Γ_1^s	$P(3)$
$\alpha^{(3)}$	p^4	$L=0$	$\Gamma_1^s + \Gamma_2$	$P(4)$
	p^4	$L=1$	$\Gamma_3 + \Gamma_{3'}$	$P(4)$
	p^4	$L=2$	$\Gamma_1^s + \Gamma_2 + \Gamma_3$	$P(4)$
	p^4	$L=3$	Γ_3	$P(4)$
	p^4	$L=4$	Γ_1^s	$P(4)$
$\alpha^{(4)}$	p^5	$L=0$	Γ_6	$P(5)$
	p^5	$L=1$	$\Gamma_1^s + \Gamma_4 + \Gamma_5 + \Gamma_{5'}$	$P(5)$
	p^5	$L=2$	$\Gamma_4 + \Gamma_5 + \Gamma_6$	$P(5)$
	p^5	$L=3$	$\Gamma_1^s + \Gamma_4 + \Gamma_5$	$P(5)$
	p^5	$L=4$	Γ_4	$P(5)$
	p^5	$L=5$	Γ_1^s	$P(5)$
$\alpha^{(5)}$	p^6	$L=0$	$\Gamma_1^s + \Gamma_{5'''} + \Gamma_9$	$P(6)$
	p^6	$L=1$	$\Gamma_5 + \Gamma_{5''} + \Gamma_{10} + \Gamma_{16}$	$P(6)$
	p^6	$L=2$	$\Gamma_1^s + \Gamma_5 + 2\Gamma_9 + \Gamma_{16}$	$P(6)$
	p^6	$L=3$	$\Gamma_5 + \Gamma_{5''} + \Gamma_9 + \Gamma_{10}$	$P(6)$
	p^6	$L=4$	$\Gamma_1^s + \Gamma_5 + \Gamma_9$	$P(6)$
	p^6	$L=5$	Γ_5	$P(6)$
	p^6	$L=6$	Γ_1^s	$P(6)$

For illustrative purposes, we now consider the case of the second rank tensor from the point of view of permutation group symmetry. Referring to Table 11.1 (which is constructed from tables in Chapter 10), we see that a second rank symmetric tensor is represented by pp, which we can consider as the generic prototype of a second rank symmetric tensor. From the discussion of Chapter 10, we found that p^2 could have angular momentum states $L = 0$, 1, 2 with the indicated permutation group symmetries, labeled "irreducible representations" in Table 11.1, and yielding a total number of states equal to $1 + 3 + 5 = 9$. From the table, it is seen that the symmetric states arise from the $L = 0$ and $L =2$ entries, corresponding to 1+5=6 states. Thus we obtain 6 independent coefficients for a symmetric second rank tensor based on permutation symmetry alone. The number of independent coefficients for the 2nd rank antisymmetric tensor (transforming Γ_1^a) is correspondingly equal to 3, and the antisymmetric contribution arises from the $L =1$ state.

A third rank symmetric tensor (such as $\overset{\leftrightarrow(2)}{\alpha}$) is more interesting from a group theoretical standpoint. Here we need to consider permutations of the type p^3, so that p^3 can be considered as the appropriate basis function of the permutation group $P(3)$ for the permutation symmetry of $\overset{\leftrightarrow(2)}{\alpha}$. Referring to Eq. 11.4, we note that the $\vec{E}\vec{E}$ fields are clearly symmetric under interchange of $\vec{E} \leftrightarrow \vec{E}$; but since Eq. 11.5 defines the general non-linear polarizability tensor $\overset{\leftrightarrow}{\alpha}$, then all terms in the expansion of $\overset{\leftrightarrow}{\alpha}$ must be symmetric under interchange of $\vec{P}$ and $\vec{E}$. From Table 11.1, we see that p^3 consists of $L = 0$, 1, 2, 3 angular momentum states. The entries for the p^3 configuration in Table 11.1 come from Table 10.4 on p. 252 which contains a variety of configurations that can be constructed from 3 electrons (or more generally 3 interchangeable vectors). The total number of states in the p^3 configuration is found by considering the degeneracy of each angular momentum state which for the $L = 0$, 1, 2, 3 multiplets is

$$(1)(1) + 3(1 + 2) + 5(2) + 7(1) = 27$$

which includes all 3^3 combinations. Of this total, the number of symmetric combinations that go with Γ_1^s is only 3(1)+7(1)=10. Similarly Table 11.1 shows that there is only one antisymmetric combination. Of

Table 11.2: Number of independent components for various tensors for the listed group symmetries

Group	Repr.[a]	angular momentum values[b]	# of independent coefficients					
			$C_{(ij)(kl)}$	$d_{k(ij)}$	$\alpha^{(1)}$	$\alpha^{(2)}$	$\alpha^{(3)}$	$\alpha^{(4)}$
$R_\infty{}^{[c]}$	$\Gamma_{l=0}$	$l = 0$	2	0	1	0	1	0
I_h	A_{1g}	$l = 0,\ 6,\ 10,\ \ldots$	2	0	1	0	1	0
O_h	A_{1g}	$l = 0,\ 4,\ 6,\ 8,\ 10,\ \ldots$	3	0	1	0	2	0
T_d	A_1	$l = 0,\ 3,\ 4,\ 6,\ 7,\ 8,\ 9,\ \ldots$	3	1	1	1	2	1
$D_{\infty h}$	A_{1g}	$l = 0,\ 2,\ 4,\ 6,\ \ldots$	5	1	2	0	3	0
$C_{\infty v}$	A_1	$l = 0,\ 1,\ 2,\ 3,\ 4,\ 5,\ \ldots$	5	4	2	2	3	3
D_{6h}	A_{1g}	$l = 0,\ 2,\ 4,\ 6,\ \ldots$	5	1	2	0	3	0
C_1	A_1	$l = 0,\ 1,\ 2,\ 3,\ 4,\ 5,\ \ldots$[d]	21	18	6	10	15	21

[a] The notation for the totally symmetric irreducible representation for each group is given.
[b] The angular momentum states that contain the A_1 (or A_{1g}) irreducible representation for the various symmetry groups (see Table 11.1).
[c] The full rotational symmetry group is denoted by R_∞.
[d] For this lowest point group symmetry, the A_1 representation occurs $2l + 1$ times. For the other groups in this table, there is only one occurrence of A_1 for each listed l value. However, for higher l's, multiple occurrences of A_1 may arise (e.g., in O_h symmetry, the $l = 12$ state has two A_{1g} modes).

—

interest (and perhaps not appreciated by many workers in the field) is the large number of combinations that are neither symmetric nor antisymmetric: $3(2)+5(2)=16$. Thus, Table 11.1 shows that on the basis of permutation symmetry, there are only 10 independent coefficients for $\overset{\leftrightarrow}{\alpha}{}^{(2)}$, assuming no additional point group symmetry. This result is summarized in Table 11.2.

As the next example, consider $\overset{\leftrightarrow}{\alpha}{}^{(3)}$ which is a fourth rank tensor that couples $\vec{P}$ and $\vec{E}\vec{E}\vec{E}$ symmetrically. The generic tensor for this case is p^4 in Table 11.1 (taken from Table 10.6 on p. 257 for 4 electrons) with 81 coefficients neglecting permutational and point group symmetries, obtained as follows:

$$(1)(1 + 2) + (3)(3 + 3) + 5(1 + 2 + 3) + 7(3) + 9(1) = 81.$$

Of these, $1+5+9=15$ are symmetric (transforms as Γ_1^s) and this entry

is included in Table 11.2. There are no antisymmetric combinations (i.e., there is no Γ_1^a for p^4 in $P(4)$).

Another commonly occurring tensor in solid state physics is the elastic modulus tensor $\mathcal{C}_{ijkl} = C_{(ij)(kl)}$ which is the direct product of two symmetric tensors, each having 6 independent components, and thus leading to 6×6=36 components for the product. But $C_{(ij)(kl)}$ is further symmetric under interchange of $ij \leftrightarrow kl$, reducing the 30 off-diagonal components of the 6×6 matrix into 15 symmetric and 15 antisymmetric combinations, in addition to the 6 diagonal symmetric components, as is explained in standard solid state physics texts. From a group theoretical standpoint, the (ij) and (kl) are each treated as p^2 units which form total angular momentum states of $L = 0$ (labeled S in Table 11.1) and $L = 2$ (labeled D). Under the permutation group $P(2)$, we can make one SS combination ($L = 0$) and one symmetric and one antisymmetric SD combination ($L = 2$), and DD combinations with $L = 0, 1, 2, 3, 4$. Adding up the total number of combinations that can be made from $C_{(ij)(kl)}$ we get

$$(1)(1) + 5(1 + 1) + 1(1) + 3(1) + 5(1) + 7(1) + 9(1) = 36,$$

in agreement with the simple argument given above. Of these 21 are symmetric (i.e., go with Γ_1^s) while 15 are antisymmetric (i.e., go with Γ_1^a), and the number 21 appears in Table 11.2. If we had instead used p^4 in Table 11.1 as the basis function for the permutation of the elastic tensor $\mathcal{C}_{ijkl}$, we would have neglected the symmetric interchange of the stress and strain tensors $(ij) \leftrightarrow (kl)$.

The final tensor that we will consider is the piezoelectric tensor $d_{i(jk)}$ formed as the symmetric direct product of a vector and a symmetric second rank tensor (3×6=18 components). The symmetries are calculated following the pS and pD combinations, using the concepts discussed for the transformation properties of the $\overset{\leftrightarrow(1)}{\alpha}$ and $C_{(ij)(kl)}$ tensors. This discussion yields 18 independent coefficients for $d_{i(jk)}$ under permutation symmetry.

In summary, each second rank symmetric tensor is composed of irreducible representations $L = 0$ and $L = 2$ of the full rotation group, the third rank symmetric tensor from $L = 1$ and $L = 3$, the fourth rank symmetric tensor from $L = 0$, $L = 2$ and $L = 4$, the elastic tensor from

$L = 0$, $2L = 2$ and $L = 4$, and the piezoelectric tensor from $2L = 1$, $L = 2$ and $L = 3$.

We use these results to find the number of independent coefficients for each symmetry group.

11.4   Independent Components of Tensors under Full Rotational Symmetry

The highest point group symmetry is the full isotropy provided by the full rotation group R_∞. The number of the independent components can also be found from Table 11.2. In §11.2, we showed that the number of independent coefficients in a tensor formed by the direct product of two tensors is the number of times this direct product contains Γ_1^s in the fully symmetric irreducible representation $L = 0$.

Referring to Table 11.1, we find that for the second rank tensor $(\Gamma_{L=0} + \Gamma_{L=2})$, $\Gamma_{L=0}$ is contained once, so that $\alpha_{11} = \alpha_{22} = \alpha_{33}$ and $\alpha_{12} = \alpha_{23} = \alpha_{31} = 0$ and the result for the number of independent components is given in Table 11.2.

Likewise Table 11.1 shows that there are no independent coefficients for $\overset{\leftrightarrow(2)}{\alpha}$ in full rotational symmetry and this tensor vanishes by symmetry (as well as all tensors of odd rank of this type). With regard to the 4th rank tensor, $\overset{\leftrightarrow(3)}{\alpha}$, Table 11.1 shows only one independent coefficient. In contrast, the $C_{(ij)(kl)}$ 4th rank tensor contains 2 independent coefficients in full rotational symmetry and the components of $d_{i(jk)}$ all vanish by symmetry.

This completes the discussion for the form of the various tensors in Table 11.2 under full rotational symmetry. Also listed in the table are the number of independent coefficients for several point group symmetries, including I_h, O_h, T_d, $D_{\infty h}$, $C_{\infty v}$, D_{6h}, and C_1. These results can be derived by considering these groups are subgroups of the full rotational group, and going from higher to lower symmetry. Some illustrative examples of the various point group symmetries are given in the following sections.

Table 11.3: Character Table and Bases for the Cubic Group O_h

Repr.	Basis	E	$3C_4^2$	$6C_4$	$6C_2$	$8C_3$	i	$3iC_4^2$	$6iC_4$	$6iC_2$	$8iC_3$
Γ_1^+	1	1	1	1	1	1	1	1	1	1	1
Γ_2^+	$x^4(y^2-z^2)+$ $y^4(z^2-x^2)+$ $z^4(x^2-y^2)$	1	1	-1	-1	1	1	1	-1	-1	1
Γ_{12}^+	x^2-y^2 $2z^2-x^2-y^2$	2	2	0	0	-1	2	2	0	0	-1
Γ_{15}^+	$xy(x^2-y^2)$ $yz(y^2-z^2)$ $zx(z^2-x^2)$	3	-1	1	-1	0	3	-1	1	-1	0
Γ_{25}^+	xy, yz, zx	3	-1	-1	1	0	3	-1	-1	1	0
Γ_1^-	$xyz[x^4(y^2-z^2)+$ $y^4(z^2-x^2)+$ $z^4(x^2-y^2)]$	1	1	1	1	1	-1	-1	-1	-1	-1
Γ_2^-	xyz	1	1	-1	-1	1	-1	-1	1	1	-1
Γ_{12}^-	$xyz(x^2-y^2)$ $xyz(2z^2-x^2-y^2)$	2	2	0	0	-1	-2	-2	0	0	1
Γ_{15}^-	x, y, z	3	-1	1	-1	0	-3	1	-1	1	0
Γ_{25}^-	$z(x^2-y^2)$ $x(y^2-z^2)$ $y(z^2-x^2)$	3	-1	-1	1	0	-3	1	1	-1	0

11.5 Tensors Arising in Non-Linear Optics

In this section we consider tensors arising in non-linear optics, including symmetric 2nd rank, 3rd rank and 4th rank tensors.

11.5.1 Cubic Symmetry $- O_h$

The character table for group O_h is shown in Table 3.33 on p. 70. Table 11.3 gives the same character table for the cubic group, but using solid state physics notation and the table furthermore contains more basis functions. We first consider the transformation properties of the linear response tensor $\overset{\leftrightarrow}{\alpha}^{(1)}$ and the non-linear polarizability tensors $\overset{\leftrightarrow}{\alpha}^{(2)}$ and $\overset{\leftrightarrow}{\alpha}^{(3)}$.

Consider for example the second rank tensor $\overset{\leftrightarrow}{\alpha}^{(1)}$ defined by

$$\vec{P} = \overset{\leftrightarrow}{\alpha}^{(1)} \cdot \vec{E}. \tag{11.12}$$

Both $\vec{P}$ and $\vec{E}$ transform as Γ_{15}^- which gives

$$\Gamma_{\vec{P}} \otimes \Gamma_{\vec{E}} = \Gamma_{15}^- \otimes \Gamma_{15}^- = \Gamma_1^+ + \Gamma_{12}^+ + \Gamma_{15}^+ + \Gamma_{25}^+. \tag{11.13}$$

But since the Γ_{15}^+ is antisymmetric under interchange of $i \leftrightarrow j$ in any of the symmetric second rank tensors, we write

$$\Gamma_{\overset{\leftrightarrow}{e}}^{(s)} = \Gamma_1^+ + \Gamma_{12}^+ + \Gamma_{25}^+, \qquad \Gamma_{\overset{\leftrightarrow}{e}}^{(a)} = \Gamma_{15}^+ \tag{11.14}$$

showing the 6 partners for the second rank symmetric tensor, and the 3 partners for the second rank antisymmetric tensor. These results can also be obtained starting from the full rotation group, considering the decomposition of the $L = 0$ and $L = 2$ states for the symmetric partners and the $L = 1$ states for the antisymmetric partners.

Since Γ_1^+ is contained only once in the direct product $\Gamma_{15}^- \otimes \Gamma_{15}^-$ in cubic O_h symmetry, there is only one independent tensor component for $\overset{\leftrightarrow}{\alpha}^{(1)}$ and we can write $\overset{\leftrightarrow}{\alpha}^{(1)} = \alpha^0 \overset{\leftrightarrow}{1}$ where $\overset{\leftrightarrow}{1}$ is the unit tensor and α^0 is a constant. As a consequence of this general result, the conductivity in cubic symmetry (O_h or T_d) is independent of the direction of the fields relative to the crystal axes and only one experiment is required to measure the polarizability or the conductivity on an unoriented cubic crystal.

In non-linear optics the lowest order non-linear term is $\overset{\leftrightarrow}{\alpha}^{(2)} \cdot \vec{E}\vec{E}$ in Eq. 11.4 where $\overset{\leftrightarrow}{\alpha}^{(2)}$ is a third rank tensor. Since $(\vec{E}\vec{E})$ is symmetric under interchange, then $(\vec{E}\vec{E})$ transforms as

$$\Gamma_{\vec{E}\vec{E}}^{(s)} = \Gamma_1^+ + \Gamma_{12}^+ + \Gamma_{25}^+, \tag{11.15}$$

where we have thrown out the Γ_{15}^+ term because it is antisymmetric under interchange of $E_i E_j \longrightarrow E_j E_i$. Thus, we obtain the irreducible representation contained in the direct product:

$$\begin{aligned} \Gamma_{\vec{P}} \otimes \Gamma_{\vec{E}\vec{E}}^{(s)} = & \ \Gamma_{15}^- \otimes \{\Gamma_1^+ + \Gamma_{12}^+ + \Gamma_{25}^+\} \\ = & \ (\Gamma_2^- + 2\Gamma_{15}^- + \Gamma_{25}^-)^{(s)} \\ + & \ (\Gamma_{12}^- + \Gamma_{15}^- + \Gamma_{25}^-) \end{aligned} \tag{11.16}$$

Table 11.4: Decomposition of angular momentum in terms of irreducible representation for the cubic group O_h.

ℓ	Γ_1^+	Γ_2^+	Γ_{12}^+	Γ_{15}^+	Γ_{25}^+	Γ_1^-	Γ_2^-	Γ_{12}^-	Γ_{15}^-	Γ_{25}^-
0	1									
1									1	
2			1		1					
3							1		1	1
4	1		1	1	1					
5								1	2	1
6	1	1	1	1	2					
7							1	1	2	2
8	1		2	2	2					
9						1	1	1	3	2
10	1	1	2	2	3					
11							1	2	3	3
12	2	1	2	3	3					
13						1	1	2	4	3
14	1	1	3	3	4					
15						1	2	2	4	4

yielding 18 partners, 10 of which are symmetric, in agreement with the general result in Table 11.1. Of particular significance is the fact that none of the 10 symmetric irreducible representations have Γ_1^+ symmetry. Thus there are **no** non-vanishing tensor components for a third rank tensor (such as $\overset{\leftrightarrow(2)}{\alpha}$) in O_h symmetry, a result which could also be obtained by going from full rotational symmetry to O_h symmetry. The 10 symmetric partners are found from Table 11.1 and includes angular momentum states $L = 1$ (corresponding to Γ_{15}^-) and $L = 3$ (corresponding to $\Gamma_2^- + \Gamma_{15}^- + \Gamma_{25}^-$) (see Table 11.4). We will now use the symmetric partners of the third rank tensor to discuss the 4th rank tensors.

The next order term in Eq. 11.4 for the non-linear response to a strong optical beam (e.g., multiple photon generation) is the fourth rank tensor $\overset{\leftrightarrow(3)}{\alpha}$ defined by

$$\vec{P}^{(3)} = \overset{\leftrightarrow(3)}{\alpha} \cdot \vec{E}\vec{E}\vec{E}. \tag{11.17}$$

If we consider the product $\vec{E}\vec{E}\vec{E}$ to arise from the symmetric combination for a 3rd rank tensor (see Eq. 11.16), then

$$\Gamma^{(s)}_{\vec{E}\vec{E}\vec{E}} = \Gamma^-_2 + 2\Gamma^-_{15} + \Gamma^-_{25} \tag{11.18}$$

in cubic O_h symmetry, and

$$\begin{aligned}
\Gamma_{\vec{P}} \otimes \Gamma^{(s)}_{\vec{E}\vec{E}\vec{E}} &= \Gamma^-_{15} \otimes \{\Gamma^-_2 + 2\Gamma^-_{15} + \Gamma^-_{25}\} \\
&= 2\Gamma^+_1 + \Gamma^+_2 + 3\Gamma^+_{12} + 3\Gamma^+_{15} + 4\Gamma^+_{25}.
\end{aligned} \tag{11.19}$$

Referring to Table 11.1 we see that the symmetric partners for p^4 correspond to $L = 0$ (giving Γ^+_1), $L = 2$ (giving $\Gamma^+_{12} + \Gamma^+_{25}$) and $L = 4$ (giving $\Gamma^+_1 + \Gamma^+_{12} + \Gamma^+_{15} + \Gamma^+_{25}$) yielding the 15 symmetric partners

$$(2\Gamma^+_1 + 2\Gamma^+_{12} + \Gamma^+_{15} + 2\Gamma^+_{25})^{(s)}.$$

Since Γ^+_1 is contained twice among the 15 symmetric partners in cubic O_h symmetry, the symmetric 4th rank tensor $\overset{\leftrightarrow}{\alpha}^{(3)}$ has 2 independent coefficients.

11.5.2   Tetrahedral Symmetry $- T_d$

The character table for T_d symmetry is given in Table 3.34 on p. 70 and the correspondence between irreducible representations in the O_h and T_d groups is given in Table 11.5. The group T_d has half the number of symmetry operations as the group O_h. In particular, the inversion operation is no longer a symmetry element. The major change in the symmetry of the tensor components of T_d crystals relative to crystals with O_h symmetry involves the 3rd rank tensors $\overset{\leftrightarrow}{\alpha}^{(2)}$. Explicitly, we see from Table 11.5 that since $\Gamma^-_2(O_h) \to \Gamma_1(T_d)$, Eq. 11.16 shows that there exists **one** nonvanishing tensor component in T_d symmetry for a 3rd rank tensor $\overset{\leftrightarrow}{\alpha}^{(2)}$. This means that zinc-blende structures such as (GaAs and InSb) can have non-vanishing non-linear optical terms in $\overset{\leftrightarrow}{\alpha}^{(2)}$ because in T_d symmetry, the symmetric partners of the direct product transform as:

$$(\Gamma_{\vec{P}} \otimes \Gamma^{(s)}_{\vec{E}\vec{E}})^{(s)} = \Gamma_1 + 2\Gamma_{25} + \Gamma_{15} \tag{11.20}$$

and the Γ_1 representation is contained once (see Table 11.2).

Table 11.5: The compatibility relations given the correspondence between groups O_h and T_d

O_h	T_d
Γ_1^+, Γ_2^-	Γ_1
Γ_1^-, Γ_2^+	Γ_2
$\Gamma_{12}^\pm$	Γ_{12}
$\Gamma_{25}^-, \Gamma_{15}^+$	Γ_{15}
$\Gamma_{15}^-, \Gamma_{25}^+$	Γ_{25}

—

11.5.3 Hexagonal Symmetry $- D_{6h}$

The character table for D_{6h} (hexagonal symmetry) is shown in Table 3.28 on p. 69. In this subsection we will use the notation found in this character table. Vector forces in hexagonal symmetry decompose into 2 irreducible representations

$$\Gamma_{\text{vector}} = A_{2u} + E_{1u}. \tag{11.21}$$

Thus the 2nd rank conductivity tensor requires consideration of

$$
\begin{aligned}
\Gamma_{\vec{P}} \otimes \Gamma_{\vec{E}} &= (A_{2u} + E_{1u}) \otimes (A_{2u} + E_{1u}) \\
&= 2A_{1g} + A_{2g} + 2E_{1g} + E_{2g} \\
&= (2A_{1g} + E_{1g} + E_{2g})^{(s)} + (A_{2g} + E_{1g})^{(a)}.
\end{aligned}
\tag{11.22}
$$

Equation 11.22 indicates that there are two independent components for a symmetric second rank tensor such as the conductivity tensor. Hence, one must measure both in-plane and out-of-plane conductivity components to determine the conductivity tensor.

The symmetric tensor components (6 partners) of Eq. 11.22 are

$$\Gamma_{\vec{E}\vec{E}}^{(s)} = 2A_{1g} + E_{1g} + E_{2g} \tag{11.23}$$

and the antisymmetric components (3 partners) are $(A_{2g} + E_{1g})$. Hence

for the symmetric 3rd rank tensor we can write

$$\begin{aligned}
\Gamma_{\vec{P}} \otimes \Gamma^{(s)}_{\vec{E}\vec{E}} = \ & (A_{2u} + E_{1u}) \otimes (2A_{1g} + E_{1g} + E_{2g}) \\
= \ & (A_{1u} + A_{2u} + B_{1u} + B_{2u} + 2E_{1u} + E_{2u})^{(s)} \qquad (11.24) \\
+ \ & (2A_{2u} + 4E_{1u} + E_{2u})
\end{aligned}$$

and there are thus no non-vanishing 3rd rank tensor components in hexagonal D_{6h} symmetry because of parity considerations.

For the 4th rank tensor we have

$$\begin{aligned}
\Gamma_{\vec{P}} \otimes \Gamma^{(s)}_{\vec{E}\vec{E}\vec{E}} = \ & (A_{2u} + E_{1u}) \otimes (A_{1u} + A_{2u} + B_{1u} + B_{2u} + 2E_{1u} + 2E_{2u}) \\
= \ & (3A_{1g} + B_{1g} + B_{2g} + 2E_{1g} + 3E_{2g})^{(s)} \\
+ \ & (3A_{2g} + 2B_{1g} + 2B_{2g} + 4E_{1g} + 3E_{2g})
\end{aligned}$$

$$(11.25)$$

and there are three independent tensor components. This result could also be obtained by going from full rotational symmetry ($L = 0$, $L = 2$, and $L = 4$), yielding the identical result

$$[A_{1g} + (A_{1g} + E_{1g} + E_{2g}) + (A_{1g} + B_{1g} + B_{2g} + E_{1g} + 2E_{2g})].$$

The results for D_{6h} and $D_{\infty h}$ (see Table 11.2) show great similarity between the behavior of all the tensors that are enumerated in this table.

11.5.4   Hexagonal Symmetry − D_{3h}

The character table for D_{3h} is shown in Table 3.31 on p. 69, and again, it is clear that D_{3h} has no inversion symmetry. Comparison of the character tables for D_{6h} and D_{3h} shows that $\Gamma^{\pm}_i(D_{6h}) \rightarrow \Gamma_i(D_{3h})$. Thus the only difference between the tensor properties in D_{6h} and D_{3d} symmetries involves odd rank tensors. Referring to Eq. 11.24 we see that for D_{3h} there are two non-vanishing 3rd rank tensor components and once again piezoelectric phenomena are symmetry allowed.

11.6 Elastic Modulus Tensor

The elastic modulus tensor represents a special case of a fourth rank tensor (see Eq. 11.8). The elastic energy is written as

$$W = \frac{1}{2}\mathcal{C}_{ijkl}e_{ij}e_{kl} \tag{11.26}$$

where W transforms as a scalar, the e_{ij} strain tensors transform as second rank symmetric tensors, and the $\mathcal{C}_{ijkl}$ matrices transform as a fourth rank tensor formed by the direct product of two symmetric second rank tensors. The symmetry of $\mathcal{C}_{ijkl}$ with regard to permutations was considered in §11.3. With regard to point group symmetry, we have the result following Eq. 11.11 that the maximum number of independent components of the $\mathcal{C}_{ijkl}$ tensor is the number of times the totally symmetric representation A_{1g} is contained in the direct product of the symmetric part of $\Gamma_{e_{ij}} \otimes \Gamma_{e_{kl}}$. In this section we provide a review of the conventions used to describe the $\mathcal{C}_{ijkl}$ tensor and then give results for a few crystal symmetries.

To make a connection between the elastic constants found in Nye's book and in conventional solid state physics books, we introduce a contracted notation for the stress tensor and the strain tensor:

$$
\begin{array}{llll}
\sigma_1 = & \sigma_{11} & \varepsilon_1 = & e_{11} \\
\sigma_2 = & \sigma_{22} & \varepsilon_2 = & e_{22} \\
\sigma_3 = & \sigma_{33} & \varepsilon_3 = & e_{33} \\
\sigma_4 = & (\sigma_{23}+\sigma_{32})/2 & \varepsilon_4 = & (e_{23}+e_{32}) \\
\sigma_5 = & (\sigma_{13}+\sigma_{31})/2 & \varepsilon_5 = & (e_{13}+e_{31}) \\
\sigma_6 = & (\sigma_{12}+\sigma_{21})/2 & \varepsilon_6 = & (e_{12}+e_{21})
\end{array}
\tag{11.27}
$$

Since both the stress and strain tensors are symmetric, then $\mathcal{C}_{ijkl}$ can have no more than 36 components. We further note from Eq. 11.26 that the $\mathcal{C}_{ijkl}$ are symmetric under the interchange of $ij \leftrightarrow kl$, thereby reducing the number of independent components to 21 for a crystal with no symmetry operations beyond translational symmetry of the lattice. Crystals with non-trivial symmetry operations such as rotations, reflections and inversions will have fewer than 21 independent coefficients. Using the notation of Eq. 11.27 for the stress and strain tensors, the

stress-strain relations can be written as

$$
\begin{bmatrix} \sigma_1 \\ \sigma_2 \\ \sigma_3 \\ \sigma_4 \\ \sigma_5 \\ \sigma_6 \end{bmatrix} = \begin{bmatrix} C_{11} & C_{12} & C_{13} & C_{14} & C_{15} & C_{16} \\ & C_{22} & C_{23} & C_{24} & C_{25} & C_{26} \\ & & C_{33} & C_{34} & C_{35} & C_{36} \\ & & & C_{44} & C_{45} & C_{46} \\ & & & & C_{55} & C_{56} \\ & & & & & C_{66} \end{bmatrix} \begin{bmatrix} \varepsilon_1 \\ \varepsilon_2 \\ \varepsilon_3 \\ \varepsilon_4 \\ \varepsilon_5 \\ \varepsilon_6 \end{bmatrix} \tag{11.28}
$$

where the contracted C_{ij} matrix is symmetric, with the 21 independent coefficients containing 15 off-diagonal components and 6 diagonal components. In the most compact form, we write

$$
\sigma_i = C_{ij}\varepsilon_j \qquad i,j = 1,\ldots 6 \tag{11.29}
$$

where the C_{ij} components are normally used in the description of the mechanical properties of solids. The introduction of additional symmetry operations reduces the number of independent components from the maximum of 21 for a monoclinic crystal group C_1 with no symmetry to a much smaller number (e.g., 2 for the full rotational group R_∞). We consider here the case of full rotational symmetry, icosahedral symmetry, cubic symmetry, full axial symmetry, and hexagonal symmetry.

Fiber reinforced composites represent an interesting application of these symmetry forms. If the fibers are oriented in three dimensional space in the six directions prescribed by icosahedral symmetry, then isotropy of the elastic modulus tensor will be obtained. In the corresponding two dimensional situation, if the fibers are oriented at 60° intervals, then isotropy is obtained in the plane. It is standard practice in the field of fiber composites to use fiber composite sheets stacked at 60° angular intervals to obtain "quasi–planar isotropy". Recent research on quasi–crystals has emphasized the connection of the icosahedral symmetry to describe the elastic properties of quasi–crystals.

11.6.1　Full Rotational Symmetry: 3D Isotropy

The highest overall symmetry for an elastic medium is the full rotation group which corresponds to "jellium". For the case of full rotational symmetry, a second rank tensor $\overset{\leftrightarrow}{T}$ transforms according to the

representation $\Gamma_{\underset{T}{\leftrightarrow}}$ where $\Gamma_{\underset{T}{\leftrightarrow}}$ can be written as a symmetric and an antisymmetric part

$$\Gamma_{\underset{T}{\leftrightarrow}} = \Gamma_{\underset{T}{\leftrightarrow}}^{(s)} + \Gamma_{\underset{T}{\leftrightarrow}}^{(a)}. \tag{11.30}$$

In Eq. 11.30 the symmetric components for full rotational symmetry transform as the irreducible representations

$$\Gamma_{\underset{T}{\leftrightarrow}}^{(s)} = \Gamma_{l=0} + \Gamma_{l=2} \tag{11.31}$$

and the antisymmetric components transform as

$$\Gamma_{\underset{T}{\leftrightarrow}}^{(a)} = \Gamma_{l=1}, \tag{11.32}$$

in which the irreducible representations of the full rotation group are denoted by their total angular momentum values l. Since the stress tensor $\vec{\nabla} \cdot \vec{F} \equiv \overset{\leftrightarrow}{X}$ and the strain tensor $\overset{\leftrightarrow}{e}$ are symmetric second rank tensors, both X_α and e_{ij} transform according to $(\Gamma_{l=0} + \Gamma_{l=2})$ in full rotational symmetry, where X_α denotes a force in the x direction applied to a plane whose normal is in the α direction.

The fourth rank symmetric $\mathcal{C}_{ijkl}$ tensor of Eq. 11.26 transforms according to the symmetric part of the direct product of two second rank symmetric tensors $\Gamma_{\underset{e}{\leftrightarrow}}^{(s)} \otimes \Gamma_{\underset{e}{\leftrightarrow}}^{(s)}$ yielding

$$(\Gamma_{l=0}+\Gamma_{l=2})\otimes(\Gamma_{l=0}+\Gamma_{l=2}) = (2\Gamma_{l=0}+2\Gamma_{l=2}+\Gamma_{l=4})^{(s)}+(\Gamma_{l=1}+\Gamma_{l=2}+\Gamma_{l=3})^{(a)}, \tag{11.33}$$

in which the direct product has been broken up into the 21 partners that transform as symmetric irreducible representations (s) and the 15 partners for the antisymmetric irreducible representations (a). In general e_{ij} is specified by 6 constants and the $\mathcal{C}_{ijkl}$ tensor by 21 constants because $\mathcal{C}_{ijkl}$ is symmetrical under the interchange of $ij \leftrightarrow kl$. Since all the symmetry groups of interest are subgroups of the full rotation group, the procedure of going from higher to lower symmetry can be used to determine the irreducible representations for less symmetric groups that correspond to the stress and strain tensors and to the elastic tensor $\mathcal{C}_{ijkl}$.

In the case of full rotational symmetry, Eq. 11.33 shows that the totally symmetric representation $(\Gamma_{l=0})$ is contained only twice in the

direct product of the irreducible representations for two second rank symmetric tensors, indicating that only two independent non–vanishing constants are needed to describe the 21 constants of the $\mathcal{C}_{ijkl}$ tensor in full rotational symmetry, a result that is well known in elasticity theory for isotropic media and discussed above (see §11.4). As stated in §11.2 and in §11.4, the number of times the totally symmetric representation (e.g., $\Gamma_{l=0}$ for the full rotational group) is contained in the irreducible representations of a general matrix of arbitrary rank determines the number of independent non–vanishing constants needed to specify that matrix.

We denote the two independent non-vanishing constants needed to specify the $\mathcal{C}_{ijkl}$ tensor by C_0 for $\Gamma_{l=0}$ and by C_2 for $\Gamma_{l=2}$ symmetry. We then use these two constants to relate symmetrized stresses and strains labeled by the irreducible representations $\Gamma_{l=0}$ and $\Gamma_{l=2}$ in the full rotation group. The symmetrized stress–strain equations are first written in full rotational symmetry, using basis functions for the partners of the pertinent irreducible representations (one for $l = 0$ and five for the $l = 2$ partners):

$$
\begin{aligned}
(X_x + Y_y + Z_z) &= C_0(e_{xx} + e_{yy} + e_{zz}) && \text{for} && l = 0, m = 0 \\
(X_x - Y_y + iY_x + iX_y) &= C_2(e_{xx} - e_{yy} + ie_{xy} + ie_{yx}) && \text{for} && l = 2, m = 2 \\
(Z_x + X_z + iY_z + iZ_y) &= C_2(e_{zx} + e_{xz} + ie_{yz} + ie_{zy}) && \text{for} && l = 2, m = 1 \\
(Z_z - \tfrac{1}{2}(X_x + Y_y)) &= C_2(e_{zz} - \tfrac{1}{2}(e_{xx} + e_{yy})) && \text{for} && l = 2, m = 0 \\
(Z_x + X_z - iY_z - iZ_y) &= C_2(e_{zx} + e_{xz} - ie_{yz} - ie_{zy}) && \text{for} && l = 2, m = -1 \\
(X_x - Y_y - iY_x - iX_y) &= C_2(e_{xx} - e_{yy} - ie_{xy} - ie_{yx}) && \text{for} && l = 2, m = -2
\end{aligned}
$$

$$(11.34)$$

From the first, second, fourth and sixth relations in Eqs. 11.34 we solve for X_x in terms of the strains, yielding

$$
X_x = \left(\frac{C_0}{3} + \frac{2C_2}{3}\right)e_{xx} + \left(\frac{C_0}{3} - \frac{C_2}{3}\right)\left(e_{yy} + e_{zz}\right). \qquad (11.35)
$$

Likewise five additional relations are then written down for the other 5 stress components in Eqs. 11.34.

$$
Y_y = \left(\frac{C_0}{3} + \frac{2C_2}{3}\right)e_{yy} + \left(\frac{C_0}{3} - \frac{C_2}{3}\right)\left(e_{zz} + e_{xx}\right), \qquad (11.36)
$$

$$
Z_z = \left(\frac{C_0}{3} + \frac{2C_2}{3}\right)e_{zz} + \left(\frac{C_0}{3} - \frac{C_2}{3}\right)\left(e_{xx} + e_{yy}\right), \qquad (11.37)
$$

$$Z_y + Y_z = C_2\left(e_{zy} + e_{yz}\right), \tag{11.38}$$

$$Y_x + X_y = C_2\left(e_{yx} + e_{xy}\right), \tag{11.39}$$

$$Z_x + X_z = C_2\left(e_{zx} + e_{xz}\right). \tag{11.40}$$

In the notation that is commonly used in elastic theory, we write the stress–strain relations as

$$\sigma_i = \sum_{j=1,6} C_{ij}\varepsilon_j, \tag{11.41}$$

where the 6 components of the symmetric stress and strain tensors are written in accordance with Eq. 11.27 as

$$
\begin{array}{lcl}
\sigma_1 = X_x & & \varepsilon_1 = e_{xx} \\
\sigma_2 = Y_y & & \varepsilon_2 = e_{yy} \\
\sigma_3 = Z_z & \text{and} & \varepsilon_3 = e_{zz} \\
\sigma_4 = \frac{1}{2}(Y_z + Z_y) & & \varepsilon_4 = (e_{yz} + e_{zy}) \\
\sigma_5 = \frac{1}{2}(Z_x + X_z) & & \varepsilon_5 = (e_{zx} + e_{xz}) \\
\sigma_6 = \frac{1}{2}(X_y + Y_x) & & \varepsilon_6 = (e_{xy} + e_{yx})
\end{array} \tag{11.42}
$$

and C_{ij} is the 6×6 elastic modulus matrix. In this notation the 21 partners that transform as $(2\Gamma_{l=0} + 2\Gamma_{l=2} + \Gamma_{l=4})$ in Eq. 11.33 correspond to the symmetric coefficients of C_{ij}. From the six relations for the six stress components (given explicitly by Eqs. 11.35 through 11.40), the relations between the C_0 and C_2 and the C_{ij} coefficients follow:

$$
\begin{aligned}
C_{11} &= \tfrac{1}{3}(C_0 + 2C_2) = C_{22} = C_{33} \\
C_{12} &= \tfrac{1}{3}(C_0 - C_2) = C_{13} = C_{23} \\
C_{44} &= \tfrac{1}{2}C_2 = C_{55} = C_{66} \\
C_{ij} &= C_{ji}
\end{aligned} \tag{11.43}
$$

from which we construct the C_{ij} matrix for a 3D isotropic medium and

involves only two independent constants C_{11} and C_{12}

$$C_{ij} = \begin{bmatrix} C_{11} & C_{12} & C_{12} & 0 & 0 & 0 \\ & C_{11} & C_{12} & 0 & 0 & 0 \\ & & C_{11} & 0 & 0 & 0 \\ & & & \frac{1}{2}(C_{11} - C_{12}) & 0 & 0 \\ & & & & \frac{1}{2}(C_{11} - C_{12}) & 0 \\ & & & & & \frac{1}{2}(C_{11} - C_{12}) \end{bmatrix} .$$

$$(11.44)$$

11.6.2 Icosahedral Symmetry

Any subgroup of the full rotation group for which the 5–fold $\Gamma_{l=2}$ level degeneracy is not lifted will leave the form of the C_{ij} matrix invariant. The icosahedral group with inversion symmetry I_h, which is a subgroup of the full rotation group, and the icosahedral group without inversion I, which is a subgroup of both the full rotation group and the group I_h, are two examples of groups which preserve the 5–fold degenerate level of the full rotation group and hence retain the form of the C_{ij} matrix given by Eq. 11.44. This result follows from at least two related arguments. The first argument relates to the compatibility relations between the full rotation group and the I_h group for which the basis functions follow the compatibility relations

$$\begin{aligned} \Gamma_{l=0} &\longrightarrow (A_g)_{I_h} \\ \Gamma_{l=2} &\longrightarrow (H_g)_{I_h}. \end{aligned}$$

$$(11.45)$$

We thus show that for the icosahedral group the irreducible representations for a symmetric second rank tensor are

$$\Gamma_{\overleftrightarrow{e}}^{(s)} = (A_g)_{I_h} + (H_g)_{I_h}. \qquad (11.46)$$

From Eq. 11.46 we see that with respect to second rank tensors no lifting of degeneracy occurs in going from full rotational symmetry to I_h symmetry from which it follows that the number of non–vanishing independent constants in the C_{ij} matrix remains at 2 for I_h (and I) symmetry.

The same conclusion follows from the fact that the basis functions for $\Gamma_{l=0}$ and $\Gamma_{l=2}$ for the full rotation group can also be used as basis

functions for the A_g and H_g irreducible representations of I_h. Therefore the same stress–strain relations are obtained in I_h symmetry as are given in Eq. 11.34. It therefore follows that the form of the C_{ij} matrix will also be the same for group I_h and full rotational symmetry, thereby completing the proof.

Clearly, the direct product $\Gamma^{(s)}_{\underset{e}{\leftrightarrow}} \otimes \Gamma^{(s)}_{\underset{e}{\leftrightarrow}}$ given by Eq. 11.33 is not invariant as the symmetry is reduced from full rotational symmetry to I_h symmetry since the 9-fold representation $\Gamma_{l=4}$ in Eq. 11.33 splits into the irreducible representations $(G_g + H_g)$ in going to the lower symmetry group I_h. But this is not of importance to the linear stress-strain equations which are invariant to this lowering of symmetry. It might be worth mentioning here that when non-linear effects are taken into account and perturbations from Eq. 11.26 are needed to specify the non-linear stress–strain relations, different mechanical behavior would be expected to occur in I_h symmetry in comparison to the full rotation group. In such a case, the compatibility relations between the irreducible representations of the full rotation group and the I_h group can be used to relate the terms in the non-linear elastic matrix for the two symmetries. This generalization is similar in concept to that discussed for the case of non-linear optics in §11.5.

11.6.3 Cubic Symmetry

It should be noted that all symmetry groups forming Bravais lattices in solid state physics have too few symmetry operations to preserve the 5-fold degeneracy of the $l = 2$ level of the full rotation group. For example, the Bravais lattice with the highest symmetry is the cubic group O_h. The $l = 2$ irreducible representation in full rotational symmetry corresponds to a reducible representation of group O_h which splits into a 3-fold and a 2-fold level (the T_{2g} and E_g levels), so that in this case we will see below, 3 elastic constants are needed to specify the 6×6 matrix for C_{ij}.

Since e_{ij} (where $i, j = x, y, z$) is a symmetric second rank tensor, the irreducible representations for e_{ij}, in cubic symmetry are found as

$$\Gamma^{(s)}_{\underset{e}{\leftrightarrow}} = \Gamma_1^+ + \Gamma_{12}^+ + \Gamma_{25}^+. \tag{11.47}$$

From the direct product we obtain

$$\Gamma^{(s)}_{\underset{e}{\leftrightarrow}}\otimes\Gamma^{(s)}_{\underset{e}{\leftrightarrow}} = (\Gamma_1^+ + \Gamma_{12}^+ + \Gamma_{25}^+)\otimes(\Gamma_1^+ + \Gamma_{12}^+ + \Gamma_{25}^+) = 3\Gamma_1^+ + \Gamma_2^+ + 4\Gamma_{12}^+ + 3\Gamma_{15}^+ + 5\Gamma_{25}^+,$$
(11.48)

which has 21 symmetric partners $(3\Gamma_1^+ + 3\Gamma_{12}^+ + \Gamma_{15}^+ + 3\Gamma_{25}^+)$ and 15 antisymmetric partners $(\Gamma_2^+ + \Gamma_{12}^+ + 2\Gamma_{15}^+ + 2\Gamma_{25}^+)$ and three independent C_{ij} coefficients. These results could also be obtained by going from higher (full rotational R_∞) symmetry to lower (O_h) symmetry using the cubic field splittings of the angular momenta shown in Table 11.4.

Forming basis functions for the irreducible representations of the stress and strain tensors in cubic O_h symmetry, we can then write the symmetrized elastic constant equations as

$$
\begin{aligned}
(X_x + Y_y + Z_z) &= C_{\Gamma_1^+}(e_{xx} + e_{yy} + e_{zz}) && \text{for} && \Gamma_1^+ \\
(X_x + \omega Y_y + \omega^2 Z_z) &= C_{\Gamma_{12}^+}(e_{xx} + \omega e_{yy} + \omega^2 e_{zz}) && \text{for} && \Gamma_{12}^+ \\
(X_x + \omega^2 Y_y + \omega Z_z) &= C_{\Gamma_{12}^+}(e_{xx} + \omega^2 e_{yy} + \omega e_{zz}) && \text{for} && \Gamma_{12}^{+*} \\
(Y_z + Z_y) &= C_{\Gamma_{25}^+}(e_{yz}) && \text{for} && \Gamma_{25x}^+ \\
(Z_x + X_z) &= C_{\Gamma_{25}^+}(e_{xz}) && \text{for} && \Gamma_{25y}^+ \\
(X_y + Y_x) &= C_{\Gamma_{25}^+}(e_{xy}) && \text{for} && \Gamma_{25z}^+
\end{aligned}
$$
(11.49)

From the first three relations in Eq. 11.49 we obtain

$$X_x = \left(\frac{C_{\Gamma_1}^+ + 2C_{\Gamma_{12}}^+}{3}\right)e_{xx} + \left(\frac{C_{\Gamma_1}^+ - C_{\Gamma_{12}}^+}{3}\right)\left(e_{yy} + e_{zz}\right) \qquad (11.50)$$

$$Y_y = \left(\frac{C_{\Gamma_1}^+ + 2C_{\Gamma_{12}}^+}{3}\right)e_{yy} + \left(\frac{C_{\Gamma_1}^+ - C_{\Gamma_{12}}^+}{3}\right)\left(e_{zz} + e_{xx}\right) \qquad (11.51)$$

$$Z_z = \left(\frac{C_{\Gamma_1}^+ + 2C_{\Gamma_{12}}^+}{3}\right)e_{zz} + \left(\frac{C_{\Gamma_1}^+ - C_{\Gamma_{12}}^+}{3}\right)\left(e_{xx} + e_{yy}\right) \qquad (11.52)$$

From Eqs. 11.49–11.52, we obtain the connections between the 3 symmetry-based elastic constants $C_{\Gamma_1}^+$, $C_{\Gamma_{12}}^+$ and $C_{\Gamma_{25}}^+$ and the C_{11}, C_{12} and C_{44} in Nye's book (and other solid state physics books)

$$
\begin{aligned}
C_{11} &= (C_{\Gamma_1}^+ + 2C_{\Gamma_{12}}^+)/3 \\[4pt]
C_{12} &= (C_{\Gamma_1} - C_{\Gamma_{12}}^+)/3 \\[4pt]
C_{44} &= C_{\Gamma_{25}}^+/2
\end{aligned}
\qquad (11.53)
$$

yielding an elastic tensor for cubic symmetry in the form

$$
C_{ij} = \begin{bmatrix}
C_{11} & C_{12} & C_{12} & 0 & 0 & 0 \\
 & C_{11} & C_{12} & 0 & 0 & 0 \\
 & & C_{11} & 0 & 0 & 0 \\
 & & & C_{44} & 0 & 0 \\
 & & & & C_{44} & 0 \\
 & & & & & C_{44}
\end{bmatrix}
\tag{11.54}
$$

11.6.4 Full Axial Symmetry

One simple method for finding the irreducible representations for full axial symmetry is to make use of the compatibility relations between the full rotation group and the group $D_{\infty h}$ (see character Table 3.36 on p. 71):

$$
\begin{aligned}
\Gamma_{l=0} &\longrightarrow A_{1g} \\
\Gamma_{l=1} &\longrightarrow A_{2u} + E_{1u} \\
\Gamma_{l=2} &\longrightarrow A_{1g} + E_{1g} + E_{2g} \\
\Gamma_{l=3} &\longrightarrow A_{2u} + E_{1u} + E_{2u} + E_{3u} \\
\Gamma_{l=4} &\longrightarrow A_{1g} + E_{1g} + E_{2g} + E_{3g} + E_{4g}.
\end{aligned}
\tag{11.55}
$$

Thus the symmetric 2nd rank tensor e_{ij} transforms according to the sum $\Gamma_{l=0} + \Gamma_{l=2}$

$$
\Gamma^{(s)}_{\overset{\leftrightarrow}{e}} = A_{1g} + (A_{1g} + E_{1g} + E_{2g}) = 2A_{1g} + E_{1g} + E_{2g}.
\tag{11.56}
$$

From the symmetric terms in Eq. 11.33 and Eq. 11.55, we find that the $\mathcal{C}_{ijkl}$ tensor transforms according to $2\Gamma_{l=0} + 2\Gamma_{l=2} + \Gamma_{l=4}$:

$$
\begin{aligned}
\Gamma_{\mathcal{C}_{ijkl}} &= (2A_{1g}) + (2A_{1g} + 2E_{1g} + 2E_{2g}) + (A_{1g} + E_{1g} + E_{2g} + E_{3g} + E_{4g}) \\
&= 5A_{1g} + 3E_{1g} + 3E_{2g} + E_{3g} + E_{4g}.
\end{aligned}
\tag{11.57}
$$

The same result as in Eq. 11.57 can be obtained by taking the direct product of $(A_{1g} + E_{1g} + E_{2g}) \otimes (A_{1g} + E_{1g} + E_{2g})$ and retaining only the symmetric terms. From Eq. 11.57, we see that there are only 5 independent elastic constants.

The splitting of the five–dimensional representation $l = 2$ into three irreducible representations (see Eq. 11.55) in $D_{\infty h}$ symmetry increases

the number of independent coefficients by two and an additional independent coefficient is needed to describe the off–diagonal coupling between the two diagonal blocks with A_{1g} symmetry.

To find the form of the elasticity matrix C_{ij} we note that the basis functions going with the irreducible representations of the second rank symmetric stress and strain tensors are:

$$
\begin{array}{cccc}
(X_x + Y_y + Z_z) & (e_{xx} + e_{yy} + e_{zz}) & l = 0, m = 0 & A_{1g} \\[4pt]
(X_x - Y_y + iY_x + iX_y) & (e_{xx} - e_{yy} + ie_{xy} + ie_{yx}) & l = 2, m = 2 & E_{2g} \\[4pt]
(X_x - Y_y - iY_x - iX_y) & (e_{xx} - e_{yy} - ie_{xy} - ie_{yx}) & l = 2, m = -2 & E_{2g} \\[4pt]
(Z_x + X_z + iY_z + iZ_y) & (e_{zx} + e_{xz} + ie_{yz} + ie_{zy}) & l = 2, m = 1 & E_{1g} \\[4pt]
(Z_x + X_z - iY_z - iZ_y) & (e_{zx} + e_{xz} - ie_{yz} - ie_{zy}) & l = 2, m = -1 & E_{1g} \\[4pt]
(Z_z - \tfrac{1}{2}(X_x + Y_y)) & (e_{zz} - \tfrac{1}{2}(e_{xx} + e_{yy})) & l = 2, m = 0 & A_{1g}.
\end{array}
$$

$$(11.58)$$

From the basis functions in Eq. 11.58 we write the stress-strain relations coupling basis functions of similar symmetry:

$$
X_x + Y_y + Z_z = C_{A_{1g},1}(e_{xx} + e_{yy} + e_{zz}) + C_{A_{1g},3}\left[e_{zz} - \tfrac{1}{2}(e_{xx} + e_{yy})\right]
$$

$$
Z_z - \tfrac{1}{2}(X_x + Y_y) = C_{A_{1g},2}\left[e_{zz} - \tfrac{1}{2}(e_{xx} + e_{yy})\right] + C_{A_{1g},4}\left[e_{xx} + e_{yy} + e_{zz}\right]
$$

$$
X_x - Y_y = C_{E_{2g}}(e_{xx} - e_{yy})
$$

$$
X_y + Y_x = C_{E_{2g}}(e_{xy} + e_{yx})
$$

$$
Y_z + Z_y = C_{E_{1g}}(e_{yz} + e_{zy})
$$

$$
Z_x + X_z = C_{E_{1g}}(e_{zx} + e_{xz}).
$$

$$(11.59)$$

We then solve Eqs. 11.59 for X_x, Y_y and Z_z and require $C_{ij} = C_{ji}$. In the case of $D_{\infty h}$, the requirement that $C_{31} = C_{13} = C_{32} = C_{23}$ yields the additional constraint $C_{A_{1g},3} = 2C_{A_{1g},4}$ which is needed to obtain the 5 independent symmetry coefficients required by Eq. 11.57: $C_{A_{1g},1}$, $C_{A_{1g},2}$, $C_{A_{1g},3}$, $C_{E_{1g}}$ and $C_{E_{2g}}$. The relations between these symmetry

coefficients and the C_{ij} coefficients are:

$$C_{11}=C_{22} = \frac{1}{2}[\frac{2}{3}C_{A_{1g},1} + \frac{1}{3}C_{A_{1g},2} - \frac{2}{3}C_{A_{1g},3} + C_{E_{2g}}]$$

$$C_{12}=C_{21} = \frac{1}{2}[\frac{2}{3}C_{A_{1g},1} + \frac{1}{3}C_{A_{1g},2} - \frac{2}{3}C_{A_{1g},3} - C_{E_{2g}}]$$

$$C_{13}=C_{23} = \frac{1}{3}[C_{A_{1g},1} - C_{A_{1g},2} + \frac{1}{2}C_{A_{1g},3}]$$

$$C_{33}=\frac{1}{3}[C_{A_{1g},1} + 2C_{A_{1g},2} + 2C_{A_{1g},3}] \qquad (11.60)$$

$$C_{44}=C_{55} = \frac{1}{2}C_{E_{1g}}$$

$$C_{66}=\frac{1}{2}C_{E_{2g}} = \frac{1}{2}(C_{22} - C_{21}) = \frac{1}{2}(C_{11} - C_{12}).$$

Combining the non-vanishing C_{ij} coefficients then yields the matrix for full axial $D_{\infty h}$ symmetry:

$$C_{ij} = \begin{bmatrix} C_{11} & C_{12} & C_{13} & 0 & 0 & 0 \\ & C_{11} & C_{13} & 0 & 0 & 0 \\ & & C_{33} & 0 & 0 & 0 \\ & & & C_{44} & 0 & 0 \\ & & & & C_{44} & 0 \\ & & & & & \frac{1}{2}(C_{11} - C_{12}) \end{bmatrix}. \qquad (11.61)$$

We see that the C_{ij} matrix in this case has the same form as for the hexagonal D_{6h} symmetry group described in the next subsection.

11.6.5 Hexagonal Symmetry

Since e_{ij} is a symmetric second rank tensor, the irreducible representations for e_{ij}, in hexagonal D_{6h} symmetry are found to be:

$$\Gamma_{\overleftrightarrow{e}} = (A_{2u} + E_{1u}) \otimes (A_{2u} + E_{1u}) = 2A_{1g} + A_{2g} + 2E_{1g} + E_{2g} \quad (11.62)$$

The antisymmetric terms are A_{2g} and E_{1g}, so that the symmetric combination is

$$\Gamma_{\overleftrightarrow{e}}^{(s)} = 2A_{1g} + E_{1g} + E_{2g} \qquad (11.63)$$

Using Eq. 11.33 and the irreducible representations contained in the angular momentum states $l = 0$, $l = 2$, and $l = 4$ in D_{6h} symmetry, we

get

$$\Gamma_{l=0} \rightarrow A_{1g}$$

$$\Gamma_{l=1} \rightarrow A_{2u} + E_{1u}$$

$$\Gamma_{l=2} \rightarrow A_{1g} + E_{1g} + E_{2g} \tag{11.64}$$

$$\Gamma_{l=3} \rightarrow A_{2u} + B_{1u} + B_{2u} + E_{1u} + E_{2u}$$

$$\Gamma_{l=4} \rightarrow A_{1g} + B_{1g} + B_{2g} + E_{1g} + 2E_{2g}$$

which gives the symmetric irreducible representations for a symmetric 4th rank tensor

$$\Gamma_{C_{(ij)(kl)}} = 2A_{1g} + 2(A_{1g} + E_{1g} + E_{2g}) + (A_{1g} + B_{1g} + B_{2g} + E_{1g} + 2E_{2g})$$

$$= 5A_{1g} + B_{1g} + B_{2g} + 3E_{1g} + 4E_{2g}$$

$$\tag{11.65}$$

yielding 5 independent C_{ij} coefficients. Since the basis functions for all the quadratic forms for $D_{\infty h}$ and D_{6h} symmetry are the same, Eq. 11.58 also provides the basis functions for the stress and strain tensor components in D_{6h} symmetry. Likewise, Eq. 11.59 also applies for the stress and strain relations in D_{6h} symmetry, giving rise to Eq. 11.60 for the relation between the C_{ij} coefficients and the 5 independent symmetry coefficients $C_{A_{1g},1}$, $C_{A_{1g},2}$, $C_{A_{1g},3}$, $C_{E_{1g}}$ and $C_{E_{2g}}$. Thus the form of the elastic tensor in D_{6h} symmetry is given by Eq. 11.61. We note the correspondence here between D_{6h} and $D_{\infty h}$ with regard to the elastic properties of solids, although D_{6h} is not a subgroup of $D_{\infty h}$.

It must be emphasized that although the form of $\mathcal{C}_{ijkl}$ is the same for both $D_{\infty h}$ and D_{6h} symmetries, tensors of rank higher than 2 (such as the non-linear elastic coefficients) will in general be expected to be different in $D_{\infty h}$ and D_{6h} symmetries.

If we now consider the elastic tensor for the group D_{4h}, we immediately see that there is only one 2-dimensional irreducible representation in group D_{4h} so that the irreducible representations contained in the second rank tensor $\Gamma_{\overleftrightarrow{e}}$ are not the same as for $D_{\infty h}$. Thus the C_{ij} tensor is expected to have more independent coefficients for the case of D_{4h} symmetry.

11.6.6 Other Symmetry Groups

The form of the elastic tensor for other lower symmetry groups is also of importance in considering the mechanical properties of solids. We only give results in these cases, leaving the derivation of the results to the reader. The derivations can either be found by direct calculation as for the case of the cubic group considered above, or by going from higher to lower symmetry, as was illustrated for the case of the group I_h derived from the group with full rotational symmetry.

For D_{2h} group symmetry which is the case of symmetry with respect to three mutually orthogonal planes (called *orthotropy* in the engineering mechanics literature), there remain nine independent components of C_{ij}. The C_{ij} tensor in this case assumes the form

$$
C_{ij} = \begin{bmatrix}
C_{11} & C_{12} & C_{13} & 0 & 0 & 0 \\
 & C_{22} & C_{23} & 0 & 0 & 0 \\
 & & C_{33} & 0 & 0 & 0 \\
 & & & C_{44} & 0 & 0 \\
 & & & & C_{55} & 0 \\
 & & & & & C_{66}
\end{bmatrix} \tag{11.66}
$$

The lowest non-trivial symmetry group for consideration of the elastic tensor is group C_{2h} with a single symmetry plane. In this case C_{ij} has 13 independent components and assumes the form

$$
C_{ij} = \begin{bmatrix}
C_{11} & C_{12} & C_{13} & 0 & 0 & C_{16} \\
 & C_{22} & C_{23} & 0 & 0 & C_{26} \\
 & & C_{33} & 0 & 0 & C_{36} \\
 & & & C_{44} & C_{45} & 0 \\
 & & & & C_{55} & 0 \\
 & & & & & C_{66}
\end{bmatrix} \tag{11.67}
$$

11.7 Selected Problems

1. Suppose that stress is applied to fcc aluminium in the (100) direction, and suppose that the effect of the resulting strain is to lower the symmetry of aluminum from cubic O_h symmetry to tetragonal D_{4h} symmetry. The situation outlined here arises in

the fabrication of superlattices using the molecular beam epitaxy technique.

   (a) How many independent elastic constants are there in the stressed Al?

   (b) What is the new symmetrized form of the stress-strain relations (see Eq. 11.34 of the notes)?

   (c) What is the form of the C_{ijkl} tensor (see Eq. 11.44 of the notes)?

2. (a) Now assume that the material in Problem 1 is non-linear elastic material and the stress-strain relation is of the form

$$\sigma_{ij} = C^{(1)}_{ijkl}\varepsilon_{kl} + C^{(2)}_{ijklmn}\varepsilon_{kl}\varepsilon_{mn} + \ldots$$

Consider the symmetry of the non-linear tensor coefficient $C^{(2)}_{ijklmn}$ explicitly. How many independent constants are there in $C^{(2)}_{ijklmn}$ assuming that the point group symmetry is C_1 (i.e., no rotational symmetry elements other than the identity operation)?

   (b) How many independent constants are there when taking into account permutation symmetry only?

   (c) How many independent constants are there when taking into account both permutation and crystal (O_h) symmetry? (Note: To do this problem, you may have to make a new entry to Table 11.1.)

3. Suppose that we prepare a quantum well using as the constituents GaAs and $GaAs_{1-x}P_x$. The lattice mismatch introduces lattice strain and lowers the symmetry. Denote by $\hat{z}$ the direction normal to the layer. Find the number of independent coefficients in the polarizability tensor, including $\overleftrightarrow{\alpha}^{(1)}$, $\overleftrightarrow{\alpha}^{(2)}$, and $\overleftrightarrow{\alpha}^{(3)}$, for:

   (a) $\hat{z} \parallel (100)$

   (b) $\hat{z} \parallel (111)$

   (c) $\hat{z} \parallel (110)$

Using these results, how can infrared and Raman spectroscopy be used to distinguish between the crystalline orientation of the quantum well?

4. Consider the third rank tensor $d_{i(jk)}$

   (a) Show from Table 11.1 that there are exactly 18 independent coefficients.

   (b) How many independent coefficients are there for group T_d?

Chapter 12

Space Groups

In this chapter we introduce the concept of translational symmetry and the space groups used to classify the translational symmetry. In addition to the point group and translation operations, we consider the compound operations of glide planes and screw axes and the space groups associated with these compound symmetry operations. The properties of the two-dimensional space groups are discussed in detail.

12.1 Simple Space Group Operations

According to the one-electron Hamiltonian for the electronic energy band structure for solids, we write Schrödinger's equation as

$$\left[-\frac{\hbar^2}{2m} \nabla^2 + V(\vec{r}) \right] \psi(\vec{r}) = E\psi(\vec{r}) \tag{12.1}$$

where $V(\vec{r})$ is a periodic potential which exhibits translational symmetry in addition to point group symmetry operations. The symmetry group of the one-electron Hamiltonian (Eq. 12.1) and of the periodic potential is the **space group** of the crystal lattice, which consists of both **point group** symmetry operations and **translational** symmetry operations. All of these symmetry operations leave the Hamiltonian invariant and consequently the operators representing these symmetry operations will commute with the Hamiltonian, and provide quantum numbers for labeling the energy eigenvalues and eigenfunctions.

The point group and translation symmetry operations which carry
the crystal into itself form a group called the **space group**. A common
notation for space group operators is

$$\{R_\alpha|\tau\} \tag{12.2}$$

where R_α denotes point group operations such as rotations, reflections,
improper rotations, inversions and τ denotes translation operations.
Pure rotations and pure translations are special cases of space group
operations:

$$
\begin{aligned}
\{\varepsilon|0\} &= \text{identity} \\
\{\alpha|0\} &= \text{pure rotations or more generally point group operations} \\
\{\varepsilon|\tau\} &= \text{pure translations by vector } \vec{\tau}
\end{aligned}
$$

We can relate the operator $\{\alpha|\tau\}$ for the space group to a coordinate
transformation

$$\vec{r'} = \overleftrightarrow{\alpha} \cdot \vec{r} + \vec{\tau} \tag{12.3}$$

where $\overleftrightarrow{\alpha}$ denotes the transformation matrix for rotation and $\vec{\tau}$ denotes
a translational transformation. Multiplication of two space group op-
erators proceeds from this identification:

$$
\begin{aligned}
\{\beta|\tau'\}\{\alpha|\tau\} &= \overleftrightarrow{\beta} \cdot \left[\overleftrightarrow{\alpha} \cdot \vec{r} + \vec{\tau}\right] + \vec{\tau'} \\
&= \overleftrightarrow{\beta} \cdot \overleftrightarrow{\alpha} \cdot \vec{r} + \overleftrightarrow{\beta} \cdot \vec{\tau} + \vec{\tau'} \\
&= \{\beta\alpha|\beta\tau + \tau'\}
\end{aligned}
$$

to yield the result for the multiplication of two space group operators

$$\{\beta|\tau'\}\{\alpha|\tau\} = \{\beta\alpha|\beta\tau + \tau'\} \tag{12.4}$$

where $\{\alpha|\tau\}$ is the first space group operator and $\{\beta|\tau'\}$ is the second.
Likewise:

$$\{\alpha|\tau\}\{\beta|\tau'\} = \overleftrightarrow{\alpha} \cdot \overleftrightarrow{\beta} \cdot \vec{r} + \overleftrightarrow{\alpha} \cdot \vec{\tau'} + \vec{\tau} \tag{12.5}$$

so that commutation of these two space group operators requires that

$$\overleftrightarrow{\alpha} \cdot \overleftrightarrow{\beta} = \overleftrightarrow{\beta} \cdot \overleftrightarrow{\alpha} \qquad \text{and} \qquad \overleftrightarrow{\beta} \cdot \vec{\tau} + \vec{\tau'} = \overleftrightarrow{\alpha} \cdot \vec{\tau'} + \vec{\tau} \tag{12.6}$$

which is not generally valid. Thus we conclude that although simple translations commute with each other, general space group operations do not commute.

To get the inverse of $\{\alpha|\tau\}$ we make use of the multiplication relation above to obtain

$$\{\alpha|\tau\}^{-1} = \{\alpha^{-1}| - \alpha^{-1}\tau\} \tag{12.7}$$

since

$$\{\alpha|\tau\}\{\alpha|\tau\}^{-1} = \{\alpha\alpha^{-1}|\alpha(-\alpha^{-1}\tau) + \tau\} = \{\varepsilon|0\}. \tag{12.8}$$

Having specified the identity operation $\{\varepsilon|0\}$, the rules for multiplication and the rules for specifying the inverse operation, and noting that the associative law applies, we see that the elements $\{\alpha|\tau\}$ **form a space group**.

To write the space group operations in matrix form, a basis

$$\begin{pmatrix} 1 \\ \vec{r} \end{pmatrix}$$

is introduced where 1 is a number and $\vec{r}$ is a column vector consisting for example of

$$\begin{pmatrix} x \\ y \\ z \end{pmatrix}.$$

The matrix representation for the space group operator is then

$$\{\alpha|\tau\} = \begin{pmatrix} 1 & 0 \\ \vec{\tau} & \overleftrightarrow{\alpha} \end{pmatrix} \tag{12.9}$$

where 1 is a number, 0 denotes a row of three zeros, $\vec{\tau}$ is a column vector, and $\overleftrightarrow{\alpha}$ is a (3×3) rotation matrix. The transformation on the coordinate system then is written as

$$\begin{pmatrix} 1 & 0 \\ \vec{\tau} & \overleftrightarrow{\alpha} \end{pmatrix} \begin{pmatrix} 1 \\ \vec{r} \end{pmatrix} = \begin{pmatrix} 1 \\ \vec{\tau} + \overleftrightarrow{\alpha} \cdot \vec{r} \end{pmatrix} = \begin{pmatrix} 1 \\ \vec{r}' \end{pmatrix}. \tag{12.10}$$

To check that the matrix of Eq. 12.9 is a representation for the space group operator $\{\alpha|\tau\}$, let us examine the multiplication and inverse

transformations. Multiplication of two matrices yields

$$\begin{pmatrix} 1 & 0 \\ \vec{\tau}' & \overleftrightarrow{\beta} \end{pmatrix} \begin{pmatrix} 1 & 0 \\ \vec{\tau} & \overleftrightarrow{\alpha} \end{pmatrix} = \begin{pmatrix} 1 & 0 \\ \vec{\tau}' + \overleftrightarrow{\beta} \cdot \vec{\tau} & \overleftrightarrow{\beta} \cdot \overleftrightarrow{\alpha} \end{pmatrix} \qquad (12.11)$$

which checks out since

$$\{\beta|\tau'\}\{\alpha|\tau\} = \{\beta\alpha|\beta\tau + \tau'\}. \qquad (12.12)$$

The inverse operation also checks out since:

$$\begin{pmatrix} 1 & 0 \\ -\overleftrightarrow{\alpha}^{-1} \cdot \vec{\tau} & \overleftrightarrow{\alpha}^{-1} \end{pmatrix} \begin{pmatrix} 1 & 0 \\ \vec{\tau} & \overleftrightarrow{\alpha} \end{pmatrix} = \begin{pmatrix} 1 & 0 \\ 0 & 1 \end{pmatrix}. \qquad (12.13)$$

If all the operations of the space group are simply point group operations on to which we add translation operations, we have a simple or **symmorphic** space group. There are 73 symmorphic space groups in all (see Table 12.1). We will illustrate the idea of symmorphic space groups using an example based on the D_{2d} point group (see Table 3.29). Suppose that we have a molecule with atoms arranged in a D_{2d} point group configuration as shown in Fig. 12.2b. We see that the D_{2d} point group has classes E, C_2 about the z axis, $2S_4$ also about the z axis, $2\sigma_d$ passing through the z axis and each of the dumbbell axes, and $2C_2'$ in (110) directions in the median plane, as shown in Fig. 12.2a, which is the top view of the molecule shown in Fig. 12.2b.

We could put such X_4 molecules into a solid in many ways and still retain the point group symmetry of the molecule. To illustrate how different space groups can be produced with a single molecular configuration, we will put the X_4 molecule with D_{2d} symmetry into two different symmorphic space groups, as shown in Fig. 12.3. Another interesting illustration of symmetry-lowering by adding a molecular configuration on a lattice site can be found for the case of the icosahedral C_{60} molecule in a FCC crystal lattice.

We note that with either of the placements of the molecule in Fig. 12.3, **all the point group operations of the molecule are also operations of the space lattice**. Conversely, if the symmetry axes of the molecule do not coincide with the symmetry axes of the lattice in which they are embedded, the combined space group symmetry is lowered.

Table 12.1: The 73 symmorphic space groups. Here P, I, F, and B, respectively, denote primitive, body centered, face centered and base centered Bravais lattices (see Fig. 12.1).

Crystal system	Bravais lattice	Space group
Triclinic	P	$P1$, $P\bar{1}$
Monoclinic	P	$P2$, Pm, $P2/m$
	B or A	$B2$, Bm, $B2/m$ (1st setting)
Orthorhombic	P	$P222$, $Pmm2$, $Pmmm$
	C, A, or B	$C222$, $Cmm2$, $Amm2^*$, $Cmmm$
	I	$I222$, $Imm2$, $Immm$
	F	$F222$, $Fmm2$, $Fmmm$
Tetragonal	P	$P4$, $P\bar{4}$, $P4/m$, $P422$, $P4mm$,
		$P42m$, $P\bar{4}m2^*$, $P4/mmm$
	I	$I4$, $I\bar{4}$, $I4/m$, $I422$, $I4mm$
		$I\bar{4}2m$, $I\bar{4}m2^*$, $I4/mmm$
Cubic	P	$P23$, $Pm3$, $P432$, $P\bar{4}3m$, $Pm3m$
	I	$I23$, $Im3$, $I432$, $I\bar{4}3m$, $Im3m$
	F	$F23$, $Fm3$, $F432$, $F\bar{4}3m$, $Fm3m$
Trigonal	P	$P3$, $P\bar{3}$ $P312$, $P321^*$, $P3m1$,
		$P1$, $P\bar{1}$
(Rhombohedral)	R	$R3$, $R\bar{3}$ $R32$, $R3m$, $R\bar{3}m$,
Hexagonal	P	$P6$, $P\bar{6}$, $P6/m$, $P622$, $P6mm$,
		$P\bar{6}m2$, $P\bar{6}m2^*$, $P6/mmm$

* The asterisks mark the seven extra space groups that are generated when the orientation of the point group operations is taken into account with respect to the Bravais cell.
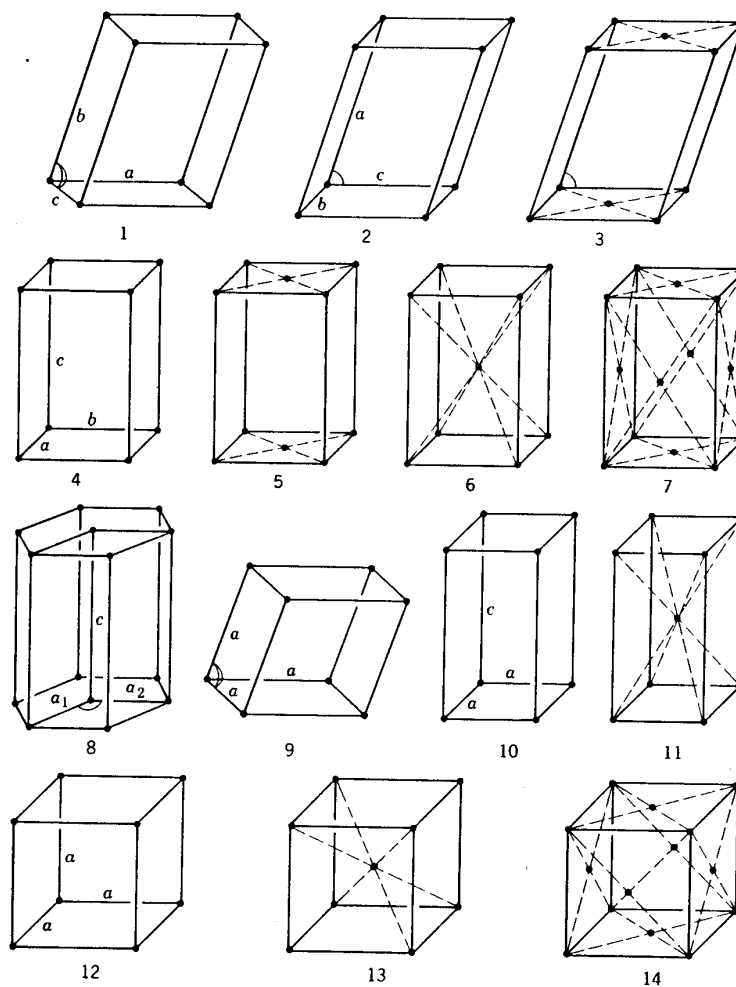
Figure 12.1: The fourteen Bravais space lattices illustrated by a unit cell of each: (1) triclinic, simple; (2) monoclinic, simple; (3) monoclinic, base centered; (4) orthorhombic, simple; (5) orthorhombic, base centered; (6) orthorhombic, body centered; (7) orthorhombic, face centered; (8) hexagonal; (9) rhombohedral; (10) tetragonal, simple; (11) tetragonal, body centered; (12) cubic, simple; (13) cubic, body centered; and (14) cubic, face centered.
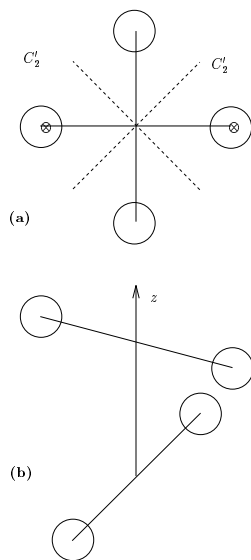
Figure 12.2: (a) Top view of a molecule X_4 with D_{2d} symmetry. The symmetry axes are indicated. (b) Schematic diagram of an X_4 molecule with point group D_{2d} ($\overline{4}2m$) symmetry.
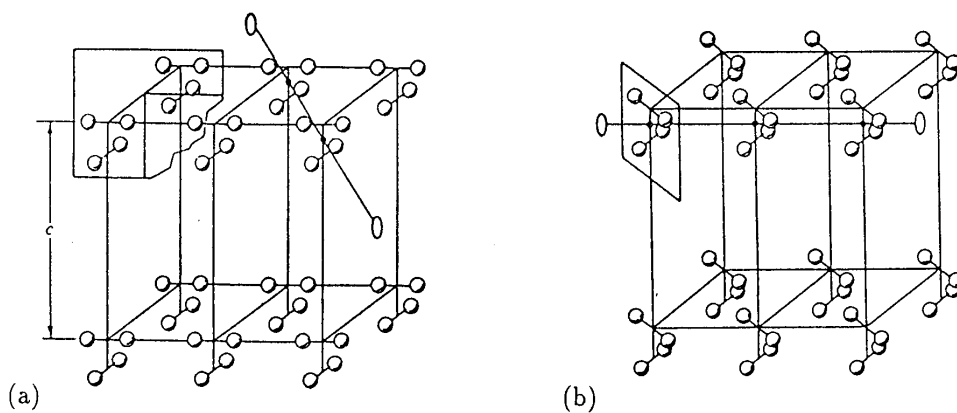
Figure 12.3: Tetragonal Bravais lattice with two possible orientations of the molecule with D_{2d} symmetry resulting in two different 3-dimensional space groups. The maximum symmetry that the tetragonal Bravais lattice can support is $D_{4h} = D_4 \otimes i$ ($4/mmm$).

In an elementary course in solid state physics we learn that there are **14 three-dimensional Bravais lattices**. Particular point group operations are appropriate to specific Bravais lattices, but the connection is homomorphic rather then isomorphic. For example, the point group operations T, T_d, T_h, O and O_h leave each of the simple cubic, face centered cubic and body centered cubic Bravais lattices invariant. Even though a given Bravais lattice is capable of supporting a high symmetry point group (e.g., the FCC structure), if we have a lower symmetry structure at each of the lattice sites (e.g., the structure in Fig. 12.2b), then the point symmetry is lowered to correspond to that structure—in this case the point group symmetry will be D_{2d}. On the other hand, the highest point group symmetry that is possible in a crystal lattice is that which is consistent with the Bravais lattice, so that the group O_h will be the appropriate point group for an FCC structure with spherical balls at each lattice site.

12.2   Space Groups and Point Groups

The space group G consists of all operations $\{R_\alpha|\tau\}$ which leave a given lattice invariant. The point group g is obtained from G by placing $\tau = 0$ for all R_α elements in G. If, with a suitable choice of origin in the direct lattice, we find that all the elements of the point group g are also elements of the space group G, then the space group G is called a **symmorphic** group.

All the elements of the space group G that are of the form $\{\varepsilon|\tau\}$ constitute the translation group T. Symmetry elements of the group T are defined by the translation vectors $\vec{R}_n = \Sigma n_i \vec{a}_i$, which leave the lattice invariant. The **translation** group is a **self-conjugate or invariant or normal subgroup of** G since

$$
\begin{aligned}
\{R_\alpha|\tau\}\{\varepsilon|t\}\{R_\alpha|\tau\}^{-1} &= \{R_\alpha|\tau\}\{\varepsilon|t\}\{R_\alpha^{-1}|-R_\alpha^{-1}\tau\} \\
&= \{R_\alpha|\tau\}\{R_\alpha^{-1}|-R_\alpha^{-1}\tau + t\} \\
&= \{\varepsilon|-R_\alpha R_\alpha^{-1}\tau + R_\alpha t + \tau\} \\
&= \{\varepsilon|R_\alpha t\}. \qquad\qquad (12.14)
\end{aligned}
$$

But $R_\alpha \vec{t}$ is just another translation vector in group T and therefore the operation $\{\varepsilon|R_\alpha t\}$ is a symmetry operation of the translation group.

Although the translation group T is an invariant subgroup of G, we cannot say that the space group G is a direct product of a translation group with a point group, since the elements $\{\varepsilon|\tau\}$ and $\{R_\alpha|0\}$ do not commute:

$$\begin{aligned}
\{\varepsilon|\tau\}\{R_\alpha|0\} &= \{R_\alpha|\tau\} \\
\{R_\alpha|0\}\{\varepsilon|\tau\} &= \{R_\alpha|R_\alpha\tau\}.
\end{aligned} \tag{12.15}$$

However, since the translation group is an invariant subgroup of G, it is of interest to study the cosets of the factor group which it defines. The right coset of the translation group considered as a subgroup of G is then

$$C_\alpha = [\{\varepsilon|\tau'\}\{R_\alpha|0\}] = [\{R_\alpha|\tau'\}] \tag{12.16}$$

where the bracket in Eq. 12.16 denotes all the terms in the coset that can be formed using all possible values of $\vec{\tau}'$. We note that C_α is also a left coset of the translation group because T is a self-conjugate (or normal) subgroup of G. We see that the **cosets C_α form a factor group** by considering the multiplication rule for the cosets:

$$C_\alpha C_\beta = [\{R_\alpha|\tau_1\}\{R_\beta|\tau_2\}] = [\{R_\alpha R_\beta|R_\alpha\tau_2 + \tau_1\}] = [\{R_\gamma|\tau_3\}] = C_\gamma \tag{12.17}$$

where $R_\alpha R_\beta = R_\gamma$ defines the group property in the point group and $\vec{\tau}_3 = R_\alpha\vec{\tau}_2 + \vec{\tau}_1$ is a translation of the lattice. Since $\vec{\tau}_1$ and $\vec{\tau}_2$ range over all possible translation vectors, the vector $\vec{\tau}_3$ also spans all possible translations.

These considerations show that the operations R_α apply to the translation vectors in accordance with the definition of the space group operations, and that the symmetry operations of the factor group G/T for symmorphic space groups are isomorphic with the point group g. Thus irreducible representations of the factor group G/T are also irreducible representations of g and are likewise irreducible representations of G. It can be shown that all irreducible representations of G can be compounded from irreducible representations of g and T, even though G is not a direct product group of g and T (see Koster's group theory article in the Seitz–Turnbull Solid State Physics series, vol. 5).
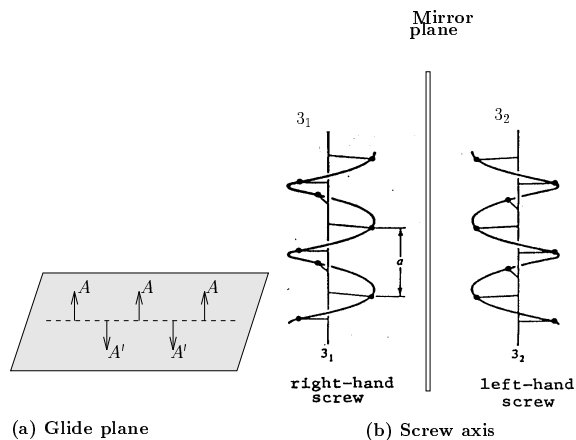
Figure 12.4: (a) The glide plane operation: (b) Right and left-hand screw axes. The right and left hand screw axes belong to closely related but different space groups.

12.3   Compound Space Group Operations

Non-symmorphic space groups are also found and there are 157 of these (230–73=157). In the non-symmorphic space groups we find instead of simple translation operations, compound translation operations such as glide planes and screw axes.

A **glide plane** consists of a translation parallel to a given plane followed by a reflection in that plane (see Fig. 12.4a). There are in fact three different types of glide planes that are identified: the **axial glide** along a symmetry axis ($\vec{a}$, $\vec{b}$, or $\vec{c}$), the **diagonal glide** or n**-glide** in two or three directions (e.g., $(\vec{a} + \vec{b})/2$ or $(\vec{a} + \vec{b} + \vec{c})/2$) and finally the **diamond glide** corresponding to $(\vec{a} + \vec{b})/4$ or $(\vec{a} + \vec{b} + \vec{c})/4$).

A **screw axis** is a translation along an axis about which a rotation is simultaneously occurring. In Fig. 12.4b we show a 3-fold screw axis, where a is the lattice constant. The tellurium and selenium structures have 3-fold screw axes similar to those shown in Fig. 12.4b. A summary of the various possible screw axes and the crystallographic notation for each is shown in Fig. 12.5. A familiar example of a **non-symmorphic space group** is the **diamond** structure shown in Fig. 12.6, where we note that there are two atoms per unit cell (the dark and light atoms).
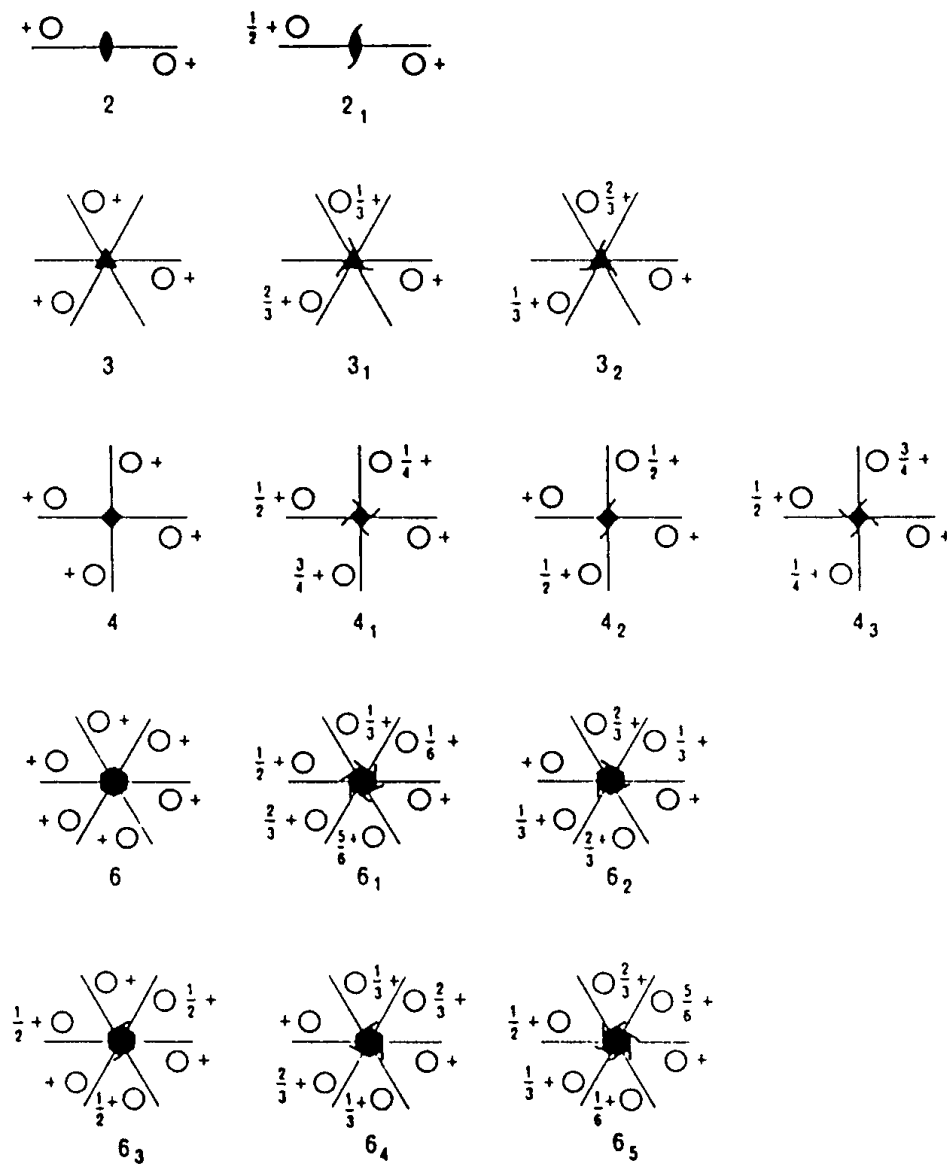
Figure 12.5: A summary of all possible screw axes.
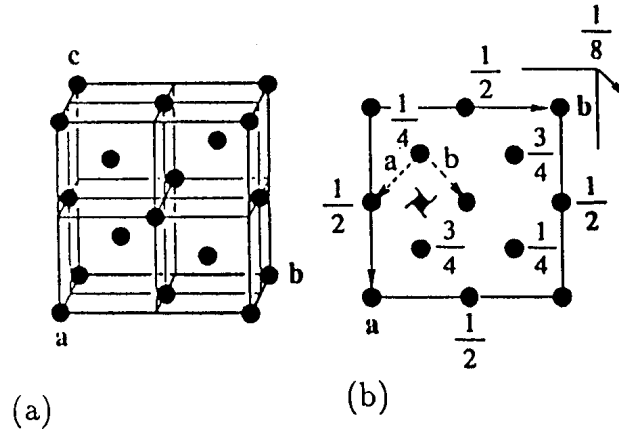
Figure 12.6: (a) Diamond structure $Fd3m$ (O_h^7, #227) showing a unit cell with 2 distinct atom site locations. For the zincblende structure (see Fig. 14.7) the atoms on the two sites are distinct. (b) The screw axis in the diamond structure.

(a)   (b)

The symmetry operations of T_d represent all the point group operations that take light atoms into light atoms and dark atoms into dark atoms. In addition, each of the operations of T_d can be compounded with a translation along $(111)/4$ which takes a light atom into a dark atom and vice versa. Because of these additional symmetry operations which are not point group operations of T_d, the diamond structure is not a Bravais lattice and is non-symmorphic. The screw axis pertinent to the diamond structure is shown in Fig. 12.6b. Further examples of non-symmorphic operations in three-dimensional space groups are given in §12.6.1 after discussion of the simpler situation occurring in 2D space groups, in §12.5.

To summarize, there are **14 Bravais lattices, 32 point groups, 230 space groups** of which **73 are symmorphic and 157 are non-symmorphic**. To demonstrate symmorphic and non-symmorphic space groups, we enumerate in §12.5 the 17 two-dimensional space groups which are important for surface science and for quasi-two dimensional systems. In §12.4 we show that a Bravais lattice can only support 1-fold, 2-fold, 3-fold, 4-fold and 6-fold rotations; a Bravais lattice is not consistent with a 5-fold (or n-fold for $n > 6$) point group symmetry.
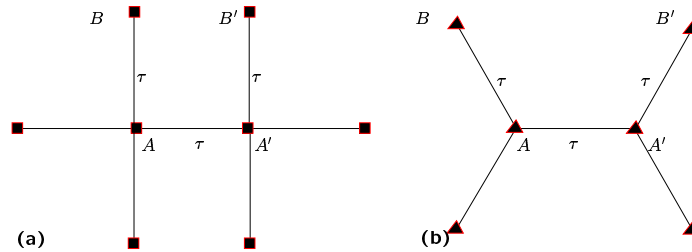
Figure 12.7: Translation–rotation symmetry for a 4–fold axis (a), and a 3–fold axis (b).

12.4 Incompatibility of Five-Fold Symmetry and Bravais Lattices

We show here that the requirements of translational symmetry limit the possible rotation angles of a Bravais lattice and in particular restrict the possible rotation axes to 1-fold, 2-fold, 3-fold, 4-fold and 6-fold. Five-fold axes do not occur. When rotational symmetry does occur in crystals, then severe restrictions on the rotation angle are imposed by the simultaneous occurrence of the repetition of the unit cells through rotations and translations.

To understand this restriction, consider the interplay of a 4–fold axis and a translation, shown in Fig. 12.7a. The 4–fold axis A requires the 4–fold repetition of the translation about itself. The translated axis A' also requires a set of translations at 90° with respect to each other. Each of these translations, in turn, requires the repetition of a 4–fold axis at the translation distance τ from another 4–fold axis. Now consider the two axes B and B'. These are derived by translation from the same axis A. Therefore B and B' are translation–equivalent, so that BB' is a translation. In this example BB' is exactly the same translation as the original $\tau = AA'$. If the same reasoning is applied to the interplay of a 3–fold axis and a translation, see Fig. 12.7b, one finds that $BB' = 2AA' = 2\tau$. In these two examples, the interplay of a rotation and a translation produces new translations which are
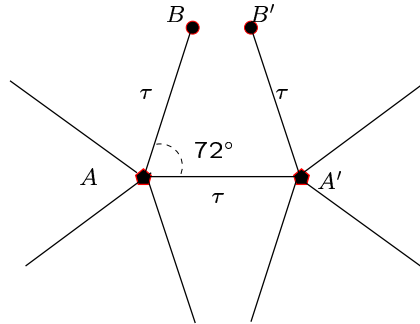
Figure 12.8: Translation–rotation symmetry for a 5–fold axis. BB' is not an integral multiple of τ, and is not a lattice vector.

consistent with the original translation.

But this is not true for all rotation angles, α. For example, it is not true for a 5–fold axis, as shown in Fig. 12.8. The 5–fold axis at A is required by translation τ to be repeated at A'. Furthermore, the rotational symmetry of A requires the translation $AA' = \tau$ to be repeated at an angular interval $\alpha = 2\pi/5 = 72°$ at AB, while the rotational symmetry of A' requires the translation $AA' = \tau$ to be repeated at $\alpha = 72°$ for $A'B'$. Since BA, AA', and $A'B'$ are all translations, BB' is a translation having the same direction as the original translation AA'. Yet the lengths of BB' and AA' are irrational with respect to one another. Thus BB' is a new translation τ' in the same direction as τ but inconsistent with it. This inconsistency can also be expressed by stating that BB' violates the initial hypothesis that τ is the shortest translation in that direction.

In general, the only acceptable values of α are those that cause BB' in Fig. 12.9 to be an integer multiple of the original translation, τ, in order to be consistent with this translation. Thus the translation b involves the condition that

$$b = m\tau, \tag{12.18}$$

Figure 12.9: Geometric construction showing the translations τ and b and the angle of rotation α (see text).
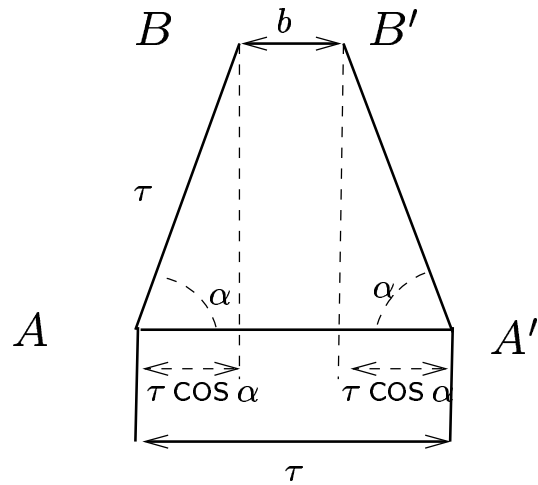
where m is an integer. But b is a simple function of α and τ, as shown in Fig. 12.9 so that

$$b = \tau - 2\tau \cos \alpha. \qquad (12.19)$$

This can be compared with Eq. 12.18, giving

$$m\tau = \tau - 2\tau \cos \alpha \qquad (12.20)$$

so that

$$m = 1 - 2 \cos \alpha. \qquad (12.21)$$

Consequently

$$2 \cos \alpha = 1 - m = M \qquad (12.22)$$

where M is also an integer. The permitted values for M, and the corresponding values of α, m, and b, are listed in Table 12.2. The permissible values of b are illustrated in Fig. 12.10.

Table 12.2: Solutions of $M = 2\cos\alpha$ for permissible periods of crystallographic axes.

M	$\cos\alpha$	α	$n = 2\pi/\alpha$	$b = \tau - 2\tau\cos\alpha$
-3	-1.5	$-$	$-$	$-$
-2	-1	π	2	3τ
-1	-0.5	$2\pi/3$	3	2τ
0	0	$\pi/2$	4	τ
1	0.5	$\pi/3$	6	0
2	1	0	∞	$-\tau$
3	1.5	$-$	$-$	$-$

Figure 12.10: Magnitudes of b in Eq. 12.18 for various crystallographic values for n (see text).

Table 12.3: Five two-dimensional Bravais lattices.

oblique	parallelogram	$a \neq b$	$\phi \neq 90°$	2
square	square	$a = b$	$\phi = 90°$	$4mm$
hexagonal	60° rhombus	$a = b$	$\phi = 120°$	$6mm$
primitive rectangular	rectangle	$a \neq b$	$\phi = 90°$	$2mm$
centered rectangular	rectangle	$a \neq b$	$\phi = 90°$	$2mm$

12.5 Two Dimensional Space Groups

12.5.1 Five Two-dimensional Bravais Lattices

There are five distinct Bravais lattices in two-dimensions as shown in Table 12.3. If we consider $\vec{a}, \vec{b}$ to be the two primitive translation vectors and ϕ to be the angle between $\vec{a}$ and $\vec{b}$, then the five lattice types are summarized in Table 12.3, and the two-dimensional space groups are given in Table 12.4.

12.5.2 Notation

The notation used for the two-dimensional space groups is illustrated by the example $p4gm$. The initial symbol ("p" in this example) indicates that the unit cell is either a primitive (p) unit cell or a centered (c) unit cell. The next symbol "4" indicates rotational symmetry about an axis perpendicular to the plane of the two-dimensional crystal. The possible n-fold rotations for a space group are 1, 2, 3, 4, and 6, as shown in §12.4. The symbols used to denote such axes are shown in Fig. 12.11. The last two symbols, when present, indicate additional symmetries for the two inequivalent in-plane axes, where "g" denotes a glide plane through the primary axis, "m" denotes a mirror plane through the primary axis, and "1" indicates that there is no additional symmetry.

We now discuss the notation for 3D groups as enumerated in Table 12.1. In the case of rectangular lattices, the inequivalent axes are both parallel to the sides of the conventional rectangular unit cell. In
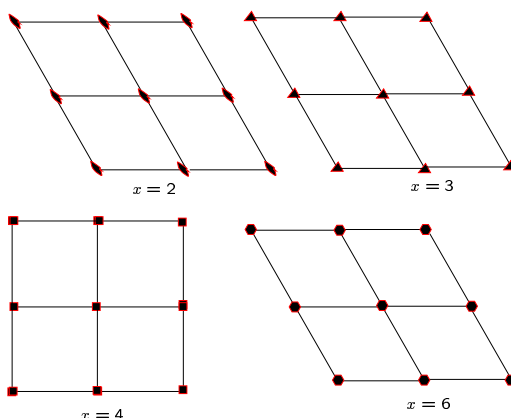
Figure 12.11: Space group symbols used at lattice points for 2-fold, 3-fold, 4-fold and 6-fold rotations ($x = n$ for an n-fold rotation).

the case of square lattices, the first set of axes is parallel to the sides and the second set is along the diagonals. In the case of hexagonal lattices, one axis is 30° away from a translation vector. Other symbols that are used for 3D space groups (see Table 12.1) include A or B for monoclinic groups, and C, A or B, I, F for orthorhombic groups. Here I refers to body centered and F to face centered groups, with F also occurring for tetragonal and cubic groups. The symbol R is used for rhombohedral groups.

12.5.3   Listing of the Space Groups

If we add two-dimensional objects, e.g., a set of atoms, to each cell of a Bravais lattice, we can change the symmetry of the lattice. If the object, sometimes called a motif, lowers the symmetry to that of another group, then the resulting symmetry space group is identified with the lower symmetry space group. Altogether there are 17 two-dimensional space groups (see Table 12.4). We give below the symmetries of each of these space groups, classified in terms of the 5 Bravais lattices given in §12.5.1. Listings from the "International Tables for X-Ray Crystallography" are given in Figs. 12.12–12.26. A listing of the 73 symmorphic space groups is given in Table 12.1.

Table 12.4: Summary of the 17 two-dimensional space groups.

Point Group	Lattice Type	International[a] Table Number	Notation Full	Type	Notation Short
1	Oblique	1	$p1$	symmorphic	$p1$
2		2	$p211$	symmorphic	$p2$
m	Rectangular	3	$p1m1$	symmorphic	pm
	(p or c)	4	$p1g1$	non-symmorphic	pg
		5	$c1m1$	symmorphic	cm
$2mm$		6	$p2mm$	symmorphic	pmm
		7	$p2mg$	non-symmorphic	pmg
		8	$p2gg$	non-symmorphic	pgg
		9	$c2mm$	symmorphic	cmm
4	Square p	10	$p4$	symmorphic	$p4$
$4mm$		11	$p4mm$	symmorphic	$p4m$
		12	$p4gm$	non-symmorphic	$p4g$
3	Hexagonal	13	$p3$	symmorphic	$p3$
$3m$		14	$p3m1$	symmorphic	$p3m1$
		15	$p31m$	symmorphic	$p31m$
6		16	$p6$	symmorphic	$p6$
$6mm$		17	$p6mm$	symmorphic	$p6m$

[a]International Tables for X-Ray Crystallography, published by the International Union of Crystallography, Kynoch Press, Birmingham, England (1952). See also G. Burns and A. M. Glazer, "Space Groups for Solid State Scientists", Academic Press, Inc.
—

12.5.4 2D Oblique Space Groups

There are 2 oblique space groups as shown in Fig. 12.12. The lowest symmetry two-dimensional space group (#1) only has translational symmetry ($p1$) and no point group operations. The diagram for $p1$ shows only one general point (x, y) with translations by lattice vectors (1,0), (0,1), and (1,1). Open circles on the left hand diagram in Fig. 12.12 are used to denote the 3 open circles obtained from the first open circle by these 3 translations.

However, by placing a motif with two-fold rotational symmetry normal to the plane, the $p211$ space group (#2) is obtained, as shown in the symmetry diagram from the International Tables for X-Ray Crystallography. The two-fold axis through the center of the rhombus (indicated by a football-shaped symbol on the right of Fig. 12.12) takes a general point (x, y) into $(-x, -y)$, shown as point symmetry type e in the table. Points obtained by rotations are indicated by open circles in Fig. 12.12. For the special points (1/2, 1/2), (1/2, 0), (0, 1/2), (0, 0), the two-fold rotation takes the point into itself or into an equivalent point separated by a lattice vector. The site symmetry for these points is listed in the table as having a two-fold axis. A general point under the action of the 2-fold axis and translation by (1,0), (0,1), and (1,1) yields the 8 open points in the figure.

12.5.5 2D Rectangular Space Groups

Primitive Lattices

Of the 7 rectangular 2D space groups, 5 are primitive and 2 are centered (see Table. 12.4). We consider these together as is done in the International Tables for X-Ray Crystallography. Of the 5 primitive rectangular space groups only two are symmorphic, and three are non-symmorphic. In general, the full rectangular point symmetry is $2mm$ (C_{2v}). The point group $2mm$ has elements E, C_{2z}, σ_x, σ_y: the identity; a two-fold axis C_{2z} perpendicular to the plane; and mirror planes parallel to the x and y axes through C_{2z}. The corresponding space group listed as space group #6 is $p2mm$ (see Fig. 12.15). When introducing a lower symmetry motif, the resulting group must be a subgroup of the original group. The lower symmetry rectangular space group
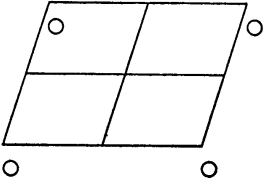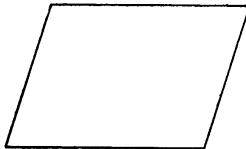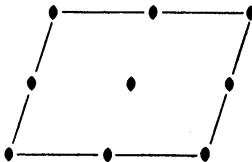
p 1   No. 1   *p* 1   1   Oblique

Origin on 1

Number of positions, Wyckoff notation, and point symmetry			Co-ordinates of equivalent positions	Conditions limiting possible reflections
				General:
1	*a*	1	*x,y.*	No conditions

p 2   No. 2   *p* 2 1 1   2   Oblique

Origin at 2

				General:
2	*e*	1	*x,y*; *x̄,ȳ.*	No conditions
				Special:
1	*d*	2	½,½.	No conditions
1	*c*	2	½,0.	
1	*b*	2	0,½.	
1	*a*	2	0,0.	

Figure 12.12: The two oblique two-dimensional space groups *p*1 and *p*2 (*p*211).

Oblique   Rectangular   *m*   *p* 1 *m* 1   No. 3   *pm*
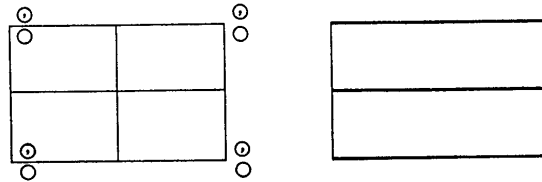
Origin on *m*

limiting lections	Number of positions, Wyckoff notation, and point symmetry			Co-ordinates of equivalent positions	Conditions limiting possible reflections
					General:
					No conditions
	2	*c*	1	*x,y*; *x̄,y*.	
					Special:
	1	*b*	*m*	½,*y*.	No conditions
Oblique	1	*a*	*m*	0,*y*.	

Rectangular   *m*   *p* 1 *g* 1   No. 4   *pg*
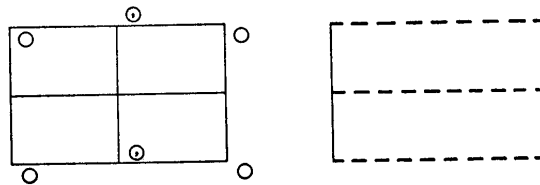
Origin on *g*

General:

hk: No conditions
0*k*: *k*=2*n*

2   *a*   1   *x,y*;   *x̄*,½+*y*.

Figure 12.13: The two-dimensional space groups *pm* and *pg*, #3 and #4, respectively.

$c\,m$

No. 5 $c\,1\,m\,1$ m Rectangular
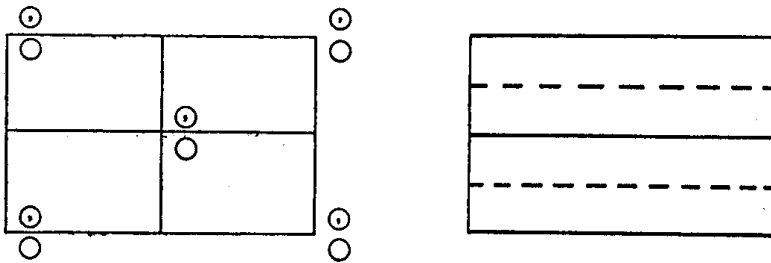
Origin on m

Number of positions, Wyckoff notation, and point symmetry			Co-ordinates of equivalent positions $(0,0;\ \tfrac{1}{2},\tfrac{1}{2})+$	Conditions limiting possible reflections
				General:
4	b	1	$x,y;\ \bar{x},y.$	$hk:\ h+k=2n$
				Special: as above only
2	a	m	$0,y.$	

Figure 12.14: The two-dimensional space group cm, #5.

Rectangular   *m m*   *p* 2 *m m*   No. 6   **pmm**

Origin at 2*mm*

Number of positions, Wyckoff notation, and point symmetry			Co-ordinates of equivalent positions	Conditions limiting possible reflections
				General:
4	*i*	1	x,y; $\bar{x},y$; $\bar{x},\bar{y}$; $x,\bar{y}$.	No conditions
				Special:
2	*h*	*m*	$\frac{1}{2},y$; $\frac{1}{2},\bar{y}$.	No conditions
2	*g*	*m*	$0,y$; $0,\bar{y}$.	
2	*f*	*m*	$x,\frac{1}{2}$; $\bar{x},\frac{1}{2}$.	
2	*e*	*m*	$x,0$; $\bar{x},0$.	
1	*d*	*mm*	$\frac{1}{2},\frac{1}{2}$.	
1	*c*	*mm*	$\frac{1}{2},0$.	
1	*b*	*mm*	$0,\frac{1}{2}$.	
1	*a*	*mm*	$0,0$.	

Figure 12.15: The rectangular two-dimensional space group *pmm*, #6.

pmg No. 7 $p\,2\,m\,g$ $m\,m$ Rectangular

Origin at 2

Number of positions, Wyckoff notation, and point symmetry			Co-ordinates of equivalent positions	Conditions limiting possible reflections
				General:
4	d	1	x,y; $\bar{x},\bar{y}$; $\frac{1}{2}+x,\bar{y}$; $\frac{1}{2}-x,y$.	hk: No conditions $h0$: $h=2n$
				Special: as above, plus
2	c	m	$\frac{1}{4},y$; $\frac{3}{4},\bar{y}$.	no extra conditions
2	b	2	$0,\frac{1}{2}$; $\frac{1}{2},\frac{1}{2}$.	$\left.\rule{0pt}{20pt}\right\}$ hk: $h=2n$
2	a	2	$0,0$; $\frac{1}{2},0$.	

Figure 12.16: The rectangular two-dimensional space group pmg, #7.

Rectangular   *m m* $p\,2\,g\,g$ No. 8 pgg
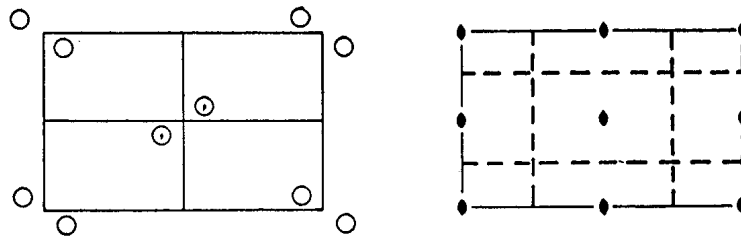
Origin at 2

Number of positions, Wyckoff notation, and point symmetry			Co-ordinates of equivalent positions	Conditions limiting possible reflections
				General:
4	*c*	1	x,y; $\bar{x},\bar{y}$; $\frac{1}{2}+x,\frac{1}{2}-y$; $\frac{1}{2}-x,\frac{1}{2}+y$.	*hk*: No conditions *h*0: $h=2n$ 0*k*: $k=2n$
				Special: as above, plus
2	*b*	2	$\frac{1}{2},0$; $0,\frac{1}{2}$.	$\Big\}$ *hk*: $h+k=2n$
2	*a*	2	$0,0$; $\frac{1}{2},\frac{1}{2}$.	

Figure 12.17: The two-dimensional rectangular space group *pgg*, #8.

c m m   No. 9   *c* 2 *m m*   *m m*   Rectangular
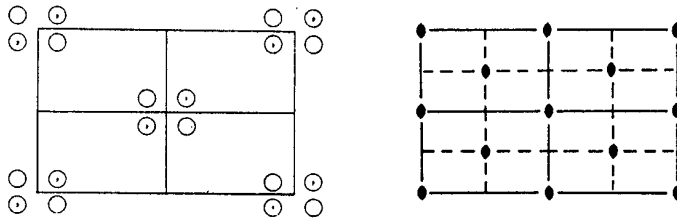
Origin at 2*mm*

Number of positions, Wyckoff notation, and point symmetry			Co-ordinates of equivalent positions $(0,0; \frac{1}{2},\frac{1}{2})+$	Conditions limiting possible reflections
				General:
8	f	1	x,y; $\bar{x},y$; $\bar{x},\bar{y}$; $x,\bar{y}$.	hk: $h+k=2n$
				Special: as above, plus
4	e	m	$0,y$; $0,\bar{y}$.	no extra conditions
4	d	m	$x,0$; $\bar{x},0$.	
4	c	2	$\frac{1}{4},\frac{1}{4}$; $\frac{1}{4},\frac{3}{4}$.	hk: $h=2n$; $(k=2n)$
2	b	mm	$0,\frac{1}{2}$.	no extra conditions
2	a	mm	$0,0$.	

Figure 12.18: The two-dimensional rectangular space group *cmm*, #9.

$p1m1$ has point group operations (E, σ_x) and is listed as space group #3 (see Fig. 12.13). We note that (E, σ_y) is equivalent to (E, σ_x) by an interchange of axes and each corresponds to point group m (C_{1h}).

Under a mirror plane operation (see Fig. 12.13) the symbols $\odot$ and $\bigcirc$ are used; the mirror plane is represented on the right by a solid horizontal line. The use of a comma inside the circle provides a sense of orientation that is preserved under translations. The three kinds of site symmetries (the general point c and the points a and b on the mirror planes) are also listed in the table for space group #3.

So far we have dealt with space groups where the point group operations are separable from the translation group operations. Such groups are symmorphic space groups.

In the case of the rectangular primitive lattice, mirror operations can be replaced by glide reflections. The glide planes are denoted by dashed lines (see diagram for space group #4 in Fig. 12.13). No distinct screw operations are possible in two-dimensions. A glide reflection symmetry operation is a compound operation consisting of a reflection combined with a fractional translation, not a primitive unit cell translation. The resulting space group is non-symmorphic.

Replacing m by g in $p1m1$ (space group #3) gives $p1g1$ (space group #4) where the translation $\vec{\tau}_1/2$ is compounded with the reflection operation; this translation can be followed by comparing the $\odot$ symbols for space groups #3 and #4.

For the case of space group #6, replacing one of the mirror planes by a glide plane gives the non-symmorphic group $p2mg$ (#7) as shown in Fig. 12.13. When both mirror planes of space group #6 are replaced by glide planes, we get $p2gg$ (#8) which has the fractional translation $\frac{1}{2}\vec{\tau}_1 + \frac{1}{2}\vec{\tau}_2$, as shown in Fig. 12.17. The compound mirror plane translation operations can be denoted by $[\sigma_x|\frac{1}{2}\vec{\tau}_1 + \frac{1}{2}\vec{\tau}_2]$, $[\sigma_y|\frac{1}{2}\vec{\tau}_1 + \frac{1}{2}\vec{\tau}_2]$.

Centered Rectangular Lattices

The centered rectangular lattice with the full centered rectangular symmetry (see Fig. 12.18) is the symmorphic space group $c2mm$ (#9). The lower symmetry subgroup, related to $p1m1$ is $c1m1$ (#5) (shown in Fig. 12.14). We note that the centering is equivalent to introducing a $\vec{\tau}_1/2$ glide plane as indicated in Fig. 12.13 for space group $c1m1$ (#5). There are no non-symmorphic centered rectangular lattices. As a more

Square   4   *p* 4   No. 10 $p\,4$

Origin at 4

Number of positions, Wyckoff notation, and point symmetry			Co-ordinates of equivalent positions	Conditions limiting possible reflections
				General:
4	*d*	1	x,y; $\bar{x},\bar{y}$; $y,\bar{x}$; $\bar{y},x$.	No conditions
				Special:
2	*c*	2	$\frac{1}{2},0$; $0,\frac{1}{2}$.	*hk*: $h+k=2n$
1	*b*	4	$\frac{1}{2},\frac{1}{2}$.	⎫
1	*a*	4	$0,0$.	⎬ No conditions ⎭

Figure 12.19: The square two-dimensional space groups $p4$ (#10).

interesting example of a centered rectangular space group, let us look at space group #9 which is denoted by *c2mm*. This space group has 2 equivalent positions (0,0) and (1/2, 1/2). The symmetry operations include a two-fold axis along the *z*-direction and two sets of intersecting mirror planes. The table shows that *c2mm* can be realized through 6 different kinds of site symmetries.

12.5.6   2D Square Space Group

There are three 2D square space groups. The square lattice space with the full $4mm$ point group symmetry is $p4mm$ (space group #11), which is shown in Fig. 12.20. The point group symmetry elements are E, C_{4z}^+, C_{4z}^-, C_{2z}, σ_y, σ_x, σ_{da}, σ_{db} corresponding to C_{4v}. The only distinct

$p\,4m$ No. 11 $p\,4\,m\,m$ $4\,m\,m$ Square

Origin at 4mm

Number of positions, Wyckoff notation, and point symmetry			Co-ordinates of equivalent positions	Conditions limiting possible reflections
8	g	1	$x,y;\;\; \bar{x},\bar{y};\;\; y,\bar{x};\;\; \bar{y},x;\;\; \bar{x},y;\;\; x,\bar{y};\;\; \bar{y},\bar{x};\;\; y,x.$	General: No conditions
4	f	m	$x,x;\;\; \bar{x},\bar{x};\;\; \bar{x},x;\;\; x,\bar{x}.$	Special: No conditions
4	e	m	$x,\frac{1}{2};\;\; \bar{x},\frac{1}{2};\;\; \frac{1}{2},x;\;\; \frac{1}{2},\bar{x}.$	
4	d	m	$x,0;\;\; \bar{x},0;\;\; 0,x;\;\; 0,\bar{x}.$	
2	c	mm	$\frac{1}{2},0;\;\; 0,\frac{1}{2}.$	$hk:\; h+k=2n$
1	b	$4mm$	$\frac{1}{2},\frac{1}{2}.$	No conditions
1	a	$4mm$	$0,0.$	
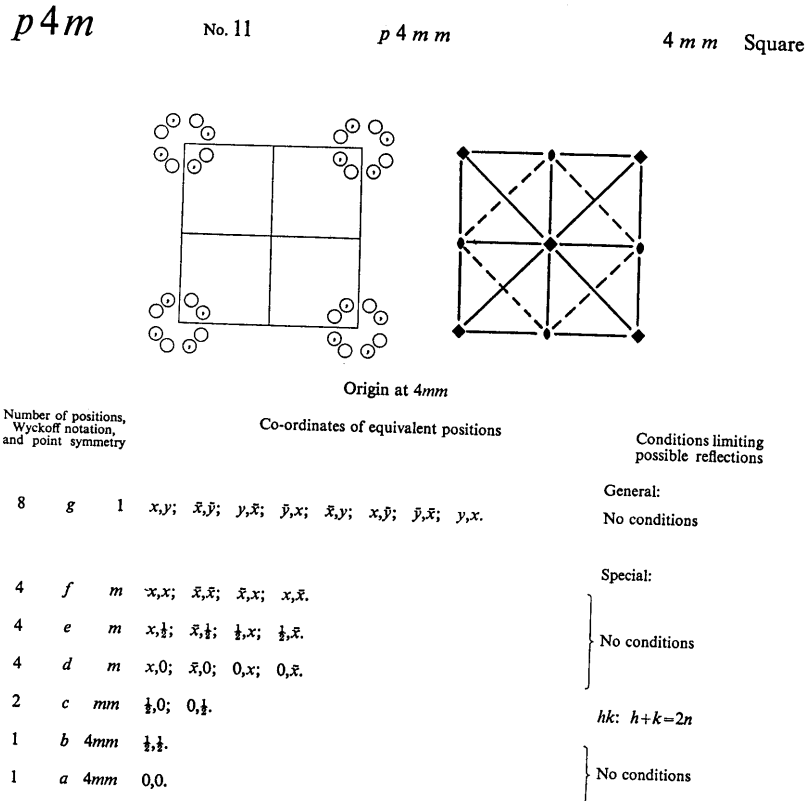
Figure 12.20: The square two-dimensional space group $p4m$ (#11).

Square   4 *m m*   *p* 4 *g m*   No. 12   *p* 4 *g*
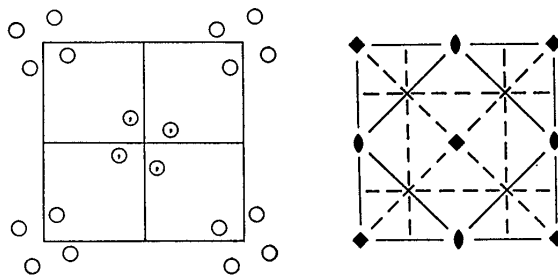
Origin at 4

Number of positions, Wyckoff notation, and point symmetry			Co-ordinates of equivalent positions	Conditions limiting possible reflections
				General:
8	*d*	1	x,y; $y,\bar{x}$; $\frac{1}{2}-x,\frac{1}{2}+y$; $\frac{1}{2}-y,\frac{1}{2}-x$; $\bar{x},\bar{y}$; $\bar{y},x$; $\frac{1}{2}+x,\frac{1}{2}-y$; $\frac{1}{2}+y,\frac{1}{2}+x$.	*hk*: No conditions *h*0: *h*=2*n* (0*k*: *k*=2*n*) *hh*: No conditions
				Special: as above, plus
4	*c*	*m*	$x,\frac{1}{2}+x$; $\bar{x},\frac{1}{2}-x$; $\frac{1}{2}+x,\bar{x}$; $\frac{1}{2}-x,x$.	no extra conditions
2	*b*	*mm*	$\frac{1}{2},0$; $0,\frac{1}{2}$.	*hk*: *h*+*k*=2*n*
2	*a*	4	$0,0$; $\frac{1}{2},\frac{1}{2}$.	

Figure 12.21: The square two-dimensional space group *p4g* (#12).

$p\,3$ No. 13 $p\,3$ 3   Hexagonal
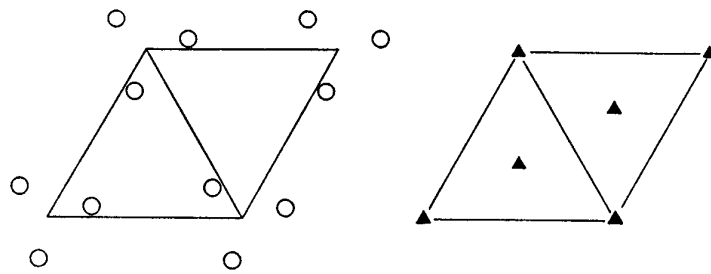
Origin at 3

Number of positions, Wyckoff notation, and point symmetry			Co-ordinates of equivalent positions	Conditions limiting possible reflections
				General:
3	d	1	$x,y;\ \ \bar{y},x-y;\ \ y-x,\bar{x}.$	No conditions
				Special:
1	c	3	$\frac{2}{3},\frac{1}{3}.$	No conditions
1	b	3	$\frac{1}{3},\frac{2}{3}.$	
1	a	3	$0,0.$	

Figure 12.22: Hexagonal two-dimensional space group

Hexagonal   3 *m*   *p* 3 *m* 1   No. 14 $p\,3\,m\,1$
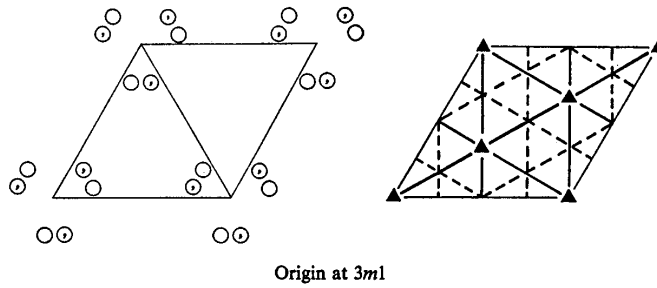
Origin at 3*m*1

Number of positions, Wyckoff notation, and point symmetry			Co-ordinates of equivalent positions	Conditions limiting possible reflections
				General:
6	*e*	1	x,y; $\bar{y},x-y$; $y-x,\bar{x}$; $\bar{y},\bar{x}$; $x,x-y$; $y-x,y$.	No conditions
				Special:
3	*d*	*m*	$x,\bar{x}$; $x,2x$; $2\bar{x},\bar{x}$.	No conditions
1	*c*	3*m*	$\frac{2}{3},\frac{1}{3}$.	
1	*b*	3*m*	$\frac{1}{3},\frac{2}{3}$.	
1	*a*	3*m*	0,0.	

Figure 12.23: Hexagonal two-dimensional space group $p3m1$ (#14).

$p\,3\,1\,m$ No. 15 $p\,3\,1\,m$ $3\,m$ Hexagonal
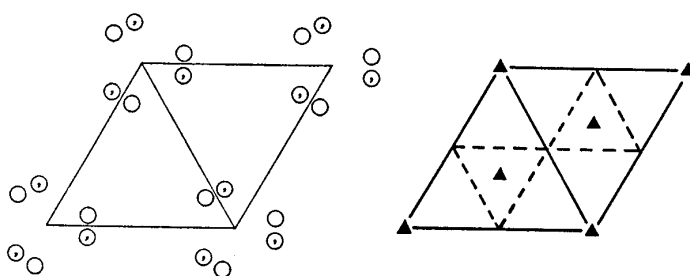
Origin at $31m$

Number of positions, Wyckoff notation, and point symmetry			Co-ordinates of equivalent positions			Conditions limiting possible reflections
						General:
6	d	1	x,y;	$\bar{y},x-y$;	$y-x,\bar{x}$;	No conditions
			y,x;	$\bar{x},y-x$;	$x-y,\bar{y}$.	
						Special:
3	c	m	$x,0$;	$0,x$;	$\bar{x},\bar{x}$.	No conditions
2	b	3	$\frac{1}{3},\frac{2}{3}$;	$\frac{2}{3},\frac{1}{3}$.		
1	a	$3m$	$0,0$.			

Figure 12.24: Hexagonal two-dimensional space group $p31m$ (#15).

Hexagonal   6 $p\,6$ No. 16 $p\,6$
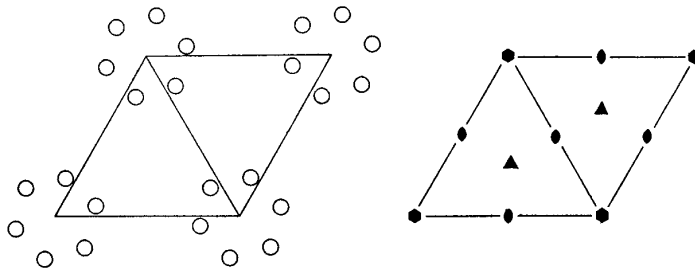
Origin at 6

Number of positions, Wyckoff notation, and point symmetry			Co-ordinates of equivalent positions	Conditions limiting possible reflections
				General:
6	d	1	$x,y;\ \ \bar{y},x-y;\ \ y-x,\bar{x};$ $\bar{x},\bar{y};\ \ y,y-x;\ \ x-y,x.$	No conditions
				Special:
3	c	2	$\frac{1}{2},0;\ \ 0,\frac{1}{2};\ \ \frac{1}{2},\frac{1}{2}.$	No conditions
2	b	3	$\frac{1}{3},\frac{2}{3};\ \ \frac{2}{3},\frac{1}{3}.$	
1	a	6	$0,0.$	

Figure 12.25: Hexagonal two-dimensional space group $p6$ (#16).

p 6 *m*   No. 17   *p* 6 *m m*   6 *m m*   Hexagonal
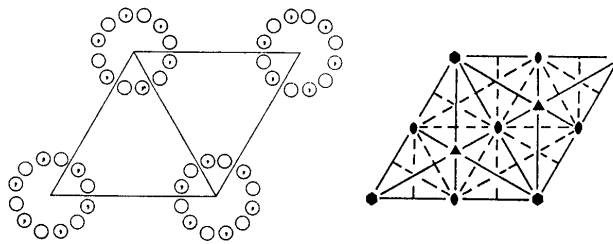
Origin at 6*mm*

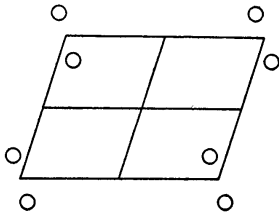| Number of positions, Wyckoff notation, and point symmetry			Co-ordinates of equivalent positions	Conditions limiting possible reflections
				General:
12	*f*	1	x,y; $\bar{y},x-y$; $y-x,\bar{x}$; y,x; $\bar{x},y-x$; $x-y,\bar{y}$; $\bar{x},\bar{y}$; $y,y-x$; $x-y,x$; $\bar{y},\bar{x}$; $x,x-y$; $y-x,y$.	No conditions
				Special:
6	*e*	*m*	$x,\bar{x}$; $x,2x$; $2\bar{x},\bar{x}$; $\bar{x},x$; $\bar{x},2\bar{x}$; $2x,x$.	No conditions
6	*d*	*m*	$x,0$; $0,x$; $\bar{x},\bar{x}$; $\bar{x},0$; $0,\bar{x}$; x,x.	
3	*c*	*mm*	$\frac{1}{2},0$; $0,\frac{1}{2}$; $\frac{1}{2},\frac{1}{2}$.	
2	*b*	3*m*	$\frac{1}{3},\frac{2}{3}$; $\frac{2}{3},\frac{1}{3}$.	
1	*a*	6*mm*	$0,0$.	

Figure 12.26: Hexagonal two-dimensional space group *p6m* (#17).

subgroup of C_{4v} is C_4 which has symmetry elements E, C_{4z}^+, C_{4z}^-, C_{2z}. In this case, the space group is $p4$ (#10 in International Tables for X-Ray Crystallography). The 4-fold axis is clearly seen on the left hand diagram in Fig. 12.19. The $\odot$ points in #11 are obtained by adding mirror planes to #10. In the diagram on the right we see lattice locations with 4-fold and with 2-fold axes, a feature found in all three 2D square lattices (see Figs. 12.19, 12.20, and 12.21).

By combining the translation $\frac{1}{2}\vec{\tau}_1 + \frac{1}{2}\vec{\tau}_2$, where $\frac{1}{2}\vec{\tau}_1$ and $\frac{1}{2}\vec{\tau}_2$ are translation vectors, with the mirror planes $\sigma_x, \sigma_y, \sigma_{da}, \sigma_{db}$ we obtain the glide reflections $[\sigma_x | \frac{1}{2}\vec{\tau}_1 + \frac{1}{2}\vec{\tau}_2]$, $[\sigma_y | \frac{1}{2}\vec{\tau}_1 + \frac{1}{2}\vec{\tau}_2]$, $[\sigma_{da} | \frac{1}{2}\vec{\tau}_1 + \frac{1}{2}\vec{\tau}_2]$, $[\sigma_{db} | \frac{1}{2}\vec{\tau}_1 + \frac{1}{2}\vec{\tau}_2]$. These glide reflections are used to form the non-symmorphic square lattice $p4gm$ (#12). We note there are mirror planes along the square diagonals and also mirror planes through the x and y axes. Space group #12 is obtained from space group #11 by translation of the comma points by $\frac{1}{2}\vec{\tau}_1 + \frac{1}{2}\vec{\tau}_2$.

12.5.7   2D Hexagonal Space Groups

There are five 2D hexagonal space groups, and all are symmorphic. The hexagonal space group with the full $6mm$ point group symmetry is $p6mm$ (#17). The point group symmetry elements are E, C_6^+, C_6^-, C_3^+, C_3^-, C_2, $\sigma_{d1}, \sigma_{d2}, \sigma_{d3}, \sigma_{v1}, \sigma_{v2}, \sigma_{v3}$. The diagram for $p6mm$ (#17) is shown in Fig. 12.26.

The four subgroups of C_{6v} are C_6, C_{3v}, C_{3d}, C_3, giving rise, respectively, to space groups $p6$ (#16), $p3m1$ (#14), $p31m$ (#15), and $p3$ (#13), as summarized in Table 12.5. The symmetry diagrams for the five 2D hexagonal space groups are shown in Figs. 12.22, 12.23, 12.24, 12.25, and 12.26.

12.6   Three Dimensional Space Groups

The fourteen Bravais space lattices (see Fig. 12.1) illustrated by a unit cell of each: (1) triclinic, simple; (2) monoclinic, simple; (3) monoclinic, base centered; (4) orthorhombic, simple; (5) orthorhombic, base centered; (6) orthorhombic, body centered; (7) orthorhombic, face centered; (8) hexagonal; (9) rhombohedral; (10) tetragonal, simple; (11)

Table 12.5: Summary of the symmetry operations of two-dimensional space groups with 3-fold symmetry.

Space Group	Point Group Elements
$p3$	E, C_3^+, C_3^-
$p3m1$	E, C_3^+, C_3^-, $\sigma_{v1}, \sigma_{v2}, \sigma_{v3}$
$p31m$	E, C_3^+, C_3^-, $\sigma_{d1}, \sigma_{d2}, \sigma_{d3}$
$p6$	E, C_6^+, C_6^-, C_3^+, C_3^-, C_2

tetragonal, body centered; (12) cubic, simple; (13) cubic, body centered; and (14) cubic, face centered.

When combined with the various point group symmetry operations there result 230 different 3D space groups. Of these 73 are symmorphic (see Table 12.1) and 157 are non-symmorphic.

12.6.1 Examples of Non-Symmorphic 3D Space Groups

Some examples of space groups with screw axes are given in Fig. 12.27 for space groups $P4_1$ (C_4^2) #75, $P4_2$ (C_4^3) #77 and $P4_3$ (C_4^4) #78. Each has point group C_4 symmetry, but a different 4-fold screw axis ($4_1, 4_2, 4_3$) is present in each case. The atom locations are given in the left hand diagrams and the symmetry operations include screw axes in the right hand diagrams.

Screw axes may also occur normal to the c-axis, as is shown in Fig. 12.28 for space group $P\overline{4}2_1m$ (D_{2d}^3) #113. Diamond glide planes along $\langle 110 \rangle$ directions also occur for this space group. The D_{2d} operations result in the occurrence of sites (x, y, z), $(-y, x, -z)$, $(-x, -y, z)$ and $(y, -x, -z)$.

Another rather complicated space group diagram is shown in Fig. 12.29 for the space group $R3c$ (C_{3v}^6) #161. The R symbol indicates a rhombohedral Bravais lattice. Two unit cells are indicated on the left hand figure, a trigonal unit cell and a rhombohedral unit cell. For this space group we see 6 point group operations (x, y, z), $(-y, x - y, z)$, $(y - x, -x, z)$, $(-y, -x, \frac{1}{2} + z)$, $(x, x - y, \frac{1}{2} + z)$, $(y - x, y, \frac{1}{2} + z)$ compounded

(a) $P4_1$ $(C_4{}^2)$
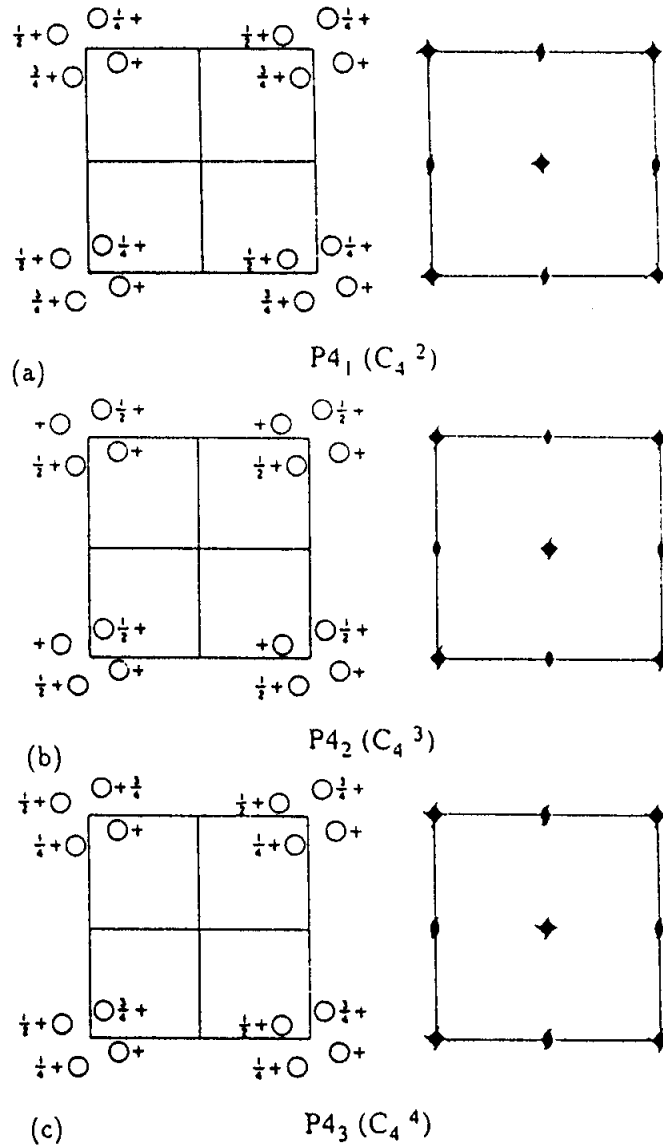
(b) $P4_2$ $(C_4{}^3)$

(c) $P4_3$ $(C_4{}^4)$

Figure 12.27: Examples of space groups with screw axes. The three examples are (a) $P4_1$ (C_4^2) #76, (b) $P4_2$ (C_4^3) #77 and (c) $P4_3$ (C_4^4) #78.
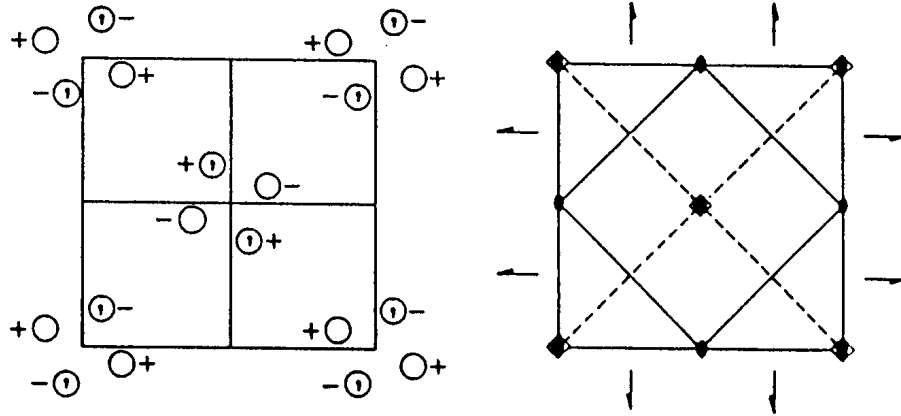
Figure 12.28: Example of a space group with a screw axis in the plane of the figure: $P\overline{4}2_1m$ (D_{2d}^3) (#113).

with 3 centerings $(0,0,0)$, $(1/3, 2/3, 2/3)$ and $(2/3, 1/3, 1/3)$ to give 18 positions. c-axis glide planes pass through the 3-fold axes in Fig. 12.29. The reader is referred to texts such as Burns and Glazer who give a detailed treatment of space group symmetries.
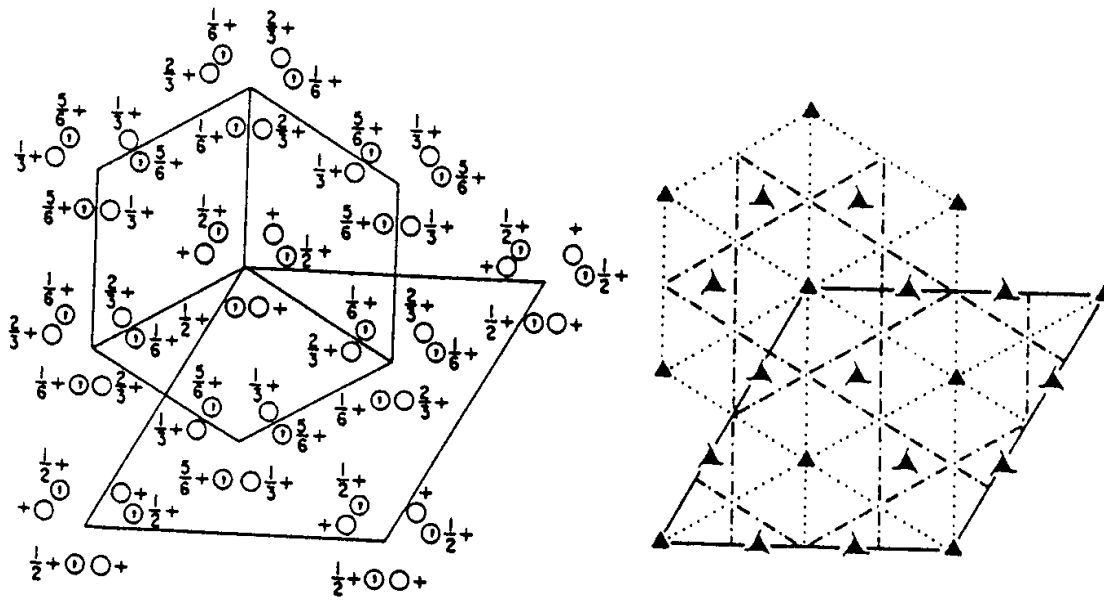
Figure 12.29: Example of a space group with many atom sites $R3c$ (C_{3v}^6) (#161).
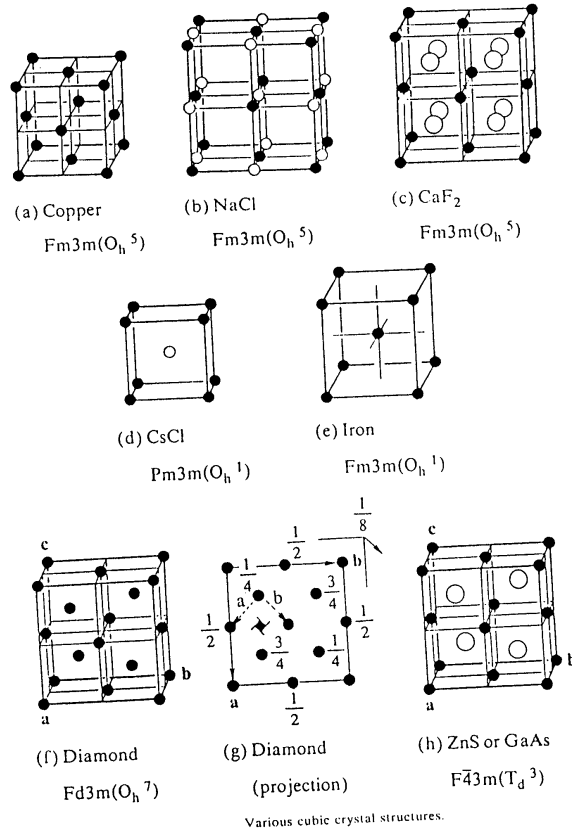
Figure 12.30: Example of cubic lattices. Here (a), (b), (c) pertain to space group #225; (d) pertains to #221 and (e) to #229; whild (f) and (g) are for #227; and (h) is for #223.

Figure 12.31: Example of 3 cubic lattices with the space group O_h^1 ($Pm3m$) (see Table **??**). (a) Simple cubic, (b) body centered cubic, and (c) perovskite structure.

CHAPTER 3   SIMPLE CRYSTAL STRUCTURES

$Pm3m$
O_h^1

No. 221 $P\,4/m\,\bar{3}\,2/m$ $m\,3\,m$ Cubic

Origin at centre ($m3m$)

Number of positions, Wyckoff notation, and point symmetry			Co-ordinates of equivalent positions						Conditions limiting possible reflections

General:

hkl: ⎫
hhl: ⎬ No conditions
0kl: ⎭

Special:
No conditions

48   n 1

$x,y,z;$ $z,x,y;$ $y,z,x;$ $x,z,y;$ $y,x,z;$ $z,y,x;$
$x,\bar{y},\bar{z};$ $z,\bar{x},\bar{y};$ $y,\bar{z},\bar{x};$ $x,\bar{z},\bar{y};$ $y,\bar{x},\bar{z};$ $z,\bar{y},\bar{x};$
$\bar{x},y,\bar{z};$ $\bar{z},x,\bar{y};$ $\bar{y},z,\bar{x};$ $\bar{x},z,\bar{y};$ $\bar{y},x,\bar{z};$ $\bar{z},y,\bar{x};$
$\bar{x},\bar{y},z;$ $\bar{z},\bar{x},y;$ $\bar{y},\bar{z},x;$ $\bar{x},\bar{z},y;$ $\bar{y},\bar{x},z;$ $\bar{z},\bar{y},x;$
$\bar{x},\bar{y},\bar{z};$ $\bar{z},\bar{x},\bar{y};$ $\bar{y},\bar{z},\bar{x};$ $\bar{x},\bar{z},\bar{y};$ $\bar{y},\bar{x},\bar{z};$ $\bar{z},\bar{y},\bar{x};$
$\bar{x},y,z;$ $\bar{z},x,y;$ $\bar{y},z,x;$ $\bar{x},z,y;$ $\bar{y},x,z;$ $\bar{z},y,x;$
$x,\bar{y},z;$ $z,\bar{x},y;$ $y,\bar{z},x;$ $x,\bar{z},y;$ $y,\bar{x},z;$ $z,\bar{y},x;$
$x,y,\bar{z};$ $z,x,\bar{y};$ $y,z,\bar{x};$ $x,z,\bar{y};$ $y,x,\bar{z};$ $z,y,\bar{x}.$

24   m m

$x,x,z;$ $z,x,x;$ $x,z,x;$ $\bar{x},\bar{x},\bar{z};$ $\bar{z},\bar{x},\bar{x};$ $\bar{x},\bar{z},\bar{x};$
$x,\bar{x},\bar{z};$ $z,\bar{x},\bar{x};$ $x,\bar{z},\bar{x};$ $\bar{x},x,z;$ $\bar{z},x,x;$ $\bar{x},z,x;$
$\bar{x},x,\bar{z};$ $\bar{z},x,\bar{x};$ $\bar{x},z,\bar{x};$ $x,\bar{x},z;$ $z,\bar{x},x;$ $x,\bar{z},x;$
$\bar{x},\bar{x},z;$ $\bar{z},\bar{x},x;$ $\bar{x},\bar{z},x;$ $x,x,\bar{z};$ $z,x,\bar{x};$ $x,z,\bar{x}.$

24   l m

$\tfrac{1}{2},y,z;$ $z,\tfrac{1}{2},y;$ $y,z,\tfrac{1}{2};$ $\tfrac{1}{2},z,y;$ $y,\tfrac{1}{2},z;$ $z,y,\tfrac{1}{2};$
$\tfrac{1}{2},\bar{y},\bar{z};$ $z,\tfrac{1}{2},\bar{y};$ $\bar{y},\bar{z},\tfrac{1}{2};$ $\tfrac{1}{2},\bar{z},\bar{y};$ $\bar{y},\tfrac{1}{2},\bar{z};$ $\bar{z},\bar{y},\tfrac{1}{2};$
$\tfrac{1}{2},y,\bar{z};$ $\bar{z},\tfrac{1}{2},y;$ $y,\bar{z},\tfrac{1}{2};$ $\tfrac{1}{2},\bar{z},y;$ $y,\tfrac{1}{2},\bar{z};$ $\bar{z},y,\tfrac{1}{2};$
$\tfrac{1}{2},\bar{y},z;$ $z,\tfrac{1}{2},\bar{y};$ $\bar{y},z,\tfrac{1}{2};$ $\tfrac{1}{2},z,\bar{y};$ $\bar{y},\tfrac{1}{2},z;$ $z,\bar{y},\tfrac{1}{2}.$

24   k m

$0,y,z;$ $z,0,y;$ $y,z,0;$ $0,z,y;$ $y,0,z;$ $z,y,0;$
$0,\bar{y},\bar{z};$ $\bar{z},0,\bar{y};$ $\bar{y},\bar{z},0;$ $0,\bar{z},\bar{y};$ $\bar{y},0,\bar{z};$ $\bar{z},\bar{y},0;$
$0,y,\bar{z};$ $\bar{z},0,y;$ $y,\bar{z},0;$ $0,\bar{z},y;$ $y,0,\bar{z};$ $\bar{z},y,0;$
$0,\bar{y},z;$ $z,0,\bar{y};$ $\bar{y},z,0;$ $0,z,\bar{y};$ $\bar{y},0,z;$ $z,\bar{y},0.$

12   j mm

$\tfrac{1}{2},x,x;$ $x,\tfrac{1}{2},x;$ $x,x,\tfrac{1}{2};$ $\tfrac{1}{2},x,\bar{x};$ $\bar{x},\tfrac{1}{2},x;$ $x,\bar{x},\tfrac{1}{2};$
$\tfrac{1}{2},\bar{x},\bar{x};$ $\bar{x},\tfrac{1}{2},\bar{x};$ $\bar{x},\bar{x},\tfrac{1}{2};$ $\tfrac{1}{2},\bar{x},x;$ $x,\tfrac{1}{2},\bar{x};$ $\bar{x},x,\tfrac{1}{2}.$

12   i mm

$0,x,x;$ $x,0,x;$ $x,x,0;$ $0,x,\bar{x};$ $\bar{x},0,x;$ $x,\bar{x},0;$
$0,\bar{x},\bar{x};$ $\bar{x},0,\bar{x};$ $\bar{x},\bar{x},0;$ $0,\bar{x},x;$ $x,0,\bar{x};$ $\bar{x},x,0.$

12   h mm

$x,\tfrac{1}{2},0;$ $0,x,\tfrac{1}{2};$ $\tfrac{1}{2},0,x;$ $x,0,\tfrac{1}{2};$ $\tfrac{1}{2},x,0;$ $0,\tfrac{1}{2},x;$
$\bar{x},\tfrac{1}{2},0;$ $0,\bar{x},\tfrac{1}{2};$ $\tfrac{1}{2},0,\bar{x};$ $\bar{x},0,\tfrac{1}{2};$ $\tfrac{1}{2},\bar{x},0;$ $0,\tfrac{1}{2},\bar{x}.$

8   g $3m$

$x,x,x;$ $x,\bar{x},\bar{x};$ $\bar{x},x,\bar{x};$ $\bar{x},\bar{x},x;$
$\bar{x},\bar{x},\bar{x};$ $\bar{x},x,x;$ $x,\bar{x},x;$ $x,x,\bar{x}.$

12.7   Selected Problems

1. (a) For the crystal structure shown below on the left, identify the space group and list the symmetry elements.

   (b) Identify the high symmetry points (and axes), and list the group of the wave vector at these high symmetry points (and axes).

   (c) Using the space group identified in (a), explain the diagrams for this space group as shown in the International Crystallography Tables.

   (d) Using the tables in (c), find the atom sites and site symmetries for the structure shown in (a).

2. (a) List the real space symmetry operations of the non-symmorphic two-dimensional square space group $p4gm$ (#12).

   (b) Explain the diagrams and the point symmetry entries for space group #12 ($p4gm$) in Fig. 12.20 which was taken from the International Crystallography Tables.

3. Show that in the diamond structure, the product of two symmetry operations involving translations τ yields a symmetry element with no translations

$$\{\alpha|\tau\}\{\beta|\tau\} = \{\gamma|0\}$$

where $\vec{\tau} = (1, 1, 1)a/4$. What is the physical significance of this result?

4. Consider the crystal structure in the diagram for Nb_3Sn, a proto-type superconductor with the A–15 (or β–W) structure used for high field superconducting magnet applications.

(a) List the symmetry elements of the space group.

(b) What is the space group designation? (Use the notation of the International Crystallography Tables.)

Chapter 13

Group of the Wave Vector and Bloch's Theorem

One of the most important applications of group theory to solid state physics relates to the symmetries and degeneracies of the dispersion relations, especially at high symmetry points in the Brillouin zone. The classification of these symmetry properties involves the **group of the wave vector**, which is the subject of this chapter. The group of the wave vector is important because it is the way in which both the **point group symmetry** and the **translational symmetry** of the crystal lattice are incorporated into the formalism that describes elementary excitations in a solid.

13.1 Introduction

If we have symmetry operations $\{R_\alpha|\tau\}$ that leave the periodic potential $V(\vec{r})$ invariant,

$$\{R_\alpha|\tau\}V(\vec{r}) = V(\vec{r}) \tag{13.1}$$

this has important implications on the form of the wave function $\psi(\vec{r})$ which satisfies Bloch's theorem (see §13.2). In particular if we consider only translation operations $\{\varepsilon|\tau\}$, we have an Abelian group because all translations

$$\hat{P}_{\{\varepsilon|\tau\}}\psi(\vec{r}) = \psi(\vec{r} + \vec{\tau}) \tag{13.2}$$

345

commute with each other.

Definition:

Since the translation operation $\vec{\tau}$ can be written in terms of translations over unit vectors $\vec{a}_i$

$$\vec{\tau} = \sum_{i=1}^{3} n_i \vec{a}_i,$$

we can think of the translation operators in each of the $\vec{a}_i$ directions as the commuting operators:

$$\{\varepsilon|\tau\} = \{\varepsilon|\tau_1\}\{\varepsilon|\tau_2\}\{\varepsilon|\tau_3\} \tag{13.3}$$

where $\vec{\tau}_i = n_i \vec{a}_i$. The commutativity of the $\{\varepsilon|\tau_i\}$ operations gives three commuting cyclic subgroups. It is convenient to use periodic boundary conditions for these cyclic subgroups. Since these subgroups are Abelian, all irreducible representations are 1-dimensional and have matrix representations or characters which are appropriate roots of unity—e.g., $e^{ik_1 n_1 a_1}$. Then the wave vector $k_1 = 2\pi m_1/L_1$ describes the irreducible representation where m_1 is an integer, and L_1 is the length of the crystal in direction $\vec{a}_1$. In this context, the wave vector serves as a quantum number for the translation operator. With this background, we can prove **Bloch's theorem**.

13.2   Bloch's Theorem

Theorem:

If an eigenfunction ψ_k transforms under the translation group according to the irreducible representation labeled by k, then $\psi_k(\vec{r})$ obeys the relation

$$\{\varepsilon|\tau\}\psi_k(\vec{r}) = \psi_k(\vec{r} + \vec{\tau}) = e^{i\vec{k}\cdot\vec{\tau}}\psi_k(\vec{r}) \tag{13.4}$$

and $\psi_k(\vec{r})$ can be written in the form

$$\psi_k(\vec{r}) = e^{i\vec{k}\cdot\vec{r}} u_k(\vec{r}) \tag{13.5}$$

where $u_k(\vec{r} + \vec{\tau}) = u_k(\vec{r})$ has the full translational symmetry of the crystal.

Proof:

Since the translation group is Abelian, all the elements of the group commute and all the irreducible representations are 1-dimensional. The requirement of the **periodic boundary condition** can be written as

$$\{\varepsilon|\tau_1 + NL_1\} = \{\varepsilon|\tau_1\} \tag{13.6}$$

where N is an integer and L_1 is the length of the crystal along basis vector $\vec{a}_1$. This results in the one-dimensional matrix representation for translation operator $\vec{\tau}_i = n_i \vec{a}_i$ of

$$D^{k_1}(n_1 a_1) = e^{ik_1 n_1 a_1} = e^{ik_1 \tau_1} \tag{13.7}$$

since

$$\hat{P}_R \psi_k(\vec{r}) = \psi_k(\vec{r}) D^k(R) \tag{13.8}$$

where $k_1 = 2\pi m_1/L_1$ corresponds to the m_1^{th} irreducible representation and $m_1 = 1, 2, \ldots, L_1/a_1$. For each m_1, there is a unique k_1, so that each irreducible representation is labeled by either m_1 or k_1, as indicated above.

We now extend these arguments to three dimensions. For a general translation

$$\vec{\tau} = \sum_{i=1}^{3} n_i \vec{a}_i \tag{13.9}$$

the matrix representation or character for the $(m_1 m_2 m_3)^{th}$ irreducible representation is

$$D^{k_1}(n_1 a_1) D^{k_2}(n_2 a_2) D^{k_3}(n_3 a_3) = e^{ik_1 n_1 a_1} e^{ik_2 n_2 a_2} e^{ik_3 n_3 a_3} = e^{i\vec{k}\cdot\vec{\tau}} \tag{13.10}$$

since

$$\{\varepsilon|\tau\} = \{\varepsilon|\tau_1\}\{\varepsilon|\tau_2\}\{\varepsilon|\tau_3\}. \tag{13.11}$$

Thus our basic formula $P_R \psi_j = \sum_\alpha \psi_\alpha D(R)_{\alpha j}$ yields

$$\{\varepsilon|\tau\}\psi(\vec{r}) = \psi(\vec{r}) e^{i\vec{k}\cdot\vec{\tau}} = e^{i\vec{k}\cdot\vec{\tau}} \psi(\vec{r}) = \psi(\vec{r} + \vec{\tau}) \tag{13.12}$$

since the representations are all 1-dimensional. This result is Bloch's theorem where we often write $\vec{\tau} = \vec{R}_n$ in terms of the lattice vector $\vec{R}_n$. This derivation shows that the phase factor $e^{i\vec{k}\cdot\vec{\tau}}$ is the eigenvalue of the translation operator $\{\varepsilon|\tau\}$.

Because of Bloch's theorem, the wave function $\psi(\vec{r})$ can be written in the form

$$\psi_k(\vec{r}) = e^{i\vec{k}\cdot\vec{r}}u_k(\vec{r}) \tag{13.13}$$

where $u_k(\vec{r})$ exhibits the full translational symmetry of the crystal. This result follows from:

$$\psi_k(\vec{r}+\vec{R}_n) = e^{i\vec{k}\cdot(\vec{r}+\vec{R}_n)}u_k(\vec{r}+\vec{R}_n) = e^{i\vec{k}\cdot\vec{R}_n}\left[e^{i\vec{k}\cdot\vec{r}}u_k(\vec{r})\right] \tag{13.14}$$

where the first equality in Eq. 13.14 is obtained simply by substitution in Eq. 13.13 and the second equality follows from Bloch's theorem. In these terms, Bloch's theorem is simply a statement of the translational symmetry of a crystal.

The wave vector $\vec{k}$ has a special significance as the **quantum number of translation** and provides a label for the irreducible representations of the translation group. If the crystal has a length L_i on a side so that n_0 different lattice translations can be made for each direction $\vec{a}_i$, then the number of $\vec{k}$ vectors must be limited to

$$k_x, k_y, k_z = 0, \pm\frac{2\pi}{n_0 a}, \pm\frac{4\pi}{n_0 a}, \ldots, \pm\frac{\pi}{a} \tag{13.15}$$

in order to insure that the number of irreducible representations is equal to the number of classes. Since the group for translations is Abelian, every group element is in a class by itself, so that the **number of irreducible representations must equal the number of possible translations**. Since the number of translation operators is very large ($\sim 10^{23}$), the quantum numbers for translations are discrete, but very closely spaced, and form a quasi-continuum of points in reciprocal space.

We note that all of these $\vec{k}$-vectors are contained within the 1st Brillouin zone. Thus, if we consider a vector in the extended zone $\vec{k} + \vec{K}$ where $\vec{K}$ is a reciprocal lattice vector, the appropriate phase factor in Bloch's theorem is

$$e^{i(\vec{k}+\vec{K})\cdot\vec{R}_n} = e^{i\vec{k}\cdot\vec{R}_n} \tag{13.16}$$

since $\vec{K}\cdot\vec{R}_n = 2\pi N$ where N is an integer.

13.3 Symmetry of $\vec{k}$ Vectors and the Group of the Wave Vector

It is convenient to deal with the symmetries of the reciprocal lattice because the quantum number of translation $\vec{k}$ is measured in reciprocal space. From the definition of the reciprocal lattice vector $\vec{K}_j$ we have

$$\vec{R}_n \cdot \vec{K}_j = 2\pi N_{nj} = 2\pi N_1 \qquad (13.17)$$

where N_{nj} is an integer depending on n, j.

If α is a symmetry operator of the point group of the crystal, then $\alpha \vec{R}_n$ leaves the crystal invariant. If $\vec{R}_n$ is a translation operator, then $\alpha \vec{R}_n$ is also a translation operator (lattice vector). Likewise $\alpha \vec{K}_j$ is a translation operator in reciprocal space. Since $\alpha \vec{R}_n$ is a lattice vector

$$(\alpha \vec{R}_n) \cdot \vec{K}_j = 2\pi N_2 \qquad (13.18)$$

where N_2 is an integer, not necessarily the same integer as N_1 in Eq. 13.17. Since α^{-1} is also a symmetry operation of the group, we have

$$(\alpha^{-1} \vec{R}_n) \cdot \vec{K}_j = 2\pi N_3 \qquad (13.19)$$

and again N_3 is not necessarily the same integer as N_1 or N_2. Furthermore, any scalar product (being a constant) must be invariant under any point symmetry operation. Thus if we perform the same symmetry operation on each member of the scalar product in Eq. 13.19, then the scalar product remains invariant

$$\alpha(\alpha^{-1} \vec{R}_n) \cdot (\alpha \vec{K}_j) = 2\pi N_3 = \vec{R}_n \cdot (\alpha \vec{K}_j). \qquad (13.20)$$

Equations 13.18–13.20 tell us that if $\vec{K}_j$ is a reciprocal lattice vector and if $\vec{R}_n$ and $\alpha^{-1} \vec{R}_n$ are lattice vectors, then $\alpha \vec{K}_j$ is also a reciprocal lattice vector. Furthermore, the **effect of α on a direct lattice vector $\vec{R}_n$ is equivalent to the operation α^{-1} on the corresponding reciprocal lattice vector $\vec{K}_j$.**

Let us now consider the action of the point group operations on a general vector $\vec{k}$ in reciprocal space, not necessarily a reciprocal lattice vector. The set of wave vectors $\vec{k}'$ which are obtained by carrying

out all the point group operations on $\vec{k}$ is called the **star of $\vec{k}$**. If $\vec{k}$ **is a general point in the Brillouin zone**, there will be only one symmetry element, namely the identity, which takes $\vec{k}$ into itself. On the other hand, if the $\vec{k}$-vector under consideration lies on a symmetry axis or is at a high symmetry point in the Brillouin zone, then perhaps several of the point group operations will transform $\vec{k}$ into itself or into an equivalent $\vec{k}$-vector $\vec{k} + \vec{K}_i$. **The set of point group operations which transform $\vec{k}$ into itself or into an equivalent $\vec{k}$-vector form the group of the wave vector**. Clearly, all the symmetry operations of the point group take the point $\vec{k} = 0$ into itself so that the point group itself forms the group of the wave vector at $\vec{k} = 0$. The group of the wave vector for non-zone center $\vec{k}$-vectors ($\vec{k} \neq 0$) is a subgroup of the point group for $\vec{k} = 0$.

An informative example for the formation of the group of the wave vector for various $\vec{k}$-vectors is provided by the 2-dimensional square lattice. Here the point group is D_4 and the symmetry operations are E, $C_2 = 2C_4^2$, $2C_4$, $2C_2'$, $2C_2''$ (diagonals). The various $\vec{k}$-vectors in the star of $\vec{k}$ are indicated in the diagrams in Fig. 13.1 for the 2-dimensional square lattice. The group elements for the group of the wave vector in each case are indicated within the parenthesis. The top three diagrams are for $\vec{k}$-vectors to interior points within the first Brillouin zone and the lower set of three diagrams are for $\vec{k}$-vectors to the Brillouin zone boundary. Thus the star of $\vec{k}$ shown in Fig. 13.1 is formed by consideration of $\alpha\vec{k}$ for all α in the point group. The group of the wave vector is formed by those α for which $\alpha\vec{k} = \vec{k} + \vec{K}_j$, where $\vec{K}_j$ is a reciprocal lattice vector (including $\vec{K}_j = 0$).

We will now consider the effect of the symmetry operations on $\vec{k}$ with regard to the eigenfunctions of Schrödinger's equation. We already know from Bloch's theorem that the action of any pure translation operator $T(\vec{R}_n)$ yields a wave function $e^{i\vec{k}\cdot\vec{R}_n}\psi_k(\vec{r})$. There will be as many wave functions of this form as there are translation vectors, each corresponding to the energy $E(\vec{k})$. These Bloch functions provide basis functions for irreducible representations for the group of the wave vector. If $\vec{k}$ is a general point in the Brillouin zone, then the star of $\vec{k}$ contains wave vectors which are all equivalent to $\vec{k}$ from a physical standpoint. The space group for a general wave vector $\vec{k}$ will

$\vec{k}$ **to an interior point in the Brillouin zone**

arbitrary $\vec{k}$ to BZ interior:
8 $\vec{k}$ in star; (E)

symmetrical $\vec{k}$ to BZ interior:
4 $\vec{k}$ in star; (E, C_2)

symmetrical $\vec{k}$ to BZ interior:
4 $\vec{k}$ in star; (E, C_2'')

$\vec{k}$ **to a point on the Brillouin zone boundary**

arbitrary $\vec{k}$ to BZ boundary:
4 $\vec{k}$ in star; (E, C_2)

symmetrical $\vec{k}$ to BZ boundary:
4 $\vec{k}$ in star; $(E, C_2, 2C_2')$

symmetrical $\vec{k}$ to BZ boundary:
4 $\vec{k}$ in star; $(E, C_2, 2C_4, 2C_2', 2C_2'')$
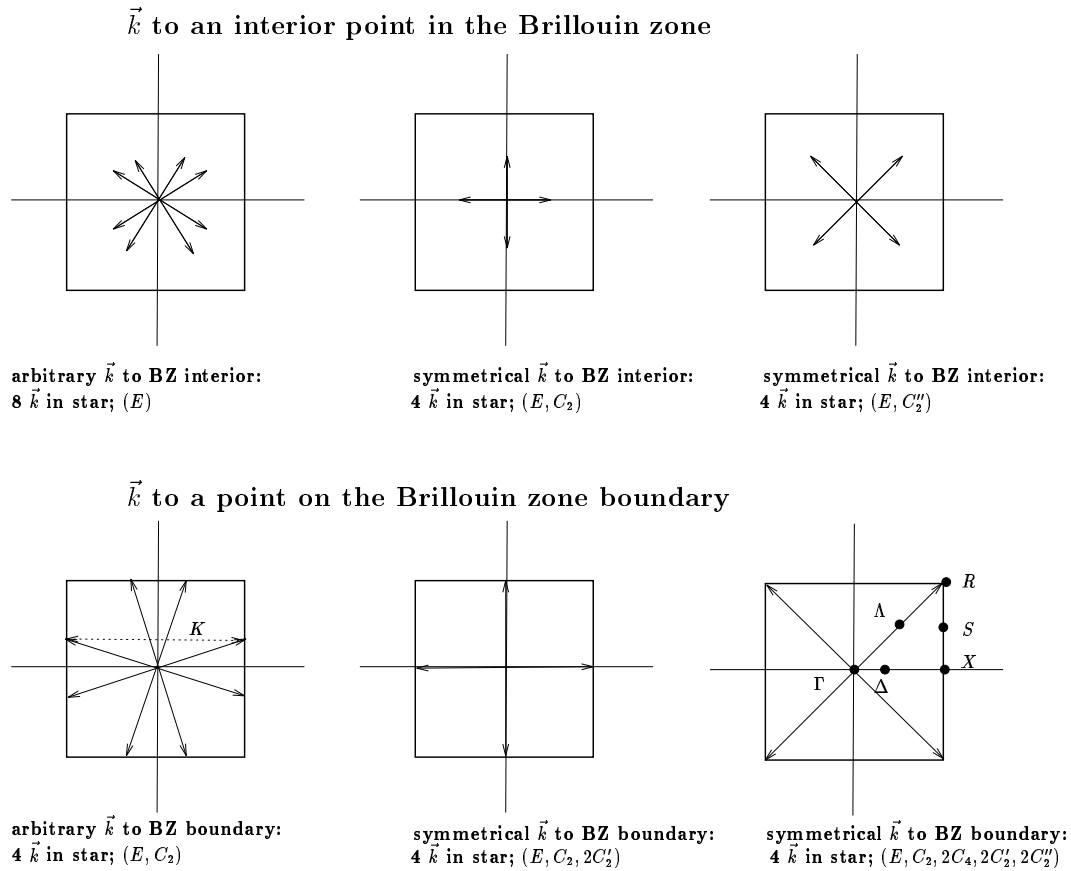
Figure 13.1: Illustration of the star of $\vec{k}$ for various wave vectors in a simple 2D square Brillouin zone. The top 3 diagrams are for $\vec{k}$-vectors to an interior point in the Brillouin zone, while the bottom 3 diagrams are for wave vectors extending to the Brillouin zone boundary. In each case the elements for the group of the wave vector are given in parentheses.

Table 13.1: Summary of the real and reciprocal lattice vectors for the two-dimensional Bravais lattices.

Type	Translation Vectors		Reciprocal Lattice Vectors	
	$\vec{\tau}_1$	$\vec{\tau}_2$	$\vec{g}_1$	$\vec{g}_2$
oblique, p	$(a, 0)$	$b(\cos\theta, \sin\theta)$	$\frac{2\pi}{a}(1, -\cot\theta)$	$\frac{2\pi}{b}(0, \csc\theta)$
rectangular, p	$(a, 0)$	$(0, b)$	$\frac{2\pi}{a}(1, 0)$	$\frac{2\pi}{b}(0, 1)$
rectangular, c	$(\frac{a}{2}, \frac{b}{2})$	$(-\frac{a}{2}, \frac{b}{2})$	$2\pi(\frac{1}{a}, \frac{1}{b})$	$2\pi(-\frac{1}{a}, \frac{1}{b})$
square, p	$(a, 0)$	$(0, a)$	$\frac{2\pi}{a}(1, 0)$	$\frac{2\pi}{a}(0, 1)$
hexagonal, p	$(0, -a)$	$a(\frac{\sqrt{3}}{2}, \frac{1}{2})$	$\frac{2\pi}{a}(\frac{1}{\sqrt{3}}, -1)$	$\frac{2\pi}{a}(\frac{2}{\sqrt{3}}, 0)$

however contain only the symmetry elements $\{\varepsilon|\vec{R}_n\}$, since in this case all the $\vec{k}$-vectors are distinct. For a wave vector with higher symmetry where the operations $\beta\vec{k} = \vec{k} + \vec{K}_j$ transform $\vec{k}$ into an equivalent wave vector, the space group of the wave vector contains $\{\beta|\vec{R}_n\}$ and the energy at equivalent $\vec{k}$ points must be equal. If the point group of the wave vector contains irreducible representations that have more than one dimension, then degeneracy in the energy bands will occur. Thus bands tend to "stick together" along high symmetry axes and at high symmetry points.

We will now illustrate the group of the wave vector for the 3-dimensional simple cubic lattice $Pm3m$ (O_h^1) #221, the BCC lattice $Im3m$ (O_h^9) #229 and the FCC lattice $Fm3m$ (O_h^5) #225.

13.3.1 Reciprocal Lattice

Reciprocal Lattice Vectors
If $\vec{\tau}_1$ and $\vec{\tau}_2$ are the primitive translation vectors, then the reciprocal lattice vectors $\vec{g}_1$ and $\vec{g}_2$ are determined by the relation

$$\vec{g}_i \cdot \vec{\tau}_j = 2\pi\delta_{ij}(i, j = 1, 2) \tag{13.21}$$

and the wave vector $\vec{k} = k_1\vec{g}_1 + k_2\vec{g}_2$. Table 13.1 contains the translation vectors and the reciprocal lattice vectors for the five two-dimensional Bravais lattices. Vectors $\vec{\tau}_1$ and $\vec{\tau}_2$ are expressed in terms of unit vectors
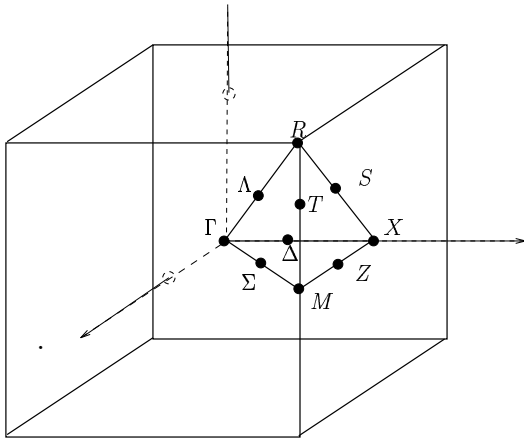
Figure 13.2: Brillouin zone for a simple cubic lattice showing the high symmetry points and axes.
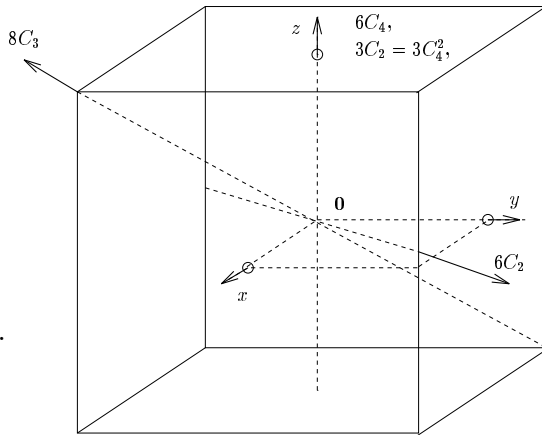
Figure 13.3: Symmetry operations for the group O.

along the orthogonal x and y directions. Vectors $\vec{g}_1$ and $\vec{g}_2$ are expressed in terms of unit vectors along the orthogonal k_x and k_y directions.

13.4 Simple Cubic Lattice

In Fig. 13.3 we see the Brillouin zone for the simple cubic lattice belonging to the space group $Pm3m$ (O_h^1) #221. The high symmetry points and axes are labeled using the standard notation. The symmetry operations of the point group are the symmetry operations of the O_h group indicated in Fig. 13.3 compounded with full inversion symmetry, $O_h = O \otimes i$. The point group corresponding to the group of the

Table 13.2: Character table for the cubic group O_h.

Repr.	Basis Functions	E	$3C_4^2$	$6C_4$	$6C_2$	$8C_3$	i	$3iC_4^2$	$6iC_4$	$6iC_2$	$8iC_3$
Γ_1	1	1	1	1	1	1	1	1	1	1	1
Γ_2	$\begin{cases} x^4(y^2-z^2)+ \\ y^4(z^2-x^2)+ \\ z^4(x^2-y^2) \end{cases}$	1	1	-1	-1	1	1	1	-1	-1	1
Γ_{12}	$\begin{cases} x^2-y^2 \\ 2z^2-x^2-y^2 \end{cases}$	2	2	0	0	-1	2	2	0	0	-1
Γ_{15}	x,y,z	3	-1	1	-1	0	-3	1	-1	1	0
Γ_{25}	$z(x^2-y^2)$, etc.	3	-1	-1	1	0	-3	1	1	-1	0
Γ_1'	$\begin{cases} xyz[x^4(y^2-z^2)+ \\ y^4(z^2-x^2)+ \\ z^4(x^2-y^2)] \end{cases}$	1	1	1	1	1	-1	-1	-1	-1	-1
Γ_2'	xyz	1	1	-1	-1	1	-1	-1	1	1	-1
Γ_{12}'	$xyz(x^2-y^2)$, etc.	2	2	0	0	-1	-2	-2	0	0	1
Γ_{15}'	$xy(x^2-y^2)$, etc.	3	-1	1	-1	0	3	-1	1	-1	0
Γ_{25}'	xy,yz,zx	3	-1	-1	1	0	3	-1	-1	1	0

wave vector at $\vec{k} = 0$ is the group O_h itself. The character table for O_h along with the basis functions for all the irreducible representations is given in Table 13.2. For the simple cubic structure this character table applies to the group of the wave vector for the Γ point and the R point, both of which have the full symmetry operations of the O_h point group (see the Brillouin zone in Fig. 13.2). We notice that to obtain basis functions for all the irreducible representations of the group O_h we need to include up to 6th order polynomials. The notation used in Table 13.2 is that traditionally used in the solid state physics literature. In this notation, Γ_{15} and Γ_{25} are odd while Γ_{15}' and Γ_{25}' are even. To get around this apparent non-uniformity of notation, we often use $\Gamma_i^{\pm}$ (e.g., $\Gamma_{15}^{\pm}$) to emphasize the parity of a wavefunction for the cubic groups.

The group of the wave vector at a point along the Δ axis (for example) has fewer symmetry operations than the group of the wave vector $\vec{k} = 0$. The symmetry operations for a point along the Δ axis for the simple cubic lattice are those of a square, rather than those of a cube and are the operations of C_{4v}. The multiplication table for the elements of the point group C_{4v} which is appropriate for a reciprocal lattice point Δ along the $\hat{x}$ axis.

Table 13.3: Character table for the group of the wave-vector Δ.[†]

Representation	Basis Functions	E	C_4^2	$2C_4$	$2iC_4^2$	$2iC_2$
Δ_1	$1, x, 2x^2 - y^2 - z^2$	1	1	1	1	1
Δ_2	$y^2 - z^2$	1	1	-1	1	-1
Δ_2'	yz	1	1	-1	-1	1
Δ_1'	$yz(y^2 - z^2)$	1	1	1	-1	-1
Δ_5	$y, z; xy, xz$	2	-2	0	0	0

Class		Operation		Designation	E	α	β	γ	δ	ε	ζ	η
E	x	y	z	E	E	α	β	γ	δ	ε	ζ	η
C_4^2	x	$-y$	$-z$	α	α	E	γ	β	ε	δ	η	ζ
$2C_4$	x	$-z$	y	β	β	γ	α	E	ζ	η	ε	δ
	x	z	$-y$	γ	γ	β	E	α	η	ζ	δ	ε
$2iC_4^2$	x	$-y$	z	δ	δ	ε	η	ζ	E	α	γ	β
	x	y	$-z$	ε	ε	δ	ζ	η	α	E	β	γ
$2iC_2$	x	$-z$	$-y$	ζ	ζ	η	δ	ε	β	γ	E	α
	x	z	y	η	η	ζ	ε	δ	γ	β	α	E

[†] The rule for using the multiplication table is that:

$$\alpha\beta = (x, -y, -z)(x, -z, y) = (x, -(-z), -(y)) = (x, z, -y) = \gamma$$

$$\beta\delta = (x, -z, y)(x, -y, z) = (x, z, y) = \eta$$

where the right operator (β) designates the row and the left operator (α) designates the column.

The character table (including basis functions) for the group of the wave vector for Δ, where $\vec{\Delta} = (\Delta, 0, 0)$ is along $\hat{x}$, is given in Table 13.3.

In Table 13.3 the C_4 rotation operation is along $\hat{x}$, the $2iC_4^2$ are along $\hat{y}, \hat{z}$, and the $2iC_2$ are along $\{011\}$. The basis functions in the character table can be found from inspection by taking linear combinations of (x^ℓ, y^m, z^n) following the discussion in Chapter 4. The basis functions for the lower symmetry groups (such as the group of Δ) are related to those of O_h by considering the basis functions of the point group O_h as reducible representations of the subgroup Δ, and decomposing these reducible representations into irreducible representations of the group Δ. For example Γ_{25}^+ of O_h is a reducible representation of C_{4v}

Table 13.4: Character table for the group of the wave vector Λ.

Character Table for the Λ Axis

$\Lambda = C_{3v}$	E	$2C_3$	$3iC_2$
Λ_1	1	1	1
Λ_2	1	1	-1
Λ_3	2	-1	0

and reduction of Γ_{25}^+ into irreducible representations of C_{4v} yields the compatibility relation

$$\left[\Gamma_{25}^+\right]_{O_h} \rightarrow \left[\Delta_{2'} + \Delta_5\right]_{C_{4v}}.$$

We note that yz is the longitudinal partner for $\vec{\Delta} = (\Delta, 0, 0)$ and corresponds to the irreducible representation Δ_2', while xy, xz are the transverse partners corresponding to Δ_5. The process of going from higher to lower symmetry defines the **compatibility relations** between irreducible representations of O_h and those of C_{4v}.

Character tables for all the high symmetry points for $\vec{k}$ vectors in the simple cubic lattice are given in this section. For example, the symmetry group for a wave vector along the (111) axis or Λ axis is C_{3v}. (See Fig. 13.2 on p. 353). The character table for a Λ point along the (111) direction with C_{3v} point group symmetry is given in Table 13.4. For a Λ point along the (111) direction, the $2C_3$ are along $\{111\}$, and the $3iC_2$ are along $(1\bar{1}0)$, $(10\bar{1})$, and $(0\bar{1}1)$ directions. For the Λ point we can do 3-fold rotations in both $\pm$ senses about ΓR. We can also do $180°$ rotations about 2-fold axes ΓM followed by inversion (see Fig. 13.2). By $\Gamma M'$ we mean the wave vector to the center of an adjacent cube edge. You will notice that a rotation by π about $\Gamma M'$ followed by inversion does not leave Λ invariant. Only 3 of the "$\Gamma M'$" axes are symmetry operations of the group; the other 3 such axes (like ΓM in the diagram) are not symmetry operations. Therefore instead of the symmetry operations $6iC_2$ which hold for the Γ and R points, the class $3iC_2$ for the group of the Λ point only has 3 symmetry elements.

In several instances, more than one high symmetry point in the

Table 13.5: Group of the wave vector for points M and X.

M	E	$2C_4^2$	$C_{4\perp}^2$	$2C_{4\perp}$	$2C_2$	i	$2iC_4^2$	$iC_{4\perp}^2$	$2iC_{4\perp}$	$2iC_2$
X	E	$2C_{4\perp}^2$	$C_{4\parallel}^2$	$2C_{4\parallel}$	$2C_2$	i	$2iC_{4\perp}^2$	$iC_{4\parallel}^2$	$2iC_{4\parallel}$	$2iC_2$
M_1, X_1	1	1	1	1	1	1	1	1	1	1
M_2, X_2	1	1	1	-1	-1	1	1	1	-1	-1
M_3, X_3	1	-1	1	-1	1	1	-1	1	-1	1
M_4, X_4	1	-1	1	1	-1	1	-1	1	1	-1
M_1', X_1'	1	1	1	1	1	-1	-1	-1	-1	-1
M_2', X_2'	1	1	1	-1	-1	-1	-1	-1	1	1
M_3', X_3'	1	-1	1	-1	1	-1	1	-1	1	-1
M_4', X_4'	1	-1	1	1	-1	-1	1	-1	-1	1
M_5, X_5	2	0	-2	0	0	2	0	-2	0	0
M_5', X_5'	2	0	-2	0	0	-2	0	2	0	0

Brillouin zone follows the same symmetry group–e.g., Δ and T (see Fig. 13.2). In considering point T, remember that any reciprocal lattice point separated by a reciprocal lattice vector from T is an equally good T point. The character table for the T-point is given in Table 13.3.

It can also happen that two symmetry points such as M and X belong to the same point group D_{4h}, but the symmetry operations for the two groups of the wave vector can refer to different axes of rotation as shown in Table 13.5. In the character Table 13.5, M and X both belong to the same point group D_{4h}, but the symmetry operations for the 2 points can refer to different rotation axes. The notation $C_{4\parallel}^2$ in Table 13.5 refers to a 2-fold axis ΓX while $2C_{4\perp}^2$ refers to the two 2-fold axes $\perp$ to ΓX. These are in different classes because in one case X is left exactly invariant, while in the other case X goes into an equivalent X point. To put it in more physical terms, if X is not exactly on the zone boundary but is at a Δ point arbitrarily close, the $C_{4\parallel}^2$ operation still holds, while the $2C_{4\perp}^2$ does not.

Character tables for other high symmetry points in the Brillouin zone for the simple cubic lattice (see Fig. 13.4) are given in Table 13.6 for the points Σ and S, and in Table 13.7 for point Z.

A word of explanation about the two C_4^2 operations in group C_{2v} which are in different classes. Consider a π rotation about the k_x axis; Z goes into an equivalent Z point on the Brillouin zone boundary. For symmetry operation iC_4^2 about the k_z axis, Z goes into itself identically,

Table 13.6: Character table for the group of the wave vector for points Σ and S

C_{2v}

Σ, S	E	C_2	iC_4^2	iC_2
Σ_1	1	1	1	1
Σ_2	1	1	-1	-1
Σ_3	1	-1	-1	1
Σ_4	1	-1	1	-1

Note that point S has extra symmetry because it is on the Brillouin zone (B.Z.) boundary.

——

Table 13.7: Character table for the group of the wave vector for the point Z

C_{2v}

		z	x	y
Z	E	C_4^2	iC_4^2	$iC_{4\perp}^2$
Z_1	1	1	1	1
Z_2	1	1	-1	-1
Z_3	1	-1	-1	1
Z_4	1	-1	1	-1
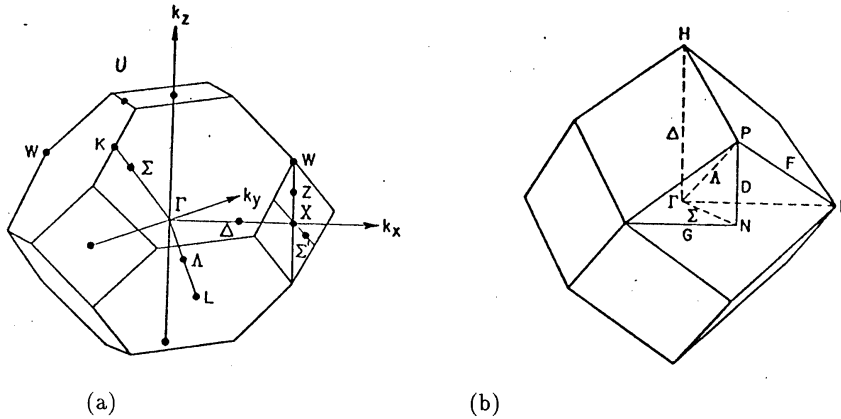
Figure 13.4: Brillouin zones for the (a) face-centered and (b) body-centered cubic lattices. Points and lines of high symmetry are indicated.

while for iC_4^2 about the k_y axis, Z goes into another Z point related to it by a reciprocal lattice vector.

13.5 High Symmetry Points and Axes and Their Character Tables for FCC and BCC Structures

The group of the wave vector for arbitrary $\vec{k}$ is a subgroup of the group of the wave vector $\vec{k} = 0$, which displays the full point group symmetry of the crystal. This situation applies to all crystal lattices, whether they are cubic, hexagonal, etc. The various character tables given in this section are for the B.C.C. (space group $Im3m$ (O_h^9) #229) and F.C.C. (space group $Fm3m$ (O_h^5) #225) structures. The basis functions are also given. The form of the basis functions is helpful in identifying s, p and d states. The subgroups of the group of the wave vector at $\vec{k} = 0$ are called the **small representations** in contrast to the full point group symmetry which is called the **large representation**.

Table 13.8: Character Table for the Group of the wave vector for X

Representation	Basis	E	$2C_{4\perp}^2$	$C_{4\parallel}^2$	$2C_{4\parallel}^2$	$2C_2$	i	$2iC_{4\perp}^2$	$iC_{4\parallel}^2$	$2iC_{4\parallel}$	$2iC_2$
X_1	$1, 2x^2-y^2-z^2$	1	1	1	1	1	1	1	1	1	1
X_2	y^2-z^2	1	1	1	-1	-1	1	1	1	-1	-1
X_3	yz	1	-1	1	-1	1	1	-1	1	-1	1
X_4	$yz(y^2-z^2)$	1	-1	1	1	-1	1	-1	1	1	-1
X_5	xy, xz	2	0	-2	0	0	2	0	-2	0	0
X_1'	$xyz(y^2-z^2)$	1	1	1	1	1	-1	-1	-1	-1	-1
X_2'	xyz	1	1	1	-1	-1	-1	-1	-1	1	1
X_3'	$x(y^2-z^2)$	1	-1	1	-1	1	-1	1	-1	1	-1
X_4'	x	1	-1	1	1	-1	-1	1	-1	-1	1
X_5'	y, z	2	0	-2	0	0	-2	0	2	0	0

Table 13.9: Character table for group of the wave vector for L.

Group of $L = (2\pi/a)\left(\frac{1}{2}, \frac{1}{2}, \frac{1}{2}\right)$

Representation	Basis	E	$2C_3$	$3C_2$	i	$2iC_3$	$3iC_2$
L_1	$1, xy+yz+xz$	1	1	1	1	1	1
L_2	$yz(y^2-z^2)+xy(x^2-y^2)+xz(z^2-x^2)$	1	1	-1	1	1	-1
L_3	$2x^2-y^2-z^2; y^2-z^2$	2	-1	0	2	-1	0
L_1'	$x(y^2-z^2)+y(z^2-x^2)+z(x^2-y^2)$	1	1	1	-1	-1	-1
L_2'	$x+y+z$	1	1	-1	-1	-1	1
L_3'	$y-z; 2x-y-z$	2	-1	0	-2	1	0

Table 13.10: Character table for group of the wave vector for W.

Group of $W = (2\pi/a)(1, \frac{1}{2}, 0)$

Representation	Basis	E	C_4^2	$2C_2$	$2iC_4$	$2iC_4^2$
W_1	$1, 2y^2-x^2-z^2$	1	1	1	1	1
W_1'	xz	1	1	1	-1	-1
W_2	xyz	1	1	-1	1	-1
W_2'	y, z^2-x^2	1	1	-1	-1	1
W_3	$xy, yz; x, z$	2	-2	0	0	0

Table 13.11: Character table for group of the wave vector for Σ.

Character Table, Group $\Sigma = (2\pi/a)(x, x, 0)$

Representation	Basis	E	C_2	iC_4^2	iC_2
Σ_1	$1, x + y$	1	1	1	1
Σ_2	$z(x - y);\ z(x^2 - y^2)$	1	1	-1	-1
Σ_3	$z;\ z(x + y)$	1	-1	-1	1
Σ_4	$x - y;\ x^2 - y^2$	1	-1	1	-1

Table 13.12: Character table for group of the wave vector for G, K, U, D, Z, S.

Character Tables of G, K, U, D, Z, S

	Z	E	C_4^2	iC_4^2	$iC_{4\perp}^2$
Represen-	G, K, U, S	E	C_2	iC_4^2	iC_2
tation	D	E	C_4^2	iC_2	$iC_{2\perp}$
K_1	$1, x + y$	1	1	1	1
K_2	$x(x - y), z(x^2 - y^2)$	1	1	-1	-1
K_3	$z, z(x + y)$	1	-1	-1	1
K_4	$x - y;\ x^2 - y^2$	1	-1	1	-1

$$G = \frac{2\pi}{a}(\tfrac{1}{2} + x, \tfrac{1}{2} - x, 0) \quad \text{(bcc)} \qquad K = \frac{2\pi}{a}(\tfrac{3}{4}, \tfrac{3}{4}, 0) \quad \text{(fcc)}$$
$$U = \frac{2\pi}{a}(1, \tfrac{1}{4}.\tfrac{1}{4}) \quad \text{(fcc)} \qquad\qquad D = \frac{2\pi}{a}(\tfrac{1}{2}, \tfrac{1}{2}, x) \quad \text{(bcc)}$$
$$Z = \frac{2\pi}{a}(1, x, 0) \quad \text{(fcc)} \qquad\qquad S = \frac{2\pi}{a}(1, x, x) \quad \text{(fcc)}$$

For a given wave vector which is contained within the first Brillouin zone for each of the simple cubic, FCC and BCC lattices, the character table for the group of the wave vector at $\vec{k} = 0$ is the same for all three kinds of lattices. Having enumerated the symmetry operations for $\vec{k}$-vectors in various cubic lattices, we are now ready to discuss the effect of point group operations on the eigenfunctions of the Hamiltonian for a solid with a periodic potential.

Table 13.13: Character table for group of the wave vector for P.

Group $P = (2\pi/a)(\frac{1}{2}, \frac{1}{2}, \frac{1}{2})$ for the BCC lattice

Representation	Basis	E	$3C_4^2$	$8C_3$	$6iC_4$	$6iC_2$
P_1	$1, xyz$	1	1	1	1	1
P_2	$x^4(y^2 - z^2) + y^4(z^2 - x^2) +$	1	1	1	-1	-1
	$z^4(x^2 - y^2)$					
P_3	$x^2 - y^2, xyz(x^2 - y^2)$	2	2	-1	0	0
P_4	$x, y, z; xy; yz; zx$	3	-1	0	-1	1
P_5	$z(x^2 - y^2)$	3	-1	0	1	-1

Table 13.14: Character table for group of the wave vector for N.

Group of $N = (2\pi/a)(\frac{1}{2}, \frac{1}{2}, 0)$ for the BCC lattice

Representation	Basis	E	C_4^2	$C_{2\parallel}$	$C_{2\perp}$	i	iC_4^2	$iC_{2\perp}$	$iC_{2\parallel}$
N_1	$1, xy, 3z^2 - r^2$	1	1	1	1	1	1	1	1
N_2	$z(x - y)$	1	-1	1	-1	1	-1	-1	1
N_3	$z(x + y)$	1	-1	-1	1	1	-1	1	-1
N_4	$x^2 - y^2$	1	1	-1	-1	1	1	-1	-1
N_1'	$x + y$	1	-1	1	-1	-1	1	1	-1
N_2'	$z(x^2 - y^2)$	1	1	1	1	-1	-1	-1	-1
N_3'	z	1	1	-1	-1	-1	-1	1	1
N_4'	$x - y$	1	-1	-1	1	-1	1	-1	1

Table 13.15: Character table for group of the wave vector for Λ and F.

$F = (2\pi/a)(\frac{1}{2} + x, \frac{1}{2} - x, \frac{1}{2} - x);\ 0 \leq x \leq \frac{1}{2}$		E	$2C_3$	$3iC_2$
Representation	Basis			
Λ_1	$1, x + y + z$	1	1	1
Λ_2	$x(y^2 - z^2) + y(z^2 - x^2) + z(x^2 - y^2)$	1	1	-1
Λ_3	$2x - y - z, y - z$	2	-1	0

13.6 Effect of Translations and Point Group Operations on Bloch Functions

We have considered the effect of the translation operator $\{\varepsilon|\tau\}$ on the eigenfunctions for an electron in a periodic potential

$$\hat{P}_{\{\varepsilon|\tau\}}\psi_k(\vec{r}) = e^{i\vec{k}\cdot\vec{\tau}}\psi_k(\vec{r}). \tag{13.22}$$

The effect of a point group operation on this eigenfunction is

$$\hat{P}_{\{R_\alpha|0\}}\psi_k(\vec{r}) = \hat{P}_{\{R_\alpha|0\}}e^{i\vec{k}\cdot\vec{r}}u_k(\vec{r}) \tag{13.23}$$

in which we have written the eigenfunction in the Bloch form. Since the effect of a point group operation on a function is equivalent to preserving the form of the function and rotating the coordinate system in the opposite sense, to maintain invariance of scalar products we require

$$\vec{k}\cdot R_\alpha^{-1}(\vec{r}) = R_\alpha(\vec{k})\cdot\vec{r}. \tag{13.24}$$

If we now define $u_{R_\alpha k}(\vec{r}) \equiv u_k(R_\alpha^{-1}\vec{r})$ and denote $R_\alpha\vec{k} \equiv \vec{k}'$, then we have

$$\hat{P}_{\{R_\alpha|0\}}\psi_k(\vec{r}) = e^{iR_\alpha\vec{k}\cdot\vec{r}}u_{R_\alpha k}(\vec{r}) \equiv \psi_{R_\alpha k}(\vec{r}) \tag{13.25}$$

which we will now show to be of the Bloch form by operating with the translation operator on $\psi_{R_\alpha k}(\vec{r})$

$$\begin{aligned}
\hat{P}_{\{\varepsilon|\tau\}}\psi_{R_\alpha k}(\vec{r}) &= \hat{P}_{\{\varepsilon|\tau\}}[e^{iR_\alpha\vec{k}\cdot\vec{r}}u_k(R_\alpha^{-1}\vec{r})] \\
&= e^{iR_\alpha\vec{k}\cdot(\vec{r}+\vec{\tau})}u_k(R_\alpha^{-1}\vec{r} + R_\alpha^{-1}\vec{\tau}). \tag{13.26}
\end{aligned}$$

Because of the periodicity of $u_k(\vec{r})$ we have

$$u_{R_\alpha k}(\vec{r}+\vec{\tau}) = u_k(R_\alpha^{-1}\vec{r} + R_\alpha^{-1}\vec{\tau}) = u_k(R_\alpha^{-1}\vec{r}) \equiv u_{R_\alpha k}(\vec{r}) \tag{13.27}$$

so that

$$\hat{P}_{\{\varepsilon|\tau\}}\psi_{R_\alpha k}(\vec{r}) = e^{iR_\alpha\vec{k}\cdot\vec{\tau}}\psi_{R_\alpha k}(\vec{r}) \tag{13.28}$$

where $u_{R_\alpha k}(\vec{r})$ is periodic in the direct lattice. The **eigenfunctions** $\psi_{R_\alpha k}(\vec{r})$ thus forms **basis functions** for the $R_\alpha k^{th}$ **irreducible representation** of the translation group T. As we saw in §13.3 on p. 349,

the set of distinct wave vectors in $\vec{k}$-space which can be generated by operating on one $\vec{k}$ vector by all the symmetry elements of the point group g is called the "star of $\vec{k}$" (see Fig. 13.1).

From the above arguments we have

$$
\begin{aligned}
\hat{P}_{\{R_\alpha|\tau\}}\psi_k(\vec{r}) &= \hat{P}_{\{\varepsilon|\tau\}}\hat{P}_{\{R_\alpha|0\}}\psi_k(\vec{r}) \\
&= \hat{P}_{\{\varepsilon|\tau\}}\psi_{R_\alpha k}(\vec{r}) \\
&= e^{iR_\alpha \vec{k}\cdot\vec{\tau}}\psi_{R_\alpha k}(\vec{r}).
\end{aligned} \tag{13.29}
$$

Similarly we obtain

$$
\hat{P}_{\{R_\beta|\tau'\}}\psi_{R_\alpha k}(\vec{r}) = e^{iR_\beta R_\alpha \vec{k}\cdot\vec{\tau}'}\psi_{R_\beta R_\alpha k}(\vec{r}). \tag{13.30}
$$

Thus the set of eigenfunctions $\{\psi_{R_\alpha k}(\vec{r})\}$ obtained by taking the star of $\vec{k}$ spans the invariant subspace of the point group g since $R_\beta R_\alpha$ is contained in g. If h is the order of the group g, there are h functions in the set $\{\psi_{R_\alpha k}(\vec{r})\}$. All of these representations are completely specified by $\vec{k}$, but they are equally well specified by any of the $\vec{k}$ vectors in the star of $\vec{k}$. Since all the functions in the set $\{\psi_{R_\alpha k}(\vec{r})\}$ correspond to the same energy, we do **not** say that the function $\psi_k(\vec{r})$ and $\psi_{R_\alpha k}(\vec{r})$ are degenerate. Instead we write $\{\psi_k(\vec{r})\}$ for all the functions in the set $\{\psi_{R_\alpha k}(\vec{r})\}$ and consider the extra point group symmetry to yield the relation $E(\vec{k}) = E(R_\alpha \vec{k})$ for all R_α. In this way, we guarantee that the energy $E(\vec{k})$ will show the full point group symmetry of the reciprocal lattice. Thus for the 2-dimensional square lattice, it is only necessary to calculate $E(\vec{k})$ explicitly for k points in 1/8 of the Brillouin zone contained within the sector $\Gamma\Lambda RSX\Delta\Gamma$ (see Fig. 13.6).

We use the term "degeneracy" to describe states with exactly the same energy **and** the same wave vector. Such degeneracies do in fact occur because of symmetry restrictions at special high symmetry points in the Brillouin zone and are called **"essential" degeneracies**. "Essential" degeneracies occur only at high symmetry or special $\vec{k}$ points, while accidental ("non-essential") degeneracies occur at arbitrary $\vec{k}$ points. "Special" high symmetry points in the Brillouin zone are those for which

$$
R_\alpha \vec{k} = \vec{k} + \vec{K} \tag{13.31}
$$
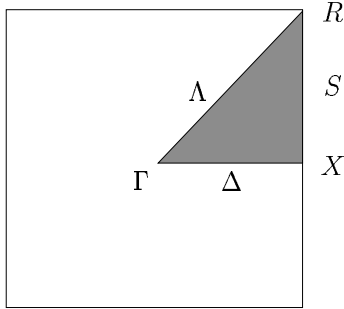
Figure 13.5: One-eighth of the simple cubic Brillouin Zone.

where $\vec{K}$ is the reciprocal lattice vector including $\vec{K} = 0$.

For these special points there are symmetry operations R_α which obey Eq. 13.31 and these symmetry operators form the group of the wave vector for wave vector $\vec{k}$. We will denote this group by g_k. When g_k is considered together with all the translation operations we denote this group by $\mathcal{G}_k$. The translations form a self-conjugate subgroup of both $\mathcal{G}_k$ and the full space group G, and define a factor group $\mathcal{G}_k/T$ and G/T for both of these cases. We label a wave function at one of these special points in the Brillouin zone as $\psi_{k\lambda}^i(\vec{r})$ where k is the quantum number of the translations, i denotes a particular irreducible representation of g_k and λ is an index denoting the partners of (i). If h_k is the order of the group of the wave vector $\vec{k}$, then if we operate on an eigenfunction with symmetry elements R_k in g_k, we obtain another eigenfunction in the set $\{\psi_{k\lambda}^{(i)}(\vec{r})\}$

$$\hat{P}_{\{R_k|0\}}\psi_{k\lambda}^{(i)}(\vec{r}) = \sum_\mu \psi_{k\mu}^{(i)}(\vec{r})D^{(i)}(\{R_k|0\})_{\mu\lambda} \qquad (13.32)$$

where the sum is on partners μ. In this way the operations $\{R_k|0\}$ in g_k will produce all partners of $\{\psi_{k\lambda}^{(i)}(\vec{r})\}$. If we have h symmetry elements in g and if we now operate with one of these symmetry elements $\{R_\beta|0\}$ which is not in g_k we obtain other functions $\{\psi_{R_\beta k\lambda}^{(i')}(\vec{r})\}$ corresponding to the star of $\vec{k}$ and there will be (h/h_k) such sets for all possible i'. In the cases where the symmetry operation yields $R_\alpha \vec{k} = \vec{k} + \vec{K}$, then the eigenfunctions have essential degeneracies because we now can have degenerate eigenfunctions with the same energy eigenvalue at

the same $\vec{k}$ vector (provided that the dimensionality of the irreducible representation ≥ 2). These essential band degeneracies are lifted as we move away from the high symmetry points to a general point in the Brillouin zone. The rules governing the lifting of these degeneracies are called **compatibility relations**, discussed in §13.7.

13.7   Compatibility Relations

To study these compatibility relations, let us follow some particular energy band around the Brillouin zone and see how its symmetry type and hence how its degeneracy changes. The problem of connectivity (connecting energy bands as we move from one $\vec{k}$ point to a neighboring $\vec{k}$ point with a different group of the wave vector) is exactly the same type of problem as that occurring in crystal field splittings (Chapter 6) as we go from a high symmetry situation to a perturbed situation of lower symmetry.

As an illustration, consider the point group O_h in a simple cubic lattice as we move along a (111) direction from $\Gamma \to \Lambda \to R$, from the center of the Brillouin zone to the zone corner. At the Γ point ($\vec{k} = 0$) we have the full point group symmetry O_h. As we now go from a higher point group symmetry O_h at Γ to a $\vec{k}$ vector along Λ, we go to a point group of lower symmetry C_{3v}. Since there are no 3-dimensional representations in C_{3v}, we know that the degeneracy of the $\Gamma_{15}^-, \Gamma_{25}^-, \Gamma_{15}^+, \Gamma_{25}^+$ levels will be at least partially lifted. We proceed as before to write down the character table for the Λ point, and below it we will write down the representations of the Γ point group, which we now treat as reducible representations of the Λ point group. We then reduce out the irreducible representations of the Λ point. This process is indicated in the table below where we list the 10 irreducible representations of O_h and indicate the irreducible representations of C_{3v} therein contained. This procedure gives a set of compatibility conditions.

Λ	E	$2C_3$	$3iC_2$	irreducible representations
Λ_1	1	1	1	
Λ_2	1	1	-1	
Λ_3	2	-1	0	
Γ_1^+	1	1	1	Λ_1
Γ_2^+	1	1	-1	Λ_2
Γ_{12}^+	2	-1	0	Λ_3
Γ_{15}^+	3	0	-1	$\Lambda_2 + \Lambda_3$
Γ_{25}^+	3	0	1	$\Lambda_1 + \Lambda_3$
Γ_1^-	1	1	-1	Λ_2
Γ_2^-	1	1	1	Λ_1
Γ_{12}^-	2	-1	0	Λ_3
Γ_{15}^-	3	0	1	$\Lambda_1 + \Lambda_3$
Γ_{25}^-	3	0	-1	$\Lambda_2 + \Lambda_3$

In a similar way, the compatibility relations for a simple cubic lattice along the Δ and Σ axes follow the progression from Γ to Δ to X and also from Γ to Σ to M as can be seen from Fig. 13.2. In going from $\Delta \to X$ we go from C_{4v} symmetry to D_{4h} symmetry, since at the Brillouin zone boundary, translation by a reciprocal lattice vector introduces additional symmetries associated with a mirror plane. Similarly in going from $\Sigma \to M$ we get 4 equivalent M points so that the symmetry group goes from C_{2v} to D_{4h}.

Tables of compatibility relations are compiled in references such as Miller and Love's book. Compatibility relations for the simple cubic lattice are summarized in Table 13.16.

As an example of using these compatibility relations, let us consider what happens as we move away from the Γ point $\vec{k} = 0$ on a 3-fold level such as Γ_{25}^+. There are many possibilities, as indicated below:

$$\Gamma_{25}^+ \to \Delta_{2'} + \Delta_5 \to X_3 + X_5 \tag{13.33}$$

$$\Gamma_{25}^+ \to \Lambda_1 + \Lambda_3 \to R_{15} \tag{13.34}$$

$$\Gamma_{25}^+ \to \Sigma_1 + \Sigma_2 + \Sigma_3 \to M_1 + M_5. \tag{13.35}$$

Suppose that we want to find a set of compatible symmetries in

Table 13.16: Compatibility Relations for the high symmetry points in the simple cubic lattice.

Compatibility Relations Between Γ and Δ, Λ, Σ.										
	Γ_1^+	Γ_2^+	Γ_{12}^+	Γ_{15}^-	Γ_{25}^+	Γ_1^-	Γ_2^-	Γ_{12}^-	Γ_{15}^+	Γ_{25}^-
(100)	Δ_1	Δ_2	$\Delta_1\Delta_2$	$\Delta_1\Delta_5$	$\Delta_{2'}\Delta_5$	$\Delta_{1'}$	$\Delta_{2'}$	$\Delta_{1'}\Delta_{2'}$	$\Delta_{1'}\Delta_5$	$\Delta_2\Delta_5$
(111)	Λ_1	Λ_2	Λ_3	$\Lambda_1\Lambda_3$	$\Lambda_1\Lambda_3$	Λ_2	Λ_1	Λ_3	$\Lambda_2\Lambda_3$	$\Lambda_2\Lambda_3$
(110)	Σ_1	Σ_4	$\Sigma_1\Sigma_4$	$\Sigma_1\Sigma_3\Sigma_4$	$\Sigma_1\Sigma_2\Sigma_3$	Σ_2	Σ_3	$\Sigma_2\Sigma_3$	$\Sigma_2\Sigma_3\Sigma_4$	$\Sigma_1\Sigma_2\Sigma_4$

Compatibility Relations Between X and Δ, Z, S									
X_1	X_2	X_3	X_4	X_5	$X_{1'}$	$X_{2'}$	$X_{3'}$	$X_{4'}$	$X_{5'}$
Δ_1	Δ_2	$\Delta_{2'}$	$\Delta_{1'}$	Δ_5	$\Delta_{1'}$	$\Delta_{2'}$	Δ_2	Δ_1	Δ_5
Z_1	Z_1	Z_4	Z_4	Z_3Z_2	Z_2	Z_2	Z_3	Z_3	Z_1Z_4
S_1	S_4	S_1	S_4	S_2S_3	S_2	S_3	S_2	S_3	S_1S_4

Compatibility Relations Between M and Σ, Z, T									
M_1	M_2	M_3	M_4	$M_{1'}$	$M_{2'}$	$M_{3'}$	$M_{4'}$	M_5	$M_{5'}$
Σ_1	Σ_4	Σ_1	Σ_4	Σ_2	Σ_3	Σ_2	Σ_3	$\Sigma_2\Sigma_3$	$\Sigma_1\Sigma_4$
Z_1	Z_1	Z_3	Z_3	Z_2	Z_2	Z_4	Z_4	Z_2Z_4	Z_1Z_3
T_1	T_2	$T_{2'}$	$T_{1'}$	$T_{1'}$	$T_{2'}$	T_2	T_1	T_5	T_5

going around a circuit using the Brillouin zone (see Fig. 13.2).

$$\Gamma \to \Sigma \to M \to Z \to X \to \Delta \to \Gamma \qquad (13.36)$$

Then we must verify that when we arrive back at Γ we have the same symmetry type as we started with. A set of such compatible symmetries designates a whole band.

To go around one of these circuits, basis functions sometimes prove very useful. Suppose that we are generating wave functions from the tight binding point of view. Then we know that s-functions transform like the identity representation so that a possible circuit would be $\Gamma_1 \to \Lambda_1 \to R_1 \to S_1 \to X_1 \to \Delta_1 \to \Gamma_1$. If we have p-functions, the basis functions are (x, y, z) and we can join up representations corresponding to these basis functions, etc. The d-functions transform as (xy, xz, yz) with Γ_{25}^+ symmetry and $(x^2 + \omega y^2 + \omega^2 z^2)$, $(x^2 + \omega^2 y^2 + \omega z^2)$ where $\omega = \exp(2\pi i/3)$, corresponding to Γ_{12}^+ symmetry. We must of course always remember that the charge distribution of an s-electron in a cubic crystal will exhibit the cubic symmetry of the crystal, and not correspond to the full rotational symmetry of the free atomic state.

As an example of how compatibility relations are used in the labeling of energy bands, we show the energy dispersion relation $E(\vec{k})$ in Fig. 13.6 for the high symmetry directions $\vec{k}_{100}$ and $\vec{k}_{111}$ for the simple cubic structure. For the band with lower energy, we have the compat-
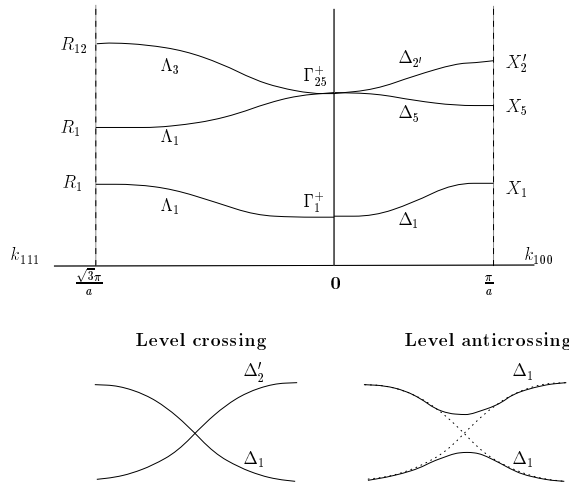
Figure 13.6: Schematic diagram of energy bands illustrating compatibility relations.

ibility relations $\Gamma_1 \to \Delta_1 \to X_1$ and $\Gamma_1 \to \Lambda_1 \to R_1$. For the upper band, a consistent set of compatibility relations is

$$
\begin{aligned}
\Gamma_{25}^+ &\to \Delta_{2'} + \Delta_5, &\Delta_{2'} \to X_{2'} \text{ and } \Delta_5 \to X_5 \\
\Gamma_{25}^+ &\to \Lambda_1 + \Lambda_3, &\Lambda_1 \to R_1 \text{ and } \Lambda_3 \to R_{12}
\end{aligned}
$$

In applying the compatibility relations as we approach the R point from the Λ direction, we note that the R point has the same group of the wave vector as $\vec{k} = 0$ and the same subscript notation can be used to label the R and Γ levels.

13.7.1 Irreducible Representations

For a symmorphic lattice, the irreducible representations for a given point in the Brillouin zone are associated with the group of the wave vector for that point.

For non-symmorphic lattices, the determination of the irreducible representation can be more difficult, except at $\vec{k} = 0$, where the irreducible representation is the same as the point group formed by ignoring the fractional translations of the space group. For each symmetry axis leading away from $\vec{k} = 0$, the character tables for those $\vec{k}$ points can be obtained by selecting the appropriate point group table and by

multiplying the character for the symmetry operations that contains a translation τ by a phase factor $\exp[i\vec{k} \cdot \vec{\tau}]$.

13.8 Selected Problems

1. (a) For the crystal structure shown below on the left, identify the space group and list the symmetry elements.

   (b) Identify the high symmetry points (and axes), and list the group of the wave vector at these high symmetry points (and axes).

   (c) Using the space group identified in (a), explain the diagrams for this space group as shown in the International Crystallography Tables.

   (d) Using the tables in (c), find the atom sites and site symmetries for the structure shown in (a).
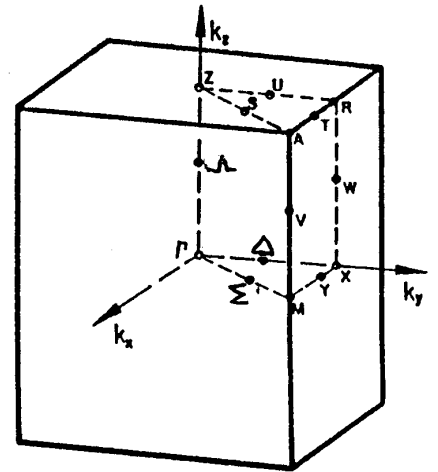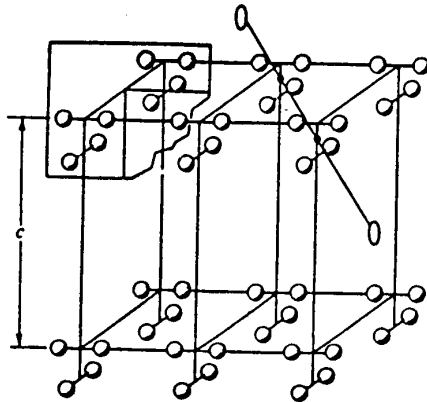
2. (a) For the crystal structure shown below on the left, list the symmetry elements of the space group.

   (b) Identify the high symmetry points (and axes), and list the group of the wave vector at these high symmetry points (and axes).

3. (a) Show that in the diamond structure (§14.3.3) the product of two symmetry operations involving translations τ yields a symmetry element with no translations

$$\{\alpha|\tau\}\{\beta|\tau\} = \{\gamma|0\}$$

where $\vec{\tau} = (1,1,1)a/4$. What is the physical significance of this result?

(b) What are the symmetry operations of the group of the wave vector for the diamond structure at $k = 0$? at the Δ point? at the L point?

(c) List the real space symmetry operations of the non-symmorphic two-dimensional square space group $p4gm$ (#12). Find the group of the wave vector for the high symmetry points in the space group $p4gm$ and compare your results with those for the symmorphic group $p4mm$ (Fig. 13.1 of the notes).

4. (a) List the real space symmetry operations of the non-symmorphic two-dimensional square space group $p4gm$ (#12).

(b) Explain the diagrams and the point symmetry entries for space group #12 ($p4gm$) in Fig. 12.20 which was taken from the International Crystallography Tables.

(c) Find the group of the wave vector for the high symmetry points in the space group $p4gm$ and compare your results with those for the symmorphic group $p4mm$ (Fig. 13.1 of the notes).

Chapter 14

Applications to Lattice Vibrations

Our first application of the space groups to excitations in periodic solids is in the area of lattice modes. Group theoretical techniques are important for lattice dynamics in formulating the normal mode secular determinant in block diagonal form, and symmetry is also important in the area of selection rules for optical processes involving lattice modes such as infrared and Raman activity. Transitions to lower symmetry through either phase transitions or strain-induced effects may lead to mode splittings. These mode splittings can be predicted using group theoretical techniques and the changes in the infrared and Raman spectra can be predicted.

14.1 Introduction

The atoms in a solid are in constant motion and give rise to lattice vibrations which are very similar to the molecular vibrations which we have discussed in Chapter 9. We discuss in this section the similarities and differences between lattice modes and molecular vibrations.

Suppose that we have a solid with N atoms which crystallize into a simple Bravais lattice with 1 atom/unit cell. For this system there are $3N$ degrees of freedom corresponding to 3 degrees of freedom/atom or 3 degrees of freedom/primitive unit cell. There are N allowed wave vector

states in the Brillouin zone which implies that there are 3 branches for
the phonon dispersion curves of a simple monatomic solid, each branch
containing solutions for N $\vec{k}$-vectors. For the case of molecules, we
subtract three degrees of freedom corresponding to the uniform trans-
lation of the molecule. In the solid, these uniform translational modes
correspond to the acoustic modes at $\vec{k} = 0$, which are subject to the
constraint that $\omega^2_{\text{acoustic}} \equiv 0$. The three modes corresponding to the
rotations of the solid about the center of mass are not specifically con-
sidered.

We have found in Chapter 13 that the translational symmetry of
a crystal is conveniently handled by labeling the N irreducible rep-
resentations of the translation group by the N $\vec{k}$ vectors which are
accommodated in the 1st Brillouin zone. So if we have a primitive
unit cell with 1 atom/unit cell, there are 3 vibrational modes for each
$\vec{k}$ value and together these 3 modes constitute the acoustic branches.
In particular, there are 3 acoustic vibrational modes for the $\vec{k} = 0$
wave vector, which exhibits the full point group symmetry of the crys-
tal; these three acoustic modes correspond to the pure **translational
modes** which have zero frequency and zero restoring force.

We review here the phonon dispersion relations in a 1-dimensional
crystal with 1 atom/unit cell (see Fig. 14.1a) and with 2 atoms/unit
cell (see Fig. 14.1b) having masses m and M where $m < M$, and a is
the distance between adjacent atoms. For the acoustic branch at $\vec{k} = 0$,
all atoms vibrate in phase with identical displacements u along the di-
rection of the atomic chain, thus corresponding to a pure translation
of the chain. The wave vector $\vec{k}$ distinguishes each normal mode of the
system by introducing a phase factor e^{ika} between the displacements on
adjacent sites. For the case of one atom/unit cell, the lattice mode at
the zone boundary corresponds to atoms moving 90° out of phase with
respect to their neighbors. For the case of 2 atoms/unit cell, the size of
the unit cell is twice as large so that the size of the corresponding Bril-
louin zone (B.Z.) is reduced by a factor of 2. The dispersion relations
and lattice modes in this case relate to those for one atom/unit cell by a
zone folding of the dispersion relation shown in Fig. 14.1a, thus leading
to Fig. 14.1b. Thus the optical mode at $\vec{k} = 0$ has neighboring atoms
moving out of phase with respect to each other. The normal mode at
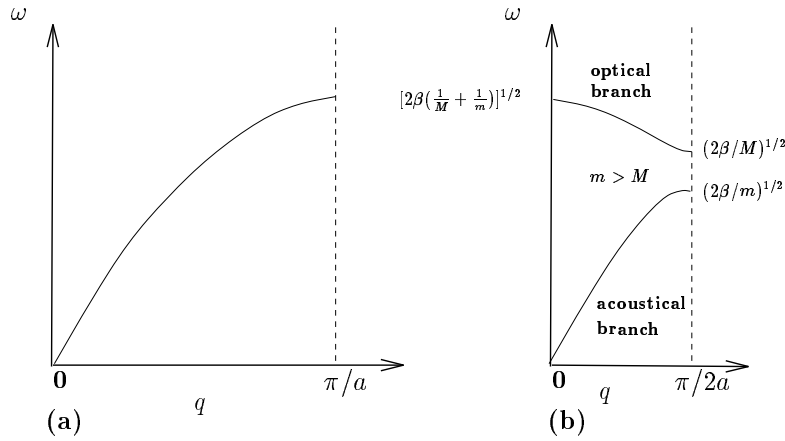
Figure 14.1: Phonon dispersion curves for a one-dimensional line of atoms with (a) a single mass and (b) two different masses m and M.

the new B.Z. boundary $k = \pi/2a$ thus corresponds to a mode where one atom is at rest, while its neighbor is in motion.

In 3-dimensions, the phonon dispersion relations for Ge with the diamond structure (with 2 atoms/unit cell) are plotted along high symmetry directions in Fig. 14.2 and the dispersion relations are labeled by the appropriate irreducible representations giving the symmetry of the corresponding normal mode. The phonon dispersion relations for **germanium** are determined from inelastic neutron scattering measurements and are plotted as points in Fig. 14.2. At a general point k in the Brillouin zone for the diamond structure, there are 3 acoustic branches and 3 optical branches. However at certain high symmetry points and along certain high symmetry directions, mode degeneracies occur as, for example, along ΓL and ΓX. Group theory allows us to identify the high symmetry points where degeneracies occur, which modes stick together, which modes cross, and which modes show anti-crossings, to be discussed further in this chapter.

The symmetry aspects of the lattice mode problem at $\vec{k} = 0$ for simple structures with 1 atom/unit cell are simply the uniform translation of the solid and no group theory is required. However, group theory is needed to deal with lattice modes away from $\vec{k} = 0$. Furthermore the lattice modes that are of interest in the current literature often involve complicated crystal structures with many atoms/unit cell or
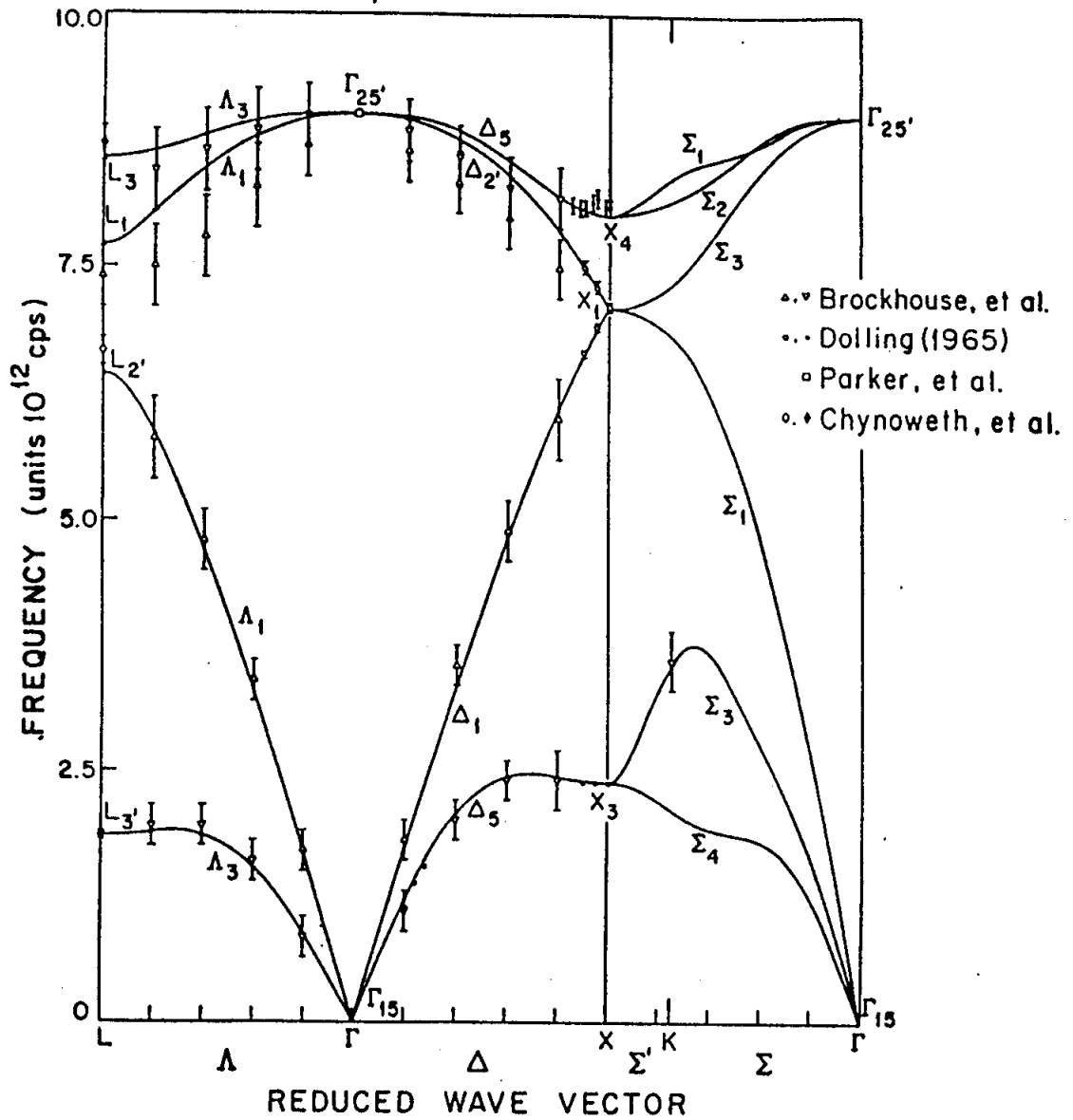
Figure 14.2: Phonon dispersion curves for Ge along certain high symmetry axes in the Brillouin zone. The data at the Γ point are from Raman scattering measurements and the data elsewhere in the zone are from neutron scattering experiments.

systems with reduced dimensionality; for such problems group theory is a powerful tool for lattice mode classification and for the determination of selection rules for infrared and Raman spectroscopy and for phonon-assisted optical transitions more generally.

The **general outline** for discussing lattice modes in solids is:

1. Find the symmetry operations for the group of the wave vector $\vec{k} = 0$, the appropriate character table and irreducible representations.

2. Find $\chi_{\text{lattice modes}} = \chi_{\text{atom sites}} \otimes \chi_{\text{vector}}$. The meaning of this relation is discussed below (item #3 in §14.2).

3. Find the irreducible representations of $\chi_{\text{lattice modes}}$. The characters for the lattice mode representation express the symmetry types and degeneracies of the lattice modes.

4. Find the normal mode patterns.

5. Which modes are IR-active?

6. Which modes are Raman-active?

7. Are there any polarization effects?

8. Find the lattice modes at other points in the Brillouin zone.

9. Using the compatibility relations, connect up the lattice modes at neighboring $\vec{k}$ points to form a phonon branch.

14.2 Unique Features of Lattice Modes Relative to Molecular Vibrations

There are several aspects of the lattice mode problem in the solid phase that differ from molecular vibrations in the gas phase (see §9.2 of Chapter 9 on p. 195):

1. **The unit cell**- In the lattice mode problem, we consider normal modes for the atoms in a unit cell rather than for a molecule. Since the symmetry is different for the various types of $\vec{k}$-vectors in the Brillouin zone, we must solve the lattice mode problem for each distinct type of $\vec{k}$-vector. On the other hand, for many experimental studies of the lattice modes we use light as our probe. Since the wavelength of light is long ($\lambda \approx 5000\text{Å}$) and the magnitude of the corresponding $\vec{k}$ vector ($k = 2\pi/\lambda$) is very small compared with Brillouin zone dimensions, our main interest is in lattice modes at or near $\vec{k} = 0$ (the Γ point). We therefore emphasize the lattice modes for $\vec{k} = 0$ in our discussions.

2. **Equivalence**- To find $\chi_{\text{atom sites}}$ for molecules, we consider the action of a symmetry operator $\hat{P}_R$ on an atomic site and examine the transformation matrix to see whether or not the site is transformed into itself under the point symmetry operation $\hat{P}_R$. In the case of a crystal, however, we consider all points separated by a lattice vector $\vec{R}_n$ as identical. Thus $\vec{r} \rightarrow \vec{r} + \vec{R}_n$ is an **identity transformation** for all $\vec{R}_n$.

3. **Counting of Lattice Modes-Phonon Branches**- For the case of molecules we have

$$\chi_{\text{molecular vibrations}} = \chi_{\text{atom sites}} \otimes \chi_{\text{vector}} - \chi_{\text{translations}} - \chi_{\text{rotations}}$$
(14.1)

whereas for lattice modes, we simply write

$$\chi_{\text{lattice modes}} = \chi_{\text{atom sites}} \otimes \chi_{\text{vector}}.$$ (14.2)

That is, we do not subtract $\chi_{\text{translations}}$ and $\chi_{\text{rotations}}$ in Eq. 14.2 for the following reasons. Each atom/unit cell has 3 degrees of freedom, yielding a normal mode for each wave vector $\vec{k}$ in the Brillouin zone. The collection of normal modes for a given degree of freedom for all $\vec{k}$ vectors forms a **phonon branch**. Thus for a structure with one atom/unit cell there are 3 phonon branches, the acoustic branches. If there is more than 1 atom/unit cell, then

$$\#\text{branches} = (\#\text{atoms/unit cell}) \times 3$$ (14.3)

of which 3 are acoustic and the remainder are optic. The translational degrees of freedom correspond to the trivial $\vec{k} = 0$ solution for the 3 acoustic branches which occur at $\omega = 0$ and are smoothly connected with non-trivial solutions as we move away from the Γ point. Since the atoms in the solid are fixed in space there are no rotational degrees of freedom to be subtracted.

We will now illustrate the application of group theory to the solution of the lattice mode problem for several illustrative structures. First we consider simple symmorphic structures. Then we consider some simple non-symmorphic structures. Our initial examples will be for the $\vec{k} = 0$ modes. This will be followed by a discussion of modes elsewhere in the Brillouin zone. In this connection, a discussion of "zone-folding" phenomena will be presented because of the connection between the zone folding of normal modes at $\vec{k} \neq 0$ to yield modes which can be excited by optical techniques.

14.3 Zone Center Phonon Modes

In this section we consider the symmetries of zone center phonon modes for some illustrative cases. The examples selected in this section are chosen to demonstrate some important aspect of the lattice mode problem.

14.3.1 In the NaCl Structure

This very simple example is selected to illustrate how the symmetries of the lattice modes are found. We take our "basic unit cell" to be the primitive unit cell of either one of the interpenetrating fcc structures (space group #225 ($Fm3m$) O_h^5), so that each unit cell will contain an Na atom and a Cl atom (see Fig. 14.3a). The primitive fcc unit cell is shown in Fig. 14.3b and the primitive lattice vectors are indicated. The larger cubic unit cell (Fig. 14.3a) contains 4 primitive unit cells with 4 Na and 4 Cl atoms (ions). The space group O_h^5 for the NaCl structure is a symmorphic structure, and the group of the wave vector at $\vec{k} = 0$ for the NaCl structure is O_h. Since the details of the translations do

NaCl Structure   #225 (Fm3m) O_h^5
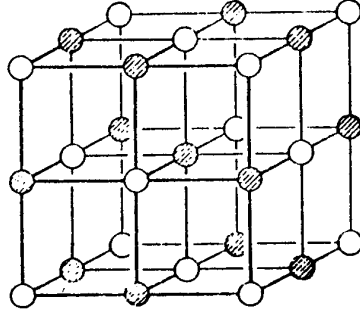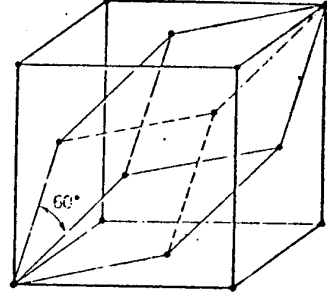
(a)   (b)

Figure 14.3: (a) The NaCl structure which is space group #225. (b) The rhombohedral primitive cell of the fcc lattice which contains one Na atom and one Cl atom.

not enter into the considerations of phonons at $\vec{k} = 0$ for symmorphic space groups, we need to consider only the point group operations for O_h.

O(432)		E	$8C_3$	$3C_2 = 3C_4^2$	$6C_2$	$6C_4$
Γ_1		A_1	1	1	1	1	1
Γ_2		A_2	1	1	1	-1	-1
Γ_{12}	$(x^2 - y^2, 3z^2 - r^2)$	E	2	-1	2	0	0
Γ_{15}	$\begin{matrix}(R_x, R_y, R_z)\\(x, y, z)\end{matrix}\Big\}$	T_1	3	0	-1	-1	1
Γ_{25}	yz, zx, xy	T_2	3	0	-1	1	-1

$$O_h = O \times i \quad (m3m)$$

Under all symmetry operations of O_h each Na and Cl atom site is transformed either into itself or into an equivalent atom site separated by a lattice vector $\vec{R}_m$. Thus,

$$\chi_{\text{atom sites}} = 2A_{1g} \tag{14.4}$$

For O_h symmetry, $\chi_{\text{vector}} = T_{1u}$, so that at $\vec{k} = 0$

$$\chi_{\text{lattice modes}} = 2A_{1g} \otimes T_{1u} = 2T_{1u}. \tag{14.5}$$

acoustic branches
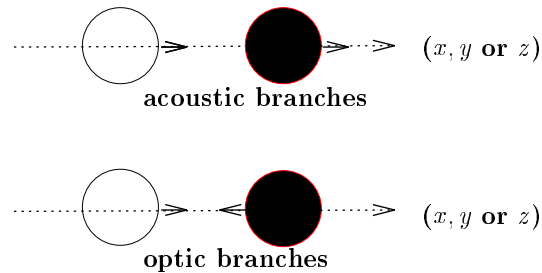
optic branches

Figure 14.4: In-phase and out-of-phase normal modes at $\vec{k} = 0$ for NaCl.

Thus both the acoustic branch and the optical branch at $\vec{k} = 0$ have T_{1u} or Γ_{15}^- symmetry. The normal modes for the acoustic branches of the NaCl structure have the two atoms moving in phase in the x, y, and z directions, while for normal modes in the optical branches the two atoms move out of phase in the x, y and z directions (see Fig. 14.4). Since the electromagnetic interaction transforms as the vector (T_{1u}), the optic branch is infrared-active. The acoustic branch is not optically excited because $\omega = 0$ at $\vec{k} = 0$. Since the optic branch for the NaCl structure has odd parity, it is not Raman-active. As we move away from the Γ point ($\vec{k} = 0$), the appropriate symmetries can be found by compatibility relations. For example along the (100) directions $\Gamma_{15}^- \rightarrow \Delta_1 + \Delta_5$ in which Δ_1 is the symmetry of the longitudinal mode and Δ_5 that for the transverse mode. We will now give several other examples of zone center modes in other structures and then return in §14.4.1 to the discussion of non-zone-center modes for the NaCl structure.

14.3.2 In the Perovskite Structure

Let us now consider lattice modes in $BaTiO_3$ (see Fig. 14.5), an example of a crystal structure with slightly more complexity, but still corresponding to a symmorphic space group. The focus of this section is to illustrate the identification of the normal modes. For the perovskite structure shown in Fig. 14.5, we have 5 atoms/unit cell and therefore we have 15 degrees of freedom, giving rise to 3 acoustic branches and 12 optical branches. The point group of symmetry at $\vec{k} = 0$ is O_h. Consider the unit cell shown in Fig. 14.5. The Ba^{++} ions at the cube
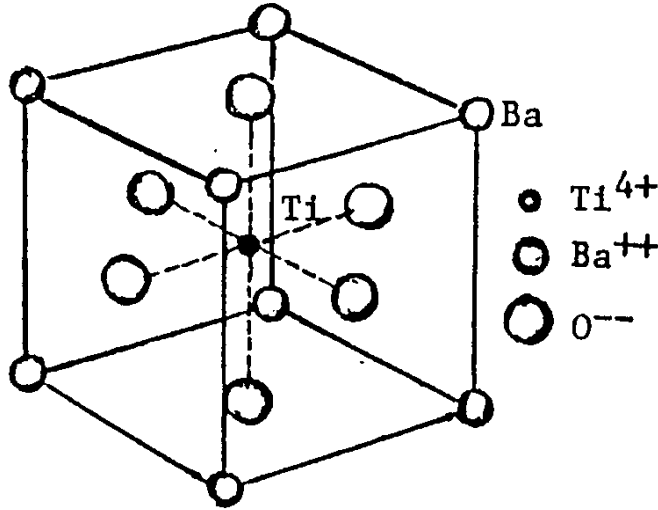
Figure 14.5: The cubic perovskite crystal structure of barium titanate, containing one Ba, one Ti and three O atoms. The Ba^{2+} ions are at the cube corners, O^{2-} ions at the face centers, and a Ti^{4+} ion at the body center. The space group is #221.

corners are shared by 8 neighboring unit cells, so that one Ba^{++} ion is considered to be associated with the unit cell shown. Likewise the O^{--} ions in the face centers are shared by two unit cells, so that $3O^{--}$ ions are treated in the unit cell shown. The Ti^{4+} ion at the cube center is of course fully contained in the unit cell shown in Fig. 14.5.

Using the diagram in Fig. 14.5, we thus obtain for $\chi_{\text{atom sites}}$

	E	$8C_3$	$3C_4^2$	$6C_2'$	$6C_4$	i	$8iC_3$	$3iC_4^2$	$6iC_2'$	$6iC_4$
$\chi_{\text{atom sites}}$	5	2	5	3	3	5	2	5	3	3
	all	Ba,Ti	all	Ba,Ti	Ba,Ti	all	Ba,Ti	all	Ba,Ti	Ba,Ti
				one O	one O				one O	one O

Looking at the character table for O_h we see that

$$\chi_{\text{atom sites}} = 3A_{1g} + E_g = 3\Gamma_1^+ + \Gamma_{12}^+. \tag{14.6}$$

We note that the Ba^{2+} and Ti^{4+} ions each transform as A_{1g} with the three oxygens transforming as $A_{1g} + E_g = \Gamma_1^+ + \Gamma_{12}^+$. In O_h symmetry

$$\chi_{\text{vector}} = T_{1u} = \Gamma_{15}^- \tag{14.7}$$

so that

$$
\begin{aligned}
\chi_{\text{lattice modes}} &= (3A_{1g} + E_g) \otimes T_{1u} = 3T_{1u} + (E_g \otimes T_{1u}) \\
&= 4T_{1u} + T_{2u} = 4\Gamma_{15}^- + \Gamma_{25}^-.
\end{aligned}
\tag{14.8}
$$

Thus at $\vec{k} = 0$ there are 5 distinct frequencies, including the acoustic branch with Γ_{15}^- symmetry and $\omega = 0$. Since the Ba^{2+} and Ti^{4+} ions transform as A_{1g}, we know that the Γ_{25}^- mode requires motion of the oxygens. In the following we illustrate how the normal mode patterns shown in Fig. 14.6 are obtained. Note the numbers assigned to the oxygens in Fig. 14.6b.

From the character table for O_h we note that the characters for C_4^z are different for the Γ_{15}^- and Γ_{25}^- modes, and for this reason C_4^z is a useful symmetry operation for finding the normal mode displacements. First we consider the effect of C_4^z on each of the 3 inequivalent oxygen sites and on each of the 3 components of the vector; this consideration is independent of the symmetry of the vibrational mode:

$$
C_4^z \begin{pmatrix} 1 \\ 2 \\ 3 \end{pmatrix} = \begin{pmatrix} 2 \\ 1 \\ 3 \end{pmatrix}
\qquad\qquad
C_4^z \begin{pmatrix} x \\ y \\ z \end{pmatrix} = \begin{pmatrix} y \\ -x \\ z \end{pmatrix}.
\tag{14.9}
$$

Finding the normal mode for the acoustic translational branch is trivial (see Fig. 14.6a). The operations of Eq. 14.9 are now applied to find the normal modes in Fig. 14.6b and e. For the Γ_{25}^- displacements, Fig. 14.6b shows the motions for the z component of the mode. The partners are found by cyclic operations on (x, y, z) and atom sites $(1, 2, 3)$, as given in Eq. 14.10. Then operation by C_4^z yields

$$
C_4^z \begin{pmatrix} -x_2 + x_3 \\ y_1 - y_3 \\ -z_1 + z_2 \end{pmatrix} = \begin{pmatrix} -y_1 + y_3 \\ -x_2 + x_3 \\ -z_2 + z_1 \end{pmatrix} = \begin{pmatrix} 0 & -1 & 0 \\ 1 & 0 & 0 \\ 0 & 0 & -1 \end{pmatrix} \begin{pmatrix} -x_2 + x_3 \\ y_1 - y_3 \\ -z_1 + z_2 \end{pmatrix}
\tag{14.10}
$$

giving a character of -1 for C_4^z in the Γ_{25}^- representation. Performing representative operations on this normal mode will show that it provides a proper basis function for the Γ_{25}^- irreducible representation in the point group O_h.
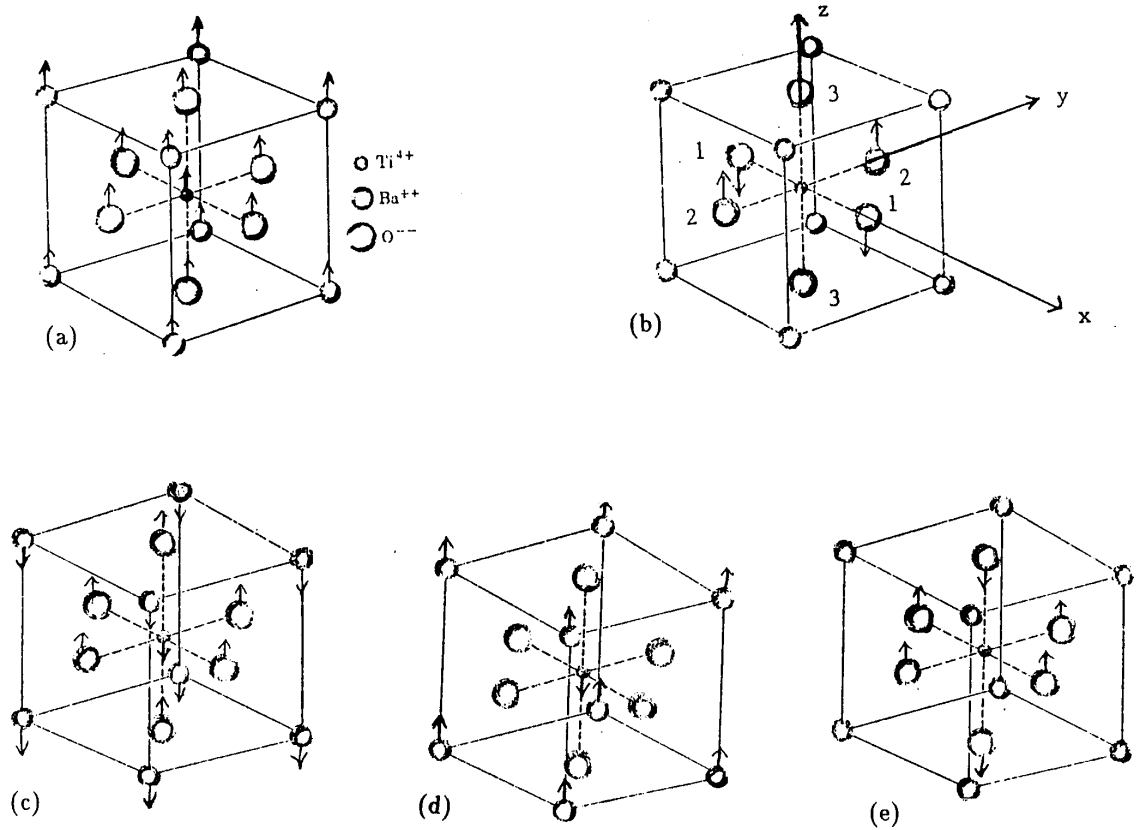
Figure 14.6: Schematic diagram of lattice modes at $\vec{k}=0$ for the $BaTiO_3$ perovskite structure. (a) Γ_{15}^- acoustic mode; (b) Γ_{25}^- mode where only 2 of the 3 distinct oxygens move; (c) Γ_{15}^- mode with the Ti and Ba vibrating against the oxygens. (d) Γ_{15}^- mode with the Ti^{4+} vibrating against the Ba^{2+} and (e) Γ_{15}^- breathing mode of transverse oxygens vs. longitudinal oxygens.

Now consider the Γ_{15}^- normal mode given in Fig. 14.6e. The displacements shown in the diagram are for the z component of the mode. To achieve no motion of the center of mass, the actual displacements must be $-z_1 - z_2 + 2z_3$ for the 3 oxygens at positions 1, 2 and 3. Using cyclic permutations we obtain the 3 components of the mode given in Eq. 14.11. Then action of C_4^z yields

$$
C_4^z \begin{pmatrix} 2x_1 - x_2 - x_3 \\ -y_1 + 2y_2 - y_3 \\ -z_1 - z_2 + 2z_3 \end{pmatrix} = \begin{pmatrix} 2y_2 - y_1 - y_3 \\ x_2 - 2x_1 + x_3 \\ -z_2 - z_1 + 2z_3 \end{pmatrix}
$$
$$
= \begin{pmatrix} 0 & 1 & 0 \\ -1 & 0 & 0 \\ 0 & 0 & 1 \end{pmatrix} \begin{pmatrix} 2x_1 - x_2 - x_3 \\ -y_1 + 2y_2 - y_3 \\ -z_1 - z_2 + 2z_3 \end{pmatrix} \tag{14.11}
$$

so that the character for this Γ_{15}^- mode is $+1$, in agreement with the character for the C_4^z operation in the $\Gamma_{15,z}^-$ irreducible representation (see the character table for O_h). Operation with typical elements in each class shows this mode provides a proper basis function for Γ_{15}^-.

Clearly all the modes shown in Fig. 14.6 have partners x, y and z, so that collectively they are all the normal modes for BaTiO$_3$. Since all modes at $\vec{k} = 0$ have odd parity, none are Raman-active, noting that for the O_h point group, Raman-active modes have A_{1g}, E_g and T_{2g} symmetries. However, the $3T_{1u}$ or $3\Gamma_{15}^-$ modes are **infrared-active**, and can be excited when the $\vec{E}$ vector for the light is polarized in the direction of the oscillating dipole moment indicated in Fig. 14.6.

14.3.3 Phonons in the Diamond Lattice: A Non-Symmorphic Structure

We now illustrate the mode symmetries for a non-symmorphic space group with 2 atoms/unit cell (specifically we illustrate the lattice modes of Ge or Si, which crystallize in the diamond structure). The two distinct atoms per unit cell are indicated in Fig. 14.7 as light atoms and dark atoms. We will take the "basic unit cell" for the diamond structure to be the fcc primitive unit cell shown in Fig. 14.3b. Again, we are most interested in the lattice modes at $\vec{k} = 0$. The set of operations $\hat{P}_R$
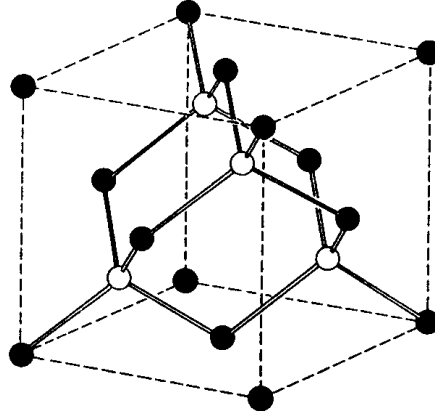
Figure 14.7: The zinc blende structure illustrating the two dissimilar lattice sites. With identical atoms at the two sites, the diamond structure results. The space group for the diamond lattice is $Fd3m$ or $\#227$ (O_h^7).

that are relevant are the 48 operations of the O_h point group. In considering the diamond structure, we think of the light atoms as being on one sublattice and the dark atoms on another sublattice. Each of the symmetry operators $\hat{P}_R$ of T_d will leave each atom on the same sublattice. However, the operations in O_h that are not in T_d when combined with a translation $\vec{\tau} = \frac{a}{4}(111)$ take each atom on one sublattice into the other. This space group is non-symmorphic because the symmetry operations of the group of the wave vector at $\vec{k} = 0$ contains translations $\tau = \frac{a}{4}(111)$. The 48 operations and 10 classes for the diamond structure at $\vec{k} = 0$ are given below. The 24 operations requiring translations τ are indicated by symmetry operations labeling the relevant classes. In computing $\chi_{\text{atom sites}}$, there are two kinds of lattice sites — one on each of the fcc sublattices. Thus an atom is considered "to go into itself" if it remains on its own sublattice and "**not** to go into itself" if it switches sublattices under a symmetry operation $\hat{P}_R$. Using this criterion the results for $\chi_{\text{atom sites}}$ for the diamond structure are given below.

	$\{E\|0\}$	$\{8C_3\|0\}$	$\{3C_2\|0\}$	$\{6C_2'\|\tau\}$	$\{6C_4\|\tau\}$
$\chi_{\text{a.s.}}$	2	2	2	0	0

	$\{i\|\tau\}$	$\{8iC_3\|\tau\}$	$\{3iC_2\|\tau\}$	$\{6iC_2'\|0\}$	$\{6iC_4\|0\}$
$\chi_{\text{a.s.}}$	0	0	0	2	2

Decomposition of $\chi_{\text{atom sites}}$ into irreducible representations of O_h leads to $\chi_{\text{a.s.}} = A_{1g} + A_{2u}$ or $\Gamma_1^+ + \Gamma_2^-$. Here Γ_1^+ is even under inversion and Γ_2^- which is odd under inversion, using the usual notation for irreducible representations for solids. We note that the operation $\{i|\tau\}$ interchanges sublattices $1 \leftrightarrow 2$. We will also make use of this result for $\chi_{\text{atom sites}}$ in discussing the electronic energy band structure of solids crystallizing in the diamond structure.

To get the characters for the lattice vibrations, we then take $\chi_{\text{vector}} = \Gamma_{15}^- = T_{1u}$ and

$$\chi_{\text{lattice modes}} = \chi_{\text{a.s.}} \otimes \chi_{\text{vector}} = (A_{1g} + A_{2u}) \otimes T_{1u} = T_{1u} + T_{2g} = \Gamma_{15}^- + \Gamma_{25}^+$$
$$(14.12)$$

For each $\vec{k}$ value, there are 6 vibrational degrees of freedom with 2 atoms/unit cell. These break up into 2 triply degenerate modes at $\vec{k} = 0$, one of which is even, the other odd under inversion. The odd mode Γ_{15}^- is the acoustic mode, which at $\vec{k} = 0$ is the pure translational mode. The other mode is a Γ_{25}^+ mode which is symmetric under inversion and represents a breathing or optical mode. The optic mode is Raman-active but not infrared-active. Furthermore, the Raman-active mode is observed only in the **off-diagonal polarization** $\vec{E}_i \perp \vec{E}_s$ for the incident and scattered light.

Let us now illustrate a screw axis operation in the diamond structure (see Fig. 14.7) and see how this operation is used in finding the normal modes. Denoting the black atoms by 1 and the white atoms by 2, consider the effect of $\{C_4^z|\tau\}$ on atom sites $\begin{pmatrix} 1 \\ 2 \end{pmatrix}$ and on the vector

$$
\begin{pmatrix} x \\ y \\ z \end{pmatrix}
$$

$$
\{C_4^z|\tau\} \begin{pmatrix} 1 \\ 2 \end{pmatrix} = \begin{pmatrix} 2 \\ 1 \end{pmatrix}
\qquad\qquad
\{C_4^z|\tau\} \begin{pmatrix} x \\ y \\ z \end{pmatrix} = \begin{pmatrix} y \\ -x \\ z \end{pmatrix}
$$

$$(14.13)$$

Using these results we can then obtain the characters for the displacements $(\vec{R}_1 + \vec{R}_2)$ which has Γ_{15}^- symmetry and is identified with the basic vibration of an fcc sublattice:

$$
\{C_4^z|\tau\} \begin{pmatrix} x_1 + x_2 \\ y_1 + y_2 \\ z_1 + z_2 \end{pmatrix} = \begin{pmatrix} y_2 + y_1 \\ -x_2 - x_1 \\ z_2 + z_1 \end{pmatrix} = \begin{pmatrix} 0 & 1 & 0 \\ -1 & 0 & 0 \\ 0 & 0 & 1 \end{pmatrix} \begin{pmatrix} x_1 + x_2 \\ y_1 + y_2 \\ z_1 + z_2 \end{pmatrix}
$$

$$(14.14)$$

yielding a character of $+1$ for $\{C_4^z|\tau\}$, in agreement with the character for $\{C_4^z|\tau\}$ in the Γ_{15}^- irreducible representation for the acoustic mode translational branches of point group O_h. If all the symmetry operations are then carried out, it is verified that $\vec{R}_1 + \vec{R}_2$ provides basis functions for the Γ_{15}^- irreducible representation of O_h.

When the 2 fcc sublattices vibrate out of phase, their parity is reversed and a mode with even parity (the Γ_{25}^+ mode) is obtained

$$
\{C_4^z|\tau\} \begin{pmatrix} x_1 - x_2 \\ y_1 - y_2 \\ z_1 - z_2 \end{pmatrix} = \begin{pmatrix} y_2 - y_1 \\ -x_2 + x_1 \\ z_2 - z_1 \end{pmatrix} = \begin{pmatrix} 0 & -1 & 0 \\ 1 & 0 & 0 \\ 0 & 0 & -1 \end{pmatrix} \begin{pmatrix} x_1 - x_2 \\ y_1 - y_2 \\ z_1 - z_2 \end{pmatrix}
$$

$$(14.15)$$

yielding a character of -1. This checks with the character for $\{C_4^z|\tau\}$ in the irreducible representation Γ_{25}^+ for the point group O_h.

As we move away from $\vec{k} = 0$ along the Δ axis or the Λ axis, the triply degenerate modes break up into longitudinal and transverse branches. The symmetries for these branches can be found from the compatibility relations (see §13.7 on p. 368). For example, as we move away from $\vec{k} = 0$ along the Δ axis toward the X point (see Fig. 14.8), we have the compatibility relations

$$
\begin{aligned}
\Gamma_{15}^- &\rightarrow \Delta_1 + \Delta_5 \\
\Gamma_{25}^+ &\rightarrow \Delta_{2'} + \Delta_5.
\end{aligned}
$$

$$(14.16)$$
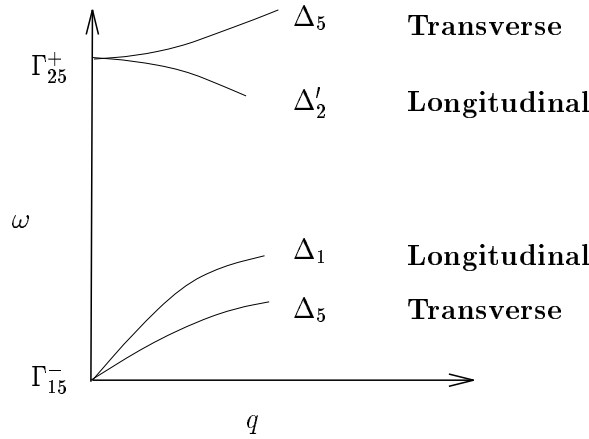
Figure 14.8: Lattice modes along the Δ-axis for the diamond structure.

Group theory gives no information on the relative frequencies of the Γ_{15}^{-} and Γ_{25}^{+} modes.

We finally note that the Raman tensor for the Raman-active Γ_{25}^{+} mode at the zone center transforms as $E_x^i E_y^s \, \alpha_{xy}(\Gamma_{25}^{+})$ plus cyclic permutations. Thus, observation of this mode requires $(\|, \perp)$ settings of the incident and scattered polarizations, respectively.

14.3.4 Phonons in the Zincblende Structure

Closely related to the diamond structure is the zincblende structure (space group $F\overline{4}3m$ #216, T_d^3) where the two fcc sublattices are distinct. This is the crystal structure for III-V semiconductor compounds such as GaAs. For this case the Ga atoms (ions) would be on one fcc sublattice and the As ions on the other fcc sublattice.

Since the sublattices are distinct, the group of the $\vec{k}$-vector at $\vec{k} = 0$ for the zincblende structure has only the operations of the point group T_d. In calculating $\chi_{\text{lattice modes}}$ we note that the vector in group T_d transforms as irreducible representation T_2. Thus from the irreducible representations contained in $\chi_{\text{atom sites}}$

$$\chi_{\text{atom sites}} = 2A_1 = 2\Gamma_1$$

we take the direct product of $\chi_{\text{atom sites}}$ with χ_{vector} to obtain

$$\chi_{\text{lattice modes}} = 2A_1 \otimes T_2 = 2T_2 = 2\Gamma_{15}. \qquad (14.17)$$

For the zincblende structure, the optic mode is both infrared-active and Raman-active since the irreducible representation T_2 for point group T_d corresponds to both T_{1u} and T_{2g} of the point group O_h. This correspondence is apparent from the character tables for T_d and O_h (see Table 13.2 on p. 354).

14.4 Lattice Modes Away From $\vec{k} = 0$

Modes at $\vec{k} \neq 0$ can be observed by optical spectroscopy when super-lattice effects are present, giving rise to zone folding. Non-zone center modes can also be observed in second-order Raman spectra (comprising phonons with wave vectors $+\vec{k}$ and $-\vec{k}$). Lattice modes at $\vec{k} \neq 0$ are routinely observed by inelastic neutron scattering techniques.

To construct phonon branches for the entire range of $\vec{k}$ vectors within the first Brillouin zone, we must consider the general procedure for finding the lattice modes at other high symmetry points and we make use of compatibility relations to relate these solutions to related solutions of neighboring $\vec{k}$-points.

The procedure for finding lattice modes at $\vec{k} \neq 0$ is outlined below:

1. Find the appropriate group of the wave vector at point $\vec{k}$.

2. Find $\chi_{\text{atom sites}}$ and χ_{vector} for this group of the wave vector.

3. Within a unit cell

$$\chi_{\text{lattice modes}} = \chi_{\text{atom site}} \otimes \chi_{\text{vector}} \qquad (14.18)$$

Find the symmetry types and mode degeneracies of $\chi_{\text{lattice modes}}$.

4. Introduce a phase factor relating unit cells with translation by $\vec{\tau}$:

$$P_{\{\varepsilon|\tau\}}\Psi_k(\vec{r}) = e^{i\vec{k}\cdot\vec{\tau}}\Psi_k(\vec{r}) \quad \text{Bloch theorem} \qquad (14.19)$$

5. Find lattice modes (including phase factor).

We illustrate these issues in terms of the NaCl structure which was previously considered with regard to its normal modes at $\vec{k} = 0$ (see §14.3.1).

14.4.1 Phonons in NaCl at the X point $k = \frac{\pi}{a}(100)$

We use essentially the same steps to get normal modes at the X point as we used for the normal modes in the Γ point (see §14.2). The group of the wave vector at point X is given in the table in §13.4. We first identify the symmetry operations of point group D_{4h}. We then obtain $\chi_{\text{atom sites}}$ for these symmetry operations.

We first review the situation for the Γ point:

Γ point	E	$8C_3$	$3C_4^2$	$6C_2'$	$6C_4$	i	$8iC_3$	$3iC_4^2$	$6iC_2'$	$6iC_4$
$\chi_{\text{atom sites}}^{\text{Na}}$	1	1	1	1	1	1	1	1	1	1
$\chi_{\text{atom sites}}^{\text{Cl}}$	1	1	1	1	1	1	1	1	1	1

Thus, we have $\chi_{\text{atom sites}}$ for the Na and Cl ions, and for χ_{vector}

$$\chi_{\text{a.s.}}^{\text{Na}} = \Gamma_{1g} = \Gamma_1^+$$
$$\chi_{\text{a.s.}}^{\text{Cl}} = \Gamma_{1g} = \Gamma_1^+$$
$$\chi_{\text{vector}} = \Gamma_{15}^-$$

so that

$$\chi_{\text{lattice vibrations}} = 2\Gamma_1^+ \otimes \Gamma_{15}^- = 2\Gamma_{15}^-.$$

Similarly for the X point, we first find $\chi_{\text{atom sites}}$ for each type of atom.

X point	E	$2C_{4\perp}^2$	$C_{4\parallel}^2$	$2C_{4\parallel}$	$2C_2$	i	$2iC_{4\perp}^2$	$iC_{4\parallel}^2$	$2iC_{4\parallel}$	$2iC_2$
$\chi_{\text{atom sites}}^{\text{Na}}$	1	1	1	1	1	1	1	1	1	1
$\chi_{\text{atom sites}}^{\text{Cl}}$	1	1	1	1	1	1	1	1	1	1

Thus, we obtain $\chi_{\text{atom sites}}$, χ_{vector}, and $\chi_{\text{lattice vector}}$ at the X point:

$$\chi_{\text{a.s.}}^{\text{Na}} = X_1$$
$$\chi_{\text{a.s.}}^{\text{Cl}} = X_1$$
$$\chi_{\text{vector}} = X_4' + X_5',$$

where X_4' corresponds to x and X_5' corresponds to (y, z). We thus obtain

$$\chi_{\text{lattice vibrations}} = 2X_1 \otimes (X_4' + X_5') = 2X_4' + 2X_5'.$$

Compatibility relations give $\Gamma_{15} \to \Delta_1 + \Delta_5 \to X_4' + X_5'$.

The action of the translation operator on a basis function (normal mode) yields

$$\hat{P}_{\{\varepsilon|\tau\}} u(\vec{r}) = e^{i\vec{k}\cdot\vec{\tau}} u(\vec{r}) \qquad (14.20)$$

where $\vec{k} = \frac{\pi}{a}\hat{x}$ at the X point under consideration. For $\vec{R}_n = a\hat{x}$ we obtain $e^{i\vec{k}\cdot\vec{\tau}} = e^{i\pi} = -1$ so that there is a π phase difference between unit cells along $\hat{x}$. However, for $\vec{R}_n = a\hat{y}$ or $a\hat{z}$, we have $e^{i\vec{k}\cdot\vec{\tau}} = e^{i(0)} = 1$, and there is no phase difference along $\hat{y}$ and $\hat{z}$.

The phase factor of Eq. 14.20 refers to the relative phase between atoms in adjacent unit cells. The relative motion between atoms within a unit cell was considered in §14.2. Thus the NaCl structure (#225) has a set of 3 acoustic branches and 3 optical branches each having X_4' and X_5' symmetries at the X point, where

$$
\begin{array}{ll}
X_4' & \to x \\
X_5' & \to y, z
\end{array}
$$

The normal modes for the 3 acoustic branches are shown in Fig. 14.9 in terms of the symmetry classifications X_4' and X_5' (2-fold) for the longitudinal and transverse branches, respectively. The corresponding normal modes for the 3 optical branches are shown in Fig. 14.10.

For rows of atoms in unit cells along the y and z directions, there will be essentially **zero** phase difference ($\delta = \pi/N$, where $N \approx 10^7$) between molecules vibrating in the acoustic mode as we move in the y and z directions. This is also true for the optical branches shown in Fig. 14.10.

14.4.2   Phonons in BaTi$_3$ at the X point

The modes in this case involve more than one atom of the same species within the unit cell so that a few new aspects enter the lattice mode problem in this case. The character table for the group of the wave

Acoustic branches $k_x = \pi/a$
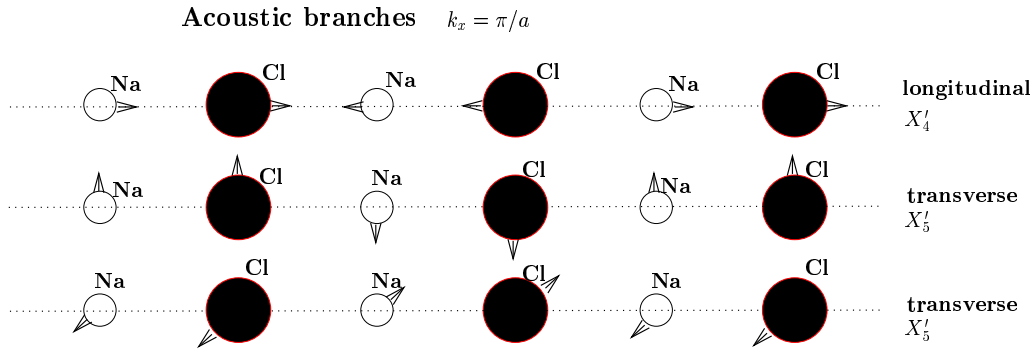
Figure 14.9: Acoustic branch for the vibrational modes of NaCl showing longitudinal and transverse modes at the X point ($k_x = \pi/a$) in the Brillouin zone for the X_4' and X_5' modes.
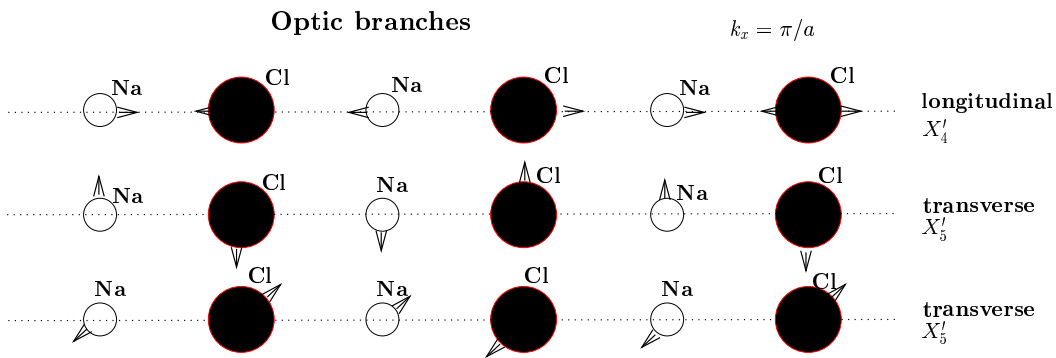
Optic branches $k_x = \pi/a$

Figure 14.10: Optic branch for the vibrational modes of NaCl showing longitudinal and transverse modes at the X point ($k_x = \pi/a$) in the Brillouin zone for the X_4' and X_5' modes.

vector at the X point for $BaTiO_3$ is the same as for NaCl. At the X point, we compute $\chi_{\text{atom sites}} \equiv \chi_{\text{a.s.}}$ using the symmetry operators for the group of the wave vector at the X point making use of the notation in Fig. 14.5.

X point	E	$2C_{4\perp}^2$	$C_{4\parallel}^2$	$2C_{4\parallel}$	$2C_2$	i	$2iC_{4\perp}^2$	$iC_{4\parallel}^2$	$2iC_{4\parallel}$	$2iC_2$
$\chi_{\text{Ba atom sites}}$	1	1	1	1	1	1	1	1	1	1
$\chi_{\text{Ti atom sites}}$	1	1	1	1	1	1	1	1	1	1
$\chi_{\text{O}_3 \text{ atom sites}}$	3	3	3	1	1	3	3	3	1	1

$$
\begin{aligned}
\chi_{\text{Ba atom sites}} &= X_1 \\
\chi_{\text{Ti atom sites}} &= X_1 \\
\chi_{\text{O}_3 \text{ atom sites}} &= 2X_1 + X_2 \\
\chi_{\text{vector}} &= X_4' + X_5'
\end{aligned}
$$

$$(14.21)$$

where X_4' corresponds to x, and X_5' to (y, z). The symmetries of the normal modes are found by taking the direct product of $\chi_{\text{atom sites}} \otimes \chi_{\text{vector}}$

$$
\begin{aligned}
\chi_{\text{Ba lattice modes}} &= X_1 \otimes (X_4' + X_5') = X_4' + X_5' \\
\chi_{\text{Ti lattice modes}} &= X_1 \otimes (X_4' + X_5') = X_4' + X_5'
\end{aligned}
$$

The Ba and Ti atoms form normal modes similar to NaCl with the Ba moving along x (X_4' symmetry) or along y or z (X_5' symmetry) with the Ti and O_3 at rest, and likewise for the Ti atoms moving along the x direction. The phase relations for atomic vibrations in adjacent unit cells in the x direction have a phase factor $e^{\pi i} = -1$, while rows of similar atoms in the y and z direction have no phase shift. For the oxygens,

$$\chi_{\text{O}_3 \text{ lattice modes}} = (2X_1 + X_2) \otimes (X_4' + X_5') = 2X_4' + X_3' + 3X_5' \quad (14.22)$$

The mode patterns at the X point for $BaTiO_3$ are given in Fig. 14.11.
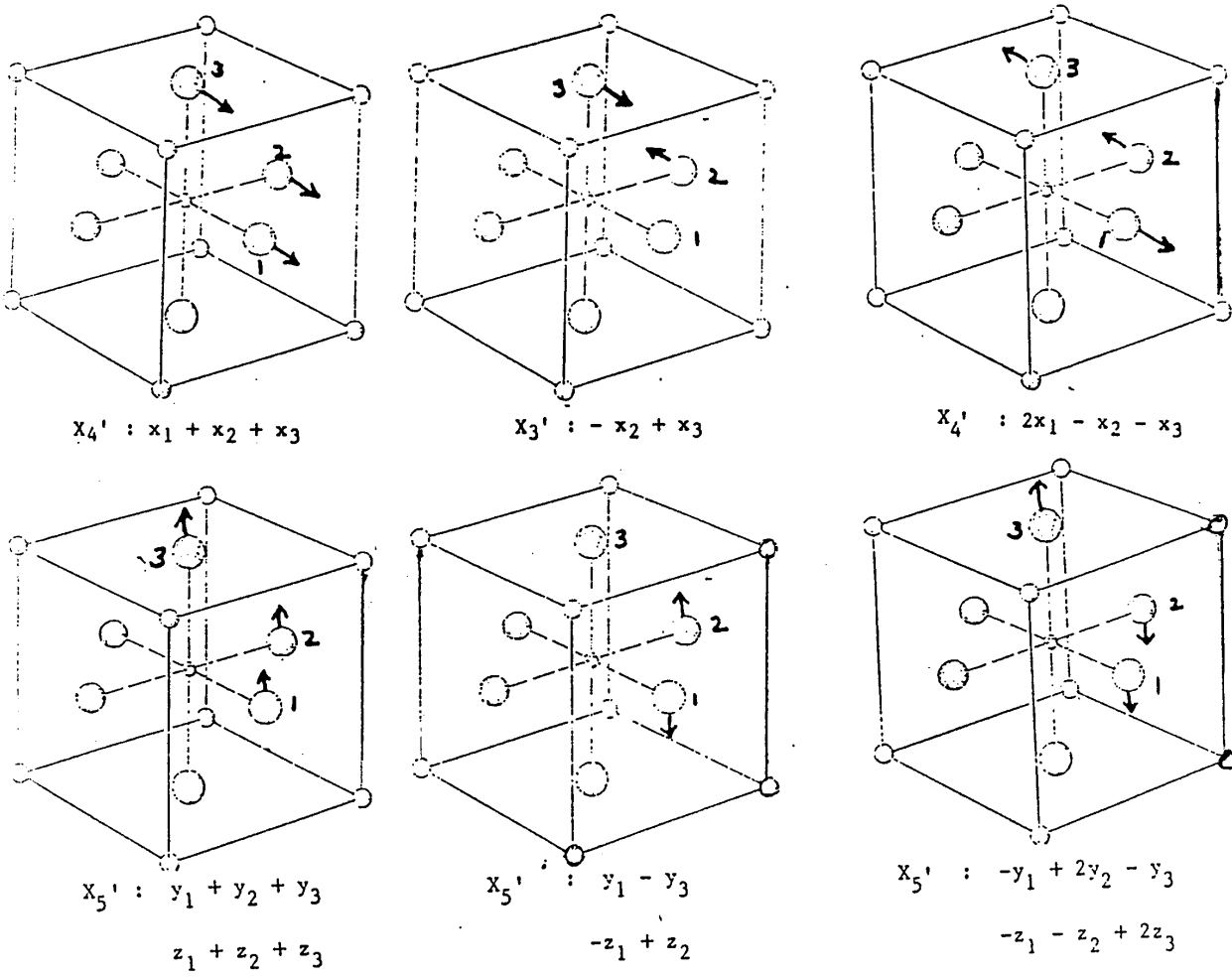
Figure 14.11: Mode patterns models for the X point modes in BaTiO$_3$. The basis functions for each normal mode are indicated.

The mode symmetry and the normal mode displacements are verified by the following considerations. Perusal of the X-point character table shows that the symmetry types are uniquely specified by the operations $C_{4\parallel}, C_2$ and i. The effect of these operations on the coordinates (x, y, z) and on the site locations are:

$$C_{4\parallel} \begin{pmatrix} 1 \\ 2 \\ 3 \end{pmatrix} = \begin{pmatrix} 1 \\ 3 \\ 2 \end{pmatrix} \qquad C_{4\parallel} \begin{pmatrix} x \\ y \\ z \end{pmatrix} = \begin{pmatrix} x \\ -z \\ y \end{pmatrix}$$

$$C_2 \begin{pmatrix} 1 \\ 2 \\ 3 \end{pmatrix} = \begin{pmatrix} 1 \\ 3 \\ 2 \end{pmatrix} \qquad C_2 \begin{pmatrix} x \\ y \\ z \end{pmatrix} = \begin{pmatrix} -x \\ z \\ y \end{pmatrix}$$

$$i \begin{pmatrix} 1 \\ 2 \\ 3 \end{pmatrix} = \begin{pmatrix} 1 \\ 2 \\ 3 \end{pmatrix} \qquad i \begin{pmatrix} x \\ y \\ z \end{pmatrix} = \begin{pmatrix} -x \\ -y \\ -z \end{pmatrix}$$

By carrying out the symmetry operations on the basis functions, we verify that the matrix representations for each of the symmetry operations have the correct characters for the X_4' irreducible representation:

$$\begin{array}{ll} C_{4\parallel}(x_1 + x_2 + x_3) = (x_1 + x_3 + x_2) & \text{so that} \quad \chi^{(C_{4\parallel})} = +1 \\ C_2(x_1 + x_2 + x_3) = -(x_1 + x_3 + x_2) & \chi^{(C_2)} = -1 \\ i(x_1 + x_2 + x_3) = -(x_1 + x_2 + x_3) & \chi^{(i)} = -1 \end{array}$$

Applying the same approach to the normal mode displacements with X_5' symmetry we have:

$$C_{4\parallel} \begin{pmatrix} y_1 + y_2 + y_3 \\ z_1 + z_2 + z_3 \end{pmatrix} = \begin{pmatrix} -z_1 - z_3 - z_2 \\ y_1 + y_3 + y_2 \end{pmatrix} = \begin{pmatrix} 0 & -1 \\ 1 & 0 \end{pmatrix} \begin{pmatrix} y_1 + y_2 + y_3 \\ z_1 + z_2 + z_3 \end{pmatrix}$$

$$i \begin{pmatrix} y_1 + y_2 + y_3 \\ z_1 + z_2 + z_3 \end{pmatrix} = \begin{pmatrix} -1 & 0 \\ 0 & -1 \end{pmatrix} \begin{pmatrix} y_1 + y_2 + y_3 \\ z_1 + z_2 + z_3 \end{pmatrix}$$

so that $\chi(C_{4\parallel}) = 0$, and $\chi(i) = -2$, which are the correct characters for the X_5' irreducible representation. Finally for the X_3' modes:

Table 14.1: Basis functions for the various irreducible representations entering the lattice modes in $BaTiO_3$.

Basis Functions	Irreducible representation
$x_3 - x_2$	X_3'
$\left.\begin{array}{l} y_1 - y_3 \\ -z_1 + z_2 \end{array}\right\}$	X_5'
$2x_1 - x_2 - x_3$	X_4'
$\left.\begin{array}{l} -y_1 + 2y_2 - y_3 \\ -z_1 - z_2 + 2z_3 \end{array}\right\}$	X_5'
$x_1 + x_2 + x_3$	X_4'
$\left.\begin{array}{l} y_1 + y_2 + y_3 \\ z_1 + z_2 + z_3 \end{array}\right\}$	X_5'

$$C_{4\parallel}(-x_2 + x_3) = (-x_3 + x_2) = -(-x_2 + x_3) \quad \rightarrow \chi(C_{4\parallel}) = -1$$
$$C_2(-x_2 + x_3) = x_3 - x_2 = (-x_2 + x_3) \quad \rightarrow \chi(C_2) = +1$$
$$i(-x_2 + x_3) = -(-x_2 + x_3) \quad \rightarrow \chi(i) = -1$$

These same calculations can be applied to the basis functions in Fig. 14.11 and their irreducible representations and the results are listed in Table 14.1.

The phase factors for oxygens separated by a lattice vector $a\hat{x}$ are $e^{\pi i} = -1$ while the oxygens separated by a lattice vector $a\hat{y}$ or $a\hat{z}$ have no phase difference (i.e., phase factor $\equiv 1$).

14.5 Phonons in Te and Quartz

In this section we discuss phonon modes for tellurium (with 3 atoms/unit cell) and show how the lattice modes for this non-symmorphic structure can be used to obtain the lattice modes for α-quartz (with 9 atoms/unit cell) which has the same space group as Te.

14.5.1   Phonons in Tellurium: A Non-Symmorphic Structure

The structure for Te (space groups $P3_121'$, #152; $P3_221'$, #154) is a spiral non-symmorphic space group as shown in Fig. 14.12. There are 3 Te atoms/unit cell and these Te atoms are at levels 0, $c/3$ and $2c/3$. The structure for right-handed Te shows a right-handed screw when viewed along $+\hat{z}$. When the atoms are arranged with the opposite screw orientation, we have left-handed Te. Three-fold rotations about the c axis must be combined with a translation $\vec{\tau} = \frac{c}{3}(001)$ to leave the crystal invariant. The 3 two-fold symmetry axes normal to the 3-fold axis do not require translations. The appropriate point group at $\vec{k} = 0$ is D_3 and the character table is shown below. Note that mirror planes are not symmetry operations.

D_3 (32)				E	$2C_3$	$3C_2'$
$x^2 + y^2, z^2$			A_1	1	1	1
		R_z, z	A_2	1	1	-1
(xz, yz) $(x^2 - y^2, xy)$ $\Big\}$		(x, y) (R_x, R_y) $\Big\}$	E	2	-1	0

Following the same procedure as was used for the non-symmorphic diamond structure (see §14.3.3), we find $\chi_{\text{atom sites}}$ by considering the number of sites within the unit cell that remain invariant (or transform into the identical site in a neighboring unit cell):

	$\{E|0\}$	$2\{C_3|\tau\}$	$3\{C_{2'}|0\}$	
$\chi_{\text{atom sites}}$	3	0	1	$= A_1 + E$

To find the lattice vibrations, we note that the vector transforms as $A_2 + E$. This allows us to separate out the lattice modes in the z-direction from those in the $x - y$ plane. For the z-**direction**

$$\chi_{\text{atom sites}} \otimes \chi_{\text{vector, z}} = (A_1 + E) \otimes A_2 = A_2 + E \qquad (14.23)$$

where the A_2 mode corresponds to pure translations in the z direction at $\vec{k} = 0$. The phonon dispersion curves for tellurium have been measured

(a)

(b)
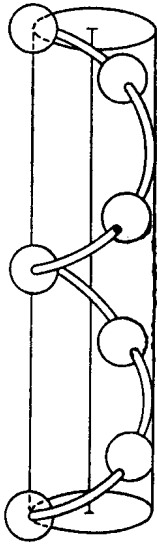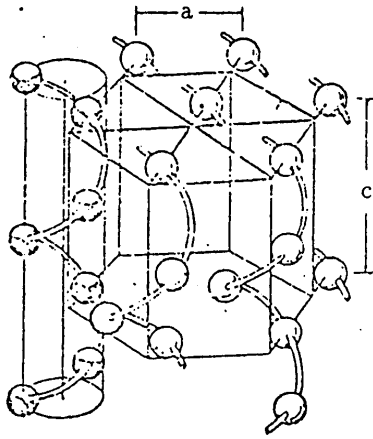
Figure 14.12: Model for the Te crystal structure.
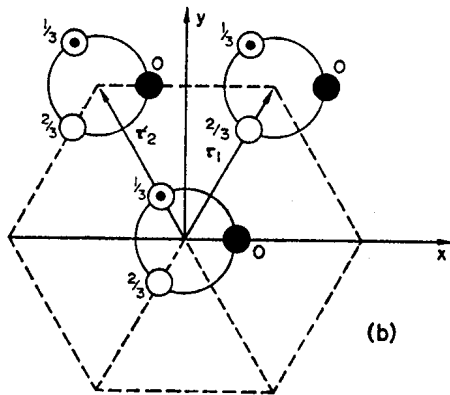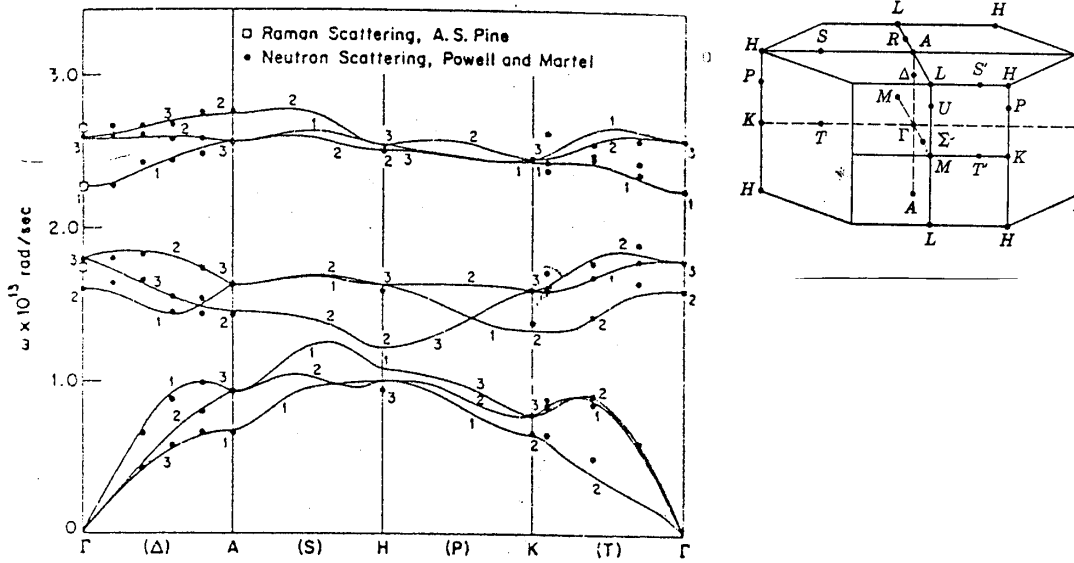
Figure 14.13: Phonon modes for Te.

by inelastic neutron scattering and the results along the high symmetry axes are shown in Fig. 14.13.

We show the normal modes with A_2 and E symmetry in Fig. 14.14. For the in-plane motion, the symmetries are obtained by computing:

$$\chi_{\text{atom sites}} \otimes \chi_{\text{vector (x,y)}} = (A_1 + E) \otimes E = E + (A_1 + A_2 + E) \quad (14.24)$$

The translational mode in the x, y directions transforms as E. The in-plane modes at $\vec{k} = 0$ are shown in Fig. 14.15. The A_2 and E modes are IR active, and the A_1 and E modes are Raman-active.

Since the Te structure has a screw axis, right and left circularly polarized light are of importance for optical experiments. For linear polarization we consider the $\vec{E}$ vector for the light in terms of x, y, z components. For circular polarization we take the linear combinations $(x + iy)$ and $(x - iy)$. From the character table, we note that $(x + iy)(x - iy) = x^2 + y^2$ transforms as A_1 and the dipole moment $\vec{u}$ is

(a)

$z_1 + z_2 + z_3$

A_2

(b)

$z_1 + \omega z_2 + \omega^2 z_3$

E

partner is c.c.
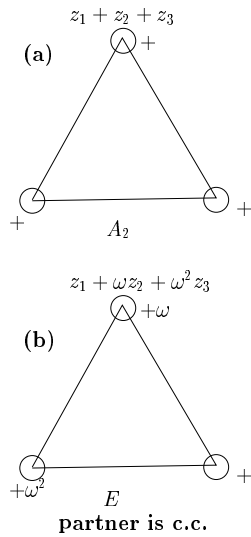
Figure 14.14: Normal modes for Te for z-axis vibrations. The A_2 mode (a) is a pure translational mode along the z-axis. The E mode has displacements along z which have phase differences of $\omega = \exp(2\pi i/3)$ with respect to one another. One partner of the E mode is shown explicitly in (b). For the other partner, the displacements correspond to the interchange of $\omega \leftrightarrow \omega^2$, yielding the complex conjugate (c.c.) of the mode that is shown.
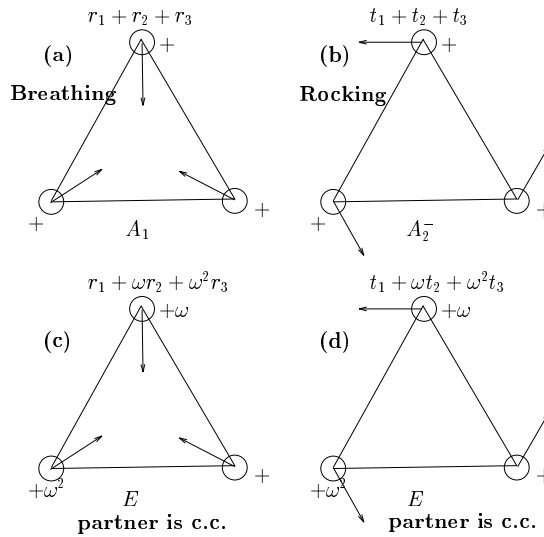
Figure 14.15: In-plane normal modes for Te. The A_1 normal mode (a) is a breathing mode, while the A_2 mode (b) is a rocking mode corresponding to rotations of the 3 tellurium atoms for each half cycle of the vibration. The two E modes (c, d) can be described as a breathing and a rocking mode with phase relations $\omega = \exp(2\pi i/3)$ between each of the atoms as indicated (with the complex conjugate partner in each case obtained by the interchange of $\omega \leftrightarrow \omega^2$).

related to the polarizability tensor $\overset{\leftrightarrow}{\alpha}$ by:

$$
\begin{pmatrix} (u_x + iu_y)/\sqrt{2} \\ (u_x - iu_y)/\sqrt{2} \\ u_z \end{pmatrix} = \begin{pmatrix} \alpha_{11} & \alpha_{12} & \alpha_{13} \\ \alpha_{21} & \alpha_{22} & \alpha_{23} \\ \alpha_{31} & \alpha_{32} & \alpha_{33} \end{pmatrix} \begin{pmatrix} (E_x + iE_y)/\sqrt{2} \\ (E_x - iE_y)/\sqrt{2} \\ E_z \end{pmatrix}
$$

$$(14.25)$$

so that the polarizability tensor for A_1 modes will have the form:

$$
\overset{\leftrightarrow}{\alpha}_{A_1'} = \begin{pmatrix} a & 0 & 0 \\ 0 & a & 0 \\ 0 & 0 & 0 \end{pmatrix}
$$

for in-plane motion with the Raman tensor having components $(E_+^i E_-^s + E_-^i E_+^s)\alpha(A_1)$. The polarizability tensor for the z-axis motion is

$$
\overset{\leftrightarrow}{\alpha}_{A_1''} = \begin{pmatrix} 0 & 0 & 0 \\ 0 & 0 & 0 \\ 0 & 0 & b \end{pmatrix}
$$

with the Raman tensor having components $E_z^i E_z^s \alpha(A_1)$. Finally for general A_1 motion, the polarizability tensor is written as:

$$
\overset{\leftrightarrow}{\alpha}_{A_1} = \begin{pmatrix} a & 0 & 0 \\ 0 & a & 0 \\ 0 & 0 & b \end{pmatrix}.
$$

$$(14.26)$$

To find the energy for aligning the dipole moment in an electric field, we need to take the dot product of the dipole moment with the electric field

$$
\vec{E}^* \cdot \vec{u} = \left([E_x - iE_y]/\sqrt{2}, (E_x + iE_y)/\sqrt{2}, E_z\right) \cdot \begin{pmatrix} (u_x + iu_y)/\sqrt{2} \\ (u_x - iu_y)/\sqrt{2} \\ u_z \end{pmatrix}
$$

so that

$$
\vec{E}^* \cdot \vec{u} = (E_-, E_+, E_z) \cdot \begin{pmatrix} u_+ \\ u_- \\ u_z \end{pmatrix}
$$
$$
= E_- u_+ + E_+ u_- + E_z u_z = E_x u_x + E_y u_y + E_z u_z = \text{real quantity.}
$$

For the electromagnetic (infrared) interaction, the pertinent symmetries are $E_+ u_-(E) + E_- u_+(E)$ for in-plane motion and $E_z u_z(A_2)$ for z-axis motion.

In considering the Raman effect, we find the energy of the Raman interaction in terms of $\vec{E}^* \cdot \overset{\leftrightarrow}{\alpha} \cdot \vec{E}$ which when properly symmetrized becomes $\frac{1}{2}\left[\vec{E}^* \cdot \overset{\leftrightarrow}{\alpha} \cdot \vec{E} + \vec{E} \cdot \overset{\leftrightarrow}{\alpha}^* \cdot \vec{E}^*\right]$. Thus for the Raman mode with A_1 symmetry, the induced dipole u_+ has the same sense of polarization as the incident electric field. However, the energy involves $\vec{E}_i^*$ and $\vec{E}_s$ or alternatively $\vec{E}_s^*$ and $\vec{E}_i$ to yield $\frac{1}{2}(E_+^i E_-^s + E_-^i E_+^s)$ which transforms as $(x + iy)(x - iy) = x^2 + y^2$ as desired for a basis function with A_1 symmetry.

For Raman modes with E symmetry we can have a dipole moment u_z induced by E_+, leading to the combination of electric fields $E_z^* E_+$. To have a symmetric polarizability tensor, we must also include the term $(E_z^* E_+)^* = E_- E_z$ since the energy must be unchanged upon interchange of electric fields $\vec{E} \leftrightarrow \vec{E}^*$. Thus the polarizability and Raman tensors must be of the form

$$\overset{\leftrightarrow}{\alpha}_{E,1} = \begin{pmatrix} 0 & 0 & 0 \\ 0 & 0 & r^* \\ r & 0 & 0 \end{pmatrix} \text{ and } \begin{cases} E_+^i E_z^s \alpha_-(E) + E_-^i E_z^s \alpha_+(E) \\ \text{or } E_z^i E_+^s \alpha_-(E) + E_z^i E_-^s \alpha_+(E) \end{cases} \quad (14.27)$$

The partner of this polarizability tensor with E symmetry will produce the displacement u_z from an electric field displacement E_- yielding

$$\overset{\leftrightarrow}{\alpha}_{E,2} = \begin{pmatrix} 0 & 0 & r \\ 0 & 0 & 0 \\ 0 & r^* & 0 \end{pmatrix}. \quad (14.28)$$

The other lattice mode for Te with E symmetry (denoted here by E') produces a dipole moment u_+ from an electric field E_-. This however involves $E_-(E_+)^* = E_-^2$ for the incident and scattered electric fields so that the polarizability tensor in this case is

$$\overset{\leftrightarrow}{\alpha}_{E',1} = \begin{pmatrix} 0 & s & 0 \\ 0 & 0 & 0 \\ 0 & 0 & 0 \end{pmatrix}; \text{ basis function } x_-^2 \quad (14.29)$$

and the corresponding partner is

$$\overleftrightarrow{\alpha}_{E',2} = \begin{pmatrix} 0 & 0 & 0 \\ s^* & 0 & 0 \\ 0 & 0 & 0 \end{pmatrix} ; \quad \text{basis function } x_+^2. \qquad (14.30)$$

The Raman tensor for the E' mode has the form $E_+^i E_+^s \alpha_+(E) + E_-^i E_-^s \alpha_-(E)$. We can relate these partners of the E' modes to the basis functions of the character table for D_3 by considering the basis functions for the partners:

$$\text{partner } \#1 \quad : \quad \frac{1}{2}(x - iy)^2 = x_-^2$$

$$\text{partner } \#2 \quad : \quad \frac{1}{2}(x + iy)^2 = x_+^2$$

$$(14.31)$$

By taking the sums and differences of these partners we obtain

$$x_+^2 + x_-^2 = \frac{1}{2}(x + iy)^2 + \frac{1}{2}(x - iy)^2 = (x^2 - y^2)$$

$$x_+^2 - x_-^2 = \frac{1}{2}(x + iy)^2 - \frac{1}{2}(x - iy)^2 = 2xy \qquad (14.32)$$

which form a set of partners listed in the character table for D_3.

14.5.2 Phonons in the Non-Symmorphic α-Quartz Structure

We will now examine the lattice modes of α-quartz (space group D_3^4, #152, $P3_1 21$ for the right hand crystal or D_3^5, #153, $P3_2 12$ for the left-hand crystal) in both its natural state and in the presence of an applied uniaxial compressive force. We will use this as a means for showing how lattice modes for crystals with several atoms per unit cell can be built up from simpler units, in this case the tellurium structure discussed in §14.5.1.

The spiral structure of α-quartz about the z-axis is shown in Fig. 14.16a where each solid ball represents a SiO_2 unit. This diagram is identical to that for tellurium (see Fig. 14.12). The projection of the atoms onto
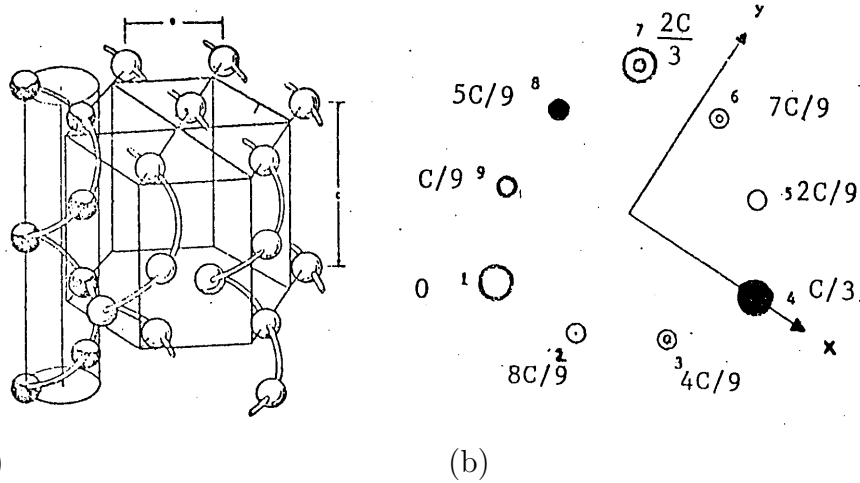
(a)   (b)

Figure 14.16: Structure of (a) right-handed α-quartz and (b) the projection of the atoms on the basal plane of α-quartz. Atoms #1, 4, 7 denote Si and the other numbers denote oxygen atoms.

the basal plane is shown in Fig. 14.16b. The Si atoms (1, 4 and 7) occupy positions at levels 0, $c/3$, $2c/3$ respectively (as for tellurium). The oxygen atoms (9, 5, 3, 8, 6 and 2) occupy positions at levels $c/9$, $2c/9$, $4c/9$, $5c/9$, $7c/9$ and $8c/9$ respectively. (These sites are of course not occupied in tellurium.) Note that the space group of α-quartz is D_3^4. Figure 14.16 shows the right-handed tellurium structure.

There are 3 molecular SiO_2 units per unit cell giving rise to 9 atoms per unit cell or **27 lattice branches** of which 24 are optic modes. By examining the atom locations in Fig. 14.16b, we can determine the point group symmetry of α-quartz. The z axis is a three-fold axis of rotation when combined with the translation $\vec{\tau} = (c/3)(001)$. In addition there is a two-fold axis from the center to each of the silicon atoms. The symmetry elements are the same as for tellurium discussed in §14.5.1. In order to determine the normal modes of vibration we first find the characters for the transformation of the atomic sites. It is convenient to make use of the results for tellurium, noting that the silicon atoms in quartz occupy the same sites as in tellurium. We thus obtain for the modes in α-quartz at $\vec{k} = 0$.

	$\{E\vert 0\}$	$2\{C_3\vert\tau\}$	$3\{C_{2'}\vert 0\}$	
$\chi_{\text{Si atom sites}}$	3	0	1	$= A_1 + E$
$\chi_{\text{oxygen atom sites}}$	6	0	0	$= A_1 + A_2 + 2E$

The lattice modes for the silicon are identical with those found previously for Te, so that part of the problem is already finished. For the 6 oxygens we have:

$$\chi_{\text{lattice modes, z}} = (A_1 + A_2 + 2E) \otimes A_2 \quad \text{for z motion}$$
$$\chi_{\text{lattice modes x,y}} = (A_1 + A_2 + 2E) \otimes E \quad \text{for x, y motion}$$

Carrying out the direct products we obtain:

$$\chi_{\text{lattice modes, z}} = A_2 + A_1 + 2E \quad \text{for z motion}$$
$$\chi_{\text{lattice modes, x,y}} = 2A_1 + 2A_2 + 4E \quad \text{for x, y motion}$$

$$(14.33)$$

where we note that for the D_3 point group $E \otimes E = A_1 + A_2 + E$.

The corresponding z-axis normal modes A_2, A_1, E and E' for the 6 oxygens are shown in Fig. 14.17. The normal mode A_2 is clearly a uniform translation of the 6 oxygens while the A_1 mode is a rocking of the two oxygens on either side of a silicon atom (one going up, while the other goes down). The two-fold E mode is derived from A_2 by introducing phases 1, ω, ω^2 for each of the pairs of oxygens around a silicon atom; the complex conjugate E mode is obtained from the one that is illustrated by the substitution $\omega \leftrightarrow \omega^2$. Finally the E' mode is obtained from the A_1 mode in a similar way as the E mode is obtained from the A_2 mode. In identifying the symmetry type for these normal modes, we note the effect of symmetry operation C_2'.

We now combine the z motion for the silicons (symmetries $A_2 + E$) with the z motion for the oxygens (symmetries $A_1 + A_2 + 2E$) to obtain $A_1 + 2A_2 + 3E$ for SiO$_2$. The resulting normal mode patterns are shown in Fig. 14.18. The z-axis translational mode for the 6 oxygens combine either in-phase or out of phase to form the two normal modes with A_2 symmetry. For the mode with A_1 symmetry, the silicon atoms remain stationary. Introducing the phases 1, ω, ω^2 for each SiO$_2$ group gives the three E normal modes along the z-direction in α-quartz.
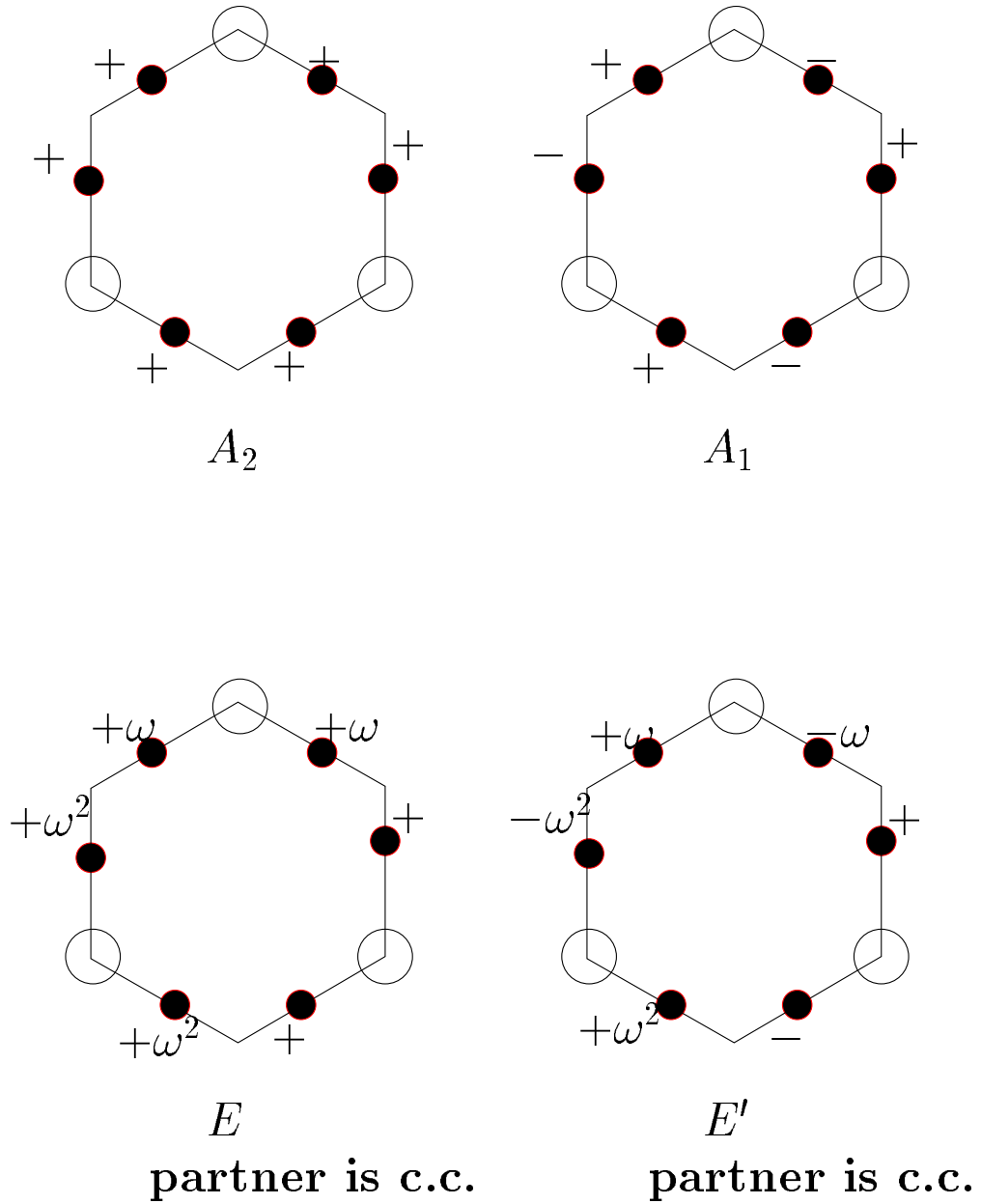
Figure 14.17: Normal modes along the z-direction for the six oxygens in the α-quartz crystal. The A_2 mode is a uniform translation while the A_1 mode is a rocking of the oxygens around the Si. The E modes are related to the A_2 and A_1 modes by combining the $1, \omega, \omega^2$ phases with the translational and rocking motions.
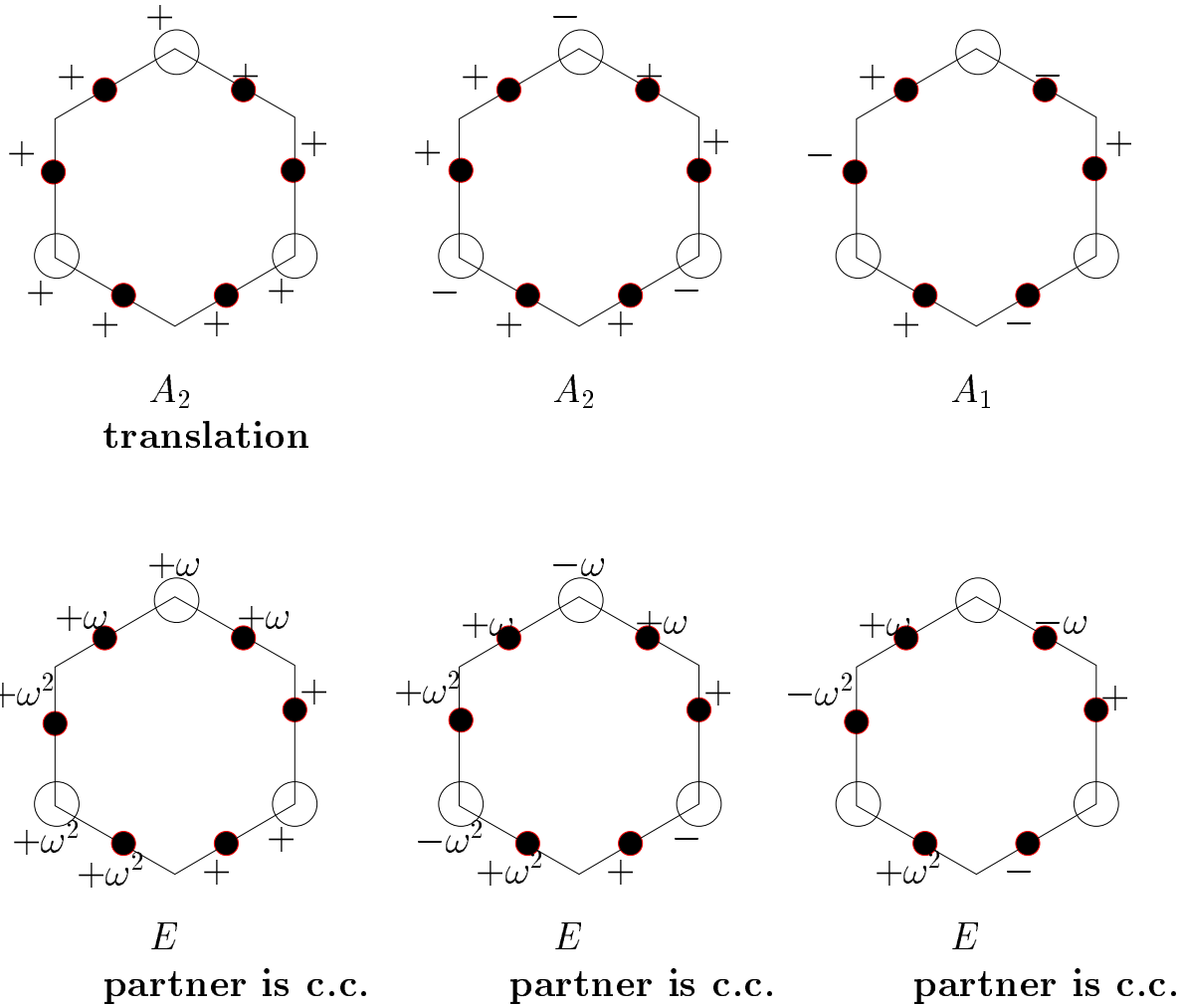
Figure 14.18: Normal modes along the z-direction for the three SiO_2 groups in α-quartz. Here the motions of the Si atoms are combined with those of the oxygens.

A_1
radial breathing

E
phased breathing

A_1
tangential breathing

A_2
radial breathing

A_2
rocking
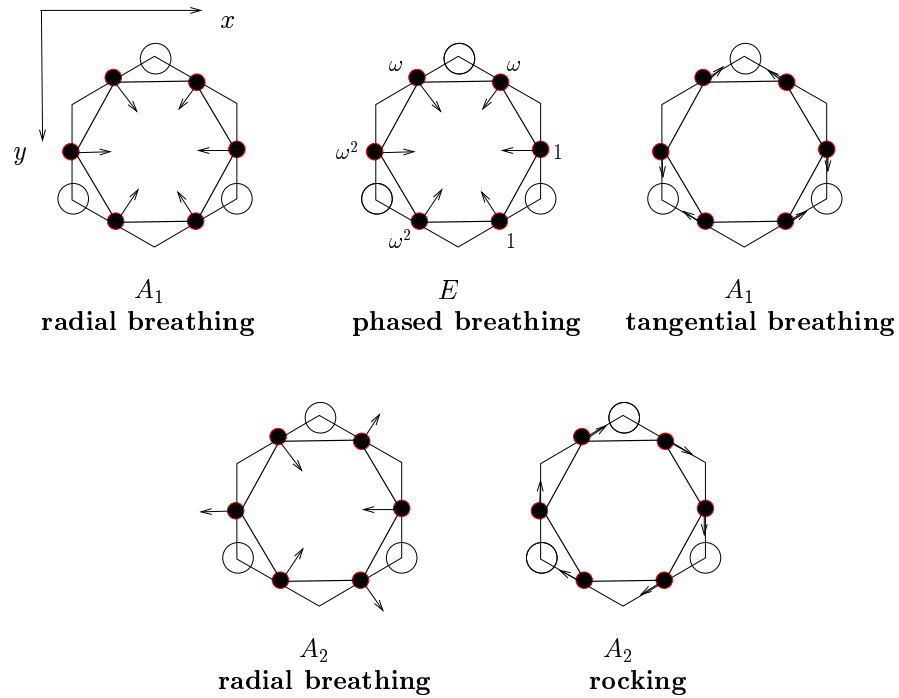
Figure 14.19: Normal modes in the $x - y$ plane for the six oxygens in the α quartz crystal. In addition, the A_1 tangential breathing mode, the A_2 radial breathing breathing mode, and the A_2 rocking mode have corresponding E modes, with phases $1, \omega, \omega^2$ for the three SiO_2 units, each having two partners related by $\omega \leftrightarrow \omega^2$. In the crystal, all modes with the same symmetry are coupled so that the actual normal mode is an admixture of the modes pictured here.

For the xy motion, the six oxygens form lattice modes with symmetries $2A_1 + 2A_2 + 4E$ and the normal mode patterns are shown in Fig. 14.19. When we now combine the silicon ($A_1 + A_2 + 2E$) and oxygens ($2A_1 + 2A_2 + 4E$) for the in-plane modes, we obtain symmetries $3A_1 + 3A_2 + 6E$ and the normal modes are shown in Fig. 14.19. For the A_1 breathing mode (a), all oxygens translate toward the center in phase, whereas for the A_2 mode (b) one oxygen of each SiO_2 group moves inward while the other moves outward. Another A_1 mode arises from each oxygen in a SiO_2 pair moving circumferentially toward the silicon atom, while an A_2 mode is formed by a circumferential trans-
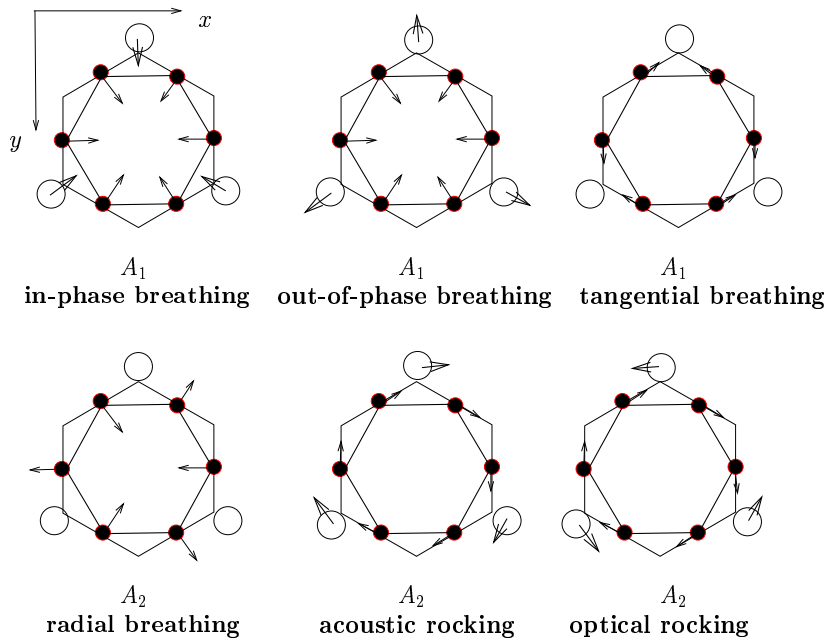
Figure 14.20: The in-plane normal modes for α-quartz obtained by superposition of the normal modes for the oxygens and the silicons. Corresponding to each of the one-dimensional modes shown here are two-dimensional E modes with phases $1, \omega, \omega^2$ for the three SiO_2 units, with the two partners related by $\omega \leftrightarrow \omega^2$.

lational rocking motion of the oxygens. Each of these 4 modes has corresponding E modes with each SiO_2 group assigned phases 1, ω, ω^2 and its complex conjugate. For the A_1 breathing mode in Fig. 14.20, we can have the silicons moving either in-phase or out of phase with respect to the oxygens, while for the A_2 mode in Fig. 14.20, the silicons remain at rest. For the circumferential translational A_2 motion, the silicons can go either in phase or they can move out of phase with respect to the oxygens. Finally the rocking motion of the oxygens with respect to static silicons forms an A_1 lattice mode. Associated with each A_1 and A_2 in-plane mode, are E modes with phases 1, ω, ω^2 as before. By superposing the normal modes of the oxygens and the silicons for the in-plane and c-axis modes, we can obtain all the normal modes (27 of them) for α-quartz.

The infrared-active modes have A_2 and E symmetries while the Raman-active modes have A_1 and E symmetries. The polarizability tensor for the A_1 and E modes is of the same form as given for the case of tellurium.

Since the E modes are infrared-active, polarization fields lift the two-fold degeneracy of every E mode giving rise to the so-called LO-TO splitting of the doubly degenerate Raman modes.

14.5.3 Effect of Uniaxial Stress on Phonons

In general, an external perturbation, when applied to a crystal, reduces the symmetry of the crystal. The fundamental principle used to deduce this lower symmetry is called the Curie principle which states that only those symmetry operations are allowed which are common to both the unperturbed system and to the perturbation itself. This condition restricts the new symmetry group to a subgroup common to the original group.

When a homogeneous uniaxial compression is applied to a crystal, the resulting strain is described by a symmetric tensor of the second rank. The strain tensor can be represented by a triaxial ellipsoid which has at least D_{2h} point group symmetry; if two of its major modes are equal, the ellipsoid acquires rotational symmetry about the third, and the point group symmetry is $D_{\infty h}$, whereas, if all three axes are equal it becomes a sphere with three dimensional continuous rotation and reflection symmetry. In order to determine the symmetry operations of the strained crystal it is necessary to know the orientation of the strain ellipsoid relative to the crystallographic axes. An alternative procedure is to treat the stress itself as the imposed condition and find the symmetry elements common to the unstrained crystal and to the symmetry of the stress tensor.

Using the symmetry properties of the stress tensor is particularly simple when the external perturbation is a uniaxial compression. In this case the stress ellipsoid has $D_{\infty h}$ point group symmetry and can be conveniently represented by a right circular cylinder with its center coinciding with the center of the crystal and its axis of revolution along the direction of the force. The symmetry operations common to the unstrained crystal and to the cylinder representing the stress can then

be easily determined by inspection.

As an illustrative case, consider the point group D_3, the point group of α-quartz. The symmetry operations of D_3 are a three-fold axis of rotation along the z axis and three two-fold axes perpendicular to the z axis, one of which is taken to be the x axis. If the force, $\vec{F}$, is applied along the z direction, all of the operations of the group are common to the symmetry of the stress and hence the symmetry remains D_3. If, however, the force is applied along the x direction, the only remaining symmetry operation is C_2. Similarly, if the force is applied along the y axis, the only remaining symmetry operation is again the two-fold axis of rotation along the x-axis and the symmetry is reduced to the point group C_2. If the force is in a direction other than along z or parallel or perpendicular to a two-fold axis, the crystal symmetry is reduced to C_1.

Once the reduced symmetry of the crystal in the presence of the external perturbation is determined, the correlation between the irreducible representations of the two groups can be obtained. From such a correlation, the removal of the degeneracy of a particular energy level can be immediately deduced.

C_2 (2)			E	C_2	
x^2, y^2, z^2, xy	R_z, z	A	1	1	
xz, yz	$\left.\begin{array}{c} x, y \\ R_x, R_y \end{array}\right\}$	B	1	-1	
Representations of D_3		A_1	1	1	A
		A_2	1	-1	B
		E	2	0	$A + B$

This group theoretical analysis thus predicts that the Raman lines of E symmetry should split and the Raman inactive A_2 mode in D_3 symmetry should become Raman-active in C_2 symmetry. We note that the basis functions that are used for C_2 are x, y, z while for D_3, the combinations $(x+iy, x-iy, z)$ are used. The form of the polarizability tensors for the Raman-active modes in D_3 and C_2 point group symmetries are given in Fig. 14.21.

Polarizability Tensors for the Raman-Active Modes
of α-quartz with

$\vec{F} = 0$ **or** $\vec{F} \parallel z$ (D_3) $\vec{F} \parallel x$ **or** $\vec{F} \perp x$ (C_2)

Basis Functions D_3 C_2 **Basis Functions**

$x^2 + y^2,\ z^2$

A_1' $\begin{bmatrix} p & 0 & 0 \\ 0 & p & 0 \\ 0 & 0 & q \end{bmatrix}$

A' $\begin{bmatrix} t & u & 0 \\ u & t & 0 \\ 0 & 0 & v \end{bmatrix}$ $x^2,\ y^2,\ z^2\ ,\ xy$

$x^2 - y^2,\ xy$ $\begin{bmatrix} 0 & m & 0 \\ m^* & 0 & 0 \\ 0 & 0 & 0 \end{bmatrix}$

E'

$xz,\ yz$ $\begin{bmatrix} 0 & 0 & r \\ 0 & 0 & r^* \\ r^* & r & 0 \end{bmatrix}$

B' $\begin{bmatrix} 0 & 0 & m \\ 0 & 0 & n \\ m & n & 0 \end{bmatrix}$ $xz,\ yz$

A_2' **Raman inactive**
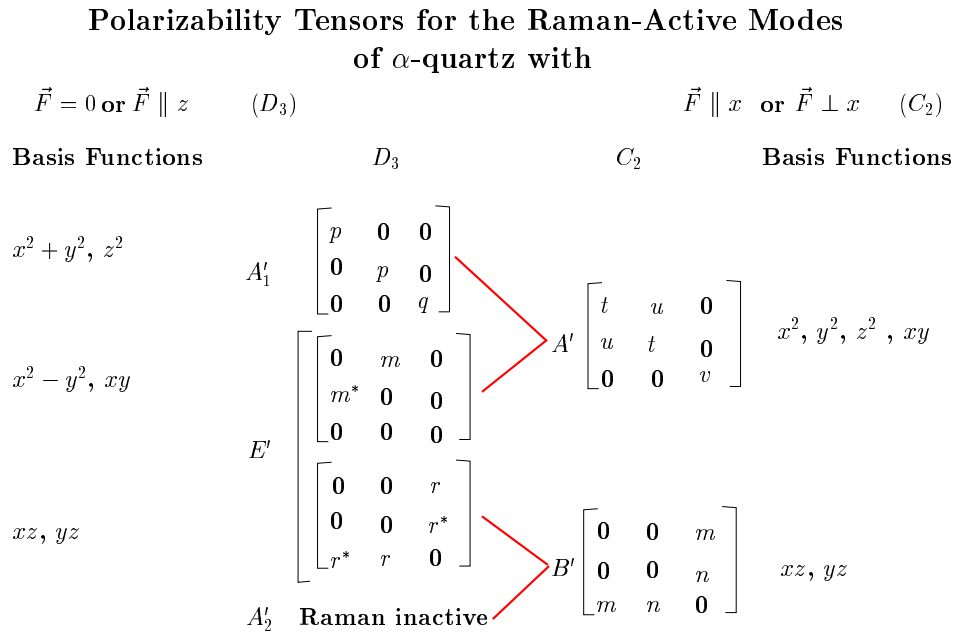
Figure 14.21: Polarizability Tensors for Raman Active Modes of α-quartz.

14.6 Lattice Modes in High T_c Related Materials

As an example of complex crystal structures of current interest, let us consider the lattice modes of high T_c related materials.

14.6.1 The K_2NiF_4 Structure

Let us now consider lattice modes in K_2NiF_4 structure. This is the structure for one of the high T_c related materials La_2CuO_4. The space group is $I4/mmm$ (D_{4h}^{17}) #139. The structure is given by Wyckoff (Vol. 3, p. 68) as:

Cu: $(2a)$	(000), $(1/2,1/2,1/2)$	
La: $(4e)$	$\pm(00u; 1/2, 1/2, u + 1/2)$	
O(1): $(4c)$	$(0, 1/2, 0)$ $(1/2, 0, 0)$, $(1/2, 0, 1/2)$, $(0, 1/2, 1/2)$	
O(2): $(4e)$	$\pm(00u; 1/2, 1/2, u + 1/2)$	

This example is slightly more complex than examples given earlier in the chapter, but still corresponds to a symmorphic space group.

Using the diagram in Fig. 14.22 and considering which atoms remain unchanged under the symmetry operations of D_{4h} or are transformed into sites separated by a lattice vector, we thus obtain for $\chi_{\text{atom sites}}$:

D_{4h}	E	$C_2 = C_4^2$	$2C_4$	$2C_2'$	$2C_2''$	i	S_2	$2S_4$	$2\sigma_v$	$2\sigma_v'$	
$\chi_{\text{Ni}_2\text{ atom sites}}$	2	2	2	2	2	2	2	2	2	2	$\Rightarrow 2A_{1g}$
$\chi_{\text{K}_4\text{ atom sites}}$	4	4	4	0	0	0	0	0	4	4	$\Rightarrow 2A_{1g} + 2A_{2u}$
$\chi_{\text{F}_4\text{ (4e) sites}}$	4	4	4	0	0	0	0	0	4	4	$\Rightarrow 2A_{1g} + 2A_{2u}$
$\chi_{\text{F}_4\text{ (4c) sites}}$	4	4	2	2	0	0	0	2	2	4	$\Rightarrow 2A_{1g} + A_{2u} + B_{1u}$

The character table for D_{4h} shown below
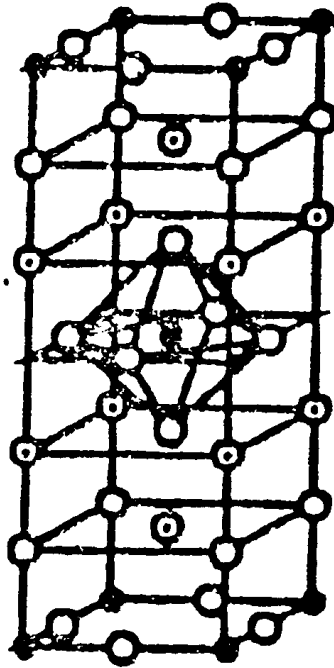
Figure 14.22: The K_2NiF_4 crystal structure, or equivalently the La_2CuO_4 structure, where La$\leftrightarrow$K, Cu$\leftrightarrow$Ni, and O$\leftrightarrow$F.

D_{4h}	E	$C_2 = C_4^2$	$2C_4$	$2C_2'$	$2C_2''$	i	S_2	$2S_4$	$2\sigma_v$	$2\sigma_v'$	
A_{1g}	1	1	1	1	1	1	1	1	1	1	$(x^2 + y^2),\ z^2$
A_{2g}	1	1	1	−1	−1	1	1	1	−1	−1	R_z
B_{1g}	1	1	−1	1	−1	1	1	−1	1	−1	$x^2 - y^2$
B_{2g}	1	1	−1	−1	1	1	1	−1	−1	1	xy
E_g	2	−2	0	0	0	2	−2	0	0	0	(xz, yz)
A_{1u}	1	1	1	1	1	−1	−1	−1	−1	−1	zR_z
A_{2u}	1	1	1	−1	−1	−1	−1	−1	1	1	z
B_{1u}	1	1	−1	1	−1	−1	−1	1	−1	1	xyz
B_{2u}	1	1	−1	−1	1	−1	−1	1	1	−1	$xyzR_z$
E_u	2	−2	0	0	0	−2	2	0	0	0	(x, y)

gives the decomposition of $\chi_{\text{atom sites}}$ as well as the irreducible representations for the vector:

$$z \to A_{2u} \quad \text{and} \quad (x, y) \to E_u$$

Thus, taking the direct product $\chi_{\text{atom sites}} \otimes \chi_{\text{vector}}$ gives

Ni$_2$	$2A_{2u} + 2E_u$
K$_4$	$2A_{1g} + 2E_g + 2A_{2u} + 2E_u$
F$_4$ (4e)	$2A_{1g} + 2E_g + 2A_{2u} + 2E_u$
F$_4$ (4c)	$A_{1g} + B_{1g} + 2E_g + 2A_{2u} + 2E_u$
(K$_2$NiF$_4$)2	$5A_{1g} + B_{1g} + 6E_g + 8A_{2u} + 8E_u$

Of these the A_{2u} and E_u modes are IR active (14 frequencies), two are acoustic modes, while the A_{1g}, B_{1g} and E_g constitute the Raman-active modes (12 frequencies). The B_{1g}, E_g and E_u modes are in-plane modes and the A_{2u} mode is a c-axis mode. The A_{1g} mode may be either an in-plane or a c-axis mode. Experimentally these mode symmetries can all be determined by a suitable sequence of settings of the polarizers.

14.6.2   Phonons in the YBa$_2$Cu$_3$O$_6$ Structure

Let us now consider lattice modes in the YBa$_2$Cu$_3$O$_6$ structure. This is the structure for one of the high T_c related materials where there is
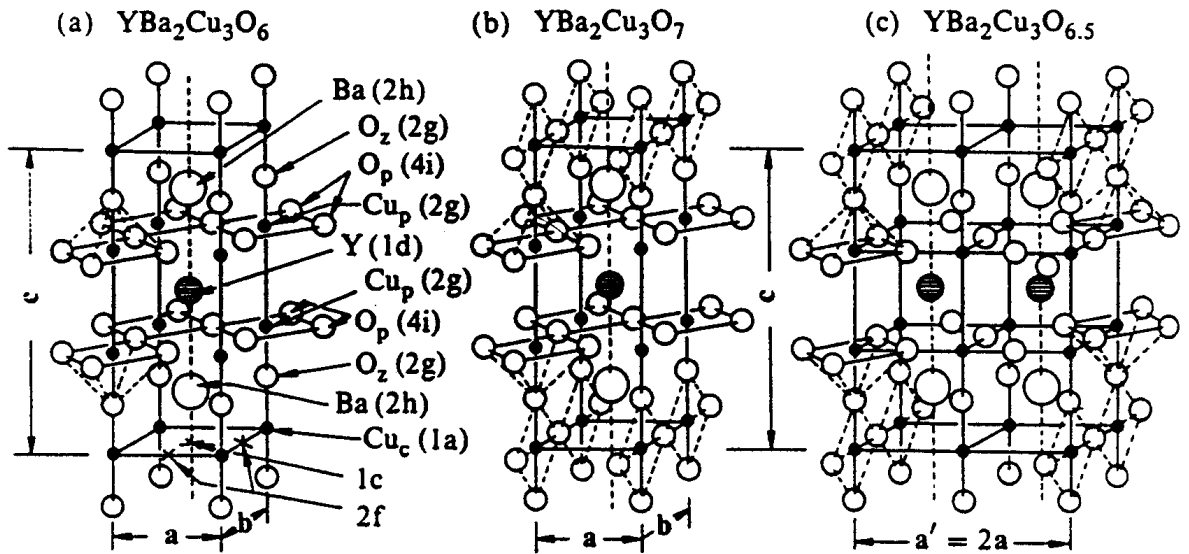
Figure 14.23: Model for the crystal structure of (a) $YBa_2Cu_3O_6$ (space group is $P4/mmm$–D_{4h}^1); (b) $YBa_2Cu_3O_7$ (space group is $Pmmm$–D_{2h}^1); and (c) $YBa_2Cu_3O_{6.5}$.

no oxygen in the chains, and the material is not conducting. The space group is the symmorphic space group $P4/mmm$ (D_{4h}^1) #123.

Using the diagram in Fig. 14.23 and considering which atoms remain unchanged under the symmetry operations of D_{4h} or are transformed into sites separated by a lattice vector, we thus obtain for $\chi_{\text{atom sites}}$

D_{4h}	E	$C_2 = C_4^2$	$2C_4$	$2C_2'$	$2C_2''$	i	S_2	$2S_4$	$2\sigma_v$	$2\sigma_v'$	
$\chi_{\text{Y atom sites}}$	1	1	1	1	1	1	1	1	1	1	$\Rightarrow A_{1g}$
$\chi_{\text{Ba}_2\text{ atom sites}}$	2	2	2	0	0	0	0	0	0	2	$\Rightarrow A_{1g} + A_{2u}$
$\chi_{\text{Cu}_3\text{ atom sites}}$	3	3	3	1	1	1	1	1	3	3	$\Rightarrow 2A_{1g} + A_{2u}$
$\chi_{\text{O}_6\text{ atom sites}}$	6	6	2	1	1	1	1	1	6	2	$\Rightarrow 2A_{1g} + 2A_{2u} + B_{1g} + B_{1u}$

Looking at the character table for D_{4h} we see that

$$z \to A_{2u} \quad \text{and} \quad (x,y) \to E_u$$

Thus, taking the direct product $\chi_{\text{atom sites}} \otimes \chi_{\text{vector}}$ gives

Y	$A_{2u} + E_u$
Ba$_2$	$A_{1g} + E_g + A_{2u} + E_u$
Cu$_3$	$A_{1g} + E_g + 2A_{2u} + 2E_u$
O$_6$	$2A_{1g} + B_{1g} + 3E_g + 2A_{2u} + B_{2u} + 3E_u$
YBa$_2$Cu$_3$O$_6$	$4A_{1g} + B_{1g} + 5E_g + 6A_{2u} + B_{2u} + 7E_u$

so that there are 2 acoustic branch modes, 11 IR active modes and 10 Raman-active modes. The in-plane and c-axis polarization of the various modes can be found from the basis functions listed in the character table.

14.6.3 In The YBa$_2$Cu$_3$O$_7$ Structure

Let us now consider lattice modes in the YBa$_2$Cu$_3$O$_7$ structure. This is the structure for one of the high T_c related materials where the chain layers contain 1 copper and 1 oxygen atom. The space group for the YBa$_2$Cu$_3$O$_7$ structure is $Pmmm$ (D_{2h}^1) #47. This example has less symmetry and is slightly more complex, but still corresponds to a symmorphic space group.

Using the diagram in Fig. 14.24 and considering which atoms remain unchanged under the symmetry operations of D_{2h} or are transformed
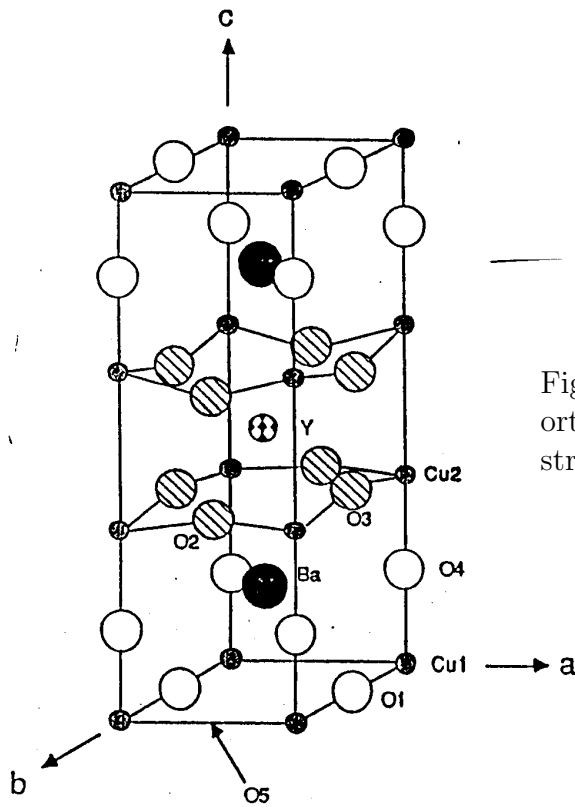
Figure 14.24: Model for the orthorhombic $YBa_2Cu_3O_7$ crystal structure ($Pmmm$ (D_{2h}^1) #47).

into sites separated by a lattice vector, we thus obtain for $\chi_{\text{atom sites}}$

D_{2h}	E	C_2	C_2'	C_2''	i	S_2	σ_h	$\sigma_v' \ \sigma_v''$	
$\chi_{\text{Y atom sites}}$	1	1	1	1	1	1	1	1	$\Rightarrow A_{1g}$
$\chi_{\text{Ba}_2 \text{ atom sites}}$	2	2	0	0	0	0	2	2	$\Rightarrow A_{1g} + B_{1u}$
$\chi_{\text{Cu}_3 \text{ atom sites}}$	3	3	1	1	1	1	3	3	$\Rightarrow 2A_{1g} + B_{1u}$
$\chi_{\text{O}_7 \text{ atom sites}}$	7	7	1	1	1	0	7	7	$\Rightarrow 4A_{1g} + 3B_{1u}$

The character table for D_{2h} is given by:

D_{2h}	E	C_2^z	C_2^y	C_2^x	i	S_2^z	S_2^y	S_2^x	
A_{1g}	1	1	1	1	1	1	1	1	$x^2, \ y^2, \ z^2$
B_{1g}	1	1	−1	−1	1	1	−1	−1	xy
B_{2g}	1	−1	1	−1	1	−1	1	−1	xz
B_{3g}	1	−1	−1	1	1	−1	−1	1	yz
A_{1u}	1	1	1	1	−1	−1	−1	−1	xyz
B_{1u}	1	1	−1	−1	−1	−1	1	1	z
B_{2u}	1	−1	1	−1	−1	1	−1	1	y
B_{3u}	1	−1	−1	1	−1	1	1	−1	x

Thus in D_{2h} symmetry we see that

$$x \to B_{3u}, \quad y \to B_{2u} \quad \text{and} \quad z \to B_{1u}$$

Thus, taking the direct product $\chi_{\text{atom sites}} \otimes \chi_{\text{vector}}$ gives

Y	$B_{1u} + B_{2u} + B_{3u}$
Ba$_2$	$A_{1g} + B_{2g} + B_{3g} + B_{1u} + B_{2u} + B_{3u}$
Cu$_3$	$A_{1g} + B_{2g} + B_{3g} + 2B_{1u} + 2B_{2u} + 2B_{3u}$
O$_7$	$3A_{1g} + 3B_{2g} + 3B_{3g} + 4B_{1u} + 4B_{2u} + 4B_{3u}$
YBa$_2$Cu$_3$O$_7$	$5A_{1g} + 5B_{2g} + 5B_{3g} + 8B_{1u} + 8B_{2u} + 8B_{3u}$

The number of IR modes in this case is 21 (3 acoustic modes). The IR selection rules are that 7 modes are seen with each polarization. The number of Raman-active modes is 15. Their polarizations can be obtained from the basis functions given in the character table and show the 5 modes are seen with $\|, \|$ polarization, 5 modes with x, z and 5 modes with y, z polarization.

14.7   Selected Problems

1. Using the results of Problem # 1:

   (a) Find the number of lattice modes at $k = 0$. What are their symmetries and what are their mode degeneracies?

   (b) What are the normal mode displacements for each of these lattice modes?

   (c) What modes are IR active, Raman active? What are the polarizations of the Raman active modes?

2. Consider the crystal structure in the diagram for Nb_3Sn, a proto-type superconductor with the A–15 (or β–W) structure used for high field superconducting magnet applications.

   (a) How many lattice modes are there at $k = 0$, what are their symmetries and what are their degeneracies?

   (b) What are the normal mode displacements for each of these lattice modes?

   (c) Which modes are IR active, Raman active? What are the polarizations of the Raman-active modes?

3. Tin oxide (SnO_2 with space group #136) is an important electronic material.

   (a) Find the lattice modes at $k = 0$, their symmetries, degeneracies and the normal mode patterns.

   (b) Indicate the IR-activity and Raman activity of these modes.

4. Bromine forms a molecular crystal.

   (a) What is the appropriate space group?

   (b) Find the lattice modes at $k = 0$, their symmetries, degeneracies and the normal mode patterns.

   (c) Indicate the IR-activity and Raman activity of these modes.

Chapter 15

Use of Standard Reference Texts

15.1   Introduction

In Chapter 14 we discussed the lattice modes for a number of crystals assuming that the crystal structure and the space group are known. In many research situations, the researcher must first identify the space group and the pertinent group of the wave vector, before solving for the lattice modes or for the electronic structure. In this chapter we discuss the procedure to be used in such cases. This procedure involves use of 3 standard reference sources:

1. Wyckoff's books which give the atom locations for hundreds of crystal structures:
   R.W.G. Wyckoff, Crystal Structures,
   QD951.W977 1963 (7 volumes).

2. The International Tables for X-ray Crystallography through which one can identify the space group from the atom locations:
   International Tables for X-ray Crystallography
   QD 945.I61 1965 (4 volumes)

3. The Character Tables for the group of the wave vector for each unique $\vec{k}$ vector for each of the 230 space groups:

Miller and Love, "Irreducible Representations of Space Groups", QA171.5 .M651

In this chapter we comment on the use of each of these standard reference texts.

15.2   Determination of the Crystal Structure

The standard determinations of crystal structures are carried out using diffraction techniques, either x-ray or neutron diffraction. The elastically scattered beams give rise to a series of diffraction peaks which can be indexed according to the points in the reciprocal lattice. The scattering intensities can be calculated using the form factors listed in the "International Tables for X-Ray Crystallography". The results of many such structural determinations for specific materials are listed in the series of books by Wyckoff (R.W.G. Wyckoff, Crystal Structures, QD 951.W977 1963 (7 volumes)).

We illustrate the use of Wyckoff's books to find the crystal structure of a particular material. We choose graphite for the illustrative material. For the crystal structure of graphite see p. 26–28 in Volume 1 of Wyckoff. The information to be extracted from Wyckoff concerns the number of allotropic structures, the site symmetries of the atoms in each of the structures and the space group designations. Wyckoff generally gives you most of the information you need. For the case of graphite, there are 3 crystal structures: ordinary hexagonal graphite, puckered graphite and rhombohedral graphite, each of which is listed in Wyckoff.

First we have ordinary graphite with 4 atoms/unit cell as shown in Fig. 15.1, containing two a-atoms at (0,0,0) and (0,0,1/2) denoted by dark circles and two b-atoms at (1/3,2/3,0) and (2/3,1/3,1/2) denoted by open circles. The lattice constants $a_0 = 2.456$Å and $c_0 = 6.696$Å are indicated in Fig. 15.1 and the layer stacking is $ABAB\ldots$. To do the various symmetry operations it is sometimes convenient to take the origin at (0,0,1/4).

The second form that is listed is puckered graphite where the two
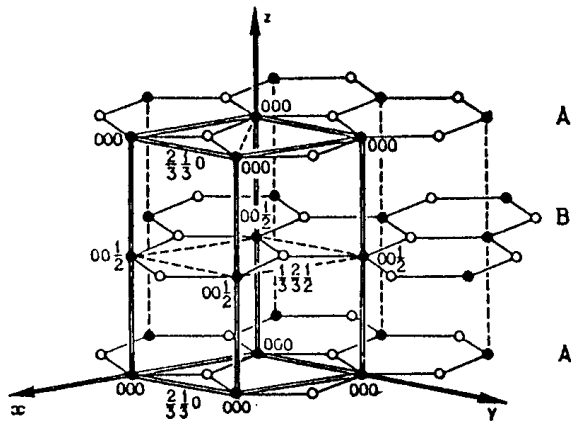
Figure 15.1: Crystal structure of hexagonal graphite.

a atoms are translated in the z direction by u and the two b atoms are translated by v in the z direction. This makes the a and b carbon atoms slightly non-planar relative to ordinary graphite, which is a sheet-like material.

In the rhombohedral form we have 3 different layer planes per unit cell, so that the repeat distance is $(3/2)(6.696)$Å$=10.044$Å in the c direction, with the 3rd layer having an atom over the $(2/3, 1/3, 1/2)$ atom but none over the $(0, 0, 1/2)$ atom. This gives 6 atoms in a hexagonal unit cell shown in Fig. 15.2 with $ABCABC\ldots$ layer stacking.

It is not always easy to see the stacking arrangements from the diagrams in Wyckoff. Sometimes you must make additional pictures, like the projection of the planar stacking for the 3 layers shown in Fig. 15.3. This stacking is equivalent to a rhombohedral unit cell with lattice constants $a_0 = 3.635$Å and $\alpha = 39°30'$ and two atoms at (u, u, u) and $(\bar{u}, \bar{u}, \bar{u})$ with $u \approx 1/6$ shown by the parallelepiped in the figure. The space group is specified in terms of the rhombohedral unit cell containing 2 carbon atoms.

Once we know the atom locations we can then use the International Tables for X-Ray Crystallography to identify the space group. In many cases the summary in Wyckoff actually gives the space group assign-
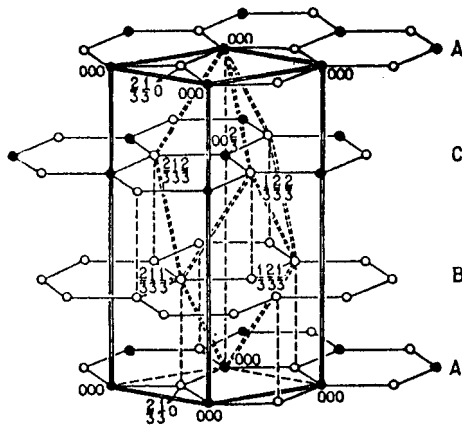
Figure   15.2:   Rhombohedral graphite showing *ABC* stacking of the individual sheets.
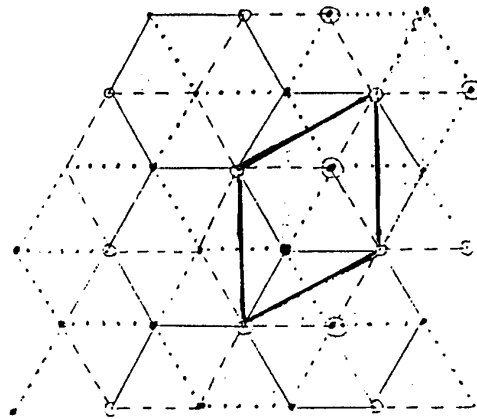
Figure 15.3: Top view of a three layered projection for rhombohedral graphite.

ment.

15.3   Determination of the Space Group

The International Tables for X-Ray Crystallography helps with the determination of the space group and the symmetry operations of the space group (International Tables for X-ray Crystallography; QD 945.I61 1965 (4 volumes)). These volumes deal with space groups in general but do not refer to specific materials, which is the central theme of Wyckoff's books. In some cases Wyckoff gives the space group designation, and if so, this will greatly simplify our work. If the space group designation is known, it should be an easy matter to match up the atom site locations in Wyckoff with the atom site locations listed under the correct space group in the International Tables. For the case of graphite we have to find three different space groups for each of the three allotropic forms.

For ordinary graphite, the space group is D_{6h}^4 ($P6_3/m\ 2/m\ 2/c$, #194). The designation D_{6h} refers to the point group at $\vec{k} = 0$ and the superscript 4 refers to a space group index based on this point group. The full symmetry listing is $P6_3/m\ 2/m\ 2/c$ and an abbreviated form is $P6_3/mmc$. Since Wyckoff does not list the space group designation we must consult the International Tables for X-ray Crystallography where the tables are arranged according to space group designation (e.g., D_{6h}^4). If Wyckoff doesn't list the space group designation, then it is necessary to use the index of the International Tables (p. 552) under the title "hexagonal systems". Under "hexagonal systems" there are 27 space groups. What needs to be done at this point is to see which of these 27 space groups is the right one. The method of identification involves matching up the atom site locations in the International Tables with the one in Wyckoff. Matching up the point group symmetry operations is often a big help in eliminating almost all of the irrelevant space groups within a given system, such as the hexagonal system. The stereograph shown in Fig. 15.4 can be used to deduce the point group symmetry operations for the space group #194.

Once this matching up is done correctly, the space group assignment with the following atom site assignments is found:

$P\,6_3/mmc$
D^4_{6h} No. 194 $P\,6_3/m\,2/m\,2/c$ $6/m\,m\,m$ Hexagonal
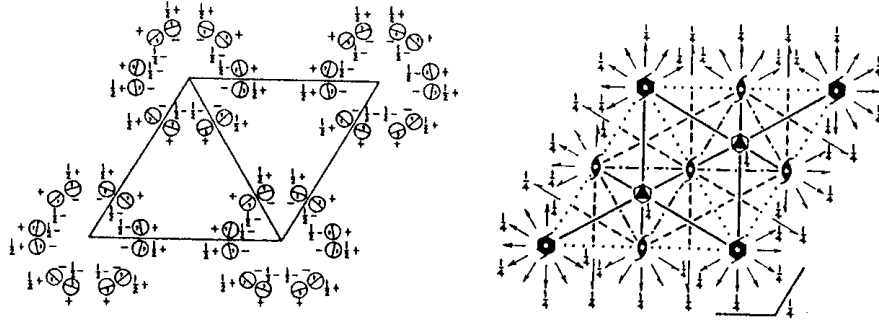
Origin at centre $(\bar{3}m1)$

Number of positions, Wyckoff notation, and point symmetry			Co-ordinates of equivalent positions	Conditions limiting possible reflections
24	l	1	x,y,z; $\bar{y},x-y,z$; $y-x,\bar{x},z$; $\bar{y},\bar{x},z$; $x,x-y,z$; $y-x,y,z$; $\bar{x},\bar{y},\bar{z}$; $y,y-x,\bar{z}$; $x-y,x,\bar{z}$; $y,x,\bar{z}$; $\bar{x},y-x,\bar{z}$; $x-y,\bar{y},\bar{z}$; $\bar{x},\bar{y},\tfrac12+z$; $y,y-x,\tfrac12+z$; $x-y,x,\tfrac12+z$; $x,y,\tfrac12-z$; $\bar{y},x-y,\tfrac12-z$; $y-x,\bar{x},\tfrac12-z$; $y,x,\tfrac12+z$; $\bar{x},y-x,\tfrac12+z$; $x-y,\bar{y},\tfrac12+z$; $\bar{y},\bar{x},\tfrac12-z$; $x,x-y,\tfrac12-z$; $y-x,y,\tfrac12-z$.	**General:** $hkil$: No conditions $hh2hl$: $l=2n$ $h\bar{h}0l$: No conditions
12	k	m	$x,2x,z$; $2\bar{x},\bar{x},z$; $x,\bar{x},z$; $\bar{x},2\bar{x},\bar{z}$; $2x,x,\bar{z}$; $\bar{x},x,\bar{z}$; $\bar{x},2\bar{x},\tfrac12+z$; $2x,x,\tfrac12+z$; $\bar{x},x,\tfrac12+z$; $x,2x,\tfrac12-z$; $2\bar{x},\bar{x},\tfrac12-z$; $x,\bar{x},\tfrac12-z$.	**Special:** as above, plus
12	j	m	$x,y,\tfrac14$; $\bar{y},x-y,\tfrac14$; $y-x,\bar{x},\tfrac14$; $\bar{y},\bar{x},\tfrac14$; $x,x-y,\tfrac14$; $y-x,y,\tfrac14$; $\bar{x},\bar{y},\tfrac34$; $y,y-x,\tfrac34$; $x-y,x,\tfrac34$; $y,x,\tfrac34$; $\bar{x},y-x,\tfrac34$; $x-y,\bar{y},\tfrac34$.	no extra conditions
12	i	2	$x,0,0$; $0,x,0$; $\bar{x},\bar{x},0$; $x,0,\tfrac12$; $0,x,\tfrac12$; $\bar{x},\bar{x},\tfrac12$; $\bar{x},0,0$; $0,\bar{x},0$; $x,x,0$; $\bar{x},0,\tfrac12$; $0,\bar{x},\tfrac12$; $x,x,\tfrac12$.	$hkil$: $l=2n$
6	h	mm	$x,2x,\tfrac14$; $2\bar{x},\bar{x},\tfrac14$; $x,\bar{x},\tfrac14$; $\bar{x},2\bar{x},\tfrac34$; $2x,x,\tfrac34$; $\bar{x},x,\tfrac34$.	no extra conditions
6	g	$2/m$	$\tfrac12,0,0$; $0,\tfrac12,0$; $\tfrac12,\tfrac12,0$; $\tfrac12,0,\tfrac12$; $0,\tfrac12,\tfrac12$; $\tfrac12,\tfrac12,\tfrac12$.	$hkil$: $l=2n$
4	f	$3m$	$\tfrac13,\tfrac23,z$; $\tfrac23,\tfrac13,\bar{z}$; $\tfrac23,\tfrac13,\tfrac12+z$; $\tfrac13,\tfrac23,\tfrac12-z$.	$hkil$: If $h-k=3n$, then $l=2n$
4	e	$3m$	$0,0,z$; $0,0,\bar{z}$; $0,0,\tfrac14+z$; $0,0,\tfrac14-z$.	$hkil$: $l=2n$
2	d	$\bar{6}m2$	$\tfrac13,\tfrac23,\tfrac34$; $\tfrac23,\tfrac13,\tfrac14$.	$hkil$: If $h-k=3n$, then $l=2n$
2	c	$\bar{6}m2$	$\tfrac13,\tfrac23,\tfrac14$; $\tfrac23,\tfrac13,\tfrac34$.	
2	b	$\bar{6}m2$	$0,0,\tfrac14$; $0,0,\tfrac34$.	$hkil$: $l=2n$
2	a	$\bar{3}m$	$0,0,0$; $0,0,\tfrac12$.	

Figure 15.4: Site locations for space group #194.

# of atoms	desig-nation	site symmetry	International Tables atom locations		Wyckoff atom locations	
2	b	$6m2$	(0,0,1/4)	(0,0,3/4)	(0,0,0)	(0,0,1/2)
2	c	$\bar{6}m2$	(1/3,2/3,1/4)	(2/3,1/3,3/4)	(1/3,2/3,0)	(2/3,1/3,1/2)

space group #194; D_{6h}^4 hexagonal $P6_3/mmc$; $P6_3/m\ 2/m\ 2/c$; $6/mmm$

The International Tables for X-ray Crystallography tell us that sites b and c each have $\bar{6}m2$ point group symmetry. The Wyckoff atom site locations differ from the International Tables atom site locations by a translation of the unit cell by $(c/4)(001)$. Once we have the correct space group, we record the space group number which is #194, because we will need this number to use Miller and Love which is discussed in §15.4, since Miller and Love only designates each space group by its number. By the way, space group #194 also describes the hexagonal close packed structure.

The expanded crystallographic notation $P6_3/m\ 2/m\ 2/c$ for space group #194 means that we have a primitive (P) lattice, the highest symmetry axis is a 6-fold screw axis along the c-direction corresponding to a translation $(3/6)$ of the length of the c-axis unit vector. Mirror planes pass through the c-axis. Perpendicular to the main symmetry directions are three two-fold axes with mirror planes through these axes $(2/m)$, and involving no translations. Also perpendicular to the main symmetry axis is a set of 2-fold axes with a glide plane or translation in the c-direction $(2/c)$. For the **ranking system** used to list the ordering of the mirror planes, the simple mirror plane is listed first, followed by glide planes perpendicular to the a, b, and c directions, followed by a net glide (n-glide) $\vec{\tau} = 1/2(\vec{a} + \vec{b})$; and finally the diamond glide (d-glide) $\tau = 1/4(\vec{a} + \vec{b}) : m > a > b > c > n > d$.

The match-up between the site locations and the space group is made as follows. We first identify the symmetry operations of the graphite lattice ($\{\varepsilon|0\}, \{C_2|\tau\}, 2\{C_3|0\}, 2\{C_6|\tau\}, 3\{C_{2'}|0\}, 3\{C_{2''}|\tau\}$, and all operations compounded with inversion). These are the point group operations of D_{6h}. There are four space groups in the hexagonal system with D_{6h} symmetry. We can immediately rule out the space group #191 ($P6_3/m\ 2/m\ 2/m$) D_{6h}^1 which is symmorphic, and we can rule out the space group #192 ($P6_3/m\ 2/c\ 2/c$) D_{6h}^2 which has two kinds of non-symmorphic translations. Group #193 D_{6h}^3 is ruled out because it does not contain the proper site locations. Group #194 (see Fig. 15.4) however contains all the proper symmetry operations and site locations.

In the puckered graphite structure the a and b atoms are no longer co-planar so that the white lattice is slightly displaced along the z direction from the dark lattice in the diagram shown in Fig. 15.1. In comparing the site symmetries between Wyckoff and the International Crystallography Tables we see that a match is found with group #186 (C_{6v}^4) another hexagonal group with $P6_3mc$ symmetry.

Combining the information in Wyckoff and the International Tables we prepare a table for the site locations of puckered graphite for space group #186; C_{6v}^4 hexagonal; $P6_3mc$; $6mm$:

# of atoms	designation in international tables	site symmetry	International Tables and Wyckoff		Comments
2	a	$3m$	$(0,0,\bar{w})$ listed as: $(0,0,u)$	$(0,0,1/2+\bar{w})$ $(0,0,1/2+u)$	In Wyckoff (International Tables) $\bar{w}$ is $u(z)$
2	b	$3m$	$(1/3,2/3,w)$ listed as: $(1/3,2/3,v)$	$(2/3,1/3,1/2+w)$ $(2/3,1/3,1/2+v)$	In Wyckoff (International Tables) w is $v(z)$

The site symmetries for the a and b sites are given as $3m$ in the International Tables. We note that puckered graphite has lower symmetry than ordinary graphite because the value of z for the site locations is arbitrary. Wyckoff tells us that $u \neq v$; in fact Wyckoff selects a coordinate system where $u = 0$ and v is small (< 0.05).

Since no space group information is provided for rhombohedral graphite in Wyckoff, we must again use the index in the International Tables (p. 552) under the heading of "Trigonal Groups". The space group that matches the site locations in Wyckoff is D_{3d}^5 #166. This space group is described in terms of rhombohedral axes (p. 272 of the International Tables) and also hexagonal axes (p. 273 of the International Tables). In terms of the rhombohedral axes we find the correct site symmetries as:

#	Designation	Site Symmetry	Site Locations
2	c	$3m$	(x,x,x); $(\bar{x},\bar{x},\bar{x})$; Wyckoff gives $x \approx 1/6$

space group D_{3d}^5 #166

The stereographs for the hexagonal and rhombohedral systems for space group #166 are shown in Fig. 15.5. Also listed in the International Tables are the site locations in the hexagonal system.
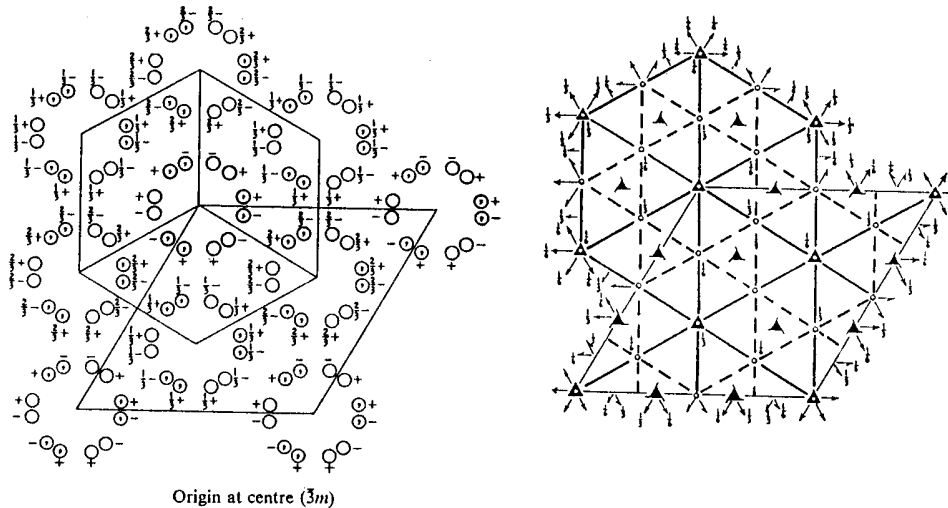
Origin at centre ($\bar{3}m$)

Number of positions, Wyckoff notation, and point symmetry			Co-ordinates of equivalent positions	Conditions limiting possible reflections

(1) RHOMBOHEDRAL AXES:

General:

No conditions

| 12 | i | 1 | x,y,z; z,x,y; y,z,x; y,x,z; z,y,x; x,z,y; $\bar{x},\bar{y},\bar{z}$; $\bar{z},\bar{x},\bar{y}$; $\bar{y},\bar{z},\bar{x}$; $\bar{y},\bar{x},\bar{z}$; $\bar{z},\bar{y},\bar{x}$; $\bar{x},\bar{z},\bar{y}$. |

Special:

No conditions

6	h	m	x,x,z; x,z,x; z,x,x; $\bar{x},\bar{x},\bar{z}$; $\bar{x},\bar{z},\bar{x}$; $\bar{z},\bar{x},\bar{x}$.
6	g	2	x,$\bar{x}$,$\frac{1}{2}$; $\bar{x}$,$\frac{1}{2}$,x; $\frac{1}{2}$,x,$\bar{x}$; $\bar{x}$,x,$\frac{1}{2}$; x,$\frac{1}{2}$,$\bar{x}$; $\frac{1}{2}$,$\bar{x}$,x.
6	f	2	x,$\bar{x}$,0; $\bar{x}$,0,x; 0,x,$\bar{x}$; $\bar{x}$,x,0; x,0,$\bar{x}$; 0,$\bar{x}$,x.
3	e	$2/m$	0,$\frac{1}{2}$,$\frac{1}{2}$; $\frac{1}{2}$,0,$\frac{1}{2}$; $\frac{1}{2}$,$\frac{1}{2}$,0.
3	d	$2/m$	$\frac{1}{2}$,0,0; 0,$\frac{1}{2}$,0; 0,0,$\frac{1}{2}$.
2	c	$3m$	x,x,x; $\bar{x},\bar{x},\bar{x}$.
1	b	$\bar{3}m$	$\frac{1}{2}$,$\frac{1}{2}$,$\frac{1}{2}$.
1	a	$\bar{3}m$	0,0,0.

(2) HEXAGONAL AXES:

$(0,0,0; \frac{2}{3},\frac{1}{3},\frac{1}{3}; \frac{1}{3},\frac{2}{3},\frac{2}{3})+$

General:

hkil: $-h+k+l=3n$
hh2$\bar{h}$l: ($l=3n$)
h$\bar{h}$0l: ($h+l=3n$)

Special: as above only

36	i	1	x,y,z; $\bar{y}$,x−y,z; y−x,$\bar{x}$,z; $\bar{x},\bar{y},\bar{z}$; y,y−x,$\bar{z}$; x−y,x,$\bar{z}$; $\bar{y},\bar{x},z$; x,x−y,z; y−x,y,z; y,x,$\bar{z}$; $\bar{x}$,y−x,$\bar{z}$; x−y,$\bar{y},\bar{z}$.
18	h	m	x,$\bar{x}$,z; x,2x,z; 2$\bar{x}$,$\bar{x}$,z; $\bar{x}$,x,$\bar{z}$; $\bar{x}$,2$\bar{x}$,$\bar{z}$; 2x,x,$\bar{z}$.
18	g	2	x,0,$\frac{1}{2}$; 0,x,$\frac{1}{2}$; $\bar{x},\bar{x}$,$\frac{1}{2}$; $\bar{x}$,0,$\frac{1}{2}$; 0,$\bar{x}$,$\frac{1}{2}$; x,x,$\frac{1}{2}$.
18	f	2	x,0,0; 0,x,0; $\bar{x},\bar{x}$,0; $\bar{x}$,0,0; 0,$\bar{x}$,0; x,x,0.
9	e	$2/m$	$\frac{1}{2}$,0,0; 0,$\frac{1}{2}$,0; $\frac{1}{2}$,$\frac{1}{2}$,0.
9	d	$2/m$	$\frac{1}{2}$,0,$\frac{1}{2}$; 0,$\frac{1}{2}$,$\frac{1}{2}$; $\frac{1}{2}$,$\frac{1}{2}$,$\frac{1}{2}$.
6	c	$3m$	0,0,z; 0,0,$\bar{z}$.
3	b	$\bar{3}m$	0,0,$\frac{1}{2}$.
3	a	$\bar{3}m$	0,0,0.

Figure 15.5: Stereographs for the hexagonal and rhombohedral systems for space group #166.

#	designation	site symmetry	International Tables site locations
6	c	$3m$	$(0, 0, z)$, $(0, 0, \bar{z})$, $(1/3, 2/3, 2/3+z)$ $(1/3, 2/3, 2/3+\bar{z})$ $(2/3, 1/3, 1/3+z)$, $(2/3, 1/3, 1/3+\bar{z})$

Agreement between the Wyckoff listing and the listing in the International Tables is obtained by taking $z = 1/6$, and $\bar{z} = -1/6$, and by translating the coordinate system by $(c/6)(0, 0, 1)$.

15.4   Finding Character Tables for all Groups of the Wave Vector

To find all the pertinent group theory information for a space group we use Miller and Love. This book contains character tables for all groups of the wave vectors for every space group. This reference is a big computer printout. Neither Miller and Love nor the International Tables refer to specific materials – these two books only refer to the space group which describes specific materials.

To find the character tables for the various points in the Brillouin zone we use Miller and Love. Let us take the case of ordinary graphite (see §15.2 for the atomic site designations) which has space group #194 (p. 356-8 Miller and Love). The first character table listed is for the Γ point ($\vec{k} = 0$) and is shown in Fig. 15.6.

The arrangement of the classes and irreducible representations is opposite to that used in Tinkham. The classes are listed on the left-hand column and follow the notation on p. 124 of Miller and Love which is reproduced in Fig. 15.7. The symmetry elements numbered $n \geq 49$ are for double group operations, to be discussed later in the course. The double group representations are $7^{\pm}, 8^{\pm}, 9^{\pm}$ and we will not be concerned with these further for discussing lattice modes of graphite. The representations with a $+(-)$ sign are even (odd) under inversion so that we need only be concerned with the first $6^{\pm}$ representations.

Applying the notation for the classes (see Fig. 15.7) in Miller and Love to Tinkham's tables, we make the following correspondence between the classes:

```
GROUP 194
GENS.= C3;C2(0,0,1/2),C2X;SIGV(0,0,1/2)
TRANSLATIONS  1=(0,0,1/2)                                                    P6₃/mmc

PT. GM  AUGMENTERS  -Y,X-Y,Z; -X,-Y,1/2+Z; X-Y,-Y,-Z; X-Y,Y,1/2+Z
REP. D AUGMENTERS                                 REP. D AUGMENTERS
GM1+ 1 (+);  E;  E;  E;  E                        GM2+ 1 (+);  E;  E; (-)E; (-)E
GM3+ 1 (+);  E; (-)E; E; (-)E                     GM4+ 1 (+);  E; (-)E; (-)E; E
GM5+ 2 (+);  5;  E;  2;  2                         GM6+ 2 (+);  5; (-)E;  2; (-)2
GM1- 1 (+);  E;  E;  E; (-)E                       GM2- 1 (+);  E;  E; (-)E;  E
GM3- 1 (+);  E; (-)E; E;  E                        GM4- 1 (+);  E; (-)E; (-)E; (-)E
GM5- 2 (+);  5;  E;  2; (-)2                       GM6- 2 (+);  5; (-)E;  2;  2
GM7+ 2 (-);  8; (+I)4; (-I)3; (-I)2               GM8+ 2 (-);  8; (-I)4; (-I)3; (+I)2
GM9+ 2 (-); (-)E; (+I)4; (-I)3; (-I)2             GM7+ 2 (-);  8; (+I)4; (-I)3; (+I)2
GM8- 2 (-);  8; (-I)4; (-I)3; (-I)2               GM9- 2 (-); (-)E; (+I)4; (-I)3; (+I)2

OPERATORS                              GM 1+ 2+ 3+ 4+ 5+ 6+ 1- 2- 3- 4- 5- 6- 7+ 8+ 9+ 7- 8- 9-
1 ......................................    1  1  1  1  2  2  1  1  1  1  2  2  2  2  2  2  2  2
49 .....................................    1  1  1  1  2  2  1  1  1  1  2  2 -2 -2 -2 -2 -2 -2
3 53 ...................................    1  1 -1 -1 -1 -1  1  1 -1 -1 -1  1  1 -2  1  1  1 -2
4,1 ....................................    1  1 -1 -1  2 -2  1  1 -1 -1  2 -2  0  0  0  0  0  0
6,1 50,1 ...............................    1  1 -1 -1  1  1  1  1 -1 -1  1 -8  8  0 -8  8  0
7 9 11 .................................    1 -1  1 -1  0  0  1 -1  1 -1  0  0  0  0  0  0  0  0
8,1 10,1 12,1 ..........................    1 -1  1 -1  0  0  1 -1  1 -1  0  0  0  0  0  0  0  0
20,1 22,1 24,1 .........................    1 -1 -1  1  0  0 -1  1  1 -1  0  0  0  0  0  0  0  0
19 21 23 ...............................    1 -1 -1  1  0  0 -1  1  1 -1  0  0  0  0  0  0  0  0
16,1 ...................................    1  1 -1 -1  2 -2 -1 -1  1  1 -2  2  0  0  0  0  0  0
14,1 66,1 ..............................    1  1 -1 -1  1  1 -1 -1  1  1 -1 -8  8 -8  0 -8  8  0
13 .....................................    1  1  1  1  2  2 -1 -1 -1 -1 -2 -2  2  2  2 -2 -2 -2
15 65 ..................................    1  1  1  1 -1 -1 -1 -1 -1 -1  1  1  1  1 -2 -1 -1  2
```

Figure 15.6: Miller and Love character table for the group of the wave vector at $\vec{k} = 0$ for space group #194.

Rhombohedral and Hexagonal Systems

Operator Number	Symbol	Effect on x, y, z	Direction Cosines of Rotation Axis and Angle of Rotation	Operator Number	Symbol	Effect on x, y, z
1	E	x, y, z	$0°$	13	I	$-x, -y, -z$
2		$x-y, x, z$	$0, 0, 1; 60°$	14		$-x+y, -x, -z$
3	$C3$	$-y, x-y, z$	$0, 0, 1; 120°$	15		$y, -x+y, -z$
4	$C2$	$-x, -y, z$	$0, 0, 1; 180°$	16	$SIGH$	$x, y, -z$
5		$-x+y, -x, z$	$0, 0, 1; 240°$	17		$x-y, x, -z$
6		$y, -x+y, z$	$0, 0, 1; 300°$	18		$-y, x-y, -z$
7	$C2X$	$x-y, -y, -z$	$1, 0, 0; 180°$	19	$SIGD$	$-x+y, y, z$
8		$x, x-y, -z$	$\frac{1}{2}\sqrt{3}, \frac{1}{2}, 0; 180°$	20		$-x, -x+y, z$
9		$y, x, -z$	$\frac{1}{2}, \frac{1}{2}\sqrt{3}, 0; 180°$	21		$-y, -x, z$
10	$C2D$	$-x+y, y, -z$	$0, 1, 0; 180°$	22	$SIGV$	$x-y; -y, z$
11		$-x, -x+y, -z$	$-\frac{1}{2}, \frac{1}{2}\sqrt{3}, 0; 180°$	23		$x, x-y, z$
12		$-y, -x, -z$	$-\frac{1}{2}\sqrt{3}, \frac{1}{2}, 0; 180°$	24		y, x, z

In addition to the symbols shown, the symbol $\bar{E}$ is used to designate the 360° rotation.

Figure 15.7: Miller and Love notation for the group elements for the rhombohedral and hexagonal systems.

Tinkham	Miller & Love	Tinkham	Miller & Love
E	1	$i \otimes E$	13
$\rightarrow C_2$	4	$i \otimes C_2$	16
$2C_3$	3,5	$i \otimes 2C_3$	15,17
$\rightarrow 2C_6$	2,6	$i \otimes 2C_6$	14,18
$3C_{2'}$	7,9,11	$i \otimes 3C_{2'}$	19,21,23
$\rightarrow 3C_{2''}$	8,10,12	$i \otimes 3C_{2''}$	20,22,24

in which indicators are used to distinguish operations with no translations (no arrows) and with translations $\vec{\tau} = \frac{c}{2}(0,0,1)$ (with arrows). The operations without arrows are all in point group $D_{3d} = D_3 \otimes i$. The operations with translations are in $D_{6h} = D_6 \otimes i$ but not in D_{3d}. Thus graphite crystallizes in a non-symmorphic space group.

The correspondence between irreducible representations in Tinkham and Miller and Love is given by the following table:

$$
\begin{array}{ll}
A_{1g} \rightarrow 1^+ & A_{1u} \rightarrow 1^- \\
A_{2g} \rightarrow 2^+ & A_{2u} \rightarrow 2^- \\
B_{1g} \rightarrow 3^+ & B_{1u} \rightarrow 3^- \\
B_{2g} \rightarrow 4^+ & B_{2u} \rightarrow 4^- \\
E_{1g} \rightarrow 6^+ & E_{1u} \rightarrow 6^- \\
E_{2g} \rightarrow 5^+ & E_{2u} \rightarrow 5^-
\end{array}
$$

With these identifications we can construct a character table from Miller and Love that looks like the character tables in Tinkham for D_6 (622), with $D_{6h} = D_6 \otimes i$. (T=Tinkham, M+L=Miller and Love). The resulting table is

	M+L	$\rightarrow$	1	4,1	3;5	2,1;6,1	7;9;11	8,1;10,1;12,1
D_6 (622)	$\downarrow$		$\{E\|0\}$	$\{C_2\|\tau\}$	$2\{C_3\|0\}$	$2\{C_6\|\tau\}$	$3\{C_{2'}\|0\}$	$3\{C_{2''}\|\tau\}$
x^2+y^2, z^2	1	A_1	1	1	1	1	1	1
R_z, z	2	A_2	1	1	1	1	-1	-1
	3	B_1	1	-1	1	-1	1	-1
	4	B_2	1	-1	1	-1	-1	1
$(xz,yz)(x,y)(R_x, R_y)$	6	E_1	2	-2	-1	1	0	0
(x^2-y^2, xy)	5	E_2	2	2	-1	-1	0	0

```
GROUP 186                                                    P6₃mc
GENS.= C3,C2(0,0,1/2),SIGV(0,0,1/2)
TRANSLATIONS   1=(0,0,1/2)

PT. GM  AUGMENTERS   -Y,X-Y,Z1 -X,-Y,1/2+Z1 X-Y,-Y,1/2+Z
REP.  D AUGMENTERS                              REP.  D AUGMENTERS
GM1   1  (+)1   E1   E1   E                     GM2   1  (+)1   E1   E1   (-)E
GM3   1  (+)1   E1   (-)E1  F                   GM4   1  (+)1   F1   (-)F1  (-)E
GM5   2  (+)1   51   E1   2                     GM6   2  (+)1   51   (-)E1  2
GM7   2  (-)1   81   (+I)41  (-I)3              GM8   2  (-)1   81   (-I)41  (-I)3
GM9   2  (-)1   (-)E1  (+I)41  (-I)3

OPERATORS                        GM 1    2    3    4    5    6    7    8    9
1 .............................. 1    1    1    1    2    2    2    2    2
49 ............................. 1    1    1    1    2    2   -2   -2   -2
3 53 ........................... 1    1    1    1   -1   -1    1    1   -2
4+1 ........................... 1    1   -1   -1    2   -2    0    0    0
6+1 50+1 ...................... 1    1   -1   -1   -1    1   -8    8    0
20+1 22+1 24+1 ................ 1   -1    1   -1    0    0    0    0    0
19 21 23 ...................... 1   -1   -1    1    0    0    0    0    0
```

Figure 15.8: Miller and Love character tables for puckered graphite, space group #186.

For puckered graphite we must use space group #186 (p. 338 in Miller and Love). We rewrite the character table for $\vec{k} = 0$ from Miller and Love (given in Fig. 15.8) in the Tinkham notation, and go through the same steps as were taken for ordinary graphite corresponding to space group #194.

In the case of rhombohedral graphite, we need to consider the high symmetry points of the rhombohedral Brillouin zone, shown in Fig. 15.9. The Miller and Love character table (p. 304) for $\vec{k} = 0$ rhombohedral graphite (space group #166) is given in Fig. 15.10. The double group irreducible representations in this case are $4^{\pm}, 5^{\pm}, 6^{\pm}$ and need not be considered here further.

15.5   Phonons in Graphite

Now that we have reviewed the use of the Standard Reference Materials we will find the phonon modes in graphite: first for ordinary hexagonal graphite, and then for puckered graphite and for rhombohedral graphite.

In terms of hexagonal coordinates, where the x and y axes are 120° apart and are at 90° relative to the z-axis, the primitive lattice and reciprocal lattice vectors are taken to have components ($\frac{1}{3}$, $-\frac{1}{3}$, $\frac{1}{3}$), ($\frac{1}{3}$, $\frac{2}{3}$, $\frac{1}{3}$), and ($-\frac{2}{3}$, $-\frac{1}{3}$, $\frac{1}{3}$). The operators and translations in the representation tables are given in hexagonal coordinates.

Symmetry Point	Hexagonal Coordinates	Coordinates in terms of primitive reciprocal lattice vectors		
GM	0, 0, 0	0,	0,	0
LD	0, 0, α	α,	α,	α
SM	α, 0, 0	α,	0,	$-\alpha$
F	$\frac{1}{2}$, 0, 0	$\frac{1}{2}$,	0,	$-\frac{1}{2}$
L	$\frac{1}{6}$, $\frac{1}{3}$, $\frac{1}{6}$	0,	$\frac{1}{2}$,	0
T	$\frac{2}{3}$, $\frac{1}{3}$, $\frac{1}{6}$	$\frac{1}{2}$,	$\frac{1}{2}$,	$-\frac{1}{2}$
Y	α, $\frac{1}{3}$, $\frac{1}{6}$	$\alpha-\frac{1}{6}$,	$\frac{1}{2}$,	$\frac{1}{6}-\alpha$
P	$\frac{2}{3}$, $\frac{1}{3}$, α	$\frac{1}{3}+\alpha$,	$\frac{1}{3}+\alpha$,	$\alpha-\frac{2}{3}$
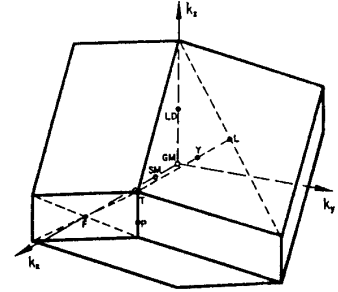
Figure 15.9: High symmetry points in the rhombohedral Brillouin zone taken from Miller and Love.

GROUP 166
GENS.= C3,I,SIGD

PT. GM AUGMENTERS   -Y,X-Y,Z; X-Y,-Y,-Z; -X+Y,Y,Z   R3m
REP. D AUGMENTERS   REP. D AUGMENTERS
GM1+ 1 (+); E; E; E   GM2+ 1 (+); F; (-)F; (-)E
GM3+ 2 (+); 5; 2; 2   GM1- 1 (+); E; E; (-)E
GM2- 1 (+); E; (-)E; E   GM3- 2 (+); 5; 2; (-)2
GM4+ 1 (-); (-)E; (+I)F; (+I)E   GM5+ 1 (-); (-)E; (-I)E; (-I)F
GM6+ 2 (-); 8; (-I)3; (-I)3   GM4- 1 (-); (-)F; (+I)E; (-I)F
GM5- 1 (-); (-)E; (-I)E; (+I)E   GM6- 2 (-); A; (-I)3; (+I)3

OPERATORS   GM 1+ 2+ 3+ 1- 2- 3- 4+ 5+ 6+ 4- 5- 6-
1   1   1   2   1   1   2   1   1   2   1   1   2
49   1   1   2   1   1   2 -1 -2 -1 -1 -1 -2
3 53   1   1 -1   1   1 -1 -1 -1   1 -1 -1   1
7 11 57 ....   1 -1   0   1 -1   0   1 -I   0   I -1   0
19 23 69 ....   1 -1   0 -1   1   0   I -I   0 -I   I   0
61   1   1   2 -1 -1 -2 -1 -1 -2   1   1   2
17 63   1   1 -1 -1 -1   1   1   1 -1 -1 -1   1

Figure 15.10: Miller and Love character table (p. 304) for space group #166 at $\vec{k} = 0$.
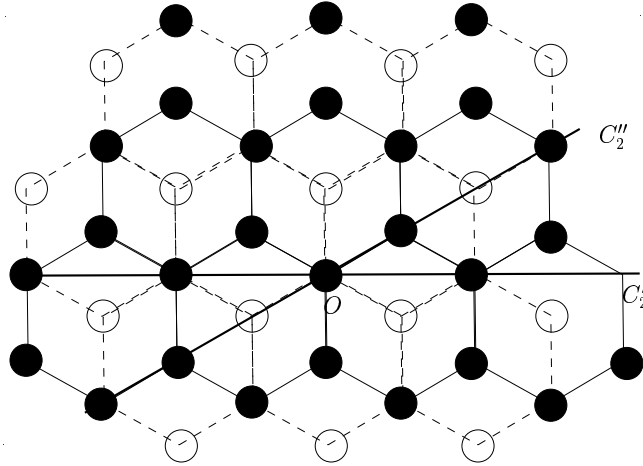
Figure 15.11: Schematic showing the symmetry operations in graphite. O labels the origin, which for convenience is taken halfway between the upper and lower planes of the unit cell.

15.5.1 Phonons in Ordinary Hexagonal Graphite

To find $\chi_{\text{atom sites}}$ we use a diagram showing the symmetry operations in graphite (see Fig. 15.11). The hexagonal Brillouin zone is shown in Fig. 15.12.

From Fig. 15.11, we compile $\chi_{\text{atom sites}} = \chi_{\text{a.s.}}$.

	$\{E\|0\}$	$\{C_2\|\tau\}$	$2\{C_3\|0\}$	$2\{C_6\|\tau\}$	$3\{C_{2'}\|0\}$	$3\{C_{2''}\|\tau\}$	$\{i\|0\}$	$\{iC_2\|\tau\}$	$2\{iC_3\|0\}$	$2\{iC_6\|\tau\}$	$3\{iC_{2'}\|0\}$	$3\{iC_{2''}\|\tau\}$
$\chi_{\text{a.s.}}$	4	0	4	0	0	4	0	4	0	4	4	0

Next we find the irreducible representations in $\chi_{\text{a.s.}}$ and χ_{vector}:

$$\chi_{\text{a.s.}} = 2A_{1g} + 2B_{2u} \tag{15.1}$$

$$\chi_{\text{vector}} = A_{2u} + E_{1u} \tag{15.2}$$

The direct product then yields

$$\chi_{\text{a.s.}} \otimes \chi_{\text{vector}} = (2A_{1g} + 2B_{2u}) \otimes (A_{2u} + E_{1u})$$

and can be decomposed into

$$\begin{aligned} \chi_{\text{in-plane lattice modes}} &= [(2A_{1g} + 2B_{2u}) \otimes E_{1u}] \\ &= 2E_{1u} + 2E_{2g} \\ \chi_{\text{z-axis lattice modes}} &= [(2A_{1g} + 2B_{2u}) \otimes A_{2u}] \\ &= 2A_{2u} + 2B_{1g} \end{aligned}$$

For the x and y primitive lattice vectors 120° apart and perpendicular to the z primitive lattice vector the x and y primitive reciprocal lattice vectors are 60° apart and perpendicular to the z-axis. In terms of hexagonal coordinates with the x and y axes 120° apart the x and y primitive reciprocal lattice vectors have components proportional to $(2, 1, 0)$ and $(1, 2, 0)$. The coordinates of the symmetry points are given in the oblique system based on the primitive reciprocal lattice vectors.

Symmetry Point	Coordinates
GM	0, 0, 0
DT	0, 0, α
LD	α, α, 0
SM	α, 0, 0
A	0, 0, ½
H	⅓, ⅓, ½
K	⅓, ⅓, 0
L	½, 0, ½
M	½, 0, 0
P	⅓, ⅓, α
Q	α, α,·½
R	α, 0, ½
S	½−α, 2α, ½
T	½−α, 2α, 0
U	½, 0, α

Figure 15.12: High symmetry points in the hexagonal Brillouin zone taken from Miller and Love.

The lattice mode diagrams are given in Fig. 15.13 for the vibrational modes. In addition there are in-plane translations (E_{1u}) and z-axis translations A_{2u} (not shown).

15.5.2 Phonons in Puckered Graphite

To find the lattice modes at $\vec{k} = 0$ for puckered graphite we use the diagram in Fig. 15.14 and the character table below:

Point Group C_{6v}	M+L	$\rightarrow$	1	4,1	3;5	2,1;6,1	19;21;23	20,1;22,1;24,1
	$\downarrow$	Tinkham	$\{E\|0\}$	$\{C_2\|\tau\}$	$2\{C_3\|0\}$	$2\{C_6\|\tau\}$	$3\{\sigma_d\|0\}$	$3\{\sigma_v\|\tau\}$
$x^2+y^2, z^2 \quad z$	1	A_1	1	1	1	1	1	1
R_z	2	A_2	1	1	1	1	-1	-1
	3	B_1	1	-1	1	-1	-1	1
	4	B_2	1	-1	1	-1	1	-1
$(xz,yz)(x,y)(R_x,R_y)$	6	E_1	2	-2	-1	1	0	0
(x^2-y^2, xy)	5	E_2	2	2	-1	-1	0	0

We also have included in the character table the basis functions for C_{6v}.

We find $\chi_{\text{atom sites}}$ for the two a atoms and for the two b atoms of puckered graphite using Fig. 15.14:

	$\{E\|0\}$	$\{C_2\|\tau\}$	$2\{C_3\|0\}$	$2\{C_6\|\tau\}$	$3\{\sigma_d\|0\}$	$3\{\sigma_v\|\tau\}$	
$\chi_{\text{a.s. a-atoms}}$	2	0	2	0	2	0	$A_1 + B_2$
$\chi_{\text{a.s. b-atoms}}$	2	0	2	0	2	0	$A_1 + B_2$

$\chi_{\text{a.s.}}$ for both the a- and b-atoms transforms as $A_1 + B_2$; also the vector transforms as $A_1 + E_1$. Thus we obtain for the lattice modes for puckered graphite

$$\chi_{\text{in-plane lattice modes}} = 2(A_1 + B_2) \otimes E_1 = 2E_1 + 2E_2$$
$$\chi_{\text{z-axis lattice modes}} = 2(A_1 + B_2) \otimes A_1 = 2A_1 + 2B_2$$

The lattice mode patterns are similar to those for ordinary graphite (see Fig. 15.13). Furthermore the A_1 and E_1 modes are infrared-active, the E_2 modes are Raman-active and the B_2 modes are silent. Thus puckered graphite would yield IR and Raman spectra similar to that observed for ordinary graphite. For the two hexagonal forms of graphite the high symmetry points in the Brillouin zone are given in Fig. 15.12 (from Miller and Love, p. 131). For each of these high symmetry points, the group of the wave vector is given in Miller and Love.

Finally we discuss the lattice modes for rhombohedral graphite. The character table from Tinkham corresponding to the the group of the
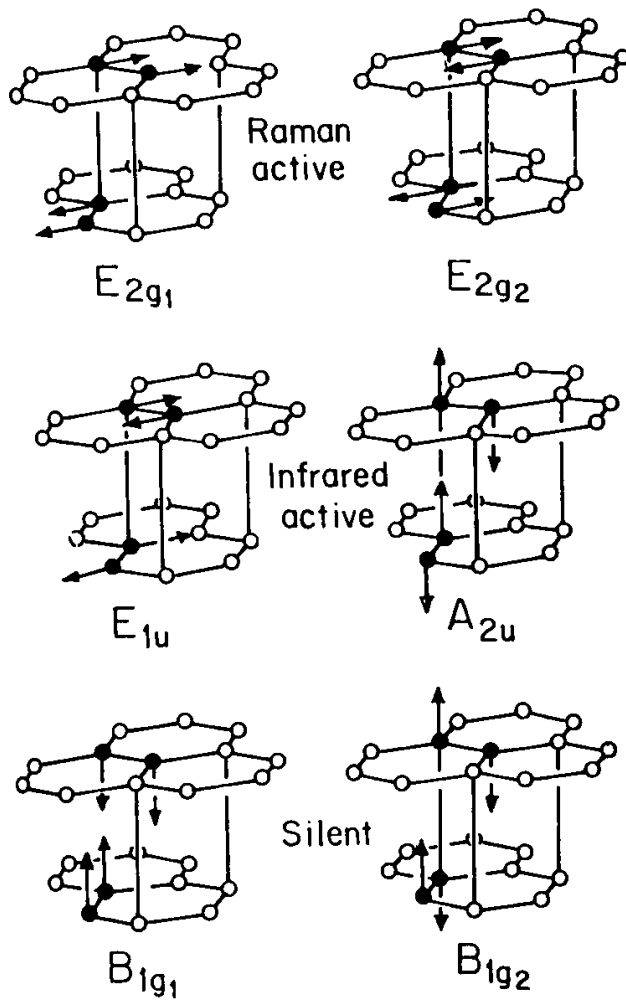
Figure 15.13: Schematic diagram showing the lattice mode displacements for hexagonal graphite.
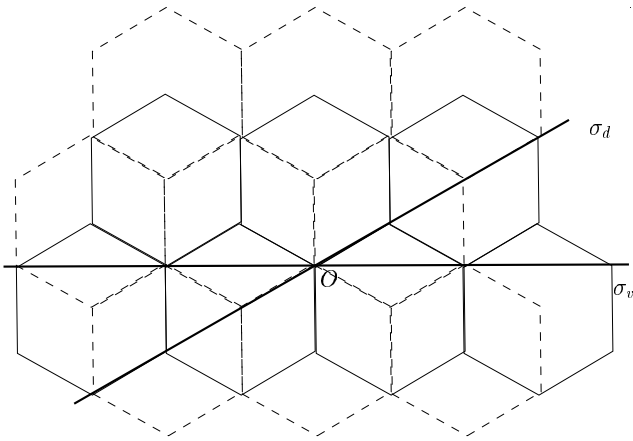
Figure 15.14: Schematic diagram showing the symmetry operations in puckered graphite.

wave vector at $\vec{k} = 0$ is written below ($D_{3d} = D_3 \otimes i$):

			1	3, 5	7, 9, 11	13	15, 17	19, 21, 23
D_3 (32)			E	$2C_3$	$3C_2'$	i	$2iC_3$	$3iC_2'$
x^2+y^2, z^2		A_1	1	1	1	1	1	1
	R_z, z	A_2	1	1	-1	1	1	-1
$\left.\begin{matrix}(xz, yz)\\(x^2-y^2, xy)\end{matrix}\right\}$	$\left.\begin{matrix}(x, y)\\(R_x, R_y)\end{matrix}\right\}$	E	2	-1	0	2	-1	0

where the correspondence in notation is:

Miller and Love	Tinkham	Miller and Love	Tinkham
1	E	1^+	A_{1g}
3, 5	$2C_3$	2^+	A_{2g}
7, 9, 11	$3C_{2'}$	3^+	E_g
13	i	1^-	A_{1u}
15, 17	$2iC_3$	2^-	A_{2u}
19, 21, 23	$3iC_{2'}$	3^-	E_u

Referring to Figs. 15.2 and 15.3 for the rhombohedral structure and layer stacking, we note that the operations E and C_3 take each carbon atom into an equivalent carbon atom (i.e., either into itself or displaced by a lattice vector), while operations $C_{2'}$ and i interchange

the two inequivalent atoms/unit cell. We also note that $iC_{2'}$ also takes each carbon into an equivalent site. We thus obtain for $\chi_{\text{atom sites}} = \chi_{\text{a.s.}}$ for rhombohedral graphite:

	E	$2C_3$	$3C_{2'}$	i	$2iC_3$	$3iC_{2'}$	
$\chi_{\text{a.s.}}$	2	2	0	0	0	2	$= A_{1g} + A_{2u}$

For D_3 symmetry

$$\chi_{\text{vector}} = A_{2u} + E_u \tag{15.3}$$

so that taking the direct product $\chi_{\text{a.s.}} \otimes \chi_{\text{vector}}$ we obtain

$$\chi_{\text{in-plane lattice modes}} = E_u \otimes (A_{1g} + A_{2u}) = E_u + E_g \tag{15.4}$$

$$\chi_{\text{z-axis lattice modes}} = A_{2u} \otimes (A_{1g} + A_{2u}) = A_{2u} + A_{1g}. \tag{15.5}$$

After identifying the A_{2u} and E_u modes with z-axis and in-plane translations, we identify the two modes with A_{1g} and E_g symmetries as optical modes at $\vec{k} = 0$. Both of these modes are Raman-active and infrared-inactive and execute the normal optical type motions.

15.6   Selected Problems

1. The electronic energy band structure of graphite near the Fermi level is of particular interest along the KH edge of the Brillouin zone (see Fig. 15.12).

    (a) "Translate" the K-point character table for graphite from Miller and Love in terms of the appropriate point group character table in Tinkham.

    (b) Find $\chi_{\text{atom sites}}$ at the K-point for the 4 atoms in the unit cell of graphite. Give the K point irreducible representations contained in $\chi_{\text{atom sites}}$.

2. Find the space groups and give the appropriate site locations for the atomic constituents from the International Crystallography Tables for the following crystalline solids:

(a) Solid molecular crystalline bromine.

(b) Crystalline SnO_2.

(c) Crystalline Nb_3Sn.

Chapter 16

Calculation of the Electronic Energy Levels in a Cubic Crystal

We now apply the space groups to the electronic dispersion relations in crystalline materials. In this chapter we will use group theory to find symmetrized plane wave solutions to the nearly free electron dispersion relations in crystalline materials.

16.1   Introduction

Suppose that we wish to calculate the electronic energy levels of a solid from a specified potential. There are many standard techniques available for this purpose based on plane waves, such as the orthogonalized plane wave method (OPW), the augmented plane wave method (APW); these are discussed in some detail in the sequence of solid state courses. In all cases these techniques utilize the **space symmetry of the crystal**. Because of the relative importance of the electronic energy bands at high symmetry points and along high symmetry axes for the interpretation of experimental data, these model calculations exploit the simplifications which result from the application of group theory.

To illustrate how group theory is utilized in these calculations, we

will consider explicitly the energy bands of the nearly free electron model. If there were no periodic potential, the energy eigenvalues would be the free electron energies

$$E(\vec{k'}) = \frac{\hbar^2 k'^2}{2m} \qquad\qquad V(\vec{r}) = 0 \qquad\qquad (16.1)$$

and the free electron eigenfunctions would be

$$\psi_{k'}(\vec{r}) = \frac{1}{\sqrt{\Omega}} e^{i\vec{k'}\cdot\vec{r}} \qquad\qquad (16.2)$$

where $\vec{k'}$ is a wave vector in the extended Brillouin zone.

The presence of a weak periodic potential imposes the symmetry of the crystal on the "empty lattice" energy bands. From a group theoretical point of view, the **free electron energy bands correspond to the symmetry of the full rotation group and the finite periodic potential serves to lower the symmetry**, as for example to O_h symmetry for a simple cubic crystal. Thus, the introduction of a periodic potential results in a situation similar to the crystal field problem which we have by now encountered in several contexts.

We consider the empty lattice energy bands in the reduced zone by writing the wave vector $\vec{k'}$ in the extended zone scheme as:

$$\vec{k'} = \vec{k} + \vec{K} \qquad\qquad (16.3)$$

where $\vec{k}$ is a reduced wave vector in the 1st Brillouin zone and $\vec{K}$ is 2π times the reciprocal lattice vector to obtain

$$E(\vec{k} + \vec{K}) = \frac{\hbar^2}{2m}(\vec{k} + \vec{K}) \cdot (\vec{k} + \vec{K}) \qquad\qquad (16.4)$$

where

$$\vec{K} = \frac{2\pi}{a}(n_1, n_2, n_3), \quad \text{and} \quad n_i = \text{integer.} \qquad\qquad (16.5)$$

We use the subscript $\vec{K}$ on the energy eigenvalues to denote the pertinent $\vec{K}$ vector when using the wave vector $\vec{k}$ within the first Brillouin zone. If we write $\vec{k}$ in dimensionless units

$$\vec{\xi} = \frac{\vec{k}a}{2\pi} \qquad\qquad (16.6)$$
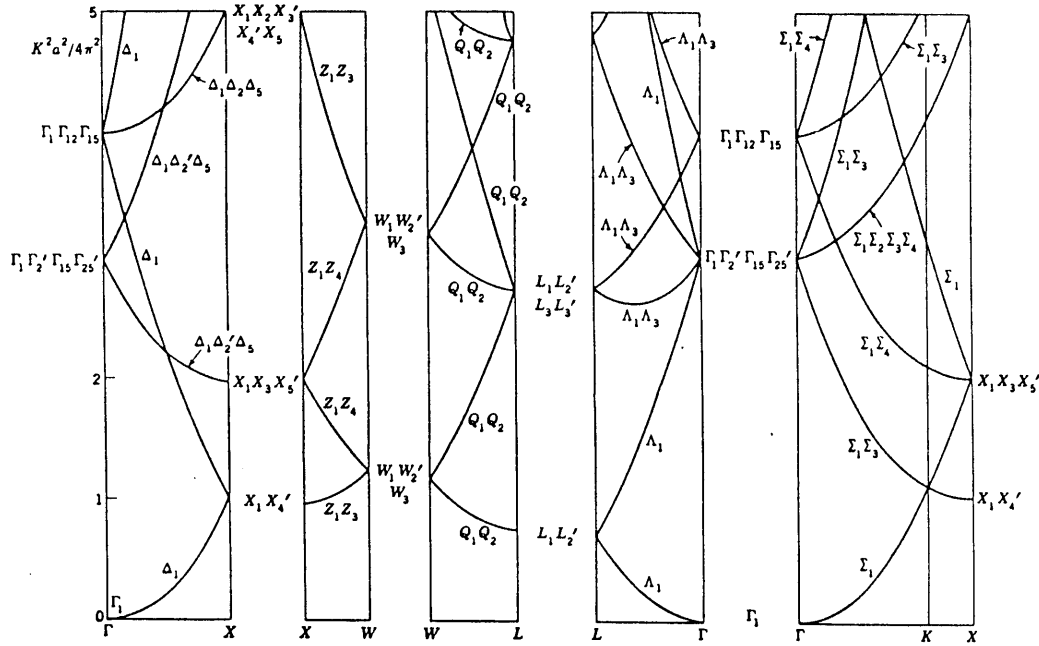
Figure 16.1: Free-electron bands in a face centered cubic structure. The labels of the high symmetry points in the fcc structure are given in Fig. 16.8(b). The band degeneracies are indicated on the diagram.

we obtain

$$E_{\vec{K}}(\vec{k}) = \frac{\hbar^2}{2m}\left(\frac{2\pi}{a}\right)^2\left[(\xi_1 + n_1)^2 + (\xi_2 + n_2)^2 + (\xi_3 + n_3)^2\right]. \quad (16.7)$$

The empty lattice energy bands for the fcc cubic structure are shown in Fig. 16.1 at the high symmetry points and along the high symmetry directions indicated by the Brillouin zone for the fcc lattice [see Fig. 16.8(b)]. The energy bands are labeled by the symmetries of the irreducible representations appropriate to the group of the wave vector corresponding to the space group. Group theory provides us with the symmetry designations and with the level degeneracies. In §16.2, we treat the symmetry designations and mode degeneracies for the simple cubic lattice at $\vec{k} = 0$, and in §16.3 and §16.4 at other symmetry points in the Brillouin zone.

In the reduced zone scheme, the wave functions for the plane wave become the Bloch functions

$$\psi_{\vec{k}'}(\vec{r}) = \frac{1}{\sqrt{\Omega}} e^{i\vec{k}'\cdot\vec{r}} = \frac{1}{\sqrt{\Omega}} e^{i\vec{k}\cdot\vec{r}} e^{i\vec{K}\cdot\vec{r}} \tag{16.8}$$

where the periodic part of the Bloch function is written as

$$u_{\vec{k}}(\vec{r}) = e^{i\vec{K}\cdot\vec{r}}. \tag{16.9}$$

According to Bloch's theorem, the effect of the translation operator is to introduce a phase factor

$$\{\varepsilon|t\}\psi_{\vec{k}}(\vec{r}) = e^{i\vec{k}\cdot\vec{t}}\psi_{\vec{k}}(\vec{r}) \tag{16.10}$$

in which $\vec{t}$ is a lattice vector such as $\vec{R}_n$.

In calculating the electronic energy bands in the nearly free electron approximation, we recognize that the main effect of the periodic potential is to lift the degeneracy of $E_{\vec{K}}(\vec{k})$. At certain high symmetry points or axes and at the Brillouin zone boundary, the degeneracy in many cases is not fully lifted because of the degeneracy of some of the pertinent irreducible representations. Group theory tells us the form of the interactions, the symmetry of the levels and their degeneracies. For each of the high symmetry points in the Brillouin zone, different symmetry operations will be applicable, depending on the appropriate group of the wave vector for the $\vec{k}$ point under consideration.

16.2   Plane Wave Solutions at $\vec{k} = 0$

The highest symmetry point in the Brillouin zone is of course the Γ point ($\vec{k} = 0$) and we will therefore illustrate the application of group theoretical considerations to the energy bands at the Γ point first. Setting $\vec{k} = 0$ in Eq. (16.7) for $E_{\vec{K}}(\vec{k})$ we obtain

$$E_{\vec{K}}(0) = \frac{\hbar^2}{2m} \left(\frac{2\pi}{a}\right)^2 \left[n_1^2 + n_2^2 + n_3^2\right] = \frac{\hbar^2}{2m} \left(\frac{2\pi}{a}\right)^2 N^2, \tag{16.11}$$

where

$$N^2 = n_1^2 + n_2^2 + n_3^2. \tag{16.12}$$

Corresponding to each reciprocal lattice vector $\vec{K}$, a value for $E_{\vec{K}}(0)$ is obtained. For most $\vec{K}$ vectors, these energies are degenerate. We will now enumerate the degeneracy of the first few levels, starting with $\vec{K} = 0$ and $n_1 = n_2 = n_3 = 0$. We then find which irreducible representations for O_h are contained in each degenerate state. If then a periodic potential is applied, the degeneracy of some of these levels will be lifted. Group theory provides a powerful tool for specifying how these degeneracies are lifted. In Table 16.1 we give the energy, the degeneracy and the set of $\vec{K}$ vectors that yield each of the five lowest energy eigenvalues $E_{\vec{K}}(0)$. The example that we explicitly work out here is for the simple cubic lattice (space group #221).

At $\vec{K} = 0$ we have $\psi_{\vec{k}}(r) = (1/\sqrt{\Omega})e^{i\vec{k}\cdot\vec{r}}$. For a general $\vec{K}$ vector, (n_1, n_2, n_3) there will in general be a multiplicity of states with the same energy. We now show how to choose a properly symmetrized combination of plane waves which transform as irreducible representations of the group of the wave vector at $\vec{k} = 0$, and therefore bring the Hamiltonian into block diagonal form. In the presence of a weak cubic periodic potential, the degeneracy of states which transform as different irreducible representations will be lifted.

By calculating $\chi_{\text{equivalence}} = \chi_{\text{atom sites}}$ we can specify which plane waves are transformed into one another by the elements of the group of the wave vector at the Γ point ($\vec{k} = 0$). From $\chi_{\text{equivalence}}$ we can find the irreducible representations of O_h which correspond to the degenerate empty lattice state and we can furthermore find the appropriate linear combination of plane wave states which correspond to a particular irreducible representation of O_h.

To calculate $\chi_{\text{equivalence}}$ we use the diagram in Fig. 16.2 which shows the cubic symmetry operations of point group O_h. The character table for O_h symmetry is given in Table 16.2, where the column on the right gives the familiar solid state notation for the irreducible representations of O_h. Computation of $\chi_{\text{equivalence}}$ is identical with the calculation of $\chi_{\text{atom sites}}$. If a given plane wave goes into itself under the symmetry operations of O_h a contribution of 1 is made to the character; otherwise no contribution is made. Using these definitions, we form $\chi_{\text{atom sites}}$ and the characters for the various plane waves are given in Table 16.3, where the various plane wave states are denoted by one of the reciprocal lat-

Table 16.1: Listing of the energy, degeneracy and the list of $\vec{K}$ vectors for the five lowest energy levels for the simple cubic lattice at $\vec{k} = 0$.

(i)	$E_{\{000\}}(0) = 0$	degeneracy=1	$\vec{K}_{\{000\}} = \frac{2\pi}{a}$	$(0,0,0)$	$N^2 = 0$
(ii)	$E_{\{100\}}(0) = \frac{\hbar^2}{2m}\left(\frac{2\pi}{a}\right)^2$	degeneracy=6	$\vec{K}_{\{100\}} = \frac{2\pi}{a}$	$\left\{\begin{array}{l}(1,0,0)\\(\bar{1},0,0)\\(0,1,0)\\(0,\bar{1},0)\\(0,0,1)\\(0,0,\bar{1})\end{array}\right.$	$N^2 = 1$

Plane Wave States:
$e^{\pm\frac{2\pi ix}{a}}, e^{\pm\frac{2\pi iy}{a}}, e^{\pm\frac{2\pi iz}{a}}$

(iii)	$E_{\{110\}}(0) = 2\frac{\hbar^2}{2m}\left(\frac{2\pi}{a}\right)^2$	degeneracy=12	$\vec{K}_{\{110\}} = \frac{2\pi}{a}$	$\left\{\begin{array}{l}(1,1,0)\\(\bar{1},1,0)\\(1,0,1)\\(\bar{1},0,1)\\(0,1,1)\\(0,\bar{1},1)\\(1,\bar{1},0)\\(\bar{1},\bar{1},0)\\(1,0,\bar{1})\\(\bar{1},0,\bar{1})\\(0,1,\bar{1})\\(0,\bar{1},\bar{1})\end{array}\right.$	$N^2 = 2$
(iv)	$E_{\{111\}}(0) = 3\frac{\hbar^2}{2m}\left(\frac{2\pi}{a}\right)^2$	degeneracy=8	$\vec{K}_{\{111\}} = \frac{2\pi}{a}$	$\left\{\begin{array}{l}(1,1,1)\\(1,\bar{1},1)\\(1,1,\bar{1})\\(\bar{1},1,1)\\(\bar{1},\bar{1},1)\\(1,\bar{1},\bar{1})\\(\bar{1},1,\bar{1})\\(\bar{1},\bar{1},\bar{1})\end{array}\right.$	$N^2 = 3$
(v)	$E_{\{200\}}(0) = 4\frac{\hbar^2}{2m}\left(\frac{2\pi}{a}\right)^2$	degeneracy=6	$\vec{K}_{\{200\}} = \frac{2\pi}{a}$	$\left\{\begin{array}{l}(2,0,0)\\(\bar{2},0,0)\\(0,2,0)\\(0,\bar{2},0)\\(0,0,2)\\(0,0,\bar{2})\end{array}\right.$	$N^2 = 4$
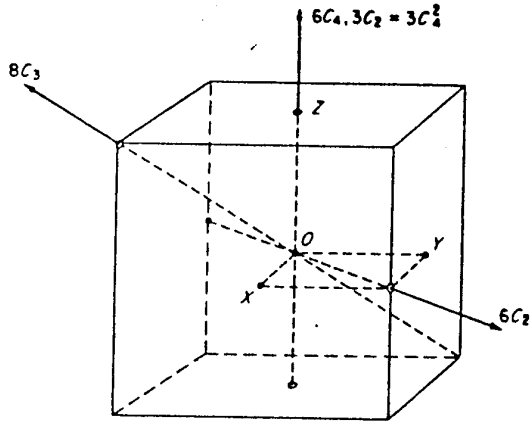
Figure 16.2: Diagram of Cubic Symmetry Operations

Table 16.2: The character table for O_h symmetry.

O (432)		E	$8C_3$	$3C_2 = 3C_4^2$	$6C_2'$	$6C_4$	
	A_1	1	1	1	1	1	Γ_1
	A_2	1	1	1	-1	-1	Γ_2
$(x^2 - y^2, 3z^2 - r^2)$	E	2	-1	2	0	0	Γ_{12}
(R_x, R_y, R_z) $\left.\begin{array}{c}\\ \\ \end{array}\right\}$ (x, y, z)	T_1	3	0	-1	-1	1	Γ_{15}
(xy, yz, zx)	T_2	3	0	-1	1	-1	Γ_{25}

$$O_h = O \otimes i \quad (m3m)$$

Table 16.3: Characters for the equivalence representation for the set of plane wave states labeled by $\{\vec{K}\}$.

$\vec{K}$	E	$3C_4^2$	$6C_2$	$8C_3$	$6C_4$	i	$3iC_4^2$	$6iC_2$	$8iC_3$	$6iC_4$	
$\{0,0,0\}$	1	1	1	1	1	1	1	1	1	1	Γ_1^+
$\{1,0,0\}$	6	2	0	0	2	0	4	2	0	0	$\Gamma_1^+ + \Gamma_{12}^+ + \Gamma_{15}^-$
$\{1,1,0\}$	12	0	2	0	0	0	4	2	0	0	$\Gamma_1^+ + \Gamma_{12}^+ + \Gamma_{15}^- + \Gamma_{25}^+ + \Gamma_{25}^-$
$\{1,1,1\}$	8	0	0	2	0	0	0	4	0	0	$\Gamma_1^+ + \Gamma_2^- + \Gamma_{15}^- + \Gamma_{25}^+$
$\{2,0,0\}$	6	2	0	0	2	0	4	2	0	0	$\Gamma_1^+ + \Gamma_{12}^+ + \Gamma_{15}^-$

tice vectors which describe each of these states using the notation of Table 16.1. The reducible representations for $\chi_{\text{equivalence}}$ for the various plane wave states in the simple cubic lattice are decomposed into irreducible representations of O_h and the results are given on the right hand side of Table 16.3.

Once we know the irreducible representations of O_h that are contained in each of the degenerate levels of the simple cubic empty lattice, we can find appropriate linear combinations of these plane wave states which will then transform as the desired irreducible representations of O_h. When a cubic periodic potential is now applied, the degeneracy of these empty lattice states will be lifted in accordance with the decomposition of the reducible representations of $\chi_{\text{equivalence}}$ into the irreducible representations of O_h. Thus the proper linear combinations of the plane wave states will bring the secular equation of the nearly free electron model energy bands into block diagonal form. As an example of how this works, let us list the six appropriate linear combinations for the $\{1,0,0\}$ set of reciprocal lattice vectors $\exp(\pm 2\pi ix/a)$, $\exp(\pm 2\pi iy/a)$, and $\exp(\pm 2\pi iz/a)$ which will bring the secular equation into block diagonal form:

$$\frac{1}{\sqrt{6}}[(1,0,0) + (\bar{1},0,0) + (0,1,0) + (0,\bar{1},0) + (0,0,1) + (0,0,\bar{1})] \;\rightarrow\; \Gamma_1^+$$

$$\left.\begin{array}{l} \frac{1}{\sqrt{6}}[(1,0,0) + (\bar{1},0,0) + \omega(0,1,0) + \omega(0,\bar{1},0) + \omega^2(0,0,1) + \omega^2(0,0,\bar{1})] \\ \frac{1}{\sqrt{6}}[(1,0,0) + (\bar{1},0,0) + \omega^2(0,1,0) + \omega^2(0,\bar{1},0) + \omega(0,0,1) + \omega(0,0,\bar{1})] \end{array}\right\} \;\rightarrow\; \Gamma_{12}^+$$

$$\left. \begin{array}{l} \frac{1}{i\sqrt{2}}[(1,0,0) - (\bar{1},0,0)] \\ \frac{1}{i\sqrt{2}}[(0,1,0) - (0,\bar{1},0)] \\ \frac{1}{i\sqrt{2}}[(0,0,1) - (0,0,\bar{1})] \end{array} \right\} \quad \rightarrow \quad \Gamma_{15}^{-},$$

$$(16.13)$$

in which we have used $(1,0,0)$ to denote $\exp(2\pi i x/a)$ and similarly for the other plane waves. Substituting

$$\begin{aligned} \tfrac{1}{2}[(1,0,0) + (\bar{1},0,0)] &= \cos(2\pi x/a) \\ \tfrac{1}{2i}[(1,0,0) - (\bar{1},0,0)] &= \sin(2\pi x/a) \end{aligned}$$

$$(16.14)$$

we obtain the following linear combinations of symmetrized plane waves from Eq. (16.13):

$$\frac{2}{\sqrt{6}} \left[\cos\left(\frac{2\pi x}{a}\right) + \cos\left(\frac{2\pi y}{a}\right) + \cos\left(\frac{2\pi z}{a}\right) \right] \quad \rightarrow \quad \Gamma_1^+$$

$$\left. \begin{array}{l} \frac{2}{\sqrt{6}}\left[\cos\left(\frac{2\pi x}{a}\right) + \omega\cos\left(\frac{2\pi y}{a}\right) + \omega^2\cos\left(\frac{2\pi z}{a}\right)\right] \\ \frac{2}{\sqrt{6}}\left[\cos\left(\frac{2\pi x}{a}\right) + \omega^2\cos\left(\frac{2\pi y}{a}\right) + \omega\cos\left(\frac{2\pi z}{a}\right)\right] \end{array} \right\} \quad \rightarrow \quad \Gamma_{12}^+$$

$$\left. \begin{array}{l} \sqrt{2}\sin\left(\frac{2\pi x}{a}\right) \\ \sqrt{2}\sin\left(\frac{2\pi y}{a}\right) \\ \sqrt{2}\sin\left(\frac{2\pi z}{a}\right) \end{array} \right\} \quad \rightarrow \quad \Gamma_{15}^-$$

$$(16.15)$$

The linear combinations of plane wave states given in Eq. (16.15) transform as irreducible representations of O_h, and bring the secular equation for $E(k = 0)$ into block diagonal form. For example, using the 6 combinations of plane wave states given in Eq. (16.15), we bring the (6×6) secular equation for $\vec{K} = \{1,0,0\}$ into a (1×1), a (2×2) and a (3×3) block, with no coupling between the blocks. Since there are 3 distinct energy levels, each corresponding to a different symmetry type, the introduction of a weak periodic potential will, in general, split the 6–fold level into 3 levels with degeneracies 1 (Γ_1^+), 2 (Γ_{12}^+) and 3 (Γ_{15}^-). This procedure is used to simplify the evaluation of $E(\vec{k})$ and $\psi_k(r)$ in first-order degenerate perturbation theory. Referring to Table 16.1, Eq. (16.15) gives the symmetrized wave functions for the six $K_{\{100\}}$ vectors. The corresponding analysis can be done for the twelve

$K_{\{110\}}$ vectors for the third lowest energy level, etc. The results for $E(\vec{k})$ for the empty lattice for the simple cubic group #221 are shown in Fig. 16.3.

The results obtained for the simple cubic lattice can be extended to other cubic lattices. The space group numbers for common cubic crystals are as follows: simple cubic (#221), fcc (#225), diamond (#227), bcc (#229). For the fcc lattice the (n_1, n_2, n_3) integers are all even or all odd so that the allowed $\vec{K}$ vectors are $\{000\}$, $\{111\}$, $\{200\}$, etc. For the bcc lattice, the integers $(n_1 + n_2 + n_3)$ must all sum to an even number, so that we can have reciprocal lattice $\vec{K}$ vectors $\{000\}$, $\{110\}$, $\{200\}$, etc. Thus Table 16.1 can be used together with an analysis such as given in this section to obtain the proper linear combination of plane waves for the pertinent $\vec{K}$ vectors for the various cubic groups.

To complete the discussion of the use of group theory for the solution of the electronic states of the empty lattice (or more generally the nearly free electron) model, we will next consider the construction of the symmetrized plane wave states $E(\vec{k})$ as we move away from $\vec{k} = 0$.

16.3   Symmetrized Plane Wave Solutions at the $\triangle$ Point

As an example of a non-zero $\vec{k}$ vector, let us consider $E(\vec{k})$ as we move from $\Gamma(\vec{k} = 0)$ toward point X $(\vec{k} = \frac{\pi}{a}(100))$. For intermediate points along the (100) direction (labeled $\triangle$ in Fig. 16.4), the appropriate point group of the wave vector is C_{4v}, with character table:

Below the character table (Table 16.4) for point group C_{4v}, are listed the characters for the three irreducible representations of $\vec{K} = \{100\}(\pi/a)$ corresponding to the $\vec{k} = 0$ solution and O_h symmetry. We consider these as reducible representations of point group C_{4v}. The decomposition of these three reducible representations in C_{4v} point group symmetry is indicated on the right of Table 16.4. This decomposition yields the compatibility relations (see §13.7):

$$\Gamma_1^+ \quad \rightarrow \quad A_1 = \Delta_1$$
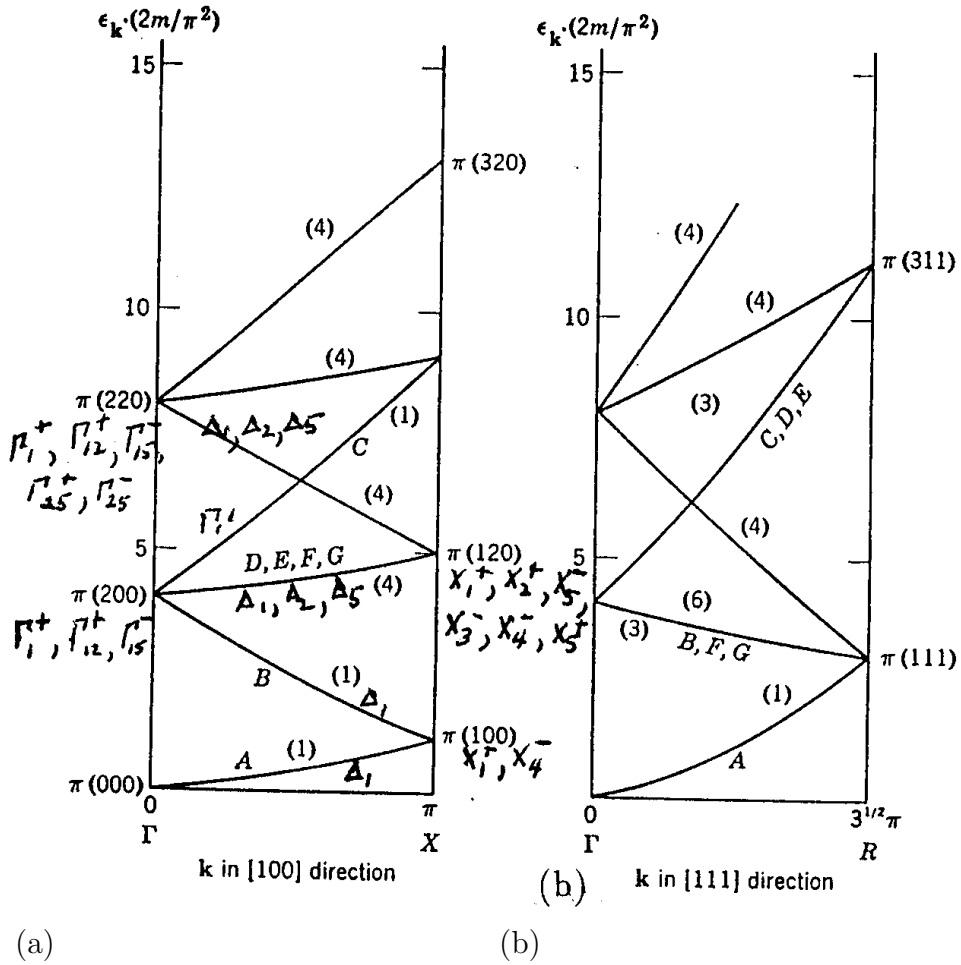
Figure 16.3: Diagram of the empty lattice energy levels along (a) $\Gamma - X$ and (b) $\Gamma - L$ for the simple cubic lattice #221.
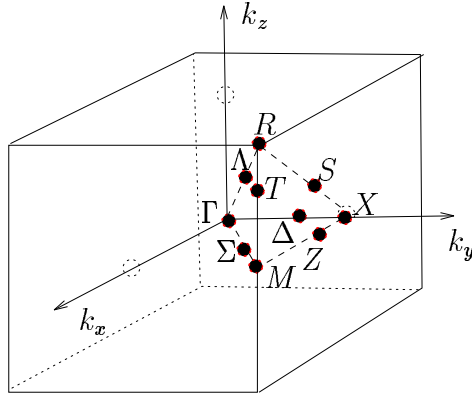
Figure 16.4: Brillouin zone for a simple cubic lattice.

Table 16.4: Character table for the point group C_{4v} and other relevant information.

C_{4v} $(4mm)$			E	C_2	$2C_4$	$2\sigma_v$	$2\sigma_d$	
$x^2 + y^2, z^2$	z	A_1	1	1	1	1	1	Δ_1
	R_z	A_2	1	1	1	−1	−1	$\Delta_{1'}$
$x^2 - y^2$		B_1	1	1	−1	1	−1	Δ_2
xy		B_2	1	1	−1	−1	1	$\Delta_{2'}$
(xz, yz)	$\begin{matrix} (x, y) \\ (R_x, R_y) \end{matrix} \Big\}$	E	2	−2	0	0	0	Γ_5
	A_{1g} (O_h)	Γ_1^+	1	1	1	1	1	A_1
	E_g (O_h)	Γ_{12}^+	2	2	0	2	0	$A_1 + B_1$
	T_{1u} (O_h)	Γ_{15}^-	3	−1	1	1	1	$A_1 + E$

$$\begin{aligned}
\Gamma_{12}^+ &\to A_1 + B_1 = \Delta_1 + \Delta_2 \\
\Gamma_{15}^- &\to A_1 + E = \Delta_1 + \Delta_5.
\end{aligned} \qquad (16.16)$$

In the above character table, the main symmetry axis is the x axis, so that the basis functions that should be used require the transformation: $x \to y$, $y \to z$, $z \to x$. The symmetry axis $\sigma_v = iC_2^{100}$ denotes the mirror planes $y = 0$ and $z = 0$, while $\sigma_d = iC_2^{1\bar{1}0}$ denotes the diagonal (011) planes, with all symmetry operations referring to reciprocal space, since we are considering the group of the wave vector at a Δ point. The results of Eq. (16.16) are of course in agreement with the compatibility relations given in §13.7 for the simple cubic structure. Compatibility relations of this type can be used to obtain the degeneracies and symmetries for all the levels at the Δ point, starting from the plane wave solution at $\vec{k} = 0$. A similar approach can be used to obtain the symmetries and degeneracies as we move away from $\vec{k} = 0$ in other directions. For an arbitrary crystal structure we have to use Miller and Love to construct the compatibility relations using the tables for the group of the wave vector given in this reference.

16.4 Plane Wave Solutions at the X Point

As we move in the Brillouin zone from a point of high symmetry to a point of lower symmetry, the solution using the compatibility relations discussed in §16.3 is unique. On the other hand, when going from a point of lower symmetry to one of higher symmetry, the solution from the compatibility relations is not unique, and we must then go back to consideration of the equivalence transformation. An example of this situation occurs when we go from the Δ point to the X-point (D_{4h} symmetry), which has higher symmetry than the Δ point (C_{4v} symmetry). The appropriate character table for the X point is $D_{4h} = D_4 \otimes i$ for the group of the wave vector shown in Table 16.5. At the X-point, the nearly free electron solutions for the simple cubic lattice given by Eq. (16.7) become:

$$E\left(\vec{k} = \frac{\pi}{a}\hat{x}\right) = \frac{\hbar^2}{2m}\left(\frac{2\pi}{a}\right)^2 \left[\left(\frac{1}{2} + n_1\right)^2 + n_2^2 + n_3^2\right]. \qquad (16.17)$$

Table 16.5: Character table for the point group D_4, showing the solid state notation in the right hand column.

D_4 (422)			E	$C_2 = C_4^2$	$2C_4$	$2C_2'$	$2C_2''$	
$x^2 + y^2, z^2$		A_1	1	1	1	1	1	X_1
	R_z, z	A_2	1	1	1	-1	-1	X_4
$x^2 - y^2$		B_1	1	1	-1	1	-1	X_2
xy		B_2	1	1	-1	-1	1	X_3
(xz, yz)	$\begin{matrix}(x, y)\\(R_x, R_y)\end{matrix}$	E	2	-2	0	0	0	X_5

The lowest energy level at the X-point is

$$E_1\left(\vec{k} = \frac{\pi}{a}\hat{x}\right) = \frac{\hbar^2}{2m}\left(\frac{2\pi}{a}\right)^2\left(\frac{1}{4}\right). \tag{16.18}$$

The pertinent plane waves which contribute to the energy level in Eq. (16.18) correspond to $\vec{K}$ vectors:

$$\begin{aligned}
\vec{K} &= (0, 0, 0)\\
\vec{K} &= \frac{2\pi}{a}(\bar{1}, 0, 0).
\end{aligned}$$

We will now find $\chi_{\text{equivalence}}$ for these plane waves, using the symmetry operations in Fig. 16.5 and in the character table for D_{4h} in which we use the transformation $x \to y$, $y \to z$, $z \to x$ to obtain the proper X-point. We note that $\vec{K} = (0, 0, 0)$ yields a plane wave $e^{\frac{\pi}{a}ix}$ while $\vec{K} = \frac{2\pi}{a}(\bar{1}, 0, 0)$ yields a plane wave $e^{\left(\frac{\pi}{a}ix - \frac{2\pi}{a}ix\right)} = e^{-\frac{\pi}{a}ix}$ and both have energies $E_1 = \frac{\hbar^2}{2m}\left(\frac{2\pi}{a}\right)^2\left(\frac{1}{4}\right)$. The plane waves denoted by $\vec{K} = (0, 0, 0)$ and $\vec{K} = \frac{2\pi}{a}(\bar{1}, 0, 0)$ form partners of a reducible representation:

	E	C_2	$2C_4$	$2C_{2'}$	$2C_{2''}$	i	iC_2	$2iC_4$	$2iC_{2'}$	$2iC_{2''}$	
$\exp(\pm\pi ix/a)$	2	2	2	0	0	0	0	0	2	2	$A_{1g} + A_{2u}$

$$A_{1g} + A_{2u} = X_1^+ + X_4^-. \tag{16.19}$$
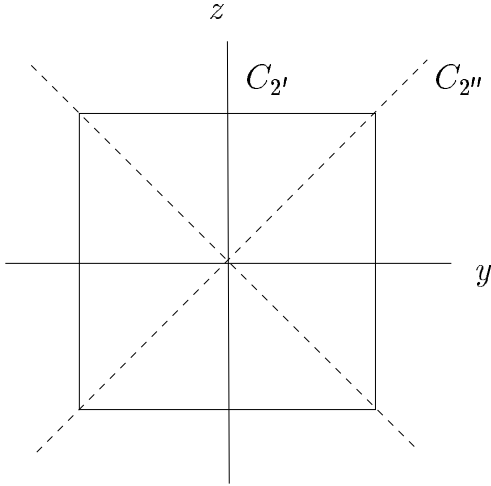
Figure 16.5: Diagram of a square showing the two-fold axes normal to the principal C_4 symmetry axis.

We thus obtain irreducible representations with X_1^+ and X_4^- symmetries for the lowest X-point level so that a periodic potential will split the degeneracy of these levels at the X-point. In this case the level separations becomes $2|V_{\vec{K}}|$ where $\vec{K} = \frac{2\pi}{a}(\bar{1},0,0)$. The appropriate linear combination of plane waves corresponding to the X_1^+ and X_4^- irreducible representations are:

$$X_1^+ \text{ symmetry } : (0,0,0) + (\bar{1},0,0) \rightarrow 2\cos\frac{\pi}{a}x$$

$$X_4^- \text{ symmetry } : (0,0,0) - (\bar{1},0,0) \rightarrow 2\sin\frac{\pi}{a}x. \qquad (16.20)$$

and each of the X_1^+ and X_4^- levels is non-degenerate.

Referring to Eq. (16.17), the next lowest energy level at the X point is:

$$E_2\left(\vec{k} = \frac{\pi}{a}\hat{x}\right) = \frac{\hbar^2}{2m}\left(\frac{2\pi}{a}\right)^2\left(\frac{5}{4}\right). \qquad (16.21)$$

The 8 pertinent plane waves for this energy level correspond to the $\vec{K}$ vectors

$$\vec{K} = \frac{2\pi}{a}(0,1,0), \frac{2\pi}{a}(0,\bar{1},0), \frac{2\pi}{a}(0,0,1), \frac{2\pi}{a}(0,0,\bar{1})$$

$$\vec{K} \;=\; \frac{2\pi}{a}(\bar{1},1,0),\frac{2\pi}{a}(\bar{1},\bar{1},0),\frac{2\pi}{a}(\bar{1},0,1),\frac{2\pi}{a}(\bar{1},0,\bar{1}).$$

More explicitly, the 8 plane waves corresponding to these $\vec{K}$ vectors are:

$$
\begin{aligned}
&\exp\left\{\tfrac{\pi ix}{a}+\tfrac{2\pi iy}{a}\right\}, && \exp\left\{\tfrac{\pi ix}{a}-\tfrac{2\pi iy}{a}\right\}, \\
&\exp\left\{\tfrac{\pi ix}{a}+\tfrac{2\pi iz}{a}\right\}, && \exp\left\{\tfrac{\pi ix}{a}-\tfrac{2\pi iz}{a}\right\}, \\
&\exp\left\{\tfrac{-\pi ix}{a}+\tfrac{2\pi iy}{a}\right\}, && \exp\left\{-\tfrac{\pi ix}{a}-\tfrac{2\pi iy}{a}\right\}, \\
&\exp\left\{-\tfrac{\pi ix}{a}+\tfrac{2\pi iz}{a}\right\}, && \exp\left\{-\tfrac{\pi ix}{a}-\tfrac{2\pi iz}{a}\right\}
\end{aligned}
\tag{16.22}
$$

To find $\chi_{\text{equivalence}}$ for the 8 plane waves of Eq. (16.22) we use the character table for D_{4h} and Fig. 16.5. The results for several pertinent plane wave combinations are given below:

	E	C_2	$2C_4$	$2C_{2'}$	$2C_{2''}$	i	iC_2	$2iC_4$	$2iC_{2'}$	$2iC_{2''}$
Eq. (16.22)	8	0	0	0	0	0	0	0	4	0
$\exp(\pm 2\pi iy/a)$ $\exp(\pm 2\pi iz/a)$	4	0	0	2	0	0	4	0	2	0

The reducible representation for the 8 plane waves given by Eq. (16.22) yields the following X point irreducible representations

$$X_1^+ + X_2^+ + X_5^- + X_4^- + X_3^- + X_5^+. \tag{16.23}$$

The same result can be obtained by considering the $e^{\pm\frac{\pi ix}{a}}$ functions as common factors of the $e^{\pm\frac{2\pi iy}{a}}$ and $e^{\pm\frac{2\pi iz}{a}}$ functions. The $\chi_{\text{equivalence}}$ for the four $e^{\pm\frac{2\pi iy}{a}}$ and $e^{\pm\frac{2\pi iz}{a}}$ plane waves is also tabulated above. The $e^{\pm\frac{\pi ix}{a}}$ functions transform as $X_1^+ + X_4^-$ (see above), and the 4 functions $e^{\pm\frac{2\pi iy}{a}}$ and $e^{\pm\frac{2\pi iz}{a}}$ transform as $X_1^+ + X_2^+ + X_5^-$. If we now take the direct product, we obtain:

$$(X_1^+ + X_4^-)\otimes(X_1^+ + X_2^+ + X_5^-) = X_1^+ + X_2^+ + X_5^- + X_4^- + X_3^- + X_5^+ \tag{16.24}$$

in agreement with the result of Eq. (16.23). The proper linear combination of the eight plane waves which transform as irreducible representations of the D_{4h} point symmetry group for the second lowest X point level is found from the $\vec{K}$ vectors given below:

$$
\begin{aligned}
X_1^+ \;:\;& (0,1,0)+(0,\bar{1},0)+(0,0,1)+(0,0,\bar{1})+(\bar{1},1,0)+(\bar{1},\bar{1},0)+(\bar{1},0,1)+(\bar{1},0,1) \\
X_4^- \;:\;& (0,1,0)+(0,\bar{1},0)+(0,0,1)+(0,0,\bar{1})-(\bar{1},1,0)-(\bar{1},\bar{1},0)-(\bar{1},0,1)-(\bar{1},0,1)
\end{aligned}
$$

$$X_2^+ \; : \; (0,1,0) - (0,0,1) + (0,\bar{1},0) - (0,0,\bar{1}) + (\bar{1},1,0) - (\bar{1},0,1) + (\bar{1},\bar{1},0) - (\bar{1},0,\bar{1})$$

$$X_3^- \; : \; (0,1,0) - (0,0,1) + (0,\bar{1},0) - (0,0,\bar{1}) - (\bar{1},1,0) + (\bar{1},0,1) - (\bar{1},\bar{1},0) + (\bar{1},0,\bar{1})$$

$$X_5^- \; : \; \left. \begin{array}{l} (0,1,0) - (0,\bar{1},0) + (\bar{1},1,0) - (\bar{1},\bar{1},0) \\ (0,0,1) - (0,0,\bar{1}) + (\bar{1},0,1) - (\bar{1},0,\bar{1}) \end{array} \right\} \text{2 partners}$$

$$X_5^+ \; : \; \left. \begin{array}{l} (0,1,0) - (0,\bar{1},0) - (\bar{1},1,0) + (\bar{1},\bar{1},0) \\ (0,0,1) - (0,0,\bar{1}) - (\bar{1},0,1) + (\bar{1},0,\bar{1}) \end{array} \right\} \text{2 partners} \tag{16.25}$$

in which the plane waves are denoted by their corresponding $\vec{K}$ vectors. We note that the wave vector $\vec{K} = \frac{2\pi}{a}(0,1,0)$ gives rise to a plane wave $\exp[\frac{\pi i x}{a} + \frac{2\pi i y}{a}]$. Likewise the wave vector $\vec{K} = \frac{2\pi}{a}(\bar{1},1,0)$ gives rise to a plane wave $\exp[\frac{\pi i x}{a} - \frac{2\pi i x}{a} + \frac{2\pi i y}{a}]$. Using this notation we find that the appropriate combinations of plane waves corresponding to Eq. (16.25) are:

$$X_1^+ \; : \; \cos\frac{\pi x}{a}\left(\cos\frac{2\pi y}{a} + \cos\frac{2\pi z}{a}\right)$$

$$X_4^- \; : \; \sin\frac{\pi x}{a}\left(\cos\frac{2\pi y}{a} + \cos\frac{2\pi z}{a}\right)$$

$$X_2^+ \; : \; \cos\frac{\pi x}{a}\left(\cos\frac{2\pi y}{a} - \cos\frac{2\pi z}{a}\right)$$

$$X_3^- \; : \; \sin\frac{\pi x}{a}\left(\cos\frac{2\pi y}{a} - \cos\frac{2\pi z}{a}\right)$$

$$X_5^- \; : \; \left. \begin{array}{l} \cos\frac{\pi x}{a}\sin\frac{2\pi y}{a} \\ \cos\frac{\pi x}{a}\sin\frac{2\pi z}{a} \end{array} \right\} \text{2 partners}$$

$$X_5^+ \; : \; \left. \begin{array}{l} \sin\frac{\pi x}{a}\sin\frac{2\pi y}{a} \\ \sin\frac{\pi x}{a}\sin\frac{2\pi z}{a} \end{array} \right\} \text{2 partners} \tag{16.26}$$

A summary of the energy levels and symmetries along $\Gamma - X$ and $\Gamma - R$ for the simple cubic lattice is given in Fig. 16.3. A similar procedure is used to find the degeneracies and the symmetrized linear combination of plane waves for any of the energy levels at each of the high symmetry points in the Brillouin zone. We show for example results in Fig. 16.3b also for the empty lattice bands along $\Gamma - R$. The corresponding results can be obtained by this same procedure for the fcc and bcc lattices as well (see Figs. 16.1 and 16.6).

In the following section we will consider the effect of non-symmorphic operations on plane waves.
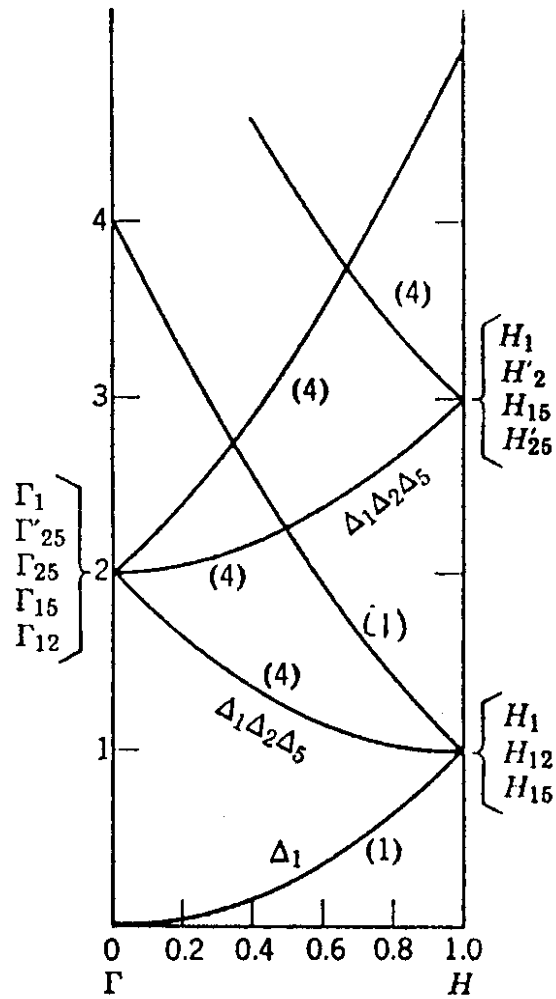
Figure 16.6: Diagram of empty lattice energy levels along $\Gamma - H$ for the bcc lattice. The irreducible representations are indicated.
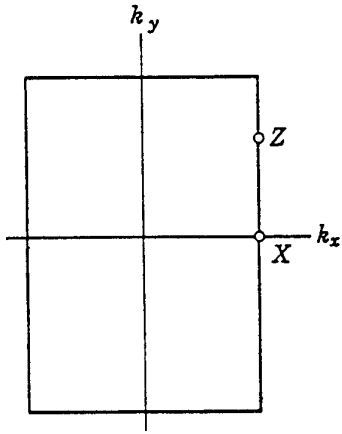
Figure 16.7: Brillouin zone for a rectangular lattice (such as $p2mg$ (#14))

16.5 Effect of Glide Planes and Screw Axes

The main effect of non-symmorphic operations connected with glide planes and screw axes is to cause energy bands to stick together along some of the high symmetry points and axes in the Brillouin zone. We first illustrate this feature using the 2D space group $p2mg$ (#14) which has a 2-fold axis, mirror planes normal to the x axis at $x = \frac{1}{4}a$ and $x = \frac{3}{4}a$, and a glide plane g parallel to the x axis for a distance $\frac{a}{2}$. In addition, group $p2mg$ has inversion symmetry. Suppose that $X(x, y)$ is a solution to Schrödinger's equation at the X point $\vec{k}_X = \frac{\pi}{a}(1, 0)$ (see Fig. 16.7). This degeneracy at the zone boundary in the two-dimensional non-symmorphic space group $p2mg$ is also found in many of the common three-dimensional non-symmorphic groups.

In the two-dimensional case for the space group $p2mg$, the mirror glide operation g implies

$$gX(x, y) = X(x + \frac{1}{2}a, -y) \tag{16.27}$$

while inversion i implies

$$iX(x, y) = X(-x, -y). \tag{16.28}$$

The mirror plane m at $x = a/4$ implies

$$mX(x,y) = X(-x + \frac{1}{2}a, y) \tag{16.29}$$

so that

$$gX(x,y) = m\,iX(x,y) \tag{16.30}$$

where m denotes reflection in a mirror plane and i denotes inversion. Since $i^2 X(x,y) = X(x,y)$ and $m^2 X(x,y) = X(x,y)$, we would expect from Eq. (16.30) that

$$g^2 X(x,y) = X(x,y). \tag{16.31}$$

But direct application of the glide operation twice yields

$$g^2 X(x,y) = X(x+a, y) = e^{ik_x a} X(x,y) = e^{\pi i} X(x,y) = -X(x,y) \tag{16.32}$$

which contradicts Eq. (16.31). This contradiction is resolved by having the solutions $\pm X(x,y)$ stick together at the X point.

In fact, if we employ time reversal symmetry (to be discussed in Chapter 21), we can show that bands $\pm\Phi_Z(x,y)$ stick together along the entire Brillouin zone edge for all Z points, i.e., $(\pi/a, k_y)$ (see Fig. 16.7). Thus in addition to the degeneracies imposed by the group of the wave vector, other symmetry relations can in some cases cause energy bands to stick together at high symmetry points and axes.

The same situation also arises for the 3D space groups. Some common examples where energy bands stick together are on the hexagonal face of the hexagonal close packed structure (space group #194, see Brillouin zone in Fig. 16.8a), and the square face in the diamond structure (#227) for which the Brillouin zone is given in Fig. 16.8b. For the case of the hexagonal close packed structure, there is only a single translation $\vec{\tau} = \frac{c}{2}(001)$ connected with non-symmorphic operations in space group #194. The character table for the group of the wave vector at the A point shows that the bands stick together, i.e., there are no non-degenerate levels at the A point. To illustrate this point, we give in Table 16.6 the character tables for the Γ point and the A point for space group #194.

For the case of the diamond structure (space group #227), Miller and Love shows that there are 3 different translations $(a/4)(110)$, $(a/4)(011)$,

Table 16.6: Character tables from Miller and Love for the Γ point and the A point for the hexagonal close packed structure (hcp) (space group #194). Note the degeneracy of all the irreducible representations at point A in the Brillouin zone.

```
GROUP 194
GENS.= C3,C2(0,0,1/2),C2X,SIGV(0,0,1/2)
TRANSLATIONS   1=(0,0,1/2)

PT. GM  AUGMENTERS  -Y,X-Y,Z; -X,-Y,1/2+Z; X-Y,-Y,-Z; X-Y,-Y,1/2+Z
REP.  D AUGMENTERS                                      REP.  D AUGMENTERS
GM1+  1  (+);   E;  E;  E;  E                           GM2+  1  (+);   E;  E;  (-)E;  (-)E
GM3+  1  (+);   E;  (-)E;  E;  (-)E                     GM4+  1  (+);   E;  (-)E;  (-)E;  E
GM5+  2  (+);   5;  E;  2;  2                            GM6+  2  (+);   5;  (-)E;  2;  (-)2
GM1-  1  (+);   E;  E;  E;  (-)E                         GM2-  1  (+);   E;  E;  (-)E;  E
GM3-  1  (+);   E;  (-)E;  E;  E                         GM4-  1  (+);   E;  (-)E;  (-)E;  (-)E
GM5-  2  (+);   5;  E;  2;  (-)2                         GM6-  2  (+);   5;  (-)E;  2;  2
GM7+  2  (-);   8;  (+I)4;  (-I)3;  (-I)2               GM8+  2  (-);   8;  (-I)4;  (-I)3;  (+I)2
GM9+  2  (-);   (-)E;  (+I)4;  (-I)3;  (-I)2            GM7-  2  (-);   8;  (+I)4;  (-I)3;  (+I)2
GM8-  2  (-);   8;  (-I)4;  (-I)3;  (-I)2              GM9-  2  (-);   (-)E;  (+I)4;  (-I)3;  (+I)2
```

OPERATORS	GM 1+	2+	3+	4+	5+	6+	1-	2-	3-	4-	5-	6-	7+	8+	9+	7-	8-	9-
1	1	1	1	1	2	2	1	1	1	1	2	2	2	2	2	2	2	2
49	1	1	1	1	2	2	1	1	1	1	2	2	-2	-2	-2	-2	-2	-2
3 53	1	1	1	1	-1	-1	1	1	1	1	-1	-1	1	1	-2	1	1	-2
4,1	1	1	-1	-1	2	-2	1	1	-1	-1	2	-2	0	0	0	0	0	0
6,1 50,1	1	1	-1	-1	-1	1	1	1	-1	-1	-1	1	-B	B	0	-B	B	0
7 9 11	1	-1	-1	-1	0	0	1	-1	1	-1	0	0	0	0	0	0	0	0
8,1 10,1 12,1	1	-1	-1	1	0	0	1	-1	-1	1	0	0	0	0	0	0	0	0
20,1 22,1 24,1	1	-1	-1	1	0	0	-1	1	1	-1	0	0	0	0	0	0	0	0
19 21 23	1	-1	-1	-1	0	0	-1	1	-1	1	0	0	0	0	0	0	0	0
16,1	1	1	-1	-1	2	-2	-1	-1	1	1	-2	2	0	0	0	0	0	0
14,1 66,1	1	1	-1	-1	-1	1	-1	-1	1	1	1	-1	B	-B	0	-B	B	0
13	1	1	1	1	2	2	-1	-1	-1	-1	-2	-2	2	2	2	-2	-2	-2
15 65	1	1	1	1	-1	-1	-1	-1	-1	-1	1	1	1	1	-2	-1	-1	2

```
PT. DT  AUGMENTERS  -Y,X-Y,Z; -X,-Y,1/2+Z; X-Y,-Y,1/2+Z
DT1 -  1  (+);   E;  TE;  TE                            DT2  1  (+);   E;  TE;  T(-)E
DT3    1  (+);   E;  T(-)E;  TE                         DT4  1  (+);   E;  T(-)E;  T(-)E
DT5    2  (+);   5;  TE;  T2                            DT6  2  (+);   5;  T(-)E;  T2
DT7    2  (-);   8;  T(-I)4;  T(-I)3                    DT8  2  (-);   8;  T(+I)4;  T(-I)3
DT9    2  (-);   (-)E;  T(-I)4;  T(-I)3
```

OPERATORS	DT 1	2	3	4	5	6	7	8	9
1	1	1	1	1	2	2	2	2	2
49	1	1	1	1	2	2	-2	-2	-2
3 53	1	1	1	1	-1	-1	1	1	-2
4,1	1,T	1,T	-1,T	-1,T	2,T	-2,T	0	0	0
6,1 50,1	1,T	1,T	-1,T	-1,T	-1,T	1,T	B,T	-B,T	0
20,1 22,1 24,1	1,T	-1,T	1,T	-1,T	0	0	0	0	0
19 21 23	1	-1	-1	1	0	0	0	0	0

```
PT. LD  AUGMENTERS  Y,X,-Z; Y,X,1/2+Z
LD1  1  (+);   E;  E                                    LD2  1  (+);   E;  (-)E
LD3  1  (+);   (-)E;  E                                 LD4  1  (+);   (-)E;  (-)E
LD5  2  (-);   (+I)4;  (-I)3
```
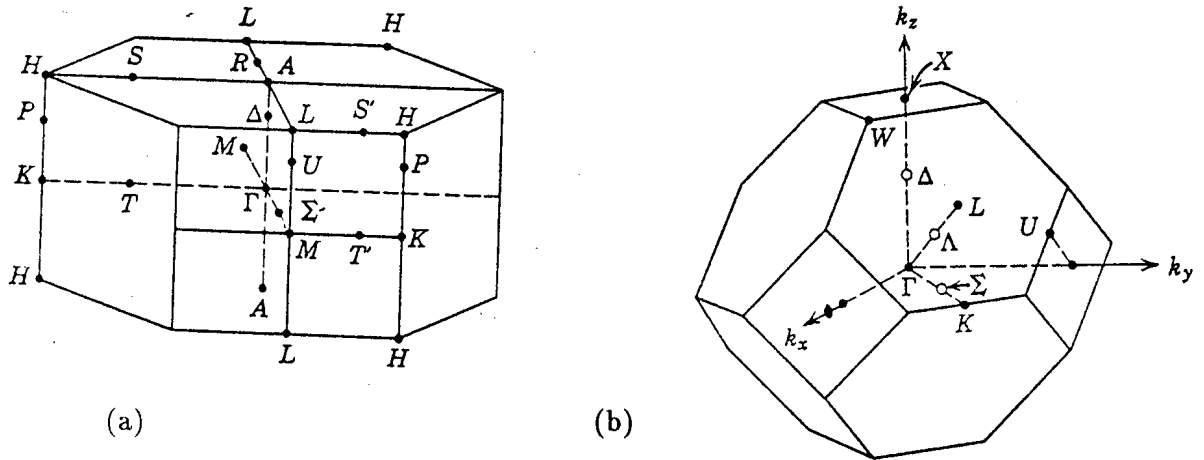
Figure 16.8: Brillouin zone for (a) the hexagonal close pack structure, D_{6h}^4, #194 and (b) the fcc structure (e.g., diamond #227).

and $(a/4)(101)$. The reason why these translations differ from those used in this section is the selection of a different origin for the unit cell. In Miller and Love the origin is selected to lie halfway between the two inequivalent lattice points. We can take the equivalent lattice points as a white atom and a black atom for discussion purposes. Miller and Love selects the origin at $\frac{a}{8}(111)$ or at $\frac{a}{8}(\bar{1}\bar{1}\bar{1})$, so that the inversion operation takes the white sublattice into a black sublattice, and vice versa. In contrast, we have taken the origin to coincide with the origin of the white sublattice so that in this case the space group operation for inversion contains a translation by $\vec{\tau} = (a/4)(111)$ and is denoted by $\{i|\tau\}$. In Table 16.7 we show the character tables appropriate for the diamond structure at the Γ point and at the X point using the origin at (000).

In all the $E(\vec{k})$ diagrams for the diamond structure (see Fig. 16.9 for $E(\vec{k})$ for Ge), we see that all the bands stick together at the X point, all being either 2-fold or 4-fold degenerate, as seen in the character table for the X point in Table 16.7. The plane wave basis functions for the irreducible representations X_1, X_2, X_3 and X_4 for the diamond structure are listed in Table 16.8.

Because of the non-symmorphic features of the diamond structure, the energy bands at the X point behave differently from the bands

Table 16.7: Character table for the diamond structure (space group #227; $Fd3m$) at the Γ point and at the X point. If we take the origin of the white sublattice at (000), then the site location of the black sublattice is at $(a/4)(111)$.

```
GROUP 227
GENS.= C2(1/4,1/4,0),C2X(0,1/4,1/4),SIGV(0,3/4,3/4),C3XYZ,SIGD
TRANSLATIONS   1=(1/4,1/4,0)  2=(0,1/4,1/4)  3=(1/4,0,1/4)

PT. GM  AUGMENTERS  1/4-X,1/4-Y,Z}  X,1/4-Y,1/4-Z}  -X,1/4+Y,1/4+Z}  Z,X,Y}  Y,X,Z
REP.  D AUGMENTERS                                      REP.  D AUGMENTERS
GM1+  1  (+)}  E}  E}  E}  E}  E                         GM2+  1  (+)}  E}  E}  E}  E}  (-)E
GM3+  2  (+)}  E}  E}  E}  5}  2                         GM4+  3  (+)}  2}  3}  3}  4}  (-)5
GM5+  3  (+)}  2}  3}  3}  4}  5                         GM1-  1  (+)}  E}  E}  (-)E}  E}  (-)E
GM2-  1  (+)}  E}  E}  (-)E}  E}  E                      GM3-  2  (+)}  E}  E}  (-)E}  5}  2
GM4-  3  (+)}  2}  3}  (-)3}  4}  5                      GM5-  3  (+)}  2}  3}  (-)3}  4}  (-)5
GM6+  2  (-)}  (+1)4}  (-1)3}  (-1)3}  6}  (-)7          GM7+  2  (-)}  (+1)4}  (-1)3}  (-1)3}  6}  7
GM8+  4  (-)}  2}  3}  3}  4}  5                         GM6-  2  (-)}  (+1)4}  (-1)3}  (+1)3}  6}  7
GM7-  2  (-)}  (+1)4}  (-1)3}  (+1)3}  6}  (-)7          GM8-  4  (-)}  2}  3}  (-)3}  4}  5
```

```
OPERATORS                              GM 1+  2+  3+  4+  5+  1-  2-  3-  4-  5-  6+  7+  8+  6-  7-  8-
1 ...................................     1   1   2   3   3   1   1   2   3   3   2   2   4   2   2   4
49 ..................................     1   1   2   3   3   1   1   2   3   3  -2  -2  -4  -2  -2  -4
2,2 3,3 4,1 .........................     1   1   2  -1  -1   1   1   2  -1  -1   0   0   0   0   0   0
26,2 27,3 28,1 ......................     1   1   2  -1  -1  -1  -1  -2   1   1   0   0   0   0   0   0
73 ..................................     1   1   2   3   3  -1  -1  -2  -3  -3  -2  -2  -4   2   2   4
6,2 7,3 9 10,2 53 56,1 59,3 60,1 .....    1   1  -1   0   0   1   1  -1   0   0   1   1  -1   1   1  -1
29 32,1 35,3 36,1 78,2 79,3 81 82,2 ..    1   1  -1   0   0  -1  -1   1   0   0  -1  -1   1   1   1  -1
37 40,1 41 42,2 45 47,3 .............     1  -1   0  -1   1  -1   1   0   1  -1   0   0   0   0   0   0
39,3 44,1 46,2 86,2 91,3 96,1 .......     1  -1   0   1  -1  -1   1   0  -1   1  -A   A   0  -A  -A   0
15,3 20,1 22,2 62,2 67,3 72,1 .......     1  -1   0   1  -1   1  -1   0   1  -1  -A   A   0  -A   A   0
13 16,1 17 18,2 21 23,3 .............     1  -1   0  -1   1   1  -1   0  -1   1   0   0   0   0   0   0
```

```
PT. X  AUGMENTERS  1/4-X,1/4-Y,Z}  X,1/4-Y,1/4-Z}  -X,1/4+Y,1/4+Z}  Z,Y,X
X1  2  (+)}  4}  4}  (-I)3}  E                 X2  2  (+)}  4}  4}  (-I)3}  (-)E
X3  2  (+)}  4}  (-)4}  (-I)3}  2              X4  2  (+)}  4}  (-)4}  (-I)3}  (-)2
X5  4  (-)}  (-)34}  33}  (-I)32}  5
```

```
OPERATORS                              X 1   2   3   4   5
1 ...................................    2   2   2   2   4
49 ..................................    2   2   2   2  -4
2,2 4,1 22,2 24,1 25 26,2 27,3 28,1
46,2 48,1 ...........................    0   0   0   0   0
3,3 ................................     2   2  -2  -2   0
45 47,3 ............................     2  -2   0   0   0
23,3 ...............................     0   0  -2   2   0
21 .................................     0   0   2  -2   0
```
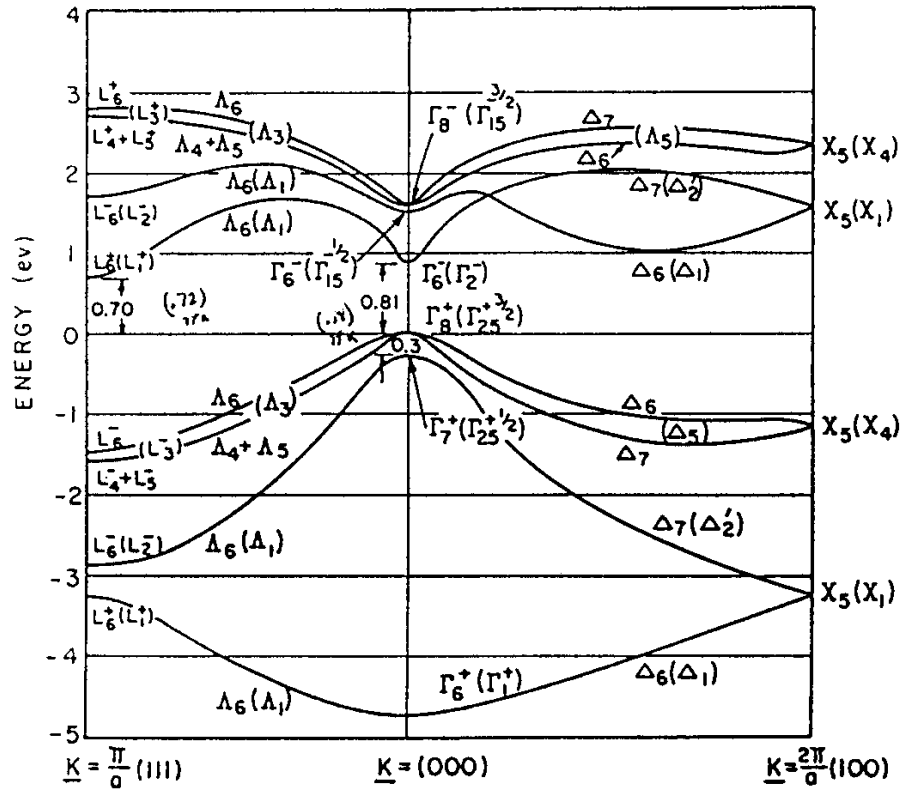
Figure 16.9: Energy band structure for germanium. Note that the bands stick together at the X point.

Table 16.8: Plane wave basis functions for the group of the wave vector for the X-point $[\frac{2\pi}{a}(100)]$ for the non-symmorphic diamond structure.

Representation	Function
X_1	$x_{11} = \cos \frac{2\pi}{a} x$
	$x_{12} = \sin \frac{2\pi}{a} x$
X_2	$x_{21} = \cos \frac{2\pi}{a} x [\cos \frac{4\pi}{a} y - \cos \frac{4\pi}{a} z]$
	$x_{22} = \sin \frac{2\pi}{a} x [\cos \frac{4\pi}{a} y - \cos \frac{4\pi}{a} z]$
X_3	$x_{31} = \sin \frac{4\pi}{a}(y+z)[\cos \frac{2\pi}{a} x + \sin \frac{2\pi}{a} x]$
	$x_{32} = \sin \frac{4\pi}{a}(y-z)[\cos \frac{2\pi}{a} x - \sin \frac{2\pi}{a} x]$
X_4	$x_{41} = \sin \frac{4\pi}{a}(y-z)[\cos \frac{2\pi}{a} x + \sin \frac{2\pi}{a} x]$
	$x_{42} = \sin \frac{4\pi}{a}(y+z)[\cos \frac{2\pi}{a} x - \sin \frac{2\pi}{a} x]$

at high symmetry points where "essential" degeneracies occur. For the case of essential degeneracies, the energy bands $E(\vec{k})$ come into the Brillouin zone with zero slope. For the X point in the diamond structure, the $E(\vec{k})$ dispersion relations with X_1 and X_2 symmetries in general have a non-zero slope, but the slopes are equal and opposite for the two levels (X_1 and X_2) that stick together. The physical reason for this behavior is that the x-ray structure factor for the Bragg reflection associated with the X point in the Brillouin zone for the diamond structure vanishes and thus no energy discontinuity in $E(\vec{k})$ is expected, nor is it observed upon small variation of k_x relative to the X point.

Explicitly the structure factor at the X point for the diamond structure is:

$$\sum_i e^{i\vec{K}_X \cdot \vec{r}_i} = 1 + e^{i\frac{4\pi}{a}(100) \cdot \frac{a}{4}(111)} = 1 - 1 \equiv 0 \qquad (16.33)$$

where the sum is over the two inequivalent atom sites in the unit cell. The vanishing of this structure factor for the reciprocal lattice vector $\vec{K}_X = (4\pi/a)(100)$ associated with the X point implies that there is no Fourier component of the periodic potential to split the degeneracy caused by having two atoms per unit cell and thus the energy bands at the X-point stick together. In fact, the structure factor in diamond vanishes for all points on the square face of the fcc Brillouin zone (see Fig. 16.8(b)), and we have energy bands sticking together across the

entire square face.

For the L-point in the Brillouin zone, the levels do not stick together because the structure factor at the L-point does not vanish:

$$\sum_i e^{i\vec{K}_L \cdot \vec{r}_i} = 1 + e^{i\frac{2\pi}{a}(111)\cdot\frac{a}{4}(111)} = 1 - i \neq 0. \qquad (16.34)$$

Thus for the non-symmorphic diamond structure, some high symmetry points behave normally (such as the L point), while for other points (such as the X point) the energy bands stick together.

To show how the energy bands at the X-point stick together, consider the operations of the inversion symmetry operator $\{i|\vec{\tau}\}$ on the basis functions for the X-point listed in Table 16.8. Similar results can be obtained by considering other operations in the point group O_h (and not in T_d), that is by considering symmetry operations involving the translation operation $\vec{\tau} = (a/4)(111)$. treat the effect of $\{i|\tau\}$ on the various functions of (x, y, z) in Table 16.8, consider first the action of $\{i|\vec{\tau}\}$ on the coordinates:

$$\{i|\vec{\tau}\} \begin{pmatrix} x \\ y \\ z \end{pmatrix} = \begin{pmatrix} -x + (a/4) \\ -y + (a/4) \\ -z + (a/4) \end{pmatrix}. \qquad (16.35)$$

Then using the trigonometric identity:

$$\begin{aligned}
\cos(\alpha + \beta) &= \cos\alpha\cos\beta - \sin\alpha\sin\beta \\
\sin(\alpha + \beta) &= \sin\alpha\cos\beta + \cos\alpha\sin\beta
\end{aligned} \qquad (16.36)$$

we obtain for the effect of $\{i|\vec{\tau}\}$ on the various trigonometric functions in Table 16.8:

$$\begin{aligned}
\{i|\vec{\tau}\}\cos(\tfrac{2\pi}{a}x) &= \cos(\tfrac{2\pi}{a}(-x) + \tfrac{\pi}{2}) = \sin(\tfrac{2\pi}{a}x) \\
\{i|\vec{\tau}\}\sin(\tfrac{2\pi}{a}x) &= \sin(\tfrac{2\pi}{a}(-x) + \tfrac{\pi}{2}) = \cos(\tfrac{2\pi}{a}x) \\
\{i|\vec{\tau}\}\cos(\tfrac{4\pi}{a}y) &= \cos(\tfrac{4\pi}{a}(-y) + \pi) = -\cos(\tfrac{4\pi}{a}y) \\
\{i|\vec{\tau}\}\sin(\tfrac{4\pi}{a}y) &= \sin(\tfrac{4\pi}{a}(-y) + \pi) = \sin(\tfrac{4\pi}{a}y) \\
\{i|\vec{\tau}\}\sin(\tfrac{4\pi}{a}(y+z)) &= \sin(\tfrac{4\pi}{a}(-y-z) + 2\pi) = -\sin(\tfrac{4\pi}{a}(y+z)) \\
\{i|\vec{\tau}\}\sin(\tfrac{4\pi}{a}(y-z)) &= \sin(\tfrac{4\pi}{a}(-y+z)) = -\sin(\tfrac{4\pi}{a}(y-z)).
\end{aligned} \qquad (16.37)$$

Thus we obtain

$$\{i|\vec{\tau}\}\begin{pmatrix} x_{11} \\ x_{12} \end{pmatrix} = \begin{pmatrix} \cos(\frac{2\pi}{a}(-x) + \frac{\pi}{2}) \\ \sin(\frac{2\pi}{a}(-x) + \frac{\pi}{2}) \end{pmatrix} = \begin{pmatrix} \sin(\frac{2\pi}{a}x) \\ \cos(\frac{2\pi}{a}x) \end{pmatrix} = \begin{pmatrix} x_{12} \\ x_{11} \end{pmatrix}$$

(16.38)

and we see that the effect of $\{i|\vec{\tau}\}$ is to interchange $x_{11} \leftrightarrow x_{12}$. Similarly the effect of $\{i|\vec{\tau}\}$ on x_{12} and x_{22} is

$$\{i|\vec{\tau}\}\begin{pmatrix} x_{21} \\ x_{22} \end{pmatrix} = \begin{pmatrix} -\sin(\frac{2\pi}{a}(x))[\cos(\frac{4\pi}{a}y) - \cos(\frac{4\pi}{a}z)] \\ -\cos(\frac{2\pi}{a}(x))[\cos(\frac{4\pi}{a}y) - \cos(\frac{4\pi}{a}z)] \end{pmatrix} = \begin{pmatrix} -x_{22} \\ -x_{21} \end{pmatrix}$$

(16.39)

so that $\{i|\vec{\tau}\}$ in this case interchanges the functions and reverses their signs $x_{21} \leftrightarrow -x_{22}$. Correspondingly, the other symmetry operations involving translations also interchange the basis functions for the X_1 and X_2 irreducible representations. The physical meaning of this phenomenon is that the energy bands $E_{X_1}(\vec{k})$ and $E_{X_2}(\vec{k})$ go right through the X point without interruption in the extended zone scheme, except for an interchange in the symmetry designations of their basis functions in crossing the X point, consistent with the $E(\vec{k})$ diagram for Ge where bands with X_1 symmetry are seen.

In contrast, the effect of $\{i|\vec{\tau}\}$ on the x_{31} and x_{32} basis functions:

$$\{i|\vec{\tau}\}\begin{pmatrix} x_{31} \\ x_{32} \end{pmatrix} = \begin{pmatrix} -\sin(\frac{4\pi}{a}(y+z))[\sin(\frac{2\pi}{a}x) + \cos(\frac{2\pi}{a}x)] \\ -\sin(\frac{4\pi}{a}(y-z))[\sin(\frac{2\pi}{a}x) - \cos(\frac{2\pi}{a}x)] \end{pmatrix} = \begin{pmatrix} -x_{31} \\ x_{32} \end{pmatrix}$$

(16.40)

does not interchange x_{31} and x_{32}. Thus the X_3 level comes into the X point with zero slope. The behavior for the X_4 levels is similar

$$\{i|\vec{\tau}\}\begin{pmatrix} x_{41} \\ x_{42} \end{pmatrix} = \begin{pmatrix} -\sin(\frac{4\pi}{a}(y-z))[\sin(\frac{2\pi}{a}x) + \cos(\frac{2\pi}{a}x)] \\ -\sin(\frac{4\pi}{a}(y+z))[\sin(\frac{2\pi}{a}x) - \cos(\frac{2\pi}{a}x)] \end{pmatrix} = \begin{pmatrix} -x_{41} \\ x_{42} \end{pmatrix}$$

(16.41)

so that the X_3 and X_4 levels behave like doubly degenerate levels. Equations 16.38 – 16.41 show that the character $\chi(\{i|\vec{\tau}\})$ vanishes at the X point for the X_1, X_2, X_3 and X_4 levels, consistent with the character table for the diamond X-point given in Table 16.7. These results also explain the behavior of the energy bands for Ge at the X-point shown in Fig. 16.9. The non-degenerate Δ_1 and $\Delta_{2'}$ energy bands going into the X point stick together and interchange their symmetry designations

on crossing the X point, while the doubly degenerate Δ_5 levels go into a doubly-degenerate X_4 level with zero slope at the Brillouin zone boundary. The doubly-degenerate X_5 levels are split by the spin-orbit interaction into Δ_6 and Δ_7 levels, and when spin-orbit interaction is taken into account all the levels at the X-point have X_5 symmetry and show sticking-together properties.

16.6   Selected Problems

1. (a) For the simple cubic lattice find the proper linear combinations of plane waves for the twelve (110) plane wave states at $\vec{k} = 0$ which transform as irreducible representations of the O_h point group.

   (b) As we move away from $\vec{k} = 0$, find the plane wave eigenfunctions which transform according to Δ_1 and Δ_5 and are compatible with the eigenfunctions for the Γ_{15}^- level at $k = 0$.

   (c) Repeat part (b) for the case of $\Gamma_{12}^- \to \Delta_1 + \Delta_2$.

2. (a) Considering the empty lattice model for the 2D triangular lattice (space group # 17 $p6mm$), find the symmetries of the two lowest energy states at the Γ point $(k = 0)$.

   (b) Find the linear combination of plane waves that transform according to the irreducible representations in part (a).

   (c) Repeat (a) and (b) for the lowest energy state at the M point shown in the diagram below.
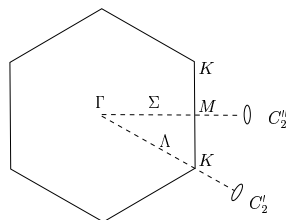
3. Using the empty lattice, find the energy eigenvalues, degeneracies and symmetry types for the two electronic levels of lowest energy for the fcc lattice at the L point.

(a) Find the appropriate linear combinations of plane waves which provide basis functions for the two lowest L-point electronic states for the fcc lattice.

(b) Which states of the lower and upper energy levels in (a) are coupled by optical dipole transitions?

(c) Repeat parts (a, b, c) for the two lowest X point energy levels for the fcc empty lattice (i.e., the X_1, $X_{4'}$ and X_1, X_3, $X_{5'}$ levels).

(d) Compare your results to those for the simple cubic lattice.

Chapter 17

Energy Band Models Based on Symmetry

Chapter 16 addressed the general application of space groups to the one-electron energy bands in a periodic solid. This chapter deals with some specific models that make extensive use of the crystal symmetry.

17.1   Introduction

Just from the symmetry properties of a particular crystal, a good deal can be deduced concerning the energy bands of a solid. Our study of the group of the wave vector illustrates that questions such as degeneracy and connectivity are answered by group theory alone. It is not necessary to solve Schrödinger's equations explicitly to find the **degeneracies and connectivity** relations for $E_n(\vec{k})$.

   There are two interpolation or extrapolation techniques for energy band dispersion relations that are based on symmetry and provide the form of $E_n(\vec{k})$ without actual solution of Schrödinger's equation. These methods are useful as interpolation schemes for experimental data or for band calculations that are carried out with great care at a few high symmetry points in the Brillouin zone. These methods are called $\vec{k} \cdot \vec{p}$ perturbation theory [extrapolation or Taylor's series expansion of $E(\vec{k})$] and the Slater–Koster Fourier expansion [interpolation or Fourier series expansion of $E(\vec{k})$]. Both of these methods are discussed in this

Chapter.

The particular example that is used here to illustrate $\vec{k} \cdot \vec{p}$ perturbation theory is the electronic structure for a material with simple cubic symmetry. This discussion is readily extended to the electronic structure of semiconductors that crystallize in the diamond structure (e.g., silicon). The valence and conduction bands for these semiconductors are formed from hybridized s- and p-bands. For the diamond structure, the s- and p-functions in the O_h point group (at $\vec{k} = 0$) transform as the Γ_1^+ and Γ_{15}^- irreducible representations, respectively. In the diamond structure there are 2 atoms/unit cell and $\chi_{\text{atom sites}}$ at $\vec{k} = 0$ transforms as $\Gamma_1^+ + \Gamma_2^-$ or $(A_{1g} + A_{2u})$. Thus we must consider 8 bands in discussing the valence and conduction bands formed by s- and p-bands. These bands have symmetries

$$
\begin{aligned}
\chi_{\text{a.s.}} \otimes \chi_{\text{s-functions}} \quad & (\Gamma_1^+ + \Gamma_2^-) \otimes \Gamma_1^+ = \Gamma_1^+ + \Gamma_2^- \\
\chi_{\text{a.s.}} \otimes \chi_{\text{p-functions}} \quad & (\Gamma_1^+ + \Gamma_2^-) \otimes \Gamma_{15}^- = \Gamma_{15}^- + \Gamma_{25}^+
\end{aligned}
\tag{17.1}
$$

We identify the Γ_1^+ and Γ_{25}^+ bands as the bonding s- and p-bands and the Γ_2^- and Γ_{15}^- bands as antibonding s- and p-bands. The reason why the bonding p-band has Γ_{25}^+ symmetry follows from the direct product $\Gamma_2^- \otimes \Gamma_{15}^- = \Gamma_{25}^+$ in Eq. (17.1).

Our discussion starts with a review of $\vec{k} \cdot \vec{p}$ perturbation theory in general. An example of $\vec{k} \cdot \vec{p}$ perturbation theory for a non-degenerate level is then given. This is followed by an example of degenerate second-order $\vec{k} \cdot \vec{p}$ perturbation theory which is appropriate to the p-bonding and antibonding levels in the diamond structure. In all of these cases, group theory tells us which are the non-vanishing matrix elements and which matrix elements are equal to each other.

17.2 $\vec{k} \cdot \vec{p}$ Perturbation Theory

An electron in a periodic potential obeys the one-electron Hamiltonian:

$$
\left[\frac{p^2}{2m} + V(\vec{r}) \right] \psi_{n,\vec{k}}(\vec{r}) = E_n(\vec{k}) \psi_{n,\vec{k}}(\vec{r})
\tag{17.2}
$$

where the eigenfunctions of the Hamiltonian are the Bloch functions

$$
\psi_{n,\vec{k}}(\vec{r}) = e^{i\vec{k} \cdot \vec{r}} u_{n,\vec{k}}(\vec{r})
\tag{17.3}
$$

and n is the band index.

Substitution of $\psi_{n,\vec{k}}(\vec{r})$ into Schrödinger's equation gives an equation for the periodic function $u_{n,\vec{k}}(\vec{r})$

$$\left[\frac{p^2}{2m} + V(\vec{r}) + \frac{\hbar \vec{k} \cdot \vec{p}}{m} + \frac{\hbar^2 k^2}{2m} \right] u_{n,\vec{k}}(\vec{r}) = E_n(\vec{k}) \, u_{n,\vec{k}}(\vec{r}). \qquad (17.4)$$

In the spirit of the $(\vec{k} \cdot \vec{p})$ method we assume that $E_n(\vec{k})$ is known at point $\vec{k} = \vec{k}_0$ either from experimental information or from direct solution of Schrödinger's equation for some model potential $V(\vec{r})$. Assume the band in question has symmetry Γ_i so that the function $u_{n,\vec{k}_0}(\vec{r})$ transforms as the irreducible representation Γ_i. Then we have

$$\mathcal{H}_{\vec{k}_0} u_{n,\vec{k}_0}^{(\Gamma_i)} = \varepsilon_n(\vec{k}_0) \, u_{n,\vec{k}_0}^{(\Gamma_i)} \qquad (17.5)$$

where

$$\mathcal{H}_{\vec{k}_0} = \frac{p^2}{2m} + V(\vec{r}) + \frac{\hbar \vec{k}_0 \cdot \vec{p}}{m} \qquad (17.6)$$

and

$$\varepsilon_n(\vec{k}_0) = E_n(\vec{k}_0) - \frac{\hbar^2 \vec{k}_0^2}{2m}. \qquad (17.7)$$

If $\varepsilon_n(\vec{k}_0)$ and $u_{n,\vec{k}_0}(\vec{r})$ are specified at $\vec{k}_0$, the $\vec{k} \cdot \vec{p}$ method prescribes the development of the periodic $u_{n,\vec{k}_0}(\vec{r})$ functions under variation of $\vec{k}$. At point $\vec{k} = \vec{k}_0 + \vec{\kappa}$, the eigenvalue problem becomes:

$$\begin{aligned}
\mathcal{H}_{\vec{k}_0+\vec{\kappa}} u_{n,\vec{k}_0+\vec{\kappa}}(\vec{r}) &= \left(\mathcal{H}_{\vec{k}_0} + \frac{\hbar \vec{\kappa} \cdot \vec{p}}{m} \right) u_{n,\vec{k}_0+\vec{\kappa}}(\vec{r}) \\
&= \varepsilon_n \left(\vec{k}_0 + \vec{\kappa} \right) u_{n,\vec{k}_0+\vec{\kappa}}(\vec{r}).
\end{aligned} \qquad (17.8)$$

In the spirit of the usual $\vec{k} \cdot \vec{p}$ perturbation theory $\vec{\kappa}$ is small so that the perturbation Hamiltonian is taken as $\mathcal{H}' = \hbar \vec{\kappa} \cdot \vec{p}/m$ and the energy eigenvalue at the displaced $\vec{k}$ vector $\varepsilon_n(\vec{k}_0 + \vec{\kappa})$ is given by Eq. (17.7), and $E_n(\vec{k}_0)$ is given by Eq. (17.2). We will illustrate this method first for a non-degenerate band (a $\Gamma_1^{\pm}$ band for the simple cubic lattice) and then for a degenerate band (a $\Gamma_{15}^{\pm}$ band for the simple cubic lattice).

17.3 $\vec{k} \cdot \vec{p}$ perturbation theory for a non-degenerate $\Gamma_1^{\pm}$ Band–Simple Cubic Lattice

Suppose the energy of the $\Gamma_1^{\pm}$ band at $\vec{k} = 0$ is established by the identification of an optical transition and measurement of its resonant photon energy. The unperturbed wave function at $\vec{k} = 0$ is $u_{n,0}^{\Gamma_1}(\vec{r})$ and its eigenvalue from Eq. (17.7) is $\varepsilon_n^{(\Gamma_1)}(0) = E_n^{(\Gamma_1)}(0)$ since $\vec{k}_0 = 0$. Then

$$\varepsilon_n^{(\Gamma_1)}(\vec{\kappa}) = E_n^{(\Gamma_1)}(0) + \left(u_{n,0}^{\Gamma_1} | \mathcal{H}' | u_{n,0}^{\Gamma_1} \right) + \sum_{n' \neq n} \frac{\left(u_{n,0}^{\Gamma_1} | \mathcal{H}' | u_{n',0}^{\Gamma_i} \right) \left(u_{n',0}^{\Gamma_i} | \mathcal{H}' | u_{n,0}^{\Gamma_1} \right)}{E_n^{\Gamma_1}(0) - E_{n'}^{\Gamma_i}(0)}$$

$$(17.9)$$

where the sum is over states n' which have symmetries Γ_i.

Now $\mathcal{H}' = \hbar \vec{\kappa} \cdot \vec{p}/m$ transforms like a vector since $\mathcal{H}'$ is proportional to the vector $\vec{p}$, which pertains to the electronic system. If we expand the eigenfunctions and eigenvalues of Eq. (17.9) about the Γ point ($\vec{k} = 0$), then $\mathcal{H}'$ transforms according to the irreducible representation Γ_{15}^- in O_h symmetry. In the spirit of $\vec{k} \cdot \vec{p}$ perturbation theory, the vector $\vec{k}_0$ determines the point symmetry group that is used to classify the wave functions and eigenvalues for the perturbation Hamiltonian.

For the $\vec{k} \cdot \vec{p}$ expansion about the Γ point, the linear term in k which arises in 1st order perturbation theory **vanishes** since $\left(u_{n,0}^{\Gamma_1^+} | \mathcal{H}' | u_{n,0}^{\Gamma_1^+} \right)$ transforms according to the direct product $\Gamma_1^+ \otimes \Gamma_{15}^- \otimes \Gamma_1^+ = \Gamma_{15}^-$ which does not contain Γ_1^+. The same result is obtained using arguments relevant to the oddness and evenness of the functions which enter the matrix elements of Eq. (17.9). At other points in the Brillouin zone, the $\vec{k} \cdot \vec{p}$ expansion may contain linear k terms.

Now let us look at the terms $\left(u_{n',0}^{\Gamma_i} | \mathcal{H}' | u_{n,0}^{\Gamma_1^+} \right)$ that arise in 2nd order perturbation theory. The product $\mathcal{H}' u_{n,0}^{\Gamma_1^+}$ transforms as $\Gamma_{15}^- \otimes \Gamma_1^+ = \Gamma_{15}^-$ so that Γ_i must be of Γ_{15}^- symmetry if a non-vanishing matrix is to

result. We thus obtain:

$$\varepsilon_n^{\Gamma_1^+}(\vec{\kappa}) = E_n^{\Gamma_1^+}(0) + \Sigma_{n' \neq n \, (\Gamma_{15}^-)} \frac{\left(u_{n,0}^{\Gamma_1^+}|\mathcal{H}'|u_{n',0}^{\Gamma_{15}^-}\right)\left(u_{n',0}^{\Gamma_{15}^-}|\mathcal{H}'|u_{n,0}^{\Gamma_1^+}\right)}{E_n^{\Gamma_1^+}(0) - E_n^{\Gamma_{15}^-}(0)} + \dots$$

(17.10)

and a corresponding relation is obtained for the non-degenerate Γ_2^- level. Thus we see that by using group theory, our $\vec{k} \cdot \vec{p}$ expansion is greatly simplified, since it is only the Γ_{15}^- levels that couple to the Γ_1^+ level by $\vec{k} \cdot \vec{p}$ perturbation theory in Eq. (17.10). These statements are completely independent of the explicit wave functions which enter the problem, but depend only on the **symmetry**. Further simplifications result from the observation that for cubic symmetry the matrix elements $\left(u_{n,0}^{\Gamma_1^+}|\mathcal{H}'|u_{n',0}^{\Gamma_{15}^-}\right)$ can all be expressed in terms of a single matrix element, if $u_{n',0}^{\Gamma_{15}^-}$ is identified with specific basis functions such as p-functions (denoted by x, y, z for brevity) and $u_{n,0}^{\Gamma_1^+}$ with an s-function (denoted by 1 for brevity). Thus for the O_h group, the selection rules (see §7.5) give

$$(1|p_x|x) = (1|p_y|y) = (1|p_z|z)$$

(17.11)

and all other cross terms of the form $(1|p_x|y)$ vanish. This result that the matrix elements of $\vec{p}$ in O_h symmetry have only one independent matrix element also follows from the discussion in Chapter 11. Combining these results with $\varepsilon_n^{\Gamma_1^+}(\vec{\kappa}) = E_n^{\Gamma_1^+}(\vec{\kappa}) - \frac{\hbar^2 \kappa^2}{2m}$ we get

$$E_n^{\Gamma_1^+}(\vec{\kappa}) = E_n^{\Gamma_1^+}(0) + \frac{\hbar^2 \kappa^2}{2m} + \frac{\hbar^2 \kappa^2}{m^2} \sum_{n' \neq n} \frac{|(1|p_x|x)|^2}{E_n^{\Gamma_1^+}(0) - E_{n'}^{\Gamma_{15}^-}(0)}$$

(17.12)

where the sum is over all states n' with Γ_{15}^- symmetry. A similar expansion formula is applicable to $E_n^{\Gamma_2^-}(\vec{k})$ which corresponds to the conduction antibonding s-band in the diamond structure. Equation 17.12 is sometimes written in the form

$$E_n^{\Gamma_1^+}(\vec{\kappa}) = E_n^{\Gamma_1^+}(0) + \frac{\hbar^2 \kappa^2}{2m_n^*}$$

(17.13)

where the effective mass parameter m_n^* is related to band couplings through the momentum matrix element:

$$\frac{m}{m_n^*} = 1 + \frac{2}{m} \sum_{n' \neq n} \frac{|(1|p_x|x)|^2}{E_n^{\Gamma_1^+}(0) - E_{n'}^{\Gamma_{15}^-}(0)} \tag{17.14}$$

in which the sum over n' is restricted to states with Γ_{15}^- symmetry. Consistent with Eq. (17.12), the effective mass m_n^* is related to the band curvature by the relation

$$\frac{\partial^2 E_n^{\Gamma_1^+}(\kappa)}{\partial \kappa^2} = \frac{\hbar^2}{m_n^*}. \tag{17.15}$$

Thus m_n^* is proportional to the inverse of the band curvature. If the curvature is large, the effective mass is small and conversely, if the bands are "flat" (essentially k-independent), the effective masses are large. Thus the $\vec{k} \cdot \vec{p}$ expansion for a non-degenerate band in a cubic crystal leads to an isotropic parabolic dependence of $E_n(\vec{k})$ on $\vec{k}$ which looks just like the free electron dispersion relation except that m is replaced by m^*.

For the case of a single band with Γ_{15}^- symmetry, the formula for the effective mass [Eq. (17.14)] becomes

$$\frac{m}{m_n^*} = 1 + \frac{2}{m} \frac{|(1|p_x|x)|^2}{\varepsilon_g} \tag{17.16}$$

which is useful for estimating effective masses, provided that we know the magnitude of the matrix element and the band gap ε_g. On the other hand, if m^* and ε_g are known experimentally, then Eq. (17.16) is useful for evaluating $|(1|p_x|x)|^2$. This is, in fact, the most common use of Eq. (17.16). The words **matrix element** or **oscillator strength** typically refer to the momentum matrix element $(u_{n,\vec{k}}|p_x|u_{n',\vec{k}})$ when discussing the optical properties of solids.

The treatment given here for the non-degenerate bands is easily carried over to treating the $\vec{k} \cdot \vec{p}$ expansion about some other high symmetry point in the Brillouin zone. For arbitrary points in the Brillouin zone, the diagonal term arising from 1st order perturbation theory does

not vanish. Also the matrix element $(u_{n,\vec{k}_0}^{\Gamma_i^{\pm}}|p_\alpha|u_{n,\vec{k}_0}^{\Gamma_j^{\mp}})$ need not be the same for each component $\alpha = x, y, z$, and for the general case six independent matrix elements would be expected. For example, along the Δ and Λ axes, the matrix element for momentum $\parallel$ to the high symmetry axis is not equal to the components $\perp$ to the axis, and there are two independent matrix elements along each of the Δ and Λ axes. These two directions are called longitudinal ($\parallel$ to the axis) and transverse ($\perp$ to the axis), and lead to longitudinal and transverse effective mass components away from the Γ point.

17.4 Two Band Model—Degenerate First-Order Perturbation Theory

One of the simplest applications of $\vec{k} \cdot \vec{p}$ perturbation theory is to two-band models for solids. These models are applicable to describe the energy $E(\vec{k})$ about a point $\vec{k}_0$ for one of two bands that are strongly coupled to each other and are weakly coupled to all other bands. The strongly coupled set is called the nearly degenerate set (NDS) and, if need be, the weakly coupled bands can always be treated in perturbation theory after the problem of the strongly interacting bands is solved. Simple extensions of the 2-band model are made to handle 3 strongly coupled bands, such as the valence band of silicon, germanium and related semiconductors or even 4 strongly coupled bands as occur in graphite.

The eigenvalue problem to be solved is

$$\left[\frac{p^2}{2m} + V(\vec{r}) + \frac{\hbar\vec{k}_0 \cdot \vec{p}}{m} + \frac{\hbar\vec{\kappa} \cdot \vec{p}}{m}\right] u_{n,\vec{k}_0+\vec{\kappa}}(\vec{r}) = \varepsilon_n\left(\vec{k}_0 + \vec{\kappa}\right) u_{n,\vec{k}_0+\vec{\kappa}}(\vec{r})$$

$$(17.17)$$

in which $\varepsilon_n(\vec{k}_0)$ is related to the solution of Schrödinger's equation $E_n(\vec{k}_0)$ by Eq. (17.7).

Let $n = i, j$ be the two bands that are nearly degenerate. Using first order degenerate perturbation theory, the secular equation is written

as

$$
\begin{array}{c}
\quad\quad\quad\quad\quad i \quad\quad\quad\quad\quad\quad\quad\quad\quad j \\
\begin{array}{c} i \\ j \end{array}
\left|
\begin{array}{cc}
\langle i|\mathcal{H}_0 + \mathcal{H}'|i\rangle - \varepsilon & \langle i|\mathcal{H}_0 + \mathcal{H}'|j\rangle \\
\langle j|\mathcal{H}_0 + \mathcal{H}'|i\rangle & \langle j|\mathcal{H}_0 + \mathcal{H}'|j\rangle - \varepsilon
\end{array}
\right| = 0
\end{array}
\qquad (17.18)
$$

in which we have explicitly written i and j to label the rows and columns. Equation 17.18 is exact within the 2-band model, i.e., all the coupling occurs between the nearly degenerate set and no coupling is made to bands outside this set. For most cases where the 2-band model is applied (e.g., bismuth, InSb, PbTe), the unperturbed wave functions $u_{n,\vec{k}_0}(\vec{r})$ are invariant under inversion. Then because of the oddness of $\mathcal{H}' = \hbar\vec{\kappa} \cdot \vec{p}/m$, the matrix elements vanish

$$
\langle i|\mathcal{H}'|i\rangle = \langle j|\mathcal{H}'|j\rangle = 0.
\qquad (17.19)
$$

Also since the "band edge" wave functions $u_{n,\vec{k}_0}(\vec{r})$ are constructed to diagonalize the Hamiltonian

$$
\mathcal{H}_0 u_{n,\vec{k}_0}(\vec{r}) = \varepsilon_n(\vec{k}_0) u_{n,\vec{k}_0}(\vec{r})
\qquad (17.20)
$$

there are no off-diagonal matrix elements of $\mathcal{H}_0$ or

$$
\langle i|\mathcal{H}_0|j\rangle = 0 \qquad \text{for } i \neq j.
\qquad (17.21)
$$

We then write

$$
\langle i|\mathcal{H}_0|i\rangle = E_i^0 \ \text{ and } \ \langle j|\mathcal{H}_0|j\rangle = E_j^0
\qquad (17.22)
$$

where for $n = i, j$

$$
E_n^0 = E_n(\vec{k}_0) - \frac{\hbar^2 k_0^2}{2m}.
\qquad (17.23)
$$

In this notation the secular equation can be written as

$$
\left|
\begin{array}{cc}
E_i^0 - \varepsilon & (\hbar/m)\vec{\kappa} \cdot \langle i|\vec{p}|j\rangle \\
(\hbar/m)\vec{\kappa} \cdot \langle j|\vec{p}|i\rangle & E_j^0 - \varepsilon
\end{array}
\right| = 0
\qquad (17.24)
$$

where $\langle i|\vec{p}|j\rangle \neq 0$ for the 2-band model. The secular equation implied by Eq. (17.24) is equivalent to the quadratic equation

$$
\varepsilon^2 - \varepsilon\left[E_i^0 + E_j^0\right] + E_i^0 E_j^0 - \frac{\hbar^2}{m^2}\vec{\kappa} \cdot \langle i|\vec{p}|j\rangle\langle j|\vec{p}|i\rangle \cdot \vec{\kappa} = 0.
\qquad (17.25)
$$
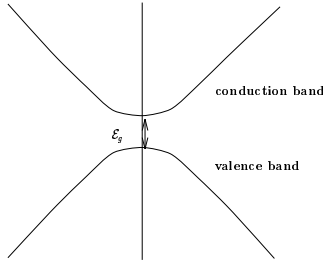
Figure 17.1: Two strongly coupled mirror bands separated by an energy ε_g at the band extremum.

We write the symmetric tensor $\overset{\leftrightarrow}{p^2_{ij}}$ coupling the 2 bands as:

$$\overset{\leftrightarrow}{p^2_{ij}} = \langle i|\vec{p}|j\rangle\langle j|\vec{p}|i\rangle \tag{17.26}$$

where i and j in the matrix elements refer to the band edge wave functions $u_{n,\vec{k}_0}(\vec{r})$ and $n = i, j$. The solution to the quadratic equation [Eq. (17.25)] yields

$$\varepsilon(\vec{\kappa}) = \frac{E_i^0 + E_j^0}{2} \pm \frac{1}{2}\sqrt{(E_i^0 - E_j^0)^2 + \frac{4\hbar^2}{m^2}\vec{\kappa}\cdot\overset{\leftrightarrow}{p^2_{ij}}\cdot\vec{\kappa}}. \tag{17.27}$$

We choose our zero of energy symmetrically such that

$$E_i^0 = \varepsilon_g/2 \qquad\qquad E_j^0 = -\varepsilon_g/2 \tag{17.28}$$

to obtain the two-band model result (see Fig. 17.1):

$$\varepsilon(\vec{\kappa}) = \pm\frac{1}{2}\sqrt{\varepsilon_g^2 + \frac{4\hbar^2}{m^2}\vec{\kappa}\cdot\overset{\leftrightarrow}{p^2_{ij}}\cdot\vec{\kappa}} \tag{17.29}$$

which at $\vec{\kappa} = 0$ reduces properly to $\varepsilon(0) = \pm\frac{1}{2}\varepsilon_g$.

Equation 17.29 gives a **non-parabolic dependence of E upon** $\vec{\kappa}$. For strongly coupled bands, the 2-band model is characterized by its non-parabolicity. In the approximation that there is no coupling to bands outside the non-degenerate set, these bands are strictly **mirror bands**—one band is described by an $E(\vec{\kappa})$ relation given by the $\oplus$ sign; the other by the identical relation with the $\ominus$ sign.

For cubic materials there is only one independent matrix element

$$\overset{\leftrightarrow}{p^2_{ij}} = \langle i|p_\alpha|j\rangle\langle j|p_\alpha|i\rangle \equiv p^2_{ij} \qquad\qquad \alpha = x, y, z \qquad (17.30)$$

and the $\overset{\leftrightarrow}{p^2_{ij}}$ tensor assumes the form

$$\overset{\leftrightarrow}{p^2_{ij}} = \begin{pmatrix} p^2_{ij} & 0 & 0 \\ 0 & p^2_{ij} & 0 \\ 0 & 0 & p^2_{ij} \end{pmatrix}. \qquad (17.31)$$

In applying the two-band model to cubic symmetry, the degeneracy of the Γ^+_{25} valence bands or the Γ^-_{15} conduction bands is ignored. The 2-band model formula then becomes

$$\varepsilon(\vec{\kappa}) = \pm\frac{1}{2}\sqrt{\varepsilon^2_g + \frac{4\hbar^2\kappa^2 p^2_{ij}}{m^2}} \quad \text{where} \ \ \kappa^2 = \kappa^2_x + \kappa^2_y + \kappa^2_z. \qquad (17.32)$$

In this form Eq. (17.32) is called the Kane 2-band model. The generalization of Eq. (17.32) to non-cubic materials is usually called the Lax 2-band model and in the case of bismuth the $\overset{\leftrightarrow}{p^2_{ij}}$ tensor has the following form

$$\overset{\leftrightarrow}{p^2_{ij}} = \begin{pmatrix} p^2_{xx} & 0 & 0 \\ 0 & p^2_{yy} & p^2_{yz} \\ 0 & p^2_{yz} & p^2_{zz} \end{pmatrix} \qquad (17.33)$$

where the x axis is a binary axis $\perp$ to the mirror plane in bismuth (space group $R\overline{3}m$, #166), and the matrix elements of Eq. (17.33) have 4 independent components.

We now show that for small κ we recover the parabolic $\varepsilon(\vec{\kappa})$ relations. For example, for the Kane 2-band model a Taylor's series expansion of Eq. (17.32) yields

$$\varepsilon(\vec{\kappa}) = \pm\frac{1}{2}\sqrt{\varepsilon^2_g + \frac{4\hbar^2\kappa^2 p^2_{ij}}{m^2}} = \pm\frac{\varepsilon_g}{2}\left[1 + \frac{4\hbar^2\kappa^2 p^2_{ij}}{\varepsilon^2_g m^2}\right]^{\frac{1}{2}} \qquad (17.34)$$

which to order κ^4 becomes:

$$\varepsilon(\vec{\kappa}) = \pm\left[\frac{\varepsilon_g}{2} + \frac{\hbar^2\kappa^2 p^2_{ij}}{\varepsilon_g m^2} - \frac{\hbar^4\kappa^4 p^4_{ij}}{\varepsilon^3_g m^4} + \dots\right] \qquad (17.35)$$

where $\varepsilon(\vec{\kappa})$ is given by Eq. (17.7), and the momentum matrix elements are given by

$$p_{ij}^2 = |(1|p_x|x)|^2 \tag{17.36}$$

and the bandgap at the band extrema by $E_n(\vec{k}_0) - E_{n'}(\vec{k}_0) = \pm\varepsilon_g$.

If the power series expansion in Eq. (17.35) is rapidly convergent (either because κ is small or the bands are not that strongly coupled– i.e., p_{ij}^2 is not too large), then the expansion through terms in κ^4 is useful. We note that within the two-band model the square root formula of Eq. (17.34) is exact and is the one that is not restricted to small κ or small p_{ij}^2. It is valid so long as the 2-band model itself is valid.

Some interesting consequences arise from these non-parabolic features of the dispersion relations. For example, the effective mass (or band curvature) is energy or κ-dependent. Consider the expression which follows from Eq. (17.35):

$$E_n(\vec{k}_0 + \vec{\kappa}) \simeq \frac{\hbar^2|\vec{k}_0 + \vec{\kappa}|^2}{2m} \pm \left[\frac{\varepsilon_g}{2} + \frac{\hbar^2\kappa^2 p_{ij}^2}{\varepsilon_g m^2} - \frac{\hbar^4\kappa^4 p_{ij}^4}{\varepsilon_g^3 m^4}\right]. \tag{17.37}$$

Take $\vec{k}_0 = 0$, so that

$$\frac{\partial^2 E}{\partial\kappa^2} = \frac{\hbar^2}{m} \pm \left[\frac{2\hbar^2 p_{ij}^2}{\varepsilon_g m^2} - \frac{12\kappa^2\hbar^4 p_{ij}^4}{\varepsilon_g^3 m^4}\right] \equiv \frac{\hbar^2}{m^*}. \tag{17.38}$$

From this equation we see that the curvature $\partial^2 E/\partial\kappa^2$ is κ dependent. In fact as we more further from the band extrema, the band curvature decreases, the bands become more flat and the effective mass increases. This result is also seen from the definition of m^* [Eq. (17.38)]

$$\frac{m}{m^*} = 1 \pm \left[\frac{2}{m}\frac{p_{ij}^2}{\varepsilon_g} - \frac{12\hbar^2\kappa^2 p_{ij}^4}{\varepsilon_g^3 m^3}\right]. \tag{17.39}$$

Another way to see that the masses become heavier as we move higher into the band (away from $\vec{k}_0$) is to work with the square root formula Eq. (17.34):

$$\varepsilon = \pm\frac{1}{2}\sqrt{\varepsilon_g^2 + \frac{4\hbar^2\kappa^2 p_{ij}^2}{m^2}}. \tag{17.40}$$

Squaring Eq. (17.40) and rewriting this equation we obtain:

$$(2\varepsilon - \varepsilon_g)(2\varepsilon + \varepsilon_g) = \frac{4\hbar^2\kappa^2 p_{ij}^2}{m^2} \tag{17.41}$$

$$(2\varepsilon - \varepsilon_g) = \frac{4\hbar^2\kappa^2 p_{ij}^2}{m^2(2\varepsilon + \varepsilon_g)}. \tag{17.42}$$

For $\kappa = 0$ we have $\varepsilon = \varepsilon_g/2$, and we then write an expression for $\varepsilon(\kappa)$:

$$\varepsilon = \frac{\varepsilon_g}{2} + \frac{2\hbar^2\kappa^2 p_{ij}^2}{m^2(2\varepsilon + \varepsilon_g)} = \frac{\varepsilon_g}{2} + \frac{\hbar^2\kappa^2 p_{ij}^2}{m^2(\varepsilon + \frac{\varepsilon_g}{2})}. \tag{17.43}$$

Therefore we obtain the non-parabolic two-band model relation

$$E(\vec{\kappa}) = \frac{\varepsilon_g}{2} + \frac{\hbar^2\kappa^2}{2m}\left[1 + \frac{2p_{ij}^2}{m(\varepsilon + \frac{\varepsilon_g}{2})}\right] \tag{17.44}$$

which is to be compared with the result for simple non-degenerate bands [Eq. (17.12)]:

$$E_i(\vec{\kappa}) = E_i(0) + \frac{\hbar^2\kappa^2}{2m}\left[1 + \frac{2p_{ij}^2}{m\varepsilon_g}\right]. \tag{17.45}$$

Equation (17.44) shows that for the non-parabolic 2-band model, the effective mass at the band edge is given by

$$\frac{m}{m^*} = \left[1 + \frac{2p_{ij}^2}{m\varepsilon_g}\right]. \tag{17.46}$$

and the effective mass becomes heavier as we move away from $\vec{k}_0$ and as we move up into the band. The magnitude of the k or energy dependence of the effective mass is very important in narrow gap materials such as bismuth. At the band edge, the effective mass parameter for electrons in Bi is $\sim 0.001m_0$ whereas at the Fermi level $m^* \sim 0.008m_0$. The number of electron carriers in Bi is only $10^{17}/\text{cm}^3$. Since the density of states for simple bands has a dependence $\rho(E) \sim m^{*\frac{3}{2}}E^{\frac{1}{2}}$, we can expect a large increase in the density of states with increasing energy in a non-parabolic band. Since bismuth has relatively low symmetry, the tensorial nature of the effective mass tensor must be considered and

the dispersion relations for the coupled bands at the L point in bismuth are generally written as

$$\varepsilon(\vec{\kappa}) = \pm \frac{1}{2} \sqrt{\varepsilon_g^2 + 2\hbar^2 \varepsilon_g \frac{\vec{\kappa} \cdot \overleftrightarrow{\alpha} \cdot \vec{\kappa}}{m}} \qquad (17.47)$$

in which $\overleftrightarrow{\alpha}$ is a reciprocal effective mass tensor.

17.5   Degenerate $\vec{k} \cdot \vec{p}$ Perturbation Theory

For many cubic crystals it is common to have triply-degenerate energy bands at $\vec{k} = 0$. Such bands are of great importance in the transport properties of semiconductors such as silicon, germanium, and the III-V compounds. The analysis of experiments such as cyclotron resonance in the valence band of these semiconductors depends upon degenerate second-order $\vec{k} \cdot \vec{p}$ perturbation theory which is discussed in this section.

Second-order degenerate $\vec{k} \cdot \vec{p}$ perturbation theory becomes a good deal more complicated than the simpler applications of perturbation theory discussed in §17.2–§17.4. Group theory thus provides a valuable tool for the solution of practical problems. As an example, we will consider how the degeneracy is lifted as we move away from $\vec{k} = 0$ for a Γ_{15}^- level; a similar analysis applies for the Γ_{25}^+ level.

Suppose that we set up the secular equation for a Γ_{15}^- level using degenerate perturbation theory

$$\begin{array}{c} \begin{array}{ccc} \quad x \quad & \quad y \quad & \quad z \quad \end{array} \\ \begin{array}{c} x \\ y \\ z \end{array} \left| \begin{array}{ccc} (x|\mathcal{H}'|x) - \varepsilon & (x|\mathcal{H}'|y) & (x|\mathcal{H}'|z) \\ (y|\mathcal{H}'|x) & (y|\mathcal{H}'|y) - \varepsilon & (y|\mathcal{H}'|z) \\ (z|\mathcal{H}'|x) & (z|\mathcal{H}'|y) & (z|\mathcal{H}'|z) - \varepsilon \end{array} \right| = 0 \end{array} \qquad (17.48)$$

where the x, y and z symbols denote the (x, y, z) partners of the basis functions in the Γ_{15}^- irreducible representation derived from atomic p-functions and the diagonal matrix elements for $\mathcal{H}'_0$ are set equal to zero at the band extremum, such as the top of the valence band. We notice that since $\mathcal{H}' = \hbar \vec{k} \cdot \vec{p}/m$, then $\mathcal{H}'$ transforms like the Γ_{15}^- irreducible representation and $(\Gamma_{15}^-|\mathcal{H}'|\Gamma_{15}^-) = 0$ since

$$\Gamma_{15}^- \otimes \Gamma_{15}^- = \Gamma_1^+ + \Gamma_{12}^+ + \Gamma_{15}^+ + \Gamma_{25}^+ \qquad (17.49)$$
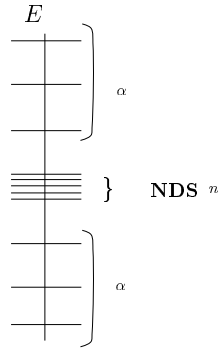
Figure 17.2: NDS ≡ nearly degenerate set. We use Roman letter subscripts for levels within the NDS and Greek indices for levels outside of the NDS.

or more simply since $\mathcal{H}'$ is odd under inversion each matrix element in Eq. (17.48) vanishes because of parity considerations. Since each of the matrix elements of Eq. (17.48) vanishes, the degeneracy of the Γ_{15}^- level is not lifted in first-order degenerate perturbation theory; thus we must use **second-order** degenerate perturbation theory to lift this level degeneracy. We show below the derivation of the form of the matrix elements for the off-diagonal matrix elements in Eq. (17.48 showing that the vanishing $\mathcal{H}'_{mn}$ is replaced by

$$\mathcal{H}'_{mn} \rightarrow \mathcal{H}'_{mn} + \sum_{\alpha} \frac{\mathcal{H}'_{m\alpha} \mathcal{H}'_{\alpha n}}{E_m^{(0)} - E_n^{(0)}}. \tag{17.50}$$

We will see below that the states given in Eq. (17.49 will serve as the intermediate states α which arise in second-order perturbation theory.

In applying second-order degenerate perturbation theory, we assume that we have a degenerate (or nearly degenerate) set of levels–abbreviated NDS. We assume that the states inside the NDS are strongly coupled and those outside the NDS are only weakly coupled to states within the NDS. (See Fig. 17.2)

The wave function for a state is now written in terms of the unperturbed wave functions and the distinction is made as to whether we are dealing with a state inside or outside of the NDS. If we now expand the wavefunction $\psi_{n'}$ in terms of the unperturbed band edge states, we obtain:

$$\psi_{n'} = \sum_{n} a_n \psi_n^{(0)} + \sum_{\alpha} a_\alpha \psi_\alpha^{(0)} \tag{17.51}$$

where $\psi_n^{(0)}$ and $\psi_\alpha^{(0)}$ are, respectively, the unperturbed wavefunctions inside (n) and outside (α) of the nearly degenerate set. Substitution into Schrödinger's equation yields

$$\mathcal{H}\psi_{n'} = E\psi_{n'} = \sum_n a_n(E_n^0 + \mathcal{H}')\psi_n^{(0)} + \sum_\alpha a_\alpha(E_\alpha^{(0)} + \mathcal{H}')\psi_\alpha^{(0)}. \quad (17.52)$$

We multiply the left hand side of Eq. (17.52) by $\psi_{m_0}^{(0)*}$ and integrate over all space, making use of the orthogonality theorem $\int \psi_m^{(0)*}\psi_n^{(0)}\vec{dr} = \delta_{mn}$ to obtain the iterative relation between the expansion coefficients (Brillouin-Wigner Perturbation Theory):

$$[E - E_m^{(0)}]a_m = a_m\mathcal{H}'_{mm} + \sum_{n'\neq m} a_{n'}\mathcal{H}'_{mn'} + \sum_\alpha a_\alpha\mathcal{H}'_{m\alpha} \quad (17.53)$$

where the sum over n' denotes coupling to states in the NDS and the sum over α denotes coupling to states outside the NDS. A similar procedure also leads to a similar equation for levels outside the NDS:

$$[E - E_\alpha^{(0)}]a_\alpha = a_\alpha\mathcal{H}'_{\alpha\alpha} + \sum_n a_n\mathcal{H}'_{\alpha n} + \sum_{\beta\neq\alpha} a_\beta\mathcal{H}'_{\alpha\beta}. \quad (17.54)$$

We now substitute Eq. (17.54) for the coefficients a_α outside the NDS in Eq. (17.53) to obtain:

$$
\begin{aligned}
[E - E_m^{(0)}]a_m = \ & a_m\mathcal{H}'_{mm} + \sum_{n'\neq m} a_{n'}\mathcal{H}'_{mn'} \\
& + \sum_\alpha \frac{\mathcal{H}'_{m\alpha}}{E-E_\alpha^{(0)}}\left\{\sum_n a_n\mathcal{H}'_{\alpha n} + a_\alpha\mathcal{H}'_{\alpha\alpha} + \sum_\beta a_\beta\mathcal{H}'_{\alpha\beta}\right\}.
\end{aligned}
$$
$$(17.55)$$

If we neglect terms in Eq. (17.55) which couple states outside the NDS to other states outside the NDS, we obtain:

$$a_m(E_m^{(0)} - E) + \sum_n a_n\mathcal{H}'_{mn} + \sum_n a_n \sum_\alpha \frac{\mathcal{H}'_{m\alpha}\mathcal{H}'_{\alpha n}}{E_m^{(0)} - E_\alpha^{(0)}} = 0 \quad (17.56)$$

in which the first sum is over all n without restriction, and for E in the denominator of the second-order perturbation term in Eq. (17.55) we replace E by $E_m^{(0)}$ in the spirit of perturbation theory. Equation 17.56 then implies the secular equation

$$\sum_{n=1}^n a_n\left[(E_m^{(0)} - E)\delta_{mn} + \mathcal{H}'_{mn} + \sum_\alpha \frac{\mathcal{H}'_{m\alpha}\mathcal{H}'_{\alpha n}}{E_m^{(0)} - E_\alpha^{(0)}}\right] = 0 \quad (17.57)$$

which yields an $n \times n$ secular equation with each matrix element given by

$$\mathcal{H}'_{mn} + \sum_\alpha \frac{\mathcal{H}'_{m\alpha}\mathcal{H}'_{\alpha n}}{E_m^{(0)} - E_\alpha^{(0)}}. \qquad (17.58)$$

In degenerate $\vec{k} \cdot \vec{p}$ perturbation theory we found that $\mathcal{H}'_{mn} = 0$ for a Γ_{15}^- level, and it was for this precise reason that we had to go to degenerate **second** order perturbation theory. In this case, each state in the NDS couples to other states in the NDS only through an intermediate state outside of the NDS.

In second-order degenerate perturbation theory Eq. (17.49) shows us that for a 3-fold Γ_{15}^- level $\vec{k} \cdot \vec{p}$ degenerate perturbation theory will involve only states of $\Gamma_1^+, \Gamma_{12}^+, \Gamma_{15}^+$, or Γ_{25}^+ symmetry as intermediate states. In our discussion of non-degenerate $\vec{k} \cdot \vec{p}$ perturbation theory (see §17.3) we found that there was only one independent matrix element of $\vec{p}$ coupling a Γ_1^+ state to a Γ_{15}^- state. We include below a useful table of matrix elements of $\vec{p}$ between states of different symmetries for Γ point levels in cubic crystals. These matrix elements are found using the basis functions for each of the irreducible representations of O_h given in Table 16.2. Table 17.1 lists the non-vanishing matrix elements appearing in the $\vec{k} \cdot \vec{p}$ perturbation theory for electronic energy bands with cubic O_h symmetry.

For the matrix element A_2 in Table 17.1 we note with the help of Table 13.2 that the pertinent basis functions are $\Gamma_2^- = xyz$ and $\Gamma_{25,x}^+ = yz$. For A_4 we note that the basis function $\Gamma_{25,z}^- = z(x^2 - y^2)$ gives $C_2 \Gamma_{25,z}^- = -\Gamma_{25,z}^-$ where C_2 is a rotation of π around the (011) axis. For A_5 we use as basis functions: $\Gamma_{15,x}^- = x$ and $\Gamma_{15,x}^+ = yz(z^2 - y^2)$ which is odd under the interchange $y \leftrightarrow z$. For A_6 we use as basis functions: $\Gamma_{25,x}^+ = yz$ and $\Gamma_{15,x}^- = x$, where $A_6 = (\Gamma_{15,x}^\pm |p_y| \Gamma_{25,z}^\mp)$. For A_7 we use as basis functions: $\Gamma_{25,x}^+ = yz$; $\Gamma_{25,x}^- = x(y^2 - z^2)$; $\Gamma_{25,z}^- = z(x^2 - y^2)$.

Let us make a few comments on this table of matrix elements for $\mathcal{H}'$. Since $\mathcal{H}'$ is odd, only states of opposite parity are coupled. For each of the 7 symmetry type couplings given in the table, there is only one independent matrix element. Likewise the coupling between the Γ_{12}^+ and Γ_{15}^- representations involve $2 \times 3 \times 3 = 18$ matrix elements but there is only one **independent** matrix element:

$$(x|p_x|f_1) = (x|p_x|f_2) = \omega(y|p_y|f_1) = \omega^2(y|p_y|f_2) = \omega^2(z|p_z|f_1) = \omega(z|p_z|f_2)$$

Table 17.1: Matrix Element Table for $\mathcal{H}' = \hbar \vec{k} \cdot \vec{p}/m$ in cubic O_h Symmetry

$(\Gamma_1^\pm \lvert \mathcal{H}' \rvert \Gamma_{15,\alpha}^\mp) = A_1 \frac{\hbar}{m} k_\alpha$	$A_1 = (\Gamma_1^\pm \lvert p_x \rvert \Gamma_{15,x}^\mp)$

$(\Gamma_2^\pm \lvert \mathcal{H}' \rvert \Gamma_{25,\alpha}^\mp) = A_2 \frac{\hbar}{m} k_\alpha$	$A_2 = (\Gamma_2^\pm \lvert p_x \rvert \Gamma_{25,x}^\mp)$

$$\left. \begin{aligned} (\Gamma_{12,1}^\pm \lvert \mathcal{H}' \rvert \Gamma_{15,x}^\mp) &= A_3 \frac{\hbar}{m} k_x \\ (\Gamma_{12,1}^\pm \lvert \mathcal{H}' \rvert \Gamma_{15,y}^\mp) &= A_3 \frac{\hbar}{m} k_y \omega^2 \\ (\Gamma_{12,1}^\pm \lvert \mathcal{H}' \rvert \Gamma_{15,z}^\mp) &= A_3 \frac{\hbar}{m} k_z \omega \end{aligned} \right\}$$

$A_3 = (f_1^\pm \lvert p_x \rvert \Gamma_{15,x}^\mp)$
$f_1 = f_2^* = x^2 + \omega y^2 + \omega^2 z^2$

$$\begin{aligned} (\Gamma_{12,2}^\pm \lvert \mathcal{H}' \rvert \Gamma_{15,x}^\mp) &= A_3^* \frac{\hbar}{m} k_x \\ (\Gamma_{12,2}^\pm \lvert \mathcal{H}' \rvert \Gamma_{15,y}^\mp) &= A_3^* \frac{\hbar}{m} k_y \omega \\ (\Gamma_{12,2}^\pm \lvert \mathcal{H}' \rvert \Gamma_{15,z}^\mp) &= A_3^* \frac{\hbar}{m} k_z \omega^2 \end{aligned}$$

$\omega = \exp(2\pi i/3)$

$$\begin{aligned} (\Gamma_{12,1}^\pm \lvert \mathcal{H}' \rvert \Gamma_{25,x}^\mp) &= A_4 \frac{\hbar}{m} k_x \\ (\Gamma_{12,1}^\pm \lvert \mathcal{H}' \rvert \Gamma_{25,y}^\mp) &= A_4 \frac{\hbar}{m} k_y \omega^2 \\ (\Gamma_{12,1}^\pm \lvert \mathcal{H}' \rvert \Gamma_{25,z}^\mp) &= A_4 \frac{\hbar}{m} k_z \omega \\ (\Gamma_{12,2}^\pm \lvert \mathcal{H}' \rvert \Gamma_{25,x}^\mp) &= A_4^* \frac{\hbar}{m} k_x \\ (\Gamma_{12,2}^\pm \lvert \mathcal{H}' \rvert \Gamma_{25,y}^\mp) &= A_4^* \frac{\hbar}{m} k_y \omega \\ (\Gamma_{12,2}^\pm \lvert \mathcal{H}' \rvert \Gamma_{25,z}^\mp) &= A_4^* \frac{\hbar}{m} k_z \omega^2 \end{aligned}$$

$A_4 = (f_1 \lvert p_x \rvert \Gamma_{25,x}^\mp)$
$f_1 = f_2^* = x^2 + \omega y^2 + \omega^2 z^2$

$$\left\{ \begin{aligned} (\Gamma_{15,x}^\pm \lvert \mathcal{H}' \rvert \Gamma_{15,x}^\mp) &= 0 \\ (\Gamma_{15,x}^\pm \lvert \mathcal{H}' \rvert \Gamma_{15,y}^\mp) &= -A_5 \frac{\hbar}{m} k_z \\ (\Gamma_{15,x}^\pm \lvert \mathcal{H}' \rvert \Gamma_{15,z}^\mp) &= A_5 \frac{\hbar}{m} k_y \\ (\Gamma_{15,y}^\pm \lvert \mathcal{H}' \rvert \Gamma_{15,x}^\mp) &= A_5 \frac{\hbar}{m} k_z \\ (\Gamma_{15,y}^\pm \lvert \mathcal{H}' \rvert \Gamma_{15,y}^\mp) &= 0 \\ (\Gamma_{15,y}^\pm \lvert \mathcal{H}' \rvert \Gamma_{15,z}^\mp) &= -A_5 \frac{\hbar}{m} k_x \\ (\Gamma_{15,z}^\pm \lvert \mathcal{H}' \rvert \Gamma_{15,x}^\mp) &= -A_5 \frac{\hbar}{m} k_y \\ (\Gamma_{15,z}^\pm \lvert \mathcal{H}' \rvert \Gamma_{15,y}^\mp) &= A_5 \frac{\hbar}{m} k_x \\ (\Gamma_{15,z}^\pm \lvert \mathcal{H}' \rvert \Gamma_{15,z}^\mp) &= 0 \end{aligned} \right.$$

$A_5 = (\Gamma_{15,y}^\pm \lvert p_x \rvert \Gamma_{15,z}^\mp)$

$$\left\{ \begin{aligned} (\Gamma_{15,x}^\pm \lvert \mathcal{H}' \rvert \Gamma_{25,x}^\mp) &= 0 \\ (\Gamma_{15,x}^\pm \lvert \mathcal{H}' \rvert \Gamma_{25,y}^\mp) &= A_6 \frac{\hbar}{m} k_z \\ (\Gamma_{15,x}^\pm \lvert \mathcal{H}' \rvert \Gamma_{25,z}^\mp) &= A_6 \frac{\hbar}{m} k_y \\ (\Gamma_{15,y}^\pm \lvert \mathcal{H}' \rvert \Gamma_{25,x}^\mp) &= A_6 \frac{\hbar}{m} k_z \\ (\Gamma_{15,y}^\pm \lvert \mathcal{H}' \rvert \Gamma_{25,y}^\mp) &= 0 \\ (\Gamma_{15,y}^\pm \lvert \mathcal{H}' \rvert \Gamma_{25,z}^\mp) &= A_6 \frac{\hbar}{m} k_x \\ (\Gamma_{15,z}^\pm \lvert \mathcal{H}' \rvert \Gamma_{25,x}^\mp) &= A_6 \frac{\hbar}{m} k_y \\ (\Gamma_{15,z}^\pm \lvert \mathcal{H}' \rvert \Gamma_{25,y}^\mp) &= A_6 \frac{\hbar}{m} k_x \\ (\Gamma_{15,z}^\pm \lvert \mathcal{H}' \rvert \Gamma_{25,z}^\mp) &= 0 \end{aligned} \right.$$

$A_6 = (\Gamma_{15,x}^\pm \lvert p_y \rvert \Gamma_{25,z}^\mp)$

$$\left\{ \begin{aligned} (\Gamma_{25,x}^\pm \lvert \mathcal{H}' \rvert \Gamma_{25,x}^\mp) &= 0 \\ (\Gamma_{25,x}^\pm \lvert \mathcal{H}' \rvert \Gamma_{25,y}^\mp) &= -A_7 \frac{\hbar}{m} k_z \\ (\Gamma_{25,x}^\pm \lvert \mathcal{H}' \rvert \Gamma_{25,z}^\mp) &= A_7 \frac{\hbar}{m} k_y \\ (\Gamma_{25,y}^\pm \lvert \mathcal{H}' \rvert \Gamma_{25,x}^\mp) &= A_7 \frac{\hbar}{m} k_z \\ (\Gamma_{25,y}^\pm \lvert \mathcal{H}' \rvert \Gamma_{25,y}^\mp) &= 0 \\ (\Gamma_{25,y}^\pm \lvert \mathcal{H}' \rvert \Gamma_{25,z}^\mp) &= -A_7 \frac{\hbar}{m} k_x \\ (\Gamma_{25,z}^\pm \lvert \mathcal{H}' \rvert \Gamma_{25,x}^\mp) &= -A_7 \frac{\hbar}{m} k_y \\ (\Gamma_{25,z}^\pm \lvert \mathcal{H}' \rvert \Gamma_{25,y}^\mp) &= A_7 \frac{\hbar}{m} k_x \\ (\Gamma_{25,z}^\pm \lvert \mathcal{H}' \rvert \Gamma_{25,z}^\mp) &= 0 \end{aligned} \right.$$

$A_7 = (\Gamma_{25,x}^\pm \lvert p_y \rvert \Gamma_{25,z}^\mp)$

$+$ denotes even and $-$ denotes odd states under inversion.

and all others vanish. Here we write

$$\left. \begin{array}{l} f_1 = x^2 + \omega y^2 + \omega^2 z^2 \\ f_2 = x^2 + \omega^2 y^2 + \omega z^2 \end{array} \right\} \tag{17.59}$$

as the basis functions for the Γ_{12}^+ representation. For Γ_{25}^+ symmetry we can take our basis functions as

$$\left\{ \begin{array}{l} yz \\ zx \\ xy \end{array} \right. \quad \text{which in the table are denoted by} \quad \left\{ \begin{array}{l} (\Gamma_{25,x}^+) \\ (\Gamma_{25,y}^+) \\ (\Gamma_{25,z}^+) \end{array} \right.$$

The three Γ_{25}^+ basis functions are derived from 3 of the 5 atomic d functions, the other two being Γ_{12}^+ functions. Using these results for the matrix elements, the secular equation Eq. (17.48) can be written as a function of k_x, k_y and k_z to yield the dispersion relations for the degenerate Γ_{15}^- bands as we move away from the Γ point $k = 0$ in the Brillouin zone.

Since $\Gamma_{15}^- \otimes \Gamma_{15}^- = \Gamma_1^+ + \Gamma_{12}^+ + \Gamma_{15}^+ + \Gamma_{25}^+$, and from Eq. (17.57), the secular equation [Eq. (**??**)] for the Γ_{15}^- levels involves the following sums:

$$
\begin{aligned}
F &= \frac{\hbar^2}{m^2} \sum_{\Gamma_1^+(n')} \frac{|(x|p_x|1)|^2}{E_n^{\Gamma_{15}^-}(0) - E_{n'}^{\Gamma_1^+}(0)} \\
G &= \frac{\hbar^2}{m^2} \sum_{\Gamma_{12}^+(n')} \frac{|(x|p_x|f_1)|^2}{E_n^{\Gamma_{15}^-}(0) - E_{n'}^{\Gamma_{12}^+}(0)} \\
H_1 &= \frac{\hbar^2}{m^2} \sum_{\Gamma_{25}^+} \frac{|(x|p_y|xy)|^2}{E_n^{\Gamma_{15}^-}(0) - E_n^{\Gamma_{25}^+}(0)} \\
H_2 &= \frac{\hbar^2}{m^2} \sum_{\Gamma_{15}^+} \frac{|(x|p_y|xy(x^2 - y^2))|^2}{E_n^{\Gamma_{15}^-}(0) - E_n^{\Gamma_{15}^+}(0)}.
\end{aligned} \tag{17.60}
$$

We are now ready to solve the secular equation [Eq. (**??**)] using Eq. (17.57 to include the various terms which occur in second-order degenerate perturbation theory. Let us consider the diagonal entries first, as for example the xx entry. We can go from an initial $\Gamma_{15,x}^-$ state to the same final state through an intermediate Γ_1^+ state which brings

down a k_x^2 term through the F term in Eq. (17.60). We can also couple the initial Γ_{15}^- state to itself through an intermediate $\Gamma_{12,1}^+$ or $\Gamma_{12,2}^+$ state, in either case bringing down a k_x^2 term through the G contribution–so far we have $Fk_x^2 + 2Gk_x^2$. We can also go from a $\Gamma_{15,x}^-$ state and back again through a $\Gamma_{25,y}^+$ or $\Gamma_{25,z}^+$ state to give a $(k_y^2+k_z^2)H_1$ contribution and also through a Γ_{15}^+ state to give a $(k_y^2 + k_z^2)H_2$ contribution. Therefore on the diagonal xx entry we get

$$Lk_x^2 + M(k_y^2 + k_z^2) \text{ where } L = F + 2G \text{ and } M = H_1 + H_2. \quad (17.61)$$

From this discussion we obtain the results for other diagonal entries yy and zz, using a cyclic permutation of indices.

Now let us consider an off-diagonal entry such as $(x|\mathcal{H}'|y)$, where we start with an initial $\Gamma_{15,x}^-$ state and go to a final $\Gamma_{15,y}^-$ state. This can be done through either of four intermediate states:

intermediate state Γ_1^+ gives $k_x k_y F$
intermediate state Γ_{12}^+ gives $(\omega^2 + \omega)k_x k_y G = -k_x k_y G$
intermediate state Γ_{15}^+ gives $-k_x k_y H_2$
intermediate state Γ_{25}^+ gives $k_x k_y H_1$

Therefore we get $Nk_x k_y = (F - G + H_1 - H_2)k_x k_y$ for the total xy entry. Using the same procedure we calculate the other four independent entries to the secular equation. Collecting terms we have the final result for the secular equation for the Γ_{15}^- degenerate p-band:

$$0 = \begin{vmatrix} Lk_x^2 + M(k_y^2 + k_z^2) - \varepsilon(k) & Nk_x k_y & Nk_x k_z \\ Nk_x k_y & Lk_y^2 + M(k_z^2 + k_x^2) - \varepsilon(k) & Nk_y k_z \\ Nk_x k_z & Nk_y k_z & Lk_z^2 + M(k_x^2 + k_y^2) - \varepsilon(k) \end{vmatrix}$$
$$(17.62)$$

The secular equation [Eq. (17.62)] is greatly simplified along the high symmetry directions. For a [100] axis, $k_y = k_z = 0$, and $k_x = \kappa$, then Eq. (17.62) reduces to

$$\begin{vmatrix} L\kappa^2 - \varepsilon(\kappa) & 0 & 0 \\ 0 & M\kappa^2 - \varepsilon(\kappa) & 0 \\ 0 & 0 & M\kappa^2 - \varepsilon(\kappa) \end{vmatrix} = 0 \qquad (17.63)$$

which has the roots

$$\varepsilon(\kappa) = L\kappa^2$$
$$\varepsilon(\kappa) = M\kappa^2 \qquad \text{twice.} \tag{17.64}$$

The result in Eq. (17.64) must be consistent with the compatibility relations about the $k = 0$ Γ-point whereby

$$\Gamma_{15}^+ = \Delta_{1'} + \Delta_5 \tag{17.65}$$

in which the $\Delta_{1'}$ level is non-degenerate and the Δ_5 level is doubly degenerate.

Along a Λ [111] axis, $k_x = k_y = k_z = \kappa$ and the general secular equation of Eq. (17.62) simplifies into

$$\begin{vmatrix} (L+2M)\kappa^2 - \varepsilon(\kappa) & N\kappa^2 & N\kappa^2 \\ N\kappa^2 & (L+2M)\kappa^2 - \varepsilon(\kappa) & N\kappa^2 \\ N\kappa^2 & N\kappa^2 & (L+2M)\kappa^2 - \varepsilon(\kappa) \end{vmatrix} = 0 \tag{17.66}$$

which can readily be diagonalized to give

$$\varepsilon(\kappa) = \frac{L + 2M + 2N}{3}\kappa^2 \qquad \text{once } (\Lambda_2 \text{ level})$$
$$\varepsilon(\kappa) = \frac{L + 2M - N}{3}\kappa^2 \qquad \text{twice } (\Lambda_3 \text{ level}) \tag{17.67}$$

where the Λ_2 level is non-degenerate and the Λ_3 level is doubly degenerate.

The secular equation for a general κ point is more difficult to solve, but it can still be done in closed form by solving a cubic equation. In practice, the problem is actually simplified by including the effects of the **electron spin** (see Chapter 19). For each partner of the Γ_{15}^- levels we get a spin up state and a spin down state so that the secular equation is now a (6×6) equation. However, we will see that spin-orbit interaction simplifies the problem somewhat and the secular equation can be solved analytically.

The band parameters L, M and N, which enter the secular equation [Eq. (17.62)], express the strength of the coupling of the Γ_{15}^- levels to the various other levels. In practice, these quantities are determined from

experimental data. The cyclotron resonance experiment carried out along various high symmetry directions provides accurate values for the band curvatures and hence for the quantities L, M and N (Dresselhaus, Kip and Kittel, Phys. Rev. <u>98</u>, 386 (1955)). In the spirit of the $\vec{k} \cdot \vec{p}$ perturbation theory, solution of the secular equation provides the most general form allowed by symmetry for $E(\vec{k})$ about $\vec{k} = 0$. The solution reduces to the proper form along the high symmetry directions, Δ, Λ and Σ. However, group theory cannot provide information about the magnitude of these coefficients. These magnitudes are most easily obtained from experimental data.

The $\vec{k} \cdot \vec{p}$ method has also been used to obtain the energy bands throughout the Brillouin zone for such semiconductors as silicon and germanium (Cardona and Pollack, Phys. Rev. <u>142</u>, 530 (1966)). In the $\vec{k} \cdot \vec{p}$ approach of Cardona and Pollack, 7 other bands outside this "nearly degenerate set" of 8 ($\Gamma_1^+, \Gamma_2^-, \Gamma_{15}^-, \Gamma_{25}^+$) are allowed to couple to these eight bands. The secular equation (a 15×15 determinantal equation in this case) is then constructed in standard first-order perturbation theory.

New features in the problem arise in going from points of lower symmetry to points of higher symmetry. Along the Λ or (111) axis, the $\vec{k} \cdot \vec{p}$ expansion will connect a Λ point to an L point. The $\vec{k} \cdot \vec{p}$ method has been made to work well and has been used for the analysis of many experiments.

17.6 Non-Degenerate $\vec{k} \cdot \vec{p}$ Perturbation Theory at a Δ Point

The momentum operator in the $\vec{k} \cdot \vec{p}$ Hamiltonian transforms as a vector. For the group of the wave vector at a Δ point (C_{4v} point group), the vector transforms as $\Delta_1 + \Delta_5$ for the longitudinal component x and for the transverse components y, z, respectively. The conduction band extrema for Si are located at the six equivalent $(\Delta, 0, 0)$ locations, where Δ is 85% of the distance from Γ to X. This level has Γ_2^- symmetry at $\vec{k} = 0$ and Δ_2' symmetry as we move away from $\vec{k} = 0$ (see the compatibility relations in §13.7).

In first-order perturbation theory we have a non-vanishing contribution along k_x of the form $(\Delta_2'|p_x|\Delta_2')$ since $\Delta_1 \otimes \Delta_2' = \Delta_2'$. Thus, there is in general a linear $\vec{k}$ term for $E(\vec{k})$ in the longitudinal direction. At the band extremum this matrix element however vanishes (not by symmetry but because of the band extremum).

The second-order contributions are as follows. The longitudinal terms $(\Delta_2'|\Delta_1|\Delta_j)$ require that the intermediate state Δ_j transforms as Δ_2' according to the compatibility relations, or else the matrix element vanishes. States with Δ_2' symmetry at a Δ point arise from Γ_{25}^+, Γ_2^- and Γ_{12}^- states at $\vec{k} = 0$. For transverse terms, the matrix element $(\Delta_2'|\Delta_5|\Delta_j)$ requires the intermediate state Δ_j to transform as Δ_5. States with Δ_5 symmetry arise from $\Gamma_{25}^{\pm}$ levels at $\vec{k} = 0$.

Since the basis function for Δ_2' is yz (see character tables in the notes), the vector component $\Delta_{5,y}$ couples to the z component of the intermediate state with symmetry $\Delta_{5,z}$ while the vector component $\Delta_{5,z}$ couples to the y component of the intermediate state with symmetry $\Delta_{5,y}$.

We thus obtain for $E(\vec{k})$ about the band extremum at $\vec{k}_0$ using the matrix element $(\Delta_{2'}|\Delta_{5,y}|\Delta_{5,z})$:

$$E(\vec{k}) = E(\vec{k}_0) + \frac{\hbar^2 k_x^2}{2m_\ell^*} + \frac{\hbar^2(k_y^2 + k_z^2)}{2m_t^*} \qquad (17.68)$$

in agreement with the expression used in all solid state physics courses.

These arguments can be extended to other points in the Brillouin zone, and to 2-band and 3-band models for materials with cubic symmetry. The $\vec{k} \cdot \vec{p}$ perturbation theory can also be extended to crystals with other symmetries.

17.7 Optical Matrix Elements

The Hamiltonian in the presence of electromagnetic fields can be written as

$$\mathcal{H} = \frac{1}{2m}(\vec{p} - \frac{e}{c}\vec{A})^2 + V \qquad (17.69)$$

Then the proper form of the Hamiltonian for an electron in a solid in the presence of an optical field is

$$\mathcal{H} = \frac{(\vec{p} - e/c\vec{A})^2}{2m} + V(\vec{r}) = \frac{p^2}{2m} + V(\vec{r}) - \frac{e}{mc}\vec{A}\cdot\vec{p} + \frac{e^2 A^2}{2mc^2} \quad (17.70)$$

in which $\vec{A}$ is the vector potential due to the optical fields, $V(\vec{r})$ is the periodic potential. Thus, the one-electron Hamiltonian without optical fields is

$$\mathcal{H}_0 = \frac{p^2}{2m} + V(\vec{r}) \quad (17.71)$$

and the optical perturbation terms are

$$\mathcal{H}' = -\frac{e}{mc}\vec{A}\cdot\vec{p} + \frac{e^2 A^2}{2mc^2}. \quad (17.72)$$

The momentum matrix elements $\langle v|\vec{p}|c\rangle$ which determine the strength of optical transitions also govern the magnitudes of the effective mass components. The coupling of the valence and conduction bands through the optical fields depends on the matrix element for the coupling to the electromagnetic field

$$\mathcal{H}' \cong -\frac{e}{mc}\vec{p}\cdot\vec{A}. \quad (17.73)$$

With regard to the spatial dependence of the vector potential we can write

$$\vec{A} = \vec{A}_0 \exp[i(\vec{K}\cdot\vec{r} - \omega t)] \quad (17.74)$$

where for a loss-less medium $K = \tilde{n}\omega/c = 2\pi\tilde{n}/\lambda$ is a slowly varying function of $\vec{r}$ since $2\pi\tilde{n}/\lambda$ is much smaller than typical wave vectors in solids. Here $\tilde{n}$, ω, and λ are respectively the real part of the index of refraction, the optical frequency, and the wavelength of light.

The relation between the momentum matrix element $\langle v|p|c\rangle$ and the effective mass components are discussed in the previous section.

17.8 Fourier Expansion of Energy Bands— Slater–Koster Method

This technique provides the most general form for the energy bands throughout the Brillouin zone which is consistent with the crystal symmetry. Like the $\vec{k}\cdot\vec{p}$ method, it is an approach whereby the energy

bands can be determined from experimental data without recourse to a definite energy band model or to a specific crystal potential. The original work on this method was done by Slater and Koster to provide an interpolation formula for calculating energy bands at high symmetry points in the Brillouin zone (Slater and Koster, Phys. Rev. <u>94</u>, 1498 (1954)) and the method was later applied to silicon and germanium (Phys. Rev. <u>160</u>, 649 (1967)). We will illustrate the method here for a simple cubic lattice (ref. "The Optical Properties of Solids", Proceedings of the International School of Physics, Enrico Fermi course XXXIV, p. 202-8).

Because of the periodicity of the lattice, the energy bands $E_n(\vec{k})$ are periodic in the extended zone

$$E_n(\vec{k} + \vec{K}) = E_n(\vec{k}) \tag{17.75}$$

where $\vec{K}$ is 2π times a reciprocal lattice vector so that $\vec{K} \cdot \vec{R_m} = 2\pi$ integer.

The energy bands $E_n(\vec{k})$ are furthermore continuous across a zone boundary and they approach this boundary with zero slope (giving the electrons zero velocity at a zone boundary). We make use of this periodicity as follows. Suppose that we have a function $V(\vec{r})$ which is periodic in the 3-dimensional lattice. This function can be Fourier expanded in the reciprocal lattice

$$V(\vec{r}) = \sum_{\vec{K}} v(\vec{K}) e^{i\vec{K} \cdot \vec{r}} \tag{17.76}$$

in which the summation is over all reciprocal lattice vectors. In the extended zone scheme, the **energy** $E_n(\vec{k})$ **is periodic** in a 3-dimensional space defined by the reciprocal lattice vectors. Therefore it is possible to Fourier expand $E_n(\vec{k})$ in a space "reciprocal" to the reciprocal lattice, i.e., in the direct lattice, to obtain:

$$E_n(\vec{k}) = \sum_{\vec{d}} \varepsilon_n(\vec{d}) e^{i\vec{k} \cdot \vec{d}} \tag{17.77}$$

where $\vec{d} = \vec{R_m}$ are Bravais lattice vectors and $\varepsilon_n(\vec{d})$ can be interpreted as an overlap integral in the tight binding approximation. Crystal symmetry restricts the number of independent expansion coefficients $\varepsilon_n(\vec{d})$.

Provided that the Fourier series of Eq. (17.77) is rapidly convergent, it is possible to describe $E_n(\vec{k})$ in terms of a small number of expansion parameters $\varepsilon_n(\vec{d})$ which can, in principle, be determined by experiment.

For example, let us consider a non-degenerate, isolated s-band in a simple cubic crystal. Such a band has Γ_1 symmetry and is invariant under the point group operations of the cubic group. The Fourier expansion would then take the form of the tight binding functions:

$$
\begin{aligned}
E_n(\vec{k}) \;=\; & \varepsilon_n(0) + \varepsilon_n(1)\Big[\cos ak_x + \cos ak_y + \cos ak_z\Big] \\
+\; & \varepsilon_n(2)\Big[\cos a(k_y + k_z) + \cos a(k_y - k_z) + \cos a(k_z + k_x) \\
+\; & \cos a(k_z - k_x) + \cos a(k_x + k_y) + \cos a(k_x - k_y)\Big] \\
+\; & \varepsilon_n(3)\Big[\cos a(k_x + k_y + k_z) + \cos a(k_x - k_y - k_z) \\
+\; & \cos a(-k_x + k_y - k_z) + \cos a(-k_x - k_y + k_z)\Big] + \ldots (17.78)
\end{aligned}
$$

where

$$
\begin{aligned}
d = 0 \quad & \text{is the zeroth neighbor at } a(0,0,0) \\
d = 1 \quad & \text{is the nearest neighbor at } a(1,0,0) \\
d = 2 \quad & \text{is the next nearest neighbor at } a(1,1,0) \\
d = 3 \quad & \text{is the next-next nearest neighbor at } a(1,1,1), \text{ etc.}
\end{aligned}
$$

In the tight binding approximation, the expansion coefficients appear as overlap integrals and transfer integrals of various kinds. Thus, the tight binding form is written to satisfy crystal symmetry and is of the Slater–Koster form.

Now for energy bands of practical interest, we will not have isolated non-degenerate bands, but rather coupled bands of some sort. We can express the problem for n coupled bands in terms of an $(n \times n)$ secular equation of the form

$$
|\langle i|\mathcal{H}|j\rangle - E_n(\vec{k})\delta_{ij}| = 0. \tag{17.79}
$$

In Eq. (17.79) the indices i and j denote Bloch wave functions which diagonalize the Hamiltonian

$$\mathcal{H} = \frac{p^2}{2m} + V(\vec{r}) \tag{17.80}$$

and are labeled by the wave vector $\vec{k}$. The matrix elements $\langle i|\mathcal{H}|j\rangle$ thus constitute a $\vec{k}$-dependent matrix. But at each $\vec{k}$ point these matrix elements are invariant under the symmetry operations of the group of the wave vector at $\vec{k}$. The Hamiltonian at $\vec{k} = 0$ has Γ_1^+ symmetry just like its eigenvalues $E_n(\vec{k})$. This matrix is also periodic in the reciprocal lattice in the extended zone scheme and therefore can be Fourier expanded.

The expansion is carried out in terms of a complete set of basis matrices which are taken as angular momentum matrices. For example, a (2×2) Hamiltonian including the electron spin (i.e., the double group representations $\Gamma_6^\pm$ or $\Gamma_7^\pm$ to be discussed in Chapter 19) would be expanded in terms of 4 basis matrices 1, S_x, S_y and S_z, representing the angular momentum matrices for spin $\frac{1}{2}$. A (3×3) Hamiltonian is expanded in terms of the 9 linearly independent basis matrices which span this space, namely, 1, S_x, S_y, S_z, S_x^2, S_y^2, $\{S_z, S_y\}$, $\{S_z, S_x\}$ and $\{S_x, S_y\}$, in which 1 is a (3×3) unit matrix, S_x, S_y, S_z are angular momentum matrices for spin 1, and $\{S_i, S_j\}$ denotes the anti-commutator for matrices S_i and S_j. Under the point group operations of the group of the wave vector, the angular momentum matrices S_i transform as an axial vector–i.e., at $\vec{k} = 0$, S_i transforms as Γ_{15}^+, while the matrix Hamiltonian still is required to be invariant. Therefore, it is necessary to take products of symmetrized combinations of the n basis matrices with appropriate symmetrized combinations of the Fourier expansion functions so that an invariant matrix Hamiltonian results.

The $(n \times n)$ matrix Hamiltonian which is denoted by $D_{\Gamma_1}(\vec{k})$ can be Fourier expanded in terms of these basis function matrices in the form

$$D_{\Gamma_1}(\vec{k}) = \sum_{\vec{d}} \alpha_{d,\Gamma_j} \vec{\mathcal{C}}_{\Gamma_j}(\vec{d}) \cdot \vec{\mathcal{S}}_{\Gamma_j} \tag{17.81}$$

which is a generalization of Eq. (17.77). In Eq. (17.81), $\mathcal{S}_{\Gamma_j}$ denotes a collection of basis matrices which transforms as Γ_j, and these sym-

Table 17.2: Symmetrized products of angular momenta for the cubic group

Order	Representation	Notation	Symmetrized Products
0	Γ_1^+	$\mathcal{S}_{\Gamma_1^+}(0)$	1
1	Γ_{15}^+	$\mathcal{S}_{\Gamma_{15}^+}^x(1)$	S_x
2	Γ_{12}^+	$\mathcal{S}_{\Gamma_{12}^+}^{(1)}(2)$	$S_x^2 + \omega S_y^2 + \omega^2 S_z^2$
	Γ_{25}^+	$\mathcal{S}_{\Gamma_{25}^+}^{(x)}(2)$	$\{S_y, S_z\}$
3	Γ_2^+	$\mathcal{S}_{\Gamma_2^+}(3)$	$S_x S_y S_z + S_x S_z S_y$
	Γ_{15}^+	$\mathcal{S}_{\Gamma_{15}^+}^{(x)}(3)$	S_x^3
	Γ_{25}^+	$\mathcal{S}_{\Gamma_{15}^+}^{(x)}(3)$	$\{S_x, (S_y^2 - S_z^2)\}$

metrized products of angular momentum matrices are given in Table 17.2. The distance $\vec{d}$ denotes the order of the expansion in Eq. (17.81) and corresponds to the distance of neighbors in the Fourier expansion in the tight binding sense. The angular momentum matrices in Table 17.2 are given by:

$$S_x = \begin{pmatrix} 0 & 0 & 0 \\ 0 & 0 & i \\ 0 & -i & 0 \end{pmatrix} \quad S_y = \begin{pmatrix} 0 & 0 & -i \\ 0 & 0 & 0 \\ i & 0 & 0 \end{pmatrix} \quad S_z = \begin{pmatrix} 0 & i & 0 \\ -i & 0 & 0 \\ 0 & 0 & 0 \end{pmatrix}$$
(17.82)

Products of the dimensionless angular momentum matrices S_i are listed in Table 17.2, using an abbreviated notation. For example, $\mathcal{S}_{\Gamma_{15}^+}^{(x)}(1)$ denotes the x component of a 3 component vector S_x, S_y, S_z and all three components would appear in Eq. (17.81). Similarly, $\mathcal{S}_{\Gamma_{12}^+}^{(i)}(2)$ is a 2 component vector with partners

$$S_x^2 + \omega S_y^2 + \omega^2 S_z^2$$

and

$$S_x^2 + \omega^2 S_y^2 + \omega S_z^2$$

and only one of the partners is listed in the table. In Table 17.2 several other 3 component matrices are found such as $\mathcal{S}_{\Gamma_{25}^+}^{(\alpha)}(2)$ where the x component is the anti-commutator $\{S_y, S_z\}$ and the y and z components of $\mathcal{S}_{\Gamma_{25}^+}^{(\alpha)}(2)$ are found by cyclic permutation of the indices x, y, z. It is worth mentioning that all of the $\mathcal{S}$ matrices in Eq. (17.81) are 3×3 matrices which are found explicitly by carrying out the indicated matrix operations. For example:

$$\{S_y, S_z\} = S_y S_z + S_z S_y = \begin{pmatrix} 0 & 0 & 0 \\ 0 & 0 & 0 \\ 0 & -1 & 0 \end{pmatrix} + \begin{pmatrix} 0 & 0 & 0 \\ 0 & 0 & -1 \\ 0 & 0 & 0 \end{pmatrix} = \begin{pmatrix} 0 & 0 & 0 \\ 0 & 0 & -1 \\ 0 & -1 & 0 \end{pmatrix}.$$
(17.83)

Also useful for carrying out matrix operations are the definitions:

$$S_x = \frac{\hbar}{i}\left(y\frac{\partial}{\partial z} - z\frac{\partial}{\partial y}\right)$$
(17.84)

so that

$$S_x \begin{pmatrix} x \\ y \\ z \end{pmatrix} = \frac{\hbar}{i}\begin{pmatrix} 0 \\ -z \\ y \end{pmatrix}.$$
(17.85)

Another point worth mentioning about Table 17.2 concerns the terms that do **not** appear. For example, in second-order we could have terms like $S_x^2 + S_y^2 + S_z^2$ but this matrix is just the unit matrix which has already been listed in the table. Similarly, the commutators $[S_y, S_z]$ which enter in second-order are matrices that have already appeared in first-order as iS_x.

We give below the nine basis matrices that span the (3×3) matrices for spin 1.

$$\mathcal{S}_{\Gamma_1^+} = \begin{pmatrix} 1 & 0 & 0 \\ 0 & 1 & 0 \\ 0 & 0 & 1 \end{pmatrix}$$
(17.86)

$$\mathcal{S}_{\Gamma_{12}^+}^{(1)} = \begin{pmatrix} -1 & 0 & 0 \\ 0 & 1+\omega^2 & 0 \\ 0 & 0 & 1+\omega \end{pmatrix} = \begin{pmatrix} -1 & 0 & 0 \\ 0 & -\omega & 0 \\ 0 & 0 & -\omega^2 \end{pmatrix}$$
(17.87)

$$\mathcal{S}^{(2)}_{\Gamma_{12}^+} = \begin{pmatrix} -1 & 0 & 0 \\ 0 & 1+\omega & 0 \\ 0 & 0 & 1+\omega^2 \end{pmatrix} \tag{17.88}$$

$$\mathcal{S}^{(x)}_{\Gamma_{15}^+} = \begin{pmatrix} 0 & 0 & 0 \\ 0 & 0 & i \\ 0 & -i & 0 \end{pmatrix} \tag{17.89}$$

$$\mathcal{S}^{(y)}_{\Gamma_{15}^+} = \begin{pmatrix} 0 & 0 & -i \\ 0 & 0 & 0 \\ i & 0 & 0 \end{pmatrix} \tag{17.90}$$

$$\mathcal{S}^{(z)}_{\Gamma_{15}^+} = \begin{pmatrix} 0 & i & 0 \\ -i & 0 & 0 \\ 0 & 0 & 0 \end{pmatrix} \tag{17.91}$$

$$\mathcal{S}^{(x)}_{\Gamma_{25}^+} = \begin{pmatrix} 0 & 0 & 0 \\ 0 & 0 & 1 \\ 0 & 1 & 0 \end{pmatrix} \tag{17.92}$$

$$\mathcal{S}^{(y)}_{\Gamma_{25}^+} = \begin{pmatrix} 0 & 0 & 1 \\ 0 & 0 & 0 \\ 1 & 0 & 0 \end{pmatrix} \tag{17.93}$$

$$\mathcal{S}^{(z)}_{\Gamma_{25}^+} = \begin{pmatrix} 0 & 1 & 0 \\ 1 & 0 & 0 \\ 0 & 0 & 0 \end{pmatrix} \tag{17.94}$$

Any arbitrary (3×3) matrix can be written as a linear combination of these nine matrices.

Table 17.2 however was constructed to be more general that to describe interacting p-bands in a 3×3 matrix formulation. The table can equally well be used to form the appropriate 16 basis matrices which are needed to deal with interacting s and p bands such as would arise in semiconductor physics. Such interacting s and p bands give rise to a 4×4 matrix Hamiltonian and therefore 16 basis matrices are needed to span the space for the secular equation in this case.

Now let use return to the Fourier expansion of Eq. (17.81). For each neighbor distance $|\vec{d}|$ there are several lattice vectors that enter, just as in the plane wave problem of Chapter 16 where we considered

sets of $\vec{K}$ vectors of equal magnitude. The terms in Eq. (17.81) can be labeled by their symmetry types so that the sum on $\vec{d}$ breaks up into a sum on the magnitude $|\vec{d}|$ and on the symmetry type Γ_j occurring at distance $\vec{d}$. The linear combinations of the exponential functions $\exp(i\vec{k} \cdot \vec{d})$ which transform as the pertinent irreducible representations of the cubic group are given in Table 17.3 out through 3rd nearest neighbor distances. Once again, if a representation is one-dimensional, the basis function itself is given. For the two-dimensional representations, only one of the functions is listed, the partner being the complex conjugate of the listed function. For the three-dimensional representations, only the x-component is listed; the partners are easily found by cyclic permutations of the indices.

The combinations of plane waves and basis functions that enter the Fourier expansion of Eq. (17.81) are the scalar products of these symmetrized Fourier functions $\vec{\mathcal{C}}_{\Gamma_j}(\vec{d})$ and the basis functions $\vec{\mathcal{S}}_{\Gamma_j}(\vec{d})$. This means that for the 2-dimensional representations, we write

$$\mathcal{C}^{(1)}_{\Gamma^+_{12}} \left(\mathcal{S}^{(1)}_{\Gamma^+_{12}} \right)^* + \mathcal{C}^{(2)}_{\Gamma^+_{12}} \left(\mathcal{S}^{(2)}_{\Gamma^+_{12}} \right)^* \tag{17.95}$$

where the second term is the complex conjugate of the first so that the sum is real. For the 3-dimensional representations we write for the scalar product

$$\mathcal{C}^x \mathcal{S}^x + \mathcal{C}^y \mathcal{S}^y + \mathcal{C}^z \mathcal{S}^z. \tag{17.96}$$

Finally, the Fourier expansion parameters α_{d,Γ_j} are just numbers that give the magnitude of all the terms which enter the Fourier expansion. These coefficients are often evaluated from experimental data.

Now suppose that we are going to do a Fourier expansion for p-bands. These have Γ^-_{15} symmetry. We ask what symmetry types can we have in the coupling between p-bands—clearly only the symmetries that enter into the direct product

$$\Gamma^-_{15} \otimes \Gamma^-_{15} = \Gamma^+_1 + \Gamma^+_{12} + \Gamma^+_{15} + \Gamma^+_{25}. \tag{17.97}$$

We will now indicate the terms which contribute at each neighbor distance to Eq. (17.81).

Table 17.3: Symmetrized Fourier functions for a simple cubic lattice.

d	Repr.	Notation	Symmetrized Fourier functions
$a(0,0,0)$	Γ_1^+	$\mathcal{C}_{\Gamma_1^+}(000)$	1
$a(1,0,0)$	Γ_1^+	$\mathcal{C}_{\Gamma_1^+}(100)$	$\cos ak_x + \cos ak_y + \cos ak_z$
	Γ_{12}^+	$\mathcal{C}_{\Gamma_{12}^+}^{(1)}(100)$	$\cos ak_x + \omega \cos ak_y + \omega^2 \cos ak_z$
	Γ_{15}^-	$\mathcal{C}_{\Gamma_{15}^-}^{(x)}(100)$	$\sin ak_x$
$a(1,1,0)$	Γ_1^+	$\mathcal{C}_{\Gamma_1^+}(110)$	$\cos a(k_y+k_z)+\cos a(k_y-k_z)+\cos a(k_z+k_x)$ $+\cos a(k_z-k_x)+\cos a(k_x+k_y)+\cos a(k_x-k_y)$
	Γ_{12}^+	$\mathcal{C}_{\Gamma_{12}^+}^{(1)}(110)$	$[\cos a(k_y+k_z)+\cos a(k_y-k_z)]$ $+\omega[\cos a(k_z+k_x)+\cos a(k_z-k_x)]$ $+\omega^2[\cos a(k_x+k_y)+\cos a(k_x-k_y)]$
	Γ_{15}^-	$\mathcal{C}_{\Gamma_{15}^-}^{(x)}(110)$	$\sin a(k_x+k_y)+\sin a(k_x-k_y)$ $+\sin a(k_x+k_z)+\sin a(k_x-k_z)$
	Γ_{25}^-	$\mathcal{C}_{\Gamma_{25}^-}^{(x)}(110)$	$\sin a(k_x+k_y)+\sin a(k_x-k_y)$ $-\sin a(k_x+k_z)-\sin a(k_x-k_z)$
	Γ_{25}^+	$\mathcal{C}_{\Gamma_{25}^+}^{(x)}(110)$	$\cos a(k_y+k_z)-\cos a(k_y-k_z)$
$a(1,1,1)$	Γ_1^+	$\mathcal{C}_{\Gamma_1^+}(111)$	$\cos a(k_x+k_y+k_z)+\cos a(k_x-k_y-k_z)$ $+\cos a(-k_x+k_y-k_z)+\cos a(-k_x-k_y+k_z)$
	Γ_2^-	$\mathcal{C}_{\Gamma_2^-}(111)$	$\sin a(k_x+k_y+k_z)+\sin a(k_x-k_y-k_z)$ $\sin a(-k_x+k_y-k_z)+\sin a(-k_x-k_y+k_z)$
	Γ_{15}^-	$\mathcal{C}_{\Gamma_{15}^-}^{(x)}(111)$	$\sin a(k_x+k_y+k_z)+\sin a(k_x-k_y-k_z)$ $-\sin a(-k_x+k_y-k_z)-\sin a(-k_x-k_y+k_z)$
	Γ_{25}^+	$\mathcal{C}_{\Gamma_{25}^+}^{(x)}(111)$	$\cos a(k_x+k_y+k_z)+\cos a(k_x-k_y-k_z)$ $-\cos a(-k_x+k_y-k_z)-\cos a(-k_x-k_y+k_z)$

where $\omega = \exp(2\pi i/3)$ and a is the lattice constant.

17.8.1 Contributions at $d = 0$:

From Table 17.3 we can have only Γ_1^+ symmetry at $d = 0$ for which the basis matrix is

$$
\begin{pmatrix}
1 & 0 & 0 \\
0 & 1 & 0 \\
0 & 0 & 1
\end{pmatrix}
\tag{17.98}
$$

and the symmetrical Fourier function is 1, so that the net contribution to Eq. (17.81) is

$$
\alpha_{0,\Gamma_1^+}
\begin{pmatrix}
1 & 0 & 0 \\
0 & 1 & 0 \\
0 & 0 & 1
\end{pmatrix}.
\tag{17.99}
$$

17.8.2 Contributions at $d = 1$:

For Γ_1^+ symmetry the contribution is in analogy to Eq. (17.99)

$$
\alpha_{1,\Gamma_1^+}\, \mathcal{C}_{\Gamma_1^+}(100)
\begin{pmatrix}
1 & 0 & 0 \\
0 & 1 & 0 \\
0 & 0 & 1
\end{pmatrix}
\tag{17.100}
$$

while for Γ_{12}^+ symmetry, the contribution is:

$$
\alpha_{1,\Gamma_{12}^+}\, \mathcal{C}_{\Gamma_{12}^+}^{(1)}
\begin{pmatrix}
\omega + \omega^2 & 0 & 0 \\
0 & 1 + \omega^2 & 0 \\
0 & 0 & 1 + \omega
\end{pmatrix}
+ \alpha_{1,\Gamma_{12}^+}\mathcal{C}_{\Gamma_{12}^+}^{(2)}
\begin{pmatrix}
\omega + \omega^2 & 0 & 0 \\
0 & 1 + \omega & 0 \\
0 & 0 & 1 + \omega^2
\end{pmatrix}
\tag{17.101}
$$

where we have used the relation $S_{\Gamma_{12}}^{(1)} = S_x^2 + \omega S_y^2 + \omega^2 S_z^2$ to obtain the appropriate matrices. We also use the relations $1 + \omega + \omega^2 = 0$ for the cube roots of unity to simplify Eq. (17.101). We note that both terms in Eq. (17.101) have the same expansion parameter α_{1,Γ_{12}^+}.

These are all the contributions for $d = 1$. The symmetry type Γ_{15}^- does not enter into this sum since there are no basis matrices with symmetries Γ_{15}^- for $\mathbf{d} = 1$ (see Table 17.2). This symmetry would however enter into treating the interaction between s and p bands. Therefore, we get no off-diagonal terms until we go to second-neighbor distances. This should not be surprising to us since this is exactly what happens in the $\vec{k} \cdot \vec{p}$ treatment of p bands. In fact, **the Fourier**

expansion technique contains in it a $\vec{k} \cdot \vec{p}$ expansion for every point in the Brillouin zone.

17.8.3 Contributions at $d = 2$:

At the second-neighbor distance Table 17.3 yields contributions from Γ_1^+, Γ_{12}^+ and Γ_{25}^+ symmetries. These contributions at $d = 2$ are:
Γ_1^+ symmetry

$$\alpha_{2,\Gamma_1^+} \, \mathcal{C}_{\Gamma_1^+}(110) \begin{pmatrix} 1 & 0 & 0 \\ 0 & 1 & 0 \\ 0 & 0 & 1 \end{pmatrix} \tag{17.102}$$

Γ_{12}^+ symmetry

$$\alpha_{2,\Gamma_{12}^+} \left[\mathcal{C}_{\Gamma_{12}^+}^{(1)}(110) \begin{pmatrix} -1 & 0 & 0 \\ 0 & -\omega & 0 \\ 0 & 0 & -\omega^2 \end{pmatrix} + c.c. \right] \tag{17.103}$$

Γ_{25}^+ symmetry

$$\alpha_{2,\Gamma_{25}^+} \begin{pmatrix} 0 & \mathcal{C}_{\Gamma_{25}^+}^{(z)}(110) & \mathcal{C}_{\Gamma_{25}^+}^{(y)}(110) \\ \mathcal{C}_{\Gamma_{25}^+}^{(z)}(110) & 0 & \mathcal{C}_{\Gamma_{25}^+}^{(x)}(110) \\ \mathcal{C}_{\Gamma_{25}^+}^{(y)}(110) & \mathcal{C}_{\Gamma_{25}^+}^{(x)}(110) & 0 \end{pmatrix} \tag{17.104}$$

Terms with Γ_{15}^- and Γ_{25}^- symmetries in Table 17.3 do not enter because there are no basis matrices with these symmetries.

17.8.4 Contributions at $d = 3$:

Symmetries Γ_1^+ and Γ_{25}^+ contribute and these are written down as above.

To get the matrix Hamiltonian we add up contributions from Eqs. (17.99–17.104). There are 6 parameters α_{d,Γ_j} that enter into the Fourier expansion through second-neighbor terms ($d = 0, 1, 2$). The Γ_1^+ representation at $d = 0$ contributes to the (1,1) position in the secular equation a term in α_{0,Γ_1^+} and at $d = 1$ contributes a term $\alpha_{1,\Gamma_1^+}(\cos ak_x + \cos ak_y + \cos ak_z)$ in which the two coefficients α_{0,Γ_1^+} and α_{1,Γ_1^+} will have different numerical values. The other entries into the (3×3) matrix are found

similarly. The resulting (3×3) matrix Hamiltonian is then diagonalized and the eigenvalues are the $E_n(\vec{k})$ we are looking for. This $E_n(\vec{k})$ properly expresses the crystal symmetry at all points in the Brillouin zone.

It is instructive to write out in detail this matrix Hamiltonian along the (100), (110) and (111) directions and to verify that all connectivity relations and symmetry requirements are automatically satisfied. It is directly shown that near $\vec{k} = 0$, the Hamiltonian of Eq. (17.81) is of the $\vec{k} \cdot \vec{p}$ form previously derived. As stated above, the Fourier expansion approach contains the $\vec{k} \cdot \vec{p}$ form for all expansion points $\vec{k}_0$ in the Brillouin zone.

17.8.5 Other Degenerate Levels

The Fourier expansion can also be applied to the two-fold Γ_{12}^+ levels in cubic symmetry arising from d-bands, or to $\Gamma_{12}^{\pm}$ levels more generally. Of particular interest is application of the Slater–Koster method to coupled s and p-bands as has been done for silicon and germanium, both of which crystallize in the diamond structure. In the case of coupled s and p bands, the 3×3 expansion in §17.8 and the s-band expansion in §17.3 are coupled with the Fourier terms from Table 17.3 having symmetries $\Gamma_i \otimes \Gamma_{15}^-$. We give an outline in this section for setting up the secular equation to solve the Fourier expansion for these two interesting cases.

The four 2×2 matrices that are used as basis matrices for Fourier expanding the $\Gamma_{12}^{\pm}$ levels are implied by $\Gamma_{12}^{\pm} \otimes \Gamma_{12}^{\pm} = \Gamma_1^+ + \Gamma_2^+ + \Gamma_{12}^+$: for Γ_1^+ symmetry

$$\mathcal{S}_{\Gamma_1^+} = \begin{pmatrix} 1 & 0 \\ 0 & 1 \end{pmatrix} \tag{17.105}$$

for Γ_2^+ symmetry

$$\mathcal{S}_{\Gamma_2^+} = \begin{pmatrix} 1 & 0 \\ 0 & -1 \end{pmatrix} \tag{17.106}$$

for Γ_{12}^+ symmetry

$$\mathcal{S}_{\Gamma_{12,1}^+} = \begin{pmatrix} 0 & 1 \\ 0 & 0 \end{pmatrix} \tag{17.107}$$

where the partner of $\mathcal{S}_{\Gamma_{12,1}^+}$ is the Hermitian transpose

$$\mathcal{S}_{\Gamma_{12,2}^+} = \mathcal{S}_{\Gamma_{12,1}^+}^* = \mathcal{S}_{\Gamma_{12,1}^+}^\dagger = \begin{pmatrix} 0 & 0 \\ 1 & 0 \end{pmatrix}. \qquad (17.108)$$

Using these matrices we see that

$$\mathcal{S}_{\Gamma_{12,1}^+}\mathcal{S}_{\Gamma_{12,1}^+}^\dagger + \mathcal{S}_{\Gamma_{12,2}^+}\mathcal{S}_{\Gamma_{12,2}^+}^\dagger = \begin{pmatrix} 1 & 0 \\ 0 & 1 \end{pmatrix} = \mathcal{S}_{\Gamma_1^+} \qquad (17.109)$$

and

$$\mathcal{S}_{\Gamma_{12,1}^+}\mathcal{S}_{\Gamma_{12,1}^+}^\dagger - \mathcal{S}_{\Gamma_{12,2}^+}\mathcal{S}_{\Gamma_{12,2}^+}^\dagger = \begin{pmatrix} 1 & 0 \\ 0 & -1 \end{pmatrix} = \mathcal{S}_{\Gamma_2^+}. \qquad (17.110)$$

The dispersion relation of $E(\vec{k})$ for a band with Γ_{12}^+ symmetry at $\vec{k} = 0$ can then be Fourier expanded throughout the Brillouin zone in terms of the basis functions in Eqs. (17.105–17.108) as:

$$\begin{aligned} E_{\Gamma_{12}^\pm}(\vec{k}) = &\sum_{\vec{d}} \alpha_{d,\Gamma_1^+} \mathcal{C}_{\Gamma_1^+}(\vec{d}) \begin{pmatrix} 1 & 0 \\ 0 & 1 \end{pmatrix} + \sum_{\vec{d}} \alpha_{d,\Gamma_2^+} \mathcal{C}_{\Gamma_2^+}(\vec{d}) \begin{pmatrix} 1 & 0 \\ 0 & -1 \end{pmatrix} \\ &+ \sum_{\vec{d}} \alpha_{d,\Gamma_{12}^+} \mathcal{C}_{\Gamma_{12}^\pm}^{(1)}(\vec{d}) \begin{pmatrix} 0 & 1 \\ 0 & 0 \end{pmatrix} + \sum_{\vec{d}} \alpha_{d,\Gamma_{12}^+} \mathcal{C}_{\Gamma_{12}^\pm}^{(2)}(\vec{d}) \begin{pmatrix} 0 & 0 \\ 1 & 0 \end{pmatrix} \end{aligned}$$
$$(17.111)$$

where $\mathcal{C}_{\Gamma_{12}^\pm}^{(2)}(\vec{d}) = \mathcal{C}_{\Gamma_{12}^\pm}^{(1)*}(\vec{d})$ and the $\mathcal{C}_{\Gamma_i^\pm}(\vec{d})$ functions are found in Table 17.3.

For the case of interacting s (Γ_1^+) and p (Γ_{15}^-) bands, the interaction terms have $\Gamma_1^+ \otimes \Gamma_{15}^- = \Gamma_{15}^-$ symmetry so the 4×4 expansion matrices must be supplemented by the matrices

$$\mathcal{S}_{\Gamma_{15}^-}^x = \begin{pmatrix} 0 & 1 & 0 & 0 \\ 1 & 0 & 0 & 0 \\ 0 & 0 & 0 & 0 \\ 0 & 0 & 0 & 0 \end{pmatrix} \qquad (17.112)$$

and the two partners

$$\mathcal{S}_{\Gamma_{15}^-}^y = \begin{pmatrix} 0 & 0 & 1 & 0 \\ 0 & 0 & 0 & 0 \\ 1 & 0 & 0 & 0 \\ 0 & 0 & 0 & 0 \end{pmatrix} \qquad \mathcal{S}_{\Gamma_{15}^-}^z = \begin{pmatrix} 0 & 0 & 0 & 1 \\ 0 & 0 & 0 & 0 \\ 0 & 0 & 0 & 0 \\ 1 & 0 & 0 & 0 \end{pmatrix} \qquad (17.113)$$

The complete treatment of the Fourier expansion for the 8 coupled s and p bonding and anti-bonding bands in the non-symmorphic diamond structure has been presented in Phys. Rev. **160**, 649 (1967) and was used to describe the Si and Ge bands throughout the Brillouin zone. The same basic treatment without the s bands was used to treat the lattice dynamics for these structures in Int. J. of Quantum Chemistry, Vol IIs, 333 (1968).

17.8.6   Summary

A discussion of the use of $\vec{k} \cdot \vec{p}$ perturbation theory extrapolation approach and the use of the Slater–Koster interpolation approach is based on the following considerations. If the available experimental data are limited to one small region in the Brillouin zone and that is all that is known, then $\vec{k} \cdot \vec{p}$ perturbation theory is adequate to describe $E(\vec{k})$. This is often the case in practice for semiconductors. If, however, the available experimental data relates to several points in the Brillouin zone, then the Slater–Koster approach is more appropriate. Experiments on various parts of the Fermi surface usually require knowledge of $E(\vec{k})$ over several regions of the Brillouin zone. Although such experiments might seem to yield unrelated information about the energy bands, the Slater–Koster approach is useful for interrelating such experiments.

In Chapter 20, the effective mass Hamiltonian will be considered in the presence of a magnetic field, taking into account the spin on the electron. In this case we form the following symmetrized combinations of wave vectors:

$$
\begin{aligned}
\Gamma_1^+ &\rightarrow k_x^2 + k_y^2 + k_z^2 \\
\Gamma_{12}^+ &\rightarrow k_x^2 + \omega k_y^2 + \omega^2 k_z^2,\ cc \\
\Gamma_{25}^+ &\rightarrow (\{k_y, k_z\},\ \{k_z, k_x\}, \{k_x, k_y\}) \\
\Gamma_{15}^+ &\rightarrow ([k_y, k_z],\ [k_z, k_x], [k_x, k_y])
\end{aligned}
\tag{17.114}
$$

treating the wave vector as an operator. This formulation of the effective mass equation is used to yield the effective g-factor for an electron in a periodic solid.

17.9 Selected Problems

1. (a) Using $\vec{k} \cdot \vec{p}$ perturbation theory, find the form of the $E(\vec{k})$ relation near the L-point in the Brillouin zone for a face centered cubic lattice arising from the lowest levels with L_1 and L'_2 symmetry that are doubly degenerate in the free electron model. Which of the non-vanishing $\vec{k} \cdot \vec{p}$ matrix elements at the L-point are equal to each other by symmetry?

   (b) Using the Slater–Koster technique, find the form for $E(\vec{k})$ for the lowest two levels for a face centered cubic lattice.

   (c) Expand your results for (b) about the L-point in a Taylor expansion.

   (d) Compare your results in (c) to those in (a).

   (e) Using $\vec{k} \cdot \vec{p}$ perturbation theory, find the form of $E(k)$ for a non-degenerate band with W_1 symmetry about the W point in the fcc lattice.

2. (a) Using $\vec{k} \cdot \vec{p}$ perturbation theory, find the form of the secular equation for the valence band of Si with Γ_{25}^+ symmetry.

   (b) Which intermediate states couple to the Γ_{25}^+ valence band states in second-order $\vec{k} \cdot \vec{p}$ perturbation theory?

   (c) Which matrix elements (listed in Table 17.1) enter the secular equation in (a)?

   (d) Write the secular equation for the Γ_{25}^+ valence bands that is analogous to Eq. (17.59) for the Γ_{15}^- band?

   (e) What result is obtained along a Λ (111) axis?

3. (a) Write down the matrices for S_x, S_y and S_z for angular momentum 3/2. Products of these and the (4×4) unit matrix form the 16 matrix basis functions which span the vector space for the (4×4) Slater–Koster secular equation for coupled s and p bands for a simple cubic lattice.

   (b) Returning to the Slater–Koster (3×3) secular determinant for a simple cubic lattice given in the class notes, write the

explicit expression for this matrix along a (100) direction. Show that the proper $\vec{k} \cdot \vec{p}$ Hamiltonian is obtained at the X point.

Chapter 18

Application of Group Theory to Valley-Orbit Interactions in Semiconductors

In this chapter, we shall discuss the application of group theory to the impurity problem of a multi-valley semiconductor, such as occurs in the donor carrier pockets in silicon and germanium. In the case of silicon the lowest conduction bands occur at the 6 equivalent (Δ,0,0) points where (Δ =0.85 on a scale where the Γ point is at the origin and the X point is at 1). In the case of germanium, the conduction band minima occur at the L points so that the Fermi surface for electrons consists of eight equivalent half-ellipsoids of revolution (4 full ellipsoids). Other cases where valley-orbit interactions are important are multi-valleyed semiconductors, such as PbTe or Te, where the conduction and valence band extrema are both away from $\vec{k} = 0$.

18.1   Introduction

Group theory tells us that the maximum degeneracy that energy levels or vibrational states can have with cubic symmetry is 3-fold degeneracy. Cubic symmetry is imposed on the problem of donor doping of a semiconductor through the valley-orbit interaction which causes a partial lifting of the n-fold degeneracy of an n-valley semiconductor.

In this presentation we show how group theory prescribes the partial lifting of this n-fold degeneracy. This effect is important in describing the ground state energy of a donor-doped n-valley semiconductor.

Our discussion of the application of group theory to the classification of the symmetries of the impurity levels in a degenerate semiconductor proceeds with the following outline:

1. Review of the one-electron Hamiltonian and the effective mass Hamiltonian for a donor impurity in a semiconductor yielding hydrogenic impurity levels for a single-valley semiconductor.

2. Discussion of the impurity states for multivalley semiconductors in the effective mass approximation.

3. Discussion of the valley-orbit interaction. In this application we consider a situation where the lower symmetry group is not a subgroup of the higher symmetry group.

18.2 Background

In this section we review the one-electron Hamiltonian, effective mass approximation and the hydrogenic impurity problem for a single-valley semiconductor. We write the one-electron Hamiltonian for an electron in a crystal which experiences a perturbation potential $U(\vec{r})$ due to an impurity:

$$\left[\frac{p^2}{2m} + V(\vec{r}) + U(\vec{r}) \right] \Psi(\vec{r}) = E\Psi(\vec{r}) \tag{18.1}$$

in which $V(\vec{r})$ is the periodic potential. In the effective mass approximation, the perturbing potential due to an impurity is taken as $U(\vec{r}) = -e^2/(\varepsilon r)$ where ε is the dielectric constant. This problem is usually solved in terms of the effective mass theorem to obtain

$$\left[\frac{p^2}{2m^*_{\alpha\beta}} + U(r) \right] f_j(\vec{r}) = (E - E_j^0) f_j(\vec{r}) \tag{18.2}$$

where $m^*_{\alpha\beta}$ is the effective mass tensor for electrons in the conduction band about the band extremum at energy E_j^0, and $f_j(\vec{r})$ is the effective mass wave function. We thus note that by replacing the periodic

potential $V(\vec{r})$ by an effective mass tensor, we have **lost most of the symmetry information** contained in the original periodic potential. This symmetry information is restored by introducing the valley-orbit interaction, as in §18.3 and §18.4.

The simplest case for an impurity in a semiconductor is that for a shallow impurity level described by hydrogenic impurity states in a non-degenerate conduction band, as for example a Si atom substituted for a Ga atom in GaAs, a direct gap semiconductor with the conduction band extremum at the Γ point ($k = 0$). To satisfy the bonding requirements in this case, one electron becomes available for conduction and a donor state is formed. The effective mass equation in this case becomes

$$\left[\frac{p^2}{2m^*} - \frac{e^2}{\varepsilon r} \right] f(\vec{r}) = (E - E_j^0) f(\vec{r}) \qquad (18.3)$$

where $U(\vec{r}) = -e^2/(\varepsilon r)$ is the screened Coulomb potential for the donor electron, ε is the low frequency dielectric constant, and the donor energies are measured from the band edge E_j^0. This screened Coulomb potential is expected to be a good approximation for $\vec{r}$ at a sufficiently **large distance from the impurity site**, so that ε can be considered to be independent of r.

The solutions to this hydrogenic problem are the hydrogenic levels

$$E_n - E_j^0 = -\frac{e^2}{2\varepsilon a_0^* n^2} \qquad\qquad n = 1, 2, \ldots \qquad (18.4)$$

where the effective Bohr radius is

$$a_0^* = \frac{\varepsilon \hbar^2}{m^* e^2}. \qquad (18.5)$$

Since $\left(E_n - E_j^0 \right) \sim m^*/\varepsilon^2$, we have **shallow** donor levels located below the band extrema. These levels are shallow because of the large value of ε and the small value of m^*, a common occurrence in many of the high mobility semiconductors.

Group theoretical considerations enter in the following way. For many III–V compound semiconductors, the valence and conduction band extrema are at $\vec{k} = 0$ so that the effective mass Hamiltonian

has full rotational symmetry. Since the hydrogenic impurity is embedded in a crystal with a periodic potential, the crystal symmetry (i.e., T_d point group symmetry) will perturb the hydrogenic levels and cause a splitting of various degenerate levels:

$$
\begin{aligned}
s \text{ levels} \quad &\rightarrow \quad \Gamma_1 \quad \text{(no splitting)} \\
p \text{ levels} \quad &\rightarrow \quad \Gamma_{15} \quad \text{(no splitting)} \\
d \text{ levels} \quad &\rightarrow \quad \Gamma_{12} + \Gamma_{15} \quad \text{(splitting occurs)} \\
f \text{ levels} \quad &\rightarrow \quad \Gamma_2 + \Gamma_{15} + \Gamma_{25} \quad \text{(splitting occurs)}
\end{aligned}
$$

In principle, if a multiplet has the same symmetry as an s or p level then an interaction can occur giving rise to an admixture of states of similar symmetries. In practice, the splittings are very small in magnitude and the effects of the crystal field are generally unimportant for shallow donor levels in single valley semiconductors.

18.3 Impurity States for Multivalley Semiconductors

Group theory plays a more important role in the determination of impurity states in multi-valley semiconductors than for the simple hydrogenic case. A common example of a multi-valley impurity state is As in Si (or in Ge). In Si there are six equivalent valleys while for Ge there are four equivalent valleys. The multi-valley aspect of the problem results in two departures from the simple hydrogenic series.

The first of these departures is associated with the fact that the constant energy surfaces in this case are ellipsoids rather than spheres. In this case we write Schrödinger's equation for a single valley in the effective mass approximation as:

$$
\left[\frac{p_x^2 + p_y^2}{2m_t} + \frac{p_z^2}{2m_\ell} - \frac{e^2}{\varepsilon r} \right] = E \, f(\vec{r}) \tag{18.6}
$$

in which m_t is the transverse mass component, m_ℓ is the longitudinal mass component, and the energy E is measured from the energy band extremum. The appropriate symmetry group for the effective mass

equation given by Eq. (18.6) is $D_{\infty h}$ rather than the full rotation group which applies to the hydrogenic impurity levels. This form for the effective mass Hamiltonian follows from the fact that the constant energy surfaces are ellipsoids of revolution, which in turn is a consequence of the selection rules for the $\vec{k} \cdot \vec{p}$ Hamiltonian at a Δ point (group of the wave vector C_{4v}) in the case of Si, and at an L point (group of the wave vector D_{3d}) in the case of Ge. The anisotropy of the kinetic energy terms corresponds to the anisotropy of the effective mass tensor. For example in the case of silicon $m_\ell/m_0 = 0.98$ (heavy mass), $m_t/m_0 = 0.19$ (light mass). This anisotropy in the kinetic energy terms results in a splitting of the impurity levels with angular momentum greater than 1, in accordance with the irreducible representations of $D_{\infty h}$. For example, in $D_{\infty h}$ symmetry we have the following correspondence with angular momentum states:

$$
\begin{aligned}
s \text{ states} &\rightarrow \Sigma_g^+ = A_{1g} \\
p \text{ states} &\rightarrow \Sigma_u^+ + \pi_u = A_{2u} + E_{1u} \\
d \text{ states} &\rightarrow \Delta_g + \pi_g + \Sigma_g^+ = A_{1g} + E_{1g} + E_{2g}.
\end{aligned}
$$

We note that s and d states are even (g) and p states are odd (u) under inversion in accordance with the character table for $D_{\infty h}$.

$D_{\infty h}$ (∞/mm)			E	$2C_\phi$	C_2'	i	$2iC_\phi$	iC_2'
x^2+y^2, z^2		$A_{1g}(\Sigma_g^+)$	1	1	1	1	1	1
		$A_{1u}(\Sigma_u^-)$	1	1	1	-1	-1	-1
	R_z	$A_{2g}(\Sigma_g^-)$	1	1	-1	1	1	-1
	z	$A_{2u}(\Sigma_u^+)$	1	1	-1	-1	-1	1
(xz, yz)	(R_x, R_y)	$E_{1g}(\Pi_g)$	2	$2\cos\phi$	0	2	$2\cos\phi$	0
	(x, y)	$E_{1u}(\Pi_u)$	2	$2\cos\phi$	0	-2	$-2\cos\phi$	0
(x^2-y^2, xy)		$E_{2g}(\Delta_g)$	2	$2\cos 2\phi$	0	2	$2\cos 2\phi$	0
		$E_{2u}(\Delta_g)$	2	$2\cos 2\phi$	0	-2	$-2\cos 2\phi$	0

Thus a $2p$ level with angular momentum $\ell = 1$ splits into a two-fold $2p^{\pm 1}$ level and a non-degenerate $2p^0$ level in which the superscripts denote the m_ℓ values. Furthermore in $D_{\infty h}$ symmetry, the splitting of d-levels gives rise to the same irreducible representation (Σ_g^+) that describes the s-levels, and consequently a mixing of these levels occurs.

Referring back to the effective mass equation [Eq. (18.6)], we note that this equation cannot be solved exactly if $m_\ell \neq m_t$. Thus, the

donor impurity levels in these indirect gap semiconductors must be deduced from some approximate technique such as a variational calculation or using perturbation theory. The effective mass approximation itself works very well for these p-states because $|\psi_p|^2$ for p states vanishes for $\vec{r} = 0$; consequently, for $\vec{r}$ values small enough for central cell corrections to be significant, the wave function has a small amplitude and thus small $\vec{r}$ values do not contribute significantly to the expectation value of the energy for p-states.

18.4   The Valley-Orbit Interaction

The second departure from the hydrogenic series in a multi-valley semiconductor is one that relates closely to group theory. This effect is most important for s-states, particularly for the $1s$ state.

For s-states, a sizable contribution to the expectation value for the energy is made by the perturbing potential for small $\vec{r}$. The physical picture of a spherically symmetric potential $U(\vec{r})$ for small $\vec{r}$ cannot fully apply because the tetrahedral bonding must become important for $|\vec{r}| \leq a$, i.e., within the unit cell dimension. This tetrahedral crystal field which is important within the central cell lifts the spherical symmetry of an isolated atom. Thus we need to consider corrections to the effective mass equation due to the tetrahedral crystal field. This tetrahedral crystal field term is called $\mathcal{H}'_{\text{valley}-\text{orbit}}$, the valley-orbit effective Hamiltonian which couples equivalent conduction band extrema in the various valleys.

Therefore to find the wave functions for the donor states in a multi-valley semiconductor, we must find linear combinations of wave functions from each of the valleys that transform as irreducible representations of the crystal field about the impurity ion. For example, in silicon, the symmetrized linear combination of valley wave functions is in the form

$$\psi^{\gamma}(\vec{r}) = \sum_{j=1}^{6} A_j^{\gamma} f_j(\vec{r}) u_{j,k_0^j}(\vec{r}) e^{i\vec{k}_0^j \cdot \vec{r}} \qquad (18.7)$$

in which $\psi^{\gamma}(\vec{r})$ denotes one of 6 possible linear combinations. The index j is the valley index and $f_j(\vec{r})$ is the envelope effective mass wave
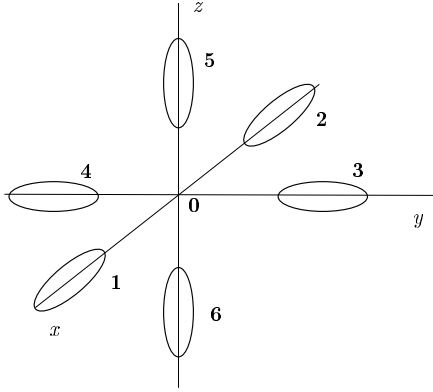
Figure 18.1: Constant energy ellipsoids of the conduction-band minima of silicon along {100} directions.

Table 18.1: Character table for the point group T_d.

T_d ($\bar{4}3m$)		E	$8C_3$	$3C_2$	$6\sigma_d$	$6S_4$	
	A_1	1	1	1	1	1	Γ_1
	A_2	1	1	1	-1	-1	Γ_2
	E	2	-1	2	0	0	Γ_{12}
(R_x, R_y, R_z)	T_1	3	0	-1	-1	1	Γ_{25}
(x, y, z)	T_2	3	0	-1	1	-1	Γ_{15}

function, while $u_{j,k_0^j}(\vec{r})$ is the periodic part of the Bloch function in which k_0^j is the wave vector to the band minimum of valley j. The 6 equivalent valleys along the (100) axes for silicon are shown in Fig. 18.1. The indices j which label the various ellipsoids or valleys in Fig. 18.1 correspond to the indices j of Eq. (18.7). The local symmetry close to the impurity center is T_d, reflecting the tetrahedral bonding at the impurity site. The character table for the T_d point group is shown in Table 18.1. The diagram which is useful for finding which valleys are invariant under the symmetry operations of T_d is given in Fig. 18.2. We ask for the number of valleys which remain invariant under the various symmetry operations of T_d. This is equivalent to finding $\chi_{\text{atom sites}}$ or $\chi_{\text{valley sites}}$, which forms a **reducible** representation of group T_d. From Figure 18.2, we immediately see that the characters for $\chi_{\text{valley sites}}$ are
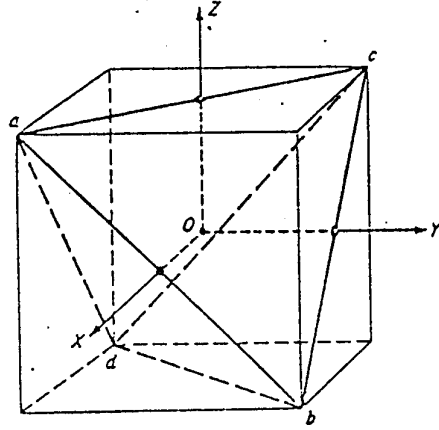
Figure 18.2: The regular tetrahedron inscribed inside a cube, illustrating the locations and symmetry operations of the six valleys.

	E	$8C_3$	$3C_2$	$6\sigma_d$	$6S_4$	
$\chi_{\text{valley sites}}$	6	0	2	2	0	$= \Gamma_1 + \Gamma_{12} + \Gamma_{15}$

and that the irreducible representations contained in $\chi_{\text{valley sites}}$ are $\Gamma_1 + \Gamma_{12} + \Gamma_{15}$. To find the splitting of a level we must take the direct product of the symmetry of the level with $\chi_{\text{valley sites}}$, **provided that the level itself transforms as an irreducible representation of group T_d:**

$$\chi_{\text{level}} \otimes \chi_{\text{valley sites}}. \tag{18.8}$$

Since χ_{level} for s-states transforms as Γ_1, the level splitting for s-states is just $\chi_{\text{valley sites}}$:

$$\begin{array}{l} \text{———}\Gamma_{15} \\ \text{———}\Gamma_{12} \\ \text{———}\Gamma_1 \end{array}$$

The appropriate linear combination of valley functions corresponding to each of these irreducible representations is [using the notation

from Eq. (18.7)]:

$$A_j^{(\Gamma_1)} = \tfrac{1}{\sqrt{6}}(1,1,1,1,1,1)$$

$$\left.\begin{array}{rl}A_j^{(\Gamma_{12},1)} &= \tfrac{1}{\sqrt{6}}(1,1,\omega,\omega,\omega^2,\omega^2) \\ A_j^{(\Gamma_{12},2)} &= \tfrac{1}{\sqrt{6}}(1,1,\omega^2,\omega^2,\omega,\omega)\end{array}\right\}$$

$$\left.\begin{array}{rl}A_j^{(\Gamma_{15},1)} &= \tfrac{1}{\sqrt{2}}(1,-1,0,0,0,0) \\ A_j^{(\Gamma_{15},2)} &= \tfrac{1}{\sqrt{2}}(0,0,1,-1,0,0) \\ A_j^{(\Gamma_{15},3)} &= \tfrac{1}{\sqrt{2}}(0,0,0,0,1,-1)\end{array}\right\} \qquad (18.9)$$

in which each of the six components refers to one of the valleys. The totally symmetric linear combination Γ_1 is a non-degenerate level, while the Γ_{12} basis functions have 2 partners which are given by $f_1 = x^2 + \omega y^2 + \omega^2 z^2$ and $f_2 = f_1^*$ and the Γ_{15} basis functions have three partners (x, y, z).

The analysis for the p-levels is more complicated because the p-levels in $D_{\infty h}$ do not transform as irreducible representations of group T_d. The p-level in group $D_{\infty h}$ transforms as a vector, with A_{2u} and E_{1u} symmetries for the longitudinal and transverse components, respectively. Since T_d does not form a subgroup of $D_{\infty h}$ we write the vector for group T_d as

$$\chi_{\text{vector}} = \chi_{\text{longitudinal}} + \chi_{\text{transverse}} \qquad (18.10)$$

where $\chi_{\text{vector}} = \Gamma_{15}$. We treat the longitudinal component of the vector as forming a σ-bond and the transverse component as forming a π-bond so that $\chi_{\text{longitudinal}} = \Gamma_1$ and $\chi_{\text{transverse}} = \Gamma_{15} - \Gamma_1$, where we note that:

$$\Gamma_{15} \otimes (\Gamma_1 + \Gamma_{12} + \Gamma_{15}) = \Gamma_{15} + (\Gamma_{15} + \Gamma_{25}) + (\Gamma_1 + \Gamma_{12} + \Gamma_{15} + \Gamma_{25}). \quad (18.11)$$

We thus obtain:

$$\chi^{2p_0} = \chi_{\text{valley sites}} \otimes \Gamma_1 = \Gamma_1 + \Gamma_{12} + \Gamma_{15} \qquad \text{for } m_\ell = 0 \qquad (18.12)$$

$$\chi^{2p_\pm} = \chi_{\text{valley sites}} \otimes (\Gamma_{15} - \Gamma_1) = 2\Gamma_{15} + 2\Gamma_{25} \qquad \text{for } m_\ell = \pm 1 \quad (18.13)$$

for group T_d. If we perform high resolution spectroscopy experiments for the donor impurity levels, we would observe transitions between the various $1s$ multiplets to the various $2p$-multiplets.

In addition to spectroscopic studies of impurity states, these donor states for multi-valley semiconductors have been studied by the EN-DOR technique (G. Feher, Phys. Rev. 114, 1219 (1959) for work on Si). Here the nuclear resonance of the ^{29}Si atoms is observed. The random distribution of the ^{29}Si sites with respect to the donor impurity sites is used to study the spatial dependence of the donor wavefunction, and to determine the location in $\vec{k}$-space of the conduction band extrema.

References for the group theoretical analysis of the valley-orbit splitting are W. Kohn and J.M. Luttinger, Phys. Rev. 97, 1721 (1955) and Phys. Rev. 98, 915 (1955). Experimental evidence for the splitting of the degeneracy of the $1s$ donor levels in silicon is provided by infrared absorption studies: R.L. Aggarwal and A.K. Ramdas, Phys. Rev. 140, A1246 (1965) and V.J. Tekippe, H.R. Chandrasekhar, P. Fisher and A.K. Ramdas, Phys. Rev. B6, 2348 (1972). An experimental trace for the excitation spectrum of phosphorus impurities in silicon is shown in Fig. 18.3 for several sample temperatures. The interpretation of this spectrum follows from the energy level diagram in Fig 18.4.

It is of interest that the valley orbit splitting effect is only important for the $1s$ levels. For the higher levels, the tetrahedral site location of the impurity atom becomes less important as the Bohr orbit for the impurity level

$$a^*_{\text{Bohr}} = \frac{\varepsilon \hbar^2}{m^* e^2} n^2 \tag{18.14}$$

increases, where n is the principal quantum number for the donor impurity level.
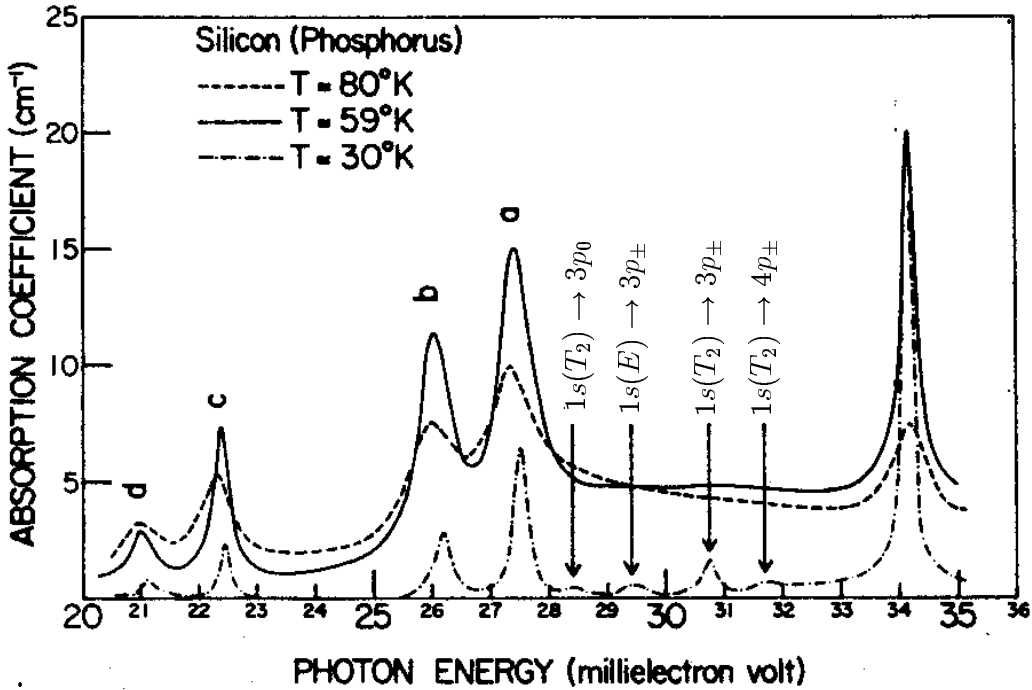
Figure 18.3: Excitation spectrum of phosphorus donors in silicon. The donor concentration $N_D \sim 5 \times 10^{15}/\text{cm}^3$. Various donor level transitions to valley-orbit split levels are indicated. The labels for the final state of the optical transitions are in accordance with the symmetries of point group T_d.
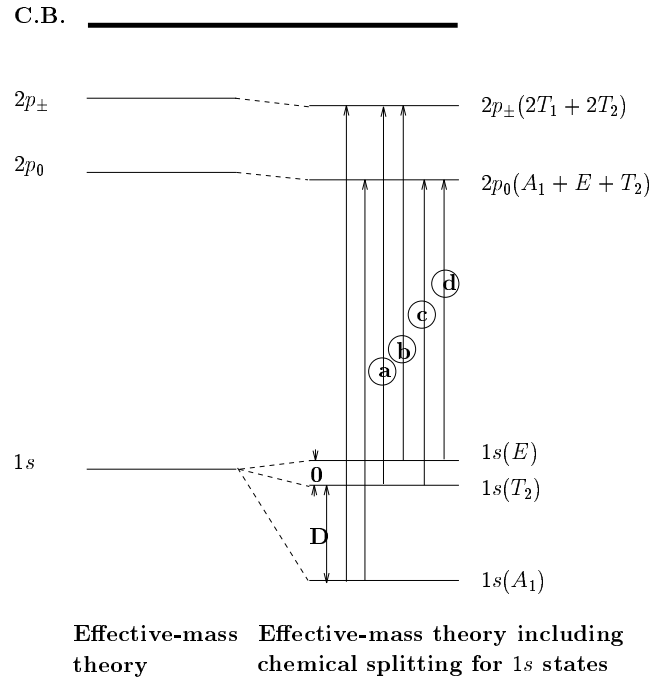
Figure 18.4: Energy-level scheme for transitions from the valley-orbit split $1s$ multiplet of states to the $2p_0, 2p_\pm$ levels. The irreducible representations for the various valley-orbit split levels in T_d symmetry are indicated. The conduction band edge (C.B.) is also indicated.

18.5   Selected Problems

1. Find the symmetries and appropriate linear combination of valley functions for the $1s$ and $2p$ donor levels for germanium (conduction band minima at the L-point in the Brillouin zone), including the effect of valley-orbit interaction. Indicate the transitions expected in the far infrared spectra for these low temperature donor level states.

Chapter 19

Spin Orbit Interaction in Solids and Double Groups

The discussion of angular momentum and the rotation group has thus far been limited to integral values of the angular momentum. The inclusion of half integral angular momentum states requires the introduction of "double groups", which is the focus of this chapter.

19.1 Introduction

The spin angular momentum of an electron is half integral or $S_z = \hbar/2$. Furthermore, associated with each electron is a magnetic moment $\mu_B = -|e|\hbar/(2mc) = 0.927 \times 10^{-20}$ erg/gauss. The magnetic moment and spin angular momentum for the free electron are related by

$$\vec{\mu} = -\frac{|e|}{mc}\vec{S} = -\frac{|e|}{mc}\frac{\hbar}{2}\frac{\vec{S}}{|\vec{S}|} \qquad (19.1)$$

and are oppositely directed. This relation between the spin angular momentum and the magnetic moment gives rise to an interaction, the spin-orbit interaction, which is important in describing the electronic structure of crystalline materials. In this section we briefly review this interaction and then in the following sections of this Chapter, we consider the group theoretical consequences of the half-integral spin and the spin-orbit interaction.

An electron in an atom sees a magnetic field because of its own orbital motion and consequently gives rise to the spin-orbit interaction whereby this internal magnetic field tends to line up its magnetic moment along the magnetic field: $\mathcal{H}_{\text{SO}} = -\vec{\mu} \cdot \vec{H}$. Substitution for $\vec{H} = -(\vec{v}/c) \times \vec{E}$ and $\vec{\mu} = -|e|/(mc)\vec{S}$ together with a factor of 1/2 to make the result correct relativistically yields

$$\mathcal{H}'_{\text{SO}} = \frac{1}{2m^2c^2}(\vec{\nabla}V \times \vec{p}) \cdot \vec{S}. \qquad (19.2)$$

For an atom the corresponding expression is written as

$$\mathcal{H}'_{\text{SO atom}} = \xi(r)\vec{L} \cdot \vec{S} \qquad (19.3)$$

since $\Delta V \sim \vec{r}/r^3$ and where $\vec{L}$ is the orbital angular momentum. A detailed discussion of the spin-orbit interaction is found in standard quantum mechanics text books.

This spin-orbit interaction gives rise to a spin-orbit splitting of atomic levels corresponding to different j values. As an example, consider an atomic p state ($\ell = 1$). Writing the total angular momentum

$$\vec{J} = \vec{L} + \vec{S} \qquad (19.4)$$

where $\vec{L}$ and $\vec{S}$ are, respectively, the orbital angular momentum operator and the spin angular momentum operator, we obtain

$$\vec{J} \cdot \vec{J} = (\vec{L} + \vec{S}) \cdot (\vec{L} + \vec{S}) = \vec{L} \cdot \vec{L} + \vec{S} \cdot \vec{S} + (\vec{L} \cdot \vec{S} + \vec{S} \cdot \vec{L}) \qquad (19.5)$$

in which the operators $\vec{L}$ and $\vec{S}$ commute. Since $\vec{L}$ and $\vec{S}$ are coupled through the spin-orbit interaction, m_ℓ and m_s are no longer good quantum numbers, though ℓ and s remain good quantum numbers. To find the magnitude of the spin-orbit interaction in Eq. (19.2), we need to take the matrix elements of $\mathcal{H}'_{\text{SO}}$ in the $|j, \ell, s, m_j\rangle$ representation. Using Eq. (19.5) for the operators $\vec{J}$, $\vec{L}$ and $\vec{S}$, we obtain the diagonal matrix element of $\vec{J} \cdot \vec{J}$

$$j(j + 1) = \ell(\ell + 1) + s(s + 1) + 2\langle \vec{L} \cdot \vec{S} \rangle / \hbar^2 \qquad (19.6)$$

so that the expectation value of $\vec{L} \cdot \vec{S}$ in the $|j, \ell, s, m_j\rangle$ representation becomes:

$$\langle \vec{L} \cdot \vec{S} \rangle = \frac{\hbar^2}{2}[j(j + 1) - \ell(\ell + 1) - s(s + 1)]. \qquad (19.7)$$
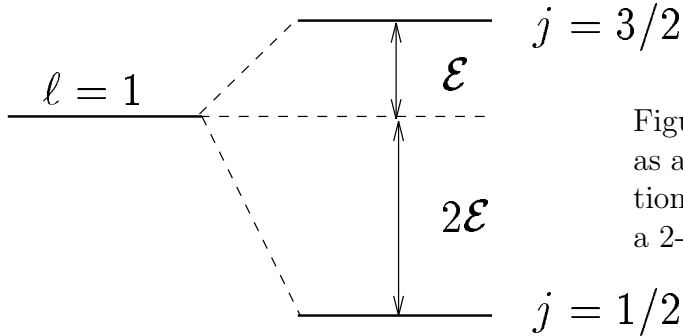
Figure 19.1: Splitting of the p levels as a result of the spin-orbit interaction into a 4-fold $j = 3/2$ level and a 2-fold $j = 1/2$ level.

For p states, we have $\ell = 1$, and $s = 1/2$ so that $j = 3/2$ or $1/2$

$$\langle \vec{L} \cdot \vec{S} \rangle = \hbar^2/2 \qquad \text{for} \quad j = 3/2$$
$$\langle \vec{L} \cdot \vec{S} \rangle = -\hbar^2 \qquad \text{for} \quad j = 1/2. \tag{19.8}$$

Thus the spin-orbit interaction introduces a splitting between the $j = 3/2$ and $j = 1/2$ angular momentum states of the p-levels, as is indicated in Fig. 19.1. From the expression for the expectation value of $\langle \vec{L} \cdot \vec{S} \rangle$, we note that the degeneracy of an s-state is unaffected by the spin-orbit interaction. On the other hand, a d-state is split up into a $D_{5/2}$ (6-fold degenerate) and a $D_{3/2}$ (4-fold degenerate). Thus, the spin-orbit interaction does not lift all the degeneracy of atomic states. To lift the remaining degeneracy, it is necessary to lower the symmetry further, for example, by the application of a magnetic field.

The magnitude of the spin-orbit interaction in atomic physics depends also on the expectation value of $\xi(r)$. For example,

$$\langle n, j, \ell, s, m_j | \mathcal{H}'_{\text{SO}} | n, j, \ell, s, m_j \rangle = \langle j, \ell, s, m_j | \vec{L} \cdot \vec{S} | j, \ell, s, m_j \rangle \int_0^\infty R_{n\ell}^* \xi(r) R_{n\ell} d\vec{r} \tag{19.9}$$

where $R_{n\ell}$ (the radial part of the wave function) has an $\vec{r}$ dependence. The magnitude of the integral in Eq. (19.9) increases rapidly with increasing atomic number Z, approximately as Z^3 or Z^4.

The physical reason behind the strong Z dependence of $\langle \mathcal{H}'_{SO} \rangle$ is that atoms with high Z have more electrons to generate larger internal

Table 19.1: Spin-orbit interaction energies for some important semi-conductors.

Semiconductor	Atomic Number	Γ-point Splitting
Diamond	$Z = 6$	$\Delta = 0.006$ eV
Silicon	$Z = 14$	$\Delta = 0.044$ eV
Germanium	$Z = 32$	$\Delta = 0.29$ eV
InSb $\{$ In	$Z = 49$	$\Delta = 0.9$ eV
Sb	$Z = 51$	

H fields and more electrons with magnetic moments to experience the interaction with these magnetic fields. References for tabulation of the spin-orbit splittings are:

1. C.E. Moore – Atomic Energy Levels (National Bureau of Standards, Circular #467), Vol. 1 (1949), Vol. 2 (1952) and Vol. 3 (1958). These references give the measured spectroscopic levels for any atom in a large number of excited configurations. The lowest Z values are in Vol. 1, the highest in Vol. 3.

2. F. Herman and S. Skillman – Atomic Structure Calculations (Prentice-Hall, Inc. 1963). This reference gives the most complete listing of the calculated atomic levels.

For most atomic species that are important in semiconducting materials, the spin-orbit interaction plays a significant role. Some typical values for the spin-orbit splitting in semiconductors are shown in Table 19.1. The listing in Table 19.1 gives the Γ-point splittings. We will see that in crystalline solids the spin-orbit splittings are k-dependent. For example, at the L-point, the spin-orbit splittings are typically about $2/3$ of the Γ-point value.

The one-electron Hamiltonian for a solid including spin-orbit interaction is

$$\mathcal{H} = \underbrace{\frac{p^2}{2m} + V(r)}_{\mathcal{H}_0} + \underbrace{\frac{1}{2m^2c^2}(\vec{\nabla}V \times \vec{p}) \cdot \vec{S}}_{\mathcal{H}'_{\text{SO}}}. \qquad (19.10)$$
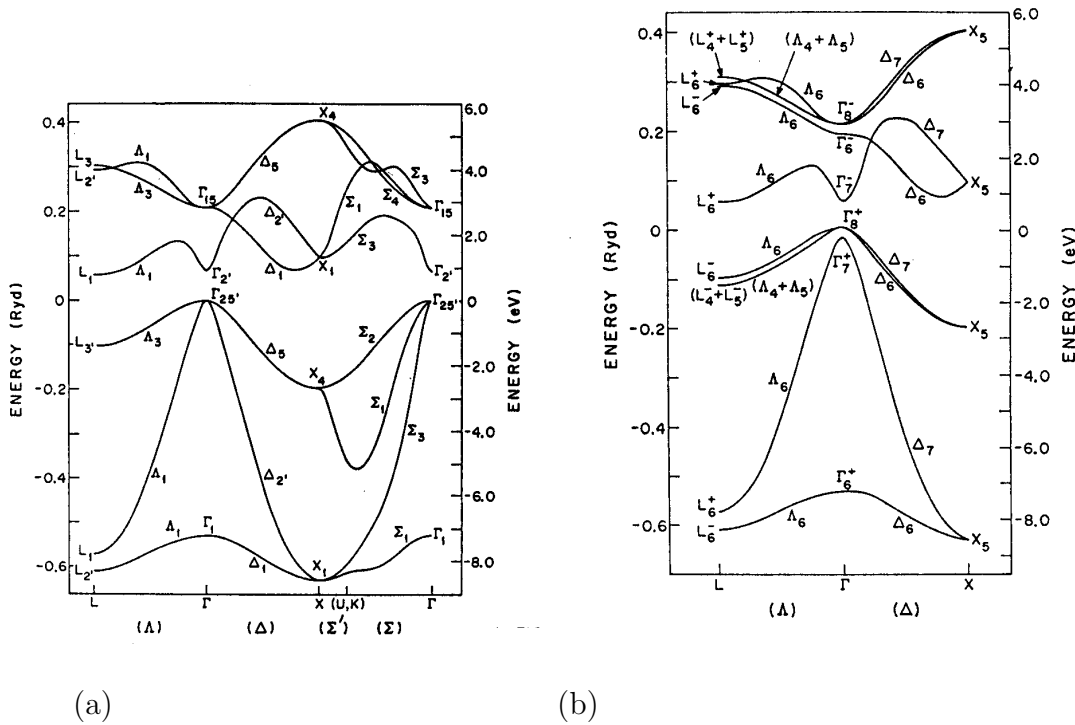
(a)   (b)

Figure 19.2: Energy versus dimensionless wave vector for a few high-symmetry directions in germanium. (a) The spin-orbit interaction has been neglected. (b) The spin-orbit interaction has been included and the bands are labeled by the double group representations.

When the spin-orbit interaction is included, the wave functions consist of a spatial part and a spin part. This means that the irreducible representations that classify the states in a solid must depend on the spin angular momentum. To show the effect of the k-dependence of the spin-orbit interaction on the energy bands of a semiconductor, consider the energy bands for germanium shown in Fig. 19.2(a) along the $\Delta(100)$ axis, $\Lambda(111)$ axis and $\Sigma(110)$ axes for no spin-orbit interaction. Here we show the four bonding and the four anti-bonding s and p bands. This picture is to be compared with the energy bands with spin-orbit interaction shown in Fig. 19.2.

    We note that the Fermi level is between the top of the highest valence band (the $\Gamma_{25'}$ or Γ_{25}^+ band) and the bottom of the lowest conduc-

tion band (the L_1 or L_1^+ band). We note that the energy band extrema for the more common semiconductors usually occur at high symmetry points.

We further note that the inclusion of the spin-orbit interaction has two major effects on the energy band structure affecting both the level degeneracies and the labeling of the energy bands. Note that the ($L_4^\pm +$ $L_5^\pm$) and ($\Lambda_4 + \Lambda_5$) are Kramers-degenerate doublet states, which means that these bands stick together at high symmetry points and along high symmetry directions, because of time reversal symmetry to be discussed in Chapter 21. The Γ_7^+ band which lies below the Γ_8^+ valence band in Fig. 19.2(b) is called the **split-off band**, and the separation between the Γ_7^+ and the Γ_8^+ bands is the Γ-point spin-orbit splitting given in Table 19.1.

19.2   Crystal Double Groups

Figure 19.2(b) shows energy bands that are labeled by irreducible representations of the **double group** for the diamond structure. Double groups come into play when we are dealing with the electron spin, whereby half-integral angular momentum states are introduced. In this section we discuss the double group irreducible representations which arise when the electron spin is introduced.

The character tables for states of half-integral angular momentum are constructed from the same basic formula as we used in Chapter 6 for finding the characters for a rotation by an angle α in the full rotation group:

$$\chi_j(\alpha) = \frac{\sin(j + 1/2)\alpha}{\sin(\alpha/2)}. \tag{19.11}$$

Not only is Eq. (19.11) valid for integral j (as we have discussed in Chapter 6) but the formula is also valid for j equal to half-integral angular momentum states. We will now discuss the special issues that must be considered for the case of half-integral spin.

We note that Eq. (19.11) behaves differently under the transformation $\alpha \to (\alpha + 2\pi)$ depending on whether j is an integral or half-integral angular momentum state. This difference in behavior is responsible for the name of double groups when j is allowed to assume half-integral

values. We first consider how rotation by $\alpha + 2\pi$ is related to a rotation by α:

$$\chi_j(\alpha + 2\pi) = \frac{\sin(j + 1/2)(\alpha + 2\pi)}{\sin\left(\frac{\alpha + 2\pi}{2}\right)} = \frac{\sin(j + 1/2)\alpha \cdot \cos(j + 1/2)2\pi}{\sin(\alpha/2) \cdot \cos\pi}$$

(19.12)

since $\sin(j + 1/2)2\pi = 0$ whether j is an integer or a half-integer. For integral values of j, $\cos(j + 1/2)2\pi = -1$ while for half-integral values of j, $\cos(j + 1/2)2\pi = +1$. Therefore we have the important relation

$$\chi_j(\alpha + 2\pi) = \chi_j(\alpha)(-1)^{2j}$$

(19.13)

which implies that for integral j, a rotation by $\alpha, \alpha \pm 2\pi, \alpha \pm 4\pi$, etc, yields identical characters (integral values of j correspond to odd-dimensional representations of the full rotation group), the dimensionality being given by $2j + 1$. For half-integral values of j, corresponding to the even-dimensional representations of the rotation group, we have

$$\begin{aligned} \chi_j(\alpha \pm 2\pi) &= -\chi_j(\alpha) \\ \chi_j(\alpha \pm 4\pi) &= +\chi_j(\alpha) \end{aligned}$$

(19.14)

so that rotation by 4π is needed to yield the same character for $\chi_j(\alpha)$. The need to rotate by 4π (rather than by 2π) to generate the identity operation leads to the concept of double groups which is the main theme of this chapter.

Although the concept of double groups goes back to 1929 (H.A. Bethe, Ann. der Phys. <u>3</u>, 133 (1929)), experimental evidence that wave functions for Fermions are periodic in 4π and not 2π was not available until 1975 (S.A. Werner, R. Colella, A.W. Overhauser and C.F. Eagen, Phys. Rev. Lett. <u>16</u>, 1053 (1975)) when an ingenious experiment was carried out to measure the phase shift of a neutron due to its precession in a magnetic field. The experiment utilizes a neutron interferometer and determines the phase shift of the neutron as it travels along path AC, where it sees a magnetic field B_{gap} as opposed to path AB where there is no magnetic field, as shown in Fig. 19.3(a). The phase shift measured by counters C_2 and C_3 shows an interference pattern that is periodic, as shown in Fig. 19.3(b), implying a magnetic field precession with a periodicity of 4π.

(a)   (b)
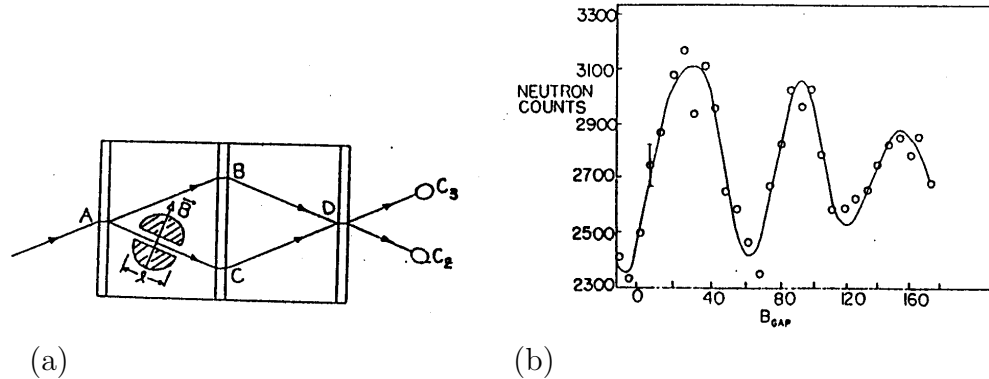
Figure 19.3: (a) A schematic diagram of the neutron interferometer used to establish the phase of the electron wave function along the path AC along which the neutrons are in a magnetic field B (0 to 500 G) for a distance ℓ (2 cm), while the path AB has no magnetic field. (b) The periodic interference pattern as a function of magnetic field, showing a periodicity of 4π, is presented on the right.

To account for this behavior of the wave function, it is convenient to **introduce a new group element** in dealing with symmetry properties of crystals for which half-integral values of the angular momentum arise as, for example, through the introduction of the electron spin.

Let $\mathcal{R}$ denote a rotation by 2π, and now let us assume that $\mathcal{R} = \pm E$ or equivalently $\mathcal{R}^2 = E$, since the rotation by 4π leaves the characters for the full rotation group invariant for both integral and half-integral j values. Suppose that the elements of the crystal group without the electron spin are $E, A_2, A_3, \ldots, A_h$. Then with spin we have twice as many group elements. That is, we have the same h elements that we had before the spin on the electron was considered, plus h new elements of the form $\mathcal{R}A_i$. Just as the matrix representation for the identity operator E is the unit matrix 1 and for $\mathcal{R}E$ it is ± 1, the matrix representation for A_i is $D^{(\Gamma_j)}(A_i)$ and for $\mathcal{R}A_i$ it is $\pm D^{(\Gamma_j)}(A_i)$, depending upon whether the representation Γ_j is related by compatibility relations to even- or odd-dimensional representations of the full rotation group. The introduction of this symmetry element $\mathcal{R}$ leads to no difficulties with the quantum mechanical description of the problem, since the wave functions ψ and $-\psi$ describe the same physical problem and

the matrices $\pm D^{(\Gamma_j)(A_i)}$ each produce the same linear combination of the basis functions.

Because of the introduction of the symmetry element $\mathcal{R}$, the point groups of the crystal have twice as many elements as before. These point groups also have more classes, but not exactly twice as many classes because some of the elements $\mathcal{R}A_i$ are in the same classes as other elements A_k. For example, according to Eq. (19.11), when j assumes **half-integral values**, then we have for a C_2 operation

$$\chi_j(\pi) = \frac{\sin(j + 1/2)\pi}{\sin(\pi/2)} = 0 \tag{19.15}$$

and

$$\chi_j(\pi \pm 2\pi) = \frac{\sin(j + 1/2)(\pi \pm 2\pi)}{\sin\left(\frac{\pi \pm 2\pi}{2}\right)} = \frac{0}{-1} = 0. \tag{19.16}$$

As presented in §19.3, for some classes of two-fold axes, the elements $\mathcal{R}C_2$ and C_2 are, in fact, in the same class.

19.3 Double Group Properties

We will now state some properties of the even-dimensional representations of the full rotation group and of double groups corresponding to the half-integral angular momentum states. These properties are given here without proof. More complete treatments can be found, for example, in Heine's book on group theory.

We list below four important rules for the properties of double groups.

1. If a set of symmetry operations $\{A_k\}$ forms a class in the original point group, then $\{A_k\}$ and the corresponding symmetry operations for the double group $\{\mathcal{R}A_k\}$ form 2 different classes in the double group, except in the case noted below under heading 2.

2. The exceptions to property 1 are classes of rotations by π, if, and only if, there is another two-fold axis $\perp$ to the 2-fold axis under consideration. In this case only, are C_2 and $\mathcal{R}C_2$ in the same class.

3. Any irreducible representation of the original group is also an irreducible representation of the double group, with the same set of characters.

4. In addition to the irreducible representations described in property 3, there must be additional double group representations, so that we have as many irreducible representations as there are classes. For these additional representations, the characters for the class $\mathcal{R}C_k$ are found from the characters of class C_k according to the relation $\chi(\mathcal{R}C_k) = -\chi(C_k)$. In the special case where property 2 applies and $\{A_k\}$ and $\{\mathcal{R}A_k\}$ are in the same class, then

$$\chi(C_k) = +\chi(\mathcal{R}C_k) = -\chi(\mathcal{R}C_k) = 0 \qquad (19.17)$$

where $\chi(C_k) = +\chi(\mathcal{R}C_k)$ since both types of symmetry operations are in same class. The relation $\chi(C_k) = -\chi(\mathcal{R}C_k)$ follows because the signs of the wavefunctions change as a result of the symmetry operation $\mathcal{R}C_k$. Therefore, for classes obeying property 2, it is always the case that $\chi(C_2)=0$.

We can now write down the characters for double group representations and relate these results to the spin-orbit interaction. In a solid, without spin-orbit coupling

$$\mathcal{H}_0 = \frac{p^2}{2m} + V(\vec{r}). \qquad (19.18)$$

Now if we include the electron spin, but still neglect the spin-orbit interaction, the Bloch functions in the simplest case can be written as

$$\psi_{nk}^{+} = e^{i\vec{k}\cdot\vec{r}}u_{nk}(\vec{r})\alpha$$

$$\psi^-_{nk} = e^{i\vec{k}\cdot\vec{r}} u_{nk}(\vec{r})\beta \tag{19.19}$$

where α, β are the spin up and spin down eigenfunctions for spin $\frac{1}{2}$, and n, k denote the band index and wave number, respectively, and for a single electron with $S_z = \pm\frac{1}{2}$. Without spin-orbit coupling, each state is doubly degenerate and is an eigenstate of S_z. If the spin-orbit interaction is included, then the states are no longer eigenstates of S_z and the wave function becomes some linear combination of the states given by Eq. (19.19):

$$\psi_{nk} = a\psi^+_{nk} + b\psi^-_{nk}. \tag{19.20}$$

The group theoretical way to describe these states is in terms of the direct product $\Gamma_i \otimes D_{1/2}$ of the irreducible representations of the spatial wave functions Γ_i with the irreducible representations of the spin function which we will denote by $D_{1/2}$.

To illustrate how we write the characters for $D_{1/2}$, let us consider cubic crystals with an O symmetry point group. (The results for O_h are immediately obtained from O by taking the direct product $O \otimes i$). From the above, the classes of the double group for O are $E, \mathcal{R}, (3C_4^2 + 3\mathcal{R}C_4^2), 6C_4, 6\mathcal{R}C_4, (6C_2 + 6\mathcal{R}C_2), 8C_3, 8\mathcal{R}C_3$. Having listed the classes (8 in this case), we can now find the characters for $D_{1/2}$ by the formula

$$\chi_j(\alpha) = \frac{\sin(j + 1/2)\alpha}{\sin(\alpha/2)} = \frac{\sin\alpha}{\sin(\alpha/2)} \tag{19.21}$$

since $j = 1/2$. For the Full Rotational Symmetry group, the characters for a rotation by α for the double O point group are:

α	$\chi_{\frac{1}{2}}(\alpha)$	$\chi_{\frac{1}{2}}(\mathcal{R}\alpha)$
0	$\frac{\alpha}{\alpha/2} = 2$	-2
π	0	0
$\frac{\pi}{2}$	$\frac{\sin\frac{\pi}{2}}{\sin\frac{\pi}{4}} = \frac{1}{\frac{1}{\sqrt{2}}} = \sqrt{2}$	$-\sqrt{2}$
$\frac{\pi}{3}$	$\frac{\sin\frac{2\pi}{3}}{\sin\frac{\pi}{3}} = \frac{\frac{\sqrt{3}}{2}}{\frac{\sqrt{3}}{2}} = 1$	-1

This procedure for finding the characters for the spinor $D_{1/2}$ is general and can be done for any point group.

Now we will write down the complete character table for the double group O. In O itself, there are 24 elements, and therefore in the double group derived from O there are $24 \times 2 = 48$ elements. There are 8 classes and therefore 8 irreducible representations. From the ordinary representations for point group O, we already have 5 irreducible representations (see Table 3.32 in Chapter 3). Using rule 2 for the character tables of double group representations, we have the following condition for the dimensionality of the three additional double group representations $(\Gamma_6, \Gamma_7, \Gamma_8)$ that are not present in the original group

$$\sum_i \ell_i^2 = h \tag{19.22}$$

$$1^2 + 1^2 + 2^2 + 3^2 + 3^2 + \ell_6^2 + \ell_7^2 + \ell_8^2 = 48, \tag{19.23}$$

yielding the following restriction on the dimensionalities of the double group irreducible representations:

$$\ell_6^2 + \ell_7^2 + \ell_8^2 = 24. \tag{19.24}$$

This allows us to fill in many of the entries in the double group character table (Table 19.2). For example, we can not have any 5-dimensional representations, because then $\ell_j^2 = 25 > 24$ for a 5-dimensional irreducible representation. Among 1, 2, 3 and 4-dimensional irreducible representations, the only combination we can make to satisfy Eq. (19.24) is:

$$2^2 + 2^2 + 4^2 = 24. \tag{19.25}$$

We already have identified a 2-dimensional irreducible representation of the double group, namely the "spinor" $D_{1/2}$. We see immediately that $D_{1/2}$ obeys all the orthogonality relations, and the characters for $D_{1/2}$ can be added to the character table.

In Table 19.2 we have also filled in zeros for the characters for all the C_2 classes in the extra representations Γ_6^+, Γ_7^+ and Γ_8^+. Using orthogonality and normalization conditions which follow from the wonderful orthogonality theorem on character, it is quite easy to complete this character table. To get the Γ_7^+ representation we have to consider the following:

Table 19.2: Worksheet for the double group characters for the group O.

	E	$\mathcal{R}$	$3C_4^2 + 3\mathcal{R}C_4^2$	$6C_4$	$6\mathcal{R}C_4$	$6C_2 + 6\mathcal{R}C_2$	$8C_3$	$8\mathcal{R}C_3$
Γ_1	1	1	1	1	1	1	1	1
Γ_2	1	1	1	-1	-1	-1	1	1
Γ_{12}	2	2	2	0	0	0	-1	-1
$\Gamma_{15'}$	3	3	-1	1	1	-1	0	0
$\Gamma_{25'}$	3	3	-1	-1	-1	1	0	0
Γ_6^+	2	-2	0	$\sqrt{2}$	$-\sqrt{2}$	0	1	-1
Γ_7^+	2	-2	0			0		
Γ_8^+	4	-4	0			0		

	E	$8C_3$	$6C_4$
Γ_6^+	2	1	$\sqrt{2}$
Γ_7^+	2	x	y

and orthogonality requires $4 + 8x + 6\sqrt{2}y = 0$ which is satisfied for $x = \pm 1$, and $y = -\sqrt{2}$. Having filled in those entries it is easy to get the 4-dimensional representation:

	E	$8C_3$	$6C_4$
Γ_6^+	2	1	$\sqrt{2}$
Γ_7^+	2	1	$-\sqrt{2}$
Γ_8^+	4	x	y

Orthogonality now requires: $8 + 8x \pm \sqrt{2}y = 0$ which is satisfied for $x = -1$, $y = 0$. So now we have the whole character table, as shown in Table 19.3.

In practice, we don't have to construct these character tables because the double group character tables have already been tabulated, e.g., Koster's article in Vol. 5 of the Seitz–Turnbull series, or the book on the "Properties of the 32 Point Groups" by Koster, Dimmock, Wheeler and Statz (QD911 .K86), or Miller and Love.

We will now apply the double group characters to a cubic crystal with O_h symmetry at the Γ point, $\vec{k} = 0$. The spin functions α and β

Table 19.3: Double group character table for the group O.

O	E	$\mathcal{R}$	$3C_4^2 + 3\mathcal{R}C_4^2$	$6C_4$	$6\mathcal{R}C_4$	$6C_2 + 6\mathcal{R}C_2$	$8C_3$	$8\mathcal{R}C_3$
Γ_1	1	1	1	1	1	1	1	1
Γ_2	1	1	1	-1	-1	-1	1	1
Γ_{12}	2	2	2	0	0	0	-1	-1
$\Gamma_{15'}$	3	3	-1	1	1	-1	0	0
$\Gamma_{25'}$	3	3	-1	-1	-1	1	0	0
Γ_6	2	-2	0	$\sqrt{2}$	$-\sqrt{2}$	0	1	-1
Γ_7	2	-2	0	$-\sqrt{2}$	$\sqrt{2}$	0	1	-1
Γ_8	4	-4	0	0	0	0	-1	1

Table 19.4: Direct products $\Gamma_i \otimes \Gamma_6^+$ for O_h symmetry.

$$
\begin{array}{l|l}
\Gamma_1^+ \otimes \Gamma_6^+ = \Gamma_6^+ & \Gamma_1^- \otimes \Gamma_6^+ = \Gamma_6^- \\
\Gamma_2^+ \otimes \Gamma_6^+ = \Gamma_7^+ & \Gamma_2^- \otimes \Gamma_6^+ = \Gamma_7^- \\
\Gamma_{12}^+ \otimes \Gamma_6^+ = \Gamma_8^+ & \Gamma_{12}^- \otimes \Gamma_6^+ = \Gamma_8^- \\
\Gamma_{15}^+ \otimes \Gamma_6^+ = \Gamma_6^+ + \Gamma_8^+ & \Gamma_{15}^- \otimes \Gamma_6^+ = \Gamma_6^- + \Gamma_8^- \\
\Gamma_{25}^+ \otimes \Gamma_6^+ = \Gamma_7^+ + \Gamma_8^+ & \Gamma_{25}^- \otimes \Gamma_6^+ = \Gamma_7^- + \Gamma_8^-
\end{array}
$$

transform as the partners of the irreducible representation $D_{1/2}$ which is written as Γ_6^+. Now we see that the appropriate double group representations (which must be used when the effects of the electron spin are included) are obtained by taking the direct product of the irreducible representation Γ_i with the spinor $(D_{1/2})$ as shown in Table 19.4.

When the spin-orbit interaction is introduced into the description of the electronic structure, then the energy bands are labeled by double group irreducible representations (e.g., $\Gamma_6^\pm, \Gamma_7^\pm$ and $\Gamma_8^\pm$ for the O_h group at $\vec{k} = 0$). Table 19.4 shows that the 1-dimensional representations without spin-orbit interaction $\Gamma_1^\pm$ and $\Gamma_2^\pm$ all become **doubly degenerate**. This result is independent of the symmetry group. When the spin-orbit interaction is introduced, all formerly non-degenerate levels therefore become double degenerate. (This effect is called the *Kramers degeneracy*.)

In the case of the O_h group, the 2-fold levels $\Gamma_{12}^{\pm}$ become 4-fold degenerate when spin is included as is shown in Table 19.4. However something different happens for the triply degenerate $\Gamma_{15}^{\pm}$ and $\Gamma_{25}^{\pm}$ states. These states would become 6-fold degenerate with spin, but the spin-orbit interaction partly lifts this degeneracy so that these 6-fold levels split into a 2-fold and a 4-fold level, just as in the atomic case. Group theory does not tell us the ordering of these levels, nor the magnitude of the splitting, but it does give the symmetry of the levels. By including the spin-orbit interaction in dealing with the valence band of a semiconductor like germanium, the 6-fold level can be partially diagonalized; the (6×6) $\vec{k} \cdot \vec{p}$ effective Hamiltonian breaks up into a (2×2) block and a (4×4) block.

Figures 19.2(a) and (b) show the effect of the spin-orbit interaction on the energy bands of germanium. We note that the magnitudes of the spin-orbit splittings are $\vec{k}$ **dependent**. These effects are largest at $\vec{k} = 0$, moderately large along the (111) direction (Λ) and at the L-point, but much smaller along the (100) direction (Δ) and at the X-point. Group theory doesn't provide information on these relative magnitudes.

As was mentioned above, the spin-orbit interaction effects tend to be very **important** in the **III–V compound semiconductors**. Since in this case the two atoms in the unit cell correspond to different species, the appropriate point group at $\vec{k} = 0$ is T_d and the bonding and anti-bonding bands both have symmetries Γ_1 and Γ_{15}. The general picture of the energy bands for the III–V compounds is qualitatively similar to that given in Figs. 19.2(a) and (b) except for a generally larger spin-orbit splitting.

Another important class of semiconductors where the spin-orbit interaction is important is the narrow gap lead salts (e.g., PbTe). Since Pb has a high atomic number it is necessary to give a more exact theory for the spin-orbit interaction in this case including relativistic correction terms. However, the group theoretical considerations given here apply equally well. Setting up a secular equation when the spin-orbit interaction is large, as for example in the lead salts, is treated in J.B. Conklin, L.E. Johnson and G.W. Pratt, Jr., Phys. Rev. <u>137</u>, A1282 (1965).

In writing down the double group irreducible representations, we see that a particular representation may be associated with various single group representations. For example, the direct products in Table 19.4 show that the Γ_7^+ irreducible double group representation could be associated with either a Γ_2^+, $a\Gamma_{15}^+$ or a Γ_{25}^+ irreducible single group representation. In dealing with basis functions in the double group representations it is often useful to know which single group representation corresponds to a particular double group representation. The standard notation used for this association is for example $\Gamma_8^+(\Gamma_{12}^+)$, in which the appropriate single group representation is put in parenthesis, indicating that Γ_8^+ arises from the direct product $\Gamma_{12}^+ \otimes \Gamma_6^+$ rather than from one of the other possibilities listed in Table 19.4.

19.4   Crystal Field Splitting Including Spin-Orbit Coupling

In our treatment of crystal field splittings in solids in chapter 6 we ignored the spin-orbit coupling. The treatment in Chapter 6 thus provided a first approximation for describing the crystal field levels for the impurity ions in a host lattice. To improve on this, we consider in this chapter the effect of the spin-orbit interaction which will allow us to treat crystal field splittings in host lattices with rare earth ions, and also to obtain a better approximation to the crystal field splittings for $3d$ transition metal ions discussed in Chapter 6.

The introduction of a transition-metal ion in an atomic d-state into an octahedral crystal field gives rise to crystal field splittings as shown in Fig. 19.4 (see §6.4).   For a single d-electron, $s = 1/2$ and the appropriate double group representation for the spinor is Γ_6^+. Thus when the spin-orbit interaction is included in the crystal field problem, the d-levels are further split. Thus the 2-fold crystal field level in cubic symmetry transforms as

$$\Gamma_{12}^+ \otimes \Gamma_6^+ = \Gamma_8^+ \tag{19.26}$$

and the 3-fold crystal field level in O_h symmetry is split according to

$$\Gamma_{25}^+ \otimes \Gamma_6^+ = \Gamma_7^+ + \Gamma_8^+. \tag{19.27}$$
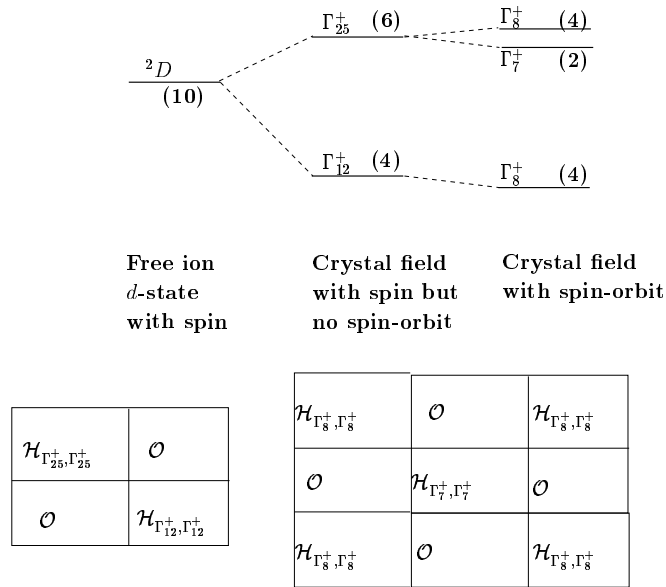
Figure 19.4: Schematic diagram of the crystal field splitting of a ^2D state, followed by further splitting by the spin-orbit interaction. This model is appropriate for a $3d$ transition metal ion in a crystal with O_h symmetry. The degeneracy of each of the levels is indicated by the parentheses. Also shown in this figure are the labels for the crystal field levels associated with each of the Γ_8^+ levels in the absence of the spin-orbit interaction. Below the crystal field splitting diagram, the form of the crystal field Hamiltonian is indicated on the left, in the absence of the spin-orbit interaction, and on the right when the spin-orbit interaction is included.
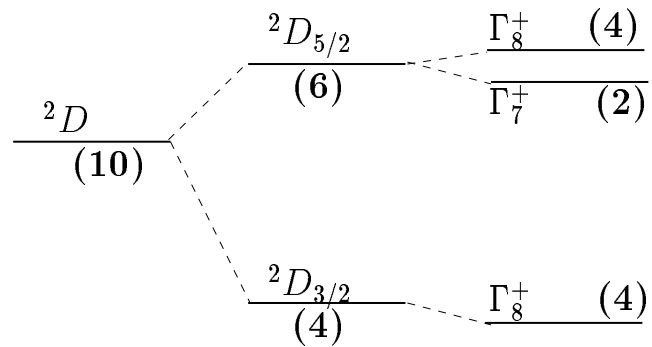
Figure 19.5: Schematic diagram of the spin-orbit splitting of a ^2D level and of the subsequent crystal field splittings of these levels in a cubic field for an ion with a spin-orbit interaction that is large compared to the crystal field splittings. The degeneracy of each level is shown in parentheses.

Table 19.5: Decomposition of double group representations for a d band.

	E	$\mathcal{R}$	$3C_4^2 + 3\mathcal{R}C_4^2$	$6C_4$	$6\mathcal{R}C_4$	$6C_2 + 6\mathcal{R}C_2$	$8C_3$	$8\mathcal{R}C_3$
$\chi(^2D_{5/2})$	6	-6	0	$-\sqrt{2}$	$\sqrt{2}$	0	0	0
$\chi(^2D_{3/2})$	4	-4	0	0	0	0	-1	1

In Eqs. (19.26) and (19.27) Γ_{12}^+ and Γ_{25}^+ denote the spatial wave-functions and Γ_6^+ denotes the spin wave-function. Here we see that the E_g level does not split further but the T_{2g} level splits into a 2-fold and a 4-fold level.

For the ^2D state of the $3d$ transition-metal ion in a host crystal, we use Fig. 19.4 (where the number of states is given in parentheses). The analysis in Fig. 19.4 is valid only if the **crystal field interaction is large compared with the spin-orbit splitting**. This situation describes the iron-group transition metal ions.

When we move down the periodic table to the palladium group ($4d$) and the platinum group ($5d$), the spin-orbit interaction is large compared with the crystal field. In this case, we consider first the spin-orbit splitting of the free ion state as the major perturbation (see Fig. 19.5). We now have to consider the effect of the crystal field on these levels. To compute the characters for the full rotation group we use the formula

$$\chi_j(\alpha) = \frac{\sin(j + 1/2)\alpha}{\sin(\alpha/2)}. \tag{19.28}$$

We then find the characters for the $^2D_{5/2}$ and $^2D_{3/2}$ states to see how they split in the cubic field (see Table 19.5). Using Table 19.5 we see immediately that

$$\chi_{^2D_{5/2}} \to \Gamma_7 + \Gamma_8 \tag{19.29}$$

$$\chi_{^2D_{3/2}} \to \Gamma_8 \tag{19.30}$$

as indicated in Fig. 19.5. The symmetries in Figs. 19.4 and 19.5 for the levels in the presence of both the spin-orbit interaction and the cubic field of the crystalline solid are $\Gamma_7^+ + 2\Gamma_8^+$ in both cases. However in Fig. 19.5, the crystal field splittings are small compared with the spin-orbit splittings in contrast to the case in Fig. 19.4.

Let us consider another example of crystal field levels that show some new features. Consider the levels of the holmium ion Ho^{3+} in a cubic field for which the atomic configuration is $4f^{10}5s^25p^6$ so that by Hund's rule the ground state after the spin-orbit interaction is included becomes $s = 2$, $l = 6$, $j = 8$ denoted by the spectroscopic notation $^5I_8$. Since $j = 8$ is an integer, application of the formula

$$\chi_j(\alpha) = \left\{ \frac{\sin(j + 1/2)\alpha}{\sin(\alpha/2)} \right\} \tag{19.31}$$

gives only ordinary irreducible representations, even though the electron spin is included. We thus get for the characters for the ground state $^5I_8$:

	E	$3C_4^2$	$6C_4$	$6C_2$	$8C_3$
$\chi(^5I_8)$	17	1	1	1	-1
$\chi(^4I_{15/2})$	16	0	0	0	-1

Decomposition of the $\chi(^5I_8)$ level into irreducible representations of O_h yields

$$\chi(^5I_8) \rightarrow \Gamma_1 + 2\Gamma_{12} + 2\Gamma_{15} + 2\Gamma_{25} \tag{19.32}$$

where there are 7 levels for 17 states.

Finding the crystal field splittings for a 17-fold level would be a very difficult problem without group theory. As another example, let us consider the erbium ion Er^{3+} in a host crystal. This ion is the basis for recent applications of amplification capabilities in optical fibers.

We consider the level splitting for the rare earth ion Er^{3+} in a $4f^{11}5s^2p^6$ which gives a $^4I_{15/2}$ ground state. The characters for the $j = 15/2$ state are given in the above table and the splitting of these states in a cubic O_h field is also included in the Table above. The $j = 15/2$ state splits in cubic symmetry into:

$$\chi(^4I_{15/2}) \rightarrow \Gamma_6 + \Gamma_7 + 3\Gamma_8.$$

In dealing with the crystal field problem, we often encounter a situation where a perturbation is applied to lower the crystal symmetry.

In such cases we follow the procedure which we have used many times before – the irreducible representation of the high symmetry group is treated as a reducible representation for the lower symmetry group and we look for the irreducible representations contained therein. The only difference in including the spin-orbit interaction is the use of double groups for all point groups – both for the high symmetry and the low symmetry groups. It is the case that the single group irreducible representations in a group of higher symmetry will always go into single group irreducible representations of the lower symmetry group. For example, the level Γ_8 in point group O goes into $\Gamma_4 + \Gamma_5 + \Gamma_6$ in point group D_3, when the symmetry is lowered.

In considering optical transitions between crystal field states which are described by either single or double group representations, the electromagnetic interaction Hamiltonian will in all cases transform as the vector within the single group representations. Thus, we can write

$$\Gamma_{15}^- \otimes \Gamma_7^- = \Gamma_7^+ + \Gamma_8^+ \tag{19.33}$$

for the coupling of the electromagnetic field to the conduction band of germanium at $\vec{k} = 0$. Thus, single group states are optically coupled to other single group states and double group states are optically coupled to other double group states,

Whereas the wave function for a single electron transforms as $D_{1/2}$ (or Γ_6^+ for O_h symmetry), a two-electron wavefunction transforms as the direct product $D_{1/2} \otimes D_{1/2}$. For O_h symmetry, we have

$$\Gamma_6^+ \otimes \Gamma_6^+ = \Gamma_1^+ + \Gamma_{15}^+ \tag{19.34}$$

where Γ_1^+ is the singlet $s = 0$ state and the Γ_{15}^+ corresponds to the triplet $s = 1$ level. We note that in both cases the levels have integral values of spin angular momentum and thus the state transforms as a single group irreducible representation. Finally we note that for a $D_{3/2}$ p-state in full rotational symmetry, the double group irreducible representation in cubic symmetry is Γ_8^- and no further splitting occurs.

19.5   Comment on the Use of the Koster et al. Reference for Double Groups

An important group theory reference book on the 32 point groups and their double groups is "Properties of the Thirty-Two Point Groups", by G.F. Koster, J.O. Dimmock, R.G. Wheeler and H. Statz (QD911 .K86). The book is especially valuable for its many useful tables including tables for double groups. In this reference you will find for each of the 32 point groups:

1. a character table including the double group representations (see e.g., Table 19.6 for groups O and T_d);

2. a table giving the decomposition of the direct product of any 2 irreducible representations (an example of such a table is given in Table 19.7);

3. tables of coupling coefficients for the product of any two basis functions (which are explained in Table 19.8);

4. compatibility tables with other point groups (Table 19.10);

5. compatibility tables with the Full Rotation Group (Table 19.11).

We will illustrate some examples of these tables for the group O, which is tabulated together with T_d (p. 88–101 in Koster's book). The first table we reproduce is (Table 19.6). Note the listing of the double group representations and basis functions for the double group representations. The basis functions for $\Gamma_4(\Gamma_{15})$ are S_x, S_y, S_z which refer to the three Cartesian components of the angular momentum (integral values of angular momentum). The **basis functions for the Γ_6 and Γ_8 irreducible representations are written in the basic form $\phi(j, m_j)$ for the angular momentum and all the m_j partners are listed**. Koster et al. use the notation $\bar{E}$ for $\mathcal{R}$ and they use $\bar{C}_3$ for $\mathcal{R}C_3$. The meaning of the time inversion entries will be explained in Chapter 21 where **time inversion symmetry** is discussed.

Table 19.7 for groups O and T_d gives the decomposition of the direct product of any irreducible representation labeling a column with one

Table 19.6: Character Table and Basis Functions for the Groups O and T_d

O	E	$\bar{E}$	$8C_3$	$8\bar{C}_3$	$3C_2$ $3\bar{C}_2$	$6C_4$	$6\bar{C}_4$	$6C_2'$ $6\bar{C}_2'$			
T_d	E	$\bar{E}$	$8C_3$	$8\bar{C}_3$	$3C_2$ $3\bar{C}_2$	$6S_4$	$6\bar{S}_4$	$6\sigma_d$ $6\bar{\sigma}_d$	Time Inv.	Bases for O	Bases for T_d
Γ_1	1	1	1	1	1	1	1	1	a	R	R or xyz
Γ_2	1	1	1	1	1	-1	-1	-1	a	xyz	$S_x S_y S_z$
$\Gamma_3(\Gamma_{12})$	2	2	-1	-1	2	0	0	0	a	$(2z^2-x^2-y^2),$ $\sqrt{3}(x^2-y^2)$	$(2z^2-x^2-y^2),$ $\sqrt{3}(x^2-y^2)$
$\Gamma_4(\Gamma_{15})$	3	3	0	0	-1	1	1	-1	a	S_x, S_y, S_z	S_x, S_y, S_z
$\Gamma_5(\Gamma_{25})$	3	3	0	0	-1	-1	-1	1	a	yz, xz, xy	x, y, z
Γ_6	2	-2	1	-1	0	$\sqrt{2}$	$-\sqrt{2}$	0	c	$\phi(1/2,-1/2),$ $\phi(1/2,1/2)$	$\phi(1/2,-1/2),$ $\phi(1/2,1/2)$
Γ_7	2	-2	1	-1	0	$-\sqrt{2}$	$\sqrt{2}$	0	c	$\Gamma_6 \otimes \Gamma_2$	$\Gamma_6 \otimes \Gamma_2$
Γ_8	4	-4	-1	1	0	0	0	0	c	$\phi(3/2,-3/2),$ $\phi(3/2,-1/2),$ $\phi(3/2,1/2),$ $\phi(3/2,3/2)$	$\phi(3/2,-3/2),$ $\phi(3/2,-1/2),$ $\phi(3/2,1/2),$ $\phi(3/2,3/2)$

Table 19.7: Table of direct products of irreducible representations for the groups O and T_d

Γ_1	Γ_2	Γ_3	Γ_4	Γ_5	Γ_6	Γ_7	Γ_8	
Γ_1	Γ_2	Γ_3	Γ_4	Γ_5	Γ_6	Γ_7	Γ_8	Γ_1
	Γ_1	Γ_3	Γ_5	Γ_4	Γ_7	Γ_6	Γ_8	Γ_2
		$\Gamma_1+\Gamma_2+\Gamma_3$	$\Gamma_4+\Gamma_5$	$\Gamma_4+\Gamma_5$	Γ_8	Γ_8	$\Gamma_6+\Gamma_7+\Gamma_8$	Γ_3
			$\Gamma_1+\Gamma_3+\Gamma_4+\Gamma_5$	$\Gamma_2+\Gamma_3+\Gamma_4+\Gamma_5$	$\Gamma_6+\Gamma_8$	$\Gamma_7+\Gamma_8$	$\Gamma_6+\Gamma_7+2\Gamma_8$	Γ_4
				$\Gamma_1+\Gamma_3+\Gamma_4+\Gamma_5$	$\Gamma_7+\Gamma_8$	$\Gamma_6+\Gamma_8$	$\Gamma_6+\Gamma_7+2\Gamma_8$	Γ_5
					$\Gamma_1+\Gamma_4$	$\Gamma_2+\Gamma_5$	$\Gamma_3+\Gamma_4+\Gamma_5$	Γ_6
						$\Gamma_1+\Gamma_4$	$\Gamma_3+\Gamma_4+\Gamma_5$	Γ_7
							$\Gamma_1+\Gamma_2+\Gamma_3$ $+2\Gamma_4+2\Gamma_5$	Γ_8

labeling a row, which is entered in the matrix position of their intersection. In our experience with Koster et al., there are a few typographical errors in the tables, so beware!

The extensive tables of coupling coefficients are perhaps the most useful tables in Koster et al. These tables give the basis functions for the irreducible representations obtained by taking the direct product of two irreducible representations. We illustrate in Table 19.8 the basis functions obtained by taking the direct product of each of the two partners of the Γ_{12} representation (denoted by Koster et al. as u_1^3 and u_2^3) with each of the 3 partners of the Γ_{15} representation (denoted as v_x^4, v_y^4, v_z^4) to yield 3 partners with Γ_{15} symmetry (denoted by $\psi_x^4, \psi_y^4, \psi_z^4$)

Table 19.8: Coupling coefficients for the indicated basis functions for single group O.

	$u_1^3 v_x^4$	$u_1^3 v_y^4$	$u_1^3 v_z^4$	$u_2^3 v_x^4$	$u_2^3 v_y^4$	$u_2^3 v_z^4$
ψ_x^4	$-1/2$	0	0	$\sqrt{3}/2$	0	0
ψ_y^4	0	$-1/2$	0	0	$-\sqrt{3}/2$	0
ψ_z^4	0	0	1	0	0	0
ψ_{yz}^5	$-\sqrt{3}/2$	0	0	$-1/2$	0	0
ψ_{xz}^5	0	$\sqrt{3}/2$	0	0	$-1/2$	0
ψ_{xy}^5	0	0	0	0	0	1

and 3 partners with Γ_{25} symmetry (denoted by $\psi_{yz}^5, \psi_{zx}^5, \psi_{xy}^5$). This is table 83 on p. 91 of Koster et al. From Table 19.8 we see that the appropriate linear combinations for the ψ^4 and ψ^5 functions are:

$$
\begin{aligned}
\psi_x^4 &= -(1/2)u_1^3 v_x^4 + (\sqrt{3}/2)u_2^3 v_x^4 \\
\psi_y^4 &= -(1/2)u_1^3 v_y^4 - (\sqrt{3}/2)u_2^3 v_y^4 \\
\psi_z^4 &= u_1^3 v_z^4 \\
\psi_{yz}^5 &= -(\sqrt{3}/2)u_1^3 v_x^4 - (1/2)u_2^3 v_x^4 \\
\psi_{xz}^5 &= (\sqrt{3}/2)u_1^3 v_y^4 - (1/2)u_2^3 v_y^4 \\
\psi_{xy}^5 &= u_2^3 v_z^4
\end{aligned}
$$

Note that the basis functions for the ψ^4 and ψ^5 functions depend on the choice of basis functions for u and v. Journal articles often use the notation

$$\Gamma_{15} \otimes \Gamma_{12} = \Gamma_{15} + \Gamma_{25} \tag{19.35}$$

where $\Gamma_4 \leftrightarrow \Gamma_{15}$ and $\Gamma_3 \leftrightarrow \Gamma_{12}$. Thus taking the direct product between irreducible representations Γ_3 and Γ_4 in O or T_d symmetries yields:

$$\Gamma_4 \otimes \Gamma_3 = \Gamma_4 + \Gamma_5 \tag{19.36}$$

where $\Gamma_5 \leftrightarrow \Gamma_{25}$.

We next illustrate the use of a typical coupling coefficient table relevant to the introduction of spin into the electronic energy level

Table 19.9: Coupling coefficient tables for the indicated basis functions for double group O_h.

	$u_x^4 v_{-1/2}^6$	$u_x^4 v_{1/2}^6$	$u_y^4 v_{-1/2}^6$	$u_y^4 v_{1/2}^6$	$u_z^4 v_{-1/2}^6$	$u_z^4 v_{1/2}^6$
$\psi_{-1/2}^6$	0	$-i/\sqrt{3}$	0	$-1/\sqrt{3}$	$i/\sqrt{3}$	0
$\psi_{1/2}^6$	$-i/\sqrt{3}$	0	$1/\sqrt{3}$	0	0	$-i/\sqrt{3}$
$\psi_{-3/2}^8$	$i/\sqrt{2}$	0	$1/\sqrt{2}$	0	0	0
$\psi_{-1/2}^8$	0	$i/\sqrt{6}$	0	$1/\sqrt{6}$	$i\sqrt{2}/\sqrt{3}$	0
$\psi_{1/2}^8$	$-i/\sqrt{6}$	0	$1/\sqrt{6}$	0	0	$i\sqrt{2}/\sqrt{3}$
$\psi_{3/2}^8$	0	$-i/\sqrt{2}$	0	$1/\sqrt{2}$	0	0

problem. In this case we need to take a direct product of Γ_6^+ with a single group representation, where Γ_6^+ is the representation for the spinor $(D_{1/2})$. For example, for a p-level $\Gamma_{15}^- \otimes \Gamma_6^+ = \Gamma_6^- + \Gamma_8^-$ and the appropriate coupling coefficient table is Table 19.9 (in Koster et al. Table 83, p. 92).

Table 19.9 gives us the following relations between basis functions:

$$\psi_{-1/2}^6 = \left|\frac{1}{2}, -\frac{1}{2}\right\rangle = -(i/\sqrt{3})(u_x^4 - iu_y^4)\uparrow + (i/\sqrt{3})u_z^4\downarrow$$

$$\psi_{1/2}^6 = \left|\frac{1}{2}, \frac{1}{2}\right\rangle = -(i/\sqrt{3})(u_x^4 + iu_y^4)\downarrow - (i/\sqrt{3})u_z^4\uparrow$$

$$\psi_{-3/2}^8 = \left|\frac{3}{2}, -\frac{3}{2}\right\rangle = (i/\sqrt{2})(u_x^4 - iu_y^4)\downarrow$$

$$\psi_{-1/2}^8 = \left|\frac{3}{2}, -\frac{1}{2}\right\rangle = (i/\sqrt{6})(u_x^4 - iu_y^4)\uparrow + (i\sqrt{2}/\sqrt{3})u_z^4\downarrow$$

$$\psi_{1/2}^8 = \left|\frac{3}{2}, \frac{1}{2}\right\rangle = -(i/\sqrt{6})(u_x^4 - iu_y^4)\downarrow + (i\sqrt{2}/\sqrt{3})u_z^4\uparrow$$

$$\psi_{3/2}^8 = \left|\frac{3}{2}, \frac{3}{2}\right\rangle = -(i/\sqrt{2})(u_x^4 + iu_y^4)\uparrow \qquad (19.37)$$

where we note that $\Gamma_{15}^- = \Gamma_4$ and $v_{1/2}^6 = \uparrow$ and $v_{-1/2}^6 = \downarrow$. The relations in Eq. (19.37) give the transformation of basis functions in the $|\ell s m_\ell m_s\rangle$ representation to the $|j\ell s m_j\rangle$ representation, appropriate to energy bands for which the spin-orbit interaction is included. These

Table 19.10: Compatibility Table

T_d	O	Γ_1	Γ_2	Γ_3	Γ_4	Γ_5	Γ_6	Γ_7	Γ_8
T	T	Γ_1	Γ_1	$\Gamma_2 + \Gamma_3$	Γ_4	Γ_4	Γ_5	Γ_5	$\Gamma_6 + \Gamma_7$
D_{2d}	D_4	Γ_1	Γ_3	$\Gamma_1 + \Gamma_3$	$\Gamma_2 + \Gamma_5$	$\Gamma_4 + \Gamma_5$	Γ_6	Γ_7	$\Gamma_6 + \Gamma_7$
$C_{3v}; E(w)$	D_3	Γ_1	Γ_2	Γ_3	$\Gamma_2 + \Gamma_3$	$\Gamma_1 + \Gamma_3$	Γ_4	Γ_4	$\Gamma_4 + \Gamma_5 + \Gamma_6$
$S_4 : H(z)$	$C_4 : H(z) : E(z)$	Γ_1	Γ_1	$\Gamma_2 + \Gamma_3$	$\Gamma_1 + \Gamma_2 + \Gamma_3$	$\Gamma_1 + \Gamma_2 + \Gamma_3$	$\Gamma_4 + \Gamma_5$	$\Gamma_4 + \Gamma_5$	$\Gamma_5 + \Gamma_6 + \Gamma_7 +$
$C_{2v} : E(z)$		Γ_1	Γ_3	$\Gamma_1 + \Gamma_3$	$\Gamma_2 + \Gamma_3 + \Gamma_4$	$\Gamma_1 + \Gamma_2 + \Gamma_4$	Γ_5	Γ_5	$2\Gamma_5$
$C_s : E(v) : H(v)$	$C_2 : E(v) : H(v)$	Γ_1	Γ_2	$\Gamma_1 + \Gamma_2$	$\Gamma_1 + 2\Gamma_2$	$2\Gamma_1 + \Gamma_2$	$\Gamma_3 + \Gamma_4$	$\Gamma_3 + \Gamma_4$	$2\Gamma_3 + 2\Gamma_4$

linear combinations are basically the **Clebsch-Gordan coefficients** in quantum mechanics. We make use of Eq. (19.37) in the next section when we discuss the introduction of spin and spin-orbit interaction into the plane wave relations of the energy eigenvalues of the empty lattice.

Table 19.10 gives the point groups that are subgroups of Groups T_d and O, and the decomposition of the irreducible representations of T_d and O into the irreducible representations of the lower symmetry group. Note in Table 19.10 that E refers to the electric field and H to the magnetic field. The table can be used for many applications such as finding the resulting symmetries under crystal field splittings as for example $O_h \rightarrow D_3$.

The notation for each of the irreducible representations is consistent with that given in the character tables of Koster's book. The decomposition of the irreducible representations of the full rotation group into irreducible representations of groups O and T_d is given in Tables 19.11 and 19.12. Note that all the irreducible representations of the full rotation group are listed, with the $\pm$ sign denoting the parity (even or odd under inversion) and the subscript giving the angular momentum quantum number (j), so that the dimensionality of the irreducible representation $D_j^{\pm}$ is $(2j + 1)$.

19.6   Plane Wave Basis Functions for Double Group Representations

In Chapter 16 we discussed the nearly free electron approximation for the energy bands in crystalline solids, neglecting the electron spin. In this case the electron wave functions were expressed in terms of symmetrized linear combinations of plane waves transforming according to irreducible representations of the group of the wave vector.

Table 19.11: Full Rotation Group Compatibility Table for the Group O

S	D_0^+	Γ_1
P	D_1^-	Γ_4
D	D_2^+	$\Gamma_3 + \Gamma_5$
F	D_3^-	$\Gamma_2 + \Gamma_4 + \Gamma_5$
G	D_4^+	$\Gamma_1 + \Gamma_3 + \Gamma_4 + \Gamma_5$
H	D_5^-	$\Gamma_3 + 2\Gamma_4 + \Gamma_5$
I	D_6^+	$\Gamma_1 + \Gamma_2 + \Gamma_3 + \Gamma_4 + 2\Gamma_5$
	$D_{1/2}^\pm$	Γ_6
	$D_{3/2}^\pm$	Γ_8
	$D_{5/2}^\pm$	$\Gamma_7 + \Gamma_8$
	$D_{7/2}^\pm$	$\Gamma_6 + \Gamma_7 + \Gamma_8$
	$D_{9/2}^\pm$	$\Gamma_6 + 2\Gamma_8$
	$D_{11/2}^\pm$	$\Gamma_6 + \Gamma_7 + 2\Gamma_8$
	$D_{13/2}^\pm$	$\Gamma_6 + 2\Gamma_7 + 2\Gamma_8$
	$D_{15/2}^\pm$	$\Gamma_6 + \Gamma_7 + 3\Gamma_8$

Table 19.12: Full Rotation Group Compatibility Table for the Group T_d

D_0^+	Γ_1	D_0^-	Γ_2
D_1^+	Γ_4	D_1^-	Γ_5
D_2^+	$\Gamma_3 + \Gamma_5$	D_2^-	$\Gamma_3 + \Gamma_4$
D_3^+	$\Gamma_2 + \Gamma_4 + \Gamma_5$	D_3^-	$\Gamma_1 + \Gamma_4 + \Gamma_5$
D_4^+	$\Gamma_1 + \Gamma_3 + \Gamma_4 + \Gamma_5$	D_4^-	$\Gamma_2 + \Gamma_3 + \Gamma_4 + \Gamma_5$
D_5^+	$\Gamma_3 + 2\Gamma_4 + \Gamma_5$	D_5^-	$\Gamma_3 + \Gamma_4 + 2\Gamma_5$
D_6^+	$\Gamma_1 + \Gamma_2 + \Gamma_3 + \Gamma_4 + 2\Gamma_5$	D_6^-	$\Gamma_1 + \Gamma_2 + \Gamma_3 + 2\Gamma_4 + \Gamma_5$
$D_{1/2}^+$	Γ_6	$D_{1/2}^-$	Γ_7
$D_{3/2}^+$	Γ_8	$D_{3/2}^-$	Γ_8
$D_{5/2}^+$	$\Gamma_7 + \Gamma_8$	$D_{5/2}^-$	$\Gamma_6 + \Gamma_8$
$D_{7/2}^+$	$\Gamma_6 + \Gamma_7 + \Gamma_8$	$D_{7/2}^-$	$\Gamma_6 + \Gamma_7 + \Gamma_8$
$D_{9/2}^+$	$\Gamma_6 + 2\Gamma_8$	$D_{9/2}^-$	$\Gamma_7 + 2\Gamma_8$
$D_{11/2}^+$	$\Gamma_6 + \Gamma_7 + 2\Gamma_8$	$D_{11/2}^-$	$\Gamma_6 + \Gamma_7 + 2\Gamma_8$
$D_{13/2}^+$	$\Gamma_6 + 2\Gamma_7 + 2\Gamma_8$	$D_{13/2}^-$	$2\Gamma_6 + \Gamma_7 + 2\Gamma_8$

In this section, we give an explicit example for O_h symmetry for the corresponding situation where the spin of the electron is included and the wave functions are described in terms of the double group irreducible representations.

It is relatively simple to include the effect of the electron spin for the irreducible representations $\Gamma_1^\pm$ and $\Gamma_2^\pm$ because there are no splittings induced by the spin-orbit coupling. Thus the basis functions in this case are simple product functions given by $\Gamma_6^\pm = \Gamma_1^\pm \otimes \Gamma_6^+$ and $\Gamma_7^\pm = \Gamma_2^\pm \otimes \Gamma_6^+$ or more explicitly

$$
\begin{aligned}
\Psi_{\Gamma_6^\pm}(\vec{K}) &= \psi_{\Gamma_1^\pm}(\vec{K}) \begin{pmatrix} \alpha \\ \beta \end{pmatrix} \\
\Psi_{\Gamma_7^\pm}(\vec{K}) &= \psi_{\Gamma_2^\pm}(\vec{K}) \begin{pmatrix} \alpha \\ \beta \end{pmatrix}
\end{aligned}
\tag{19.38}
$$

in which the $\psi_{\Gamma_1^\pm}(\vec{K})$ and $\psi_{\Gamma_2^\pm}(\vec{K})$ denote symmetrized plane wave combinations considered in Chapter 16, ignoring the effect of the electron spin, while α and β denote spin up and spin down functions, respectively, which form partners of the Γ_6^+ double group irreducible representation.

For the degenerate plane wave combinations such as those with $\Gamma_{12}^\pm$, $\Gamma_{15}^\pm$ and $\Gamma_{25}^\pm$ symmetries, one method to find an appropriate set of basis functions when the electron spin is included is to use the Koster tables discussed in §19.5. For example, basis functions for the four partners for $\Gamma_8^\pm = \Gamma_3^\pm \otimes \Gamma_6^+$ can be found in the following Koster table:

	$u_1^3 v_{-1/2}^6$	$u_1^3 v_{+1/2}^6$	$u_2^3 v_{-1/2}^6$	$u_2^3 v_{+1/2}^6$
$\psi_{-3/2}^8$	0	0	0	1
$\psi_{-1/2}^8$	1	0	0	0
$\psi_{+1/2}^8$	0	-1	0	0
$\psi_{+3/2}^8$	0	0	-1	0

where the Koster functions u_1^3, u_2^3 for Γ_3 are related to the $\psi_{\Gamma_{12}}$ of Table 17.3 on p. 507 by:

$$
\begin{aligned}
u_1^3 &\propto 3z^2 - r^2 \sim [\omega \psi_{\Gamma_{12}^+} + \omega^2 \psi_{\Gamma_{12}^+}^*] \\
u_2^3 &\propto \sqrt{3}(x^2 - y^2) \sim [\omega \psi_{\Gamma_{12}^+} - \omega^2 \psi_{\Gamma_{12}^+}^*]
\end{aligned}
\tag{19.39}
$$

and

$$v^6_{+1/2} \propto \alpha$$
$$v^6_{-1/2} \propto \beta. \tag{19.40}$$

Thus the application of Koster's table gives:

$$\Psi_{\Gamma_8^{\pm}}(\vec{K}) = \tfrac{1}{\sqrt{2}} \begin{pmatrix} \sqrt{3}(x^2 - y^2)\alpha \\ (3z^2 - r^2)\beta \\ -(3z^2 - r^2)\alpha \\ -\sqrt{3}(x^2 - y^2)\beta \end{pmatrix} \tag{19.41}$$

A more symmetric set of basis functions for $\Gamma_8^{\pm} = \Gamma_{12}^{\pm} \otimes \Gamma_6^+$ is

$$\Psi_{\Gamma_8^{\pm}}(\vec{K}) = \tfrac{1}{\sqrt{2}} \begin{pmatrix} [\omega^2 \psi^*_{\Gamma_{12}^{\pm}}(\vec{K}) + \omega \psi_{\Gamma_{12}^{\pm}}(\vec{K})]\alpha \\ -i[\omega^2 \psi^*_{\Gamma_{12}^{\pm}}(\vec{K}) - \omega \psi_{\Gamma_{12}^{\pm}}(\vec{K})]\beta \\ i[\omega^2 \psi^*_{\Gamma_{12}^{\pm}}(\vec{K}) - \omega \psi_{\Gamma_{12}^{\pm}}(\vec{K})]\alpha \\ -[\omega^2 \psi^*_{\Gamma_{12}^{\pm}}(\vec{K}) + \omega \psi_{\Gamma_{12}^{\pm}}(\vec{K})]\beta \end{pmatrix} \tag{19.42}$$

in which $\psi_{\Gamma_{12}^+}(\vec{K}) = x^2 + \omega y^2 + \omega^2 z^2$.

Since the 3-dimensional levels $\Gamma_{15}^{\pm}$ and $\Gamma_{25}^{\pm}$ split under the spin-orbit interaction

$$\Gamma_{15}^{\pm} \otimes D_{1/2} = \Gamma_6^{\pm} + \Gamma_8^{\pm}$$
$$\Gamma_{25}^{\pm} \otimes D_{1/2} = \Gamma_7^{\pm} + \Gamma_8^{\pm}$$

the basis functions for these levels are somewhat more complicated. In these cases we can use the following tables from Koster's Table 83 on coupling coefficients (see Table 19.9):

	$u_x^4 v_{-1/2}^6$	$u_x^4 v_{+1/2}^6$	$u_y^4 v_{-1/2}^6$	$u_y^4 v_{+1/2}^6$	$u_z^4 v_{-1/2}^6$	$u_z^4 v_{+1/2}^6$
$\psi_{-1/2}^6$	0	$-i/\sqrt{3}$	0	$-1/\sqrt{3}$	$i/\sqrt{3}$	0
$\psi_{+1/2}^6$	$-i/\sqrt{3}$	0	$1/\sqrt{3}$	0	0	$-i/\sqrt{3}$
$\psi_{-3/2}^8$	$i/\sqrt{2}$	0	$1/\sqrt{2}$	0	0	0
$\psi_{-1/2}^8$	0	$i/\sqrt{6}$	0	$1/\sqrt{6}$	$i\sqrt{2}/\sqrt{3}$	0
$\psi_{+1/2}^8$	$-i/\sqrt{6}$	0	$1/\sqrt{6}$	0	0	$i\sqrt{2}/\sqrt{3}$
$\psi_{+3/2}^8$	0	$-i/\sqrt{2}$	0	$1/\sqrt{2}$	0	0

and

	$u_x^5 v_{-1/2}^6$	$u_x^5 v_{+1/2}^6$	$u_y^5 v_{-1/2}^6$	$u_y^5 v_{+1/2}^6$	$u_z^5 v_{-1/2}^6$	$u_z^5 v_{+1/2}^6$
$\psi_{-1/2}^7$	0	$-i/\sqrt{3}$	0	$-1/\sqrt{3}$	$i/\sqrt{3}$	0
$\psi_{+1/2}^7$	$-i/\sqrt{3}$	0	$1/\sqrt{3}$	0	0	$-i/\sqrt{3}$
$\psi_{-3/2}^8$	$-i/\sqrt{6}$	0	$1/\sqrt{6}$	0	0	$i\sqrt{2}/\sqrt{3}$
$\psi_{-1/2}^8$	0	$i/\sqrt{2}$	0	$-1/\sqrt{2}$	0	0
$\psi_{+1/2}^8$	$-i/\sqrt{2}$	0	$-1/\sqrt{2}$	0	0	0
$\psi_{+3/2}^8$	0	$i/\sqrt{6}$	0	$1/\sqrt{6}$	$i\sqrt{2}/\sqrt{3}$	0

from which we obtain for the two-fold levels:

$$\Psi_{\Gamma_6^\pm}(\vec{K}) = \frac{1}{\sqrt{3}} \begin{pmatrix} \left[-i\left(\psi_{\Gamma_{15}^\pm}^x(\vec{K}) - i\psi_{\Gamma_{15}^\pm}^y(\vec{K})\right)\alpha + i\psi_{\Gamma_{15}^\pm}^z(\vec{K})\beta\right] \\ \left[-i\left(\psi_{\Gamma_{15}^\pm}^x(\vec{K}) + i\psi_{\Gamma_{15}^\pm}^y(\vec{K})\right)\beta - i\psi_{\Gamma_{15}^\pm}^z(\vec{K})\alpha\right] \end{pmatrix}$$

$$\Psi_{\Gamma_7^\pm}(\vec{K}) = \frac{1}{\sqrt{3}} \begin{pmatrix} \left[-i\left(\psi_{\Gamma_{25}^\pm}^x(\vec{K}) - i\psi_{\Gamma_{25}^\pm}^y(\vec{K})\right)\alpha + i\psi_{\Gamma_{25}^\pm}^z(\vec{K})\beta\right] \\ \left[-i\left(\psi_{\Gamma_{25}^\pm}^x(\vec{K}) + i\psi_{\Gamma_{25}^\pm}^y(\vec{K})\right)\beta - i\psi_{\Gamma_{25}^\pm}^z(\vec{K})\alpha\right] \end{pmatrix}$$

(19.43)

The corresponding 4-fold levels are also found from the same two Koster tables:

$$\Psi_{\Gamma_8^\pm}(\vec{K}) = \frac{1}{\sqrt{6}} \begin{pmatrix} \left[i\sqrt{3}\left(\psi_{\Gamma_{15}^\pm}^x(\vec{K}) - i\psi_{\Gamma_{15}^\pm}^y(\vec{K})\right)\right]\beta \\ \left[i\left(\psi_{\Gamma_{15}^\pm}^x(\vec{K}) - i\psi_{\Gamma_{15}^\pm}^y(\vec{K})\right)\alpha + 2i\psi_{\Gamma_{15}^\pm}^z(\vec{K})\beta\right] \\ \left[-i\left(\psi_{\Gamma_{15}^\pm}^x(\vec{K}) + i\psi_{\Gamma_{15}^\pm}^y(\vec{K})\right)\beta + 2i\psi_{\Gamma_{15}^\pm}^z(\vec{K})\alpha\right] \\ \left[-i\sqrt{3}\left(\psi_{\Gamma_{15}^\pm}^x(\vec{K}) + i\psi_{\Gamma_{15}^\pm}^y(\vec{K})\right)\right]\alpha \end{pmatrix}$$

(19.44)

and

$$\Psi_{\Gamma_8^\pm}(\vec{K}) = \frac{1}{\sqrt{6}} \begin{pmatrix} \left[-i\left(\psi_{\Gamma_{25}^\pm}^x(\vec{K}) + i\psi_{\Gamma_{25}^\pm}^y(\vec{K})\right)\beta + 2i\psi_{\Gamma_{25}^\pm}^z(\vec{K})\alpha \right] \\[2ex] \left[i\sqrt{3}\left(\psi_{\Gamma_{25}^\pm}^x(\vec{K}) + i\psi_{\Gamma_{25}^\pm}^y(\vec{K})\right)\right]\alpha \\[2ex] \left[-i\sqrt{3}\left(\psi_{\Gamma_{25}^\pm}^x(\vec{K}) - i\psi_{\Gamma_{25}^\pm}^y(\vec{K})\right)\right]\beta \\[2ex] \left[i\left(\psi_{\Gamma_{25}^\pm}^x(\vec{K}) - i\psi_{\Gamma_{25}^\pm}^y(\vec{K})\right)\alpha + 2i\psi_{\Gamma_{25}^\pm}^z(\vec{K})\beta \right] \end{pmatrix}$$

$$(19.45)$$

in which the $\psi_{\Gamma_i}(\vec{K})$ for the single group are the plane wave combinations obtained in Chapter 16 for the plane wave solutions to the electronic problem, and α, β are, respectively, the spin up and spin down spin states. The basis functions for $\Gamma_8^\pm(\Gamma_{15}^\pm)$ are given in Eq. (19.44) and the basis functions for $\Gamma_8^\pm(\Gamma_{25}^\pm)$ are given in Eq. (19.45).

If no special precautions are taken, the various partners of the $\Gamma_8^\pm$ representation will differ from one another, depending on whether they come from a $\Gamma_3^\pm$, a $\Gamma_4^\pm$ or a $\Gamma_5^\pm$ orbital state. In all cases, the sets of partners for the $\Gamma_8^\pm$ representation will be related to one another through a unitary transformation. However, for some applications it is desirable that the unitary matrix be the identity or unit matrix so that all partners for a given irreducible representation look the same, independent of origin. Koster's tables generally require use of a unitary transformation (other than the unitary matrix) to relate the various $\Gamma_8^\pm$ basis functions. Despite this possible undesirable feature, the completeness of coverage in Koster's book make it a very useful resource for research problems in this topic.

To treat the plane wave states at other points in the Brillouin zone, we again use the direct product approach. For the orbital wave functions we use the procedures outlined in Chapter 16 to get the appropriate symmetrized combinations of plane waves for each of the high symmetry points and axes in the Brillouin zone using the character tables for the group of the wave vector at these symmetry points. For the same group of the wave vector, we use the appropriate Koster table for coupling coefficients which give the basis functions for the direct

product between the orbital plane wave states and the spinors. In this way the $E(\vec{k})$ relations in the nearly free electron approximation can be found, including the effect of the electron spin and the spin-orbit interaction.

19.7 Use of Reference Books to Find the Group of the Wave Vector for Non-Symmorphic Groups

In Chapters 16 and 17 we discussed the form of the $E(\vec{k})$ relations for symmorphic space groups, neglecting the spin and the spin-orbit interaction. In the case of non-symmorphic space groups we found in §16.5 that bands are often required to stick together at certain high symmetry points on the Brillouin zone boundary where the structure factor vanishes. In §16.5 it was explicitly shown that for the diamond structure the non-degenerate Δ_1 and $\Delta_{2'}$ levels come into the X point with equal and opposite non-zero slopes, so that in the extended Brillouin zone, the $E(\vec{k})$ curves pass through the X point continuously together with all their derivatives, as they interchange their symmetry designations. The physical basis for bands sticking together in this way is that if the structure factor vanishes, it is as if there was no Brillouin zone boundary and the energy eigenvalues continue through the symmetry point without interruption.

In this section, we consider the corresponding situation including the electron spin and the spin-orbit interaction. Explicitly we illustrate the sticking together of energy bands in terms of space group #194 for the hexagonal close packed structure. Another objective of this section is to illustrate the use of Koster's tables for double group irreducible representations. Space group #194 was previously discussed in §15.3, §15.4 and §15.5 in relation to lattice modes in graphite. In the case of lattice modes we only made use of the single group representations. Mention of space group #194 was also made in §16.5 in connection with bands sticking together at the zone boundary in cases where the structure factor vanishes for non-symmorphic groups.

Consider the character table of space group #194 in Miller and Love

Table 19.13: Miller and Love character table for the group of the wave vector at $\vec{k} = 0$ (the Γ point) for space group #194 $P6_3/mmc$, which is applicable to the hexagonal close packed structure and to graphite.

```
GENS.= C3;C2(0,0,1/2),C2X;S10V(0,0,1/2)
TRANSLATIONS   1=(0,0,1/2).

PT. OM  AUGMENTERS   -Y,X-Y,Z1  -X,-Y,1/2+Z1  X-Y,-Y,-Z1  X-Y,-Y,1/2+Z
REP.  D AUGMENTERS                                      REP.  D AUGMENTERS
OM1+  1  (+)1   E1   E1   E1   E                        OM2+  1  (+)1   E1   E1   (-)E1  (-)E
OM3+  1  (+)1   E1  (-)E1  E1  (-)E                     OM4+  1  (+)1   E1  (-)E1  (-)E1  E
OM5+  2  (+)1   51   E1   21   2                        OM6+  2  (+)1   51  (-)E1  21  (-)2
OM1-  1  (+)1   E1   E1   E1  (-)E                      OM2-  1  (+)1   E1   E1  (-)E1  E
OM3-  1  (+)1   E1  (-)E1  E1   E                       OM4-  1  (+)1   E1  (-)E1  (-)E1  (-)E
OM5-  2  (+)1   51   E1   21  (-)2                      OM6-  2  (+)1   51  (-)E1  21   2
OM7+  2  (-)1   81  (+)1)41  (-1)31  (-1)2              OM8+  2  (-)1   81  (-1)41  (-1)31  (+1)2
OM9+  2  (-)1  (-)E1  (+1)41  (-1)31  (-1)2             OM7-  2  (-)1   81  (+1)41  (-1)31  (+1)2
OM8-  2  (-)1   81  (-1)41  (-1)31  (-1)2               OM9-  2  (-)1  (-)E1  (+1)41  (-1)31  (+1)2

OPERATORS                         OM  1+   2+   3+   4+   5+   6+   1-   2-   3-   4-   5-   6-   7+   8+   9+   7-   8-   9-
 1 ....................................  1    1    1    1    2    2    1    1    1    1    2    2    2    2    2    2    2    2
 49 ...................................  1    1    1    1    2    2    1    1    1    1    2    2   -2   -2   -2   -2   -2   -2
 3 53 ................................   1    1    1    1   -1   -1    1    1    1   -1   -1   -1    1    1   -2    1    1   -2
 4,1 .................................   1    1   -1   -1    2   -2    1    1   -1   -1    2   -2    0    0    0    0    0    0
 6,1 50,1 ............................   1    1   -1   -1   -1    1    1    1   -1   -1   -1    1   -8    8    0   -8    8    0
 7 9 11 ..............................   1   -1    1   -1    0    0    1   -1    1   -1    0    0    0    0    0    0    0    0
 8,1 10,1 12,1 .......................   1   -1   -1    1    0    0    1   -1   -1    1    0    0    0    0    0    0    0    0
 20,1 22,1 24,1 ......................   1   -1   -1    1    0    0   -1    1    1   -1    0    0    0    0    0    0    0    0
 19 21 23 ............................   1   -1    1   -1    0    0   -1    1   -1    1    0    0    0    0    0    0    0    0
 16,1 ................................   1    1   -1   -1    2   -2   -1   -1    1    1   -2    2    0    0    0    0    0    0
 14,1 66,1 ...........................   1    1   -1   -1   -1    1   -1   -1    1    1    1   -1    8   -8    0   -8    8    0
 13 ..................................   1    1    1    1    2    2   -1   -1   -1   -1   -2   -2    2    2    2   -2   -2   -2
 15 65 ...............................   1    1    1    1   -1   -1   -1   -1   -1   -1    1    1    1    1   -2   -1   -1    2
```

for the Γ point shown in Table 19.13. The related point group symmetry at the Γ point is D_{6h}. The double group character table for D_{6h} from Koster et al. is given in Table 19.14. We then make the identification of the symmetry elements and classes between Miller and Love and Koster. On top of the labels of the classes given in Koster's character table (Table 19.14) we have included the Miller and Love symmetry operations of the space group #194 including the translation operation $\tau = (0, 0, c/2)$ for the classes which have translations. For example, the symmetry operation $\{C_4|\tau\}$ in Table 19.14 is identified with the operation '4, 1' in Miller and Love where '4' refers to the C_4 rotation and ',1' refers to the translation τ.

In the character table for the Γ point (corresponding to the D_{6h} point group) from Miller and Love (Table 19.13), we note that half of the operations in #194 have translations τ. The operations in D_{6h} that are also in $D_{3d} \equiv D_3 \otimes i$ have no translations while those in

Figure 19.6: Brillouin zone for a hexagonal Bravais lattice.

$D_{6h} \equiv D_6 \otimes i$ and not in D_{3d} do have the translation $\vec{\tau} = (c/2)(001)$. Irreducible representations $6^\pm$, $7^\pm$ and $8^\pm$ in Miller and Love are double group representations and correspond to $\Gamma_7^\pm$, $\Gamma_8^\pm$ and $\Gamma_9^\pm$ in Table 19.14 from Koster. The Miller and Love notation for the irreducible representations for the group of the wave vector at $\vec{k} = 0$ are included in Table 19.14 on the left margin.

Comparing Miller and Love with Koster identifies B (which appears in Table 19.13) with $B = \sqrt{3}$. In Table 19.14, we note the mixing of symmetry elements '3' and '53' in the same class, where element '53' is a double group symmetry operation related to symmetry element '5' compounded with $\bar{E}$ (rotation by 2π). Note that the representations $\Gamma_1^\pm$ through $\Gamma_6^\pm$ are even under multiplication by $\bar{E}$, while representations $\Gamma_7^\pm$ through $\Gamma_9^\pm$ are odd, as required for double groups.

As we move away from the Γ point in the k_z direction, the symmetry is lowered and the appropriate group of the wave vector is that for a Δ point. Miller and Love give the character table for the group of the wave vector at the Δ point which is reproduced in Table 19.15. The corresponding point group is C_{6v} which has the classes:

$$E, \bar{E}, \left\{ \begin{array}{c} C_2 \\ \bar{C}_2 \end{array} \right., 2C_3, 2\bar{C}_3, 2C_6, 2\bar{C}_6, \left\{ \begin{array}{c} 3\sigma_d \\ 3\bar{\sigma}_d \end{array} \right., \left\{ \begin{array}{c} 3\sigma_v \\ 3\bar{\sigma}_v \end{array} \right. .$$

Table 19.14: Character Table and Basis Functions for the Group D_{6h} from Koster.

D_{6h}	E	$\bar{E}$	$C_2 / \bar{C}_2$	$2C_3$	$2\bar{C}_3$	$2C_6$	$2\bar{C}_6$	$3C'_2 / 3\bar{C}'_2$	$3C''_2 / 3\bar{C}''_2$	I	$\bar{I}$	σ_h	$2S_6$	$2\bar{S}_6$	$2S_3$	$2\bar{S}_3$	$3\sigma_d / 3\bar{\sigma}_d$	$3\sigma_v / 3\bar{\sigma}_v$	Time Inv.	Bases
Γ_1^+	1	1	1	1	1	1	1	1	1	1	1	1	1	1	1	1	1	1	a	R
Γ_2^+	1	1	1	1	1	1	1	-1	-1	1	1	1	1	1	1	1	-1	-1	a	S_z
Γ_3^+	1	1	-1	1	1	-1	-1	1	-1	1	1	-1	1	1	-1	-1	1	-1	a	$z(x^3-3xy^2)$
Γ_4^+	1	1	-1	1	1	-1	-1	-1	1	1	1	-1	1	1	-1	-1	-1	1	a	$z(y^3-3yx^2)$
Γ_5^+	2	2	-2	-1	-1	1	1	0	0	2	2	-2	-1	-1	1	1	0	0	a	$(S_x-iS_y),$ $-(S_x+iS_y)$
Γ_6^+	2	2	2	-1	-1	-1	-1	0	0	2	2	2	-1	-1	-1	-1	0	0	a	$\Gamma_5^+ \times \Gamma_3^+$
Γ_1^-	1	1	1	1	1	1	1	1	1	-1	-1	-1	-1	-1	-1	-1	-1	-1	a	zS_z
Γ_2^-	1	1	1	1	1	1	1	-1	-1	-1	-1	-1	-1	-1	-1	-1	1	1	a	z
Γ_3^-	1	1	-1	1	1	-1	-1	1	-1	-1	-1	1	-1	-1	1	1	-1	1	a	y^3-3yx^2
Γ_4^-	1	1	-1	1	1	-1	-1	-1	1	-1	-1	1	-1	-1	1	1	1	-1	a	x^3-3xy^2
Γ_5^-	2	2	-2	-1	-1	1	1	0	0	-2	-2	2	1	1	-1	-1	0	0	a	$(x-iy),-(x+iy)$
Γ_6^-	2	2	2	-1	-1	-1	-1	0	0	-2	-2	-2	1	1	1	1	0	0	a	$\Gamma_5^+ \times \Gamma_3^-$
Γ_7^+	2	-2	0	1	-1	$\sqrt{3}$	$-\sqrt{3}$	0	0	2	-2	0	1	-1	$\sqrt{3}$	$-\sqrt{3}$	0	0	c	$\phi(1/2,-1/2),$ $\phi(1/2, 1/2)$
Γ_8^+	2	-2	0	1	-1	$-\sqrt{3}$	$\sqrt{3}$	0	0	2	-2	0	1	-1	$-\sqrt{3}$	$\sqrt{3}$	0	0	c	$\Gamma_7^+ \times \Gamma_3^+$
Γ_9^+	2	-2	0	-2	2	0	0	0	0	2	-2	0	-2	2	0	0	0	0	c	$\phi(3/2,-3/2),$ $\phi(3/2, 3/2)$
Γ_7^-	2	-2	0	1	-1	$\sqrt{3}$	$-\sqrt{3}$	0	0	-2	2	0	-1	1	$-\sqrt{3}$	$\sqrt{3}$	0	0	c	$\Gamma_7^+ \times \Gamma_1^-$
Γ_8^-	2	-2	0	1	-1	$-\sqrt{3}$	$\sqrt{3}$	0	0	-2	2	0	-1	1	$\sqrt{3}$	$-\sqrt{3}$	0	0	c	$\Gamma_7^+ \times \Gamma_5^-$
Γ_9^-	2	-2	0	-2	2	0	0	0	0	-2	2	0	2	-2	0	0	0	0	c	$\Gamma_9^+ \times \Gamma_1^-$

Table 19.15: Miller and Love character table for the group of the wave vector at the Δ point for space group #194.

```
PT. DT  AUGMENTERS  -Y,X-Y,Z1 -X,-Y,1/2+Z1 X-Y,-Y,1/2+Z
DT1 - 1  (+)1  E1  TE1  TE                              DT2  1  (+)1  E1  TE1  T(-)E
DT3   1  (+)1  E1  T(-)E1  TE                           DT4  1  (+)1  E1  T(-)E1  T(-)E
DT5   2  (+)1  51  TE1  T2                              DT6  2  (+)1  51  T(-)E1  T2
DT7   2  (-)1  81  T(-I)41  T(-I)3                      DT8  2  (-)1  A1  T(+I)41  T(-I)3
DT9   2  (-)1  (-)E1  T(-I)41  T(-I)3

OPERATORS                                    DT 1     2      3      4       5      6      7      8      9
1 ...............................................  1      1      1      1      2      2      2      2      2
49 ..............................................  1      1      1      1      2      2     -2     -2     -2
3 53 ............................................  1      1      1      1     -1     -1      1      1     -2
4,1 ............................................  1,T    1,T   -1,T   -1,T    ?,T   -2,T     0      0      0
6,1 50,1 .......................................  1,T    1,T   -1,T   -1,T   -1,T    1,T    B,T   -B,T     0
20,1 22,1 24,1 .................................  1,T   -1,T    1,T   -1,T     0      0      0      0      0
19 21 23 .......................................  1     -1     -1      1       0      0      0      0      0
```

These classes are identified with the listing given in the character table from Miller and Love, Table 19.15, by comparison with the character table for the Γ point (Table 19.14). The character table for the double point group C_{6v} from Koster is given in Table 19.16 and the correspondence is explicitly given between symmetry operations in Miller and Love and in Koster's table. Again $B = \sqrt{3}$ relates the characters in Miller and Love with those in Koster. All characters corresponding to symmetry operations containing τ must be multiplied by a phase factor $\alpha = \exp[ick_z]$ which is indicated in Table 19.15 as T.

We note that elements '3' and '53' are in class $2C_3$ as are elements '5' and '51' in class $2\bar{C}_3$. Similarly elements '6,1' and '50,1' are in class $2\{C_6|\tau\}$ as are elements '2,1' and '54,1' in class $2\{\bar{C}_6|\tau\}$. All characters with operations containing τ must be multiplied by a phase factor $\alpha = \exp[ick_z]$, indicated by arrows on the bottom of Table 19.16. From Tables 19.14 and 19.16 we can write down compatibility relations between the Γ point and the Δ point representations (see Table 19.17). In the limit $k \to 0$ the phase factors $\alpha \to 0$, so that the compatibility relations are satisfied as $\Delta \to \Gamma$.

In §16.5 we discussed the phenomenon of bands sticking together for the case where the electron spin and the spin-orbit interaction was neglected. A typical high symmetry point in the Brillouin zone where energy bands for the non-symmorphic hexagonal close packed lattice stick together is the A point (see Fig. 19.7). Reference: Phys. Rev. 140, A401 (1965). The character table for the A point taken from Miller

Table 19.16: Character Table and Basis Functions for the Group C_{6v} from Koster.

C_{6v}	E	$\bar{E}$	$\begin{array}{c}C_2\\ \bar{C}_2^2\end{array}$	$2C_3$	$2\bar{C}_3$	$\begin{array}{c}2C_6\\ \text{c}\end{array}$	$\begin{array}{c}2\bar{C}_6\\ \text{c}\end{array}$	$\begin{array}{c}3\sigma_d\\ 3\bar{\sigma}_d\end{array}$	$\begin{array}{c}3\sigma_v\\ 3\bar{\sigma}_v\end{array}$	Time Inv.	Bases for C_{6v}
Γ_1	1	1	1	1	1	1	1	1	1	a	R or z
Γ_2	1	1	1	1	1	1	1	-1	-1	a	S_z
Γ_3	1	1	-1	1	1	-1	-1	1	-1	a	x^3-3xy^2
Γ_4	1	1	-1	1	1	-1	-1	-1	1	a	y^3-3yx^2
Γ_5	2	2	-2	-1	-1	1	1	0	0	a	$(S_x-iS_y),$ $-(S_x+iS_y)$
Γ_6	2	2	2	-1	-1	-1	-1	0	0	a	$\Gamma_3\times\Gamma_5$
Γ_7	2	-2	0	1	-1	$\sqrt{3}$	$-\sqrt{3}$	0	0	c	$\phi(1/2,-1/2),$ $\phi(1/2,1/2)$
Γ_8	2	-2	0	1	-1	$-\sqrt{3}$	$\sqrt{3}$	0	0	c	$\Gamma_7\times\Gamma_3$
Γ_9	2	-2	0	-2	2	0	0	0	0	c	$\phi(3/2,-3/2),$ $\phi(3/2,3/2)$

$B = \sqrt{3}$

M+L
1
2
4
3
6
5
7
8
9

Table 19.17: Compatibility relations between irreducible representations at Γ and Δ for space group #194 using both Koster and Miller and Love notations.

Γ point reps.			Δ point reps.		Γ point reps.			Δ point reps.	
Koster	M&L		M&L	Koster	Koster	M&L		M&L	Koster
Γ_1^+	1^+	$\rightarrow$	1	Δ_1	Γ_1^-	1^-	$\rightarrow$	2	Δ_2
Γ_2^+	2^+	$\rightarrow$	2	Δ_2	Γ_2^-	2^-	$\rightarrow$	1	Δ_1
Γ_3^+	3^+	$\rightarrow$	4	Δ_3	Γ_3^-	3^-	$\rightarrow$	3	Δ_3
Γ_4^+	4^+	$\rightarrow$	3	Δ_4	Γ_4^-	4^-	$\rightarrow$	4	Δ_4
Γ_5^+	6^+	$\rightarrow$	6	Δ_5	Γ_5^-	6^-	$\rightarrow$	6	Δ_6
Γ_6^+	5^+	$\rightarrow$	5	Δ_6	Γ_6^-	5^-	$\rightarrow$	5	Δ_5
Γ_7^+	8^+	$\rightarrow$	7	Δ_7	Γ_7^-	8^-	$\rightarrow$	7	Δ_7
Γ_8^+	7^+	$\rightarrow$	8	Δ_8	Γ_8^-	7^-	$\rightarrow$	8	Δ_8
Γ_9^+	9^+	$\rightarrow$	9	Δ_9	Γ_9^-	9^-	$\rightarrow$	9	Δ_9

and Love illustrates the sticking together of bands at the Brillouin zone boundary (see Table 19.18).

At the A point we have 6 irreducible representations, 3 of which are ordinary irreducible representations and 3 of which are double group representations. There are only 6 classes with non-vanishing characters (see Table 19.19 which lists the characters for all the symmetry operations at the A point). The compatibility relations below

$$
\begin{array}{ccccccc}
\text{(A)} & 1 & 2 & 3 & 4 & 5 & 6 \\
& \downarrow & \downarrow & \downarrow & \downarrow & \downarrow & \downarrow \\
\text{(}\Delta\text{)} & (1+4) & (2+3) & (5+6) & 9 & 9 & (7+8)
\end{array}
$$

show that in the vicinity of the A point we have band crossings for all the single group bands with A_1, A_2 and A_3 symmetry. These band crossings are based on the compatibility relations and the non-vanishing of the p_z matrix element for the first-order $\vec{k} \cdot \vec{p}$ perturbation is shown in Fig. 19.7. Since the structure factor vanishes at A, the energy bands pass through the A point without interruption and merely change their

Table 19.18: Character table for point A in space group #194 from Miller and Love.

```
PT. A   AUGMENTERS   -Y,X-Y,Z1 -X,-Y,1/2+Z1 X-Y,-Y,-Z1 X-Y,-Y,1/2+Z
A1    2  (+)1   E1  (+1)41   21  (+1)4                          A2    2  (+)1   E1  (+1)41   21  (-1)4
A3    4  (+)1   71  141   91  5                                 A4    2  (-)1   (-)E1  41  (+1)E1  2
A5    2  (-)1  (-)E1  41  (-1)E1  2                             A6    4  (-)1  101  191  111  13

OPERATORS                                      . A   1    2    3    4    5    6
1 ..........................................    2    2    4    2    2    4
49 .........................................    2    2    4   -2   -2   -4
3 53 .......................................    2    2   -2   -2   -2    2
2,1 4,1 6,1 8,1 10,1 12,1 13 14,1 15
16,1 17 18,1 20,1 22,1 24,1 ...........         0    0    0    0    0    0
7 11 57 ....................................     0    0    0   21  -21    0
19 21 23 ...................................     2   -2    0    0    0    0
```

Table 19.19: Character table for the group of the wave vector at the point A adapted from character tables in Koster.

D_{6h}	E	$\bar{E}$	C_2 $\bar{C_2}$ $\frac{1}{\tau}$	$2C_3$ 53	$2\bar{C_3}$ 5	$2C_6$ $6,1$ τ	$2\bar{C_6}$ $5Y,1$ τ	$3C_2'$ $3C_2'$ τ	$3C_2''$ $3C_2''$ τ	I	$\bar{I}$	$\frac{\sigma_h}{\bar{\sigma_h}}$ τ	$2S_6$ 17	$2\bar{S_6}$ 65	$2S_3$ τ	$2\bar{S_3}$ τ	$3\sigma_d$ $3\bar{\sigma_d}$	$3\sigma_v$ $3\bar{\sigma_v}$ τ	Time Inver.
1	2	2	0	2	2	0	0	0	0	0	0	0	0	0	0	0	2	0	a
2	2	2	0	2	2	0	0	0	0	0	0	0	0	0	0	0	-2	0	a
3	4	4	0	-2	-2	0	0	0	0	0	0	0	0	0	0	0	0	0	a
4	2	-2	0	-2	2	0	0	$2i$	0	0	0	0	0	0	0	0	0	0	b
5	2	-2	0	-2	2	0	0	$-2i$	0	0	0	0	0	0	0	0	0	0	b
6	4	-4	0	2	-2	0	0	0	0	0	0	0	0	0	0	0	0	0	c
p_z	1	1	1	1	1	1	1	-1	-1	-1	-1	-1	-1	-1	-1	1	1	
p_x, p_y	2	2	-2	-1	-1	1	1	0	0	-2	-2	2	1	1	-1	-1	0	0	

symmetry designations at the A point, as for example $\Delta_1 \to A_1 \to \Delta_4$. Bands for doubly degenerate double group irreducible representations Δ_7 and Δ_8 stick together as an A_6 band at the A point. At the A point $(k_z = \pi/c)$ the phase factor $\exp[i(c/2)k_z]$, associated with the symmetry operations containing τ such as $\{C_6|\tau\}$, becomes $e^{i\pi/2} = i$. Energy bands with double group representations A_4 and A_5 have complex characters and are complex conjugates of each other. In Chapter 21 we will see that such bands stick together because of time reversal symmetry. Thus two Δ_9 levels come into the A point to form $A_4 + A_5$ levels and leave the A point with the same Δ_9 symmetry (see Fig. 19.7). The p_z matrix element couples the A_4 and A_5 levels (see Table 19.19) and since the A_4 and A_5 levels are degenerate by time reversal symmetry there is once again a finite slope of the Δ_9 levels as they approach the A-point. We note that for the non-symmorphic groups at points in the Brillouin zone where the structure factor vanishes (such as the A point for group #194), the various components of the momenta need not transform as irreducible representations of the non-symmorphic group.
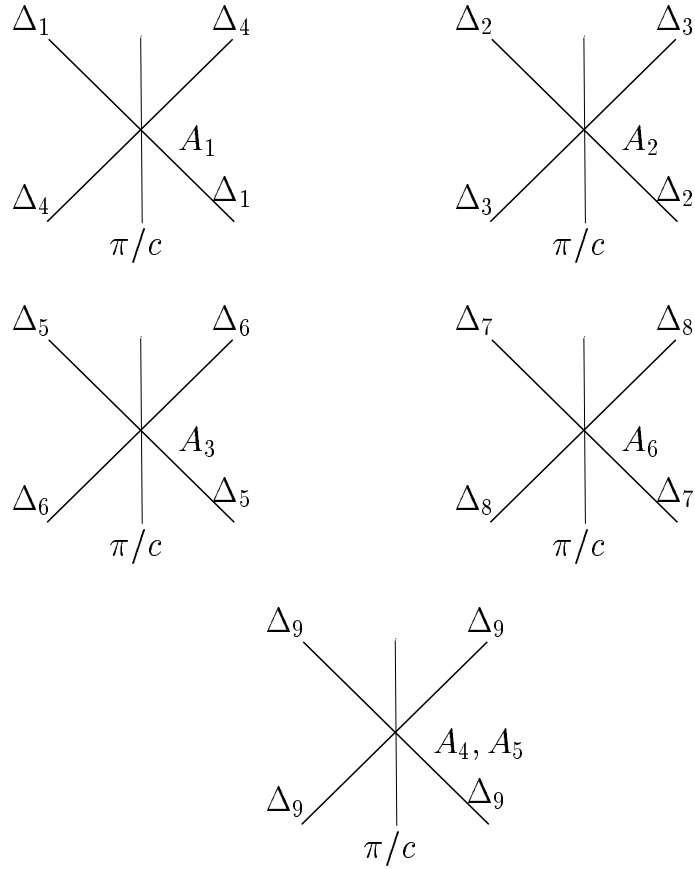
Figure 19.7: Energy band splittings near the A point for bands going through the A point without interruption because of the vanishing structure factor at the A point. Note that A_4, A_5, A_6, Δ_7, Δ_8 and Δ_9 are double group representations. The A_4 and A_5 levels stick together because of time reversal symmetry discussed in Chapter 21.

19.8   Selected Problems

1. Consider an Er^{3+} rare earth ion entering an insulating ionic crystal in a position with point group symmetry D_{4h}.

   (a) Find the double group irreducible representations of the crystal field (D_{4h} point group symmetry) corresponding to the ground state configuration for the free ion. Compare with the crystal field splitting that would occur for icosahedral point group symmetry I_h.

   (b) Use Charlotte Moore's tables to identify the lowest energy optical transitions that can be induced from the ground state level of the free Er^{3+} ion. Find the corresponding optical transitions for the Er^{3+} ion in a crystal field with I_h point group symmetry.

   (c) Repeat part (b) for the case of D_{4h} point group symmetry.

   (d) What changes in the spectra (part c) are expected to occur if a stress is applied in the z-direction? In the x-direction?

   (e) Now suppose that a Dy^{3+} rare earth ion is introduced in the same lattice instead of the Er^{3+} ion. What are the symmetry types for levels to which optical transitions can be induced from a multiplet corresponding to the ground state level of the free ion. (Use Hund's rule to obtain the ground state energies.) Work the problem only for the D_{4h} point group symmetry. Comment on the expected difference in the optical spectrum for the Dy^{3+} and the Er^{3+} ions in part (c).

Chapter 20

Application of Double Groups to Energy Bands with Spin

In this chapter we apply the group theoretical background for the electron spin and the spin-orbit interaction (which is discussed in Chapter 19) to the treatment of energy band models for solids (which are discussed in Chapters 16 and 17). By including the spin-orbit interaction we can also discuss the effective g-factor, which together with the effective mass tensor, characterizes the properties of a semiconductor in a magnetic field.

20.1   Introduction

The one-electron Hamiltonian including spin-orbit interaction is written as:

$$\mathcal{H} = \frac{p^2}{2m} + V(\vec{r}) + \frac{\hbar}{4m^2c^2}(\vec{\nabla}V \times \vec{p}) \cdot \vec{\sigma} \qquad (20.1)$$

where $\vec{\sigma}$ is the dimensionless spin operator. The first two terms of Eq. (20.1) denote the kinetic energy and periodic potential of the one-electron Hamiltonian in a simple periodic potential $V(\vec{r})$, and the third

term denotes the spin-orbit interaction $\mathcal{H}'_{SO}$

$$\mathcal{H}'_{SO} = \frac{\hbar}{4m^2c^2}(\vec{\nabla}V \times \vec{p}) \cdot \vec{\sigma} \tag{20.2}$$

where $\mathcal{H} = \mathcal{H}_0 + \mathcal{H}'_{SO}$. The Hamiltonian [Eq. (20.1)] is appropriate when the spin-orbit splittings are significant compared with typical energy gaps. The presence of the spin operator $\vec{\sigma}$ in the spin-orbit term $\mathcal{H}'_{SO}$ requires the use of spin-dependent wave functions with double group symmetry designations for the energy bands. Since the magnitude of the spin-orbit interaction is comparable to energy band gaps for many important electronic materials, it is important to consider the spin-orbit interaction when carrying out energy band calculations.

Thus explicit band calculations of $E(\vec{k})$ with spin-orbit interaction have been carried out using all the standard techniques for energy band calculations. Quite independent of the particular calculational technique that is used, group theoretical techniques are introduced to classify the states and to bring the secular equation into block diagonal form. To illustrate these points we consider explicitly the use of group theory (i.e., double groups as discussed in Chapter 19) to treat the energy bands for the empty lattice (nearly free electron approximation) and for $\vec{k} \cdot \vec{p}$ perturbation theory. These examples are designed to provide some experience with the handling of double groups.

20.2 The $\vec{k} \cdot \vec{p}$ Perturbation with Spin-Orbit Interaction

Schrödinger's equation including the spin-orbit interaction can be written as:

$$\left[\frac{p^2}{2m} + V(\vec{r}) + \frac{\hbar}{4m^2c^2}(\vec{\nabla}V \times \vec{p}) \cdot \vec{\sigma}\right]\psi_{n\vec{k}}(\vec{r}) = E_n(\vec{k})\psi_{n\vec{k}}(\vec{r}) \tag{20.3}$$

in which the Bloch functions $\psi_{n\vec{k}}(\vec{r})$ for $\mathcal{H}'_{SO}$ become spinors $\psi_{n\vec{k}\uparrow}(\vec{r})$ and $\psi_{n\vec{k}\downarrow}(\vec{r})$ rather than simple wave functions. These spinor basis functions can be written in more expanded notation as

$$\psi_{n\vec{k}\uparrow}(\vec{r}) = e^{i\vec{k}\cdot\vec{r}}u_{n\vec{k}\uparrow}(\vec{r})$$

$$\psi_{n\vec{k}\downarrow}(\vec{r}) \;=\; e^{i\vec{k}\cdot\vec{r}} u_{n\vec{k}\downarrow}(\vec{r}) \tag{20.4}$$

where the arrow on $\psi_{n\vec{k}\uparrow}(\vec{r})$ means that the state is generally spin up or the expectation value of σ_z in this state is positive, and the down arrow gives a negative expectation value for σ_z so that

$$\begin{aligned} \langle \psi_{n\vec{k}\uparrow} | \sigma_z | \psi_{n\vec{k}\uparrow} \rangle \;&> 0 \\ \langle \psi_{n\vec{k}\downarrow} | \sigma_z | \psi_{n\vec{k}\downarrow} \rangle \;&< 0. \end{aligned} \tag{20.5}$$

The Bloch states are only pure spin up or spin down states when the spin-orbit interaction is neglected ($\mathcal{H}'_{SO} \equiv 0$). The spin-orbit interaction mixes the spin-up and spin-down partners, and, as was discussed in Chapter 19 for the atomic case, the $|j, \ell, s, m_j\rangle$ representation becomes the appropriate irreducible representation for the spin-orbit coupled system rather than the $|\ell, s, m_\ell, m_s\rangle$ representation.

Let us focus our attention on one of the spinor $u_{n\vec{k}}(\vec{r})$ functions (either of the components which diagonalize the Schrödinger equation [Eq. (20.3)]. Using $\vec{k} \cdot \vec{p}$ perturbation theory, the corresponding differential equation for $u_{n\vec{k}}(\vec{r})$ is

$$\left[\frac{p^2}{2m} + V(\vec{r}) + \frac{\hbar}{4m^2c^2} (\vec{\nabla}V \times \vec{p}) \cdot \vec{\sigma} \right] u_{n\vec{k}}(\vec{r}) \;+$$

$$\frac{\hbar\vec{k}}{m} \cdot \left(\vec{p} + \frac{\hbar}{4mc^2} \vec{\sigma} \times \vec{\nabla}V \right) u_{n\vec{k}}(\vec{r}) \;= \tag{20.6}$$

$$\left[E_n(\vec{k}) - \frac{\hbar^2 k^2}{2m} \right] u_{n\vec{k}}(\vec{r})$$

in which we have made use of the vector identities:

$$(\vec{A} \times \vec{B}) \cdot \vec{C} = (\vec{B} \times \vec{C}) \cdot \vec{A} = (\vec{C} \times \vec{A}) \cdot \vec{B}, \tag{20.7}$$

or more explicitly

$$(\vec{\nabla}V \times \vec{p}) \cdot \vec{\sigma} e^{i\vec{k}\cdot\vec{r}} u_{n\vec{k}}(\vec{r}) = (\vec{\sigma} \times \vec{\nabla}V) \cdot \vec{p}\, e^{i\vec{k}\cdot\vec{r}} u_{n\vec{k}}(\vec{r}) \tag{20.8}$$

and

$$\vec{p}\, e^{i\vec{k}\cdot\vec{r}} u_{n\vec{k}}(\vec{r}) = e^{i\vec{k}\cdot\vec{r}} \left(\hbar\vec{k} u_{n\vec{k}}(\vec{r}) + \vec{p} u_{n\vec{k}}(\vec{r}) \right). \tag{20.9}$$

If we identify terms in Eq. (20.6) with an unperturbed Hamiltonian $\mathcal{H}_0$ and a perturbation Hamiltonian $\mathcal{H}'_{\vec{k}\cdot\vec{p}}$ we obtain

$$\mathcal{H}_0 = \frac{p^2}{2m} + V(\vec{r}) + \frac{\hbar}{4m^2c^2}(\vec{\nabla}V \times \vec{p}) \cdot \vec{\sigma} \qquad (20.10)$$

and

$$\mathcal{H}'_{\vec{k}\cdot\vec{p}} = \frac{\hbar\vec{k}}{m} \cdot \left(\vec{p} + \frac{\hbar}{4mc^2}\vec{\sigma} \times \vec{\nabla}V\right) \qquad (20.11)$$

so that Rayleigh-Schrödinger perturbation theory for energy bands near $k = 0$ yields the following expression for the non-degenerate state Γ_i [see Eq. (17.4)]

$$E_n^{\Gamma_i}(\vec{k}) = E_n^{\Gamma_i}(0) + (u_{n,0}^{\Gamma_i}|\mathcal{H}'|u_{n,0}^{\Gamma_i}) + \sum_{n'\neq n} \frac{(u_{n,0}^{\Gamma_i}|\mathcal{H}'|u_{n',0}^{\Gamma_j})(u_{n',0}^{\Gamma_j}|\mathcal{H}'|u_{n,0}^{\Gamma_i})}{E_n^{\Gamma_i}(0) - E_{n'}^{\Gamma_j}(0)}$$
$$(20.12)$$

in which the unperturbed functions $u_{n,0}^{\Gamma_i}$ are evaluated at $\vec{k} = 0$ (the expansion point for the $\vec{k}\cdot\vec{p}$ perturbation) and Γ_j labels the irreducible representations for bands n'. The sum in Eq. (20.12) is over states Γ_j that couple to state Γ_i through the $\vec{k}\cdot\vec{p}$ perturbation Hamiltonian given by Eq. (20.11). We note that Eq. (20.12) has the same form as the corresponding expression without spin-orbit interaction [Eq. (17.4)] **except** that in Eq. (20.12):

1. The unperturbed Hamiltonian yielding the energy eigenvalues at $\vec{k} = 0$ explicitly contains a spin-orbit term.

2. The $\vec{k}\cdot\vec{p}$ perturbation explicitly contains the spin operator and a spin-orbit term.

3. The irreducible representations Γ_i and Γ_j are both double group representations.

For example, if the spin-orbit interaction is neglected for a crystal with O_h symmetry, then a non-degenerate Γ_1^+ state is coupled by the $\vec{k}\cdot\vec{p}$ perturbation Hamiltonian only to a Γ_{15}^- intermediate state. When the

spin-orbit interaction is included, the Γ_1^+ and Γ_{15}^- states become double group states:

$$
\begin{aligned}
\Gamma_1^+ &\rightarrow \Gamma_6^+ \\
\Gamma_{15}^- &\rightarrow \Gamma_6^- + \Gamma_8^-
\end{aligned}
\tag{20.13}
$$

so that with the spin-orbit interaction a Γ_6^+ band will couple to bands with Γ_6^- and Γ_8^- symmetries. We note that bands with Γ_8^- symmetry can arise from single-group bands with $\Gamma_{12}^-, \Gamma_{15}^-$ and Γ_{25}^- symmetries. In this sense the spin-orbit interaction gives more possibilities for immediate states.

In treating $\vec{k} \cdot \vec{p}$ perturbation theory (see Chapter 17), we have 3 possibilities: non-degenerate levels, degenerate (or nearly degenerate) levels that are treated in first-order degenerate perturbation theory, and degenerate levels that are treated in second-order degenerate perturbation theory. In all three of these cases, we use group theory to determine which are the non-vanishing matrix elements of a vector operator taken between double group states, and which of the non-vanishing matrix elements are equal to each other. More explicitly, for the case of a crystal with O_h symmetry, all the Γ_i and Γ_j representations have either $\Gamma_6^{\pm}, \Gamma_7^{\pm}$ and $\Gamma_8^{\pm}$ symmetry since the spatial part of the wavefunctions transform according to one of the five ordinary irreducible representations and the direct product of an ordinary irreducible representation with D_6^+ yields one of the double group representations. By inspection, we find that for the O_h group all the irreducible representations Γ_i are at least 2-fold degenerate. But this degeneracy is maintained for all $\vec{k}$ values and is lifted only by the application of an external (or internal) magnetic field. This 2-fold degeneracy, know as the **Kramers degeneracy** is generally found in the absence of a magnetic field. We therefore look for this degeneracy when working practical problems, because it greatly reduces the labor in dealing with problems involving spin). Because of this Kramers degeneracy, we can effectively use **non-degenerate perturbation theory** to deal with 2-fold levels such as the $\Gamma_6^{\pm}$ and $\Gamma_7^{\pm}$ levels in many applications.

Group theory can be used to greatly simplify the $\vec{k} \cdot \vec{p}$ expansion for one of the $\Gamma_6^{\pm}$ or $\Gamma_7^{\pm}$ levels. For example, take $\Gamma_i = \Gamma_6^+$ and note that

the momentum operator including the spin-orbit interaction

$$\vec{P} = \vec{p} + \frac{\hbar}{4mc^2}\vec{\sigma} \times \vec{\nabla}V \qquad (20.14)$$

transforms like the Γ_{15}^- irreducible representation. The momentum operator $\vec{P}$ transforms as Γ_{15}^- whether or not the spin-orbit interaction is included, since $\vec{p}$ is a vector and so is $(\vec{\sigma} \times \vec{\nabla}V)$, both being radial vectors. Since $\Gamma_6^+ \otimes \Gamma_{15}^- = \Gamma_6^- + \Gamma_8^-$ and Γ_6^+ are orthogonal to Γ_6^- and Γ_8^-, we have no linear $\vec{k}$ term in the $\vec{k} \cdot \vec{p}$ expansion of Eq. (20.12). In the quadratic term we can only have intermediate states with Γ_6^- and Γ_8^- symmetry. Again we can use group theory to show relations between the various non-vanishing matrix elements of $\vec{p}$, and as before, only a very small number of matrix elements are independent. To study these matrix elements we will need to look at the basis functions for the double group irreducible representations, which are discussed in the next section, §20.3.

20.3   Basis Functions for Double Group Representations

We will use the notation for single electron spin states:

$$
\begin{aligned}
\uparrow = & \quad \text{spin up} \quad = \begin{pmatrix} 1 \\ 0 \end{pmatrix} \\
\downarrow = & \quad \text{spin down} \quad = \begin{pmatrix} 0 \\ 1 \end{pmatrix}.
\end{aligned}
\qquad (20.15)
$$

Operation by the **Pauli spin matrices** σ_x, σ_y and σ_z

$$
\begin{aligned}
\sigma_x &= \begin{pmatrix} 0 & 1 \\ 1 & 0 \end{pmatrix} \\
\sigma_y &= \begin{pmatrix} 0 & -i \\ i & 0 \end{pmatrix} \\
\sigma_z &= \begin{pmatrix} 1 & 0 \\ 0 & -1 \end{pmatrix}
\end{aligned}
\qquad (20.16)
$$

on the pure spin up and spin down states yields

$$
\begin{aligned}
\sigma_x \uparrow &= \downarrow \\
-i\sigma_y \uparrow &= \downarrow \\
\sigma_z \uparrow &= \uparrow \\
\sigma_x \downarrow &= \uparrow \\
-i\sigma_y \downarrow &= -\uparrow \\
\sigma_z \downarrow &= -\downarrow
\end{aligned}
\tag{20.17}
$$

The Pauli spin matrices $\sigma_x, \sigma_y, \sigma_z$ together with the (2×2) unit matrix

$$
1 = \begin{pmatrix} 1 & 0 \\ 0 & 1 \end{pmatrix}
\tag{20.18}
$$

span a 2×2 space, so that every matrix can be expressed in terms of these four matrices, 1, σ_x, $-i\sigma_y$, σ_z. Also the raising and lowering operators are defined by

$$
\sigma_\pm = \sigma_x \pm i\sigma_y
\tag{20.19}
$$

so that

$$
\frac{1}{2}\sigma_- \uparrow = \downarrow \qquad \text{and} \qquad \frac{1}{2}\sigma_+ \downarrow = \uparrow \ .
\tag{20.20}
$$

One set of basis functions for Γ_6^+ is the pair $\uparrow, \downarrow$ which form partners for Γ_6^+. Any other pair can be found from multiplication of this pair by another basis function for Γ_1^+, since $\Gamma_6^+ = \Gamma_1^+ \otimes \Gamma_6^+$. We will see below how very different-looking basis functions can be used for Γ_6^+ depending on the single group representation with which Γ_6^+ is connected, such as a Γ_1^+ or a Γ_{15}^+ state. Thus, it is convenient to label the basis functions for any double group representation with the single group representation from which it comes. Thus the pair $\uparrow, \downarrow$ would be associated with a $\Gamma_6^+(\Gamma_1^+)$ state.

To understand this problem better, consider the $\Gamma_8^+(\Gamma_{15}^+)$ state which comes from the direct product $\Gamma_{15}^+ \otimes \Gamma_6^+ = \Gamma_6^+ + \Gamma_8^+$. For the Γ_{15}^+ state we may take the **basis functions** L_x, L_y, L_z (angular momentum components). Then the 6 functions $L_x \uparrow, L_x \downarrow, L_y \uparrow, L_y \downarrow, L_z \uparrow, L_z \downarrow$ make up basis functions for the combined Γ_6^+ and Γ_8^+ representations, assuming

no spin-orbit interaction. However, when the spin-orbit interaction is included, we must now find the correct linear combinations of the above 6 functions so that two of these transform as Γ_6^+ and four transform as Γ_8^+. The **correct linear combinations** are found by identifying these basis functions which arise in the energy band problem with basis functions that occur in the angular momentum problem. If the group theory problem is solved for the angular momentum functions, then the same solution can be applied to the energy band eigenfunctions more generally. This approach was taken in writing down basis functions in §19.6.

20.4 Basis Functions for $j = 3/2$ and $1/2$ States

For the angular momentum functions in the $|\ell s m_\ell m_s\rangle$ representation, the 6 eigenfunctions correspond to the orbital states $\ell = 1$, $m_\ell = 1, 0, -1$ and the spin states $s = 1/2$, $m_s = 1/2, -1/2$. The transformations we are looking for will transform these states into $j = 3/2$, $m_j = 3/2, 1/2, -1/2, -3/2$ and $j = 1/2$, $m_j = 1/2, -1/2$. The matrices which carry out these transformations generate what are known as the Clebsch-Gordan coefficients.

Tables of Clebsch-Gordan coefficients are found in quantum mechanics and group theory books for many of the useful combinations of spin and orbital angular momentum that occur in practical problems. A set that is appropriate for $\ell = 1$, $s = 1/2$ is given below for a Γ_8^+ double group state derived from a Γ_{15}^+ single group state (see §19.6)

$$
\begin{array}{ll}
|j, m_j\rangle \text{ State} & \text{Basis Function} \\
|\frac{3}{2}, \frac{3}{2}\rangle & \xi_1 = \frac{1}{\sqrt{2}}(L_x + iL_y) \uparrow \\
|\frac{3}{2}, \frac{1}{2}\rangle & \xi_2 = \frac{1}{\sqrt{6}}[(L_x + iL_y) \downarrow +2L_z \uparrow] \\
|\frac{3}{2}, -\frac{1}{2}\rangle & \xi_3 = \frac{1}{\sqrt{6}}[(L_x - iL_y) \uparrow +2L_z \downarrow] \\
|\frac{3}{2}, -\frac{3}{2}\rangle & \xi_4 = \frac{1}{\sqrt{2}}(L_x - iL_y) \downarrow
\end{array}
\tag{20.21}
$$

in which we have used the fundamental relations for raising operators

$$
L_+|\ell, m_\ell\rangle = \sqrt{(\ell - m_\ell)(\ell + m_\ell + 1)} \ |\ell, m_\ell + 1\rangle
$$

$$J_+|j, m_j\rangle \ = \ \sqrt{(j - m_j)(j + m_j + 1)} \ |j, m_j + 1\rangle. \quad (20.22)$$

We further note that the state $|j = 3/2, m_j = -3/2\rangle$ is identical with the state for $\ell = 1, s = 1/2$ and $|m_\ell = -1, m_s = -1/2\rangle$. Therefore, we start with the $j = 3/2$, $m_j = -3/2$ state and apply the raising operator to obtain the other states:

$$J_+ \left|j = 3/2, \ m_j = -3/2\right\rangle \ = \ \sqrt{\left(\frac{3}{2} + \frac{3}{2}\right)\left(\frac{3}{2} - \frac{3}{2} + 1\right)} \left|j = 3/2, \ m_j = -1/2\right\rangle$$

$$= (L_+ + S_+)\left|m_\ell = -1, \ m_s = -1/2\right\rangle \ = \ \sqrt{(1+1)(1-1+1)} \left|m_\ell = 0, m_s = -1/2\right\rangle$$

$$+ \ \sqrt{\left(\frac{1}{2} + \frac{1}{2}\right)\left(\frac{1}{2} - \frac{1}{2} + 1\right)} \left|m_\ell = -1, m_s = 1/2\right\rangle.$$

Collecting terms, we obtain

$$\left|j = \frac{3}{2}, m_j = -\frac{1}{2}\right\rangle = \frac{\sqrt{2}}{3}\left|m_\ell = 0, m_s = -\frac{1}{2}\right\rangle + \frac{1}{\sqrt{3}}\left|m_\ell = -1, m_s = \frac{1}{2}\right\rangle.$$
$$(20.23)$$

We make the identification:

$$m_\ell = +1 \ \rightarrow \ \frac{1}{\sqrt{2}}(L_x + iL_y)$$

$$m_\ell = 0 \ \rightarrow \ L_z$$

$$m_\ell = -1 \ \rightarrow \ \frac{1}{\sqrt{2}}(L_x - iL_y)$$

$$m_s = \frac{1}{2} \ \rightarrow \ \uparrow$$

$$m_s = -\frac{1}{2} \ \rightarrow \ \downarrow.$$

from which we obtain the basis functions

$|j, m_j\rangle$ State	Basis Function	
$\left|\frac{3}{2}, -\frac{3}{2}\right\rangle$	$\frac{1}{\sqrt{2}}(L_x - iL_y) \downarrow$	(20.24)
$\left|\frac{3}{2}, -\frac{1}{2}\right\rangle$	$\frac{1}{\sqrt{6}}[(L_x - iL_y) \uparrow + 2L_z \downarrow].$	

Similarly, operation of J_+ on the state $|j = 3/2, m_j - 1/2\rangle$ results in a state $|j = 3/2, m_j = 1/2\rangle$ and operation of $L_+ + S_+$ on the corresponding functions of $|m_\ell = 0, m_s = -1/2\rangle$ and $|m_\ell = -1, m_s = 1/2\rangle$ results

in states $|m_\ell = 0, m_s = 1/2\rangle$ and $|m_\ell = +1, m_s = -1/2\rangle$. In this way we obtain all the basis functions for $\Gamma_8^+(\Gamma_{15}^+)$ given in Eq. (20.21).

We will now proceed to obtain the basis functions for $\Gamma_6^+(\Gamma_{15}^+)$ which are

$$
\begin{array}{lll}
|j, m_j\rangle \text{ State} & \text{Basis Function} & \\
|\frac{1}{2}, \frac{1}{2}\rangle & \lambda_1 = \frac{1}{\sqrt{3}}[(L_x + iL_y)\downarrow - L_z\uparrow] & (20.25) \\
|\frac{1}{2}, -\frac{1}{2}\rangle & \lambda_2 = \frac{1}{\sqrt{3}}[-(L_x - iL_y)\uparrow + L_z\downarrow].
\end{array}
$$

The notation "ξ_i" was used in Eq. (20.21) to denote the four $\Gamma_8^+(\Gamma_{15}^+)$ basis functions for $j = 3/2$ and "λ_i" for the two $\Gamma_6^+(\Gamma_{15}^+)$ basis functions for $j = 1/2$. This notation "ξ_i" and "λ_i" is arbitrary and not standard in the literature.

To obtain the $\Gamma_6^+(\Gamma_{15}^+)$ basis functions we note that the appropriate (m_ℓ, m_s) quantum numbers corresponding to $j = 1/2$ and $m_j = \pm 1/2$ are

$$
\begin{array}{llll}
m_\ell = 0 & & m_s & = \pm\frac{1}{2} \\
m_\ell = 1 & & m_s & = -\frac{1}{2} \\
m_\ell = -1 & & m_s & = +\frac{1}{2}
\end{array}
$$

so that the corresponding basis functions are completely specified by making them orthogonal to the $|j = 3/2, m_j = +1/2\rangle$ and $|j = 3/2, m_j = -1/2\rangle$ states. For example, the function orthogonal to

$$
\sqrt{\frac{2}{3}}\left|m_\ell = 0, m_s = -\frac{1}{2}\right\rangle + \frac{1}{\sqrt{3}}\left|m_\ell = -1, m_s = +\frac{1}{2}\right\rangle \tag{20.26}
$$

is the function

$$
\frac{1}{\sqrt{3}}\left|m_\ell = 0, m_s = -\frac{1}{2}\right\rangle - \sqrt{\frac{2}{3}}\left|m_\ell = -1, m_s = +\frac{1}{2}\right\rangle \tag{20.27}
$$

which yields the basis functions for the $|j = 1/2, m_j = -1/2\rangle$ state:

$$
\frac{1}{\sqrt{3}}\left|L_z\downarrow - (L_x - iL_y)\uparrow\right\rangle. \tag{20.28}
$$

Similarly the basis function for the $|j = 1/2, m_j = +1/2\rangle$ state can be found by application of the raising operators J_+ and $(L_+ + S_+)$ to the $|j = 1/2, m_j = -1/2\rangle$ state, or alternatively by requiring orthogonality to the $|j = 3/2, m_j = +1/2\rangle$ state. Applying the raising operator to the state

$$\frac{1}{\sqrt{3}}\left|m_\ell = 0, m_s = -\frac{1}{2}\right\rangle - \sqrt{\frac{2}{3}}\left|m_\ell = -1, m_s = +\frac{1}{2}\right\rangle \qquad (20.29)$$

yields:

$$\frac{1}{\sqrt{3}}\left|m_\ell = 0, m_s = +\frac{1}{2}\right\rangle - \sqrt{\frac{2}{3}}\left|m_\ell = +1, m_s = -\frac{1}{2}\right\rangle = \frac{1}{\sqrt{3}}[(L_x + iL_y)\downarrow - L_z \uparrow]$$
$$(20.30)$$

which is seen to be orthogonal to

$$\frac{1}{\sqrt{6}}[(L_x + iL_y)\downarrow + 2L_z \uparrow]. \qquad (20.31)$$

In finding the basis functions for $\Gamma_8^+(\Gamma_{15}^+)$ we have made use of the symmetry properties of the angular momentum operators. As far as the symmetry properties are concerned, it makes no difference whether $\vec{L}$ is an angular momentum function or an energy band wave function with Γ_{15}^+ symmetry. This concept allows us to write down wave functions with Γ_8^+ symmetry derived from other single group states, and tables of these results are given in §19.6, taken from Koster's book, where tables of coupling coefficients for all point groups are given.

20.5 Basis Functions for Other Γ_8^+ States

Basis functions for the $\Gamma_8^{\pm}$ state derived from $\Gamma_8^-(\Gamma_{15}^-)$, $\Gamma_8^+(\Gamma_{25}^+)$, $\Gamma_8^-(\Gamma_{25}^-)$, etc. can be found from Γ_8^+ (Γ_{15}^+) and Γ_6^+ (Γ_{15}^+). All we have to do is to replace

$$L_x, L_y, L_z \rightarrow x, y, z$$

in the Eqs. (20.21) of §20.4 to obtain the basis functions for $\Gamma_8^-(\Gamma_{15}^-)$. Likewise to obtain $\Gamma_8^+(\Gamma_{25}^+)$, we have to replace

$$L_x, L_y, L_z \rightarrow \varepsilon_x, \varepsilon_y, \varepsilon_z \ ,$$

where $\varepsilon_x = yz, \varepsilon_y = zx, \varepsilon_z = xy$. By using this prescription, the basis functions for $\Gamma_8^\pm$ will be of the same form for all symmetry-related partners, whether the basis functions are derived from a $\Gamma_{15}^\pm$ or a $\Gamma_{25}^\pm$ single group representation. This correspondence is a highly desirable feature for working practical problems.

We note that the $\Gamma_8^+(\Gamma_{12}^+)$ representation can also be produced by considering the electron spin for a Γ_{12}^+ spinless level: $\Gamma_6^+ \otimes \Gamma_{12}^+ = \Gamma_8^+$. We can always make a set of 4 basis functions for this representation out of $f_1 \uparrow, f_1 \downarrow, f_2 \uparrow, f_2 \downarrow$ where $f_1 = x^2 + \omega y^2 + \omega^2 z^2, f_2 = f_1^*$ and $\omega = \exp(2\pi i/3)$. This makes up a perfectly good representation, but the partners look very different from those of $\Gamma_8^+(\Gamma_{15}^+)$ or $\Gamma_8^+ (\Gamma_{25}^+)$. We can however make a unitary transformation of these 4 functions so that they look like the $\Gamma_8^+ (\Gamma_{15}^+)$ set.

We can make use of these double group basis functions in many ways. For example, these basis functions are used to determine the non-vanishing $\vec{k} \cdot \vec{p}$ **matrix elements** $(u_{n,0}^{\Gamma_i}|\mathcal{H}'|u_{n,0}^{\Gamma_j})$ in Eq. (20.12). These basis functions also determine which of the non-vanishing matrix elements are equal to each other for a given group of the wave vector.

One technique that can be used to determine the number of non-vanishing matrix elements in cases involving multidimensional representations is as follows. If the relevant matrix element is of the form $(\Gamma_i|\Gamma_{\text{interaction}}|\Gamma_j)$ then the **number of independent matrix elements** is the number of times the identity representation (Γ_1^+) is contained in the triple direct product $\Gamma_i \otimes \Gamma_{\text{interaction}} \otimes \Gamma_j$. For example, the direct product of the matrix element $(\Gamma_1^+|\Gamma_{15}^-|\Gamma_{15}^-)$ is:

$$\Gamma_1^+ \otimes \Gamma_{15}^- \otimes \Gamma_{15}^- = \Gamma_1^+ + \Gamma_{12}^+ + \Gamma_{15}^+ + \Gamma_{25}^+.$$

and since all non-vanishing matrix elements must be invariant under all symmetry operations of the group, only the Γ_1^+ term leads to a non-vanishing matrix element. Of the 9 possible combinations of partners, there is only one independent non-vanishing matrix element.

For the case of double groups, the matrix element $(\Gamma_6^+|\Gamma_{15}^-|\Gamma_6^-)$ has $2 \times 3 \times 2 = 12$ possible combinations. Now $\Gamma_6^+ \otimes \Gamma_{15}^- \otimes \Gamma_6^- = \Gamma_1^+ + \Gamma_{15}^+ + \Gamma_{12}^+ + \Gamma_{15}^+ + \Gamma_{25}^+$, so that once again there is only one independent matrix element. Finally, for the case $(\Gamma_6^+|\Gamma_{15}^-|\Gamma_8^-)$ there are 24 possible

combinations. The direct product $\Gamma_6^+ \otimes \Gamma_{15}^- \otimes \Gamma_8^- = \Gamma_1^+ + \Gamma_2^+ + \Gamma_{12}^+ + 2\Gamma_{15}^+ + 2\Gamma_{25}^+$, and once again there is one independent matrix element. Furthermore, if Γ_6^- and Γ_8^- are both related through a Γ_{15}^- interaction term, then the **same independent matrix element** applies to both $(\Gamma_6^+|\Gamma_{15}^-|\Gamma_6^-)$ and $(\Gamma_6^+|\Gamma_{15}^-|\Gamma_8^-)$. We illustrate this simplifying feature in §20.6.

20.6 $E(\vec{k})$ for a Non-Degenerate Band Including Spin-Orbit Interaction

We are now ready to give the form of $E(\vec{k})$ for a non-degenerate band using non-degenerate $\vec{k} \cdot \vec{p}$ perturbation theory [see Eq. (20.12)] by considering the form of the $\vec{k} \cdot \vec{p}$ matrix elements implied by group theory. As an example, consider a non-degenerate Γ_6^+ band. We take as basis functions for the Γ_6^+ state:

$$\Gamma_6^+ : \quad \left\{ \begin{array}{l} 1 \uparrow \\ 1 \downarrow \end{array} \right. . \tag{20.32}$$

Within the framework of $\vec{k} \cdot \vec{p}$ perturbation theory, the Γ_6^+ state couples only to Γ_6^- and Γ_8^- since $\Gamma_6^+ \otimes \Gamma_{15}^- = \Gamma_6^- + \Gamma_8^-$. For the Γ_6^- and Γ_8^- states we use the basis functions derived from Eq. (20.21) and Eq. (20.25), so that for $\Gamma_6^+(\Gamma_{15}^+)$ we write

$|j, m_j\rangle$ State	Basis Function	
$|\frac{1}{2}, \frac{1}{2}\rangle$	$(\frac{1}{\sqrt{3}})[(x + iy) \downarrow -z \uparrow]$	(20.33)
$|\frac{1}{2}, -\frac{1}{2}\rangle$	$(\frac{1}{\sqrt{3}})[-(x - iy) \uparrow +z \downarrow]$	

and for $\Gamma_8^+(\Gamma_{15}^+)$ we write

$|j, m_j\rangle$ State	Basis Function	
$|\frac{3}{2}, \frac{3}{2}\rangle$	$(\frac{1}{\sqrt{2}})(x + iy) \uparrow$	
$|\frac{3}{2}, \frac{1}{2}\rangle$	$(\frac{1}{\sqrt{6}})[(x + iy) \downarrow +2z \uparrow]$	(20.34)
$|\frac{3}{2}, -\frac{1}{2}\rangle$	$(\frac{1}{\sqrt{6}})[(x - iy) \uparrow +2z \downarrow]$	
$|\frac{3}{2}, -\frac{3}{2}\rangle$	$(\frac{1}{\sqrt{2}})(x - iy) \downarrow$	

We can read off the basis functions relating the $|j, m_j\rangle$ representation and the $|\ell s m_\ell m_s\rangle$ representation for the Γ_6^- ($j = 1/2$) and Γ_8^- ($j = 3/2$) states that are derived from the Γ_{15}^- level directly from Eqs. (20.33) and (20.34). The x, y and z in Eqs. (20.33) and (20.34) refer to the three partners of the Γ_{15}^+ state. For this case there are no non-vanishing matrix elements in Eq. (20.12) in first-order perturbation theory. In second-order, the non-vanishing terms are:

$$\left(1 \uparrow |P_x| \left(\frac{1}{\sqrt{2}}\right)(x + iy) \uparrow\right) = \left(\frac{1}{\sqrt{2}}\right)(1|P_x|x)$$

$$\left(1 \uparrow |P_y| \left(\frac{1}{\sqrt{2}}\right)(x + iy) \uparrow\right) = \left(\frac{i}{\sqrt{2}}\right)(1|P_y|y)$$

$$\left(1 \uparrow |P_z| \left(\frac{1}{\sqrt{6}}\right)\{(x + iy) \downarrow +2z \uparrow\}\right) = \left(\frac{2}{\sqrt{6}}\right)(1|P_z|z)$$

$$\left(1 \uparrow |P_x| \left(\frac{1}{\sqrt{6}}\right)\{(x - iy) \uparrow +2z \downarrow\}\right) = \left(\frac{1}{\sqrt{6}}\right)(1|P_x|x)$$

$$\left(1 \uparrow |P_y| \left(\frac{1}{\sqrt{6}}\right)\{(x - iy) \uparrow +2z \downarrow\}\right) = -\left(\frac{i}{\sqrt{6}}\right)(1|P_y|y)$$

$$\left(1 \uparrow |P_z| \left(\frac{1}{\sqrt{3}}\right)\{(x + iy) \downarrow -z \uparrow\}\right) = -\left(\frac{1}{\sqrt{3}}\right)(1|P_z|z)$$

$$\left(1 \uparrow |P_x| \left(\frac{1}{\sqrt{3}}\right)\{(-x + iy) \uparrow +z \downarrow\}\right) = -\left(\frac{1}{\sqrt{3}}\right)(1|P_x|x)$$

$$\left(1 \uparrow |P_y| \left(\frac{1}{\sqrt{3}}\right)\{(-x + iy) \uparrow +z \downarrow\}\right) = \left(\frac{i}{\sqrt{3}}\right)(1|P_y|y). \quad (20.35)$$

Summing up the second-order terms and utilizing the equality

$$(1|P_x|x) = (1|P_y|y) = (1|P_z|z) \quad (20.36)$$

we obtain

$$E^{\Gamma_6^+}(\vec{k}) = E^{\Gamma_6^+}(0) + \frac{\hbar^2|(1|P_x|x)|^2}{m^2 E_g}\left\{\frac{1}{3}k_x^2 + \frac{1}{3}k_y^2 + \frac{1}{3}k_z^2\right\}$$

$$+ \frac{\hbar^2|(1|P_x|x)|^2}{m^2(E_g + \Delta)}\left\{\frac{1}{2}k_x^2 + \frac{1}{2}k_y^2 + \frac{2}{3}k_z^2 + \frac{1}{6}k_x^2 + \frac{1}{6}k_y^2\right\}$$

$$= E^{\Gamma_6^+}(0) + \frac{\hbar^2 k^2}{m^2}|(1|P_x|x)|^2\left\{\frac{1}{3E_g} + \frac{2}{3(E_g + \Delta)}\right\} \quad (20.37)$$
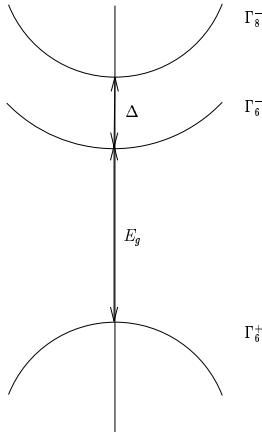
Figure 20.1: Energy versus k at the Γ point showing the effect of the spin-orbit interaction in splitting the p-level. The relevant bands are labeled by the double group representations.

where E_g and $E_g + \Delta$ are defined in Fig. 20.1.

20.7 $E(\vec{k})$ for Degenerate Bands Including Spin-Orbit Interaction

In dealing with $\vec{k} \cdot \vec{p}$ perturbation theory for degenerate states we again use basis functions such as are given by Eqs. (20.21) and (20.25) to classify the degenerate states. For example, instead of the ($3 \times$ 3) secular equation for p-bands (Γ_{15}^- symmetry) that was discussed in § 17.5, inclusion of the spin-orbit interaction leads to solution of a (6×6) secular equation. This (6×6) equation assumes block diagonal form containing a (4×4) and a (2×2) block, because the spin functions transform as $D_{1/2}$ or Γ_6^+ and because

$$\Gamma_6^+ \otimes \Gamma_{15}^- = \Gamma_6^- + \Gamma_8^- \tag{20.38}$$

where Γ_6^- corresponds to a $j = 1/2$ state and Γ_8^- to a $j = 3/2$ state (see Fig. 20.1).

An important application of degenerate $\vec{k} \cdot \vec{p}$ perturbation theory including the effects of spin-orbit interaction is to the valence band of the group IV and III-V compound semiconductors. A description of $E(\vec{k})$ for the valence band is needed to construct the constant energy surfaces for holes in these semiconductors. This method is useful for

analysis of cyclotron resonance measurements on holes in group IV and III-V semiconductors.

One way to solve for the energy levels of the valence band of a group IV semiconductor about the valence band maximum $\vec{k} = 0$ (Γ_{25}^+ single group level) is to start with the (6×6) matrix labeled by the double group basis functions. The secular equation is constructed by considering

$$\mathcal{H} = \mathcal{H}_0 + \mathcal{H}'_{\vec{k}\cdot\vec{p}} \tag{20.39}$$

in which the matrix elements for $\mathcal{H}'_{\vec{k}\cdot\vec{p}}$ vanish in first-order. Therefore in degenerate second-order perturbation theory we must replace each matrix element $\langle i|\mathcal{H}'|j\rangle$ by

$$\langle i|\mathcal{H}'|j\rangle + \sum_{\alpha} \frac{\langle i|\mathcal{H}'|\alpha\rangle\langle\alpha|\mathcal{H}'|j\rangle}{E_i - E_\alpha} \tag{20.40}$$

in which $\mathcal{H}'$ denotes the $\vec{k}\cdot\vec{p}$ perturbation Hamiltonian (see §17.5), and i, j, α all denote double group irreducible representations. In this case we obtain the appropriate basis functions for the Γ_7^+ and Γ_8^+ states from the combination that we previously derived using the raising operator $J_+ = L_+ + S_+$ [see Eqs. (20.21) and (20.25)]. Thus for the $\Gamma_7^+ (\Gamma_{25}^+)$ states, the basis functions are

$$
\begin{array}{lll}
|j, m_j\rangle \text{ State} & \text{Basis Function} & \\
|\frac{1}{2}, \frac{1}{2}\rangle & \mu_1 = \frac{1}{\sqrt{3}}[(\varepsilon_x + i\varepsilon_y)\downarrow -\varepsilon_z\uparrow] & (20.41) \\
|\frac{1}{2}, \frac{1}{2}\rangle & \mu_2 = \frac{1}{\sqrt{3}}[-(\varepsilon_x - i\varepsilon_y)\uparrow +\varepsilon_z\downarrow] &
\end{array}
$$

and for the $\Gamma_8^+ (\Gamma_{25}^+)$ states, the basis functions are

$$
\begin{array}{lll}
|j, m_j\rangle \text{ State} & \text{Basis Function} & \\
|\frac{3}{2}, \frac{3}{2}\rangle & \nu_1 = \frac{1}{\sqrt{2}}(\varepsilon_x + i\varepsilon_y)\uparrow & \\
|\frac{3}{2}, \frac{1}{2}\rangle & \nu_2 = \frac{1}{\sqrt{6}}[(\varepsilon_x + i\varepsilon_y)\downarrow +2\varepsilon_z\uparrow] & (20.42) \\
|\frac{3}{2}, -\frac{1}{2}\rangle & \nu_3 = \frac{1}{\sqrt{6}}[(\varepsilon_x - i\varepsilon_y)\uparrow +2\varepsilon_z\downarrow] & \\
|\frac{3}{2}, -\frac{3}{2}\rangle & \nu_4 = \frac{1}{\sqrt{2}}(\varepsilon_x - i\varepsilon_y)\downarrow &
\end{array}
$$

in which the states Γ_7^+ and Γ_8^+ are labeled by $|j, m_j\rangle$ and the components of the function ε_i relate to x, y, z partners according to

$$
\begin{aligned}
\varepsilon_x &= yz \\
\varepsilon_y &= zx \\
\varepsilon_z &= xy.
\end{aligned} \tag{20.43}
$$

In solving for $E(\vec{k})$ for the valence band of a semiconductor such as germanium we use the unperturbed and perturbed Hamiltonians given by Eqs. (20.10) and (20.11), respectively. The states used to solve the eigenvalue problem are labeled by the wave functions that diagonalize the "unperturbed" Hamiltonian $\mathcal{H}_0$ of Eq. (20.10). Since $\mathcal{H}'_{\vec{k}\cdot\vec{p}}$ transforms as Γ_{15}^- and $\Gamma_{15}^- \otimes \Gamma_7^+ = \Gamma_7^- + \Gamma_8^-$, $\mathcal{H}'_{\vec{k}\cdot\vec{p}}$ does not couple band Γ_7^+ to band Γ_7^+. This result follows more easily just from parity arguments.

A solution to the (6×6) secular equation involves explicit computation of matrix elements as was done for the spinless case in §17.5. For brevity, we will not include a detailed evaluation of all the matrix elements, but we will instead just summarize the results. For the $\Gamma_7^+ (\Gamma_{25}^+)$ level, $E(\vec{k})$ assumes the form

$$E(\Gamma_7^+) = k^2 \left(\frac{\hbar^2}{2m} + 4C_1 + \frac{4}{3}C_2 + C_3 \right) \qquad (20.44)$$

where

$$
\begin{aligned}
C_1 &= \frac{\hbar^2}{m^2} \left\{ \sum_{\Gamma_8^-(\Gamma_{12}^-)} \frac{|\langle \Gamma_7^+|P_x|\Gamma_8^-\rangle|^2}{E_0 - E_\ell} + \sum_{\Gamma_8^-(\Gamma_{25}^-)} \frac{|\langle \Gamma_7^+|P_x|\Gamma_8^-\rangle|^2}{E_0 - E_\ell} \right\} \\
C_2 &= \frac{\hbar^2}{m^2} \sum_{\Gamma_8^-(\Gamma_{15}^-)} \frac{|\langle \Gamma_7^+|P_x|\Gamma_8^-\rangle|^2}{E_0 - E_\ell} \\
C_3 &= \frac{\hbar^2}{m^2} \sum_{\Gamma_7^-(\Gamma_2^-)} \frac{|\langle \Gamma_7^+|P_z|\Gamma_7^-\rangle|^2}{E_0 - E_\ell}
\end{aligned} \qquad (20.45)
$$

in which

$$\vec{P} = \vec{p} + \frac{\hbar}{4m^2c^2}(\vec{\sigma} \times \vec{\nabla}V) \qquad (20.46)$$

and E_ℓ is an intermediate state. Since bands with Γ_{12}^- and Γ_{25}^- symmetries do not lie close to the valence band Γ_{25}^+ in germanium we would expect C_1 to be much smaller than C_2 or C_3.

The solution for the Γ_8^+ level is a good deal more complicated and yields the result

$$E[\Gamma_8^+(\Gamma_{25}^+)] = Ak^2 \pm \sqrt{B^2k^4 + C^2(k_x^2k_y^2 + k_y^2k_z^2 + k_z^2k_x^2)} \qquad (20.47)$$

where

$$
\begin{aligned}
A = {} & \tfrac{\hbar^2}{2m} + \tfrac{2}{3}E_1 + 2E_2 + E_3 + 5E_4 + \tfrac{1}{2}E_5 \\
B^2 = {} & \tfrac{4}{9}E_1^2 + 4E_2^2 + 16E_4^2 + \tfrac{1}{4}E_5^2 - \tfrac{8}{3}E_1E_2 + \tfrac{16}{3}E_1E_4 \\
& - \tfrac{2}{3}E_1E_5 - 16E_2E_4 + 2E_2E_5 - 4E_4E_5 \\
C^2 = {} & -\tfrac{9}{16}E_5^2 + 16E_1E_2 - 32E_1E_4 + E_1E_5 - 9E_2E_5 + 18E_4E_5
\end{aligned}
\tag{20.48}
$$

and where

$$
\begin{aligned}
E_1 &= \frac{\hbar^2}{m^2} \sum_{\Gamma_6^-\,(\Gamma_{15}^-)} \frac{|\langle \Gamma_8^+|P_x|\Gamma_6^-\rangle|^2}{E_0 - E_\ell} \\[2ex]
E_2 &= \frac{\hbar^2}{m^2} \sum_{\Gamma_7^-\,(\Gamma_2^-)} \frac{|\langle \Gamma_8^+|P_x|\Gamma_7^-\rangle|^2}{E_0 - E_\ell} \\[2ex]
E_3 &= \frac{\hbar^2}{m^2} \sum_{\Gamma_8^-\,(\Gamma_{15}^-)} \frac{|\langle \Gamma_8^+(\Gamma_{25}^+)|P_z|\Gamma_8^-(\Gamma_{15}^-)\rangle|^2}{E_0 - E_\ell} \\[2ex]
E_4 &= \frac{\hbar^2}{m^2} \sum_{\Gamma_8^-\,(\Gamma_{25}^-)} \frac{|\langle \Gamma_8^+(\Gamma_{25}^+)|P_z|\Gamma_8^-(\Gamma_{25}^-)\rangle|^2}{E_0 - E_\ell} \\[2ex]
E_5 &= \frac{\hbar^2}{m^2} \sum_{\Gamma_8^-\,(\Gamma_{12}^-)} \frac{|\langle \Gamma_8^+(\Gamma_{25}^+)|P_z|\Gamma_8^-(\Gamma_{12}^-)\rangle|^2}{E_0 - E_\ell}.
\end{aligned}
\tag{20.49}
$$

In Eqs. (20.49), E_4 and E_5 are expected to be small. Because of the $E_0 - E_\ell$ denominator that enters second-order degenerate perturbation theory, the most important contributions to $\vec{k} \cdot \vec{p}$ perturbation theory come from bands lying close in energy to the E_0 level, which in this case are the Γ-point valence band energy extrema. For germanium the levels lying close to the Fermi level have $\Gamma_{25}^+, \Gamma_1^+, \Gamma_2^-$ and Γ_{15}^- symmetries (see Fig. 19.2) so that only the double group states derived from these states will contribute significantly to the sums in Eqs. (20.49). The far-lying levels only contribute small correction terms.

Although the spin-orbit perturbation term contained in $\mathcal{H}_0$ in Eq. (20.10) does not depend on $\vec{k}$, the resulting energy bands show a $\vec{k}$-dependent spin-orbit splitting. For example, in Figure 19.2 we note that the spin-orbit splitting of the Γ_8^+ (Γ_{25}^+) level is $\Delta = 0.29$ eV at the Γ point while along the Λ axis, the splitting is only about 2/3 this value and remains

constant over most of the Λ axis. For the corresponding levels along the Δ or (100) direction, the spin-orbit splitting is very much smaller. When the spin-orbit interaction is weak, it is convenient to deal with this interaction in perturbation theory. We note that the spin-orbit interaction can be written in diagonal form using the $|j, m_j\rangle$ representation. Therefore instead of writing the wavefunctions for the unperturbed problem in the $|\ell, s, m_\ell, m_s\rangle$ representation, it is convenient to use the $|j, m_j\rangle$ representation for the whole perturbation theory problem. A classic work on spin-orbit interaction in solids is R.J. Elliott, Phys. Rev. $\underline{96}$, 266 (1954). An application to $\vec{k} \cdot \vec{p}$ perturbation theory is found in Phys. Rev. $\underline{98}$, 368 (1955).

20.8 Effective g–Factor

One of the important applications of double groups in solid state physics is to the treatment of the effective g–factor. In calculating the effective g-factor (g_{eff}), we employ $\vec{k} \cdot \vec{p}$ perturbation theory with spin, and show that in a magnetic field B, new terms arise in the one-electron Hamiltonian. Some of these new terms have the symmetry of an axial vector (e.g., the magnetic moment μ_{eff}), giving rise to an interaction $\vec{\mu}_{\text{eff}} \cdot \vec{B}$. We review first the origin of the effective g–factor in solid state physics and show the important role of group theory in the evaluation of the pertinent matrix elements. In this problem we consider 3 perturbations

1. spin-orbit interaction

2. $\vec{k} \cdot \vec{p}$ perturbation

3. perturbation by a magnetic field.

We will see that the effective one-electron Hamiltonian for an electron in a solid in an applied magnetic field can be written as

$$\mathcal{H}_{\text{eff}} = \frac{1}{2m^*_{\alpha\beta}} \left(\vec{p} - \frac{e}{c}\vec{A} \right)^2 - g_{\text{eff}}\mu_B m_s B \qquad (20.50)$$

which implies that in effective mass theory, the periodic potential is replaced by both an effective mass tensor and an effective g-factor.

Just as the effective mass of an electron can differ greatly from the free electron value, so can the effective g–factor differ greatly from the free electron value of 2. To see how this comes about, let us consider energy bands about a band extrema in a crystal with O_h symmetry. The discussion given here follows closely that given for $\vec{k} \cdot \vec{p}$ perturbation theory in Chapter 17.

Every entry in the secular equation for the $\vec{k} \cdot \vec{p}$ Hamiltonian is of the following form since there are no entries in first-order that couple the degenerate states:

$$\frac{\hbar^2 k^2}{2m} \delta_{n,n'} + \sum_{n''} \frac{\langle n | \mathcal{H}' | n'' \rangle \langle n'' | \mathcal{H}' | n' \rangle}{E_n - E_{n''}} \tag{20.51}$$

where $\sum_{n''}$ denotes the sum over states outside the nearly degenerate set (NDS) and where we are assuming that every member in the NDS is of approximately the same energy, like the situation for degenerate p-bands or of strongly coupled s and p bands. The $\vec{k} \cdot \vec{p}$ perturbation Hamiltonian is $\mathcal{H}' = \frac{\hbar}{m} \vec{k} \cdot \vec{p}$ for the spinless problem or $\mathcal{H}' = \frac{\hbar}{m} \vec{k} \cdot \vec{P}$ for the problem with spin, where $\vec{P} = \vec{p} + \frac{\hbar}{4mc^2} \vec{\sigma} \times \vec{\nabla} V$. With this identification of $\mathcal{H}'$ we can rewrite the entries to the secular equation as

$$\sum_{\alpha\beta} D_{nn'\alpha\beta} k_\alpha k_\beta = \sum_{\alpha\beta} k_\alpha k_\beta \left\{ \frac{\hbar^2}{2m} \delta_{nn'} \delta_{\alpha\beta} + \frac{\hbar^2}{m^2} \sum_{n''} \frac{\langle n | P_\alpha | n'' \rangle \langle n'' | P_\beta | n' \rangle}{E_n^{(0)} - E_{n''}^{(0)}} \right\} \tag{20.52}$$

where $\sum_{\alpha\beta}$ denotes a sum on components of the $\vec{k}$ vectors, and $\sum_{n''}$ denotes a sum over members outside the NDS, and where $D_{nn'\alpha\beta}$ denotes the term in curly brackets, and depends on the band indices n, n'. The eigenvalues are found by solving the secular equation

$$\sum_{n'} \left[\sum_{\alpha\beta} D_{nn'\alpha\beta} k_\alpha k_\beta - E \delta_{nn'} \right] f_{n'} = 0. \tag{20.53}$$

Equation 20.53 is the eigenvalue problem in zero magnetic field. The same form for the secular equation also applies when $B \neq 0$. This equation symbolically represents the problem with spin if the $f_{n'}$ functions are taken to transform as irreducible representations of the crystal double group and the $\vec{P}$ vectors are chosen so that they include the spin-orbit interaction $\vec{P} = \vec{p} + \frac{\hbar}{4mc^2} (\vec{\sigma} \times \vec{\nabla} V)$.

In an external magnetic field we replace the operator $\vec{p} \to \vec{p} - \frac{e}{c}\vec{A}$ in the Hamiltonian and from this it follows generally that in Eq. (20.53) we must replace

$$\hbar\vec{k} \to \frac{\hbar}{i}\vec{\nabla} - \frac{e}{c}\vec{A} \tag{20.54}$$

when a magnetic field is applied. The relation Eq. (20.54) is called the Kohn–Luttinger transcription and is widely used in the solution of magnetic field problems in semiconductor physics. As a result of Eq. (20.54), $\vec{k}$ in a magnetic field becomes a non-commuting operator, rather than just a simple commuting operator. Let us, for example, select a gauge for the vector potential

$$\begin{aligned} A_x &= -By \\ A_y &= 0 \\ A_z &= 0 \end{aligned} \tag{20.55}$$

so that $\vec{B} = B\hat{z}$,

$$\hbar k_x = \frac{\hbar}{i}\frac{\partial}{\partial x} + \frac{e}{c}By \tag{20.56}$$

$$\hbar k_y = \frac{\hbar}{i}\frac{\partial}{\partial y} \tag{20.57}$$

which results in the commutation relation

$$[k_x, k_y] = \frac{ieB}{\hbar c}. \tag{20.58}$$

The commutation relation [Eq. (20.58)] tells us that the amount by which the operators k_x and k_y fail to commute is proportional to B. We note that all other pairs of wave vector components, such as $[k_x, k_z]$ etc., commute. Since the order of operators is important in a magnetic field, we will need to rewrite the secular equation [Eq. (20.53)] when $B \neq 0$ in terms of a symmetric and an antisymmetric part:

$$D_{nn'\alpha\beta}k_\alpha k_\beta = \frac{1}{2}D^S_{nn'\alpha\beta}\underbrace{\{k_\alpha, k_\beta\}}_{\text{anticommutator}} + \frac{1}{2}D^A_{nn'\alpha\beta}\underbrace{[k_\alpha, k_\beta]}_{\text{commutator}} \tag{20.59}$$

where the symmetric part is

$$D^S_{nn'\alpha\beta} = \frac{1}{2}\left[D_{nn'\alpha\beta} + D_{nn'\beta\alpha}\right] \tag{20.60}$$

and the antisymmetric part is

$$D^A_{nn'\alpha\beta} = \frac{1}{2} \left[D_{nn'\alpha\beta} - D_{nn'\beta\alpha} \right]. \tag{20.61}$$

Thus the symmetric part can be written explicitly as

$$D^S_{nn'\alpha\beta} = \frac{\hbar^2}{2m}\delta_{nn'}\delta_{\alpha\beta} + \frac{\hbar^2}{2m^2} \sum_{n''} \frac{\langle n|P_\alpha|n''\rangle\langle n''|P_\beta|n'\rangle + \langle n|P_\beta|n''\rangle\langle n''|P_\alpha|n'\rangle}{E_n(0) - E_{n''}(0)} \tag{20.62}$$

and gives the effective mass tensor through the relation

$$\frac{1}{m^*_{\alpha\beta}} = \frac{\partial^2 E_n}{\hbar^2 \partial k_\alpha \partial k_\beta}. \tag{20.63}$$

Since the electron spin is included, the states in Eq. (20.62) are labeled by irreducible representations of the double groups and $\vec{P}$ is a function of $\vec{\sigma}$, as seen in Eq. (20.11).

The antisymmetric part $D^A_{nn'\alpha\beta}$ is from the above definition:

$$D^A_{nn'\alpha\beta} = \frac{\hbar^2}{2m^2} \sum_{n''} \frac{\langle n|P_\alpha|n''\rangle\langle n''|P_\beta|n'\rangle - \langle n|P_\beta|n''\rangle\langle n''|P_\alpha|n'\rangle}{E_n(0) - E_{n''}(0)}. \tag{20.64}$$

In the case of a spinless electron in a cubic crystal, $D^A_{nn'\alpha\beta}$ would vanish identically because there is only one independent momentum matrix element in cubic O_h symmetry in the absence of a magnetic field. If now we also include the electron spin and the double group representations, these arguments do not apply and we will find that $D^A_{nn'\alpha\beta}$ does not generally vanish and in fact contributes strongly to the effective g-factor.

By way of comparison, the zero magnetic field eigenvalue problem is

$$\sum_{n'} \left[\sum_{\alpha\beta} D_{nn'\alpha\beta} k_\alpha k_\beta - E\delta_{nn'} \right] f_{n'} = 0 \tag{20.65}$$

and the magnetic field eigenvalue problem then becomes

$$\sum_{n'} \left\{ \sum_{\alpha\beta} \frac{1}{2} \left[D^S_{nn'\alpha\beta}\{k_\alpha, k_\beta\} + D^A_{nn'\alpha\beta}[k_\alpha, k_\beta] \right] - \mu_B \vec{\sigma} \cdot \vec{B} - E\delta_{nn'} \right\} f_{n'} = 0 \tag{20.66}$$

where μ_B is the Bohr magneton

$$\mu_B = -\frac{|e|\hbar}{2mc}$$

and $\vec{\sigma} = 2\vec{S}/\hbar$. The term $D^S_{nn'\alpha\beta}$ gives rise to a replacement of the periodic potential by an effective mass tensor. In computing $m^*_{\alpha\beta}$ we ordinarily neglect the difference between $\vec{p}$ and $\vec{P}$.

In the presence of a magnetic field, the wavevectors $\vec{k}$ are operators which act on the effective mass wave functions $f_{n'}$. From Eq. (20.58) we see that the components of the wave vector operator do not commute, so that

$$[k_\alpha, k_\beta] = \frac{ieB_\gamma}{\hbar c} \tag{20.67}$$

and the commutator in Eq. (20.67) vanishes in zero magnetic field, as it should. Here the α, β, γ directions form a right-handed coordinate system. The term $D^A_{nn'\alpha\beta}$ vanishes if there is no spin. The commutator $[k_\alpha, k_\beta]$ transforms as an axial vector. Because of the form of $D^A_{nn'\alpha\beta}$ given in Eq. (20.64), we see that $D^A_{nn'\alpha\beta}$ also transforms as an axial vector. Therefore the term $D^A_{nn'\alpha\beta}$ has the same symmetry properties as $-\mu_B\vec{\sigma}$ and gives rise to an effective magnetic moment different from the free electron value of the Bohr magneton μ_B. If we now write

$$[k_x, k_y] = \frac{ieB_z}{\hbar c} = iB_z\left(\frac{e\hbar}{2mc}\right)\left(\frac{2m}{\hbar^2}\right) = i\mu_B B_z \frac{2m}{\hbar^2} \tag{20.68}$$

then

$$D^A_{nn'xy}[k_x, k_y] = \frac{iB_z}{m}\mu_B \sum_{n''} \frac{\langle n|P_x|n''\rangle\langle n''|P_y|n'\rangle - \langle n|P_y|n''\rangle\langle n''|P_x|n'\rangle}{E_n(0) - E_{n''}(0)} \tag{20.69}$$

so that the effective magnetic moment of an electron in a crystal is

$$\mu^*_{\alpha\beta} = |\mu_B|\left[\delta_{\alpha\beta} + \frac{i}{m}\sum_{n''} \frac{\langle n|P_\alpha|n''\rangle\langle n''|P_\beta|n\rangle - \langle n|P_\beta|n''\rangle\langle n''|P_\alpha|n\rangle}{E_n(0) - E_{n''}(0)}\right] \tag{20.70}$$

where the effective g–factor is related to $\mu^*_{\alpha\beta}$ by $g_{\text{eff }\alpha\beta} = 2\mu^*_{\alpha\beta}/\mu_B$.

We recall that the energy levels of a free electron in a magnetic field are

$$E_{m_s} = g\mu_B m_s B \tag{20.71}$$

so that for spin $1/2$, the spin splitting of the levels is $2\mu_B B$. In a crystalline solid, the spin splitting becomes $2\mu^* B$.

For comparison we include the formula for the effective mass tensor component

$$\frac{1}{m^*_{\alpha\beta}} = \frac{\delta_{\alpha\beta}}{m} + \frac{1}{m^2}\sum_{n''}\frac{\langle n|P_\alpha|n''\rangle\langle n''|P_\beta|n\rangle + \langle n|P_\beta|n''\rangle\langle n''|P_\alpha|n\rangle}{E_n(0) - E_{n''}(0)}$$

(20.72)

in which

$$\vec{P} = \vec{p} + \frac{\hbar}{4mc^2}\vec{\sigma}\times\vec{\nabla}V. \tag{20.73}$$

Thus an electron in a magnetic field and in a periodic potential acts as if the periodic potential can be replaced by letting $m \to m^*_{\alpha\beta}$ and $\mu_B \to \mu^*_{\alpha\beta}$. Thus, symbolically we would write an effective Hamiltonian as

$$H_{\text{eff}} = \frac{1}{2m^*}\left(p - \frac{e}{c}A\right)^2 - \mu^*\vec{\sigma}\cdot\vec{B} \tag{20.74}$$

where

$$\mu^* = \mu_B g_{\text{eff}}/2. \tag{20.75}$$

In deriving the formula for the effective g–factor above, we did not pay much attention to whether $\vec{P}$ was merely the momentum operator $\vec{p}$ or the more complete quantity including the spin-orbit interaction

$$\vec{p} + \frac{\hbar}{4mc^2}(\vec{\sigma}\times\vec{\nabla}V).$$

It turns out that it is not very important whether we distinguish between matrix elements of $\vec{p}$ and of $\vec{P}$ since the matrix element of

$$\frac{\hbar}{4mc^2}(\vec{\sigma}\times\vec{\nabla}V)$$

is generally quite small. However, what is important, and even crucial, is that we consider the states n, n', n'' as states characterized by the irreducible representations of the crystal double groups.

Let us illustrate how we would proceed to calculate an effective g–factor for a typical semiconductor. Let us consider the effective g-factor for germanium at the Γ point ($\vec{k} = 0$). In Fig. 20.2 we let E_g denote the
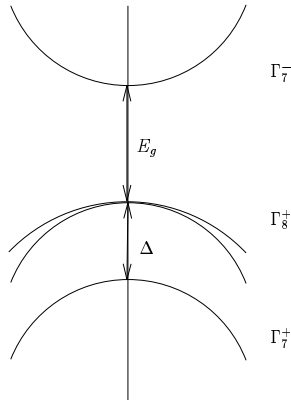
Figure 20.2: Level ordering at the Γ point in Ge.

energy gap between the conduction band and the uppermost valence band, and Δ denote the spin-orbit splitting of the valence band. In germanium $E_g \sim 0.8\text{eV}$ and $\Delta \sim 0.3\text{eV}$. We will assume in this simple example that these are the only bands to be included in carrying out the sum on n''.

To evaluate μ^* and m^* in Eqs. (20.70) and (20.72) we use the basis function discussed in §20.4 to find the non-vanishing matrix elements of $\hbar \vec{k} \cdot \vec{p}/m$. We write the basis functions for $\Gamma_8^+(\Gamma_{25}^+)$ and $\Gamma_7^+(\Gamma_{25}^+)$ in a symbolic form from Eqs. (20.41) and (20.42) so that we can make use of all the group theory ideas that were discussed in §17.5 in connection with the corresponding problem without spin. This approximation is valid if $\Delta \ll E_g$ and each double group level can be clearly identified with the single group level from which it originates. Otherwise the Γ_8^+ levels mix appreciably with one another and all matrix elements must be evaluated in the double group representation directly, so that the numerical estimates obtained here would have to be revised.

Take the basis functions for the Γ_7^- state to be $(\gamma^- \uparrow, \gamma^- \downarrow)$ where γ^- is a basis function for the Γ_2^- representation. Now let us evaluate the matrix elements that go into Eq. (20.70) for μ^*. For example, we obtain

$$\langle \gamma^- \uparrow |p_x| \frac{3}{2}, \frac{3}{2} \rangle = \langle \gamma^- \uparrow |p_x| \frac{1}{\sqrt{2}} (\varepsilon_x + i\varepsilon_y) \uparrow \rangle \qquad (20.76)$$

using the basis functions for Γ_8^+ (Γ_{25}^+)

$$
\begin{array}{ll}
|j, m_j\rangle \text{ State} & \text{Basis Function} \\
|\frac{3}{2}, \frac{3}{2}\rangle & \nu_1 = \frac{1}{\sqrt{2}}(\varepsilon_x + i\varepsilon_y) \uparrow \\
|\frac{3}{2}, \frac{1}{2}\rangle & \nu_2 = \frac{1}{\sqrt{6}}[(\varepsilon_x + i\varepsilon_y) \downarrow +2\varepsilon_z \uparrow] \\
|\frac{3}{2}, -\frac{1}{2}\rangle & \nu_3 = \frac{1}{\sqrt{6}}[(\varepsilon_x - i\varepsilon_y) \uparrow +2\varepsilon_z \downarrow] \\
|\frac{3}{2}, -\frac{3}{2}\rangle & \nu_4 = \frac{1}{\sqrt{2}}(\varepsilon_x - i\varepsilon_y) \downarrow
\end{array}
\tag{20.77}
$$

From §17.5 we have $(\Gamma_2^\pm|\mathcal{H}'|\Gamma_{25,\alpha}^\mp) = A_2\hbar k_\alpha/m$ where $A_2 = (\Gamma_2^\pm|p_x|\Gamma_{25,x}^\mp)$ is the only independent matrix element connecting these symmetry types, where we note that the basis function for Γ_2- symmetry is xyz.

Using the basis functions for $\Gamma_8^+(\Gamma_{25}^+)$ given by Eq. (20.77) we obtain

$$
\langle\gamma^- \uparrow |p_x|\frac{3}{2}, \frac{3}{2}\rangle = \frac{1}{\sqrt{2}}A_2
$$

$$
\langle\gamma^- \uparrow |p_x|\frac{3}{2}, \frac{1}{2}\rangle = 0
$$

$$
\langle\gamma^- \uparrow |p_x|\frac{3}{2}, -\frac{1}{2}\rangle = \frac{1}{\sqrt{6}}A_2
$$

$$
\langle\gamma^- \uparrow |p_x|\frac{3}{2}, -\frac{3}{2}\rangle = 0
$$

where we consider the ortho-normality of both the spin and orbital states. For the p_y matrix, the same procedure gives

$$
\langle\gamma^- \uparrow |p_y|\frac{3}{2}, \frac{3}{2}\rangle = \frac{i}{\sqrt{2}}A_2
$$

$$
\langle\gamma^- \uparrow |p_y|\frac{3}{2}, \frac{1}{2}\rangle = 0
$$

$$
\langle\gamma^- \uparrow |p_y|\frac{3}{2}, -\frac{1}{2}\rangle = -\frac{i}{\sqrt{6}}A_2
$$

$$
\langle\gamma^- \uparrow |p_y|\frac{3}{2}, -\frac{3}{2}\rangle = 0.
$$

To find the contribution to μ^*/μ_B, we sum Eq. (20.70) over the four Γ_8^+ levels we obtain

$$\sum_i \left[\langle \gamma^- \uparrow |p_x|\nu_i\rangle\langle\nu_i|p_y|\gamma^- \uparrow\rangle - \langle\gamma^- \uparrow |p_y|\nu_i\rangle\langle\nu_i|p_x|\gamma^- \uparrow\rangle \right]/E_g$$
$$= \frac{1}{E_g}\left[\left\{\frac{A_2}{\sqrt{2}}\right\}\left\{-\frac{iA_2^*}{\sqrt{2}}\right\} + \left\{\frac{A_2}{\sqrt{6}}\right\}\left\{\frac{iA_2^*}{\sqrt{6}}\right\} - \left\{\frac{iA_2}{\sqrt{2}}\right\}\left\{\frac{A_2^*}{\sqrt{2}}\right\} - \left\{-\frac{iA_2}{\sqrt{6}}\right\}\left\{\frac{A_2^*}{\sqrt{6}}\right\} \right]$$
$$= \frac{|A_2|^2}{E_g}\left[-\frac{2i}{3}\right].$$

(20.78)

We thus obtain for the contribution from the $\Gamma_8^+(\Gamma_{25}^+)$ levels to $\left(\frac{\mu^*}{\mu_B}\right)$ a value of

$$\frac{i}{m}\left(-\frac{2i}{3}\right)\frac{|A_2|^2}{E_g} = \frac{2|A_2|^2}{3mE_g}.$$

(20.79)

Let us now find the contribution to μ^*/μ_B from the spin-orbit split-off bands. Here we use the basis functions for $\Gamma_7^+(\Gamma_{25}^+)$

$$
\begin{array}{lll}
|j,m_j\rangle \text{ State} & \text{Basis Function} \\
|\frac{1}{2},\frac{1}{2}\rangle & \mu_1 = \frac{1}{\sqrt{3}}[(\varepsilon_x + i\varepsilon_y)\downarrow -\varepsilon_z \uparrow] & (20.80) \\
|\frac{1}{2},-\frac{1}{2}\rangle & \mu_2 = \frac{1}{\sqrt{3}}[-(\varepsilon_x - i\varepsilon_y)\uparrow +\varepsilon_z \downarrow]
\end{array}
$$

so that the matrix elements for p_x and p_y become

$$\langle\gamma^- \uparrow |p_x|\frac{1}{2},\frac{1}{2}\rangle = 0$$
$$\langle\gamma^- \uparrow |p_x|\frac{1}{2},-\frac{1}{2}\rangle = -\frac{1}{\sqrt{3}}A_2$$
$$\langle\gamma^- \uparrow |p_y|\frac{1}{2},\frac{1}{2}\rangle = 0$$
$$\langle\gamma^- \uparrow |p_y|\frac{1}{2},-\frac{1}{2}\rangle = \frac{i}{\sqrt{3}}A_2.$$

We thus obtain the contribution of

$$\frac{i}{m(E_g+\Delta)}\left[\frac{2i}{3}|A_2|^2\right] = -\frac{2}{3}\frac{|A_2|^2}{m(E_g+\Delta)}.$$

(20.81)

to μ^*/μ_B in Eq. (20.70) from the $\Gamma_7^+(\Gamma_{25}^+)$ levels. Adding up the two contributions from Eqs. (20.79) and (20.81) we finally obtain

$$\left(\frac{\mu^*}{\mu_B}\right)_{\text{orbital}} = -\frac{2|A_2|^2}{3m}\left[\frac{1}{E_g+\Delta} - \frac{1}{E_g}\right] + 1$$

(20.82)

where $+1$ is the free electron contribution.

We can now evaluate $|A_2|^2$ in terms of the conduction band effective mass using the symmetric contribution $D^S_{nn'\alpha\beta}$ and for this term we can use the relation

$$\frac{m}{m^*} = 1 + \frac{2}{m} \sum_n \frac{|\langle \gamma^- \uparrow |p_x|n\rangle|^2}{E_{\Gamma_{2'}}(0) - E_n(0)}. \tag{20.83}$$

Evaluating the matrix elements in Eq. (20.83) we thus obtain

$$\frac{m}{m^*} = 1 + \frac{2}{m} \left[\frac{|A_2|^2}{2E_g} + \frac{|A_2|^2}{6E_g} + \frac{|A_2|^2}{3(E_g + \Delta)} \right] \approx \frac{2}{3m} |A_2|^2 \left[\frac{2}{E_g} + \frac{1}{E_g + \Delta} \right] \tag{20.84}$$

where the free electron term of unity is usually small compared to other terms in the sum in Eq. (20.84) and can be neglected in many cases. Neglecting this term, we now substitute for $|A_2|^2$ in terms of m^* to obtain

$$g_{\text{eff}} = \frac{2\mu^*}{\mu_B} = 2 - \frac{2m}{m^*} \left(\frac{\Delta}{3E_g + 2\Delta} \right). \tag{20.85}$$

In the limit, $\Delta \to 0$, then $g \to 2$ in agreement with the results for the free electron g-factor. In the limit $\Delta \gg E_g$

$$g_{\text{eff}} \to 2 - \frac{m}{m^*} \tag{20.86}$$

which implies $g_{\text{eff}} \to -\frac{m}{m^*}$ for very light masses.

For germanium, for which $m^*/m \sim 0.12$, $\Delta \sim 0.3\text{eV}$, and $E_g \sim 0.8\text{eV}$, the effective g–factor mostly cancels the free electron contribution:

$$g_{\text{eff}} = 2 \left[1 - \frac{1}{0.12} \frac{0.3}{3(0.8) + 2(0.3)} \right] = 2 \left[1 - \frac{1}{1.2} \right] \simeq \frac{1}{3}. \tag{20.87}$$

For InSb, the spin-orbit splitting is large compared with the direct band gap $m^*/m \sim 0.013$, $\Delta \sim 0.9\text{eV}$, and $E_g \sim 0.2\text{eV}$

$$g_{\text{eff}} \sim 2 \left[1 - \frac{1}{0.013} \frac{0.9}{3(0.2) + 2(0.9)} \right] \sim 2(1 - 28) \simeq -54 \tag{20.88}$$

leading to the picture for InSb shown in Figure 20.3. In InSb, the spin splitting is almost as large as the Landau level separation. However,

Landau levels **Landau levels**
(no spin) **(with spin)**
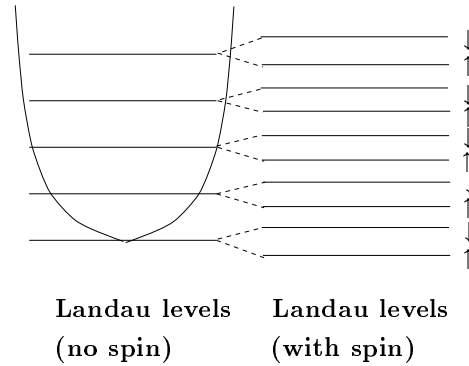
Figure 20.3: Landau levels in InSb showing the spin splitting resulting from the large negative effective g-factor.

the g_{eff} has the opposite sign as compared with free electron spin g–value, where we note that because of the negative sign of the charge on the electron and on the Bohr magneton, the free electron spin state of lowest energy is aligned antiparallel to the applied field. Sometimes it is convenient to define the spin effective mass by the relation

$$\frac{\mu^*}{\mu_B} = \frac{m}{m_s^*} \qquad (20.89)$$

where m_s^* denotes spin effective mass, so that $g_{\text{eff}} = 2m/m_s^*$.

In general, the spin and orbital effective masses will not be the same. If they are, the Landau level spacing is equal to the spacing between spin levels. The physical reason why these masses are not expected to be equal is that the orbital mass is determined by a momentum matrix element (which transforms as a radial vector). Since the spin mass depends on the coupling between bands through an operator which transforms as an axial vector, different bands are coupled for the 2 cases.

In treating cyclotron resonance transitions, the transitions are spin conserving and the g–factors usually cancel out. They are, however, important for interband Landau level transitions even though the transitions are spin conserving, since the g–factors in the valence and conduction bands can be different. Thus spin up and spin down transitions can occur at different energies. The effective g–factors are directly observed in spin resonance experiments which occur between the same
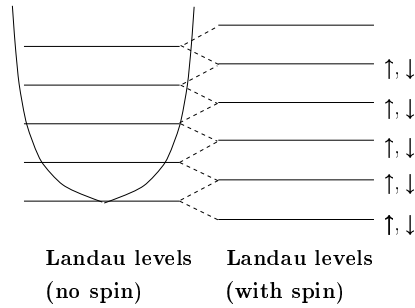
Figure 20.4: Strict 2-band model where the Landau level separation is equal to the spin splitting as for the case of a free electron gas. This limit applies quite well to the L-point Landau levels in bismuth.

Landau level but involve a spin flip.

Of interest also is the case where the spin effective mass and the orbital effective mass are equal. In a strict 2-band model this must be the case. For bismuth the strongly coupled 2-band model is approximately valid and $m_s^* \simeq m^*$ (see Figure 20.4). Landau level separations equal to the spin splitting also occur for the free electron magnetic energy levels. However, for band electrons, the Landau level separations are proportional to the inverse cyclotron effective mass rather than the inverse free electron mass.

For high mobility (low effective mass) materials with a small spin-orbit interaction, the Landau level separation is large compared with the spin splitting (see Fig. 20.3). On the other hand, some high mobility narrow gap semiconductors with a large spin-orbit interaction can have spin splittings larger than the Landau level separations; such a situation gives rise to interesting phenomena at high magnetic fields.

References for Effective g–Factors

Luttinger, Phys. Rev. <u>102</u>, 1030 (1956).
Yafet, Vol. 14 of Seitz-Turnbull Solid State Physics Series.
Roth, Phys. Rev. <u>118</u>, 1534 (1960).
Cohen and Blount, Phil. Mag. <u>5</u>, 115 (1960).
Wolff, J. Phys. Chem. Solids <u>25</u>, 1057 (1964).

20.9 Selected Problems

1. Bismuth is a semimetal which crystallizes in a rhombohedral structure (see Wyckoff vol. 1 p. 32) which is a slight distortion from a simple cubic structure. These distortions result in the semimetallic behavior for Bi with small electron pockets about the L points and a small hole pocket around the T point in the Brillouin zone. See the diagram below for the Bi band structure. As this distortion becomes small, the T-point becomes degenerate with the L-point.

Fig. 1. Bi. Band structure of bismuth along various symmetry lines and planes. The electronic structure was obtained from pseudopotential calculations. The energy unity 1 hartree equals 27.21 eV or 2 Ry [68G].
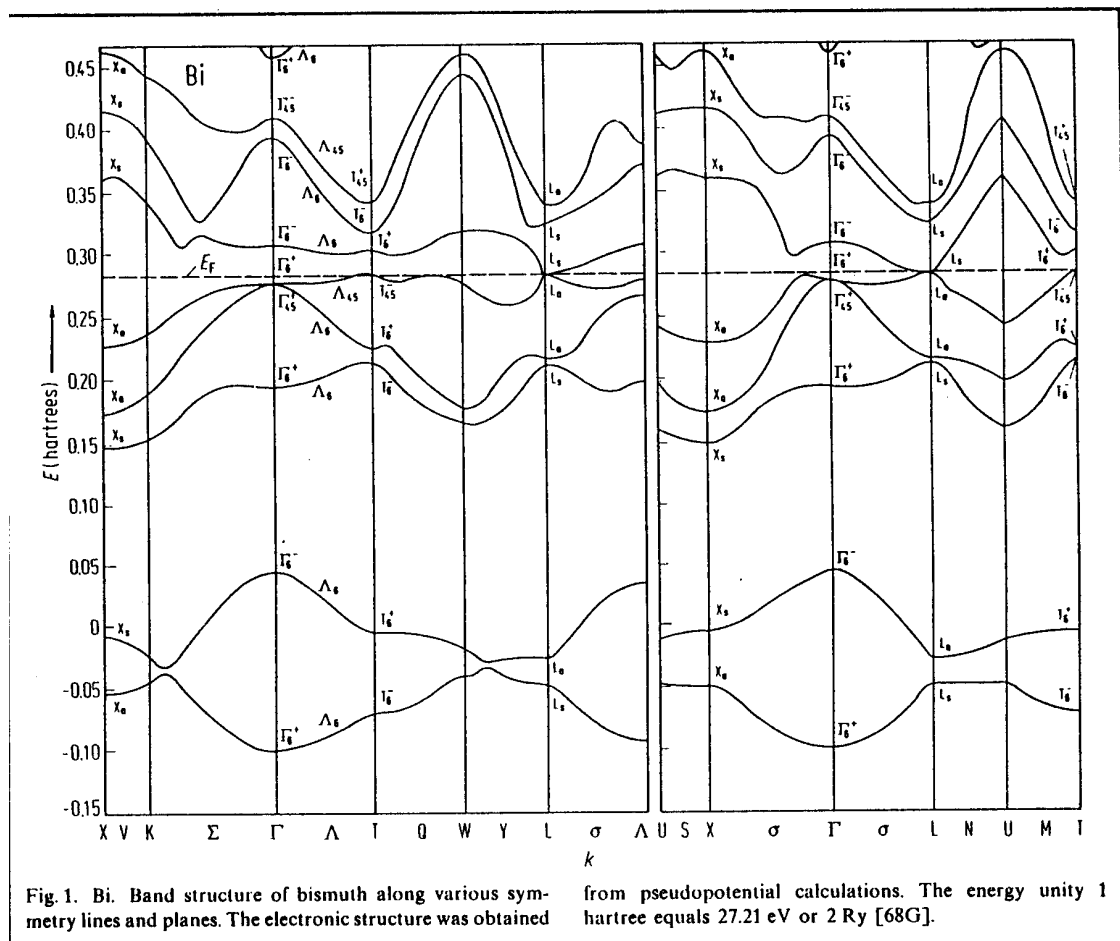
(a) Using double group $\vec{k} \cdot \vec{p}$ perturbation theory, find the form of $E(\vec{k})$ for the L point occupied conduction bands. How many L point electron pockets are there? (Note that in the cubic limit where the distortion vanishes, the L and T points of bismuth all become equivalent "L points" for a fcc Brillouin zone.) In the bismuth band structure shown below, the conduction band has $L_s = L_5 + L_6$ symmetry while the filled valence band strongly coupled to L_s has $L_a = L_7 + L_8$ symmetry, where L_s and L_a are, respectively, symmetric and antisymmetric under time reversal symmetry.

(b) Between which energy bands and where in the Brillouin zone do the far infrared transitions occur?

(c) Between which energy bands and where in the Brillouin zone do allowed optical transitions in the visible range occur?

Chapter 21

Time Reversal Symmetry

In this chapter we consider the properties of the time reversal operator for the case of no spin and when the spin-orbit interaction is included. The effect of time reversal symmetry on the energy dispersion relations is then considered, first for the case of no spin and then including the spin-orbit interaction.

In high energy physics, arguments regarding time inversion were essential in providing guidance for the development of a theory for the fundamental particles. The CPT invariance in particle physics deals with charge conjugation (C) which is the reversal of the sign of the electrical charge, parity (P) which is spatial inversion, and time inversion (T).

21.1   The Time Reversal Operator

Knowledge of the state of a system at any instant of time t and the deterministic laws of physics are sufficient to determine the state of the system both into the future and into the past. If $\psi(\vec{r}, t)$ specifies the time evolution of state $\psi(\vec{r}, 0)$, then $\psi(\vec{r}, -t)$ is called the **time-reversed conjugate** of $\psi(\vec{r}, t)$. The time-reversed conjugate state is achieved by running the system backwards in time or reversing all the velocities (or momenta) of the system.

The time evolution of a state is governed by Schrödinger's equation

(one of the deterministic laws of physics)

$$i\hbar\frac{\partial\psi}{\partial t} = \mathcal{H}\psi \tag{21.1}$$

which is satisfied by a time-dependent wave function of the form

$$\psi(\vec{r},t) = e^{\frac{-i\mathcal{H}t}{\hbar}}\psi(\vec{r},0) \tag{21.2}$$

where $\tilde{T} \equiv \exp\left[-i\mathcal{H}t/\hbar\right]$ is the time evolution operator. Under time reversal $t \to -t$ we note that $\psi \to \psi^*$ so that

$$\hat{T}\psi(\vec{r},t) = \psi(\vec{r},-t) = \psi^*(\vec{r},t). \tag{21.3}$$

In the following section, we derive some of the important properties of $\hat{T}$.

21.2   Properties of the Time Reversal Operator

The important properties of the time reversal operator include:

1. commutation: $[\hat{T},\mathcal{H}] = 0$
   Because of **energy conservation**, the time reversal operator $\hat{T}$ commutes with the Hamiltonian $\hat{T}\mathcal{H} = \mathcal{H}\hat{T}$. Since $\hat{T}$ commutes with the Hamiltonian, eigenstates of the time reversal operator are also eigenstates of the Hamiltonian.

2. anti-linear: $\hat{T}i = -i\hat{T}$
   From Schrödinger's equation (Eq. 21.1), it is seen that the reversal of time corresponds to a change of $i \to -i$, which implies that $\hat{T}i = -i\hat{T}$. We call an operator **anti-linear** if its operation on a complex number yields the complex conjugate of the number rather than the number itself $\hat{T}a = a^*\hat{T}$.

3. action on wave functions: $\hat{T}\psi = \psi^*\hat{T}$
   Since $\hat{T}\psi = \psi^*\hat{T}$, the action of $\hat{T}$ on a scalar product is

$$\hat{T}(\psi,\phi) = \int \phi^*(\vec{r})\psi(\vec{r})d^3r \ \hat{T} = (\psi,\phi)^*\hat{T} \tag{21.4}$$

4. In the case of no spin $\hat{T} = \hat{K}$ where $\hat{K}$ is the complex conjugation operator. With spin, we show below that $\hat{T} = \hat{K}\sigma_y$ where σ_y is the Pauli spin operator,

$$\sigma_y = \begin{pmatrix} 0 & -i \\ i & 0 \end{pmatrix}.$$

We will see below that both $\hat{T}$ and $\hat{K}$ are anti-unitary operators. From Schrödinger's equation (no spin), the effect of $\hat{T}$ on $\vec{p}$ is to reverse $\vec{p}$ (time goes backward) and $\hat{T}$ leaves $V(\vec{r})$ invariant, so that indeed $\mathcal{H}$ is invariant under $\hat{T}$; and furthermore $\hat{T} = \hat{K}$ for the case of no spin. When spin is included, however, the Hamiltonian $\mathcal{H}$ must still be invariant under $\hat{T}$. We note that $\hat{T}\vec{p} = -\vec{p}$ and $\hat{T}\vec{L} = -\vec{L}$ (orbital angular momentum). We likewise require that $\hat{T}\vec{S} = -\vec{S}$ where $\vec{S} = $ spin angular momentum. If these requirements are imposed, we show below that the $\mathcal{H}$ is still invariant under $\hat{T}$ (i.e., $\mathcal{H}$ commutes with $\hat{T}$) when the spin-orbit interaction is included:

$$\mathcal{H} = \frac{p^2}{2m} + V(\vec{r}) + \frac{\hbar}{4m^2c^2}\vec{\sigma} \cdot (\vec{\nabla}V \times \vec{p}). \qquad (21.5)$$

We note that $\hat{K}[\sigma_x, \sigma_y, \sigma_z] = [\sigma_x, -\sigma_y, \sigma_z]$ when the spin components are written in terms of the Pauli matrices

$$\begin{aligned} \sigma_x &= \begin{pmatrix} 0 & 1 \\ 1 & 0 \end{pmatrix} \\ \sigma_y &= \begin{pmatrix} 0 & -i \\ i & 0 \end{pmatrix} \\ \sigma_z &= \begin{pmatrix} 1 & 0 \\ 0 & -1 \end{pmatrix} \end{aligned}$$

$$(21.6)$$

since only the Pauli matrix σ_y contains i. Thus $\hat{K}$ by itself is not sufficient to describe the time reversal operation on the Hamiltonian $\mathcal{H}$ (Eq. 21.5) when the spin-orbit interaction is included. We will see below that the product $\hat{K}\sigma_y$ can describe time reversal of $\mathcal{H}$.

Let us now consider the effect of $\hat{K}\sigma_y$ on the spin matrices $\hat{K}\sigma_y[\sigma_x, \sigma_y, \sigma_z]$. We note that

$$\sigma_y\sigma_x = -\sigma_x\sigma_y \qquad \text{so that} \qquad \hat{K}\sigma_y\sigma_x = -\hat{K}\sigma_x\sigma_y = -\sigma_x\hat{K}\sigma_y$$

$$\sigma_y\sigma_z = -\sigma_z\sigma_y \qquad \text{so that} \qquad \hat{K}\sigma_y\sigma_z = -\hat{K}\sigma_z\sigma_y = -\sigma_z\hat{K}\sigma_y$$

$$\hat{K}\sigma_y\sigma_y = -\sigma_y\hat{K}\sigma_y \quad \text{since, from above} \quad \hat{K}\sigma_y = -\sigma_y\hat{K}.$$

Thus we obtain

$$\hat{K}\sigma_y\vec{\sigma} = -\vec{\sigma}\hat{K}\sigma_y$$

so that the operator $\hat{K}\sigma_y$ transforms $\vec{\sigma}$ (or $\vec{S}$) into $-\vec{\sigma}$ (or $-\vec{S}$). Clearly σ_y does not act on any of the other terms in the Hamiltonian. We note that $\hat{K}$ cannot be written in matrix form.

Since $\hat{K}\hat{K} = \hat{K}^2 = 1$, we can write the important relation $\hat{T} = \hat{K}\sigma_y$ which implies $\hat{K}\hat{T} = \sigma_y = $ **unitary operator**. Thus $\sigma_y^\dagger\sigma_y^{-1} = 1$ and since $\sigma_y^2 = \sigma_y\sigma_y = 1$ we have $\sigma_y^\dagger = \sigma_y$ and $\sigma_y^{\dagger 2} = 1$, where the symbol † is used to denote the adjoint of an operator.

5. In the case of no spin $\hat{T}^2 = 1$, since $\hat{K}^2 = 1$ and $\hat{T} = \hat{K}$. With spin we will now show that $\hat{T}^2 = -1$. Since $\hat{T} = \hat{K}\sigma_y$ when the effect of the electron spin is included,

$$\hat{T}^2 = (\hat{K}\sigma_y)(\hat{K}\sigma_y) = -(\sigma_y\hat{K})(\hat{K}\sigma_y) = -\sigma_y\hat{K}^2\sigma_y = -\sigma_y\sigma_y = -1.$$

More generally if we write $\hat{K}\hat{T} = U = $ unitary operator (not necessarily σ_y), we can then show that $\hat{T}^2 = \pm 1$. Since two consecutive operations by $\hat{T}$ on a state ψ must produce the same physical state ψ, we have $\hat{T}^2 = C1$ where C is a phase factor $e^{i\phi}$ of unit magnitude. Since $\hat{K}^2 = 1$, we can write

$$\hat{K}^2\hat{T} = \hat{T} = \hat{K}U = U^*\hat{K} \tag{21.7}$$

$$\hat{T}^2 = \hat{K}U\hat{K}U = U^*\hat{K}^2U = U^*U = C1 \tag{21.8}$$

We show below that $C = \pm 1$. Making use of the unitary property $U^\dagger U = UU^\dagger = 1$, we obtain by writing $U^* = U^*UU^\dagger = CU^\dagger$,

$$U^* = CU^\dagger = C\tilde{U}^* \tag{21.9}$$

Taking the transpose of both sides of Eq. 21.9 yields

$$\tilde{U}^* = U^\dagger = CU^* = C(C\tilde{U}^*) = C^2 U^\dagger \ \text{ or } \ C^2 = 1 \text{ and } C = \pm 1.$$
(21.10)

We thus obtain either $\hat{T}^2 = +1$ or $\hat{T}^2 = -1$.

6. Operators $H, \vec{r}, V(\vec{r})$ are even under time reversal $\hat{T}$; operators $\vec{p}, \vec{L}, \vec{\sigma}$ are odd under $\hat{T}$. Operators are either even or odd under time reversal. We can think of spin angular momentum classically as due to a current loop in a plane $\perp$ to the z-axis. Time reversal causes the current to flow in the opposite direction.

7. $\hat{T}$ and $\hat{K}$ are anti-unitary operators, as shown below.

In this subsection we show that $\hat{T}\hat{T}^\dagger = -1$ and $\hat{K}\hat{K}^\dagger = -1$, which is valid whether or not the spin is considered explicitly. The properties of the inverse of $\hat{T}$ and $\hat{K}$ are readily found. Since $\hat{K}^2 = 1$, then $\hat{K}\hat{K} = 1$ and $\hat{K}^{-1} = \hat{K}$. If for the case where the spin is treated explicitly $\hat{T}^2 = -1$, then $\hat{T}\hat{T} = -1$ and $\hat{T}^{-1} = -\hat{T}$; $\hat{T} = \hat{K}\sigma_y$ for the case of spin. For the spinless case, $\hat{T}^2 = 1$ and $\hat{T}^{-1} = \hat{T}$.

Since complex conjugation changes $i \rightarrow -i$, we can write $\hat{K}^\dagger = -\hat{K}$ so that $\hat{K}$ is anti-unitary.

We now use this result to show that both $\hat{T}$ and $\hat{K}$ are **anti-unitary**. This is the most important property of $\hat{T}$ from the point of view of group theory. Since $\hat{K} = \hat{T}$ in the absence of spin, and since $\hat{K}$ is anti-unitary, it follows that $\hat{T}$ is anti-unitary in this case. However, when spin is included, $\hat{T} = \hat{K}\sigma_y$ and

$$\begin{aligned} \sigma_y &= \hat{K}\hat{T} \\ \sigma_y^\dagger &= \hat{T}^\dagger \hat{K}^\dagger. \end{aligned}$$
(21.11)

Since σ_y is a unitary operator, thus $\hat{T}^\dagger \hat{K}^\dagger \hat{K}\hat{T} = 1$ but since $\hat{K}^\dagger \hat{K} = -1$ it follows that $\hat{T}^\dagger \hat{T} = -1$, showing that $\hat{T}$ is also **anti-unitary**.

Furthermore $\hat{K}$ and $\hat{T}$ behave differently from all the operators that we have thus far encountered in group theory, such as the point group operations (rotations, improper rotations, mirror planes, inversion and $\mathcal{R}=$ rotation of 2π for spin problems). Thus in considering symmetry

operations in group theory, we treat all the unitary operators separately by use of character tables and all the associated apparatus, and then we treat **time reversal symmetry** as an **additional symmetry constraint**. We will see in Chapter 22 how time reversal symmetry enters directly as a symmetry element for magnetic point groups.

We discuss first in §21.3 and §21.4 the general effect of $\hat{T}$ on the form of $E(\vec{k})$ for the case of electronic bands (a) neglecting spin and (b) including spin. After that, we will consider the question of degeneracies imposed on energy levels by time reversal symmetry (the Herring Rules).

21.3   The Effect of $\hat{T}$ on $E(\vec{k})$, Neglecting Spin

If for the moment we neglect spin, then the time reversal operation acting on a solution of Schrödinger's equation yields

$$\hat{T}\psi(\vec{r}) = \psi^*(\vec{r}). \tag{21.12}$$

Since the Hamiltonian commutes with $\hat{T}$, then both $\psi(\vec{r})$ and $\psi^*(\vec{r})$ satisfy Schrödinger's equation for the same energy eigenvalue, so that a two-fold degeneracy occurs. We will now show that time reversal symmetry leads to two symmetry properties for the energy eigenvalues for Bloch states: the evenness of the energy eigenvalues $E(\vec{k}) = E(-\vec{k})$, and the zero slope of $E_n(\vec{k})$ at the Brillouin zone boundaries.

The effect of the translation operation on a Bloch state is

$$\psi_k(\vec{r} + \vec{R}_n) = e^{i\vec{k}\cdot\vec{R}_n}\psi_k(\vec{r}) \tag{21.13}$$

and the effect of time reversal is

$$\hat{T}\psi_k(\vec{r}) = \psi_k^*(\vec{r}). \tag{21.14}$$

We can write the following relation for the complex conjugate of Bloch's theorem

$$\psi_k^*(\vec{r} + \vec{R}_n) = e^{-i\vec{k}\cdot\vec{R}_n}\psi_k^*(\vec{r}) \tag{21.15}$$

and we can also rewrite Eq. 21.15 in terms of $\vec{k} \rightarrow -\vec{k}$ as

$$\psi^*_{-k}(\vec{r} + \vec{R}_n) = e^{i\vec{k}\cdot\vec{R}_n}\psi^*_{-k}(\vec{r}) \tag{21.16}$$

which upon comparing Eqs. 21.13, 21.15 and 21.16 implies that for non-degenerate levels the time reversal operator transforms $\vec{k} \rightarrow -\vec{k}$

$$\hat{T}\psi_k(\vec{r}) = \psi_{-k}(\vec{r}) = \psi^*_k(\vec{r}). \tag{21.17}$$

If the level is doubly degenerate and $\psi_k(\vec{r})$ and $\phi_k(\vec{r})$ are the corresponding eigenstates, then if $\hat{T}\psi_k(\vec{r}) = \phi_k(\vec{r}) = \psi_{-k}(\vec{r})$, no additional degeneracy is required by time reversal symmetry. Time reversal symmetry thus implies that for a spinless system

$$E_n(\vec{k}) = E_n(-\vec{k}) \tag{21.18}$$

and the energy is an even function of wave vector $\vec{k}$ whether or not there is inversion symmetry.

Using this result (Eq. 21.18) and the $E(\vec{k}) = E(\vec{k} + \vec{K})$ periodicity in $\vec{k}$ space, we obtain:

$$E\left(\frac{\vec{K}}{2} - \delta\vec{k}\right) = E\left(-\frac{\vec{K}}{2} + \delta\vec{k}\right) = E\left(\frac{\vec{K}}{2} + \delta\vec{k}\right) \tag{21.19}$$

where $\delta\vec{k}$ is an infinitesimal distance to the Brillouin zone boundary. Thus referring to Fig. 21.1, $E(\vec{k})$ comes into the zone boundary with **zero slope** for both the lower and upper branches of the solutions in Fig. 21.1. For the case where there is degeneracy at the zone boundary, the upper and lower bands will have **equal and opposite slopes**.

We have been using the symmetry properties in Eqs. 21.18 and 21.19 throughout our solid state physics courses. In the most familiar cases, $E(\vec{k})$ depends on k^2. Figure 21.1 taken from Kittel illustrates the symmetry properties of Eqs. 21.18 and 21.19 for a simple parabolic band at $\vec{k} = 0$.

Let us now consider the consequences of these ideas from a group theoretical point of view, and enumerate Herring's rules. If $\psi(\vec{r})$ belongs to the irreducible representation D, then $\hat{T}\psi(\vec{r}) = \psi^*(r)$ will transform
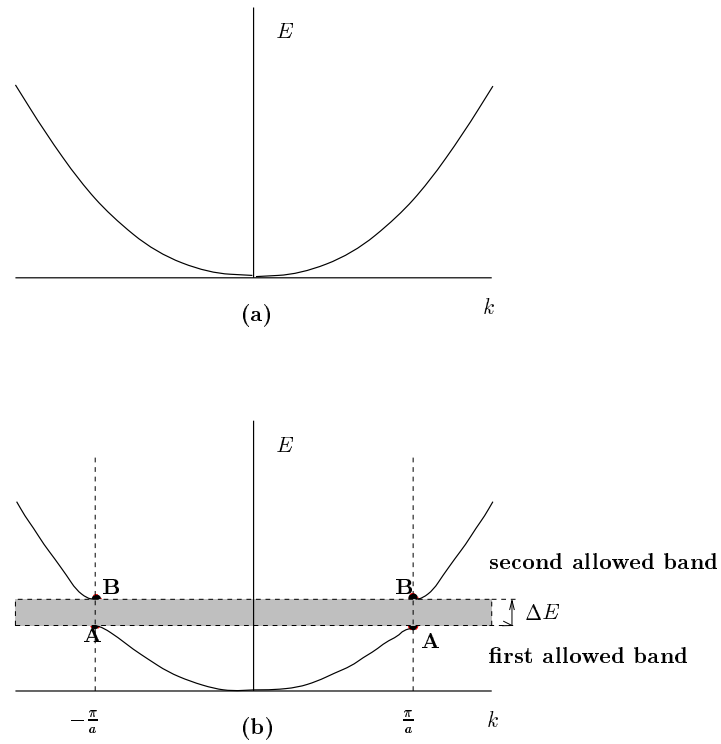
Figure 21.1: Simple $E(\vec{k})$ diagram from Kittel for a spinless electron illustrating both $E(\vec{k}) = E(-\vec{k})$ and the zero slope of $E(\vec{k})$ at the Brillouin zone boundary.

Table 21.1: Character table for point group C_4.

C_4 (4)			E	C_2	C_4	C_4^3	Time reversal
x^2+y^2, z^2	R_z, z	A	1	1	1	1	(a)
x^2-y^2, xy		B	1	1	-1	-1	(a)
(xz, yz)	(x, y) (R_x, R_y) $\Big\}$	E	1	-1	i	$-i$	(b)
			1	-1	$-i$	i	(b)

according to D^* which consists of the complex conjugate of all the matrices in D.

We can distinguish three different possibilities in the case of **no spin**:

(a) All of the matrices in the representation D can be written as real matrices. In this case, the time reversal operator leaves the representation D invariant and no additional degeneracies in $E(\vec{k})$ result.

(b) If the representations D and D^* cannot be brought into equivalence by a unitary transformation, there is a doubling of the degeneracy of such levels due to time reversal symmetry. Then the representations D and D^* are said to form a **time reversal symmetry pair** and these levels will stick together.

(c) If the representations D and D^* can be made equivalent under a suitable unitary transformation, but the matrices in this representation cannot be made real, then the time reversal symmetry also requires a doubling of the degeneracy of D and the bands will stick together.

To illustrate these possibilities, consider the point group C_4 (see Table 21.1). Here irreducible representations A and B are of type (a) above and each of these representations correspond to non-degenerate energy levels. However, the two representations labeled E are complex conjugates of each other and are of type (b) since there is no unitary transformation that can bring them into equivalence. Thus because of

the time reversal symmetry requirement, representation E corresponds to a doubly degenerate level. This is an example where time reversal symmetry gives rise to an additional degeneracy.

The time reversal partners are treated as different representations when applying the following rules on character:

1. The number of irreducible representations is equal to the number of classes.

2. $\sum_i \ell_i^2 = h$.

Using the character table for the group of the wave vector, we can distinguish which of the 3 cases apply for a given irreducible representation using the Herring test (ref. C. Herring, Phys. Rev. 52, 361 (1937)). Let Q_0 be an element in the space group which transforms $\vec{k}$ into $-\vec{k}$. Then Q_0^2 is an element in the group of the wave vector $\vec{k}$ and all elements in the group of the wave vector are elements of Q_0^2. If the inversion operator i is contained in the group of the wave vector $\vec{k}$, then all the elements Q_0 are in the group of the wave vector $\vec{k}$. If i is not an element of the group of the wave vector $\vec{k}$, then the elements Q_0 may or may not be an element in the group of the wave vector. Let h equal the number of elements Q_0. The Herring space group test is then

$$
\begin{aligned}
\sum_{Q_0} \chi(Q_0^2) \quad &= h \quad &\text{case (a)} \\
&= 0 \quad &\text{case (b)} \\
&= -h \quad &\text{case (c)}
\end{aligned}
$$

where χ is the character for a representation of the group of the wave vector $\vec{k}$. These tests can be used to decide whether or not time reversal symmetry introduces any additional degeneracies to this representation. Information on the Herring test is contained for every one of the 32 point groups in the character tables in Koster's book.

To apply the Herring test to the point group C_4, and consider the group of the wave vector for $\vec{k} = 0$. Then all four symmetry operations take $\vec{k} \to -\vec{k}$ since $\vec{k} = 0$. Furthermore, $E^2 = E, C_2^2 = E, C_4^2 = C_2$ and $(C_4^3)^2 = C_2$ so that for representations A and B

$$
\sum_{Q_0} \chi(Q_0^2) = 1 + 1 + 1 + 1 = 4 \tag{21.20}
$$

from which we conclude that A and B correspond to case (a), in agreement with Koster's tables.

On the other hand, for each representation under E,

$$\sum_{Q_0} \chi(Q_0^2) = 1 + 1 + (-1) + (-1) = 0 \tag{21.21}$$

from which we conclude that representations E correspond to case (b). Therefore the two irreducible representations under E correspond to the same energy and the corresponding $E(\vec{k})$ will stick together. The two representations under E are called **time reversal conjugate representations**.

21.4 The Effect of $\hat{T}$ on $E(\vec{k})$, Including the Spin-Orbit Interaction

When the **spin-orbit interaction is included**, then the Bloch functions transform as irreducible representations of the double group. The degeneracy of the energy levels is different from the spinless situation, and in particular every level is at least doubly degenerate.

When the spin-orbit interaction is included, $\hat{T} = \hat{K}\sigma_y$ and not only do we have $\vec{k} \rightarrow -\vec{k}$, but we also have $\vec{\sigma} \rightarrow -\vec{\sigma}$ under time reversal symmetry. This is written schematically as:

$$\hat{T}\psi_{n,k\uparrow}(\vec{r}) = \psi_{n,-k\downarrow}(\vec{r}) \tag{21.22}$$

so that the time reversal conjugate states are

$$E_{n\uparrow}(\vec{k}) = E_{n\downarrow}(-\vec{k}) \tag{21.23}$$

and

$$E_{n\downarrow}(\vec{k}) = E_{n\uparrow}(-\vec{k}). \tag{21.24}$$

If inversion symmetry exists as well,

$$E_n(\vec{k}) = E_n(-\vec{k}) \tag{21.25}$$

then

$$E_{n\uparrow}(\vec{k}) = E_{n\uparrow}(-\vec{k}) \text{ and } E_{n\downarrow}(\vec{k}) = E_{n\downarrow}(-\vec{k}) \tag{21.26}$$

making $E_{n\uparrow}(\vec{k})$ and $E_{n\downarrow}(\vec{k})$ degenerate. In more detail, since $\hat{T} = \hat{K}\sigma_y$ and since

$$\sigma_y \uparrow = \begin{pmatrix} 0 & -i \\ i & 0 \end{pmatrix} \begin{pmatrix} 1 \\ 0 \end{pmatrix} = i \begin{pmatrix} 0 \\ 1 \end{pmatrix} = i \downarrow$$

$$\sigma_y \downarrow = \begin{pmatrix} 0 & -i \\ i & 0 \end{pmatrix} \begin{pmatrix} 0 \\ 1 \end{pmatrix} = -i \begin{pmatrix} 1 \\ 0 \end{pmatrix} = -i \uparrow$$

we obtain

$$\hat{T}\psi_{n,k\uparrow}(\vec{r}) = \hat{T}e^{i\vec{k}\cdot\vec{r}} \left[u_{n,k\uparrow} \begin{pmatrix} 1 \\ 0 \end{pmatrix} \right] = e^{-i\vec{k}\cdot\vec{r}} \left[iu_{n,k\uparrow}^* \begin{pmatrix} 0 \\ 1 \end{pmatrix} \right] = e^{-i\vec{k}\cdot\vec{r}} u_{n,-k\downarrow} \begin{pmatrix} 0 \\ 1 \end{pmatrix}$$

$$(21.27)$$

which is a Bloch state for wave vector $-\vec{k}$ and spin $\downarrow$. Likewise

$$\hat{T}\psi_{n,k\downarrow}(\vec{r}) = \hat{T}e^{i\vec{k}\cdot\vec{r}} \left[u_{n,k\downarrow} \begin{pmatrix} 0 \\ 1 \end{pmatrix} \right] = e^{-i\vec{k}\cdot\vec{r}} \left[-iu_{n,k\downarrow}^* \begin{pmatrix} 1 \\ 0 \end{pmatrix} \right] = e^{-i\vec{k}\cdot\vec{r}} u_{n,-k\uparrow} \begin{pmatrix} 1 \\ 0 \end{pmatrix}$$

$$(21.28)$$

which is a Bloch state for wave vector $-\vec{k}$ and spin $\uparrow$ in which we have written

$$iu_{n,k\uparrow}^* = u_{n,-k\downarrow}$$

and

$$-iu_{n,k\downarrow}^* = u_{n,-k\uparrow}.$$

For a general point in the Brillouin zone, and in the absence of spin-orbit coupling but including the spin on the electron, the energy levels have a **necessary 2-fold spin degeneracy** and also exhibit the property $E(\vec{k}) = E(-\vec{k})$, whether or not there is inversion symmetry. This is illustrated in Fig. 21.2(a). When the spin-orbit interaction is turned on and there **is** inversion symmetry then we get the situation illustrated in Fig. 21.2(b) where the 2-fold degeneracy remains. However, if there is no inversion symmetry, then the only relationships that remain are those of Eqs. 21.23 and 21.24 shown in Fig. 21.2(c), and the Kramers degeneracy results in $E_{\uparrow}(\vec{k}) = E_{\downarrow}(-\vec{k})$ and $E_{\downarrow}(\vec{k}) = E_{\uparrow}(-\vec{k})$.

The role of inversion symmetry is also important for the $E(\vec{k})$ relations for degenerate bands. This is illustrated in Fig. 21.3 for degenerate bands near $\vec{k} = 0$. We take as examples: (a) diamond for which the
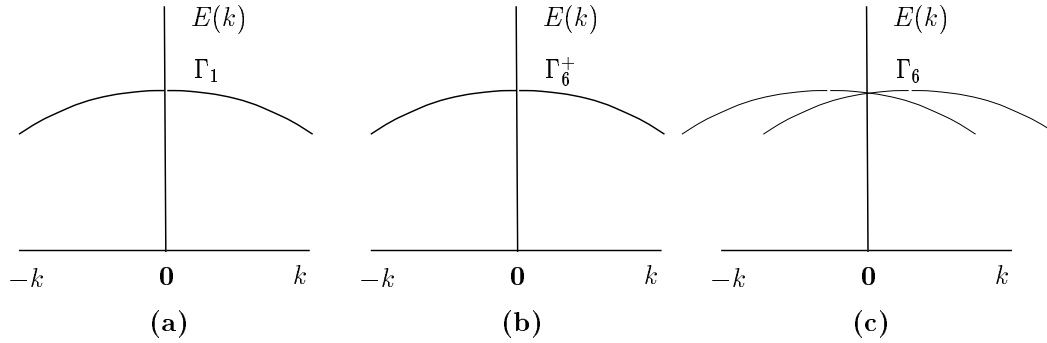
Figure 21.2: Schematic example of Kramers degeneracy in a crystal in the case of: (a) no spin-orbit interaction where each level is doubly degenerate $(\uparrow, \downarrow)$, (b) both spin-orbit interaction and inversion symmetry are present and the levels are doubly degenerate, (c) spin-orbit interaction and no spatial inversion symmetry where the relations 21.23 and 21.24 apply.

spin-orbit interaction can be neglected and all levels are doubly degenerate at a general point in the Brillouin zone, (c) InSb or GaAs which have T_d symmetry (lacking inversion) so that relations 21.23 and 21.24 apply and the two-fold Kramers degeneracy is lifted, (b) Ge or Si which have O_h symmetry (including inversion) and the two-fold Kramers degeneracy is retained at a general point in the Brillouin zone.

We give in Table 21.2 the Herring rules (see §21.3) whether or not the spin-orbit interaction is included. When the spin-orbit interaction

Table 21.2: Summary of rules regarding degeneracies and time reversal.

Case	Relation between D and D^*	Frobenius-Schur test	Spinless electron	Half-integral spin electron
Case (a)	D and D^* are equivalent to the same real irreducible representation	$\sum_R \chi(Q_0^2) = h$	No extra degeneracy	Doubled degeneracy
Case (b)	D and D^* are inequivalent	$\sum_R \chi(Q_0^2) = 0$	Doubled degeneracy	Doubled degeneracy
Case (c)	D and D^* are equivalent to each other but not to a real representation	$\sum \chi(Q_0^2) = -h$	Double degeneracy	No extra degeneracy
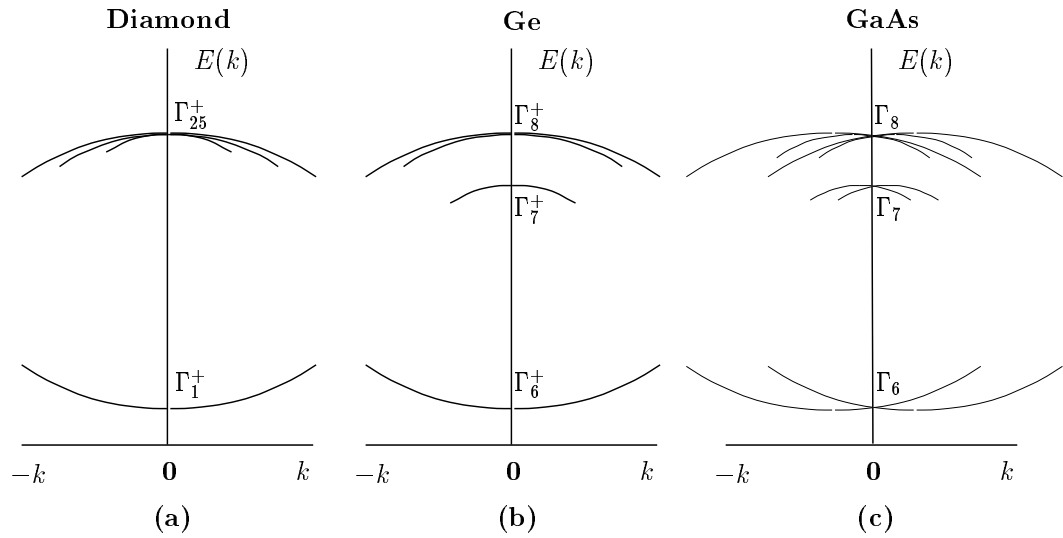
Figure 21.3: Schematic examples of energy bands $E(\vec{k})$ in diamond, Ge and GaAs near $\vec{k} = 0$. (a) Without spin-orbit coupling, each band in diamond has a two-fold spin degeneracy. (b) Splitting by spin-orbit coupling in Ge, with each band remaining doubly degenerate. (c) Splitting of the valence bands by the spin-orbit coupling in GaAs. The magnitudes of the splittings are not to scale.

is included, there are also three cases which can be distinguished. When the time reversal operator $\hat{T}$ acts on a spin dependent wavefunction ψ which transforms according to an irreducible representation D, then we have three possibilities:

(a) If the representation D is real, or can be transformed by a unitary transformation into a set of real matrices, then the action of $\hat{T}$ on these matrices will yield the same set of matrices. To achieve the required additional degeneracy, we must have D occur twice.

(b) If representations D and D^* cannot be brought into equivalence by a unitary transformation, then the corresponding levels must stick together in pairs to satisfy the time reversal degeneracy requirement.

(c) If representations D and D^* can be brought into equivalence but neither can be made all real, then no additional degeneracy need be introduced and both make up the time reversal degenerate pair.

These results are summarized in Table 21.2 for both the case of no spin and when spin-orbit interaction is included. We now illustrate these rules with two cases:

1. the double group representations of the point group C_4 (symmorphic)

2. the double group representation at the L point in Ge (or Si) where the levels are degenerate by time reversal symmetry (nonsymmorphic)

For the first illustration, we give the character table for the double group C_4 taken from Koster et al. in Table 21.3. We note that the Koster table contains an entry for time inversion, which summarizes the results discussed in §21.1 for the spinless bands. Inspection of this character table shows that the double group representations involve the 4th roots of unity (as shown below) and obey the relation $\chi(A_i) = -\chi(\bar{A}_i)$ for each of the pairs of symmetry operations A_i and $\bar{A}_i$. Note that the character table originally given in Koster has some misprints with

Table 21.3: Character table for C_4

C_4	E	$\bar{E}$	C_4	$\bar{C}_4$	C_2	$\bar{C}_2$	C_4^{-1}	$\bar{C}_4^{-1}$	Time Inv.	Bases for C_4
Γ_1	1	1	1	1	1	1	1	1	a	z or S_z
Γ_2	1	1	-1	-1	1	1	-1	-1	a	xy
Γ_3	1	1	i	i	-1	-1	$-i$	$-i$	b	$-i(x+iy)$ or $-(S_x + iS_y)$
Γ_4	1	1	$-i$	$-i$	-1	-1	i	i	b	$i(x-iy)$ or $(S_x - iS_y)$
Γ_5	1	-1	ω	$-\omega$	i	$-i$	$-\omega^3$	ω^3	b	$\phi(1/2, 1/2)$
Γ_6	1	-1	$-\omega^3$	ω^3	$-i$	i	ω	$-\omega$	b	$\phi(1/2, -1/2)$
Γ_7	1	-1	$-\omega$	ω	i	$-i$	ω^3	$-\omega^3$	b	$\phi(3/2, -3/2)$
Γ_8	1	-1	ω^3	$-\omega^3$	$-i$	i	$-\omega$	ω	b	$\phi(3/2, 3/2)$

regard to $\chi(C_4^{-1}) = -\chi(\bar{C}_4^{-1})$, which are corrected in Table 21.3. This character table shows that the characters for the Γ_5 and Γ_6 irreducible representations are time reversal degenerate pairs, and likewise for the Γ_7 and Γ_8 irreducible representations:

	E	$\bar{E}$	C_4	$\bar{C}_4$	C_2	$\bar{C}_2$	C_4^{-1}	$\bar{C}_4^{-1}$
Γ_5:	ω^0	ω^4	ω	ω^5	ω^2	ω^6	ω^7	ω^3
Γ_6:	ω^0	ω^4	ω^7	ω^3	ω^6	ω^2	ω	ω^5
Γ_7	ω^0	ω^4	ω^5	ω	ω^2	ω^6	ω^3	ω^7
Γ_8:	ω^0	ω^4	ω^3	ω^7	ω^6	ω^2	ω^5	ω

Application of the Frobenius–Schur test for Γ_5 yields:

$$\begin{aligned}
\sum \chi(Q_0^2) &= (1)(-1) + (1)(-1) - \omega^2 - \omega^2 + 1 + 1 - \omega^6 - \omega^6 \\
&= -1 - 1 - i - i + 1 + 1 + i + i = 0
\end{aligned}$$

(21.29)

where we note that for the double group representations we consider the character $\chi(Q_0 \bar{Q}_0)$ in the Frobenius–Schur test. We thus find that the representations Γ_6, Γ_7 and Γ_8 are also of the b type with respect to time reversal symmetry and this information is also given in Table 21.3.

Table 21.4: Character Table and Basis Functions for the Group D_{3d}

D_{3d}		E	$\bar{E}$	$2C_3$	$2\bar{C}_2$	$3C_2'$	$3\bar{C}_2'$	I	$\bar{I}$	$2S_6$	$2\bar{S}_6$	$3\sigma_d$	$3\bar{\sigma}_d$	Time Inv.	Bases
L_1^+	Γ_1^+	1	1	1	1	1	1	1	1	1	1	1	1	a	R
L_2^+	Γ_2^+	1	1	1	1	-1	-1	1	1	1	1	-1	-1	a	S_x
L_3^+	Γ_3^+	2	2	-1	-1	0	0	2	2	-1	-1	0	0	a	$(S_x - iS_y),$ $-(S_x + iS_y)$
L_1^-	Γ_1^-	1	1	1	1	1	1	-1	-1	-1	-1	-1	-1	a	zS_z
L_2^-	Γ_2^-	1	1	1	1	-1	-1	-1	-1	-1	-1	1	1	a	z
L_3^-	Γ_3^-	2	2	-1	-1	0	0	-2	-2	1	1	0	0	a	$(x - iy),$ $-(x + iy)$
L_6^+	Γ_4^+	2	-2	1	-1	0	0	2	-2	1	-1	0	0	c	$\phi(1/2, -1/2)$
L_4^+	Γ_5^+	1	-1	-1	1	i	$-i$	1	-1	-1	1	i	$-i$	b	$\phi(3/2, -3/2)$ $-i\phi(3/2, 3/2)$
L_5^+	Γ_6^+	1	-1	-1	1	$-i$	i	1	-1	-1	1	$-i$	i	b	$-(\phi(3/2, 3/2)$ $-i\phi(3/2, -3/2))$
L_6^-	Γ_4^-	2	-2	1	-1	0	0	-2	2	-1	1	0	0	c	$\Gamma_4^+ \times \Gamma_1^-$
L_4^-	Γ_5^-	1	-1	-1	1	i	$-i$	-1	1	1	-1	$-i$	i	b	$\Gamma_5^+ \times \Gamma_1^-$
L_5^-	Γ_6^-	1	-1	-1	1	$-i$	i	-1	1	1	-1	i	$-i$	b	$\Gamma_6^+ \times \Gamma_1^-$

For the L-point levels in Ge, see the $E(\vec{k})$ diagram in Fig. 19.2b for the case where the spin-orbit interaction is included. The character table appropriate to the L-point is given in Table 21.4. The designation for the L-point representations have been added on the left column of Koster's table.

For a Λ point, the operations $E, 2C_3$ and $3C_2$ take $\vec{k} \rightarrow -\vec{k}$. For the L-point, all operations are of the Q_0 type, so that for the representations L_1, L_2 and L_3, we have $\Sigma\chi(Q_0^2) = 12$, yielding representations of type a, in agreement with the character table for D_{3d} (Table 21.4).

For the double group representation L_6^+ we obtain

$$L_6^+ = \Sigma\chi(Q_0^2) = -4 - 2 + 0 - 4 - 2 + 0 = -12 \quad \text{type (c)} \quad (21.30)$$

where again we write $Q_0\bar{Q}_0$ for Q_0^2. For the double group representation L_4^+ the Frobenius–Schur test yields:

$$L_4^+ : \Sigma\chi(Q_0^2) = -1 - 2 + 3 - 1 - 2 + 3 = 0 \quad \text{type (b)} \quad (21.31)$$

Likewise L_5^+ is of type b. Since L_4^+ and L_5^+ are complex conjugate representations, L_4^+ and L_5^+ form time reversal degenerate pairs. Similarly, L_4^- and L_5^- are type b representations and form time reversal degenerate pairs (see Fig. 19.2b).

With this discussion of time reversal symmetry, we have explained all the entries to the character tables, and have explained why because of time reversal symmetry certain bands stick together on the $E(\vec{k})$ diagrams. In the following Chapter we see how the time reversal operator becomes a symmetry element in magnetic point groups.

21.5   Selected Problems

1. Consider the space group D_{6h}^4 (#194) which we discussed in connection with the lattice modes for graphite. We will now concern ourselves with the electronic structure. Since the Fermi surfaces are located close to the HK axes in the Brillouin Zone it is important to work with the group of the wave vector at points H, K and P (see diagram).
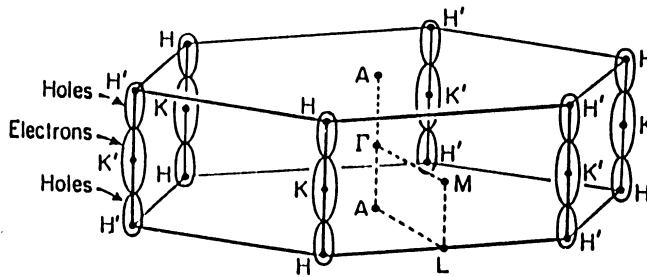
   (a) Using Miller and Love, and Koster et al., give the character table including double groups for the group of the wave vector at point K. Classify each of the irreducible representations according to whether they behave as a, b or c under time reversal symmetry.

   (b) Find the compatibility relations as we move away from K toward H.

Chapter 22

Magnetic Groups

If atoms at each lattice site, can be represented as a charge distribution $\rho(\vec{r})$ with no particular spin symmetry (paramagnetic or diamagnetic), the ordinary space groups are used. If, however, we have ordered arrangements of spins, then the time reversal operator (which reverses the spin direction) can be combined with other group elements to form elements of a new type of symmetry group. Groups in which the time reversal operator forms group elements are called **magnetic space groups** and the corresponding point groups are called **magnetic point groups**.

In this chapter we present some of the essential properties of magnetic space groups and give some examples of interest to solid state physics.

22.1   Introduction

When magnetically ordered phases are taken into account, the magnetic unit cell is often larger than the chemical unit cell, as for example in an antiferromagnetic system. Additional symmetry elements are introduced (see §22.2), and as a result many more point groups and space groups are possible (see §22.3).

There are, in fact, **122** (58 + 2×32) magnetic point groups (rather than 32), and **1651** (1191 + 2×230) magnetic space groups (rather than 230), and 36 (22 + 14) magnetic Bravais lattices rather than 14.

623

The magnetic Bravais lattices which are important for describing anti-ferromagnetic structures are shown in Fig. 22.1(b), and for comparison the 14 ordinary Bravais lattices are also shown in Fig. 22.1(a), and are further explained below. We will confine our discussion in this chapter to magnetic single groups (not double groups), and we shall only discuss magnetic point groups.

22.2   Types of Elements

Magnetic groups have symmetry elements corresponding to unitary operators (denoted by A_i) and anti-elements $M_k = \hat{T}A_k$ corresponding to anti-unitary operators, where $\hat{T}$ is the anti-unitary time reversal operator (see Chapter 21). We show in Fig. 22.2(a) a one-dimensional lattice in which $\hat{T}$ when combined with a translation is a symmetry operation. However, by displacing the non-magnetic white atoms in Fig. 22.2(b) relative to Fig. 22.2(a), we see that $\hat{T}$ is no longer a symmetry operation. If we neglect spin, then $\hat{T} = \hat{K}$ where $\hat{K}$ is the complex conjugation operator (see Chapter 21), and $\hat{T}^2 = \hat{K}^2 = 1$. The product of two unitary elements A_i or of two anti-unitary elements M_k yields a unitary element, while the product of a unitary element A_i with an anti-unitary element M_k yields an anti-unitary element:

$$
\begin{aligned}
A_i A_{i'} &= A_{i''} \\
A_i M_k &= M_{k'} \\
M_k A_i &= M_{k''} \\
M_{k'} M_{k'} &= A_{i'''}
\end{aligned}
\tag{22.1}
$$

To satisfy these relations, group properties and the rearrangement theorem, there must be **equal numbers** of elements of the type A_i and of the type M_k in a magnetic point group.

22.3   Types of Magnetic Point Groups

In classifying the magnetic point groups we must consider three types of point groups:
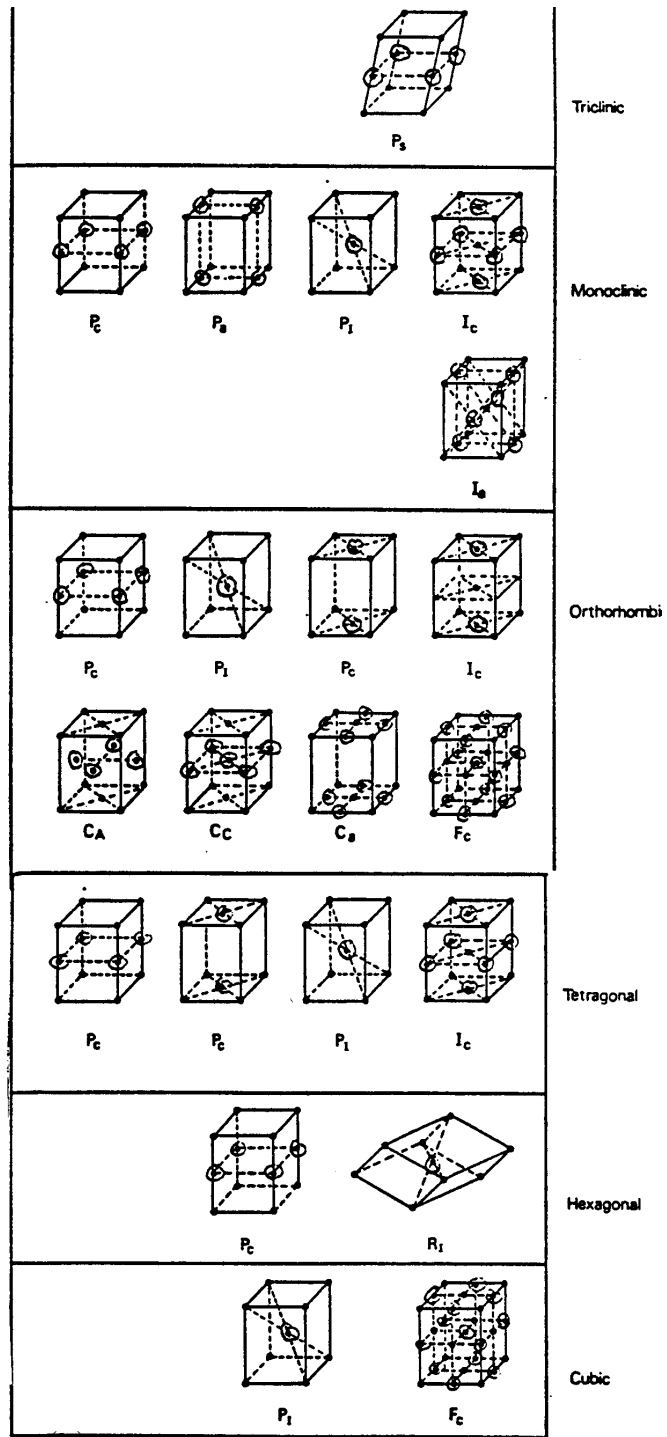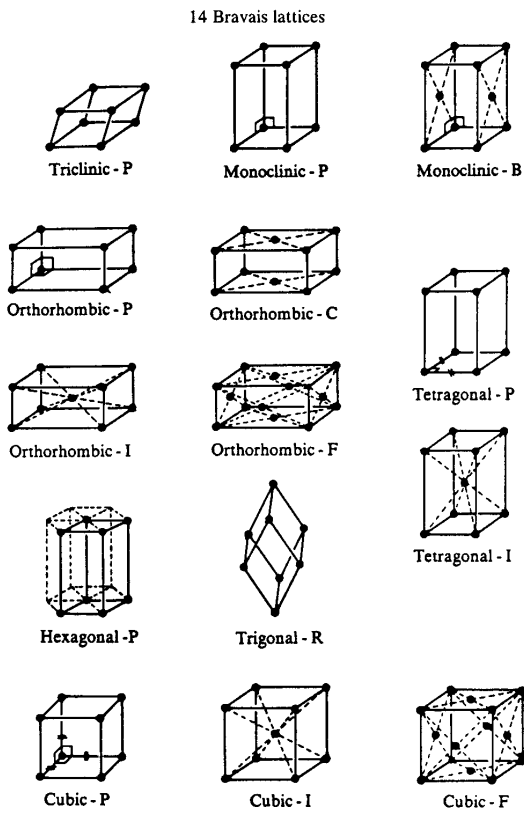
Figure 22.1: (a) The 14 ordinary Bravais lattices and (b) the 22 additional magnetic Bravais lattices. The open circles represent the time reversed sites.
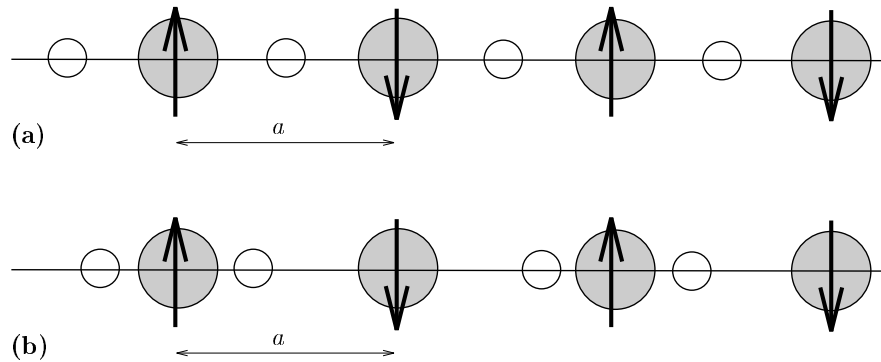
Figure 22.2: Diagram showing a one-dimensional lattice where: (a) the operation $\hat{T}$ is combined with the translation symmetry operation, (b) $\hat{T}$ is not a symmetry operation even if combined with translations.

(a) 32 ordinary point groups G' where $\hat{T}$ is not an element

(b) 32 ordinary point groups $G' \otimes \hat{T}$. In these magnetic point groups, all elements A_i of G' are contained together with all elements $\hat{T}A_i$.

(c) 58 point groups G in which half of the elements are $\{A_i\}$ and half are $\{M_k\}$ where $M_k = \hat{T}A_k$ and the $\{A_i, A_k\}$ form an ordinary point group G'. Also $\{A_i\}$ is a subgroup of G'.

Summing the number of types (a), (b), and (c) we obtain $(32 + 32 + 58) = 122$ magnetic point groups. Case (a) can apply to non-magnetic materials and some ferromagnetic materials. Case (b) can apply to some antiferromagnetic materials. Case (c) can apply to magnetic materials with a variety of spin orderings.

We list in Table 22.1 (from Tinkham) the 58 magnetic point groups of type (c) and denoted by G; also included in the table are the 32 ordinary point groups of type (a) which are denoted by G'. The 32 point groups of type (b), obtained from those in type (a) as $G' \otimes \hat{T}$, are not listed. The magnetic groups of type (c) are related to elements of a group G' and a subgroup H_r and are denoted by $G'(H_r)$. The

appropriate group G' contains the symmetry elements $\{A_i, A_k\}$ while the subgroup H_r of G' only has elements $\{A_i\}$.

22.4 Properties of the 58 Magnetic Point Groups $\{A_i, M_k\}$

We list below some of the properties of the magnetic point groups [type (c)] that contain both unitary and anti-unitary symmetry elements, A_i and $M_k = \hat{T} A_k$, respectively. We denote a typical magnetic point group of this category by $G = \{A_i, M_k\}$.

1. $\hat{T}$ is not an element in the magnetic point group G (since the identity element is one of the elements of $\{A_i\}$ but not of $\{A_k\}$).

2. A_i and A_k are distinct, so that no element in the set $\{A_i\}$ is also in $\{A_k\}$ where $\{M_k\} = \{\hat{T} A_k\}$. (If there were one A_j in common, then we could have $\hat{T} A_j$ in $\{M_k\}$ and A_j^{-1} in $\{A_i\}$, which on multiplication $\hat{T} A_j A_j^{-1}$ implies that $\hat{T}$ is in G, in contradiction with property (1)).

3. $G' \equiv \{A_i, A_k\}$ is one of the 32 ordinary point groups.

4. The set $H_r = \{A_i\}$ forms an invariant unitary subgroup of G. This subgroup is self-conjugate because conjugation of an element in A_i with any element in $\{M_k\}$ written as $M_k A_i M_k^{-1}$ yields an element in $\{A_i\}$ as a result of Eq. (22.1), and likewise the conjugation $A_i M_k A_i^{-1}$ yields an element in $\{M_k\}$.

5. The number of unitary operators $A_i =$ the number of anti-unitary operators M_k, to satisfy the multiplication rules in Eq. 22.1 and the group properties of G.

6. $\{A_i\}$ is the only coset of H_r in G and $\{A_k\}$ is the only coset of H_r in G'.

7. Since H_r and G' are groups, and properties (5) and (6) apply, then G is a group of the form

Table 22.1: The magnetic point groups of type (a) and type (c).

Crystal system	Group G'	Number of elements	Invariant unitary subgroup H	Shubnikov notation	International notation	Magnetic order
Triclinic	C_1	1	C_1	1	1	F
	$S_2(C_i)$	2	S_2	$\underline{2}$	$\bar{1}$	F
			C_1	$\underline{2}$	$\bar{1}$	AF
Monoclinic	C_{1h}	2	C_{1h}	m	m	F
			C_1	$\underline{m}$	$\underline{m}$	F
	C_2	2	C_2	2	2	F
			C_1	$\underline{2}$	$\underline{2}$	F
	C_{2h}	4	C_{2h}	$2{:}m$	$2/m$	F
			C_i	$\underline{2}{:}\underline{m}$	$\underline{2}/\underline{m}$	AF
			C_2	$2{:}\underline{m}$	$2/\underline{m}$	AF
			C_{1h}	$\underline{2}{:}m$	$\underline{2}/m$	AF
Rhombic	C_{2v}	4	C_{2v}	$2\cdot m$	$2mm$	AF
			C_{1h}	$\underline{2}\cdot m$	$\underline{2}mm$	F
			C_2	$2\cdot\underline{m}$	$2\underline{mm}$	F
	D_2	4	D_2	$2{:}2$	222	AF
			C_2	$2{:}\underline{2}$	$2\underline{22}$	F
	D_{2h}	8	D_{2h}	$m\cdot2{:}m$	mmm	AF
			C_{2h}	$\underline{m}\cdot2{:}m$	$\underline{m}mm$	F
			C_{2v}	$m\cdot2{:}\underline{m}$	$mm\underline{m}$	AF
			D_2	$\underline{m}\cdot2{:}\underline{m}$	$\underline{m}mm$	AF
Tetragonal	C_4	4	C_4	4	4	F
			C_2	$\underline{4}$	$\underline{4}$	AF
	S_4	4	S_4	$\bar{4}$	$\bar{4}$	F
			C_2	$\underline{\bar{4}}$	$\underline{\bar{4}}$	AF
	C_{4h}	8	C_{4h}	$4{:}m$	$4/m$	F
			C_{2h}	$\underline{4}{:}m$	$\underline{4}/m$	AF
			C_4	$4{:}\underline{m}$	$4/\underline{m}$	AF
			S_4	$\underline{4}\cdot\underline{m}$	$\underline{4}/\underline{m}$	AF
	D_{2d}	8	D_{2d}	$\bar{4}\cdot m$	$\bar{4}2m$	AF
			C_{2v}	$\underline{\bar{4}}\cdot m$	$\underline{\bar{4}}2m$	AF
			D_2	$\underline{\bar{4}}\cdot\underline{m}$	$\underline{\bar{4}}2\underline{m}$	AF
			S_4	$\bar{4}\cdot\underline{m}$	$\bar{4}2\underline{m}$	F
	C_{4v}	8	C_{4v}	$4\cdot m$	$4mm$	AF
			C_{2v}	$\underline{4}\cdot m$	$\underline{4}mm$	AF
			C_4	$4\cdot\underline{m}$	$4\underline{mm}$	F
	D_4	8	D_4	$4{:}2$	$42(422)$	AF
			D_2	$\underline{4}{:}2$	$\underline{4}2$	AF
			C_4	$4{:}\underline{2}$	$4\underline{2}$	F
	D_{4h}	16	D_{4h}	$m\cdot4{:}m$	$4/mmm$	AF
			D_{2h}	$m\cdot\underline{4}{:}m$	$\underline{4}/mmm$	AF
			C_{4h}	$\underline{m}\cdot4{:}m$	$4/m\underline{mm}$	F
			D_{2d}	$m\cdot\underline{4}{:}\underline{m}$	$\underline{4}/m\underline{mm}$	AF
			C_{4v}	$m\cdot4{:}\underline{m}$	$4/\underline{mmm}$	AF
			D_4	$\underline{m}\cdot4{:}\underline{m}$	$4/\underline{mmm}$	AF

Table 22.1: CONTINUED: The magnetic point groups of type (a) and type (c).

Crystal system	Group G'	Number of elements	Invariant unitary subgroup H	Shubnikov notation	International notation	Magnetic order
Rhombohedral	C_3	3	C_3	3	3	F
	S_6	6	S_6	$\bar{6}$	$\bar{3}$	F
			C_3	$\underline{6}$	$\underline{\bar{3}}$	AF
	C_{3v}	6	C_{3v}	$3{\cdot}m$	$3m$	AF
			C_3	$3{\cdot}\underline{m}$	$3\underline{m}$	F
	D_3	6	D_3	$3{:}2$	32	AF
			C_3	$3{:}\underline{2}$	$3\underline{2}$	F
	D_{3d}	12	D_{3d}	$\bar{6}{\cdot}m$	$\bar{3}m$	AF
			S_6	$\bar{6}{\cdot}\underline{m}$	$\bar{3}\underline{m}$	F
			C_{3v}	$\underline{\bar{6}}{\cdot}m$	$\underline{\bar{3}}m$	AF
			D_3	$\underline{\bar{6}}{\cdot}\underline{m}$	$\underline{\bar{3}}\underline{m}$	AF
Hexagonal	C_{3h}	6	C_{3h}	$3{:}m$	$\bar{6}$	F
			C_3	$3{:}\underline{m}$	$\underline{\bar{6}}$	AF
	C_6	6	C_6	6	6	F
			C_3	$\underline{6}$	$\underline{6}$	AF
	C_{6h}	12	C_{6h}	$6{:}m$	$6/m$	F
			S_6	$\underline{6}{:}m$	$\underline{6}/m$	AF
			C_{3h}	$\underline{6}{:}m$	$\underline{6}/m$	AF
			C_6	$6{:}\underline{m}$	$6/\underline{m}$	AF
	D_{3h}	12	D_{3h}	$m{\cdot}3{:}m$	$\bar{6}m2$	AF
			C_{3v}	$m{\cdot}3{:}\underline{m}$	$\underline{\bar{6}}m2$	AF
			D_3	$m{\cdot}3{:}\underline{m}$	$\bar{6}m2$	AF
			C_{3h}	$\underline{m}{\cdot}3{:}m$	$\bar{6}m2$	F
	C_{6v}	12	C_{6h}	$6{\cdot}m$	$6mm$	AF
			C_{3v}	$\underline{6}{\cdot}m$	$\underline{6}mm$	AF
			C_6	$6{\cdot}\underline{m}$	$6\underline{mm}$	F
	D_6	12	D_6	$6{:}2$	$62(622)$	AF
			D_3	$\underline{6}{:}2$	$\underline{6}2$	AF
			C_6	$6{:}\underline{2}$	$6\underline{2}$	F
	D_{6h}	24	D_{6h}	$m{\cdot}6{:}m$	$6/mmm$	AF
			D_{3d}	$m{\cdot}\underline{6}{:}\underline{m}$	$\underline{6}/\underline{m}mm$	AF
			C_{6h}	$\underline{m}{\cdot}6{:}m$	$6/m\underline{mm}$	F
			D_{3h}	$m{\cdot}\underline{6}{:}m$	$\underline{6}/mmm$	AF
			C_{6v}	$m{\cdot}6{:}\underline{m}$	$6/\underline{mmm}$	AF
			D_6	$\underline{m}{\cdot}6{:}\underline{m}$	$6/\underline{mmm}$	AF
Cubic	T	12	T	$3/2$	23	AF
	T_h	24	T_h	$\bar{6}/2$	$m3$	AF
			T	$\underline{6}/2$	$\underline{m}3$	AF
	T_d	24	T_d	$3/\bar{4}$	$\bar{4}3m$	AF
			T	$3/\underline{\bar{4}}$	$\underline{\bar{4}}3m$	AF
	O	24	O	$3/4$	$43(432)$	AF
			T	$3/\underline{4}$	$4\underline{3}$	AF
	O_h	48	O_h	$\bar{6}/4$	$m3m$	AF
			T_h	$\bar{6}/4$	$m3\underline{m}$	AF
			T_d	$\underline{\bar{6}}/4$	$m3\underline{m}$	AF
			O	$\underline{\bar{6}}/4$	$m3\underline{m}$	AF

Table 22.2: Character Table for Group C_{2h}

C_{2h} $(2/m)$			E	C_2	σ_h	i
x^2, y^2, z^2, xy	R_z	A_g	1	1	1	1
	z	A_u	1	1	-1	-1
xz, yz	R_x, R_y	B_g	1	-1	-1	1
	x, y	B_u	1	-1	1	-1

$$G = H_r + \hat{T}(G' - H_r) \tag{22.2}$$

8. From property (7), we see that the procedure for finding magnetic point groups is to start with one of the 32 point groups G' and find all invariant subgroups of **index 2**. Denoting each such subgroup by H_r we can form

$$G_r = H_r + \hat{T}(G' - H_r). \tag{22.3}$$

We denote each magnetic group G_r thus formed by $G'(H_r)$ in which the relevant G' and H_r for each G_r are listed. This notation is used in Table 22.1 and the various $G'(H_r)$ can be found in Table 22.1.

To illustrate the elements of magnetic point groups, consider the 4 entries under C_{2h} in Table 22.1. We list below the symmetry elements of each of the $C_{2h}(H_r)$ magnetic point groups.

$$
\begin{aligned}
C_{2h}(C_{2h}) &: \quad E, C_2, i, iC_2 \ \ (iC_2 = \sigma_h) \\
C_{2h}(C_2) &: \quad E, C_2, \hat{T}i, \hat{T}iC_2 \\
C_{2h}(C_i) &: \quad E, i, \hat{T}C_2, \hat{T}iC_2 \\
C_{2h}(C_{1h}) &: \quad E, iC_2, \hat{T}i, \hat{T}C_2
\end{aligned}
\tag{22.4}
$$

in which the magnetic point group $C_{2h}(C_{2h})$ is of type (a), and the other three are of type (c). Not listed is the magnetic space group $C_{2h} \otimes \hat{T}$ of type (b) which contains the eight symmetry elements $\{A_i\} = \{E, C_2, i, iC_2\}$ and $\{\hat{T} \otimes A_i\} = \{\hat{T}, \hat{T}C_2, \hat{T}i, \hat{T}iC_2\}$. The character table for the ordinary point group C_{2h} is given as Table 22.2.

Table 22.3: Character Table for Group D_2

D_2 (222)			E	C_2^z	C_2^y	C_2^x
x^2, y^2, z^2		A_1	1	1	1	1
xy	R_z, z	B_1	1	1	-1	-1
xz	R_y, y	B_2	1	-1	1	-1
yz	R_x, x	B_3	1	-1	-1	1
	$D_{2h} = D_2 \otimes i$					

We note that the time reversal operator of $\hat{T}$ reverses the sign of a spin, while the **inversion operator** i **leaves a spin invariant** (since the angular momentum $\vec{L}$ is even under inversion while $\vec{r}$ and $\vec{p}$ are each odd).

22.5 Examples of Magnetic Structures

22.5.1 Orthorhombic Ferromagnetic Unit Cell with $D_{2h}(C_{2h})$ Symmetry

The notation D_{2h} (C_{2h}) for a magnetic point group denotes a point group D_{2h} from which the subgroup (C_{2h}) forms the set of symmetry elements $\{A_i\}$ and the remaining symmetry elements of G' are of the form $\{A_k\}$ where the elements M_k in G are of the form $M_k = \hat{T}A_k$. We note from Table 22.1 that D_{2h} (C_{2h}) corresponds to a ferromagnetic structure such as the one shown in Fig. 22.3. In the paramagnetic state, the proper symmetry group for this structure in D_{2h}.

The symmetry operations for $D_{2h} = D_2 \otimes i$ are: E, C_{2x}, C_{2y}, C_{2z}, i, iC_{2x}, iC_{2y}, iC_{2z} (see Table 22.3). It is immediately seen that the subgroup of D_{2h} which leaves the spin invariant consists of the elements $\{A_i\} = E$, C_{2z}, i, iC_{2z}, since both orbital and spin angular momentum are invariant under inversion. These four elements form the group $C_{2h} = C_2 \otimes i$, noting again that the spin angular momentum S is even under inversion. The remaining elements of D_{2h} reverse the spins, so that the time reversal operator $\hat{T}$ is needed to keep all the spins ferro-
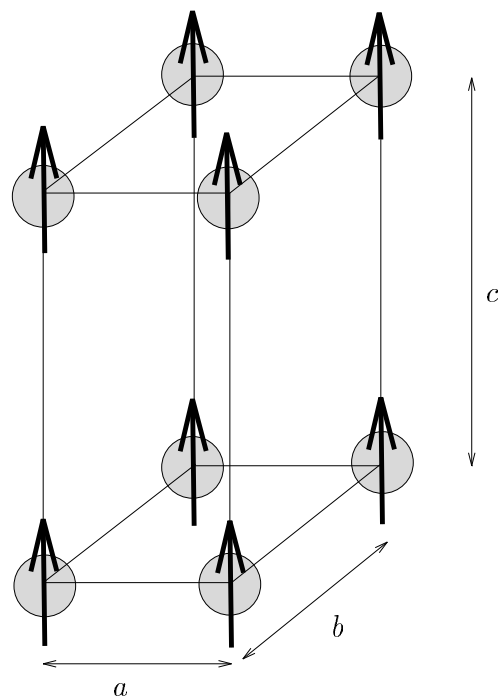
Figure 22.3: Magnetic spin arrangement in $D_{2h}(C_{2h})$ for an orthorhombic ferromagnetic system.

D_{2h} (C_{2h}) **symmetry**

magnetically aligned. We therefore obtain $\{M_k\} = \hat{T}C_{2x}, \hat{T}C_{2y}, \hat{T}iC_{2x}$ and $\hat{T}iC_{2y}$ for the remaining symmetry elements of D_{2h} (C_{2h}). The appropriate Bravais lattice in this case is the orthorhombic Bravais lattice #4 for the non-magnetic groups [see Fig. 22.1(a)].

22.5.2 Antiferromagnets with the Rutile Structure

The antiferromagnets MnF_2, FeF_2 and CoF_2 crystallize in the rutile structure shown in Fig. 22.4. The open circles are the F ions while the shaded circles with spins denote the magnetic cations. The point group for this structure in the paramagnetic state is $D_{4h} = D_4 \otimes i$. In the antiferromagnetic state, each unit cell has one spin up and one spin down cation. The chemical and magnetic unit cells contain the atoms shown in Fig. 22.4. The space group symmetry operations for D_{4h} pertinent to the rutile structure are the 16 operations listed below:

$$
\begin{array}{llll}
1. & \{E|0\} & 9. & \{i|0\} \\
2. & \{C_2|0\} & 10. & \{\sigma_h|0\} = \{C_2|0\}\{i|0\} \\
3. & \{C_{2\xi}|0\} & 11. & \{\sigma_{d\xi}|0\} = \{C_{2\xi}|0\}\{i|0\} \\
4. & \{C_{2\nu}|0\} & 12. & \{\sigma_{d\nu}|0\} = \{C_{2\nu}|0\}\{i|0\} \\
5. & \{C_4|\tau_0\} & 13. & \{S_4^{-1}|\tau_0\} = \{C_4|\tau_0\}\{i|0\} \\
6. & \{C_4^{-1}|\tau_0\} & 14. & \{S_4|\tau_0\} = \{C_4^{-1}|\tau_0\}\{i|0\} \\
7. & \{C_{2x}|\tau_0\} & 15. & \{\sigma_{vx}|\tau_0\} = \{C_{2x}|\tau_0\}\{i|0\} \\
8. & \{C_{2y}|\tau_0\} & 16. & \{\sigma_{vy}|\tau_0\} = \{C_{2y}|\tau_0\}\{i|0\}
\end{array}
\tag{22.5}
$$

where the axes $\xi = (110)$ and $\nu = (1\bar{1}0)$ denote two-fold axes and the translation $\vec{\tau}_0 = \frac{1}{2}(\vec{a_1} + \vec{a_2} + \vec{a_3})$ is to the body center of the unit cell (see Fig. 22.4). The point group D_{4h} corresponding to these space group operations is found by setting $\vec{\tau}_0 = 0$. The character table for D_4 is given in Table 22.4 where $D_{4h} = D_4 \otimes i$. Thus the operations in Eq. (22.5) correspond to the space group for the chemical unit cell.

The unitary subgroup that forms the symmetry group for antiferromagnetic MF_2 (M=magnetic cation) consists of the 4 elements of the symmetry group D_2 $\{E|0\}$, $\{C_2|0\}$, $\{C_{2x}|\tau_0\}$, $\{C_{2y}|\tau_0\}$ and 4 additional elements formed by combining these with inversion. These 8 elements constitute $\{A_i\}$ which corresponds to the group $D_{2h} = D_2 \otimes i$ (see Table 22.3). Note that the operations C_{2x} and C_{2y} invert the spins. The
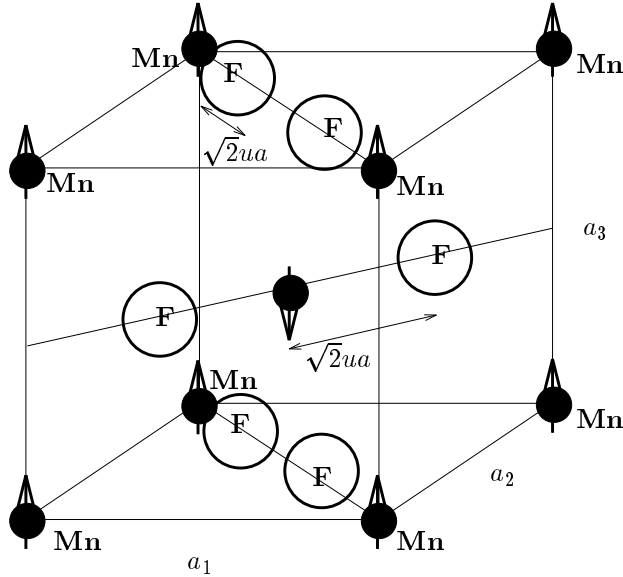
Figure 22.4: The common antiferromagnets MnF_2, FeF_2 and CoF_2 crystallize in the rutile structure with $|a_1| = |a_2| = a$; $|a_3| = c$; $c \neq a$. The diagram shows the magnetic point group D_{4h} (D_{2d}) which describes the antiferromagnetic spin alignment.

Table 22.4: Character Table for Group D_4 (422)

D_4 (422)			E	$C_2 = C_4^2$	$2C_4$	$2C_2'$	$2C_2''$
$x^2 + y^2, z^2$		A_1	1	1	1	1	1
	R_z, z	A_2	1	1	1	-1	-1
$x^2 - y^2$		B_1	1	1	-1	1	-1
xy		B_2	1	1	-1	-1	1
(xz, yz)	$\left.\begin{array}{c}(x,y)\\(R_x, R_y)\end{array}\right\}$	E	2	-2	0	0	0

$D_{4h} = D_4 \otimes i$

appropriate Bravais lattice for MnF_2 is the tetragonal Bravais lattice P_I for the magnetic groups (see Fig. 22.1).

If we ignore the fluorine anions, the chemical unit cell would be half as large containing only one magnetic cation. The magnetic unit cell would then be twice as large as the chemical unit cell. Nevertheless the magnetic point group for the magnetic antiferromagnetic system remains $D_{4h}(D_{2h})$.

22.5.3 The Magnetic States of EuSe

Because the nearest and next-nearest exchange constants are of approximately equal magnitude and of opposite sign, EuSe exhibits several different magnetic phases, depending on the magnetic field and temperature variables. In Figs. 22.5a, 22.5b, 22.5c we see, respectively, the spin arrangement for the antiferromagnetic (AF-II) two spin ($\uparrow\downarrow$) phase, the ferrimagnetic three spin ($\uparrow\uparrow\downarrow$) phase, and the antiferromagnetic (AF-I) four spin ($\uparrow\uparrow\downarrow\downarrow$) phase.

A ferromagnetic phase is also found upon application of a high applied magnetic field. In all 4 magnetically ordered phases, the spins in a given $(1\bar{1}1)$ plane are parallel to each other and are oriented along the $[011]$ direction. The resulting magnetic space group has very low symmetry. For the AF-II phase, the symmetry elements are: $\{E|0\}, \{i|0\}, \hat{T}\{E|\vec{\tau_0}\}, \hat{T}\{i|\vec{\tau_0}\}$ in which the vector $\vec{\tau_0}$ takes the spins from one sublattice to the other

$$\vec{\tau_0} = \frac{1}{4}(a_x, 0, a_z) \tag{22.6}$$

Thus the magnetic point group is $S_2 \otimes \hat{T}$.

If, however, the spins were oriented instead along $[1\bar{1}1]$ and $[\bar{1}1\bar{1}]$ directions in alternate (111) planes, then the magnetic symmetry of the group increases and is $C_3 \otimes \hat{T}$. Thus the spin direction is important in determining the magnetic point group and the magnetic space group. We note that the number of sublattices (1, 2, 3, or 4) is also important in determining the symmetry operations in the magnetic space groups. For some cases it is useful to ignore the spin directions and just to consider each atom on a given sublattice as a colored atom. Such

(a) **AF-II phase** (↑↓)

(b) **Ferrimagnetic phase** (↑↑↓)
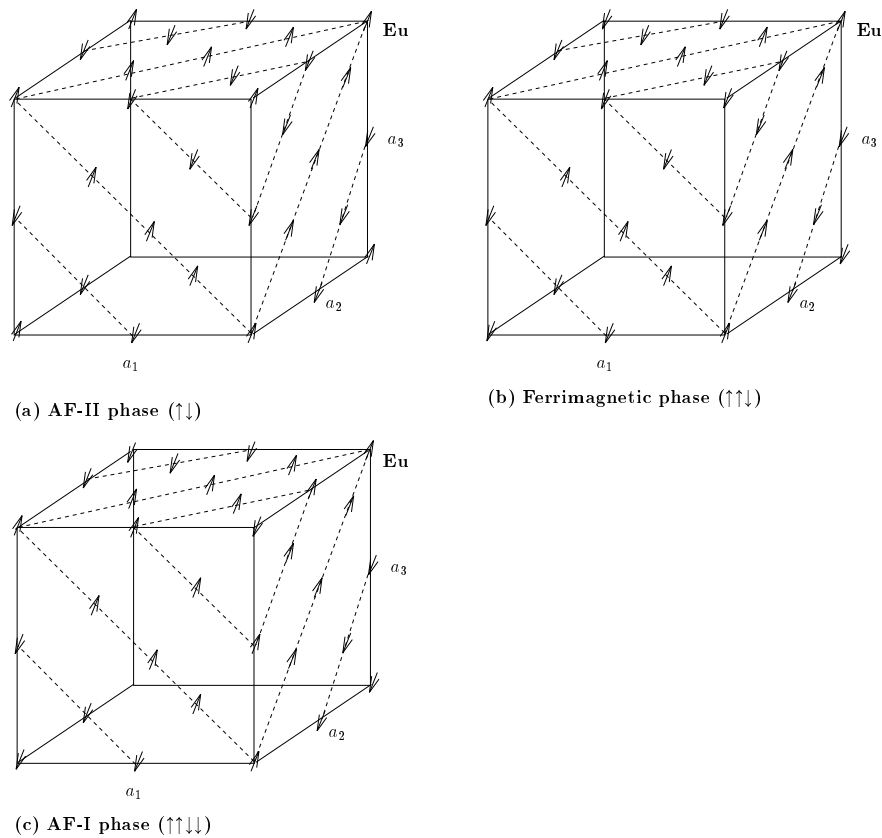
(c) **AF-I phase** (↑↑↓↓)

Figure 22.5: Magnetic structure of EuSe in (a) the AF-II phase (↑↓), (b) the ferrimagnetic phase (↑↑↓), and (c) the antiferromagnetic AF-I phase (↑↑↓↓).

groups are called **color groups**. Color groups have more symmetry than the magnetic groups.

22.6 Selected Problems

1. Suppose that we have a magnetic compound MX (where M is the magnetic species) that crystallizes in the zincblende structure. Suppose that at the Neél temperature the magnetic species undergo a magnetic phase transition to an antiferromagnetic two sublattice phase such that by treating the M↑ and M↓ as different species, the magnetic crystal is described by the chalcopyrite structure. Find the change in the Raman spectra associated with this magnetic phase transition from the zincblende to the chalcopyrite structures.

In the prototype chalcopyrite structure, shown on the right for ZnGeP$_2$, the lattice is compressed slightly along the vertical direction and the phosphorus atoms are slightly displaced from the positions they would have in the zincblende structure.
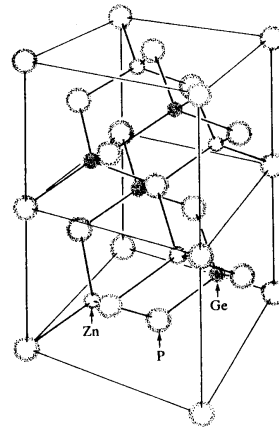
Chapter 23

Symmetry Considerations of Fullerene Molecules and Carbon Nanotubes

Many of the special properties that fullerenes exhibit are directly related to the very high symmetry of the C_{60} molecule, where the 60 equivalent carbon atoms are at the vertices of a truncated icosahedron. The regular truncated icosahedron is obtained from the regular icosahedron by passing planes normal to each of the six five-fold axes passing through the center of the icosahedron so that the edges of the pentagonal faces thus formed are equal in length to the edges of the hexagonal faces. Figure 23.1 shows this soccer-ball configuration for C_{60}. This structure is thought to have been constructed by Leonardo da Vinci in about 1500, and Fig. 23.1 shows the location of the carbon atoms at the vertices of the truncated icosahedron. The first application of the icosahedral group to molecules was by Tisza in 1933.

In this chapter the group theory for the icosahedron is reviewed, and mathematical tables are given for simple applications of the icosahedral group symmetry to the vibrational and electronic states of the icosahedral fullerenes. The effect of lowering the icosahedral symmetry is discussed in terms of the vibrational and electronic states. Symmetry considerations related to the isotopic abundances of the ^{12}C and ^{13}C nuclei are discussed. The space group symmetries appropriate to several crystalline phases of C_{60} are reviewed. The symmetry properties of

Table 23.1: Character table^{a,b,c} for the point group I_h.

$\mathcal{R}$	E	$12C_5$	$12C_5^2$	$20C_3$	$15C_2$	i	$12S_{10}^3$	$12S_{10}$	$20S_3$	$15\sigma_v$
A_g	1	$+1$	$+1$	$+1$	$+1$	$+1$	$+1$	$+1$	$+1$	$+1$
F_{1g}	3	$+\tau^c$	$1-\tau$	0	-1	$+3$	$+\tau$	$1-\tau$	0	-1
F_{2g}	3	$1-\tau$	$+\tau$	0	-1	$+3$	$1-\tau$	$+\tau$	0	-1
G_g	4	-1	-1	$+1$	0	$+4$	-1	-1	$+1$	0
H_g	5	0	0	-1	$+1$	$+5$	0	0	-1	$+1$
A_u	1	$+1$	$+1$	$+1$	$+1$	-1	-1	-1	-1	-1
F_{1u}	3	$+\tau$	$1-\tau$	0	-1	-3	$-\tau$	$\tau-1$	0	$+1$
F_{2u}	3	$1-\tau$	$+\tau$	0	-1	-3	$\tau-1$	$-\tau$	0	$+1$
G_u	4	-1	-1	$+1$	0	-4	$+1$	$+1$	-1	0
H_u	5	0	0	-1	$+1$	-5	0	0	$+1$	-1

^{a}Note: the symmetry operations about the 5-fold axes are in two different classes, labeled $12C_5$ and $12C_5^2$ in the character table. Then $iC_5 = S_{10}^{-1}$ and $iC_5^{-1} = S_{10}$ are in the classes labeled $12S_{10}^3$ and $12S_{10}$, respectively. Also $iC_2 = \sigma_v$.
^{b} See Table 23.2 for a complete listing of the basis functions for the I_h point group in terms of spherical harmonics.
^{c} In this table $\tau \equiv (1 + \sqrt{5})/2$.

symmorphic and non-symmorphic carbon nanotubes are also discussed.

23.1   Icosahedral Symmetry Operations

The truncated icosahedron (see Fig. 23.1) has 12 pentagonal faces, 20 hexagonal faces, 60 vertices and 90 edges. The 120 symmetry operations for the icosahedral point group are listed in the character table given in Table 23.1, where they are grouped into 10 classes, as indicated in this character table. These classes are the identity operator which is in a class by itself, the 12 primary five-fold rotations (12 C_5 and 12 C_5^2) going through the centers of the pentagonal faces, the 20 secondary 3-fold rotations going through the centers of the 20 hexagonal faces, and the 30 secondary 2-fold rotations going through the 30 edges joining two adjacent hexagons. Each of these symmetry operations is compounded with the inversion operation. Also listed in the character

C$_{60}$

5-fold axis
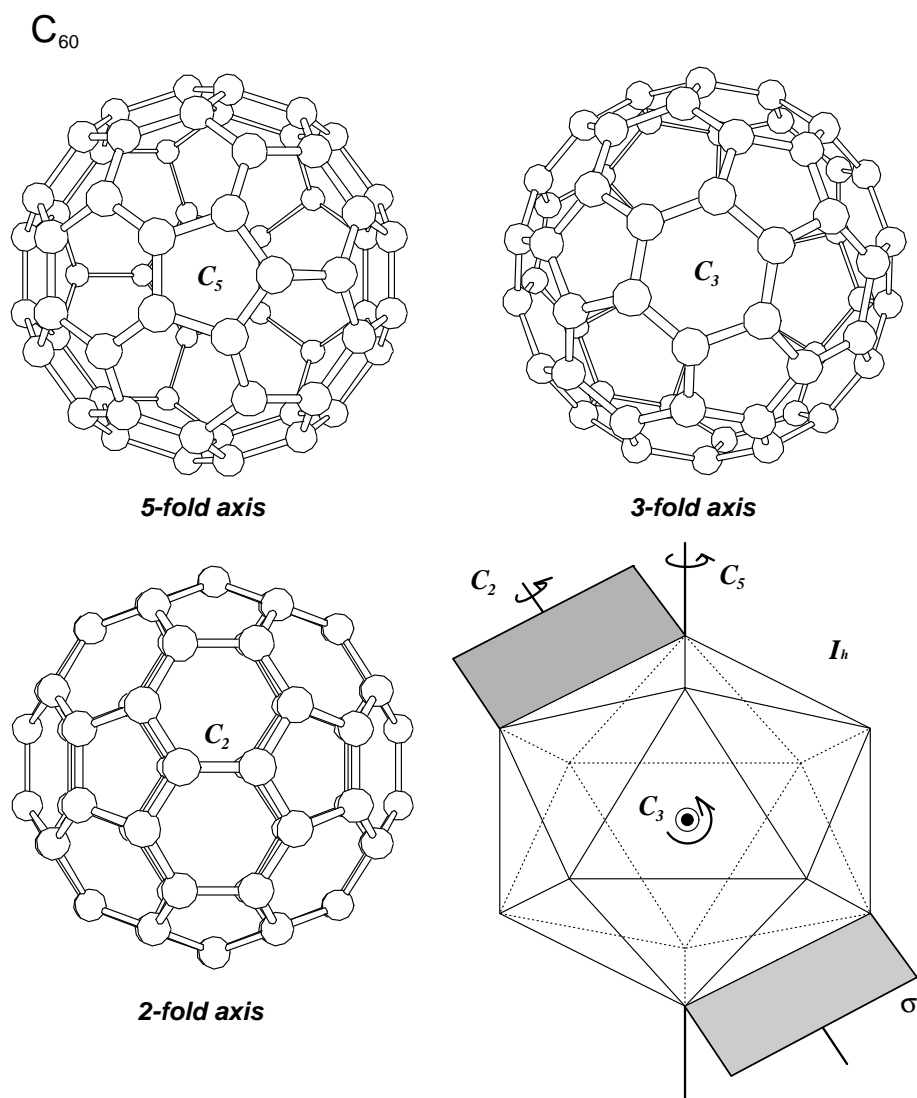
3-fold axis

2-fold axis

Figure 23.1: Symmetry operations of the regular truncated icosahedron. (a) The 5-fold axis, (b) the 3-fold axis, (c) the 2-fold axis, and (d) a composite of the symmetry operations of the point group I_h.

table are the 10 irreducible representations of the point group I_h.

The C_{60} molecule has carbon atoms at the 60 equivalent vertices of a truncated icosahedron for which the lengths of the pentagonal edges are slightly longer ($a_5 = 1.46$ Å) than the bond lengths shared by two hexagons ($a_6 = 1.40$ Å). If we take this difference in bond length into account, then the C_{60} cage forms a truncated icosahedron, but not a *regular* truncated icosahedron where all bond lengths would be equal. Nevertheless, from a symmetry point of view, the truncated icosahedron describes the C_{60} molecule group symmetry, as does the regular truncated icosahedron.

Since the truncated icosahedron is close in shape to a sphere, it is suggestive to relate the basis functions of the icosahedron to those of the sphere, namely the spherical harmonics. Basis functions for each irreducible representation and each partner for group I_h are listed in Table 23.2 in terms of spherical harmonics $Y_{\ell,m}$ with minimal ℓ values. Many physical problems dealing with fullerenes, such as the electronic states or vibrational modes, are treated in terms of spherical harmonics which are basis functions for the full rotational group. The spherical harmonics therefore form reducible representations of the I_h point group for $\ell > 2$, and irreducible representations for $\ell = 0, 1, 2$. Odd and even integers ℓ, respectively, correspond to odd and even representations of the group I_h. The basis functions for group I_h in an l-dimensional manifold are obtained by solving the eigenvalue problem for irreducible tensor operations. The decomposition of the spherical harmonics into irreducible representations of the point group I is given in Table 23.3 for both integral and half integral values of the angular momentum J, where groups I and I_h are related by $I_h = I \otimes i$. The integral values of J are pertinent to the vibrational spectra (§23.2), while the half integral J values are also needed to describe the electronic states when electron spin is included in the wave function (§23.3).

Five-fold symmetry is not often found in solid state physics, because it is impossible to construct a Bravais lattice based on five-fold symmetry (see §12.4). Thus fullerenes in the solid state crystallize into solids of lower point group symmetries, such as the fcc lattice (e.g., C_{60} at room temperature) or the hcp lattice (e.g., some phases of C_{70}). Nevertheless, the local point group symmetry of the individual fullerene molecules is very important because they crystallize into highly molec-

Table 23.2: Basis functions for each of the irreducible representations $\mathcal{R}$ of point group I_h expressed as spherical harmonics $Y_{l,m}$. For the multi-dimensional representations, the basis functions for each partner are listed.

$\mathcal{R}$	Basis function
A_g	$Y_{0,0}$; and $\frac{\sqrt{7}}{5}(Y_{6,5} - Y_{6,-5}) + \frac{\sqrt{11}}{5}Y_{6,0}$
F_{1g}	$\begin{cases} -\sqrt{3/5}Y_{6,-6} + \sqrt{66}/10Y_{6,-1} + \sqrt{22}/10Y_{6,4} \\ \sqrt{1/2}(Y_{6,5} + Y_{6,-5}) \\ \sqrt{3/5}Y_{6,6} + \sqrt{66}/10Y_{6,1} - \sqrt{22}/10Y_{6,-4} \end{cases}$
F_{2g}	$\begin{cases} -\sqrt{28/125}Y_{8,-8} + \sqrt{39/500}Y_{8,-3} + \sqrt{143/250}Y_{8,2} - \sqrt{63/500}Y_{8,7} \\ \sqrt{1/2}(Y_{8,5} + Y_{8,-5}) \\ -\sqrt{28/125}Y_{8,8} - \sqrt{39/500}Y_{8,3} + \sqrt{143/250}Y_{8,-2} + \sqrt{63/500}Y_{8,-7} \end{cases}$
G_g	$\begin{cases} \sqrt{8/15}Y_{4,-4} + \sqrt{7/15}Y_{4,1} \\ \sqrt{1/15}Y_{4,-3} + \sqrt{14/15}Y_{4,2} \\ -\sqrt{1/15}Y_{4,3} + \sqrt{14/15}Y_{4,-2} \\ \sqrt{8/15}Y_{4,4} - \sqrt{7/15}Y_{4,-1} \end{cases}$
H_g	$\begin{cases} Y_{2,-2} \\ Y_{2,-1} \\ Y_{2,0} \\ Y_{2,1} \\ Y_{2,2} \end{cases}$
A_u	$-\frac{\sqrt{5\cdot7\cdot11\cdot13}}{250}(Y_{15,15} + Y_{15,-15}) - \frac{\sqrt{2\cdot3\cdot5\cdot11\cdot29}}{250}(Y_{15,10} - Y_{15,-10})$ $+\frac{\sqrt{23\cdot29}}{50}(Y_{15,5} + Y_{15,-5})$
F_{1u}	$\begin{cases} Y_{1,-1} \\ Y_{1,0} \\ Y_{1,1} \end{cases}$
F_{2u}	$\begin{cases} -\sqrt{2/5}Y_{3,-3} + \sqrt{3/5}Y_{3,2}) \\ Y_{3,0} \\ \sqrt{2/5}Y_{3,3} + \sqrt{3/5}Y_{3,-2}) \end{cases}$
G_u	$\begin{cases} \sqrt{3/5}Y_{3,-3} + \sqrt{2/5}Y_{3,2} \\ Y_{3,-1} \\ Y_{3,1} \\ -\sqrt{3/5}Y_{3,3} + \sqrt{2/5}Y_{3,-2} \end{cases}$
H_u	$\begin{cases} \sqrt{3/10}Y_{5,-4} + \sqrt{7/10}Y_{5,1} \\ \sqrt{3/5}Y_{5,-3} - \sqrt{2/5}Y_{5,2} \\ \sqrt{1/2}(Y_{5,5} + Y_{5,-5}) \\ \sqrt{3/5}Y_{5,3} + \sqrt{2/5}Y_{5,-2} \\ -\sqrt{3/10}Y_{5,4} + \sqrt{7/10}Y_{5,-1} \end{cases}$

Table 23.3: Decomposition of angular momenta basis functions in the full rotation group labeled by J into irreducible representations of the double group of I. Both integral and half-integral angular momentum basis functions are included.[a]

J	Γ_1 A	Γ_2 F_1	Γ_3 F_2	Γ_4 G	Γ_5 H	J	Γ_6	Γ_7	Γ_8	Γ_9
0 (S)	1					$\frac{1}{2}$	1			
1 (P)		1				$\frac{3}{2}$			1	
2 (D)					1	$\frac{5}{2}$				1
3 (F)			1	1		$\frac{7}{2}$		1		1
4 (G)				1	1	$\frac{9}{2}$			1	1
5 (H)		1	1		1	$\frac{11}{2}$	1		1	1
6 (I)	1	1		1	1	$\frac{13}{2}$	1	1	1	1
7 (K)		1	1	1	1	$\frac{15}{2}$			1	2
8 (L)			1	1	2	$\frac{17}{2}$		1	1	2
9 (M)		1	1	2	1	$\frac{19}{2}$	1	1	1	2
10 (N)	1	1	1	1	2	$\frac{21}{2}$	1		2	2
11 (O)		2	1	1	2	$\frac{23}{2}$	1	1	2	2
12 (Q)	1	1	1	2	2	$\frac{25}{2}$	1	1	1	3
13 (R)		1	2	2	2	$\frac{27}{2}$		1	2	3
14 (T)		1	1	2	3	$\frac{29}{2}$	1	1	2	3
15 (U)	1	2	2	2	2	$\frac{31}{2}$	2	1	2	3
16 (V)	1	2	1	2	3	$\frac{33}{2}$	1	1	3	3
17 (W)		2	2	2	3	$\frac{35}{2}$	1	1	2	4
18 (X)	1	1	2	3	3	$\frac{37}{2}$	1	2	2	4
19 (Y)		2	2	2	4	$\frac{39}{2}$	1	1	3	4
20 (Z)	1	2	2	2	4	$\frac{41}{2}$	2	1	3	4
21	1	3	2	3	3	$\frac{43}{2}$	2	2	3	4
22	1	2	2	3	4	$\frac{45}{2}$	1	1	3	5
23		2	3	3	4	$\frac{47}{2}$	1	2	3	5
24	1	2	2	4	4	$\frac{49}{2}$	2	2	3	5
25	1	3	3	3	4	$\frac{51}{2}$	2	1	4	5
26	1	3	2	3	5	$\frac{53}{2}$	2	2	4	5
27	1	3	3	4	4	$\frac{55}{2}$	2	2	3	6
28	1	2	3	4	5	$\frac{57}{2}$	1	2	4	6
29		3	3	4	5	$\frac{59}{2}$	2	2	4	6
30	2	3	3	4	5	$\frac{61}{2}$	3	2	4	6
31	1	4	3	4	5	$\frac{63}{2}$	2	2	5	6
32	1	3	3	4	6	$\frac{65}{2}$	2	2	4	7
33	1	3	4	4	5	$\frac{67}{2}$	2	3	4	7
34	1	3	3	4	6	$\frac{69}{2}$	2	2	5	7
35	1	4	4	4	6	$\frac{71}{2}$	3	2	5	7
36	2	4	3	5	6	$\frac{72}{2}$	3	3	5	7
$\vdots$	$\vdots$	$\vdots$	$\vdots$	$\vdots$	$\vdots$	$\vdots$	$\vdots$	$\vdots$	$\vdots$	$\vdots$

[a] As an example in using the table, $\Gamma(J = 5) = \Gamma_2(F_1) + \Gamma_3(F_2) + \Gamma_5(H)$.

Table 23.4: Characters $\chi^{\text{a.s.}}$ for the equivalence transformation of various atomic sites in icosahedral I_h symmetry.[a] The corresponding irreducible representations of group I_h are listed in Table 23.5.

Cluster	E	C_5	C_5^2	C_3	C_2	i	S_{10}^3	S_{10}	S_6	σ_v
# elements	1	12	12	20	15	1	12	12	20	15
X_{12}	12	2	2	0	0	0	0	0	0	4
C_{20}	20	0	0	2	0	0	0	0	0	4
X_{30}	30	0	0	0	2	0	0	0	0	4
C_{60}	60	0	0	0	0	0	0	0	0	4
C_{80}	80	0	0	2	0	0	0	0	0	8
C_{140}	140	0	0	2	0	$-^a$	$-^a$	$-^a$	$-^a$	$-^a$
C_{180}	180	0	0	0	0	0	0	0	0	4
C_{240}	240	0	0	0	0	0	0	0	0	8

[a]Since C_{140} lacks inversion symmetry, entries in the table are made only for the classes that are pertinent to point group I.

ular solids in which the electronic and vibrational states are closely related to those of the free molecule. Therefore we summarize in this chapter the group theoretical considerations that are involved in finding the symmetries and degeneracies of the vibrational and electronic states of the C_{60} molecule, with some discussion also given to higher mass fullerenes.

To describe the symmetry properties of the vibrational modes and of the electronic levels, it is necessary to find the equivalence transformation for the carbon atoms in the molecule. The characters for the equivalence transformation $\chi^{a.s.}$ for the 60 equivalent carbon atom sites (a.s.) for the C_{60} molecule in icosahedral I_h symmetry are given in Table 23.4. Also listed in Table 23.4 are the characters for the equivalence transformation for the 12 five-fold axes, the 20 three-fold axes and the 30 two-fold axes which form classes of the icosahedral I_h group. The decomposition of the reducible representations of Table 23.4 into their irreducible constituents is given in Table 23.5, which directly gives the number of π-orbitals for each irreducible representation. For example, if guest species X are attached to each 5-fold axis at an equal distance from the center of the icosahedron to yield a molecule

Table 23.5: Irreducible representations contained in the various $\chi^{\text{a.s.}}$ in the icosahedral group I_h given in Table 23.4.[a]

Cluster	$\chi^{\text{a.s.}}$
X_{12}	$A_g, H_g,$ F_{1u}, F_{2u}
C_{20}	$A_g, G_g, H_g,$ F_{1u}, F_{2u}, G_u
X_{30}	$A_g, G_g, 2H_g,$ F_{1u}, F_{2u}, G_u, H_u
C_{60}	$A_g, F_{1g}, F_{2g}, 2G_g, 3H_g,$ $2F_{1u}, 2F_{2u}, 2G_u, 2H_u$
C_{80}	$2A_g, F_{1g}, F_{2g}, 3G_g, 4H_g,$ $3F_{1u}, 3F_{2u}, 3G_u, 2H_u$
C_{140}	$3A, 7F_1, 7F_2, 10G, 11H$
C_{180}	$2A_g, 5F_{1g}, 5F_{2g}, 6G_g, 8H_g$ $A_u, 4F_{1u}, 5F_{2u}, 6G_u, 7H_u$
C_{240}	$3A_g, 5F_{1g}, 5F_{2g}, 8G_g, 11H_g,$ $A_u, 7F_{1u}, 7F_{2u}, 8G_u, 9H_u$

[a]Since C_{140} lacks inversion symmetry, the irreducible representations for $\chi^{\text{a.s.}}$ refer to the group I.

$X_{12}C_{60}$, then the full icosahedral I_h symmetry is preserved. Table 23.4 also lists $\chi^{\text{a.s.}}$ for a few higher icosahedral fullerenes which are specified by C_{n_C} with $n_C = 20(m^2 + n^2 + mn)$. Thus C_{60} corresponds to $(m, n) = (1, 1)$, C_{80} has $(n, m) = (2, 0)$, C_{140} has $(n, m) = (2, 1)$, and C_{240} has $(n, m) = (2, 2)$. We note that fullerenes with either $m = 0$, or $n = 0$, or those with $m = n$ have inversion symmetry and therefore are described by group I_h. Other icosahedral fullerenes with $m \neq n \neq 0$ lack inversion symmetry (e.g., C_{140} and C_{180}) and are described by the point group I. The decomposition of the equivalence transformation $\Gamma^{\text{a.s.}}$ which is a reducible representation of the group I_h (or I) into its irreducible constituents is given in Table 23.5 for every entry in Table 23.4, and the even and odd constituents are listed on separate lines.

23.2   Symmetry of Vibrational Modes

In this section we review the symmetries and degeneracies of the vibrational modes for the C_{60} molecule. There are 180 degrees of freedom (3×60) for each C_{60} molecule. Three of these degrees of freedom correspond to translations and three to rotation, leaving 174 vibrational degrees of freedom. Since icosahedral symmetry gives rise to a large number of degenerate modes, only 46 distinct mode frequencies are expected for the C_{60} molecule. The number of distinct modes N_ω for C_{60} and other icosahedral configurations is given in Table 23.6. The results given in Table 23.6 follow directly from group theoretical arguments, using the entries given in Table 23.4 for the characters for the equivalence transformation $\chi^{\text{a.s.}}(C_{60})$ for the 60 equivalent carbon atoms in C_{60}. Taking the direct product of $\chi^{\text{a.s.}}(C_{60})$ with the characters for the vector (which transforms according to the irreducible representation F_{1u}), as given in Table 23.1, and subtracting off the irreducible representations for pure rotations (F_{1g}) and pure translations (F_{1u}), yields the irreducible representations for the vibrational modes of C_{60}. The symmetries of the resulting vibrational modes are listed in Table 23.6, where the multiplicities for each symmetry type are given. For example, X_{12} in I_h symmetry has $N_\omega = 8$ distinct modes, and the symmetry types that are found include $A_g + G_g + 2H_g + F_{1u} + F_{2u} + G_u + H_u$ where $2H_g$ indicates that there are two distinct mode frequencies cor-

Table 23.6: Symmetry properties of vibrational modes in molecules with icosahedral symmetry.

Cluster	$N_\omega{}^a$	$A_g{}^b$	F_{1g}	F_{2g}	G_g	$H_g{}^c$	A_u	$F_{1u}{}^d$	F_{2u}	G_u	H_u
X_{12}	8	1			1	2		1	1	1	1
X_{20}	14	1		1	2	3		1	2	2	2
X_{30}	22	1	1	2	3	4		2	3	3	3
C_{60}	46	2	3	4	6	8	1	4	5	6	7
$X_{12}C_{60}$	56	3	4	4	7	10	1	6	6	7	8
C_{80}	62	3	6	5	8	10	1	5	6	8	10
$C_{140}{}^e$	110	7	20	20	28	35	–	–	–	–	–
C_{240}	190	7	17	17	24	31	5	17	19	24	29

[a] The number of distinct mode frequencies in icosahedral symmetry is denoted by N_ω.

[b] Raman-active mode is seen only in $\parallel, \parallel$ polarization.

[c] Raman-active mode is seen in both $\parallel, \parallel$ and $\parallel, \perp$ polarizations.

[d] Infrared-active mode symmetry.

[e] In I symmetry, there are no gerade or ungerade modes. In this case the F_1 modes are IR-active and the A and H modes are Raman-active.
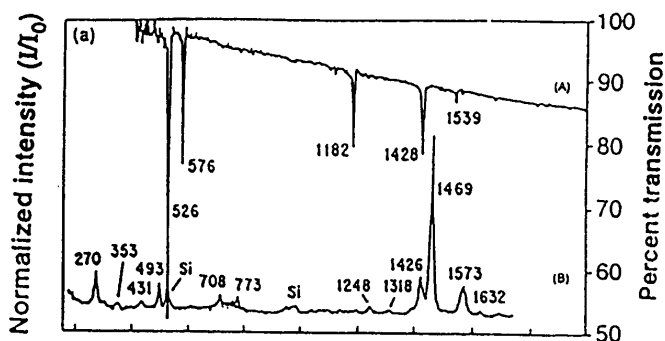
Figure 23.2: First-order infrared (A) and Raman (B) spectra for C_{60} taken with low incident optical power levels (<50 /mm^2)

responding to $(5 \times 2) = 10$ normal modes. We note that for the C_{60} molecule, every irreducible representation is contained at least once. In carrying out the direct product $\chi^{\text{a.s.}} \otimes \chi_{F_{1u}}$ the entries in Table 23.7 for the decomposition of direct products for the point group I are useful, noting that $I_h = I \otimes i$.

The Raman-active modes have A_g and H_g symmetry (corresponding to the basis functions for all symmetrical quadratic forms, and the antisymmetric F_{1g} does not contribute to the Raman scattering). The infrared-active modes have F_{1u} symmetry (the linear forms associated with a vector). One can see from the basis functions listed in Table 23.2 that the symmetry of the Raman tensor allows $\|, \|$ scattering for A_g modes, and both $\|, \|$ and $\|, \perp$ scattering for H_g modes, where the directions $\|$ and $\perp$ refer to the polarization directions of the incident and scattered photon electric fields. For example, $\|, \perp$ implies that the polarizations for the incident and scattered beams are orthogonal. Table 23.6 shows that of the 46 distinct vibrational mode frequencies for C_{60}, only four are infrared active with symmetry F_{1u}, and only 10 are Raman active (two with A_g symmetry and eight with H_g symmetry), while the remaining 32 modes are silent in the first-order infrared and Raman spectra. The experimental observation of the infrared and Raman spectra for C_{60} is shown in Fig. 23.2. Many of these silent modes can, however, be observed by inelastic neutron scattering, electron energy loss spectroscopy, as vibronic sidebands on the photoluminescence spectra, and most sensitively in the higher-order infrared and Raman spectra, because of the different selection rules governing these higher-

Table 23.7: Decomposition of direct products[a] in the icosahedral point group I.

$\mathcal{R}$	Γ_1 (A)	Γ_2 (F_1)	Γ_3 (F_2)	Γ_4 (G)	Γ_5 (H)
Γ_1 (A)	Γ_1	Γ_2	Γ_3	Γ_4	Γ_5
Γ_2 (F_1)	Γ_2	Γ_1 Γ_2 Γ_5	Γ_4 Γ_5	Γ_3 Γ_4 Γ_5	Γ_2 Γ_3 Γ_4 Γ_5
Γ_3 (F_2)	Γ_3	Γ_4 Γ_5	Γ_1 Γ_3 Γ_5	Γ_2 Γ_4 Γ_5	Γ_2 Γ_3 Γ_4 Γ_5
Γ_4 (G)	Γ_4	Γ_3 Γ_4 Γ_5	Γ_2 Γ_4 Γ_5	Γ_1 Γ_2 Γ_3 Γ_4 Γ_5	Γ_2 Γ_3 Γ_4 $2\Gamma_5$
Γ_5 (H)	Γ_5	Γ_2 Γ_3 Γ_4 Γ_5	Γ_2 Γ_3 Γ_4 Γ_5	Γ_2 Γ_3 Γ_4 $2\Gamma_5$	Γ_1 Γ_2 Γ_3 $2\Gamma_4$ $2\Gamma_5$
Γ_6	Γ_6	Γ_6 Γ_8	Γ_9	Γ_7 Γ_9	Γ_8 Γ_9
Γ_7	Γ_7	Γ_9	Γ_6 Γ_8	Γ_6 Γ_9	Γ_8 Γ_9
Γ_8	Γ_8	Γ_6 Γ_8 Γ_9	Γ_7 Γ_8 Γ_9	Γ_8 $2\Gamma_9$	Γ_6 Γ_7 Γ_8 $2\Gamma_9$
Γ_9	Γ_9	Γ_7 Γ_8 $2\Gamma_9$	Γ_6 Γ_8 $2\Gamma_9$	Γ_6 Γ_7 $2\Gamma_8$ $2\Gamma_9$	Γ_6 Γ_7 $2\Gamma_8$ $3\Gamma_9$

[a] As an example of using this table, the direct product $\Gamma_4 \otimes \Gamma_2 = \Gamma_3 + \Gamma_4 + \Gamma_5$.

order processes. The observation that the Raman spectra for C_{60} remain essentially unchanged for isolated C_{60} molecules in solution and in a crystalline film is indicative of the very weak coupling between the C_{60} molecules in the solid.

Various possible attachments could be made to the C_{60} molecule without lowering its symmetry (e.g., by attaching 12 equivalent guest species (X) along the 12 five-fold axes, or 20 guest species along the 20 three-fold axes, or 30 guest species along the two-fold axes). To preserve the I_h symmetry, all the equivalent sites must be occupied. However, if only some of these sites are occupied, the symmetry is lowered (see §23.4). Table 23.4 gives the characters $\chi^{a.s.}$ for the equivalence transformation for special arrangements of guest species that preserve the I_h or I symmetries, and these guest species may be attached through doping or a chemical reaction. The corresponding vibrational modes associated with such guest species are included in Table 23.6, both separately and in combination with the C_{60} molecule, as for example $X_{12}C_{60}$, where we might imagine a guest atom to be located at the center of each pentagonal face, as occurs in the alkali metal coated $Li_{12}C_{60}$. Any detailed solution to the normal mode problem will involve solutions of a dynamical matrix in which tangential and radial modes having the same symmetry will mix.

Vibrational modes that are silent in the first-order spectrum can, however, contribute to the second- and higher-order Raman and infrared spectra. Anharmonic terms in the potential couple the normal mode solutions of the harmonic potential approximation, giving rise to overtones ($n\omega_i$) and combination modes ($\omega_i \pm \omega_j$), many of which are observable in the second-order spectra. Group theory requires that the direct product of the second-order combination modes $\Gamma_i \otimes \Gamma_j$ (see Table 23.7) must contain the irreducible representations F_{1u} to be observable in the second-order infrared spectrum, and A_g or H_g to be observable in the second-order Raman spectrum. By parity considerations alone, overtones (or harmonics) can be observed in the Raman spectrum, but are not symmetry-allowed in the second-order infrared spectrum, since all second-order overtones have even parity. Because of the highly molecular nature of crystalline C_{60}, the second-order infrared and Raman spectra are especially strong in crystalline films. Whereas only about 10 strong features are seen experimentally in the first-order

Raman spectrum, over 100 features are resolved and identified in the second-order Raman spectrum. The observation of a multitude of sharp lines in the higher-order infrared and Raman spectra is a unique aspect of the spectroscopy of highly molecular solids. For typical crystals, dispersion effects in the solid state broaden the higher-order spectra, so that detailed features commonly observed in the gas phase spectra can no longer be resolved in the crystalline phase. Nevertheless, analysis of the second-order infrared and Raman spectra of fcc C_{60} provides a powerful method for the determination of the silent modes of C_{60}.

Although the icosahedral C_{80}, C_{140}, and C_{240} icosahedral molecules have not yet been studied by Raman or infrared spectroscopy, the symmetry analysis for these molecules is included in Table 23.6. The corresponding symmetry analysis for fullerene molecules of lower symmetry is given in §23.4.

23.3   Symmetry for Electronic States

Symmetry considerations are also important for describing the electronic states of fullerenes and their related crystalline solids. In this section we consider a simple description of the electronic states of fullerene molecules. The basic concepts presented in this section can be extended to the electronic states in crystalline solids and to carbon nanotubules.

To treat the electronic energy levels of a fullerene molecule it is necessary to consider a many-electron system with the point group symmetry appropriate to the fullerene. From a group theoretical standpoint, treatment of the electronic states for the neutral C_{60} molecule or the charged $C_{60}^{\pm n}$ molecular ion requires consideration of both integral and half-integral angular momentum states. To describe the half-integral states, it is necessary to use the double group based on the point group I_h. The character table for the double group I is given in Table 23.8.

The double group of I_h is found from that for I by taking the direct product group $I \otimes i$, and the irreducible representations and characters for the double group are obtained by taking appropriate direct products of the characters in Table 23.8 with those of the inversion group C_i consisting of two elements (the identity and the inversion operator) and having two irreducible representations $(1, 1)$ and $(1, -1)$.

Table 23.8: Character table[a,b] for the double point group I.

$\mathcal{R}$	E	$\overline{E}$	C_5	$\overline{C}_5$	C_5^2	$\overline{C}_5^2$	C_3	$\overline{C}_3$	C_2
# elements	1	1	12	12	12	12	20	20	30
Γ_1 (A)	1	+1	+1	+1	+1	+1	+1	+1	+1
Γ_2 (F_1)	3	+3	$+\tau$	$+\tau$	$1-\tau$	$1-\tau$	0	0	-1
Γ_3 (F_2)	3	+3	$1-\tau$	$1-\tau$	$+\tau$	$+\tau$	0	0	-1
Γ_4 (G)	4	+4	-1	-1	-1	-1	+1	+1	0
Γ_5 (H)	5	+5	0	0	0	0	-1	-1	+1
Γ_6	2	-2	$+\tau$	$-\tau$	$-(1-\tau)$	$1-\tau$	+1	-1	0
Γ_7	2	-2	$1-\tau$	$-(1-\tau)$	$-\tau$	$+\tau$	+1	-1	0
Γ_8	4	-4	+1	-1	-1	+1	-1	+1	0
Γ_9	6	-6	-1	+1	+1	-1	0	0	0

[a] Note: C_5 and C_5^{-1} are in different classes, labeled $12C_5$ and $12C_5^2$ in the character table. The class $\overline{E}$ represents a rotation by 2π and classes $\overline{C}_n$ represent rotations by $2\pi/n$ between 2π and 4π. In this table $\tau = (1+\sqrt{5})/2$, while $-1/\tau = 1-\tau$, and $\tau^2 = 1+\tau$.
[b] The basis functions for $\Gamma_1 - \Gamma_5$ are given in Table 23.2 and for the double group irreducible representations $\Gamma_6 - \Gamma_9$ are given in Table 23.9.

Table 23.9: Basis functions for the double group irreducible representations $\mathcal{R}$ of point group I expressed as half-integer spherical harmonics ϕ_{j,n_j}.

$\mathcal{R}$	Basis function
Γ_6	$\phi_{1/2,-1/2}, \phi_{1/2,1/2}$
Γ_7	$\begin{cases} (\sqrt{(7/10)}\phi_{7/2,-3/2} - \sqrt{(3/10)}\phi_{7/2,7/2}) \\ (\sqrt{(7/10)}\phi_{7/2,3/2} + \sqrt{(3/10)}\phi_{7/2,-7/2}) \end{cases}$
Γ_8	$\phi_{3/2,-3/2}, \phi_{3/2,-1/2}, \phi_{3/2,1/2}, \phi_{3/2,3/2}$
Γ_9	$\begin{cases} \phi_{5/2,-5/2} \\ \phi_{5/2,-3/2} \\ \phi_{5/2,-1/2} \\ \phi_{5/2,1/2} \\ \phi_{5/2,3/2} \\ \phi_{5/2,5/2} \end{cases}$

Basis functions for each of the irreducible representations of the double group of I are also listed in Table 23.9. Spin states enter both in the application of the Pauli principle and in considering the effect of the spin-orbit interaction. Though the spin-orbit interaction of carbon is small, it has been determined in graphite by means of detailed electron spin resonance (ESR) measurements.

Each C_{60} molecule with icosahedral symmetry can be considered to have $60 \times 3 = 180$ σ electrons making bonds along the surface of the icosahedron and 60 π electrons with higher-lying energy levels than the σ-bonds for a given angular momentum state. On a graphene sheet (denoting a single layer of the graphite crystal), the bonding π states have nearest-neighbor orbitals parallel to one another, and the anti-bonding states have antiparallel orbitals. More generally, for fullerenes with n_C carbon atoms, the molecular electronic problem involves n_C π electrons.

The electronic levels for the π electrons for a fullerene molecule can be found by starting with a spherical approximation where spherical harmonics can be used to specify the electronic wave functions according to their angular momentum quantum numbers. As stated above, for $\ell > 2$ these spherical harmonics form reducible representations for the icosahedral group symmetry. By lowering the symmetry from full rotational symmetry to icosahedral symmetry (see Table 23.3), the irreducible representations of the icosahedral group are found. In general, the bonding σ levels will lie well below the Fermi level in energy and are not as important for determining the electronic properties as the π electrons.

To obtain the symmetries for the 60 π electrons for C_{60} we focus our attention on the 60 bonding π electrons whose energies lie close to the Fermi level. Assigning angular momentum quantum numbers to this electron gas, we see from the Pauli principle that 60 π electrons will completely fill angular momentum states up through $\ell = 4$, leaving 10 electrons in the $\ell = 5$ level which can accommodate a total of 22 electrons. In Table 23.10 we list the number of electrons that can be accommodated in each angular momentum state ℓ, as well as the splitting of the angular momentum states in the icosahedral field.

Table 23.10 thus shows that the $\ell = 4$ level is totally filled by the C_{50} molecule or by $n_C = 50$. The filled states in icosahedral symmetry

Table 23.10: Filled shell configurations for fullerene molecules.[a]

ℓ	electrons/state	n_C	HOMO in I_h symmetry
0	2	2	a_g^2
1	6	8	f_{1u}^6
2	10	18	h_g^{10}
3	14	24	f_{2u}^6
		26	g_u^8
		32	$(f_{2u}^6 g_u^8)$
4	18	40	g_g^8
		42	h_g^{10}
		50	$(g_g^8 h_g^{10})$
5	22	56	f_{1u}^6 or f_{2u}^6
		60	h_u^{10}
		62	$f_{1u}^6 f_{2u}^6$
		66	$(f_{1u}^6 h_u^{10})$ or $(f_{2u}^6 h_u^{10})$
		72	$(f_{1u}^6 f_{2u}^6 h_u^{10})$
6	26	74	a_g^2
		78	f_{1g}^6
		80	g_g^8 or $(a_g^2 f_{1g}^6)$
		82	h_g^{10} or $(a_g^2 g_g^8)$
		84	$(a_g^2 h_g^{10})$
		88	$(f_{1g}^6 g_g^8)$
		90	$(a_g^2 f_{1g}^6 g_g^8)$ or $(f_{1g}^6 h_g^{10})$
		92	$(a_g^2 g_g^8 h_g^{10})$
		96	$(f_{1g}^6 g_g^8 h_g^{10})$
		98	$(a_g^2 f_{1g}^6 g_g^8 h_g^{10})$
$\vdots$	$\vdots$	$\vdots$	$\vdots$

[a] The angular momentum quantum number for a spherical shell of π electrons is denoted by ℓ, while n_C denotes the number of π electrons for fullerenes with closed shell (^1A_g) ground state configurations in icosahedral symmetry. The last column gives the symmetries of all the levels of the ℓ value corresponding to the highest occupied molecular orbital (HOMO). The superscript on the symmetry label indicates the total spin and orbital degeneracy of the level. All of the listed levels are assumed to be occupied.

for $\ell = 4$ are labeled by the irreducible representations g_g^8 and h_g^{10} to accommodate a total of 18 electrons. On filling the $\ell = 4$ level, possible ground states occur when either the g_g level is filled with 8 electrons at $n_C = 40$ or when the h_g level is filled with 10 electrons at $n_C = 42$, or when the complete shell $\ell = 4$ is filled (i.e., $g_g^8 h_g^{10}$) at $n_C = 50$. Following the same line of reasoning, the 22-fold degenerate $\ell = 5$ level in full rotational symmetry will be filled by C_{72} which splits into the irreducible representations $H_u + F_{1u} + F_{2u}$ of the icosahedral group with filled shell occupations for these levels of 10, 6, and 6 electrons, respectively. Ten electrons in the $\ell = 5$ angular momentum states of C_{60} are sufficient to completely occupy the h_u level, leaving the f_{1u} and f_{2u} levels completely empty, so that the highest occupied molecular orbital (HOMO) corresponds to the h_u level and the lowest unoccupied molecular orbital (LUMO) corresponds to the f_{1u} level, in agreement with Hückel calculations for the one-electron molecular orbitals. It should be noted that for Hückel calculations the next lowest unoccupied molecular orbital is not an f_{2u} level but rather an f_{1g} level, associated with the angular momentum state $\ell = 6$. The reason why an $\ell = 6$ derived level becomes lower than an $\ell = 5$ derived level is due to the form of the atomic potential. In fact, the C_{60} molecule has sufficiently large icosahedral splittings so that some of the $\ell = 6$ states lie lower than the highest $\ell = 5$ state, so taht the lowest $\ell = 6$ state becomes occupied before the $\ell = 5$ shell is completely filled. Such level crossings occur even closer to the HOMO level as n_C increases.

Not only C_{60}, but also other higher mass fullerenes, have icosahedral symmetry. As discussed previously, all icosahedral fullerenes can be specified by C_{n_C} where $n_C = 20(n^2 + nm + m^2)$. Using the same arguments as for C_{60}, the angular momentum states and electronic configurations for the n_C π electrons in these larger fullerenes (up to $n_C = 780$) can be found (see Table 23.11). In this table, the symmetry of each icosahedral fullerene is given. Fullerenes with (n, m) values such that $n = 0$, $m = 0$ or $m = n$ have I_h symmetry (including the inversion operation), while other entries have I symmetry, lacking inversion. Also listed in this table is $\ell_{\max}$, the maximum angular momentum state that is occupied, from which n_{tot}, the maximum number of electrons needed

Table 23.11: Symmetries and configurations of the π-electrons for icosahedral fullerenes.

C_{n_C}	$\ell_{max}{}^a$	$n_{tot}{}^b$	$n_v{}^c$	Config.^{d}	J_{Hund}	I_h (or I) Symmetries^e
C_{20}	3	32	2	$\ldots f^2$	4	G_g, H_g
C_{60}	5	72	10	$\ldots g^{18}h^{10}$	0	A_g
C_{80}	6	96	8	$\ldots h^{22}i^8$	16	$A_g, 2F_{1g}, F_{2g}, 2G_g, 3H_g$
C_{140}	8	162	12	$\ldots k^{30}l^{12}$	24	$A, 2F_1, 2F_2, 4G, 4H$
C_{180}	9	200	18	$\ldots l^{34}m^{18}$	0	A_g
C_{240}	10	242	40	$\ldots m^{38}n^{40}$	20	$A_g, 2F_{1g}, 2F_{2g}, 2G_g, 4H_g$
C_{260}	11	288	18	$\ldots n^{42}o^{18}$	36	$2A, 4F_1, 3F_2, 5G, 6H$
C_{320}	12	338	32	$\ldots o^{46}q^{32}$	72	$\ldots$
C_{380}	13	392	42	$\ldots q^{50}r^{42}$	96	$\ldots$
C_{420}	14	450	28	$\ldots r^{54}t^{28}$	0	A
C_{500}	15	512	50	$\ldots t^{58}u^{50}$	120	$\ldots$
C_{540}	16	578	28	$\ldots u^{62}v^{28}$	56	$\ldots$
C_{560}	16	578	48	$\ldots u^{62}v^{48}$	144	$\ldots$
C_{620}	17	648	42	$\ldots v^{66}w^{42}$	112	$\ldots$
C_{720}	18	722	72	$\ldots w^{70}x^{72}$	36	$2A_g, 4F_{1g}, 3F_{2g}, 5G_g, 6H_g$
C_{740}	19	800	18	$\ldots x^{74}y^{18}$	180	$\ldots$
C_{780}	19	800	58	$\ldots x^{74}y^{58}$	200	$\ldots$
C_{860}	20	882	60	$\ldots y^{78}z^{60}$	220	$\ldots$
C_{960}	21	968	78	$\ldots z^{82}a^{78}$	144	$\ldots$
C_{980}	22	1058	12	$\ldots a^{86}b^{12}$	192	$\ldots$
$\vdots$	$\vdots$	$\vdots$	$\vdots$	$\vdots$	$\vdots$	$\vdots$

^{a} ℓ_{max} represents the maximum value of the angular momentum for the HOMO level.

^{b} $n_{tot} = 2(\ell_{max} + 1)^2$ is the number of electrons needed for a filled shell.

^{c} n_v represents the number of electrons in the HOMO level.

^{d} The notation for labeling the angular momentum states is consistent with Table 23.3.

^{e} The splittings of the Hund's rule ground state J_{Hund} in icosahedral symmetry.

to fill a spherical shell can be calculated according to

$$n_{\text{tot}} = 2(\ell_{\text{max}} + 1)^2. \tag{23.1}$$

The number of valence electrons in the HOMO level n_{v} is included in Table 23.11, which also lists the full electronic configuration of the π electrons, the J_{Hund} value for the ground state configuration according to Hund's rule and the icosahedral symmetries for the valence electron states. Then by decomposing these angular momentum states into irreducible representations of the icosahedral group (using Table 23.3 and the notation for the electronic configurations in Table 23.3), the symmetry designation for the ground state energy levels (according to Hund's rule) in icosahedral symmetry can be found (see Table 23.11). For example, the icosahedral C_{80} molecule has a sufficient number of π electrons to fill the $\ell = 5$ level, with 8 electrons available for filling states in the $\ell = 6$ level. Hückel calculations for this molecule suggest that the f_{1u} and f_{1g} levels are completely filled, and the h_u level is partially filled with 8 electrons.

There are, in general, many Pauli-allowed states that one can obtain from the spherical molecule configurations listed in Table 23.11. For example, the hypothetical C_{20} icosahedral molecule with the $s^2 p^6 d^{10} f^2$ (or simply f^2) configuration has Pauli-allowed states with $S = 0$, $L = 0, 2, 4, 6$ and with $S = 1$, $L = 1, 3, 5$. The Hund's rule ground state is the $J_{\text{Hund}} = 4$ state that comes from $S = 1$, $L = 5$. The symmetries of these Hund's rule ground states are listed in the column labeled J_{Hund} in Table 23.11 together with the decomposition of these states of the J_{Hund} reducible representation into the appropriate irreducible representations of the icosahedral group. If the perturbation to the spherical symmetry by the icosahedral potentials is small, and Hund's rule applies, then the ground state will be as listed. If, however, the icosahedral perturbation is large compared with the electron correlation and exchange energies, then the icosahedral splitting must be considered first before the electrons are assigned to the spherical symmetry angular momentum states.

23.4 Going from Higher to Lower Symmetry

A lowering of the symmetry from full icosahedral symmetry occurs in a variety of fullerene-derived structure-property relations. One example of symmetry lowering results from elongation of the icosahedral shape of the C_{60} fullerene molecules to a rugby-ball shape for the C_{70} molecule, as discussed below. Another example involves the introduction of chirality into the fullerene molecule. A third example is found in many chemical or photochemical reactions which add side-groups at various sites, and with various symmetries. In these cases the symmetry-lowering effect is specific to the side-groups that are added. A fourth example is the introduction of fullerenes into a crystal lattice. Since no Bravais lattice with five-fold symmetry is possible, symmetry-lowering must occur in this case. As a fifth example, carbon nanotubes can be considered to be related to fullerenes through a symmetry-lowering process (see §23.6).

23.4.1 Symmetry Considerations for C_{70}

The most common fullerene which has lower than icosahedral symmetry is C_{70}, and the structure and properties of this fullerene have also been studied in some detail. The C_{70} molecule can be constructed from C_{60} by appropriately bisecting the C_{60} molecule normal to a five-fold axis, rotating one hemisphere relative to the other by 36° (thereby losing inversion symmetry), then adding a ring of 5 hexagons around the equator (or belt), and finally reassembling these three constituents (see Fig. 23.3). The elongation of the icosahedral C_{60} in this way to yield C_{70} results in a lowering of the symmetry of the molecule from I_h to D_{5h}. The point group D_{5h} does not have inversion symmetry, but does have a mirror plane normal to the five-fold axis. In contrast, group I_h has inversion symmetry but no mirror plane. If a second ring of 5 hexagons is added around the equator, we then obtain a C_{80} molecule with D_{5d} symmetry, which is symmetric under inversion but has no σ_h mirror plane. The character tables for the point groups D_{5h} and D_{5d} are given in Tables 23.12 and Tables 23.13, respectively, and the corre-
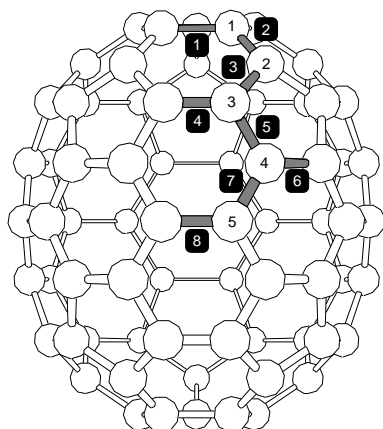
Figure 23.3: Geometry of the C_{70} molecule with D_{5h} symmetry. In the C_{70} cluster, there are five inequivalent atomic sites (1–5) and eight kinds of bonds (boxed numbers).

sponding basis functions are given in Table 23.14. The corresponding compatibility relations for the irreducible representations of the point group I_h in going to lower symmetry groups (I, T_h, D_{5d}, D_5, and C_{1h}) are provided in Table 23.15. Since the group D_{5d} has inversion symmetry, the irreducible representations of I_h form reducible representations of D_{5d}, so that the compatibility relations between the two groups are easily written. For the group D_{5h} which has a mirror plane but no inversion symmetry, one must use the lower symmetry icosahedral group I for relating the icosahedral irreducible representations to those in D_5, which is a subgroup of I. The compatibility relations for $I \to D_5$ are also included in Table 23.15, in addition to compatibility tables for groups $I_h \to T_h$ and $I \to C_{1h}$.

In treating the electronic levels and vibrational modes for the C_{70} molecule, we can either go from full rotational symmetry (see Table 23.3) to D_{5h} symmetry in analogy to §23.3, or we can first go from full rotational symmetry to I symmetry, and then treating D_5 as a subgroup of I, go from I to D_5 in the sense of perturbation theory. Referring to Table 23.16, which shows the decomposition of the various angular momentum states ℓ into irreducible representations of point group I and then to group D_5 (or directly from $\ell = 5$ to point group D_5), we obtain

$$\Gamma_{\ell=5} \to H + F_1 + F_2 \to A_1 + 2A_2 + 2E_1 + 2E_2 \qquad (23.2)$$

Table 23.12: Character table for point group D_{5h}.

$\mathcal{R}$	E	$2C_5$	$2C_5^2$	$5C_2'$	σ_h	$2S_5$	$2S_5^3$	$5\sigma_v$
A_1'	$+1$	$+1$	$+1$	$+1$	$+1$	$+1$	$+1$	$+1$
A_2'	$+1$	$+1$	$+1$	-1	$+1$	$+1$	$+1$	-1
E_1'	$+2$	$\tau - 1$	$-\tau$	0	$+2$	$\tau - 1$	$-\tau$	0
E_2'	$+2$	$-\tau$	$\tau - 1$	0	$+2$	$-\tau$	$\tau - 1$	0
A_1''	$+1$	$+1$	$+1$	$+1$	-1	-1	-1	-1
A_2''	$+1$	$+1$	$+1$	-1	-1	-1	-1	$+1$
E_1''	$+2$	$\tau - 1$	$-\tau$	0	-2	$1 - \tau$	τ	0
E_2''	$+2$	$-\tau$	$\tau - 1$	0	-2	τ	$1 - \tau$	0

In the table $\tau \equiv (1 + \sqrt{5})/2$ and $\sigma_v = C_2' \otimes \sigma_h$.

Table 23.13: Character table for point group D_{5d}.

$\mathcal{R}$	E	$2C_5$	$2C_5^2$	$5C_2'$	i	$2S_{10}^{-1}$[a]	$2S_{10}$	$5\sigma_d$
A_{1g}	$+1$	$+1$	$+1$	$+1$	$+1$	$+1$	$+1$	$+1$
A_{2g}	$+1$	$+1$	$+1$	-1	$+1$	$+1$	$+1$	-1
E_{1g}	$+2$	$\tau - 1$	$-\tau$	0	$+2$	$\tau - 1$	$-\tau$	0
E_{2g}	$+2$	$-\tau$	$\tau - 1$	0	$+2$	$-\tau$	$\tau - 1$	0
A_{1u}	$+1$	$+1$	$+1$	$+1$	-1	-1	-1	-1
A_{2u}	$+1$	$+1$	$+1$	-1	-1	-1	-1	$+1$
E_{1u}	$+2$	$\tau - 1$	$-\tau$	0	-2	$1-\tau$	$+\tau$	0
E_{2u}	$+2$	$-\tau$	$\tau - 1$	0	-2	$+\tau$	$1-\tau$	0

[a]Note: In this table $\tau \equiv (1+\sqrt{5})/2$, while $iC_5 = S_{10}^{-1}$ and $iC_5^2 = S_{10}$. Also $iC_2' = \sigma_d$

Table 23.14: Basis functions for the irreducible representations of groups D_{5h} and D_{5d}.

D_{5h}	D_{5d}	Basis functions
A_1'	A_{1g}	$x^2 + y^2, z^2$
A_2'	A_{2g}	R_z
E_1'	E_{1u}	$(x, y), (xz^2, yz^2), [x(x^2 + y^2), y(x^2 + y^2)]$
E_2'	E_{2g}	$(x^2 - y^2, xy), [y(3x^2 - y^2), x(x^2 - 3y^2)]$
A_1''	A_{1u}	$-$
A_2''	A_{2u}	$z, z^3, z(x^2 + y^2)$
E_1''	E_{1g}	$(R_x, R_y), (xz, yz)$
E_2''	E_{2u}	$[xyz, z(x^2 - y^2)]$

Table 23.15: Compatibility relations between the icosahedral groups, I_h, I, and several point groups of lower symmetry.

I_h	I	T_h	D_{5d}	D_5	C_{1h}
A_g	A	A_g	A_{1g}	A_1	A_1
F_{1g}	F_1	T_g	$A_{2g} + E_{1g}$	$A_2 + E_1$	$A_1 + 2A_2$
F_{2g}	F_2	T_g	$A_{2g} + E_{2g}$	$A_2 + E_2$	$A_1 + 2A_2$
G_g	G	$A_g + T_g$	$E_{1g} + E_{2g}$	$E_1 + E_2$	$2A_1 + 2A_2$
H_g	H	$E_g + T_g$	$A_{1g} + E_{1g} + E_{2g}$	$A_1 + E_1 + E_2$	$3A_1 + 2A_2$
A_u	A	A_u	A_u	A_1	A_2
F_{1u}	F_1	T_u	$A_{2u} + E_{1u}$	$A_2 + E_1$	$2A_1 + A_2$
F_{2u}	F_2	T_u	$A_{2u} + E_{2u}$	$A_2 + E_2$	$2A_1 + A_2$
G_u	G	$A_u + T_u$	$E_{1u} + E_{2u}$	$E_1 + E_2$	$2A_1 + 2A_2$
H_u	H	$E_u + T_u$	$A_{1u} + E_{1u} + E_{2u}$	$A_1 + E_1 + E_2$	$3A_1 + 2A_2$

Table 23.16: Decomposition of spherical angular momentum states labeled by ℓ (for $\ell \leq 10$) into irreducible representations of lower symmetry groups.[a]

ℓ	I_h	T_h	D_{5d}	D_{5h}	C_{1h}
0	A_g	A_g	A_{1g}	A'_1	A_1
1	F_{1u}	T_u	$\begin{cases} A_{2u} \\ E_{1u} \end{cases}$	$\begin{cases} A''_2 \\ E''_1 \end{cases}$	$\begin{cases} 2A_1 \\ A_2 \end{cases}$
2	H_g	$\begin{cases} E_g \\ T_g \end{cases}$	$\begin{cases} A_{1g} \\ E_{1g} \\ E_{2g} \end{cases}$	$\begin{cases} A'_1 \\ E'_1 \\ E'_2 \end{cases}$	$\begin{cases} 3A_1 \\ 2A_2 \end{cases}$
3	$\begin{cases} F_{2u} \\ G_u \end{cases}$	$\begin{cases} A_u \\ 2T_u \end{cases}$	$\begin{cases} A_{2u} \\ E_{1u} \\ 2E_{2u} \end{cases}$	$\begin{cases} A''_2 \\ E''_1 \\ 2E''_2 \end{cases}$	$\begin{cases} 4A_1 \\ 3A_2 \end{cases}$
4	$\begin{cases} G_g \\ H_g \end{cases}$	$\begin{cases} A_g \\ E_g \\ 2T_g \end{cases}$	$\begin{cases} A_{1g} \\ 2E_{1g} \\ 2E_{2g} \end{cases}$	$\begin{cases} A'_1 \\ 2E'_1 \\ 2E'_2 \end{cases}$	$\begin{cases} 5A_1 \\ 4A_2 \end{cases}$
5	$\begin{cases} F_{1u} \\ F_{2u} \\ H_u \end{cases}$	$\begin{cases} E_u \\ 3T_u \end{cases}$	$\begin{cases} A_{1u} \\ 2A_{2u} \\ 2E_{1u} \\ 2E_{2u} \end{cases}$	$\begin{cases} A''_1 \\ 2A''_2 \\ 2E''_1 \\ 2E''_2 \end{cases}$	$\begin{cases} 6A_1 \\ 5A_2 \end{cases}$
6	$\begin{cases} A_g \\ F_{1g} \\ G_g \\ H_g \end{cases}$	$\begin{cases} 2A_g \\ E_g \\ 3T_g \end{cases}$	$\begin{cases} 2A_{1g} \\ A_{2g} \\ 3E_{1g} \\ 2E_{2g} \end{cases}$	$\begin{cases} 2A'_1 \\ A'_2 \\ 3E'_1 \\ 2E'_2 \end{cases}$	$\begin{cases} 7A_1 \\ 6A_2 \end{cases}$
7	$\begin{cases} F_{1u} \\ F_{2u} \\ G_u \\ H_u \end{cases}$	$\begin{cases} A_u \\ E_u \\ 4T_u \end{cases}$	$\begin{cases} A_{1u} \\ 2A_{2u} \\ 3E_{1u} \\ 3E_{2u} \end{cases}$	$\begin{cases} A''_1 \\ 2A''_2 \\ 3E''_1 \\ 3E''_2 \end{cases}$	$\begin{cases} 8A_1 \\ 7A_2 \end{cases}$
8	$\begin{cases} F_{2g} \\ G_g \\ 2H_g \end{cases}$	$\begin{cases} A_g \\ 2E_g \\ 4T_g \end{cases}$	$\begin{cases} 2A_{1g} \\ A_{2g} \\ 3E_{1g} \\ 4E_{2g} \end{cases}$	$\begin{cases} 2A'_1 \\ A'_2 \\ 3E'_1 \\ 4E'_2 \end{cases}$	$\begin{cases} 9A_1 \\ 8A_2 \end{cases}$
9	$\begin{cases} F_{1u} \\ F_{2u} \\ 2G_u \\ H_u \\ 5T_u \end{cases}$	$\begin{cases} 2A_u \\ E_u \\ 5T_u \end{cases}$	$\begin{cases} A_{1u} \\ 2A_{2u} \\ 4E_{1u} \\ 4E_{2u} \end{cases}$	$\begin{cases} A''_1 \\ 2A''_2 \\ 4E''_1 \\ 4E''_2 \end{cases}$	$\begin{cases} 10A_1 \\ 9A_2 \end{cases}$
10	$\begin{cases} A_g \\ F_{1g} \\ F_{2g} \\ G_g \\ 2H_g \end{cases}$	$\begin{cases} 2A_g \\ 2E_g \\ 5T_g \end{cases}$	$\begin{cases} 3A_{1g} \\ 2A_{2g} \\ 4E_{1g} \\ 4E_{2g} \end{cases}$	$\begin{cases} 3A'_1 \\ 2A'_2 \\ 4E'_1 \\ 4E'_2 \end{cases}$	$\begin{cases} 11A_1 \\ 10A_2 \end{cases}$

[a] Note that $D_{5d} = D_5 \otimes i$ and $D_{5h} = D_5 \otimes \sigma_h$

Table 23.17: Characters of atomic sites $\chi^{\text{a.s.}}$ for D_{5h} of relevance to the C_{70} molecule[a,b].

$\chi^{\text{a.s.}}(D_{5h})$	E	$2C_5$	$2C_5^2$	$5C_2'$	σ_h	$2S_5$	$2S_5^3$	$5\sigma_v$
$C_{10}(\text{cap}^0)$	10	0	0	0	0	0	0	2
$C_{20}(\text{off-belt})$	20	0	0	0	0	0	0	0
$C_{10}(\text{belt})$	10	0	0	0	10	0	0	0

[a] See text for a discussion of $C_{10}(\text{cap}^0)$, $C_{20}(\text{off-belt})$, and $C_{10}(\text{belt})$. The same building blocks listed in this table are found in C_{50}, C_{70}, C_{90}, etc.

[b] The irreducible representations for each $\chi^{\text{a.s.}}$ in this table are given in Table 23.18.

Table 23.18: Irreducible representations of atomic sites $\chi^{\text{a.s.}}$ for D_{5h} of relevance to the C_{70} molecule[a].

$\chi^{\text{a.s.}}(D_{5h})$	Irreducible representations
$C_{10}(\text{cap}^0)$	$A_1' + A_2'' + E_1' + E_1'' + E_2' + E_2''$
$C_{20}(\text{off-belt})$	$A_1' + A_2' + A_1'' + A_2'' + 2E_1' + 2E_1'' + 2E_2' + 2E_2''$
$C_{10}(\text{belt})$	$A_1' + A_2' + 2E_1' + 2E_2'$

[a] The characters for the equivalence transformation for these sets of carbon atoms are given in Table 23.17.

where the irreducible representations of group I go into irreducible representations of group D_5

$$\begin{aligned} H &\rightarrow A_1 + E_1 + E_2 \\ F_1 &\rightarrow A_2 + E_1 \\ F_2 &\rightarrow A_2 + E_2 \end{aligned} \qquad (23.3)$$

using the results of Table 23.15. Since $\ell = 5$ corresponds to states that are odd under reflection in the mirror plane, the proper states in D_{5h} symmetry for $\ell = 5$ $A_1'' + 2A_2'' + 2E_1'' + 2E_2''$, as given in Table 23.16.

Symmetry considerations also play a major role in classifying the normal modes of the C_{70} molecule. To find the symmetries of the normal mode vibrations of C_{70}, we first find the symmetries for the transformation of the 70 carbon atoms denoted by $\chi^{\text{a.s.}}(C_{70})$ for the

Table 23.19: Characters of atomic sites $\chi^{\text{a.s.}}$ for D_{5d} of relevance to the D_{5d} isomer of the C_{80} molecule[a].

$\chi^{\text{a.s.}}(D_{5d})$	E	$2C_5$	$2C_5^2$	$5C_2'$	i	$2S_{10}^{-1}$	$2S_{10}$	$5\sigma_d$
C_{10} (cap^0)	10	0	0	0	0	0	0	2
C_{20} (cap^1)	20	0	0	0	0	0	0	0
C_{20} (off–belt)	20	0	0	0	0	0	0	0
C_{20} (belt)	20	0	0	0	0	0	0	0

[a] For an explanation about the notation for the atom sites, see text. Irreducible representations contained in $\chi^{\text{a.s.}}$ are given in Table 23.20.

Table 23.20: Irreducible representations of atomic sites $\chi^{\text{a.s.}}$ for D_{5d} of relevance to the D_{5d} isomer of the C_{80} molecule[a].

$\chi^{\text{a.s.}}(D_{5d})$	Irreducible representations
C_{10} (cap^0)	$\begin{cases} A_{1g} + A_{2u} \\ +E_{1g} + E_{1u} + E_{2g} + E_{2u} \end{cases}$
$\left. \begin{matrix} C_{20} \text{ (cap}^1) \\ C_{20} \text{ (off–belt)} \\ C_{20} \text{ (belt)} \end{matrix} \right\}$	$\begin{cases} A_{1g} + A_{1u} + A_{2g} + A_{2u} \\ +2E_{1g} + 2E_{1u} + 2E_{2g} + 2E_{2u} \end{cases}$

[a] The characters for $\chi^{\text{a.s.}}$ in this table are given in Table 23.19.

Table 23.21: Symmetries of molecular vibrational modes^{a,b} for groups of carbon atoms with D_{5h} symmetry.

D_{5h}	A_1'	A_2'	E_1'	E_2'	A_1''	A_2''	E_1''	E_2''
$C_{10}^{\text{axial}}(\text{cap}^0)$	1	0	1	1	0	1	1	1
$C_{10}^{\text{radial}}(\text{cap}^0)$	2	2	2	1	2	2	2	1
$C_{20}^{\text{axial}}(\text{off-belt})$	2	2	2	1	2	2	2	1
$C_{20}^{\text{radial}}(\text{off-belt})$	2	2	2	1	2	2	2	1
$C_{10}^{\text{axial}}(\text{belt})$	1	0	1	1	0	1	1	1
$C_{10}^{\text{radial}}(\text{belt})$	2	2	2	1	2	2	2	1
$C_{70+20j}^{\text{axial}}$	$4+j$	$1+j$	$6+2j$	$6+2j$	$3+j$	$4+j$	$8+2j$	$8+2j$
$C_{70+20j}^{\text{radial}}$	$8+2j$	$8+2j$	$15+4j$	$16+4j$	$6+2j$	$6+2j$	$11+4j$	$12+4j$

^{a} One A_2'' mode corresponding to translations of the center of mass of the free molecule along the 5-fold axis and one A_2' mode corresponding to rotations of the free molecule about the 5-fold axis have been subtracted.

^{b} One E_1' mode corresponding to translations of the center of mass of the free molecule normal to the 5-fold axis and one E_1'' mode corresponding to rotations of the free molecule about axes normal to the 5-fold axis have been subtracted.

Table 23.22: Symmetries of molecular vibrational modes[a,b] for groups of carbon atoms with D_{5d} symmetry.

D_{5d}	A_{1g}	A_{2g}	E_{1g}	E_{2g}	A_{1u}	A_{2u}	E_{1u}	E_{2u}
$C_{10}^{\text{axial}}(\text{cap}^0)$	1	0	1	1	0	1	1	1
$C_{10}^{\text{radial}}(\text{cap}^0)$	2	2	2	1	2	2	2	1
$C_{20}^{\text{axial}}(\text{off-belt})$	2	2	2	1	2	2	2	1
$C_{20}^{\text{radial}}(\text{off-belt})$	2	2	2	1	2	2	2	1
$C_{20}^{\text{axial}}(\text{belt})$	1	0	1	1	0	1	1	1
$C_{20}^{\text{radial}}(\text{belt})$	2	2	2	1	2	2	2	1
$C_{80+20j}^{\text{axial}}$	$5 + j$	$2 + j$	$8 + 2j$	$8 + 2j$	$3 + j$	$4 + j$	$8 + 2j$	$8 + 2j$
$C_{80+20j}^{\text{radial}}$	$8 + 2j$	$8 + 2j$	$15 + 4j$	$16 + 4j$	$8 + 2j$	$8 + 2j$	$15 + 4j$	$16 + 4j$

[a] One A_{2u} mode corresponding to translations of the center of mass of the free molecule along the 5-fold axis and one A_{2g} mode corresponding to rotations of the free molecule about the 5-fold axis have been subtracted.

[b] One E_{1u} mode corresponding to translations of the center of mass of the free molecule normal to the 5-fold axis and one E_{1g} mode corresponding to rotations of the free molecule about axes normal to the 5-fold axis have been subtracted.

point group D_{5h} where "a.s." refers to atom sites (as in Table 23.5 for icosahedral symmetry). Because of the large number of degrees of freedom in fullerenes, it is advantageous to break up the 70 atoms in C_{70} into subunits which themselves transform as a subgroup of D_{5h}. This approach allows us to build up large fullerene molecules by summing over these building blocks. The equivalence transformation ($\chi^{\text{a.s.}}$) for each of the building blocks can be written down by inspection.

The characters for the equivalence transformation for $\chi^{\text{a.s.}}$ for these subgroup building blocks, which are expressed in terms of sets of atoms normal to the 5-fold axis, are listed in Table 23.17. The symmetry operations of the group transform the atoms within each of these subgroups into one another. The $\chi^{\text{a.s.}}$ entries in Table 23.17 under the various symmetry operations denote the number of carbon atoms that remain invariant under the various classes of symmetry operations. The set $C_{10}(\text{cap}^0)$ denotes the 5 carbon atoms around the two pentagons (10 atoms in total) through which the 5-fold axis passes. Another 10 carbon atoms that are nearest neighbors to the 10 atoms on the axial pentagons transform in the same way as the set $C_{10}(\text{cap}^0)$. The set $C_{10}(\text{belt})$ refers to the 10 equatorial atoms in the 5 hexagons on the equator that form a subgroup. There are also two sets of 20 carbon atoms on hexagon double bonds, labeled $C_{20}(\text{off-belt})$, that form another subgroup. The characters for the equivalence transformation for C_{70} are found by summing the contributions from the various layers appropriately:

$$\chi^{\text{a.s.}}(C_{70}) = 2\chi^{\text{a.s.}}[C_{10}(\text{cap}^0)] + 2\chi^{\text{a.s.}}[C_{20}(\text{off–belt})] + \chi^{\text{a.s.}}[C_{10}(\text{belt})].$$
$$(23.4)$$

From Tables 23.17 and 23.21 and from . (23.4), we then obtain the irreducible representations of D_{5h} contained in the equivalence transformation for C_{70} as a whole:

$$\chi^{\text{a.s.}}(C_{70}) = 5A_1' + 3A_2' + 2A_1'' + 4A_4'' + 8E_1' + 8E_2' + 6E_1'' + 6E_2''. \quad (23.5)$$

If instead of C_{70}, we were to consider an isomer of C_{90} with D_{5h} symmetry, the same procedure as in Eqs. (23.4) and (23.5) would be used, except that an additional $\chi^{\text{a.s.}}(\text{off-belt})$ would be added to Eq. (23.4). The same building block approach could be used to describe C_{80} or C_{100} isomers with D_{5d} symmetry using Tables 23.19 and 23.20.

Table 23.23: The D_{5h} irreducible representations ($\mathcal{R}$) together with the number of distinct eigenvalues (N_ω) and the corresponding degeneracies g of the normal modes of the C_{70} molecule. The symbols N_ω^{belt} and N_ω^{cap} denote the number of distinct eigenvalues associated with the "belt" and "cap" modes, respectively, for each irreducible representation.

$\mathcal{R}$	N_ω^{belt}	N_ω^{cap}	N_ω	g
A_1'	2	10	12	1
A_2'	2	7	9	1
E_1'	4	17	21	2
E_2'	4	18	22	2
A_1''	1	8	9	1
A_2''	1	9	10	1
E_1''	2	17	19	2
E_2''	2	18	20	2

The symmetries of the molecular vibrations $\chi^{\text{m.v.}}$ (see Table 23.23) are then found using the relation

$$\chi^{\text{m.v.}}(C_{70}) = \chi^{\text{a.s.}}(C_{70}) \otimes \chi^{\text{vector}} - \chi^{\text{translations}} - \chi^{\text{rotations}} \qquad (23.6)$$

in which the direct product is denoted by $\otimes$ and the irreducible representations for the χ^{vector}, $\chi^{\text{translation}}$, and χ^{rotation} for group D_{5h} are given by

$$\begin{aligned} \chi^{\text{vector}} &= A_2'' + E_1' \\ \chi^{\text{translation}} &= A_2'' + E_1' \\ \chi^{\text{rotation}} &= A_2' + E_1''. \end{aligned} \qquad (23.7)$$

Table 23.21 lists the number of axial and radial molecular vibrations associated with each of the layers of carbon atoms of C_{70}. This division into axial and radial molecular modes is only approximate but often gives a good description of the physics of the molecular vibrations. The terms axial and transverse refer to modes associated with motions along and perpendicular to the 5-fold axis, respectively. Also included in Table 23.21 are the total number of axial and radial modes for C_{70+20j}, which contains summaries of the mode symmetries for C_{70}, C_{90}, etc.

From Table 23.21 and Eq. (23.5), we see that the number of distinct mode frequencies for C_{70} is 122. It is sometimes useful to consider these

modes as being approximately divided into cap modes and belt modes. Thus the 122 modes for C_{70} are classified as 104 cap modes (corresponding to the 60 carbon atoms of the two hemispheres of C_{60}) and 18 are belt modes. This division into cap and belt modes becomes more important in the limit of carbon nanotubes which are discussed elsewhere. The symmetries and degeneracies of the distinct mode frequencies for C_{70} are given in Table 23.23.

Among the modes given in Table 23.23, those that transform according to the A'_1, E'_2 or E''_1 irreducible representations are Raman active, with the A'_1 modes being observed only in the $(\|,\|)$ polarization geometry and the E''_1 mode observed in the $(\|,\perp)$ polarization. The E'_2 symmetry mode is seen in both polarization geometries. The modes with A''_2 and E'_1 symmetries are infrared active.

23.4.2 Symmetry Considerations for Higher Mass Fullerenes

Similar arguments can be made to classify the symmetries of the molecular vibrations of the rugby-shaped C_{80} (see Fig. 23.3) which follows symmetry group D_{5d}. Table 23.19 lists the characters for the equivalence transformations for groups of carbon atoms comprising the C_{80} isomer with D_{5d} symmetry. Each of these equivalence transformations forms a reducible representation of D_{5d} and the decomposition of $\chi^{\text{a.s.}}$ into irreducible representations of D_{5d} is given in Table 23.20. The vibrations associated with these groups of atoms are found using a variant of Eq. (23.6), and the classification of the vibrational modes into irreducible representations of D_{5d} is given in Table 23.22. Finally in Table 23.24, we give the number of distinct eigenfrequencies for the C_{80} isomer with D_{5d} symmetry, listed according to their symmetry type, and again distinguishing between the cap and belt modes. It should be noted that the building block approach using point group D_{5h} can be used to obtain $\chi^{\text{a.s.}}$ and $\chi^{\text{m.v.}}$ for C_{50}, C_{70}, C_{90}, etc., and using group D_{5d} the corresponding information can simply be found for D_{5d} isomers of C_{80}, C_{100}, etc. The building block approach provides a simple method for constructing the dynamical matrix of large fullerenes molecules or for treating their electronic structure when using explicit potentials.

Table 23.24: The D_{5d} irreducible representations ($\mathcal{R}$) together with the number of distinct eigenvalues (N_ω) and the corresponding degeneracies g of the normal modes of the C_{80} molecule. The symbols N_ω^{belt} and N_ω^{cap} denote the number of distinct eigenvalues associated with the "belt" and "cap" modes, respectively, for each irreducible representation.

$\mathcal{R}$	N_ω^{belt}	N_ω^{cap}	N_ω	g
A_{1g}	3	10	13	1
A_{2g}	2	8	10	1
E_{1g}	3	20	23	2
E_{2g}	2	22	24	2
A_{1u}	2	9	11	1
A_{2u}	3	9	12	1
E_{1u}	3	20	23	2
E_{2u}	2	22	24	2

23.5 Symmetry Considerations for Isotopic Effects

Carbon has two stable isotopes: ^{12}C which is 98.892% abundant and has a molecular weight of 12.011 and a zero nuclear spin, and ^{13}C with atomic weight 13.003, a natural abundance of 1.108%, and a nuclear spin of $\frac{1}{2}$. It is the nuclear spin of the ^{13}C isotope that is exploited in the NMR experiments on fullerenes.

Though small in abundance, the ^{13}C isotope occurs on approximately half of the C_{60} molecules synthesized using the natural abundance of carbon isotopes as shown in Table 23.25. The probability p_m for m isotopic substitutions to occur on an n_C atom fullerene C_{n_C} is given by

$$p_m(C_{n_C}) = \left(\begin{array}{c} n_C \\ m \end{array} \right) x^m (1-x)^{n_C - m}, \qquad (23.8)$$

where x is the fractional abundance of the isotope and the binomial coefficient appearing in Eq. (23.8) is given by

$$\left(\begin{array}{c} n_C \\ m \end{array} \right) = \frac{n_C!}{(n_C - m)!m!}. \qquad (23.9)$$

For the natural abundance of carbon isotopes ($x = 0.01108$), we obtain the results for the C_{60} and C_{70} molecules listed in Table 23.25 and shown graphically in Fig. 23.4. Less than 1% of the C_{60} and C_{70} fullerenes have more than three ^{13}C isotopes per fullerene. Also included in the table are the corresponding results for an isotopic enrichment to 5% and 10% ^{13}C. The results in Table 23.25 show that as x increases (and also as n_C increases in C_{n_C}), the peak in the distribution moves to larger m values and the distribution gets broader. These conclusions follow from binomial statistics, where the average $\bar{m}$ and the standard deviation $\Delta m \equiv \langle (m - \bar{m})^2 \rangle^{1/2}$ give

$$\bar{m} = n_C x \tag{23.10}$$

and

$$\Delta m = \sqrt{n_C x (1 - x)}, \tag{23.11}$$

respectively. For example, for a fullerene with $x = 0.05$, then Eqs. (23.10) and (23.11) yield $\bar{m} = 3$ and $\Delta m = 1.7$. Thus as x increases, so does $\bar{m}$ and Δm, thereby accounting for the broader distribution with increasing x. In general, for isotopically enriched samples, the distribution $p_m(C_{n_C})$ is sufficiently shifted and broadened so that graphical displays are desirable, such as shown in Fig. 23.4.

The results of Table 23.25 have important consequences for both symmetry considerations and the rotational levels of fullerene molecules. The molecules containing one or more ^{13}C atoms show much lower symmetry than that of the full I_h point group. In fact, the singly ^{13}C substituted molecule $^{13}C_1{}^{12}C_{59}$ has only one symmetry operation, a single reflection plane (point group C_{1h}, see Table 23.26); two or more substitutions generally show no symmetry, i.e., they belong to point group C_1 and have no symmetry-imposed degeneracies, which implies that all levels (electronic, vibrational, rotational, etc.) are non-degenerate and every state is both IR and Raman active. Group theory predicts this symmetry-lowering, but the intensity of IR and Raman lines do not change much upon addition of ^{13}C isotopes. Inactive modes before the isotopic symmetry lowering effect remain mostly inactive, and the optically-active modes still show strong intensity.

The isotopic distribution has unique consequences with regard to the rotational levels of the C_{60} molecule and hence also regarding the

Table 23.25: The probability $p_m(C_{n_C})$ of ^{13}C occurring among C_{60} and C_{70} fullerenes.[a]

x	m	$p_m(C_{60})$	$p_m(C_{70})$
0.0001	0	0.9940	0.9930
0.0005	0	0.9704	0.9656
0.001	0	0.9417	0.9324
0.005	0	0.7403	0.7041
0.01	0	0.5472	0.4948
0.01108	0	0.5125	0.4584
0.01108	1	0.3445	0.3595
0.01108	2	0.1139	0.1390
0.01108	3	0.0247	0.0353
0.01108	4	0.0039	0.0066
0.05	0	0.0461	0.0276
0.05	1	0.1455	0.1016
0.05	2	0.2259	0.1845
0.05	3	0.2298	0.2201
0.05	4	0.1724	0.1941
0.05	5	0.1016	0.1348
0.05	6	0.0490	0.0769
0.10	0	0.0018	0.00063
0.10	1	0.0120	0.00487
0.10	2	0.0393	0.01868
0.10	3	0.0844	0.04705
0.10	4	0.1336	0.08756
0.10	5	0.1662	0.12843
0.10	6	0.1693	0.15459
0.10	7	0.1451	0.15704

[a]Here x is the isotopic abundance, m is the number of ^{13}C per fullerene, and $p_m(C_{n_C})$ is the probability a fullerene C_{n_C} has m ^{13}C atoms. Although the table would normally be used for small concentrations of ^{13}C in ^{12}C, the same probabilities as given in the table apply to: 1.108% ^{12}C in 98.892% ^{13}C; or to 5% ^{12}C in 95% ^{13}C; or to 10% ^{12}C in 90% ^{13}C.
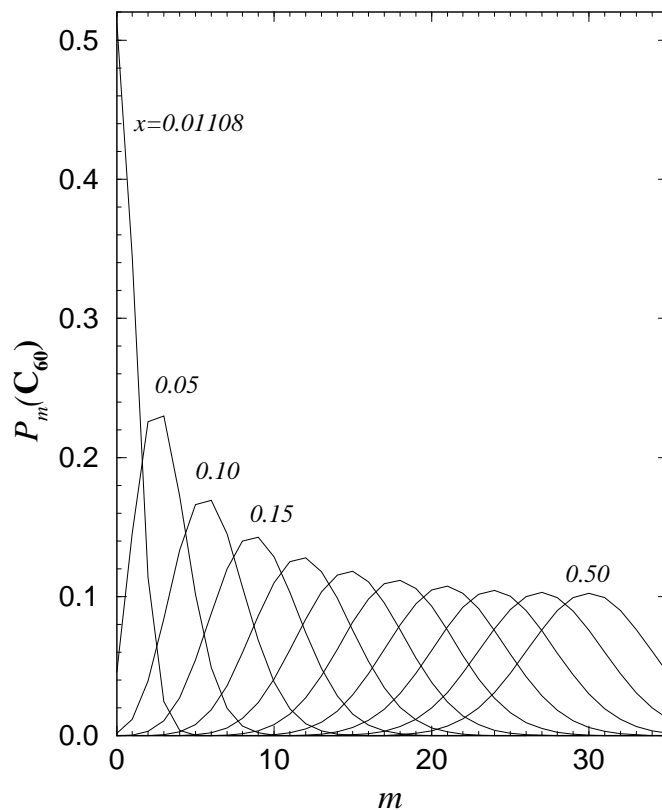
Figure 23.4: Plot of the m dependence of $p_m(C_{60})$ the distribution of C_{60} molecules with m ^{13}C atoms for various concentrations of x from 5% to 50% in steps of 5%. A plot of $p_m(C_{60})$ for x equal to the natural abundance is also shown.

Table 23.26: Character table for point group C_{1h}.

$\mathcal{R}$	E	σ_h	basis functions
A_1	1	1	1; x; y; x^2; etc.
A_2	1	-1	z; xz; yz; etc.

librational states of the corresponding solid. Other experiments sensitive to the isotopic abundance include NMR measurements and studies of the isotope effect regarding the superconducting transition temperature T_c.

23.6 Symmetry Properties of Carbon Nanotubes

Although the symmetry of the 2D graphene layer (a single honeycomb layer plane of the graphite structure) is greatly lowered in the 1D nanotube, the single-walled nanotubes have interesting symmetry properties that lead to nontrivial physical effects, namely a necessary degeneracy at the Fermi surface for certain geometries.

23.6.1 Relation between Carbon Nanotubes and Fullerenes

In this section we consider first two simple examples of single-walled carbon nanotubes based on the C_{60} fullerene. The concept of a single-walled nanotube is then generalized to specify the idealized structure of single-walled nanotubes in general.

In analogy to a C_{60} molecule, we can specify a single-walled C_{60}-derived nanotube by bisecting a C_{60} molecule at the equator and joining the two resulting hemispheres with a cylindrical tube one monolayer thick and with the same diameter as C_{60}. If the C_{60} molecule is bisected normal to a fivefold axis, the "armchair" nanotube shown in Fig. 23.5(a) is formed. If the C_{60} molecule is bisected normal to a threefold axis, the "zigzag" nanotube in Fig. 23.5(b) is formed. Armchair and zigzag carbon nanotubes of larger diameter, and having correspondingly larger caps, are described below.

Figures 23.6 (a) and (b) show the only nanotube types that have the σ_h symmetry operation. Other nanotubes, such as (c), belong to a nonsymmorphic translational group which only has pure spiral symmetry operations. From the shape of the cross sections of the nanotubes shown in Fig. 23.5 and listed in Table 23.27, carbon nanotubes with high sym-
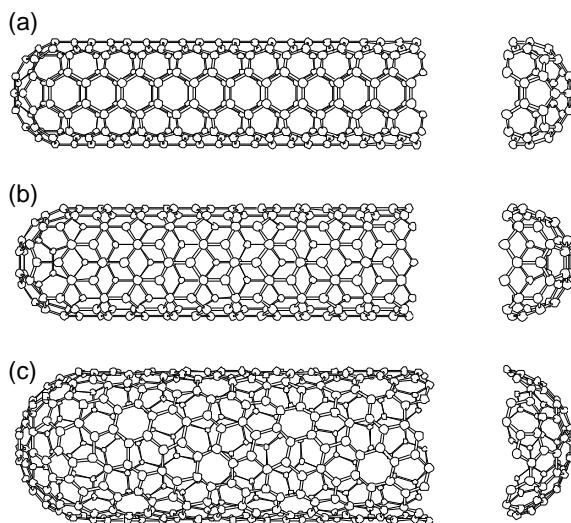
Figure 23.5: By rolling up a graphene sheet (a single layer from a 3D graphite crystal) as a cylinder and capping each end of the cylinder with half of a fullerene molecule, a "fullerene-derived carbon nanotube," one atomic layer in thickness, is formed. Shown here is a schematic theoretical model for a single-wall carbon nanotube with the nanotube axis normal to: (a) the $\theta = 30°$ direction (an "armchair" nanotube), (b) the $\theta = 0°$ direction (a "zigzag" nanotube), and (c) a general direction $\overrightarrow{OB}$ (see Fig. 23.8) with $0 < \theta < 30°$ (a "chiral" nanotube). The actual nanotubes shown in the figure correspond to (n, m) values of: (a) (5, 5), (b) (9, 0), and (c) (10, 5).
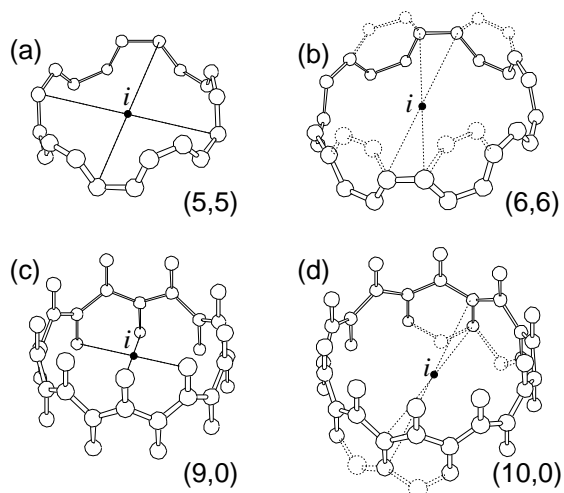
Figure 23.6: Symmetry of armchair (a,b) and zigzag (c,d) tubules with odd (a,c) and even (b,d) numbers of the unit cell around the circumferential direction: (a) (5,5) armchair, (b) (6,6) armchair (c) (9,0) zigzag and (d) (10,0) zigzag tubes. Here we show the inversion centers.

metry are called (a) armchair and (b) zigzag nanotubes, respectively, and are described by symmorphic space groups. All nanotubes, except for the armchair and zigzag nanotubes, are called chiral nanotubes.[1] The classification of carbon nanotubes is listed in Table 23.27.

In addition to the armchair and zigzag nanotubes, a large number of chiral carbon nanotubes can be formed with a screw axis along the axis of the nanotube and with a variety of hemispherical caps. These carbon nanotubes can be specified mathematically in terms of the nanotube diameter d_t and chiral angle θ, which are shown in Fig. 23.8, where the chiral vector $\vec{C}_h$

$$\vec{C}_h = n\hat{a}_1 + m\hat{a}_2 \qquad (23.12)$$

is shown, as well as the basic translation vector $\vec{T}$ for the nanotube, which is discussed below. In Fig. 23.8, the chiral vector $\vec{C}_h$ connects two crystallographically equivalent sites A and A' on a two-dimensional (2D) graphene sheet where a carbon atom is located at each vertex of the honeycomb structure. The construction in Fig. 23.8 shows the chiral

---

[1]The name for the chiral nanotube comes from the designation of spiral symmetry by 'axial chirality' in chemistry. Axial chirality is commonly discussed in connection with optical activity.
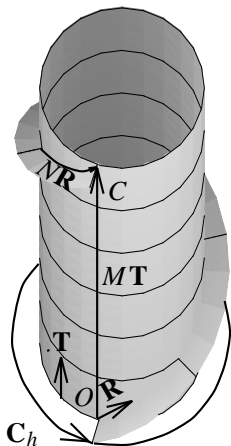
Figure 23.7: The vector $N\vec{R} = (\psi|\tau)^N$ is shown on the cylindrical surface. After rotating by 2π around the tube M times, the vector $N\vec{R}$ reaches a lattice point equivalent to point O, but separated from O by $M\vec{T}$. In the figure we show the case $\vec{C}_h = (4, 2)$ where $M = 6$.

angle θ of the nanotube with respect to the zigzag direction ($\theta = 0$) and the unit vectors $\hat{a}_1$ and $\hat{a}_2$ of the hexagonal honeycomb lattice. The armchair nanotube [Fig. 23.5(a)] corresponds to $\theta = 30°$ on this construction. An ensemble of possible chiral vectors can be specified by Eq. (23.12) in terms of pairs of integers (n, m) and this ensemble is shown in Fig. 23.8(b). Each pair of integers (n, m) defines a different way of rolling up the graphene sheet to form a carbon nanotube. We now show how the construction in Fig. 23.8(a) specifies the geometry of the carbon nanotube.

The cylinder connecting the two hemispherical caps of Fig. 23.5 is formed by superimposing the two ends OA of the vector $\vec{C}_h$. The cylinder joint is made by joining the line AB' to the parallel line OB in Fig. 23.8(a), where lines OB and AB' are perpendicular to the vector $\vec{C}_h$ at each end. distortion of bond angles other than distortions caused by the cylindrical curvature of the nanotube. Differences in chiral angle θ and in the nanotube diameter d_t give rise to differences in the properties of the various carbon nanotubes. In the (n, m) notation for specifying the chiral vector $\vec{C}_h$ in Eq. (23.12), the vectors $(n, 0)$ denote zigzag nanotubes and the vectors (n, n) denote armchair nanotubes, and the larger the value of n, the larger the nanotube diameter. Both
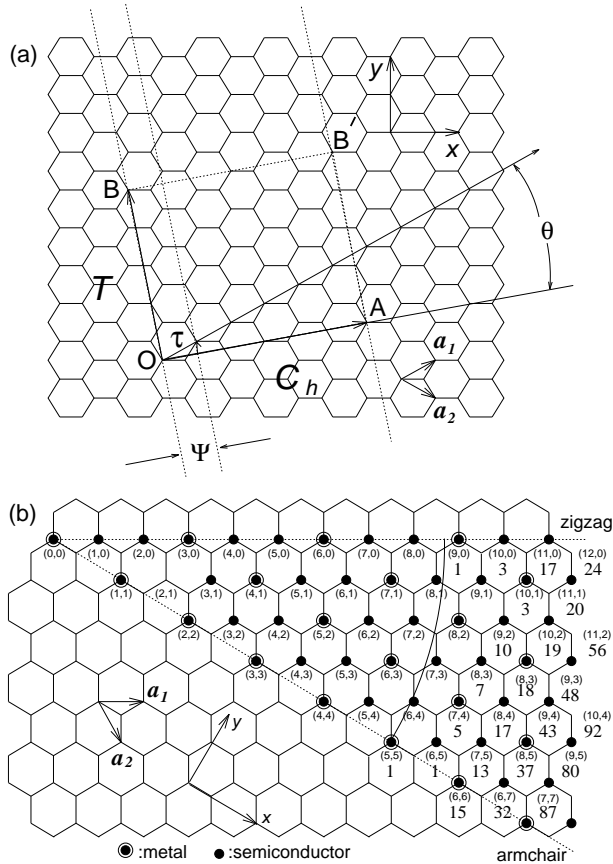
Figure 23.8: (a) The chiral vector $\overrightarrow{OA}$ or $\vec{C}_h = n\hat{a}_1 + m\hat{a}_2$ is defined on the honeycomb lattice of carbon atoms by unit vectors $\hat{a}_1$ and $\hat{a}_2$ and the chiral angle θ is defined with respect to the zigzag axis. Along the zigzag axis $\theta = 0°$. Also shown are the lattice vector $\overrightarrow{OB} = \vec{T}$ of the 1D nanotube unit cell and the rotation angle ψ and the translation τ which constitute the basic symmetry operation $R = (\psi|\tau)$ for the carbon nanotube. The diagram is constructed for $(n, m) = (4, 2)$. (b) Chiral vectors specified by the pairs of integers (n, m) for carbon nanotubes, including zigzag, armchair, and chiral nanotubes. Below each pair of integers (n, m) is listed the number of distinct caps that can be joined continuously to the carbon nanotube denoted by (n, m). The encircled dots denote metallic nanotubes while the small dots are for semiconducting nanotubes.

the $(n, 0)$ and (n, n) nanotubes have especially high symmetry, corresponding to symmorphic space groups, as discussed in §23.6.4, and exhibit a mirror symmetry plane normal to the nanotube axis. All other vectors (n, m) correspond to chiral nanotubes. Since both right- and left-handed chirality are possible for chiral nanotubes, it is expected that chiral nanotubes are optically active to either right or left circularly polarized light. In terms of the integers (n, m), the nanotube diameter d_t is given by

$$d_t = C_h/\pi = \sqrt{3}a_{C-C}(m^2 + mn + n^2)^{1/2}/\pi \qquad (23.13)$$

where a_{C-C} is the nearest-neighbor C–C distance (1.421 Å in graphite), C_h is the length of the chiral vector $\vec{C}_h$, and the chiral angle θ is given by

$$\theta = \tan^{-1}[\sqrt{3}m/(m + 2n)]. \qquad (23.14)$$

For example, a zigzag nanotube ($\theta = 0°$) specified by $(9, 0)$ has a theoretical nanotube diameter of $d_t = 9\sqrt{3}a_{C-C}/\pi = 7.05$ Å, while an armchair nanotube specified by $(5, 5)$ has $d_t = 15a_{C-C}/\pi = 6.83$ Å, both derived from hemispherical caps for the C_{60} molecule and assuming an average $a_{C-C} = 1.43$ Å appropriate for C_{60}. If the graphite value of $a_{C-C} = 1.421$ Å is used, slightly smaller values for d_t are obtained. Substitution of $(n, m) = (5, 5)$ into Eq. (23.14) yields $\theta = 30°$ while substitution of $(n, m) = (9, 0)$ and $(0, 9)$ yields $\theta = 0°$ and $60°$, respectively. The nanotubes $(0, 9)$ and $(9, 0)$ are equivalent, because of the sixfold symmetry of the graphene layer. Because of the point group symmetry of the honeycomb lattice, several different integers (n, m) give rise to equivalent nanotubes. To define each nanotube uniquely, we restrict ourselves to consideration of nanotubes arising from the $30°$ wedge of the 2D Bravais lattice shown in Fig. 23.8(b). Because of the small diameter of a carbon nanotube (~ 10 Å) and the large length-to-diameter ratio ($> 10^4$), carbon nanotubes provide an important system for studying one-dimensional physics, both theoretically and experimentally.

Many of the carbon nanotubes that were observed experimentally in early work were multilayered, consisting of capped concentric cylinders separated by ~ 3.5 Å. In a formal sense, each of the constituent

cylinders can be specified by the chiral vector $\vec{C}_h$ in terms of the indices (n, m) of Eq. (23.12), or equivalently by the nanotube diameter d_t and chiral angle θ. Because of the different numbers of carbon atoms around the various coaxial cylinders, it is not possible to achieve the ABAB... interlayer graphite stacking in carbon nanotubes. Thus, an interlayer spacing closer to that of turbostratic graphite (3.44 Å) is expected, subject to the quantized nature of the (n, m) integers, which determine $\vec{C}_h$.

23.6.2 Specification of Lattice Vectors in Real Space

To specify the symmetry properties of carbon nanotubes as 1D systems, it is necessary to define the lattice vector $\vec{T}$ along the nanotube axis and normal to the chiral vector $\vec{C}_h$ defined by Eq. (23.12) and Fig. 23.8(a). The vector $\vec{T}$ thus defines the unit cell of the 1D nanotube. The length T of the translation vector $\vec{T}$ corresponds to the first lattice point of the 2D graphene sheet through which the vector $\vec{T}$ passes. From Fig. 23.8(a) and these definitions, we see that the translation vector $\vec{T}$ of a general chiral nanotube as a function of n and m, can be written as:

$$\vec{T} = [(2m + n)\vec{a}_1 - (2n + m)\vec{a}_2]/d_R \qquad (23.15)$$

with a length

$$T = \sqrt{3}C_h/d_R \qquad (23.16)$$

where the length C_h is given by Eq. (23.13), d is the highest common divisor of (n, m), and

$$d_R = \begin{cases} d & \text{if } n - m \text{ is not a multiple of } 3d \\ 3d & \text{if } n - m \text{ is a multiple of } 3d. \end{cases} \qquad (23.17)$$

Thus for the $(5, 5)$ armchair nanotube $d_R = 3d = 15$, while for the $(9, 0)$ zigzag nanotube $d_R = d = 9$. The relation between the translation vector $\vec{T}$ and the symmetry operations on carbon nanotubes is discussed below and in §23.6.3. As a simple example, $T = \sqrt{3}a_{C-C}$ for a $(5, 5)$ armchair nanotube and $T = 3a_{C-C}$ for a $(9, 0)$ zigzag nanotube, where a_{C-C} is the nearest-neighbor carbon–carbon distance. We note that the

length T is greatly reduced when (n, m) have a common divisor and when $(n - m)$ is a multiple of 3.

Having specified the length T of the smallest translation vector for the 1D carbon nanotube, it is useful to determine the number of hexagons, N, per unit cell of a chiral nanotube specified by integers (n, m) having a highest common divisor of d. From the size of the unit cell of the 1D carbon nanotube defined by the orthogonal vectors $\vec{T}$ and $\vec{C}_h$, the number N is given by

$$N = \frac{2(m^2 + n^2 + nm)}{d_R} \tag{23.18}$$

where d_R is given by Eq. (23.17) and we note that each hexagon contains two carbon atoms. As an example, application of Eq. (23.18) to the $(5, 5)$ and $(9, 0)$ nanotubes yields values of 10 and 18, respectively, for N. We will see below that these unit cells of the 1D nanotube contain, respectively, five and nine unit cells of the 2D graphene lattice, each 2D unit cell containing two hexagons of the honeycomb lattice. This multiplicity is used in the application of zone-folding techniques to obtain the electronic and phonon dispersion relations for carbon nanotubes.

Referring to Fig. 23.8(a), we see that the basic space group symmetry operation of a chiral fiber consists of a rotation by an angle ψ combined with a translation $\vec{\tau}$, and this space group symmetry operation is denoted by $R = (\psi|\tau)$ and corresponds to the vector $\vec{R} = p\vec{a}_1 + q\vec{a}_2$ shown in Fig. 23.9. The physical significance of the vector $\vec{R}$ is that the projection of $\vec{R}$ on the chiral vector $\vec{C}_h$ gives the angle ψ scaled by $C_h/2\pi$, while the projection of $\vec{R}$ on $\vec{T}$ gives the translation vector $\vec{\tau}$ of the basic symmetry operation of the 1D space group. The integer pair (p, q) which determines $\vec{R}$ is found using the relation

$$mp - nq = d \tag{23.19}$$

subject to the conditions $q < m/d$ and $p < n/d$. Taking the indicated scalar product $\vec{R} \cdot \vec{T}$ in Fig. 23.9 we obtain the expressions for the length of τ

$$\tau = Td/N \tag{23.20}$$

where d is the highest common divisor of (n, m), T is the magnitude of the lattice vector $\vec{T}$, and N is the number of hexagons per 1D unit
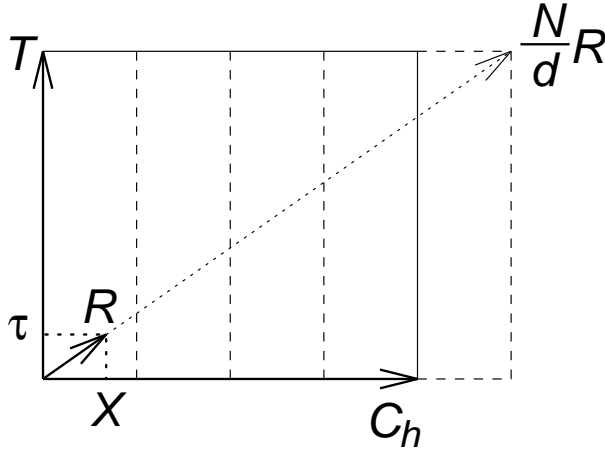
Figure 23.9: Relation between the fundamental symmetry vector $\vec{R} = p\vec{a}_1 + q\vec{a}_2$ of the 1D unit cell and the two vectors that specify the carbon nanotube (n, m): the chiral vector $\vec{C}_h$ and translation vector $\vec{T}$. The projections of $\vec{R}$ on the $\vec{C}_h$ and $\vec{T}$ axes, respectively, yield ψ and $\vec{\tau}$ (see text). After (N/d) translations, $\vec{R}$ reaches a lattice point B'' (see text). The vertical dashed lines divide the vector $\vec{C}_h$ into d sectors.

cell, given by Eq. (23.18). For the armchair and zigzag nanotubes, Eq. (23.20) yields $\tau = T/2$ and $\tau = \sqrt{3}T/2$, respectively.

Regarding the angle of rotation, the scalar product $\vec{R} \cdot \vec{C}_h$ yields

$$\psi = 2\pi \left[\frac{\Omega}{Nd} + \frac{\lambda}{d} \right] \qquad (23.21)$$

where $\lambda = 0, 1, \ldots, d - 1$ and

$$\Omega = [p(m + 2n) + q(n + 2m)](d/d_R) \qquad (23.22)$$

in which the integers (p, q) determine the vector $\vec{R}$ (see Fig. 23.9). Thus (p, q) denotes the coordinates reached when the symmetry operation $(\psi|\tau)$ acts on an atom at (0,0), i.e., $(\psi|\tau)(0, 0) = (p, q)$.

If $(\psi|\tau)$ is a symmetry operation for the nanotube, then $(\psi|\tau)^2$, $(\psi|\tau)^3, \ldots (\psi|\tau)^{N/d}$ are all distinct symmetry operations where $(\psi|\tau)^{N/d} = E$ is the identity operation, bringing the lattice point O to an equivalent lattice point B'', where

$$\overrightarrow{OB}'' = (N/d)\vec{R} = (1/d)[\Omega\vec{C}_h + \vec{T}\, d]. \qquad (23.23)$$

Table 23.27: Values for characterization parameters[a] for selected carbon nanotubes labeled by (n, m).

(n, m)	d	d_R	d_t (Å)	L/a_0	T/a_0	N	$\psi/2\pi$	τ/a_0	Ω/d
$(4, 2)$	2	2	4.14	5	$\sqrt{21}$	28	$5/28$	$\sqrt{21}/14$	5
$(5, 5)$	5	15	6.78	$\sqrt{75}$	1	10	$1/10$	$1/2$	1
$(9, 0)$	9	9	7.05	9	$\sqrt{3}$	18	$-1/18$	$\sqrt{3}/2$	-1
$(6, 5)$	1	1	7.47	$\sqrt{91}$	$\sqrt{273}$	182	$149/182$	$\sqrt{3/364}$	149
$(7, 4)$	1	3	7.55	$\sqrt{93}$	$\sqrt{31}$	62	$17/62$	$1/\sqrt{124}$	17
$(8, 3)$	1	1	7.72	$\sqrt{97}$	$\sqrt{291}$	194	$71/194$	$\sqrt{3/388}$	71
$(10, 0)$	10	10	7.83	10	$\sqrt{3}$	20	$-1/20$	$\sqrt{3}/2$	-1
$(6, 6)$	6	18	8.14	$\sqrt{108}$	1	12	$1/12$	$1/2$	1
$(10, 5)$	5	5	10.36	$\sqrt{175}$	$\sqrt{21}$	70	$1/14$	$\sqrt{3/28}$	5
$(20, 5)$	5	15	17.95	$\sqrt{525}$	$\sqrt{7}$	70	$3/70$	$1/(\sqrt{28})$	3
$(30, 15)$	15	15	31.09	$\sqrt{1575}$	$\sqrt{21}$	210	$1/42$	$\sqrt{3/28}$	5
$\vdots$	$\vdots$	$\vdots$	$\vdots$	$\vdots$	$\vdots$	$\vdots$	$\vdots$	$\vdots$	$\vdots$
(n, n)	n	$3n$	$\sqrt{3}na/\pi$	$\sqrt{3}n$	1	$2n$	$1/2n$	$1/2$	1
$(n, 0)$	n	n	na/π	n	$\sqrt{3}$	$2n$	$-1/2n$	$\sqrt{3}/2$	-1

[a] Ω is given by Eq. (23.22); T is given by Eq. (23.16) with $a_0 = \sqrt{3}a_{C-C}$; L is the length of the chiral vector πd_t given by Eq. (23.13); N is given by Eq. (23.18); ψ is given by Eq. (23.21); τ is given by Eq. (23.20); Ω/d is the number of complete 2π revolutions about the nanotube axis for one cycle.

Referring to Fig. 23.9, we see that after N/d symmetry operations $(\psi|\tau)$, the vector $(N/d)\vec{R}$ along the zigzag direction reaches a lattice point, which we denote by B''. Correspondingly, after N/d symmetry operations $(\psi|\tau)^{N/d}$, the translation $(N/d)\vec{\tau}$ yields one translation of the lattice vector $\vec{T}$ of the nanotube and (Ω/d^2) revolutions of 2π around the nanotube axis. Although Ω/d is an integer, Ω/d^2 need not be. In Table 23.27 we list the characteristic parameters of carbon nanotubes specified by (n, m), including d, the highest common divisor of n and m, and the related quantity d_R given by Eq. (23.17). Also listed in Table 23.27 are the nanotube diameter d_t in units of Å, the translation repeat distance T of the 1D lattice in units of the lattice constant $a_0 = \sqrt{3}a_{C-C}$ for a 2D graphene sheet, the number N of hexagons per

unit cell of the 1D nanotube, the rotation angle ψ expressed in units of $C_h/2\pi$, and the translation τ of the symmetry operation $R = (\psi|\tau)$ expressed in units of a_0. The length of the chiral vector L ($L \equiv C_h = \pi d_t$) is listed in Table 23.27 in units of a_0. For cases where n and m have a common divisor d, the angle of rotation ψ is defined modulo $2\pi/d$ instead of 2π, so that the group $C'_{N/\Omega}$ has N/d elements. To illustrate use of Table 23.27 we refer to the $(4, 2)$ nanotube illustrated in Fig. 23.8(a), which has $N = 28$, $d = d_R = 2$, and $T = 14\tau = \sqrt{21}a_0$ and also $C_h = \sqrt{28}a_0$. Thus for the $(4, 2)$ nanotube, while $(N/d)\psi = (5/2)(2\pi)$ corresponding to 5π rotations around the nanotube axis, (N/d) translations $\vec{R}$ reach a lattice point.

As a second example, we consider the case of the nanotube specified by $(7, 4)$. For this nanotube, there are no common divisors, so $d = 1$, but since $n-m = 3$, we obtain $d_R = 3$. Solution of Eq. (23.19) for (p, q) gives $p = 2$ and $q = 1$, which yields the rotation angle (in units of 2π) $N\psi = \Omega/d = 17(2\pi)$, where $N = 62$. Thus, after 62 operations $(\psi|\tau)^N$, the origin O is transformed into a new lattice point a distance T from O along the T axis, after having completed 17 rotations of 2π around the nanotube axis. For the armchair nanotube $(5, 5)$, the highest common divisor is 5, and since $n - m = 0$, we have $d_R = 3 \times 5 = 15$, yielding $N = 10$ and $N\psi = 2\pi$. Regarding translations, use of Eq. (23.20) yields $\tau = a_0/2 = T/2$. Finally, we give the example of the smallest zigzag nanotube $(0, 9)$, for which $d = d_R = 9$ and $N = 18$. Using $p = 1$ and $q = 0$ and $N = 18$, we obtain $N\psi = 2\pi$ and $\tau = \sqrt{3}a_0/2 = T/2$.

23.6.3 Symmetry for Symmorphic Carbon Nanotubes

In this section we consider the symmetry properties of the highly symmetric armchair and zigzag carbon nanotubes, which can be described by symmorphic groups. We then summarize the symmetry operations for the general chiral nanotube in §23.6.4 which is described by a nonsymmorphic space group.

For symmorphic groups, the translations and rotations are decoupled from each other, and we can treat the rotations simply by point group operations. Since symmorphic groups generally have higher sym-

Table 23.28: Character table for point group $D_{(2j+1)}$.

$\mathcal{R}$	E	$2C^1_{\phi_j}$ ^{a}	$2C^2_{\phi_j}$	$\ldots$	$2C^j_{\phi_j}$	$(2j+1)C'_2$
A_1	1	1	1	$\ldots$	1	1
A_2	1	1	1	$\ldots$	1	-1
E_1	2	$2\cos\phi_j$	$2\cos 2\phi_j$	$\ldots$	$2\cos j\phi_j$	0
E_2	2	$2\cos 2\phi_j$	$2\cos 4\phi_j$	$\ldots$	$2\cos 2j\phi_j$	0
$\vdots$	$\vdots$	$\vdots$	$\vdots$	$\vdots$	$\vdots$	$\vdots$
E_j	2	$2\cos j\phi_j$	$2\cos 2j\phi_j$	$\ldots$	$2\cos j^2\phi_j$	0

^{a} Where $\phi_j = 2\pi/(2j+1)$.

metry than the nonsymmorphic groups, it might be thought that group theory plays a greater role in specifying the dispersion relations for electrons and phonons for symmorphic space groups and in discussing their selection rules. It is shown in §23.6.4 that group theoretical considerations are also very important for the nonsymmorphic groups, leading to important and simple classifications of their dispersion relations.

In discussing the symmetry of carbon nanotubes, it is assumed that the nanotube length is much larger than its diameter, so that the nanotube caps can be neglected when discussing the electronic and lattice properties of the nanotubes. Hence, the structure of the infinitely long armchair nanotube ($n = m$) or zigzag nanotube ($m = 0$) is described by the symmetry groups D_{nh} or D_{nd} for even or odd n, respectively, since inversion is an element of D_{nd} only for odd n and is an element of D_{nh} only for even n. Character tables for groups D_{5h} and D_{5d} are given in §17.7 under Tables 3.38 and 3.37, respectively. We note that group D_{5d} has inversion symmetry and is a subgroup of group I_h, so that compatibility relations can be specified between the lower symmetry group D_{5d} and I_h, as given in Table 23.15. In contrast, D_{5h} is not a subgroup of I_h, although D_5 is a subgroup of I.   Character tables for D_{6h} and D_{6d} are readily available in standard group theory texts. For larger diameter nanotubes, appropriate character tables can be constructed from the generalized character tables for the D_n group given in Table 23.28 (for odd $n = 2j + 1$) and in Table 23.29 (for even $n = 2j$), and the basis functions are listed in Table 23.30. These tables

Table 23.29: Character Table for Group $D_{(2j)}$

$\mathcal{R}$	E	C_2	$2C_{\phi_j}^1$ [a]	$2C_{\phi_j}^2$	$\ldots$	$2C_{\phi_j}^{j-1}$	$(2j)C_2'$	$(2j)C_2''$
A_1	1	1	1	1	$\ldots$	1	1	1
A_2	1	1	1	1	$\ldots$	1	-1	-1
B_1	1	-1	1	1	$\ldots$	1	1	-1
B_2	1	-1	1	1	$\ldots$	1	-1	1
E_1	2	-2	$2\cos\phi_j$	$2\cos 2\phi_j$	$\ldots$	$2\cos(j-1)\phi_j$	0	0
E_2	2	2	$2\cos 2\phi_j$	$2\cos 4\phi_j$	$\ldots$	$2\cos 2(j-1)\phi_j$	0	0
$\vdots$	$\vdots$	$\vdots$	$\vdots$	$\vdots$	$\vdots$	$\vdots$	$\vdots$	$\vdots$
E_{j-1}	2	$(-1)^{j-1}2$	$2\cos(j-1)\phi_j$	$2\cos 2(j-1)\phi_j$	$\ldots$	$2\cos(j-1)^2\phi_j$	0	0

[a] Where $\phi_j = 2\pi/(2j)$.

Table 23.30: Basis Functions for Groups $D_{(2j)}$ and $D_{(2j+1)}$

Basis functions		$D_{(2j)}$	$D_{(2j+1)}$	$C_{N/\Omega}$
(x^2+y^2, z^2)		A_1	A_1	A
	z	A_2	A_1	A
	R_z	A_2	A_2	A
(xz, yz)	$\left.\begin{array}{c}(x,y)\\(R_x,R_y)\end{array}\right\}$	E_1	E_1	E_1
(x^2-y^2, xy)		E_2	E_2	E_2
		$\vdots$	$\vdots$	$\vdots$

are adapted from the familiar character table for the semi-infinite group $D_{\infty h}$.

The character table for group D_{nd} for odd integers $n = 2j + 1$ is constructed from Table 23.28 for group D_n [or group $(n2)$ in the international notation] by taking the direct product $D_n \otimes i$ where i is the two element inversion group containing E and i. In addition to the identity class E, the classes of D_n in Table 23.28 constitute the nth roots of unity where $\pm\phi_j$ rotations belong to the same class, and in addition there is a class $(2j+1)C_2'$ of n twofold axes at right angles to the main symmetry axis C_{ϕ_j}. Thus, Table 23.28 yields the character tables

for D_{nd}, or D_{5d}, D_{7d}, ... for symmorphic nanotubes with odd numbers of unit cells around the circumference $[(5,5)$, $(7,7)$, .. armchair nanotubes, and $(9,0)$, $(11,0)$, ... zigzag nanotubes]. Likewise, the character table for D_{nh}, or D_{6h}, D_{8h}, ... for even n is found from Table 23.29 by taking the direct product $D_n \otimes i = D_{nh}$. Table 23.29 shows two additional classes for group D_{2j} because rotation by π about the main symmetry axis is in a class by itself. Also the $2j$ twofold axes nC_2' form a class and are in a plane normal to the main symmetry axis C_{ϕ_j}, while the nC_2'' dihedral axes, which are bisectors of the nC_2' axes, also form a class for group D_n when n is an even integer. Correspondingly, there are two additional one-dimensional representations (B_1 and B_2) in D_{2j}, since the number of irreducible representations equals the number of classes. Table 23.30 lists the irreducible representations and basis functions for the various 1D nanotube groups and is helpful for indicating the symmetries that are infrared active (transform as the vector x, y, z) and Raman active (transform as the symmetric quadratic forms).

23.6.4   Symmetry for Nonsymmorphic Carbon Nanotubes

The symmetry groups for carbon nanotubes can be either symmorphic (as for the special case of the armchair and zigzag nanotubes) or nonsymmorphic for the general case of chiral nanotubes. For chiral nanotubes the chiral angle in Eq. (23.14) is in the range $0 < \theta < 30°$ and the space group operations $(\psi|\tau)$ given by Eqs. (23.20) and (23.21) involve both rotations and translations, as discussed in §23.6.2. Figure 23.9 shows the symmetry vector $\vec{R}$ which determines the space group operation $(\psi|\tau)$ for any carbon nanotube specified by (n, m). From the symmetry operation $R = (\psi|\tau)$ for nanotube (n, m), the symmetry group of the chiral nanotube can be determined. If the nanotube is considered as an infinite molecule, then the set of all operations R^j, for any integer j, also constitutes symmetry operators of the group of the nanotube. Thus from a symmetry standpoint, a carbon nanotube is a one-dimensional crystal with a translation vector $\vec{T}$ along the cylinder axis and a small number of carbon hexagons associated with the circumferential direction.

Table 23.31: The character table for the group $C_{N/\Omega}$ for chiral nanotubes, where N and Ω have no common divisor, corresponding to (n, m) having no common divisor.

$C_{N/\Omega}$	E	C^1	C^2	$\cdots$	C^ℓ	$\cdots$	C^{N-1}
A	1	1	1	$\cdots$	1	$\cdots$	1
B	1	-1	1	$\cdots$	$(-1)^\ell$	$\cdots$	-1
E_1	$\begin{cases} 1 \\ 1 \end{cases}$	$\begin{matrix} \epsilon \\ \epsilon^* \end{matrix}$	$\begin{matrix} \epsilon^2 \\ \epsilon^{*2} \end{matrix}$	$\cdots$	$\begin{matrix} \epsilon^\ell \\ \epsilon^{*\ell} \end{matrix}$	$\cdots$	$\begin{matrix} \epsilon^{N-1} \\ \epsilon^{*(N-1)} \end{matrix}$
E_2	$\begin{cases} 1 \\ 1 \end{cases}$	$\begin{matrix} \epsilon^2 \\ \epsilon^{*2} \end{matrix}$	$\begin{matrix} \epsilon^4 \\ \epsilon^{*4} \end{matrix}$	$\cdots$	$\begin{matrix} \epsilon^{2\ell} \\ \epsilon^{*2\ell} \end{matrix}$	$\cdots$	$\begin{matrix} \epsilon^{2(N-1)} \\ \epsilon^{*2(N-1)} \end{matrix}$
$\vdots$	$\vdots$	$\vdots$	$\vdots$	$\vdots$	$\vdots$	$\vdots$	$\vdots$
$E_{\frac{N}{2}-1}$	$\begin{cases} 1 \\ 1 \end{cases}$	$\begin{matrix} \epsilon^{\frac{N}{2}-1} \\ \epsilon^{*\frac{N}{2}-1} \end{matrix}$	$\begin{matrix} \epsilon^{2(\frac{N}{2}-1)} \\ \epsilon^{*2(\frac{N}{2}-1)} \end{matrix}$	$\cdots$	$\begin{matrix} \epsilon^{\ell(\frac{N}{2}-1)} \\ \epsilon^{*\ell(\frac{N}{2}-1)} \end{matrix}$	$\cdots$	$\begin{matrix} \epsilon^{(N-1)(\frac{N}{2}-1)} \\ \epsilon^{*(N-1)(\frac{N}{2}-1)} \end{matrix}$

[a] The complex number ϵ is $e^{2\pi i \Omega/N}$.

The symmetry groups for the chiral nanotubes are Abelian groups. All Abelian groups have a phase factor ϵ, such that all h symmetry elements of the group commute, and are obtained from any symmetry element by multiplication of ϵ by itself an appropriate number of times, such that $\epsilon^h = E$, the identity element. To specify the phase factors for the Abelian group, we introduce the quantity Ω of Eq. (23.22), where Ω/d is interpreted as the number of 2π rotations which occur after N/d rotations of ψ. The phase factor ϵ for the Abelian group for a carbon nanotube then becomes $\epsilon = \exp(2\pi i \Omega/N)$ for the case where (n, m) have no common divisors (i.e., $d = 1$). If $\Omega = 1$ and $d = 1$, then the symmetry vector $\vec{R}$ in Fig. 23.9 reaches a lattice point after a 2π rotation. Many of the actual nanotubes with $d = 1$ have large values for Ω; for example, for the $(6, 5)$ nanotube, $\Omega = 149$, while for the $(7, 4)$ nanotube $\Omega = 17$, so that many 2π rotations around the nanotube axis are needed to reach a lattice point of the 1D lattice.

The character table for the Abelian group of a carbon nanotube is given in Table 23.31 for the case where (n, m) have no common divisors and is labeled by $C_{N/\Omega}$. The number of group elements is N,

all symmetry elements commute with each other, and each symmetry operation is in a class by itself. The irreducible representation A in Table 23.31 corresponds to a 2π rotation, while representation B corresponds to a rotation by π. Except for the irreducible representations A and B, all other irreducible representations are doubly degenerate. The E representations correspond to two levels which stick together by time reversal symmetry, for which the corresponding eigenvectors are related to one another by complex conjugation. Since N can be quite large, there can be a large number of symmetry operations in the group $C_{N/\Omega}$, all of which can be represented in terms of a phase factor $\epsilon = \exp(i\psi) = \exp(2\pi i \Omega/N)$ and the irreducible representations are related to the Nth roots of unity. The number of classes and irreducible representations of group $C_{N/\Omega}$ is thus equal to N, counting each of the partners of the E representations as distinct. Various basis functions for group $C_{N/\Omega}$ that are useful for determining the infrared and Raman activity of the chiral nanotubes are listed in Table 23.30. We note that the irreducible representations A and E_1 are infrared active and A, E_1, and E_2 are Raman active.

For nanotubes where (n, m) have a common divisor d, then after N translations τ, a length Td is produced, and Ω unit cells of area (C_hT) are generated. For $d \neq 1$ the character table for the Abelian group in Table 23.31 contains $1/d$ as many elements, so that the order of the Abelian group becomes N/d. This case is discussed further below.

The space group for a chiral nanotube specified by (n, m) is given by the direct product of two Abelian groups

$$\mathcal{C} = C_{d'} \otimes C_{Nd/\Omega} \qquad (23.24)$$

where d' is the highest common divisor of Ω/d and d, while d is the highest common divisor of (n, m). The symmetry elements in group $C_{d'}$ which is of order d' include

$$C_{d'} = \{E, C_{d'}, C_{d'}^2, ..., C_{d'}^{d'-1}\}, \qquad (23.25)$$

and, correspondingly, the symmetry elements in group $C_{Nd/\Omega}$ include

$$C_{Nd/\Omega} = \{E, C_{Nd/\Omega}, C_{Nd/\Omega}^2, ..., C_{Nd/\Omega}^{(N/d')-1}\}, \qquad (23.26)$$

and group $C_{Nd/\Omega}$ is of order N/d'. The irreducible representations of the groups $C_{d'}$ and $C_{Nd/\Omega}$ in Eq. (23.24) are given in Table 23.31 and are appropriate roots of unity. For the two-dimensional E_n irreducible representations, the characters of the symmetry operations $C_{d'}$ and $C_{Nd/\Omega}$ are given by

$$\chi_{E_n}(C_{d'}) = \begin{cases} e^{i2\pi n/d'} \\ e^{-i2\pi n/d'} \end{cases} \tag{23.27}$$

where $1 \leq n \neq d'$ and

$$\chi_{E_n}(C_{Nd/\Omega}) = \begin{cases} e^{i2\pi n\Omega/Nd} \\ e^{-i2\pi n\Omega/Nd} \end{cases} \tag{23.28}$$

For the chiral nanotubes a vector transforms according to the basis functions for the A and E_1 irreducible representations, whereas quadratic terms in the coordinates form basis functions for the A, E_1, and E_2 irreducible representations, as shown in the Table 23.30.

Referring to Fig. 23.8(a) for the $(4, 2)$ nanotube, we have $\psi = 2\pi(5/28)$ and $\Omega/d = 5$, so that N rotations produce a total rotation of $2\pi(5)$. Since $d = 2$, N translations produce a distance $2T$, so that $N\vec{R}$ is the length of the diagonal of a rectangle that contains $\Omega = 10$ times the area of the 1D nanotube unit cell. The first lattice point is, however, reached at $(N/d)\vec{R} = [(5/2)C_h, T]$ of the 1D nanotube lattice. The number of elements in the Abelian group $C_{Nd/\Omega}$ is N/d, which is 14 in this case. The value of d' which is the highest common divisor of d and Ω/d is $d' = 1$, so that $C_{d'}$ is the identity group containing only one symmetry element. This example shows that for those (n, m) having a common divisor d, a lattice point is reached after $(N/d)\vec{R}$ translations, so that Ω/d^2 is not necessarily a multiple of 2π.

We now give some examples to show that if either $d > 1$ or $n - m = 3r$ (so that $d_R = 3d$), the 1D nanotube unit cell is reduced in size, and the number of $\vec{R}$ vectors to reach a lattice point is reduced. For example, nanotube $(7, 5)$ has a diameter of 8.18 Å, $N = 218$ symmetry operations, and 91 translations $\vec{R}$ are needed to reach a lattice point. Since the integers $(7, 5)$ have no common divisor, and since $n - m \neq 3r$, the unit cell is large. If we now consider a nanotube with $(n, m) = (8, 5)$ with a diameter of 8.89 Å, nearly 10% larger than the diameter for the

$(7,5)$ nanotube, we note that since $n-m$ is a multiple of 3, then $N = 86$ for the $(8,5)$ nanotube, where N is much smaller than for the $(7,5)$ nanotube. Likewise, for the $(8,5)$ nanotube, the length $T = 16.1$ Å is much shorter than $T = 44.5$ Å for the $(7,5)$ nanotube, and a lattice point is reached after 53 translations. An even smaller unit cell is obtained for the nanotube corresponding to $(n,m) = (10,5)$, despite the larger nanotube diameter of 10.36 Å. For the $(10,5)$ nanotube, N is only 70, and a lattice point is reached after only five translations $\vec{R}$. Although the number of symmetry operations of the nonsymmorphic groups tends to increase with nanotube diameter, those nanotubes for which either $n - m = 3r$, where r is an integer, or (n,m) contains a common divisor d, the size of the unit cell and therefore the number of symmetry operations is reduced by factors of 3 and d, respectively.

The symmorphic groups corresponding to the armchair and zigzag nanotubes have relatively small unit cells with $T = a_0$ and $T = \sqrt{3}a_0$, respectively, where $a_0 = 2.46$ Å$= \sqrt{3}a_{\mathrm{C-C}}$. The basic rotation angle ψ for both the (n,n) armchair nanotube and the $(n,0)$ zigzag nanotube is $\psi = 2\pi/n$.

23.6.5   Reciprocal Lattice Vectors

To express the dispersion relations for electrons and phonons in carbon nanotubes, it is necessary to specify the basis vectors in reciprocal space $\vec{K}_i$ which relate to those in real space $\vec{R}_j$ by

$$\vec{R}_j \cdot \vec{K}_i = 2\pi \delta_{ij}. \tag{23.29}$$

The lattice vectors and the unit cells in real space are discussed in §23.6.2. In Cartesian coordinates we can write the two real space lattice vectors as

$$\begin{aligned}
\vec{C}_h &= (a_0/2d_R)\Big(\sqrt{3}(n+m), (n-m)\Big), \\
\vec{T} &= (3a_0/2d_R)\Big(-(n-m)/\sqrt{3}, (n+m)\Big)
\end{aligned} \tag{23.30}$$

where d_R is defined by Eq. (23.17) and the length a_0 is the lattice constant of the 2D graphene unit cell, $a_0 = a_{\mathrm{C-C}}\sqrt{3}$. From Eq. (23.30),
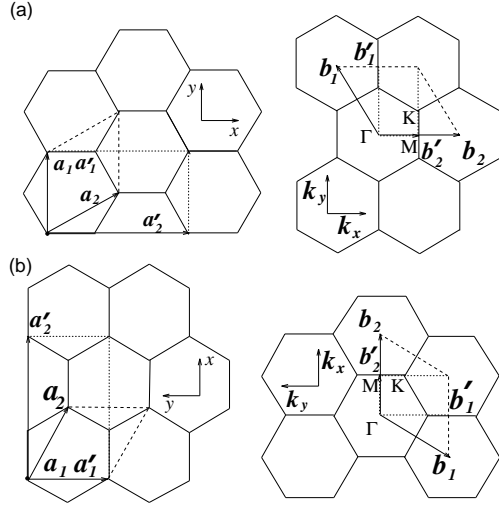
Figure 23.10: Real space unit cell and Brillouin zone for (a) armchair and (b) zigzag nanotubes (dotted lines). Those for a 2D graphene sheet (dashed lines) are shown for comparison.

it is easy to see that the lengths of $\vec{C}_h$ and $\vec{T}$ are in agreement with Eqs. (23.13) and (23.16). Then using Eqs. (23.29) and (23.30), we can write the corresponding reciprocal lattice vectors $\vec{K}_1$ and $\vec{K}_2$ in Cartesian coordinates as

$$
\begin{aligned}
\vec{K}_1 &= (2\pi/Na_0)\left(\sqrt{3}(n+m),(n-m)\right), \\
\vec{K}_2 &= (2\pi/Na_0)\left(-(n-m)/\sqrt{3},(n+m)\right).
\end{aligned}
\tag{23.31}
$$

For the case of the armchair and zigzag nanotubes, it is convenient to choose a real space rectangular unit cell in accordance with Fig. 23.10. The area of each real space unit cell for both the armchair and zigzag nanotubes contains two hexagons or four carbon atoms. It should be noted that the real space unit cell defined by the vectors $\vec{T}$ and $\vec{C}_h$ is n times larger than the real space unit cells shown in Fig. 23.10. Also shown in this figure are the real space unit cells for a 2D graphene layer. It should be noted that the real space unit cell for the zigzag nanotubes follows from the definition given for the unit cells for chiral nanotubes

[Fig. 23.8(a)], but the unit cell for the armchair nanotube is specially selected for convenience.

Having specified the real space unit cells in Fig. 23.10, the corresponding unit cells in reciprocal space (or Brillouin zones) are determined by Eqs. (23.29) and (23.31) and are shown in Fig. 23.10 in comparison to the reciprocal space unit cell for a 2D graphene sheet. We note that for both the armchair and zigzag nanotubes, the 1D reciprocal space unit cells shown in Fig. 23.10 are half as large as those for the 2D graphene sheet. On the graphene sheet, the real space lattice vectors $\vec{C}_h$ and $\vec{T}$ form a rectangular unit cell for the zigzag or armchair nanotubes. This unit cell has an area N times larger than the area of the corresponding primitive cell in the graphene sheet, where N is given by Eq. (23.18), spans the circumference of the cylinder of the nanotube.

The one-dimensional Brillouin zone of the chiral nanotube is a segment along the vector $\vec{K}_2$ of Eq. (23.31). The extended Brillouin zone for the nanotube is a collection of N wave vector segments of length $|\vec{K}_2|$, each separated from the next segment by the vector $\vec{K}_1$. Thus, by zone folding the N wave vector segments of the 2D dispersion relations of the graphene layer back to the first Brillouin zone of the 1D nanotube, the 1D dispersion relations for the N electron energy bands (or phonon branches) of the nanotube are obtained. For the special cases of the armchair and zigzag nanotubes, the real space unit cells in Fig. 23.10 correspond to four carbon atoms and two hexagons, while the reciprocal space unit cells also contain two wave vectors. Therefore each dispersion relation for the (n, n) armchair nanotubes and the $(n, 0)$ zigzag nanotubes is zone folded $n = N/2$ times in the extended Brillouin zone to match the 1D Brillouin zone of the nanotube.

23.7   Suggested Problems

1. A regular dodecahedron has 12 regular pentagonal faces, 20 vertices and 30 edges.

    (a) What are the symmetry classes for the regular dodecahedron?

(b) Is this symmetry group isomorphic to that for the regular icosahedron? Explain.

(c) Show (by finding the characters of the rotation group) that the d-level for a transition metal impurity in a quasicrystal with I_h point symmetry is not split by the icosahedral crystal field.

2. Suppose that we stretch the $B_{12}H_{12}$ molecule pictured in Fig. 3.3 along one of the 5-fold axes.

(a) What are the resulting symmetry elements on the stretched molecule?

(b) What is the appropriate point group?

(c) Consider the G_u and H_g irreducible representations of group I_h as reducible representation of the lower symmetry group of a 4-fold level transforming as G_u and a 5-fold level transforming as H_g in the I_h group. Assuming the basis functions given in the character table, give the corresponding basis functions for the levels in the stretched molecule.